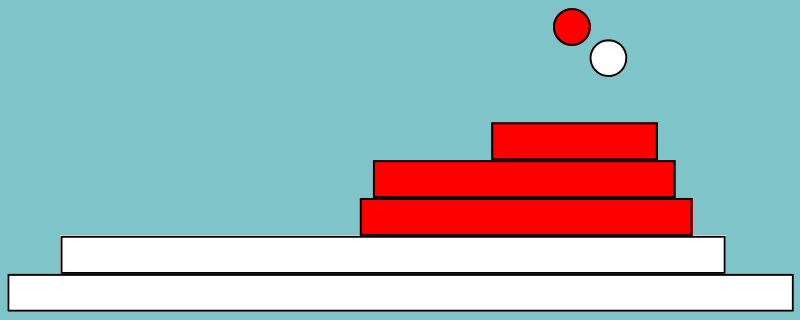

# Proceedings of ICTF14

## &RSD2008

R. De Gryse
D. Depla
D. Poelman
S. Mahieu
W.P. Leroy
H. Poelman

Proceedings of ICTF14&RSD2008
R. De Gryse, D. Depla, D. Poelman, S. Mahieu,
W.P. Leroy and H. Poelman

ISBN 978 90 334 7347 0

# Preface

Organizing an international conference with a limited number of people, is quite a challenge. It is hard work, and the work adds just to the daily work. Two research groups within the department of Solid State Sciences of Ghent University took the challenge, and one can ask why.

When processing this book of proceedings and abstracts for the International Conference on Thin Films the answer came. The reason is the common interest of all participants. Indeed, isn't just great ? To notice that more than 750 names are registered in the index list of this book, and all these people have a common interest: thin films! To know that we will meet some of these people, listening to their oral contributions, and discussing their scientific work over a poster, has given the organizing committee the spirit to keep on going.

The large interest in thin films, is to our opinion, not a surprise, realizing the impact of thin films on our daily life. Thin films have a broad application field. During the four days of the International Conference on Thin Films, most aspects of thin films are covered. Ranging from fundamental studies of thin film growth, over characterization to specialized applications. Browsing through this book with proceedings and abstracts gives pretty much an idea about the new trends in thin film deposition and applications. Together with the sponsors of this book, we hope, by registering this book with an ISBN number, that we give the international scientific community a good overview of the present status of thin film research. And … if a few persons get new ideas or view points when browsing through this book, the hard work of the organizing committee was worth the effort.

The organizing committee,

# A vision for Thin Film Applications in photovoltaic technology and the renewable energy sector

**W. Hoffmann**

Dr. Hoffmann is president of the European Photovoltaic Industry Association (EPIA), the world's largest industry association devoted to the solar electricity market. He is also an executive committee member with the German Solar Industry Association (BSW). Currently, Dr. Hoffmann is chief technology officer of the Solar Business Group and a member of the management board of Applied Materials GmbH, where he is responsible for technology development for Applied Materials in the US, Europe and Asia. Dr. Hoffmann was previously the chairman of the management board at RWE Schott Solar GmbH, chairman of the board of Applied Solar Energy (ASE) Americas and leader of the solar division at NUKEM. Dr. Hoffmann is a member of the Scientific Advisory Board of the Fraunhofer Institute for Solar Energy Systems (fhG-ISE) in Freiburg, and a member of the supervisory board of the Institute for Solar Energy Research (ISFH) in Hameln, Germany.

# Development of Highly Functional $TiO_2$ Thin Films by a RF Magnetron Sputtering Method and their Applications in Visible-Light-responsive Photocatalysts and Dye-Sensitizer-free Thin Film Solar Cells

**M. Anpo**
Department of Applied Chemistry, Graduate School of Engineering
Osaka Prefecture University
1-1 Gakuen-cho, Sakai, Osaka 599-8531, JAPAN

Environmentally harmonious, clean and safe chemical technologies and processes to address pollution and climatic change are the subject of much research and discussion. Photocatalysis, in which the abundant and clean energy of solar light could be harnessed, would be a major advance in the development of sustainable and non-hazardous technologies. Such photocatalytic reactions using light can be classified into two categories, i.e., "down-hill" and "up-hill", and the application of "down-hill" reactions is yet a great challenge to scientists. However, investigations on $TiO_2$ photocatalysts have been especially promising and, significantly, the photo-induced super-hydrophilic properties of $TiO_2$ thin films for such applications as self-cleaning and anti-fogging in mirrors and windows have already being realized. One of the most significant "up-hill" reactions known is the photosynthesis in green plants. However, unlike natural photosynthesis, typical $TiO_2$ photocatalysts make use of only 3-4 % of the solar irradiation reaching the earth, necessitating the use of an UV light source. There is, thus, an urgent need to develop highly reactive and functional $TiO_2$ materials, or second-generation $TiO_2$ photocatalysts, able to operate efficiently and effectively under weak UV as well as natural sunlight or visible light. The present work presents the development of highly functional $TiO_2$ thin film photocatalysts by applying a RF magnetron sputtering deposition method, enabling the thin films to absorb visible light of longer than 550 nm. The method was found to be one of the most promising approaches in the development of highly functional $TiO_2$ thin film catalysts for application in devices for the splitting of $H_2O$ into $H_2$ and $O_2$ with their separate evolution as well as to design thin film solid solar cells without the use of any organic dye sensitizers. In summary, our findings clearly show that these newly developed $TiO_2$ thin film materials can be considered potential candidates in innovative reactions and processes that can efficiently utilize solar energy.

M. Anpo, et al., *Annu. Rev. Mater. Res.,* Ed. J. M. Thomas, **35**, 233 (2005), and references therein.
M. Kitano and M. Anpo, et al., *Current Appl. Physics*, **6**, 982 (2006), and references therein.
M. Kitano, H. Kikuchi, M. Anpo, et al., *J. Phys. Chem.*, **110**, 5537 and 25266 (2006).
M. Kitano, M. Matauoka, M. Ueshima, M. Anpo, *Appl. Catal., A: Genera*l, **325,** 1 (2007).
M. Kitano, M. Anpo, et al., *Materials Science Form*, **544-545**, 107 (2007), and references therein.
M. Kitano, M. Takeuchi, M. Matsuoka, M. Anpo, et al., *Catal. Today*, **120**, 133 (2007).
M. Matsuoka, M. Kitano, M. Takeuchi, M.Anpo, J. M. Thomas, *Catal. Today*, **122**, 51 (2007).
M. Kitano, M. Anpo, W. T. Lin, and H. C. Chen, unpublished data (2006-2007).

# Organic Thin Films: Basic properties and device applications

**K. Leo**
Institut für Angewandte Photophysik, TU Dresden, 01062 Dresden, Germany, www.iapp.de
Fraunhofer-Institute for Photonic Microsystems, 01109 Dresden

Organic semiconductors are currently investigated intensively, both because the basic physics are little understood and because of attractive application possibilities, such as flat-panel displays based on organic light emitting diodes (OLED). Despite the fact that organic semiconductors have, in particular as thin films, rather low mobilities, they perform surprisingly well in optoelectronic devices.
In contrast to classical semiconductor technology, where device applications started when it was possible to control the carrier concentration, doping in organics has been less considered. I will discuss results of a comprehensive study of controlled n- and p-type doping of various molecular organic materials.
We have recently shown that these electrical doping concepts can be successfully applied in devices: the concept of molecular doping allows to realise green OLED devices with the highest efficiencies reported so far, well exceeding the efficiency of current inorganic GaN devices! White OLED have recently achieved efficiencies comparable to fluorescent tubes, opening the path to a new form of high-efficiency area lighting devices. Surprisingly, the field of OLED is currently dominated by vapor-deposited small-molecule devices, despite the fact that initially, polymer OLED which allow liquid processing were seen as the more direct and cost-effective approach to devices.
Also, I will discuss organic solar cells. In particular, I will address novel absorber materials for small-molecule solar cells and the use of electrically doped transport layers. The latter approach is very helpful for an optimized optical design since it yields large freedom in the choice of window layer thickness.

For an overview about this work, see the review article K. Walzer et al., Chem. Rev. 107, 1233 (2007).

# Atomistic processes during thin film and nanostructure growth

**Daniel Gall**
Rensselaer Polytechnic Institute
http://www.rpi.edu/~galld

Developing a true atomic-level understanding of thin film and nanostructure formation during physical vapor deposition requires a quantitative study bridging multiple length-scales. A combination of experimental and computational methods is employed to investigate (i) microstructural evolution of entire layers, (ii) surface roughening and island kinetics, and (iii) single atom and molecule diffusion and reaction processes, in order to develop an atomistic understanding of transition-metal nitride layer growth. Atomic shadowing, anisotropic surface diffusion, and ion-surface interactions are exploited to create unique nanostructures, including nanopipes, nanostaircases, nanosprings, and nanorods, with potential applications as sensors, hard self-lubricating coatings, gas filtration, and fuel-cell electrodes.

# From PVD to CVD to ALD for Semiconductor Manufacturing

**S.M. Rossnagel**
IBM Research, PO 218 Yorktown Heights, NY 10598 USA

With the advent of Damascene integration for microprocessor fabrication, sputter deposition (PVD) of films into deep, high aspect ratio features was deemed obsolete due to the broad angular distribution of the sputtered flux. Over the past 20 years, numerous iterative upgrades to PVD technology, such as collimation and ionization, have allowed PVD to remain as the domiant film deposition process for interconnects, contacts and silicides. Chemical Vapor Deposition (CVD) has long been anticipated as the solution to the fundamental problem of PVD, which is conformality. However, CVD techniques have not been broadly accepted due to the complexities of the deposition process chemistry and secondary manufacturing problems. Recent CVD work with oversupply of the product species during deposition has resulted in significant increases in conformality control. Issues remain with the very early stages of deposition, which become increasingly critical as functional film thicknesses approach the 2-3nm level in manufacturing. Atomic Layer Deposition (ALD) was envisioned as the logical extension of CVD and overcomes both conformality control issues as well as very-thin-film nucleation problems. ALD, however, is a slow technology and has only become viable as film thicknesses shrink to the nm scale. This talk will address these and related deposition technologies and their application to interconnects, contacts, and also gate technology.

# Nanostructures- à la carte: From size controlled Si nanocrystals to ordered arranged ZnO Nanowires

**Margit Zacharias**
Inst. of Microsystems Engineering (IMTEK), Georges Koehler Alley 103, Albert Ludwigs University of Freiburg, 79110 Freiburg, Germany

The aim of a future nanotechnology should be the growth of nanostructures with defined properties and defined dimension, may be in a periodic arrangement, and at a predefined position of the substrate. This means that the process of complete "self-organization" has to be influenced and controlled. In this talk examples based on Si nanocrystals as well as ZnO nanowires will be presented.

The visible room temperature luminescence of Si nanocrystals in porous Si observed in 1990 triggered a strong interest in the controlled fabrication of Si nanocrystals. Basic fundamental questions concerning quantum confinement in indirect semiconductors as well as potential applications such as non volatile Si NC based memories or light emitting devices are still in the focus of attention. For clarifying the origin of the observed luminescence signal as well as for applications, tight control over the size of the nanocrystals is essential. The talk will give an overview about ways for size controlled Si nanocrystals, their basic properties and future applications. [1, 2]

World wide the synthesis of semiconductor nanowires has been studied intensively for a wide spectrum of materials. Such low-dimensional nanostructures are not only interesting for fundamental research due to their unique structural and physical properties compared to their bulk counterparts, but also offer a fascinating potential for future technological applications. Strategies for position-controlled and nano-patterned growth of nanowire arrays will be demonstrated by selected examples based on ZnO nanowires as well as discussed in terms of larger scale realization and future prospects.[3] The properties of single ZnO nanowires will be presented on selected examples. Recently, we demonstrated the transfer of core-shell nanowires into spinel nanotubes via Kirkendall effect and solid-state reaction.[4] We expect that the nanoscaled Kirkendall effect provides a general fabrication route to hollow nanostructures, including high aspect ratio nanotubes.[5]

[1] J. Heitmann, F. Müller, L.X. Yi, M. Zacharias, D. Kovalev, F. Eichhorn, Excitons in Si nanocrystals: confinement and migration effects. Phys. Rev. B69 (2004) 195309.
[2] J. Heitmann, F. Müller, M. Zacharias, U. Gösele. Silicon nanocrystals: Size matters. Adv. Mat. 17 (2005) 795.
[3] H.J. Fan, P. Werner, M. Zacharias, Semiconductor nanowires: from self-organization to growth control Small 2 (2006) 700.
[4] H.J. Fan, M. Knez, R. Scholz, K. Nielsch, E. Pippel, D. Hesse, M. Zacharias; U. Gösele, Monocrystalline spinel nanotube fabrication based on Kirkendall effect. Nature Materials 5 (2006) 627.
[5] H.J. Fan, U. Gösele, M. Zacharias, Formation of nanotubes and hollow nanoparticles based on Kirkendall and diffusion processes: A review, Small 3 (2007) 1660.

# In-situ, real-time observation of Thin film deposition : Roughening, zeno, boundary crossing barrier, and steering

**Marcel J. Rost**
Kamerlingh Onnes Laboratory, P.O.Box 9504, 2300 RA Leiden, The Netherlands

Thin polycrystalline metal films are becoming increasingly important, as is reflected in the multitude of applications in nanotechnology, nanooptics, microelectronics, vacuum coating, catalysis, medical science, sensor elements, wear protection layers, decorative coatings, and the synthesis of new materials.
As thin film properties are intrinsically linked to the precise film structure, one would like to control the overall film morphology down to the nanometer scale.
This clearly demands fundamental research that links well-known atomic processes, such as diffusion and nucleation, with the mesoscopic film evolution during film growth.
Applying video-rate Scanning Tunneling Microscopy (STM) [1], we succeeded in visualizing film growth with atomic-scale resolution in real-time [2]. We evaporated several tens of monolayers of gold on top of a well-annealed polycrystalline gold film, *while* continuously observing the evolving surface with the microscope. These measurements directly visualize atomic processes that take place *during* film growth.
Analyzing the evolving film structure, we observe a significant increase in the film roughness, which we explain by considering both “well-known”, single crystalline growth modes in combination with additional polycrystalline effects [2, 3]. The grain boundaries play a crucial role in the evolution, as they initiate mound formation, thereby significantly increasing the total film roughness. A possible additional roughness contribution comes from atom steering, which also can delay the film closure in the early stages during film growth.

[1] M.J. Rost et al.; Rev. Sci. Instr. **76**, 053710-1 (2005)
[2] M.J. Rost; Phys. Rev. Lett. **99**, 266101 (2007)
[3] M.J. Rost et al.; Phys. Rev. Lett. **91**, 026101 (2003)

# Tailoring surface properties for advanced biomaterials devices and applications

**M.Anderle**

Fondazione Bruno Kessler, 38050 Povo, Trento, Italy

The design of bio-functional interfaces on solid surfaces is a fast developing and highly interdisciplinary field with numerous scientific and practical applications. Examples are medical implants in the human body, biosensors and biochips for diagnostics, drug delivery systems, tissue engineering, bioelectronics and biomimetic materials. Biofunctional surfaces have also a fundamental interest giving the opportunity to explore the interaction between biological components and surfaces and to address the physical basis of biomembrane self-assembly and lipid/protein interaction mechanisms. In this presentation different strategies in surface biofunctionalization will be described, ranging from surface plasma treatment, to covalent bonding of organic molecules, to the use of electrochemically deposited biopolymer layers for controlling the biocompatible character of the surface. Examples will cover bacteria proliferation control on catheter surfaces and enhanced growth of gingival cells on artificial dental implants. In the nano and micro scale range, surface treatments for extraction, purification and amplification of DNA from whole blood to develop microfluidic devices for genomic analysis will be presented, as well as carbon nanotubes functionalization as a novel substrate for DNA and protein binding for biosensing, drug delivery, and implant applications.

# QUADRUPOLES FOR ADVANCED SCIENCE

## PRECISION GAS ANALYSIS

Instruments for residual gas analysis (RGA)
Evolved gas analysis
TPD/TPR
Vacuum process monitoring


## UHV SURFACE SCIENCE

UHV specific pulse counting detector
Photon and electron stimulated desorption
Molecular beam studies
Temperature programmed desorption
SIMS - high sensitivity surface analysis

## PLASMA CHARACTERISATION

EQP ion mass and energy analyser
RF, DC, ECR and pulsed plasma
Neutrals and neutral radicals
Time resolved analysis

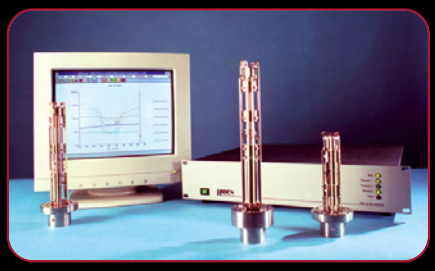

HIDEN ANALYTICAL

for further details of Hiden Analytical products contact:

info@hiden.co.uk
www.HidenAnaytical.com

Quadrupoles for advanced science

## LayTec
## from academic vision – to market leadership

In the late 1990s, LayTec's innovative in-situ measuring technology created a sensation in the already adrenalin-pumped compound semiconductor market. Because our in-situ sensors proved indispensable for optimising material quality and obtaining run-to-run reproducibility in epitaxy-based opto-electronic and electronic applications, LayTec quickly became the market leader in compound semiconductor monitoring instrumentation for epitaxial thin-film growth (MOVPE, MBE), replacing conventional ex-situ models of characterisation.

Our sensors measure growth rate, layer thickness, doping levels, ternary material composition, surface roughness, substrate temperature and strain-induced substrate bowing with an extreme precision already during the deposition process.

Our **EpiCurve® TT** type of sensors allows simultaneous and waferselective temperature, reflectance and wafer bowing measurements with an outstanding resolution up to 0.3 $km^{-1}$. Our EpiTT sensors are the first choice today for LED production world-wide and provide emissivity corrected temperature measurements based on the combination of pyrometry and refl ectance measurements at two optimized wavelengths. **EpiRAS® TT** is still the most advanced multiwafer in-situ sensor for cubic compound semiconductors. It is a unique tool for the R&D of GaAs- and InP-based opto-electronic devices.

We balance the spirit of innovative, pioneering invention with solid production efficiency. Fast-paced product development is inspired by a continuing dialogue with our customers. Supported through an international network of local distributors, LayTec sensors are in use at leading institutes and manufacturing facilities around the world.

All of LayTec's high-precision instruments are built in our in-house production facilities. This gives us the added capability to respond quickly to potential engineering needs for sensor customisation and OEM integration.

Our customers know that in-situ monitoring dramatically reduces development cycles, increases yield, enables superior quality control and provides best possible reproducibility.

# Reactively Sputtered Zinc Oxide Based Transparent Window Layers for $CuInS_2$ Thin Film Solar Cells

**M. Resch [1], M. Kanis [1], K. Ellmer [1]**

1. Helmholtz Centre for Materials and Energy, Dept. Solar Energetics, Glienicker Str. 100, 14109 Berlin, Germany

Copper indium disulfide ($CuInS_2$) is an attractive absorber material for thin film solar cells [1]. It has a suitable band gap of $E_g$=1.53 eV for solar energy conversion and a high absorption coefficient (> 105 cm-1) and it is already commercialized for thin film solar modules [2].
Compared to the related material Cu(In,Ga)Se2, which yields in the laboratory efficiencies of up to 19.9 %, $CuInS_2$ shows up to now a much lower efficiency in the range from 11 to 12.3 %, which is mainly caused by an open circuit voltage, which is too low, compared to the band gap voltage of $CuInS_2$. Since this fact is independent on the preparation method of the films, it seems to be an intrinsic property of the absorber material itself and/or of the heterojunction $CuInS_2$/CdS/ZnO/ZnO:Al. This lack of open circuit voltage is observed not only for $CuInS_2$ but also for other wide-band gap compound semiconductors [3]. One idea is, that this is due to a wrong band alignement between absorber and window layer.
In this work other transparent, conductive oxide layers, derived from ZnO are investigated with respect to its optical and electrical properties. The main goal was to deposit $ZnMe_xO_y$ films with lower electron affinities in order to improve the band alignement.
The $ZnMe_xO_y$ films were prepared by reactive magnetron sputtering from oxidic targets in $Ar/O_2$ or $Ar/H_2$ gas mixtures. The plasma was excited by radio frequency (13.56 MHz). The optical absorption coefficient and the band gap were determined from reflection and transmission measurements by a double-beam spectrometer in the wavelength range from 200 to 3200 nm. The electrical parameters were derived from Hall and conductivity measurements. The measurement of the electron affinity was performed by photoelectron spectroscopy (PES). For this purpose, the films were transferred under high-vacuum from the deposition to the PES chamber. With optimized $ZnMe_xO_y$ films, solar cells with $CuInS_2$ absorbers were prepared in the base line of our institute and IV characteristics were measured.
While the electron affinity and the band gap of $ZnMe_xO_y$ films can be modified by the addition of group II elements to ZnO, the open circuit voltage improved only slightly. Reasons for this behaviour are discussed.

[1] R. Scheer, T. Walter, H. W. Schock, M. L. Fearheiley and H. J. Lewerenz, Appl. Phys. Lett. 63 3294 (1993)
[2] N. Meyer, A. Meeder and D. Schmid, in: Proc. E-MRS 2006 Spring Meeting, Nice (France), May 29 to June 2, 4 (2006)
[3] U. Rau and M. Turcu, Mat. Res. Soc. Symp. Proc. 763 335 (2003)

# Influence of a-Si:H Fermi-energy on a-Si:H/c-Si hetero-interface passivation

**S. De Wolf [1,2], M. Kondo [1]**

1. National Institute of Advanced Industrial Science and Technology (AIST), Tsukuba, Japan
2. Now at Neuchâtel University, Switzerland

The doped hydrogenated amorphous silicon (a-Si:H) / crystalline silicon (c-Si) hetero-structure is an attractive solution to avoid the presence of highly recombinative metal contacts at the surfaces of c-Si based solar cells. To assure good interface passivation, insertion of a few nanometer thin device-grade intrinsic a-Si:H(i) film between c-Si substrate and doped a-Si:H layer is recommended (where the latter typically is also only a few nanometer thin) [1]. In this presentation, we focus on the role that such buffer-layer plays for the interface passivation. Post-deposition annealing offers in a straightforward way a single parameter to vary both electronic and material properties of the samples under study. Two fundamentally different recombination mechanisms that may critically affect heterostructure device performance have been identified in this way. Firstly, for the intrinsic buffer layer, whereas for abrupt a-Si:H / c-Si interfaces typically the interface passivation quality benefits from post deposition annealing, it is shown this is not the case when epitaxially grown Si material is present at the interface [2]. Likely, this difference in annealing behavior is related to the hydrogen-configuration and -content at the interface between film and substrate [3]. Secondly, in case the buffer layer is covered by a doped a Si:H overlayer, annealing may again be detrimental for the interface passivation [4]. Bringing the Fermi-level closer to either the conduction or valence band edge generally may lower the native acceptor or donor formation energy in a semiconductor [5]. For a-Si:H films, perhaps this corresponds to an observed lowered Si-H bond rupture energy for doped material. This offers an explanation why such doped films are typically more defect-rich and why it is beneficial to insert a lower defected intrinsic buffer-layer in between the doped a Si:H film and the substrate. Nevertheless, the presence of such a doped a Si:H overlayer on an intrinsic a-Si:H buffer layer may also shift the Fermi-energy in the latter film. Hence, the energy required for Si-H bond rupture is lowered slightly in the underlying intrinsic buffer layer as well. Principally, this may be the reason why the presence of a doped overlayer is detrimental to the c-Si:H / a-Si:H(i) interface passivation during annealing.

[1] M. Tanaka, M. Taguchi, T. Matsuyama, T. Sawada, S. Tsuda, S. Nakano, H. Hanafusa, and Y. Kuwano, Jpn. J. Appl. Phys., Part 1 31, 3518 (1992).
[2] S. De Wolf and M. Kondo, Appl. Phys. Lett. 90, 042111 (2007).
[3] S. De Wolf, S. Olibet and C. Ballif, Appl. Phys. Lett. 93, 032101 (2008).
[4] S. De Wolf and M. Kondo, Appl. Phys. Lett 91, 112109 (2007).
[5] A. Zunger, Appl. Phys. Lett. 83, 57 (2003).

# A novel approach for thin-film polycrystalline silicon on glass

**A. Illiberi, K.Sharma, A. Branca, M. Creatore, M.C.M. van de Sanden**
Eindhoven University of Technology, Department of Applied Physics, 5600 MB Eindhoven, The Nederlands

Thin film technology is starting to emerge as a new and promising approach for industrial production of PV modules [1]: polycrystalline silicon (Poly-Si) films are fabricated by crystallization of a-Si films, grown on low-cost supporting materials (glass substrate). In this framework, we are developing a new approach for the production of Poly-Si thin films: the a-Si layers are deposited by using the expanding chemical vapor deposition (ETP-CVD) technique, which has previously demonstrated device grade a-Si:H at high deposition rate (7-11 nm/s) [2].
The crystallization process has been induced by means of both Solid Phase Crystallization (SPC) and Rapid Thermal Annealing (RTA) techniques. Fourier Transform Infrared (FTIR) and Spectroscopic Ellipsometry (SE) diagnostics have been used to characterize both the as deposited and annealed a-Si:H layers, by measuring the thickness, hydrogen content, bonding configuration and optical constants of the films.
The imaginary part of the pseudo-dielectric function has been measured by means of SE to give insight into the crystallization degree of the annealed a-Si:H films [3]. The results have been confirmed by Raman diagnostic.
Structural material quality of the Poly-Si films has been investigated by means of cross-section Transmission Electron Microscopy (TEM): many crystal grains (1um lateral dimension) extend over the entire thickness (1um) of the annealed (via SPC) a-Si:H films on glass. This result indicates that a-Si:H films deposited in the ETP set-up are well suited in order to produce high quality Poly-Si films on low cost supporting material.

[1] "Photovoltaic technology: the case for thin film solar cells" A. Shah et al. Nature 285, 692 (1999)
[2] "Hydrogenated amorphous silicon deposited at very high growth rates by an expanding Ar-$H_2$-$SiH_4$ plasma" E. Kessels at al., J. Appl. Phys. 89, 2404, (2001)
[3] B. Hoex et al., 17th international PVSEC, Fukuoka, Japan, 1305, (2007)

# Chalcogenides films for non linear optical properties

**V. Nazabal [1], M. Chauvet [2], G. Fanjoux [2], G. Boudebs [4], K. P. Huy [2], S.-P. Gorza [5], F. Charpentier[1], M. Cathelinaud [3], T. Billeton [5], J.L.Adam [1]**

1. Sciences Chimiques de Rennes, UMR 6226, Université de Rennes 1, 35042 Rennes, France
2. Institut FEMTO-ST, UMR CNRS 6174, Département d'optique, Besançon Antwerp University,
3. Institut Fresnel, UMR CNRS 6133, Marseille. Laboratoire POMA, FRE CNRS, Angers
4. Laboratoire de physique des lasers (LPL), UMR CNRS 7538, Villetaneuse.
5. Université Libre de Bruxelles, service OPERA, Bruxelles

In this work, we are interested in the study of chalcogenides amorphous thin films for non linear applications. Chalcogenide glasses (ChG) are known for their good transmission from visible (sulphide) or near infrared (selenide, telluride) to middle infrared (mid-IR). This optical property is related to high atomic masses and weak bond strengths shifting increasingly the multiphonon absorption to the mid-infrared following sulphide, selenide and telluride series. Their refractive index is generally high (~2-3), and one particularly important potential rely on their photosensitivity to band gap light. ChG have also attracted significant attention in recent years as a promising nonlinear material for all optical devices. In addition, these chalcogenides can be deposited in amorphous thin film for optical coatings but also for opto-electronic components or opto-chemical sensors considering complex integrated optical structures. With their specific physico-chemical properties, these materials can be used like optical coatings, such as for example band pass filters for telecom or spatial applications in the infrared range. Moreover, the photoinduced refractive index change of chalcogenide films can be exploited for selective writing of Bragg gratings or channels waveguide. The transmission of amorphous chalcogenide films until 20μm can be exploited for Mid-IR micro-sensors with their inherent molecular selectivity, allow qualitative and quantitative analysis of various chemical and biological species. Finally, integrated all-optical devices rely on operation based on a third-order nonlinearity (e.g., ultra fast Kerr effect) for which chalcogenide films can play a leading role. Within this framework, we studied different types of sulphide and selenide films. These particular compositions were chosen because of their remarkable properties: large optical window covering the spectral region from 500 nm to 11 μm for sulphide glasses and between 1.3 μm and 18 μm for selenide glasses, excellent resistance to devitrification, good durability towards water and solvent corrosion, and high linear and non linear refractive index. We have investigated the chalcogenide films deposition by two deposition methods, electron beam deposition (EBD) and magnetron RF sputtering, both of them having their own advantages and disadvantages. As it is commonly accepted, the sputtering method generally allows preparation of thin films of complex composition since all components from the target can be deposited at once while the EBD technique is able to form large surface films with homogeneous thickness. We will also present experimental results on beam self-focusing in these films at telecommunication wavelength using the Kerr effect which represents preliminary results towards realisation of reconfigurable optical interconnects.

# Reactive Magnetron Sputtering of Sulfides for Thin Film Solar Cells

**S. Seeger [1], R. Grötzschel [2], K. Ellmer [1]**

1. Helmholtz Zentrum für Materialien und Energie, Dept. Solar Energetics, Glienicker Str. 100, 14109 Berlin, Germany

2. Forschungszentrum Rossendorf, Dept. Ion Beam Physics and Material Science, D-01328 Dresden, Bautzner Landstr. 128, Germany

Reactive magnetron sputtering is a well-known large-area deposition technique, which is already used to fabricate layers for thin film solar cells: the back contact (molybdenum) and front contact (zinc oxide) or metallic precursors, but NOT for the preparation of the light absorbing semiconductor layers in a one-step process [1]. In general, magnetron sputtering has the following advantages due to the ion-assistance: (i) deposition at lower temperatures compared to thermal processes, (ii) high chemical reactivity and (iii) compact and well adherent films. However, for the deposition of active electronic films, the high-energetic particles in magnetron discharge can pose problems due to the generation of recombination active defects. In this work the reactive magnetron sputtering from metallic copper, indium and tungsten targets in $Ar/H_2S$ atmospheres at substrate temperatures up to 700 °C is investigated. The plasma excitation was performed by DC and RF (13.56 and 27.12 MHz) power supplies. For the plasma characterization a Langmuir probe and a plasma monitor for the measurement of ion-energy distributions has been used. The deposition rate was determined by a quartz crystal monitor, while the film composition was analyzed by Rutherford backscattering (RBS). The electronic quality of the films has been checked by Hall and conductivity measurements, by photoluminescence (PL) spectroscopy and by time-resolved microwave conductivity (TRMC) analysis. While for tungsten disulfide ($WS_2$) films direct reactive magnetron sputtering is NOT suited for the preparation of photoactive absorber films due to the generation of defects, photoactive $In_2S_3$ and $CuInS_2$ films can be prepared. Due to the electronegative sulfur species in the discharges, high energetic negative ions ($S^-$), accelerated from the target towards the substrate, are responsible for the defect generation. The concentration of these defects depends on the bond-strength of the semiconductor, which is deposited. For WS2, which exhibits weak van der Waals bonds, a sequential process was developed, where an amorphous sulfur-rich WSx film is thermally crystallized by metal-induced crystallization [2]. For high frequency (27.56 MHz) plasma excitation, the target voltages are significantly lower compared to DC excitation and hence the energy of particles in the plasma is reduced considerably. Another advantage of RF excitation is the much higher chemical reactivity of the reactive species. The efficiency of the $CuInS_2$ solar cells depends strongly on the film morphology of the absorber layer. High copper excess during the deposition leads to porous films, which are responsible for shunting problems between back und front contacts in the solar cells.

[1] K. Ellmer, in "Low Temperature Plasmas. Fundamentals Technologies and Techniques "; Vol. 2, Ed.: R. Hippler, H. Kersten, M. Schmidt and K. H. Schoenbach (Wiley-VCH, Berlin, 2008) (ISBN 978-3-527-40673-9)

[2] S. Brunken, R. Mientus, S. Seeger, K. Ellmer, J. Appl. Phys. 103 (2008) 063501

# Growth of GaSb-based Thin Films for Optoelectronic Applications

**E.V. Kunitsyna, I.A. Andreev, T.V. L'vova, Ya.V. Terent'ev, A.N. Semenov, V.A. Solov'ev, B.Ya. Meltser, S.V. Ivanov, Yu.P. Yakovlev**
Ioffe Physical-Technical Institute RAS, 26 Politekhnicheskaya, 194021 St Petersburg, Russia

We present the aspects of the LPE and MBE growth, processing and characterization of GaSb-based thin films for IR photodiode applications, as well as R&D of the n-GaInAsSb/p-GaAlAsSb photodiodes. The crystalline quality of the grown epitaxial layers, the surface morphology and interface abruptness have been studied with PL, SEM, AFM, TEM, X-ray diffraction methods. Passivation of the n-GaInAsSb/p-GaAlAsSb heterostructure photodiodes in $Na_2S$ water solutions reduced the dark current.

## 1. INTRODUCTION

In recent years much effort has been devoted to photodiodes, solar cells and thermophotovoltaic devices for IR spectral range [1-3]. GaSb-related semiconductors demonstrate huge potential in these applications. This class of materials is of interest from both the fundamental physics viewpoint and viewpoint of optoelectronic devices. Over the past few years, molecular-beam epitaxy (MBE) and metal organic vapor phase epitaxy (MOCVD) have been used for the growth of high quality GaSb-based thin films. However, the simplicity and relative low cost of liquid phase epitaxy (LPE) makes it an attractive method for III-V growth. The main drawback of a near-equilibrium technique such as LPE is the existence of a wide range of solid composition which can not be obtained because of fundamental thermodynamic limitations [4]. Although MBE is generally accepted as a nonequilibrium technique, it reveals some difficulties in growing high quality GaSb-based alloys inside the immiscibility region [5]. The paper presents the growth, processing and characterization of GaSb-based thin films for IR photodiodes.

## 2. Growth of GaSb-based photodiode heterostructures

In the case of MBE growth the n-GaInAsSb/p-GaAlAsSb heterostructures (Table) lattice matched to n-GaSb(100) substrate were obtained using a RIBER 32P setup. Conventional solid source effusion cells were applied to produce In, Al and $Sb_4$ fluxes, whereas $As_4$ flux was supplied from a VAC-500 valved cracking cell. The GaSb surface was monitored *in situ* by RHEED. The composition of AlGaAsSb and GaInAsSb layers was determined using a CAMEBAX X-ray spectral microanalyzer and by double-crystal X-ray diffractometry (XRD) [6]. The microanalysis data on the composition of the metal components were used in the analysis and simulation of the XRD rocking curves for more exact determination of the lattice mismatch between a layer and a substrate. The lattice mismatch is less than $10^{-3}$ at $T=20^0C$.
In LPE growth of the n-GaInAsSb/p-GaAlAsSb heterostructures (Table) standard LPE system was used. The substrates were Te-doped GaSb(100). For GaInAsSb thin films the GaSb,

InAs, InSb binary compounds were applied for the melt preparation. As melt ingredients for GaAlAsSb layers we used Ga, Al with purity 99.9999 wt. % and GaSb. Arsenic was introduced into the melt from the additional GaAs substrate. According to XRD data, the lattice mismatch between the GaInAsSb layer and substrate was $(2\text{-}5)\times10^{-4}$ at T=$20^0$C. In case of LPE growth substrate-layer interface abruptness and high crystalline quality of the grown layers are achieved.

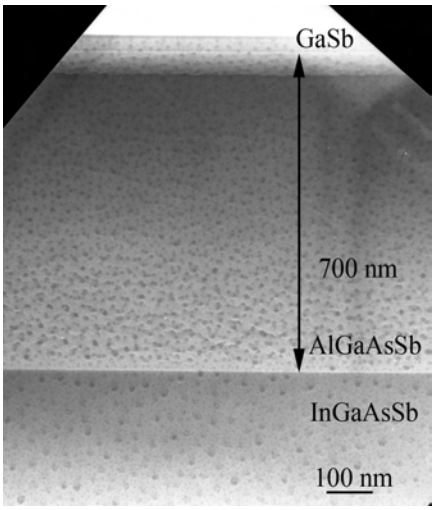


Figure 1. TEM image of the n-GaInAsSb/p-GaAlAsSb heterostructure grown by MBE.

| Composition | **Growth method** | **Growth temperature, $^0$C** | **Thickness, μm** | **Band gap $E_g$ at 300K, eV** |
|---|---|---|---|---|
| $Ga_{0.78}In_{0.22}As_{0.18}Sb_{0.82}$ | LPE | 600 | 2.2-2.5 | 0.53 |
| $Ga_{0.79}In_{0.21}As_{0.19}Sb_{0.81}$ | MBE | 500 | 1.5 | 0.512 |
| $Ga_{0.66}Al_{0.34}As_{0.025}Sb_{0.97}$ | LPE | 599 | 2.0 | 1.24 |
| $Ga_{0.6}Al_{0.4}As_{0.04}Sb_{0.96}$ | MBE | 500 | 1 | 1.35 |

Table 1. Parameters of GaSb-based solid solutions for photodiode applications.

Main requirements for the materials in photodiode terms are low carrier density in n-GaInAsSb active layer and high carrier density in p-GaAlAsSb "window". We employed Te as a compensating donor impurity for GaInAsSb layers and Ge (Be) as an acceptor impurity for GaAlAsSb layers.

It should be noted that the main advantage of LPE is possibility to grow the high-quality bulk GaInAsSb layers with composition near the miscibility gap boundary. At the same time main advantage of MBE technique in our case is the chance to reach the long-wavelength photosensitivity threshold $\lambda_{th}$=2.51 μm for GaInAsSb/GaAlAsSb heterostructures on (100)-oriented GaSb substrate.

## 3. n-GaInAsSb/p-GaAlAsSb PHOTODIODES

Our investigations of the n-GaInAsSb/p-GaAlAsSb MBE photodiodes indicate that the half maximum wavelength of the spectral sensitivity $\lambda_{50\%}$ determined by energy gap of the GaInAsSb solid solution (Eg=0.512 eV) is $\lambda_{50\%}$=2.42 μm at T=$20^0$C. The short wavelength cutoff is caused by absorption in the GaAlAsSb wide-gap "window" ($E_g$=1.35 eV). The temperature coefficient of variation of the band gap $\Delta E_g/\Delta T$, defined in the temperature range of 90-295 K, is $-4\times10^{-4}$ eV/K. The monochromatic current sensitivity at the maximum of

spectrum ($\lambda$=2.0-2.2 μm) was $S_I$=0.8-1.1 A/W, which corresponds to a quantum efficiency $\eta$=0.5-0.6 (without any antireflection coating). The capacitance at zero reverse bias is $C_0$ < 950 pF for the devices with diameter of 1.0 mm. The dark current density of the photodiodes was $j=(3\text{-}5)\times10^{-2}$ A/cm$^2$ at reverse bias 0.2-0.5 V. We believe that dark current may be significantly reduced by using higher quality GaSb-substrates and more accurately lattice-matching solid alloys.

For the n-GaInAsSb/p-GaAlAsSb LPE photodiodes parameters are the following: $\lambda_{50\%}$ = 2.32 μm at T=20$^0$C; $\Delta E_g/\Delta T = -4\times10^{-4}$ eV/K in the temperature range of 90-295 K; $S_I$ = 0.9-1.2 A/W ($\eta$=0.6-0.7); $C_0$ < 500 pF for the of the photodiode with 1.0 mm diameter; $j=3\times10^{-3}$ A/cm$^2$ of the best photodiodes at reverse bias 0.2-0.5 V.

## 4. Wet chemical passivation

One of main problems of the GaSb-based photodiode heterostructures is a relatively high level of the dark current. This is due to the fact that GaSb demonstrates high chemical activity causing a quick formation of surface oxides. The influence of mesa geometry formation techniques on the leakage currents of the photodiodes was studied. It was found that kinetics of etching for GaSb, GaInAsSb, GaAlAsSb materials were essentially different in the mesa formation process. It leads to non-uniformity of the mesa etching profiles for the GaSb-based photodiode heterostructures (Fig.2). Consequently, considerable advances in processing technology, including surface passivation techniques are required for further development of GaSb-based heterojunction photodiodes. Anodic oxidation of the mesa sidewall protects the surface from environment influence, but it does not improve the photodiode parameters fundamentally (Fig.3). To address this situation, we employ wet chemical passivation in $Na_2S$ water solutions for reducing the surface leakage current. According to our data, the chemical treatment of GaSb-related compounds in 1M $Na_2S$ water solution removes the surface oxides and forms instead it a thin film protecting the surface from further oxidation.

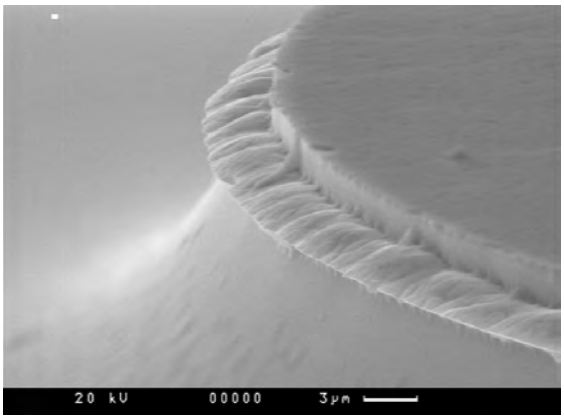


Figure 2. SEM image of the S-passivated n-GaInAsSb/p-GaAlAsSb photodiode mesa sidewall.

As seen in Figure 4, wet $Na_2S$ passivation of the GaInAsSb/GaAlAsSb photodiode mesa sidewall reduced the dark current. No degradation of the photodiode performance has been found for 4 months after the passivation.

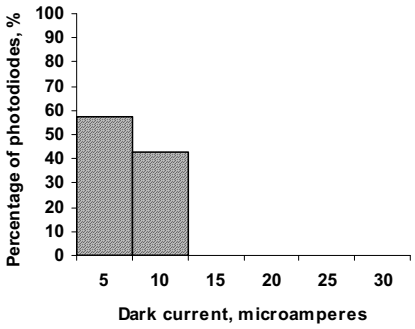


Figure 3. Histogram of the dark current distribution for the p-GaInAsSb/n-GaAlAsSb photodiodes with anodic oxidation of the mesa sidewall (57 in number, heterostructure M217, t=20C, U= –0.2V

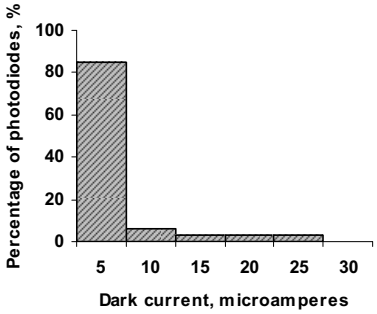


Figure 4. Histogram of the dark current distribution for the p-GaInAsSb/n-GaAlAsSb photodiodesafter $Na_2S$ surface passivation of the mesa sidewall (33 in number, heterostructure M217, t=20C, U=–0.2V).

## 5. CONCLUSIONS

In summary, we have developed reproducible LPE and MBE techniques for creating GaSb-based photodiodes with the long-wavelength photosensitivity threshold $\lambda_{th}$=2.4 μm and $\lambda_{th}$=2.51μm. These devices are extremely important now for laser diode spectroscopy of gases and molecules, IR optical fiber communication, ecological monitoring and medicine.

The work is supported by the Russian Foundation of Basic Research (RFBR) under Grant No.07-02-01359.

## 6. REFERENCES

[1] M.H.M. Reddy, J.T. Olesberg et al., Semicond. Sci. Technol. 21 267 (2006)
[2] M.G. Mauk and V.M. Andreev, Semicond. Sci. Technol. 18 191 (2003)
[3] E.V. Kunitsyna, I.A. Andreev, M.P. Mikhailova et al., Proc. SPIE. 4340 244 (2000)
[4] A.M. Litvak and N.A. Charykov, Zh.Fiz. Khim. 66 (4) 923 (1992)
[5] H. Miyoshi, Y. Horikoshi, J. Cryst.Growth. 227-228 571 (2001)
[6] A.N. Semenov et al., J. Cryst.Growth. 278 203 (2005)

# Electrochemistry of thin film battery materials prepared by Low Pressure Chemical Vapor Deposition

**J.F.M. Oudenhoven [1], T. van Dongen [2], R.A.H. Niessen [2], M.H.J.M. de Croon [1] and P.H.L. Notten [1,2]**

1. Eindhoven University of Technology, Department of Chemistry and Chemical Engineering, Den Dolech 2, 5612 AZ Eindhoven, The Netherlands

2. Philips Research Laboratories, Eindhoven, High Tech Campus 4, 5656 AE Eindhoven, The Netherlands

With miniaturization of electronics, nowadays a large part of the volume of standalone electronic devices is occupied by the power storage. The development of thin film lithium ion batteries did help in the miniaturization of electrochemical power storage [1], but the volumetric energy density of these batteries remains relatively low. An increase in energy density can be obtained with an increase of the surface area of the substrate on which the thin film battery is deposited. This can be achieved by etching microstructures into a silicon substrate, increasing the energy storage capacity by simply using the bulk of the substrate [2,3]. Etching of three-dimensional structures into silicon substrates is a well developed field in semiconductor industry [4], but the deposition of active battery materials onto these structures requires techniques that are somewhat unconventional for thin film batteries, e.g. Atomic Layer Deposition (ALD) and Low Pressure Chemical Vapor Deposition (LPCVD).

To evaluate the suitability of LPCVD as a method for the production of 3D thin film lithium ion batteries, first the deposition of battery materials on planar substrates needs to be thoroughly understood. To gain this knowledge, commercially available LPCVD equipment was modified for the deposition of metal oxide films. One of these metal oxides, $LiCoO_2$, a standard cathode material for lithium ion batteries, was deposited in planar thin film form and evaluated. These investigations focused on the effects of the deposition variables, e.g. the deposition temperature and the reactant ratio. The consequences of annealing on the electrode morphology were also investigated. Using the observation of the influence of these variables on the thin film properties, the deposition was optimized with respect to physical, chemical and electrochemical characteristics.

## 1. INTRODUCTION

Lithium ion batteries play a key-role in the development of micro-electronic devices. The recent development of all-solid-state thin film micro-batteries has created possibilities for on-board electrochemical energy storage in these devices [1]. To enhance the volumetric energy density of these batteries (which remained, until now, relatively low) a technique can be applied that is already relatively mature in semiconductor industry: by etching microstructures into silicon substrates, a battery with a larger effective surface area can be created, with possible capacity enhancements up to a factor of 25 [2,3].

Techniques that are somewhat unconventional for thin film batteries, e.g. Atomic Layer Deposition (ALD) and Low Pressure Chemical Vapor Deposition (LPCVD), are required to

deposit step-conformal thin films into three-dimensional structures. LPCVD is already an established technique to deposit metal oxides, like $LiCoO_2$, which are common cathodes for lithium ion batteries [5,6]. However, before LPCVD $LiCoO_2$ can be applied in 3D micro-batteries first the deposition on planar substrates needs to be thoroughly understood. Therefore the influence of various deposition parameters on film properties was investigated.

## 2. MEHODS

### *2.1 Low Pressure Chemical Vapor Deposition*

A commercial horizontal cold walled LPCVD reactor (Aixtron 200RF) was employed for the deposition of $LiCoO_2$ thin films. Bubblers filled with cobalt dicarbonyl cyclopentadienyl and tert-butyl lithium (both from Epichem, United Kingdom) were used as precursor sources, with argon as a carrier gas. Oxygen was mixed with argon and delivered to the deposition reactor via a separate system. The cobalt and lithium precursor were allowed to mix with oxygen in the deposition chamber.

Circular silicon wafers with a diameter of approximately 3 cm were used as substrates. A thin layer of platinum served as a conductive back contact for samples used for electrochemistry. During deposition, the substrates were placed on a graphite susceptor which was heated via RF. The influence of the ratio of reactants and of the susceptor temperature on the film properties was investigated.

### *2.3 Analysis and Electrochemistry*

X-ray diffraction and electrochemistry were used for sample characterization. X-ray diffraction was performed on a Panalytical X'Pert PRO MDP diffractometer using a Cu Kα X-ray source. Electrochemical measurements were done in an argon filled glove-box at room temperature using an Ecochemie PGSTAT30 potentiostat/galvanostat. For these measurements the $LiCoO_2$ films were employed as working electrodes, while lithium metal foils were used as reference and counter electrode. Cyclic Voltammetry (CV) was performed at 1 mV/s between 3.3 and 4.3 V (all potentials are given *versus* the $Li/Li^+$ reference electrode couple).

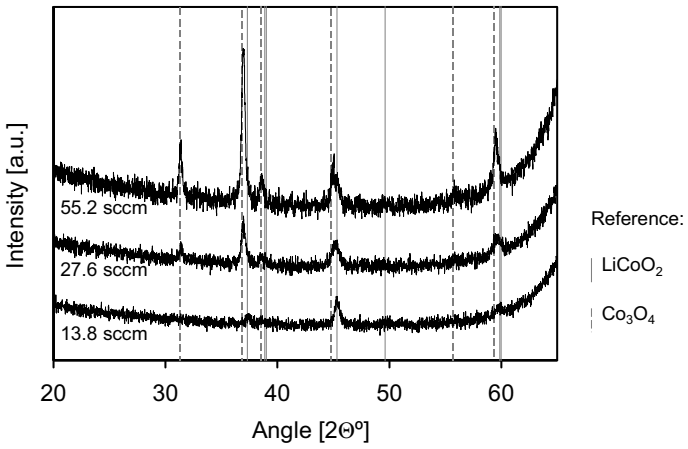


Figure 1. X-ray diffraction of samples deposited at various flow rates of cobalt precursor. Also shown are $LiCoO_2$ and $Co_3O_4$ references [7].

## 3. RESULTS

### *3.1 Reactant ratio*

The flow of argon through the cobalt precursor bubbler was varied to obtain samples in a range of stoichiometries. These samples were investigated by XRD, to determine the amount of $LiCoO_2$ formed and to detect the by-product $Co_3O_4$ (Fig. 1). The results show that a higher cobalt precursor flow leads to a higher $Co_3O_4$ concentration, while hardly any of it is formed at the lowest flow used. This can be observed most clearly from the 220 $Co_3O_4$ diffraction line at an angle of 31.3 º and the 311 at 36.9 º, which do not appear for the sample deposited at a flowrate of 13.8 sccm. This flow was chosen as a standard for subsequent experiments.

### *3.2 Deposition temperature*

To investigate the influence of the susceptor temperature on the film properties, five layers were deposited at temperatures between 300 and 500 ºC with an interval of 50 ºC. XRD analysis of these samples (Fig. 2) shows that deposition at low susceptor temperatures (below 400 ºC) yields no, or a negligible amount of crystalline material. Layers deposited at higher temperatures consist of a crystalline $LiCoO_2$ phase, which can be derived most clearly from the presence of the 101 and 104 diffraction lines at 37.3 and 45.3 º respectively. Also some $Co_3O_4$ is formed: the 220 diffraction (31.3 º) as well as the 311 line (36.9 º) are observed in the diffractograms. The sample deposited at 450 ºC shows the strongest $Co_3O_4$ peaks, whereas at 500 ºC a smaller amount of this compound is formed.

CV plots of the samples deposited at 400, 450 and 500 ºC (Fig. 3) show the typical large phase transition peak for $LiCoO_2$ near 3.9 V, and the two well-known smaller peaks around 4.1 and 4.2 V [8]. Samples deposited at lower temperatures (not shown here) gave a much weaker and less defined electrochemical response. Also a trend is observed that samples deposited at higher temperatures show a higher peak intensity and therefore a higher lithium ion storage capacity, since the peak area in CV measurements is directly related to the intercalated charge.

Combining the electrochemical and XRD results it is concluded that, within the experimental range, 500 ºC is the optimal deposition temperature: well defined crystalline $LiCoO_2$ is formed, a small amount of $Co_3O_4$ is present and the highest electrochemical charge is found.

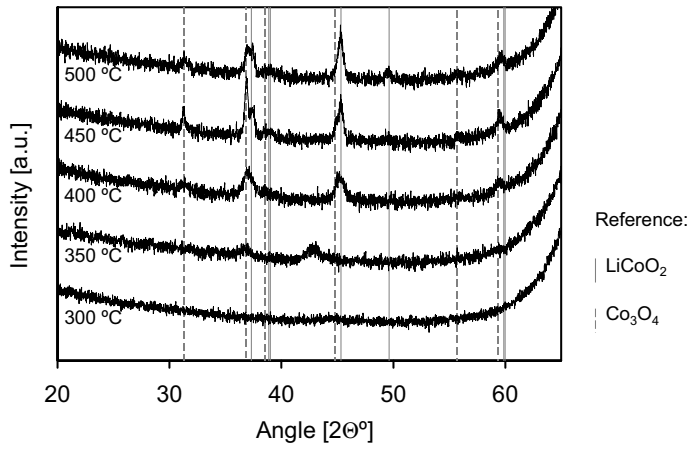


Figure 2. X-ray diffraction of $LiCoO_2$ samples deposited at 300-500 ºC, also indicated are $LiCoO_2$ and $Co_3O_4$ reference lines [7].

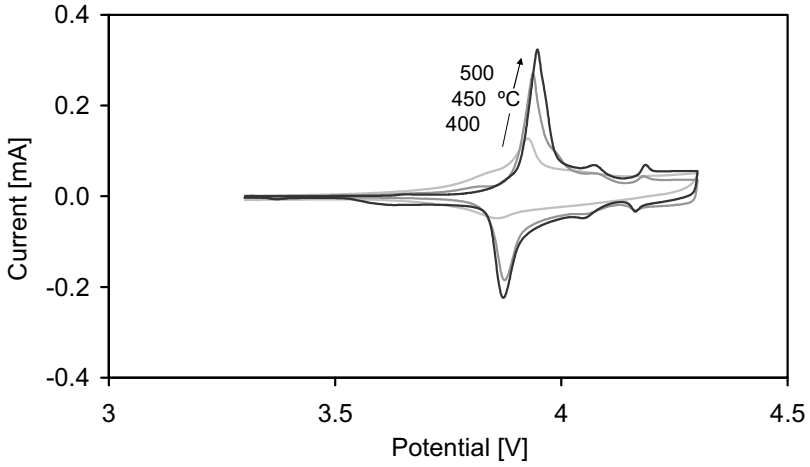


Figure 3. Cyclic Voltammetry on three $LiCoO_2$ samples deposited at 400, 450 and 500 ºC.

## 4. CONCLUSIONS

The influence of various deposition parameters on the quality of $LiCoO_2$ thin film cathodes for all solid state lithium ion batteries was reported. It was concluded that both the ratio of the reactants and the deposition temperature influence the layer properties significantly.

To deposit a low amount of $Co_3O_4$ in the $LiCoO_2$, a relatively low argon flow through the cobalt precursor delivery bubbler has to be chosen. When this low flow is combined with a high susceptor temperature of typically 500 ºC, films are formed that consist of crystalline $LiCoO_2$, which are electrochemically active. The well-known phase transitions are observed, indicating that well defined $LiCoO_2$ is formed.

These investigations show that LPCVD is a technique that is attractive for the deposition of planar thin film cathodes for all solid state batteries. Further experiments will have to evaluate the feasibility of LPCVD for Lithium ion battery anodes and electrolytes, and eventually for the deposition of all-solid-state 3D thin film micro-batteries.

## 5. REFERENCES

[1] J.B. Bates, N.J. Dudney, D.C. Lubben, G.R. Gruzalski, B.S. Kwak, Xiaohua Yu, R.A. Zuhr, J. Power Sources. 54 58 (1995)

[2] P.H.L. Notten, F. Roozeboom, R.A.H. Niessen, L. Baggetto, Adv. Mater. 19 4564 (2007)

[3] L. Baggetto, R.A.H. Niessen, F. Roozeboom and P.H.L. Notten, Adv. Funct. Mater. 18 1057 (2008)

[4] F. Roozeboom, R. Elfrink, J. Verhoeven, J. van den Meerakker, F. Holthuysen, Microelectronic Eng. 53 581 (2000)

[5] P. Fragnaud, R. Nagarajan, D.M. Schleich, and D. Vujic, J. Power Sources, 54, 362 (1995)

[6] S.I. Cho and S.G. Yoon, J. Electrochem. Soc., 149, A1584 (2002)

[7] X-ray powder diffraction file of the International Centre for Diffraction Data (ICDD). JCPDS cards 44-0145 and 42-1467

[8] J.N. Reimers and J.R. Dahn, J. Electrochem. Soc., 139, 2091 (1992)

# The Use of Modulated Pulse Power During High Power Pulse Magnetron Sputtering

**B. Mishra [1], J. J. Moore [1], J. Lin [1], W. D. Sproul [1,2], R, Chistyakov [3], and B. Abraham [3]**

1. Colorado School of Mines, Department of Metallurgical & Materials Engineering, Nathaniel P. Hill Hall, 15th Street & Arapahoe, Golden, CO, 80401

2. Reactive Sputtering, Inc., 2152 Goya Place, San Marcos, CA 92078

3. Zond, Inc./Zpulser, LLC, 137A High Street, Mansfield, MA, 02048

Modulated pulse power (MPP) sputtering is a variation of high power pulse magnetron sputtering that overcomes the rate loss issue through modulation of the pulse shape, intensity, and duration. With MPP, the pulse shape and duration and plasma perturbations directly affect the degree of ionization of the sputtered material. A typical MPP pulse, which can have a duration up to 2 msec, usually has 3 distinct parts to it. The first is the high voltage pulse to ignite the plasma, the second is the stabilization of a weakly ionized plasma, and the third is the generation of a strongly ionized plasma that occurs when the voltage is increased on the target. By using different pulse lengths and shapes, it is possible to modulate the energy delivered to the cathode during each of these different pulses. In this study, two different alternating pulse shapes and durations were used with each target material during the reactive sputtering of TiAlN and CrN films resulting in a layered deposition of these two materials. The effect of this energy modulation during the deposition of each layer was to change the structure and properties of the films. For the TiAlN coatings, the microstructure was reduced to a very fine columnar structure, and for the CrN films, the columnar structure, as observed in a scanning electron microscope, changed to an equiaxed structure. The hardness and elastic modulus were measured for the films, and for the CrN films a peak hardness of 38 GPa was found when the substrate bias voltage was only -25 V. Details of the coating process and of the characterization of the films will be presented.

# Thin film approach to Reactive Hydride Composites

**M. Gonzalez-Silveira [1], R. Gremaud [2], H. Schreuders [1], J. H. Rector [1], E. D. Batyrev [1], A. Rougier [3], L. Dupont [3], B. Dam [1]**

1. Condensed Matter Physics, Dept. of Physics and Astronomy, VU University, Amsterdam, The Netherlands

2. Hydrogen & Energy laboratory, Empa Materials Sciences & Technology, Überlandstrasse 129, CH-8600 Dübendorf, Switzerland

3. Laboratoire de Réactivité et Chimie des Solides, Amiens, France

Hydrogen is the ideal means of energy storage, transportation and conversion in a comprehensive clean-energy concept. However the storage of hydrogen is still a bottleneck for further deployment of hydrogen as an energy carrier. Storage in metals seems the most feasible option but the material that satisfactorily fulfills all the requirements has not yet been found. A promising route is the combination of Mg-based hydrides with other light-metal hydrides. These systems are denoted reactive hydride composites (RHC) when all the compounds react during the hydrogen sorption process. Interesting examples of Mg-based RHC with high storage capacities are composites with borohydrides, such as $MgH_2 + NaBH_4$, $MgH_2 + LiBH_4$ and $MgH_2 + Ca(BH_4)_2$ [1]. We present here a new approach to investigate these systems. Since diffusional problems are still one of the main limiting factors for hydrogen ab-/desorption, especially in complex hydrides where metal atom diffusion has to be considered, the use of thin films provides an interesting alternative to bulk. Since the microstructure of metallic thin films is in the nano-range, kinetic limitations should be much smaller than for bulk samples. In this study we focus our attention on the formation of borohydrides as a product of the reaction between $MgB_2$ and $CaH_2$, LiH and NaH. Thin films of the precursor compounds have been successfully deposited by reactive sputtering from the metallic compounds on a mixture of $Ar/H_2$ and have been thoroughly analyzed by optical spectroscopy, TEM and XPS. Different combinatorial thin films configurations such as co-sputtered films or multilayers have been used to analyze the reactivity of these precursors under hydrogen absorption conditions.

[1] G. Barkhordarian, T. Klassen, M. Dornheim, R. Bormann J. Alloys Comp. 440 L18-L21 (2007)

# Application of visible light-responsive $TiO_2$ thin film photocatalysts to highly efficient $H_2$ production from aqueous solutions of biomass

**S. Fukumoto, A. Ebrahimi, M. Takeuchi, M. Matsuoka, M. Anpo***
Osaka Prefecture University, Department of Applied Chemistry, 1-1 Gakuen-cho, Naka-ku, Sakai, Osaka 599-8531, Japan

Photocatalytic $H_2$ productions using semiconductor electrodes such as $TiO_2$ thin films have been considered a promising environmentally harmonious energy production process. Previously, we have reported on the successful development of visible light-responsive $TiO_2$ (Vis-$TiO_2$) thin films by controlling the substrate temperatures using a radio frequency magnetron sputtering (RF-MS) deposition method. It was also found that Vis-$TiO_2$ thin films can decompose $H_2O$ stoichiometrically and separately into $H_2$ and $O_2$ under solar light irradiation [1, 2]. Meanwhile, biofuels that can be produced from biomass have attracted much attention as alternative fuels. In the present work, we have investigated the separate evolution of $H_2$ on Vis-$TiO_2$ thin film photocatalysts from aqueous solutions of various kinds of alcohol, i.e., model compounds of biomass, by employing an H-type glass container. The Vis-$TiO_2$ thin films were prepared by an RF-MS deposition method using a calcined $TiO_2$ plate as the source material and Ar gas as the sputtering gas. The films were prepared on a Ti metal substrate at a substrate temperature (Ts) of 873 K and RF power of 300 W. Evaluation of the photocatalytic activity was carried out by photoelectrochemical measurements and the evolution of pure $H_2$ from an aqueous solution of the biomass. The photoelectrochemical properties of the Vis-$TiO_2$/Ti electrode were examined with an aqueous solution of 0.1 M $HClO_4$. The photocurrents were found to increase after the addition of 10 vol% alcohol into the $HClO_4$ aqueous solution under UV and visible light irradiation, indicating that the photooxidation of alcohol occurred in preference to that of $H_2O$ and that the charge recombination was suppressed by the addition of alcohol due to its hole scavenging effect. In order to evaluate the photocatalytic activity of the Vis-$TiO_2$ thin film, the separate evolution of $H_2$ from an aqueous solution of methanol was carried out in an H-type glass container under visible light of wavelengths longer than 450 nm. Pt was deposited on the opposite side of the Vis-$TiO_2$ on the Ti foil substrate with an RF power of 70 W at Ts = 298 K. The prepared photocatalyst was then mounted on an H-type glass container, separating the two aqueous solutions. The $TiO_2$ side of the photocatalyst was immersed in 1.0 M NaOH aqueous solution and the Pt side in 0.5 M $H_2SO_4$ aqueous solution in order to add a small chemical bias to assist the electron transfer from the $TiO_2$ to Pt side through the metal substrate. By adding 10 vol% methanol to 1.0 M NaOH aqueous solution at the $TiO_2$ side, the evolution rate of $H_2$ increased from 0.08 to 0.52 μmol / h, indicating that the use of alcohol was an effective method in improving the photocatalytic activity. The details of these results will be reported.

[1] M. Kitano, M. Takeuchi, M. Matsuoka, J.M. Thomas, M. Anpo, Catal. Today, 120, 133 (2007).
[2] M. Kitano, K. Tsujimaru, M. Anpo, Appl. Catal. A: General, 314, 179 (2006).

# Epitaxy by ion beam nitridation of liquid-Ga covered substrates

**J.W. Gerlach [1], C. Patzig [1], L. Neumann [1], B. Rauschenbach [1]**
1. Leibniz-Institute of Surface Modification (IOM), Permoserstrasse 15, D-04318 Leipzig, Germany

In the epitaxial growth of high-quality gallium nitride (GaN) films, the nitrogen flux to gallium flux ratio is a crucial parameter. For instance, during GaN film growth by ion-beam assisted molecular-beam epitaxy (IBA-MBE), an enhancement of the adatom mobility is achieved by simultaneous irradiation of the deposited Ga atoms with hyperthermal nitrogen ions at N ion/Ga MBE, slightly Ga-rich growth conditions are required, as a liquid-like Ga bilayer is formed on the film surface leading to an enhanced surface mobility of Ga atoms [2]. The present contribution focuses on the border case of most extreme Ga-rich growth conditions, i.e. the separate deposition of pure gallium at an elevated substrate temperature and subsequent post-nitridation of the as-deposited liquid Ga by a hyperthermal nitrogen ion beam. A constricted glow-discharge (hollow-anode) ion beam source was applied for this purpose, delivering hyperthermal nitrogen ions with kinetic energies lower than 25 eV [3]. The substrate temperature during Ga deposition and nitridation was kept constant at 630 °C. GaN films of 25 to 30 nm thickness were formed on the surfaces of different single crystal substrates, 6H-SiC(0001) and $Al_2O_3(0001)$, $Al_2O_3(1\bar{1}02)$, and γ-$LiAlO_2(100)$, that are known to force epitaxial growth with the c-, a-, and m-plane, respectively, of wurtzitic GaN parallel to this planes. In situ investigations of the crystallization process during the ion beam nitridation of Ga were performed using reflection high energy electron diffraction (RHEED) at an acceleration voltage of 30 kV, as well as using a CCD camera monitoring the 1×1 cm² sized sample surface. The investigations exhibited that the nitridation process leads to epitaxial GaN films via an epitaxial crystallization mechanism. X-ray diffraction (XRD) structure and texture analysis confirmed the epitaxial nature of the formed GaN films and revealed the occurring epitaxial relationships. Additionally, the films were examined by scanning electron microscopy (SEM) to study the present mechanism of epitaxial GaN formation. The surface topography before and after the ion beam nitridation process reveals a conversion of liquid Ga droplets into densely arranged GaN crystallites of relatively homogeneous thickness, as obtained by x-ray reflectometry (XRR). The observed growth mechanism is compared for the different substrate surfaces, i.e. for different polar and non-polar GaN lattice orientations. The results are discussed taking into account wetting phenomena like spreading and changes in surface energy due to ion beam nitridation.

[1] S. Sienz, J.W. Gerlach, T. Höche, A. Sidorenko, B. Rauschenbach, Thin Solid Films 458 63 (2004)
[2] G. Mula, C. Adelmann, S. Moehl, J. Oullier, B. Daudin, Phys. Rev. B 64 195406 (2001)
[3] A. Anders, M. Kühn, Rev. Sci. Instr. 69 1340 (1998)

# Biaxially textured polycrystalline Ag films on amorphous Si by ion beam assisted deposition

**D.F. Foerster, S. Bleikamp, T. Michely**
University of Cologne, Institute of Physics 2, Zuelpicher Str. 77, 50937 Koeln, Germany

Controlling the texture of polycristalline thin films is crucial for their performance, i.e. in integrated circuits or as IR-reflective coatings. We studied the early growth stages of Ag thin films on amorphous silicon as a model system by scanning tunneling microscopy. If grown by physical vapour phase deposition, these films develop a <111> fiber texture. In order to obtain biaxially textured films, ion beam assisted deposition is performed using 4 keV Argon ions. Three channeling directions, corresponding to ion beam angles of 20°, 35° and 85° with respect to the surface normal are tested at different ion-to-atom arrival rates. For the grazing incidence angle of 85° at an 1/10 arrival rate a pronounced biaxial texture is found. Details of the in-plane texture may be understood by considering the different interaction of the grazing ion beam with terraces and step edges.

# Sputtering yield amplification for targets operated in reactive mode

**T.Kubart [1,2], T.Nyberg [1], A. Pflug [3], D. Kohl [4], M. Wuttig [4], S. Berg [1]**

1. The Angstrom laboratory, Uppsala university, Box 534, 751 21 Uppsala, Sweden
2. Department of Applied Mathematics, Faculty of Transportation Sciences, Czech Technical University in Prague, Na Florenci 25, Prague 1, 110 00, Czech Republic
3. Fraunhofer IST, Bienroder Weg 54e, D-38108 Braunschweig
4. Institute of Physics (IA), RWTH Aachen University, 52056 Aachen, Germany

In this work, we present simulations of the partial sputtering yields for individual elements in multielement targets sputtered in a reactive atmosphere. It has been previously demonstrated that it is possible to significantly increase the sputtering rate from a target by doping if with a few percent of a heavier element. This phenomenon is referred to as the sputtering yield amplification effect and is investigated for oxide depositions here. The Monte Carlo based TRIDYN computer code has been used for the simulations. We have used this code to find out optimum doping conditions to obtain maximum partial sputtering yield for different target materials. In particular, we have focused on the deposition process for $TiO_2$. The maximum sputtering yields from metal and oxide target are discussed. Further, the influence of the sputtering yield amplification on the hysteresis behaviour is analyzed. The results indicate that a substantial increase in the deposition rate may be achieved for Ti. The transition between metal and compound mode is shifted towards higher oxygen flows as a result of the increased yield. Substoichiometic targets are suggested as a way of accomplishing hysteresis free deposition process that takes the full advantage of increased yield.

## 1. INTRODUCTION

Many reactive sputter deposition applications require high deposition rates. The primary limiting parameters are the target power dissipation and sputtering yields of the target elements. A well established technique to obtain high rate deposition processes is to include a feedback control system for control of the reactive gas partial pressure [1]. By the feedback control it is possible to operate the target in the transition area thereby maintaining a relatively high deposition rate. An alternative technique may be to manipulate the target in order to increase its sputtering yield. Such a sputter rate improving modification technique have been described by Berg and Katardjiev [2] and was named the Sputtering Yield Amplification (SYA). The SYA is based on the possibility to influence the penetration depth of the sputtering collision cascade. By adding a few percents of a heavy metal into the matrix of a light element target, a fraction of the cascading light atoms will be reflected back towards the target surface by collisions with the added heavy atoms. Since the collision cascade takes place closer to the target surface the probability for ejection of surface atoms may increase substantially. Altogether, this effect results in an increase of the partial sputtering yield of the lighter matrix element. It has previously been shown that for some materials it is possible to increase the sputtering yield as much as 300% [3]. These results indicate that it may be

attractive to involve the SYA in reactive deposition processes in order to increase the sputter erosion rate.
Production of targets for SYA turned out to be the main obstacle hindering demonstration of the effect. If the components are not mixed on atomic scale, SYA does not occur. Targets produced by traditional techniques are usually composed of grains of different composition and hence not suitable for SYA. One way to obtain atomic mixing at the target surface is serial co-sputtering. In this configuration, the sputter source consists of a primary rotatable sputter target of material A and a secondary target of material B. During operation of the primary sputter target, a thin metallic film of the material sputtered from target B is deposited onto its backside. In the primary sputtering process, this film gets implanted into the primary target material A, thereby enabling an increased sputtering rate of the metallic or reactive deposition of doped layers with an adjustable doping concentration B/A [4]. Here, we report on simulations of SYA effects in reactive sputtering. In order to simplify the study, a homogenous target composition is assumed, hence we don't consider the transitional effects in a serial co-sputtering setup. The main purpose of this study is to evaluate possible benefits which could be achieved by SYA.

## 2. MODEL

The ion surface interaction has been simulated using the Tridyn code [5]. Tridyn is a binary collision approximation (BCA) Monte-Carlo code frequently used for simulation of sputtering [6]. In the program, the target surface region is divided into depth slabs, initially equidistant. The changes in composition and thickness of each slab as a result of ion impact and subsequent collision cascades are followed. In order to account for sputtering of targets containing oxygen, the original Tridyn_FZR v1.0 has been modified. In the modified code, the total sum of all oxygen is limited, independent of whether the oxygen is originating from the target or reactive atmosphere. Maximum oxygen concentration has been set to the stoichiometric concentration, 66.7% of O for $TiO_2$ with the excess oxygen diffusing towards the surface [7]. Argon incorporation is neglected in this study.
There are three components in the beam bombarding the target surface. Argon atoms have an energy of 300 eV, energetic $O_2^+$ molecules are assumed to dissociate during the first collision with the target and hence the flux is simulated as 150 eV $O^+$ ions [6]. Neutral oxygen is again simulated as a flux of O atoms, in this case with zero energy and the sticking probability of 0.5. The ratio between components is adjusted according to the partial pressure of each gas, assuming equal ionization probability of Ar and $O_2$. Total fluence of energetic particles ($Ar^+$ and $O^+$) of $10^{19}$ $cm^{-2}$ was used on a target area of 30x30 $Å^2$ ($10^6$ pseudoparticles). Depending on the $O_2$ pressure, a dose of neutral O was added to the total fluence. In order to reduce the computational speed, cut-off energy of 4 eV was used. Constant surface binding energy of 7 eV was used for oxygen. 4.89 eV and 10 eV was used for metallic and oxidised Ti, respectively.

## 3. RESULTS and DISCUSSION

The normalized Ar sputtering yields of Ti doped with various elements are shown in figure 1 as a function of dopant concentration. The sputtering yield of pure Ti was 0.38, which is in good agreement with literature [8]. Sputtering yield in the figure is normalized to the value of pure Ti. As seen in figure 1, typical manifestation of SYA is an increase of Ti yield at lower doping levels and a then decrease for higher contents, where the dopant itself constitutes substantial part of the sputtered flux. Maximum SYA is achieved for high atomic mass dopant with high density. The results show that one of the most efficient dopants is tungsten, hence we focus on the Ti-W system in the rest of this study. Similar results is achieved for Ta. Nb, however, is much lighter and less effective in influencing the collision cascade.

For the selected material combination, i.e. Ti doped with W, a series of simulations of reactive sputtering has been carried out. The results are shown in figure 2 for different W contents. The effect of SYA is clearly visible. While in nonreactive mode, figure 1, the maximum yield increase is about 30 %, in reactive mode it may reach several times. For instance, at 5 mPa of $O_2$ the Ti yield ratio between 5 % W and undoped target is about 360 %.

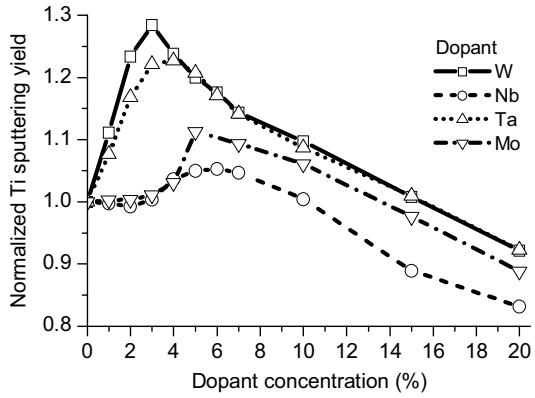


Figure 1. Simulated Ti partial sputtering yield for different dopants. The yield is normalized to the value of pure Ti metal target.

The amplitude of the increase is related to the operation in the transition area. Thanks to the rate increase, the doped target may still be in metal mode at the $O_2$ pressure for which the pure Ti target is already poisoned. The relative sputtering yield then reaches very high values. The maximum of the Ti deposition rate shifts towards higher W content for higher oxygen pressures. This could be related to a more pronounced preferential sputtering of O from W surfaces, as a result of higher ratio of the atomic masses. In compound mode, at 20 mPa of oxygen in figure 2, the target stays in the compound mode for the whole range of W concentration. The yield increase is again only relatively moderate, about 50 % for 5 % of W.

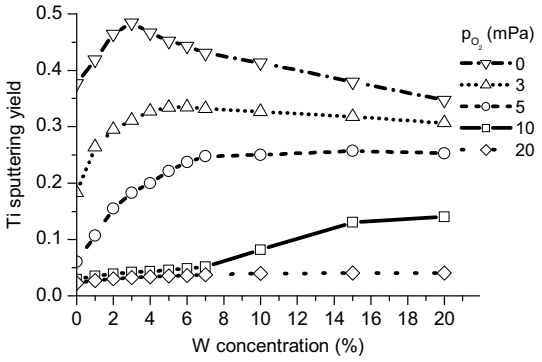


Figure 2. Sputtering yield of Ti as a function of W content for different oxygen partial pressures..

The model used in this study assumes the oxygen pressure as an independent variable. This corresponds to a sputtering process with partial pressure feedback control. For most sputtering systems with a simple reactive gas flow control, the transition area is unstable and it is possible to operate only in metal or compound mode due to the hysteresis. It has been shown earlier that by using substoichiometric $TiO_x$ targets, the hysteresis may be completely

eliminated [9]. By combining the SYA effect and hysteresis free process, it is possible to take full advantage of the increased deposition rate. To examine such an approach, sputtering from targets containing 0, 25 and 50% of oxygen was simulated. Undoped and 5% of W containing targets were considered.
The difference in Ti yield between metal (pure Ar) and compound mode is substantially reduced for oxide targets, figure 3. With increasing oxide content in the target bulk, the initial deposition rate decreases, while in compound mode all surfaces reaches the same, stoichiometric, composition and corresponding deposition rate. Since the hysteresis is related to the sputtering rate difference, with increasing O content the hysteresis is reduced. Relative yield of doped targets is decreased accordingly.

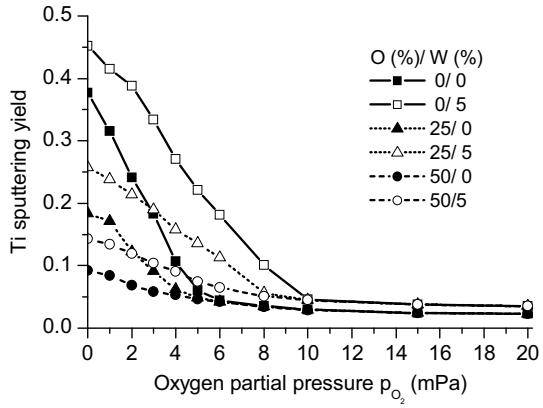


Figure 3. Titanium sputtering yield for metal and suboxide targets. Pure targets (full symbols) and targets with 5% of tungsten (open symbols) were simulated.

It may be argued that the relative Ti yield is not the correct parameter for performance evaluation. Higher oxygen partial pressure has to be used for higher deposition rate to achieve the same composition of the growing films. In most cases, stoichiometric oxide is the desired coating. We can compare the oxygen pressure required for the same deposition rate from different targets. At higher $O_2$ pressure, the deposition results in more oxygen rich coatings as a result of higher oxygen flux to the surfaces. Hence, for the same deposition rate, the doped target results in better stoichiometry. As shown in figure 3, the use of a doped target makes it possible to use nearly double the $O_2$ pressure for the same Ti sputter erosion rate.

## 4. Acknowledgement

This work was supported by Volkswagen Foundation. Part of the project was also funded by the Swedish Strategic Research Centre $MS^2E$. The authors are grateful to Prof. W. Möller for assistance with Tridyn.

## 5. References

[1] Sproul, W. D., Christie, D. J., Carter, D. C. Thin Solid Films 491 1 (2005)
[2] Berg, S., Barklund, A. M., Nender, C., Katardjiev, I. V., Barankova, H. Surf. Coat. Technol. 54 131 (1992)
[3] Berg, S., Katardjiev, I. V. J. Vac. Sci. Technol. A 17 1916 (1999)
[4] Belkind, A. J. Vac. Sci. Technol. A 11 1501 (1993)
[5] Moller, W., Eckstein, W., Biersack, J. P. Computer Physics Comm. 51 355 (1988)
[6] Moller, W., Guttler, D. J. Appl. Phys. 102 094501 (2007)
[7] Moller, W., Posselt, M. TRIDYN User Manual, 2002
[8] Eckstein, W., Moller, W. Nucl. Ins. Meth. B. 7-8 727 (1985)
[9] Kubart, T., Depla, D., Martin, D. M., Nyberg, T., Berg, S. Appl. Phys. Lett. 92 221501 (2008)

# Production of thick metallic lithium layer by sputter evaporation

**C. Rigaux, A. Lafort, F. Bodart, S. Lucas**
University of Namur (FUNDP), Research center in Physics of Matter and Radiation (PMR),
Rue de Bruxelles 61, 5000 Namur, Belgium

Lithium coatings on various substrates have numerous applications: Boron Neutron Capture Therapy, super conducting tocamak, … Traditionally they are produced by well known techniques like electrochemistry, evaporation... In this work, we investigate a new method based on sputter-evaporation in order to build thick coatings (≈ 30 μm) on various substrates in a short duration. In order to minimize the process time, evaporation can be used but it suffers from coating quality. Moreover it is well-know that DC magnetron sputtering allows for deposition of good quality coatings (smoothness, density, adhesion) but suffers low deposition rate. Thus we combine these two techniques to obtain the sputter-evaporation and keep the advantages of each. Li was placed in a stainless steel crucible (cathode), and heated by the plasma generated by a magnetron discharge. The Li temperature was measured by a thermocouple welded on the cathode and measured at different plasma power densities. The deposition rate has been measured by quartz balance and by profilometry, for several temperatures (from 0 to 580 °C) of lithium. For numerous applications, the great concentration of lithium in the coatings must be near 100% and there should not be diffusion in the substrates. Thus to check the purity of the coatings, we depth profiled it by measuring the production of gammas of the reaction $^{7}Li(p,\gamma)^{7}$ at different proton energy. In addition to the concentration, some characteristics like the density and the crystallography of a layer are also important. Thus we have studied the evolution in time of the density estimated by weight and profilometry measurements. The evolutions in time of the components of the layer and their crystallography have also been determined by X-ray grazing diffraction and powder diffraction. These physical properties have been investigated for various sample bias during deposition.

# Physical Characterization of ALD $Al_2O_3$ Films Deposited on GaAs Substrates

**A. Franquet [1], T. Conard [1], W. Vandervorst [1,2], S. Sioncke [1], M. Caymax [1], A. Delabie [1], M. Heyns [1], M. Meuris [1], G. Brammertz [1], J.L. van Hemmen [3], W. Keuning [3], W.M.M. Kessels [3]**

1. Imec, Kapeldreef 75, B-3001 Leuven, Belgium
2. KU Leuven, Electrical Engineering Department, INSYS, Kasteelpark Arenberg 10, B-3001 Leuven, Belgium
3. Department of Applied Physics, Eindhoven University of Technology, 5600 MB Eindhoven, The Netherlands

The continuous improvement of performances of IC's passes through the use of substrate with higher mobilities, including the use of III-V materials. To this end, the necessity to have a dielectric layer of good quality deposited on the GaAs substrate is of major importance. Among the different existing deposition techniques, Atomic Layer Deposition (ALD) allows depositing ultra thin films with good thickness control, uniformity and step coverage. ALD films can be deposited either using the "conventional" thermal process, i.e. dissociation of the precursors into reactive species performed by heating, either using the plasma enhanced process (PE-ALD), in which one of the precursors is the plasma gas.

This paper will focus on the physical characterization of ALD $Al_2O_3$ layers deposited on GaAs substrates. A comparison of the two different deposition processes, i.e. thermal and PE-ALD, will be made, and the influence of the surface pretreatments of the GaAs substrate prior to ALD deposition will be studied. To this end, several characterization techniques have been used, such as Angle Resolved-X-ray Photoelectron Spectroscopy (AR-XPS), Time Of Flight Secondary Ion Mass Spectroscopy (TOFSIMS), Spectroscopic Ellipsometry (SE), Total X-ray Reflectance Fluorescence (TXRF) and Atomic Force Microscopy (AFM).

Emphasis will be put first on the chemical composition, oxide thickness and contamination of the GaAs surface as a function of the pretreatment and will be further developed by a comparison of results concerning the growth modes of both PE and thermal ALD processes. Characteristics such as layer closure and growth per cycle, will be presented for PE and thermal ALD deposited $Al_2O_3$. Finally, the interface layer between the $Al_2O_3$ layers and the GaAs substrate will be investigated.

# Impact of metal-doping and annealing on the structure and constitution of amorphous carbon films

**C. Adelhelm [1], M. Balden, M. Rasinski [1], M. Rinke [2], M. Stüber [2], M. Sikora [3]**

1 Max-Planck-Institut für Plasmaphysik, Materials Research, EURATOM Association, D-85748 Garching, Germany

2 Forschungszentrum Karlsruhe, Institute of Materials Research I, Hermann-von-Helmholtz-Platz 1, D-76344 Eggenstein-Leopoldshafen, Germany

3 European Synchrotron Radiation Facility, 6 rue Jules Horowitz, 38043 Grenoble, France

Amorphous metal-doped carbon films (a-C:Me) with low metal concentration were deposited by non-reactive magnetron sputtering using graphite and metal targets at room temperature without applying a substrate bias. The films were characterized by XAFS, XRD, TEM and XES to obtain information about the metal bonding state and distribution. The influence of the metal type (Me=Ti, V, Zr, W), concentration (<15 at%) and annealing temperature (up to 1300 K) on the formation of carbide phases and evolution of crystallite sizes were investigated. The carbon matrix was analyzed by XRD and Raman spectroscopy. All metals used in this study show a carbide-like bonding character and are mainly distributed atomically disperse in an amorphous environment after deposition. Annealing in vacuum leads to the formation of carbide crystallites of several nm; the crystallite size generally increases with annealing temperature, metal concentration, and type (ZrC<TiC<VC). In the case of a-C:W films, $W_2C$ crystallites are formed at 1300 K as indicated by XAFS; the XRD spectra of a-C:W films exhibit very broad peaks, and no phase identification was possible. At lower temperatures, the carbide phase could not be resolved. It is suggested, that these coatings are a mixture of very small and distorted carbide crystallites ($W_2C$, $WC_{1-x}$). Bulk sensitive synchrotron X-ray emission spectroscopy (XES) was used to monitor the growth of carbide crystallites in a-C:V and to analyze the atomic vanadium environment with chemical sensitivity. The occurrence of oxygen atoms in the V environment could be shown in samples annealed up to 1300 K. Calculation of I(D)/I(G) from Raman spectra showed that addition of up to 15 at% metal leads to a continuous increase of the average aromatic cluster size in the as-deposited samples, compared to pure a-C. The strongest effect was observed for Ti and Zr; the lowest for W. The difference between the dopants regarding the clustering of the sp2 phase vanishes by annealing. After heating to 1100 K, the aromatic cluster size is the same as for a-C, independent of metal type and content. For that temperature, the a-C:Me film structure can be described as nanocomposite of carbide crystallites embedded in a-C. The carbon structure is then only determined by the annealing temperature.

# Characterization of $Mg_xAl_yO_z$ thin films grown by reactive magnetron sputtering

**M. Saraiva [1], H. Chen [2], W. P. Leroy [1], S. Mahieu [1], N. Jehanathan [3], O. Lebedev [3], V. Georgieva [4], R. Persoons [2], D. Depla [1]**

1. Ghent University, Department of Solid State Sciences, Krijgslaan 281 (S1),9000 Gent, Belgium
2. Flemish Institute for Technological Research (VITO), Boeretang 200, B-2400 Mol, Belgium.
3 Electron Microscopy for Materials Research (EMAT), University of Antwerp, Groenenborgerlaan 171, B2020 Antwerpen, Belgium
4 PLASMANT Research Group, Department of Chemistry, University of Antwerp, Universiteitsplein 1, 2610 Antwerp, Belgium

Thin film technology is pervasive in many applications. Progress in each of these areas depends upon the ability to selectively and controllably deposit thin films with specified physical properties. This, in turn, requires control of the film microstructure and microchemistry. This knowledge is acquired by combining know-how in producing thin films by reactive sputter deposition and on the other hand in the evaluation of properties of thin films.

In the present work, reactive magnetron sputtering in DC mode was used to grow thin films of complex oxides, starting from two separate pure metal targets. This set-up is not used very often, although it has many advantages such as higher deposition rate than when oxide targets are used. Furthermore, it enables one to have an absolute control of the metals ratio, which is not the case with compound metallic targets.

Several deposition parameters were varied in order to control the stoichiometry of the oxide thin film. In this way, a series of coatings were produced with a stoichiometry going from MgO, over $Mg_xAl_yO_z$ to $Al_2O_3$. All these thin films were characterized in order to obtain a relation between intrinsic and extrinsic properties. The characterization was focused on optical and mechanical properties such as optical constants of the dielectric function and hardness, respectively. A relationship between all the properties was found. By this work, the understanding of the Mg-Al-O system was improved.

# Effect of surface pre-treatment on the initial, thermal oxidation of Al-1.12 at% Mg surfaces

**E. Panda, L.P.H. Jeurgens, E.J. Mittemeijer**
Max Planck Institute for Metals Research, Heisenbergstrasße 3, D-70569, Stuttgart, Germany

The effect of surface pre-treatment and oxidizing temperature on the growth kinetics and developing microstructure of ultra-thin (< 2 nm) oxide films grown on bare Al – 1.12 at.% Mg alloy surfaces has been studied by a combined experimental approach of angle-resolved X-ray photoelectron spectroscopy (AR-XPS), real-time in situ spectroscopic ellipsometry (RISE) and high resolution transmission electron microscopy (HR-TEM). First, the native oxide and other contaminants on the alloy surface were removed by sputter-cleaning under UHV conditions. Next, ultra-thin oxide films were grown by exposure of the sputter-cleaned alloy surfaces to pure oxygen gas (at $P_{O2} = 1\times10^{-4}$ Pa) at a temperature range 300 - 485 K. As a second surface pre-treatment, the sputter-cleaned surfaces were exposed to a short in-vacuo annealing step (at 460 K) prior to oxidation. It follows that, depending on the oxidizing temperature and surface pre- treatment, a single or a combination of different chemical states occurs for the Al and Mg cations incorporated in the grown oxide films (resembling states observed for bulk $Al_2O_3$, MgO and $MgAl_2O_4$). For $T <$ 450 K, the oxide-film growth kinetics and the chemical state of the ions in the grown oxide films depend on the surface pre-treatment. The overall Al-to-Mg-ratio of the grown oxide film decreases with increasing oxide-film thickness, which eventually results in the thermodynamically preferred formation of a MgO-type of oxide film.

# Properties of nanocrystalline and amorphous W-Zr thin films deposited by co-sputtering

**D.Horwat [1], M. Dehmas [2], E.Aubry [1], J. Zollinger [2], S. Migot [3], J.F. Pierson [1]**

1. Laboratoire de Science et Génie des Surfaces (UMR CNRS 7570), Ecole des Mines, Parc de Saurupt, CS 14234, 54042 NANCY cedex, France

2.Laboratoire de Science et Génie des Matériaux Métalliques (UMR CNRS 7584), Ecole des Mines, Parc de Saurupt, CS 14234, 54042 NANCY cedex, France

3.Laboratoire de Physique des Matériaux (UMR 7556), Ecole des Mines, Parc de Saurupt, CS 14234, 54042 NANCY cedex France

Zr-W thin glassy films are expected to act as active thermally stable catalyst. In this study we investigate the relationships between the structural, electrical and optical properties of nano-crystalline and glassy thin $W_xZr_{1-x}$ films. $W_xZr_{1-x}$ thin films with $x \leq 0.81$ were deposited by magnetron co-sputtering by varying the current dissipated by the tungsten target while the current was maintained constant on the zirconium one. As the evolution of chemical composition measured by electron probe microanalysis (EPMA) increases with the current applied to the tungsten target, the thickness does not increase monotonically indicating the presence of structural events. Varying the composition induces modifications in the structural organization from XRD amorphous to nanocrystalline. Different local organizations of the coatings were deduced from the combination of structural, electrical (4 point probe measurements) and optical (UV-Visible-Near Infrared spectrometry) analyses. While the amount of tungsten increases, the transitions occur from a XRD amorphous solid solution of W in Zr to true amorphous $W_xZr_{1-x}$ to nanocrystalline $ZrW_2$ and finally to a nanocrystalline solid solution of Zr in W. The structural organisations of the films exhibiting $ZrW_2$ and amorphous XRD structures were confirmed by transmission electron microscopy. The grain size deduced from X-Ray diffraction analysis ranged from 1.3 nm to 16 nm depending on the composition, the resistivity of the films is driven by the total volume perturbed by the grain boundaries.

# Fullerene-Like Phosphorus-Carbide Thin Solid Films

**A. Furlan [1], G.K. Gueorguiev [1], S. Braun [1], Zs. Czigány [2], V Darakchieva [1], H. Högberg [1], S. Stafström [1], L. Hultman [1]**

1. Linköping University, Department of Physics, Chemistry and Biology, 581 83 Linköping, Sweden

2. Research Institute for Technical Physics and Materials Science, P.O. Box 49, 1525 Budapest, Hungary

Phosphorus-carbide ($CP_x$) thin solid films with a fullerene-like (FL) structure have been deposited on Si(100) substrates by DC magnetron sputtering from pressed graphite-phosphorus with a composition of 5 at% to 12 at% of red phosphorus and a substrate temperature ranging from 150 $^{o}$C to 600 $^{o}$C. The target composition was chosen following previous theoretical modeling [1,2], suggesting a preferred phosphorus content between 5-15 at% for deposition of (FL) compounds within this materials system. The deposited $CP_x$ ($0.025 \leq x \leq 0.15$) films were characterized by X-ray photoelectron spectroscopy (XPS), Auger electron spectroscopy (AES), transmission electron microscopy and diffraction, nanoindentation, elastic recoil detection analysis, infra-red ellipsometry, and Raman spectroscopy. For $CP_x$ ($0.05 \leq x \leq 0.15$) and a temperature of 300 $^{o}$C the films display an amorphous structure, but with presence of curved graphene planes, according to TEM. XPS analysis of P2p photoelectrons show P-C bonding, indicating that the phosphorus atoms are incorporated into the graphene network and not as phosphorus clusters. The formation of a FL compound is also supported by selected area electron diffraction patterns, showing broad rings at positions different from those of other carbon allotropes, as well as from patterns obtained from FL-$CN_x$. Nanoindentation shows that films are mechanically resilient with hardness values of at least 24 GPa and with an elastic recovery of more than 70 %. Thin film growth performed at a lower temperature of 150 $^{o}$C and with a target composition of 12 at% results in both an increased phosphorus content of the films as well as a reduced oxygen content. However, these growth conditions deteriorate the mechanical properties by reducing the hardness to around 9 GPa and the elastic recovery around 40 %. To compensate for this we have studied targets with less phosphorus content.

[1] G.K. Gueorguiev, A. Furlan, H. Högberg, S. Stafström, L. Hultman, Chem. Phys. Lett. 426 374 (2006)

[2] A. Furlan, G.K. Gueorguiev, Zs. Czigány, H. Högberg, S. Braun, S. Stafström, L. Hultman, Phys. Stat. Sol. (RRL) 2 191(2008)

# Thin Film ITO Coatings obtained using Rotary Sputtering Targets

**P. Lippens [1], E. Medvedovski [1], A. Hellmich [2], C. Szepesi [1], K. Leitner [1] and R. Linsbod [1]**

1. Umicore Thin Film Products, p/a Kasteelstraat 7, B-2250 Olen, Belgium

2. AKT, Display Products Group, Applied Materials GmbH & Co. KG, Siemensstrasse 100, D-63755 Alzenau, Germany

Rotary sputter magnetrons have received increasing interest in all segments of large area vacuum coating since several years. Besides the main advantage of better target utilization, which has a major impact on cost reduction, especially for expensive materials, also the stability of the sputter process is strongly improved. In case of IndiumTinOxide (ITO) sputter deposition, higher deposition rates and a more stable process could be achieved using ceramic ITO sputter targets, at least for planar magnetrons. The vacuum deposition community has always wanted to combine those two technologies, however, cylindrical rotatable ceramic ITO targets present a major challenge to materials' manufacturers and were simply not available. Recently, Umicore Thin Film Products successfully developed a unique process for manufacturing of such targets. This presentation will give an overview of such process and will present some of the results that have been achieved in actual large area coating applications. The technology is also applicable to other transparent conducting oxides such as AZO (Al:ZnO).

## INTRODUCTION

IndiumTinOxide (ITO) has been the Transparent Conducting Oxide (TCO) of choice in the Flat Panel Display (FPD) industry since more than ten years now. Also in the Photovoltaic (PV) industry, this TCO is gaining increased interest, mainly for the production of flexible thin film solar cells (a-Si, CIGS and CdTe). In almost all these applications, ITO is sputter deposited using planar DC magnetrons. For depositing other, both metallic and ceramic, thin films, rotary or rotatable magnetrons have been in use since quite some time [1].

There are a number of drivers for making the transition to this advanced technology in the vacuum sputter deposition industry: higher target utilization (up to 90 %) compared to planar magnetrons which is not only important for expensive target materials but also reduces equipment idle time; higher sputter power possible (as the racetrack is smeared out over almost the entire target surface); increased process stability as the entire target surface is eroded (no re-deposition and constant target potential over the entire target surface); quasi no variations of knock-on angle for inert gas atoms over the target life (which can be important for critical oxides such as Al:ZnO, [2]), much faster and less frequent target exchange, … . All these advantages result normally in a lower cost of ownership. Calculations show that, even if the kilogram cost of ITO in case of rotatable targets is much higher than the

corresponding planar ITO kg cost, then still rotatable ITO targets can yield a total cost of ownership advantage of typically 20 %.
Unfortunately and until recently, ITO couldn't be sputtered using rotary targets as high density (> 99 % of theoretical density) and high purity (> 3N5) targets were not available. Some manufacturers launched plasma sprayed ITO targets [3], but such parts suffered from low density (typically 93 – 95 % of TD), reduced chemical purity and limited target thickness (typic. 3 mm). Recently however, Umicore Thin Film Products was able to launch ceramic rotatable ITO targets with an ITO-layer thickness of 6 mm. The aim of this article is to show the potential of this type of targets for large area coating in the FPD and PV industries.

## ROTARY CERAMIC ITO TARGET MANUFACTURING.

Tubular rotary targets have been manufactured in the following way. First, ceramic ITO hollow cylindrical bodies with a wall thickness of 5 – 9 mm have been manufactured using an advanced ceramic sintering technology starting from in house manufactured high purity precursor materials [4]. Contrary to plasma sprayed ITO-targets, this technique resulted in cylindrical ITO bodies with a density > 99.5 % of theoretical density.
In a second stage, several of those hollow cylindrical components were bonded to seamless titanium (Ti) backing tubes using liquid indium (In) solder. The choice of Ti as the backing tube material was mainly dictated by its coefficient of thermal expansion which is quasi similar to ITO and by its specific weight. Using this methodology, targets up to 2.8 meter length have been manufactured. Even longer targets as used e.g. in the architectural glass coating industry, can also be produced. For the further discussion in this paper, performance data were collected for targets with a length of 1.2 m. They have been tested in an industrial sputter coater such as the ones used in the display industry in collaboration with AKT, Display Products Group, a renowned equipment manufacturer for this industry. Figure 1 shows a picture of such a multi-segment target used on a vertical cantilever type magnetron.

Figure 1. Picture of an industrial size, multi-segment ITO ceramic rotary target.

## BEHAVIOUR OF CERAMIC ROTARY ITO TARGETS.

Figure 2 shows the target erosion profile for a target with an initial ITO thickness of 5 mm (outer diameter 145 mm), eroded by DC magnetron sputtering with a total energy of 2400 kWh. The target has been tested during several long duration sputter runs in which power was often around 10 kW/m. Looking at the remaining ITO thickness of 1.8 mm in the race track closing at both ends and a step height towards the middle zone of the target of about 0.5 mm, it can be concluded that this target can be utilized for at least 80 % on this specific magnetron.

Of course, by optimizing the magnetic field at the racetrack closing at both ends of the target, the target utilization can still be improved. In any case, even with the same magnet array, it will be better for longer magnetrons as the effect of the non sputter eroded edges and racetrack closing will reduce.

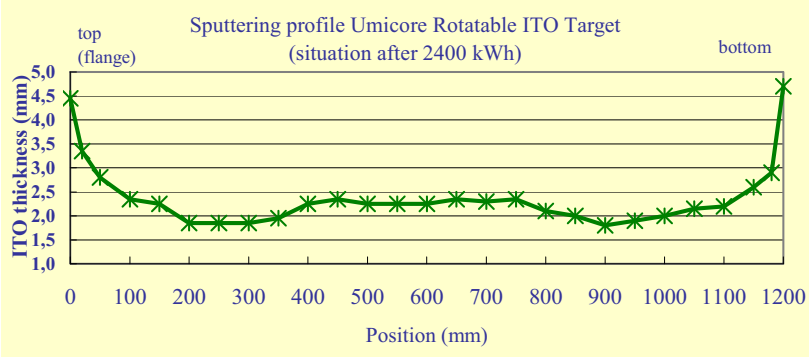


Figure 2. Sputter erosion profile as measured on the target surface after total sputter energy of 2400 kWh was used.

No cracks were observed, arc traces were completely absent. Contrary to sputtering with planar ITO-targets, the targets didn't show any signs of nodule formation except for a few traces at the two very edges of the target (see fig. 3a and 3b). With planar targets, the nodules consist mainly of Indium-suboxide ($In_2O$) which is formed by re-deposition on and beyond the racetrack edge [5]. High target temperature, an oxygen deficient atmosphere above the target, low target density and low materials' purity have been suggested as reasons for this nodule formation. As quasi the entire target surface is being sputter eroded with rotary magnetrons, only the very edges of the rotary target are prone to nodule formation. But even then, such formation is almost absent. Remark however that nodules develop when metallic rotary In/Sn targets are reactively sputtered. Therefore, the better target cooling with rotatable magnetrons is clearly not enough to result in a nodule free process.

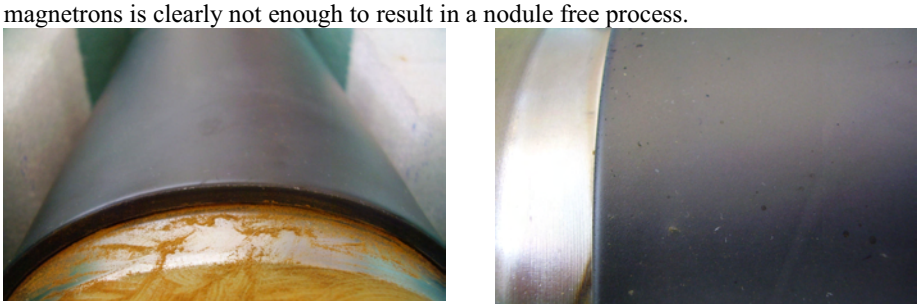

A B

Figure 3a/b. Views of ITO target surface after 2400 kWh of sputter erosion. The arrow points to a few emerging nodules at the very edge of the target (b).

In general, target nodules are not only extremely annoying in an industrial operation (as they require process interruptions for mechanical target cleaning), but even more importantly, they reduce product yield (due to arcing and particle formation) and increase costs (equipment down time for cleaning, removing nodules means lost sputter material).

## COATING PROPERTIES.

One of the most important coating properties for ITO coatings is their electrical resistivity. Figure 4 compares this parameter for coatings deposited from both planar and rotatable

magnetrons in function of the composition of the Ar/O2 reactive gas mixture. Those coatings were deposited on glass at elevated substrate temperature (typic. 235°C) without using Plasma Emission (PEM) control [6] for the reactive gas flow. The graph clearly indicates high similarity in coating properties. Remark that all the as deposited ITO–coatings with a resistivity below 2.E-04 ohm.cm from figure 3 had an optical transmittance at 550 nm of about 93 %, regardless of the deposition magnetron.

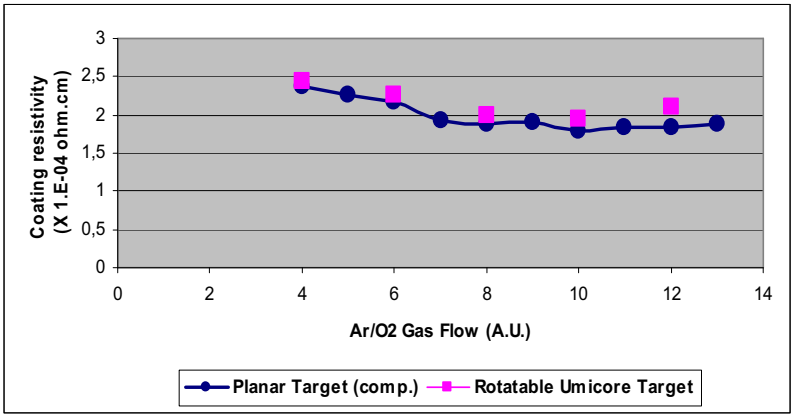


Figure 4. Comparison of coating resistivity for ITO-coatings deposited from a planar resp. rotatable ceramic sputtering target.

## CONCLUSIONS AND OUTLOOK.

Large scale multi-segment ceramic ITO rotary targets have been developed and can be produced in industrial quantities. The cylindrical ITO segments are bonded to a Ti backing tube. Such targets sputter nodule free without cracking or arcing at high power levels (up to 10 kW/m of target length). Target utilization depends heavily on the magnetron design but is typically over 80 %. Coatings deposited with such targets have similar properties than coatings deposited with planar ITO ceramic targets. In the mean time, ceramic rotary multi-segment Al:ZnO targets produced via a slightly different manufacturing technique have also been launched.

## REFERENCES

[1] T. Minami, “New n-Type Transparent Conducting Oxides”, MRS Bulletin, Aug. 2000 pp. 38-44.

[2] P. Lippens et al., “Soft-magnetic sputtered coatings on pet-substrate for electronic article surveillance”, Surface & Coatings Techn. 93 (1997), pp. 46-50.

[3] W. De Bosscher et al.,”Cylindrical ITO Targets for Large-Area Coating”, J. Soc. Vacuum Coaters, 48, pp. 111-115 (2005).

[4] E. Medvedovski et al., American Ceramic Soc. Bulletin, Vol. 87, N° 2, pp. 39-42.

[5] Lippens et al., “Chemical instability of the target surface during DC-magnetron sputtering of ITO-coatings”, Thin Solid Films 317 (1998), pp. 405-408.

[6] N. Schiller et al., “Reactive DC High-Rate Sputtering as production technology”, Surf. & Coatings Techn. 33 (1987), pp. 405-423

# In situ study of the effect of Sn doping on the electrical properties of indium oxide

**A. Rogozin, M. Vinnichenko, N. Shevchenko, U. Kreissig, A. Kolitsch, W. Moeller**
Research Center Dresden-Rossendorf

Indium oxide ($In_2O_3$) and ITO ($In_2O_3$ :Sn) amorphous films grown by pulsed reactive magnetron sputtering have been annealed in vacuum. The film structure and properties have been studied during annealing using in-situ diagnostics. The evolution of the film structure has been continuously monitored by synchrotron X-ray diffraction at the European Synchrotron Radiation Facility in Grenoble, France. Four point probe measurements, spectroscopic ellipsometry, and elastic recoil detection analysis have been undertaken to determine and correlate with the structure in real time the evolution of the film resistivity (ρ), the free electron density (Ne), and the film stoichiometry. At the start of annealing both the $In_2O_3$ and the ITO films show a fast decrease in ρ and an increase in Ne, which is explained by the formation of oxygen vacancies and reordering of the amorphous phase. Subsequent film crystallization does not influence the $In_2O_3$ film electrical properties, but causes a further decrease in ITO resistivity due to the Sn donor activation. The estimated efficiency of the Sn donor activation is 40%. All the films show during annealing a resistivity decrease which is caused not only by an increase in the free carrier density, but also by a rise in the electron mobility.

# Influence of structure and microstructure on electrical properties in $Sm_{0.6}Nd_{0.4}NiO_3$ thin films

**C. Girardot [1, 2], M. Boudard [1, 3], N. Caillault [2], J. Kreisel [1], F. Weiss [1], S. Pignard [1]**

[1] LMGP, Laboratoire des Matériaux et du Génie Physique (UMR 5628 CNRS / Grenoble-INP) - Minatec - 3, parvis Louis Néel , BP 257, 38016 GRENOBLE CEDEX 1, France

[2] Schneider Electric Industries S.A., 37, Quai Paul Louis Merlin- 38050 GRENOBLE Cedex, France

[3] SIMAP, Science et Ingénierie des Matériaux et Procédés (UMR5266 CNRS/ Grenoble-INP /UJF), 1130, rue de la piscine, BP 75, 38402 St Martin d'Hères Cedex, France

Rare earth nickelates with the generic formula $RENiO_3$ (*RE* = rare earth) have attracted a lot of research interest since the report of a sharp metal-to-insulator (MI) transition whereof the critical temperature $T_{MI}$ can be tuned with the rare earth size. In the case of $Sm_{1-x}Nd_xNiO_3$, $T_{MI}$ can be readably adjusted between 200 K to 400 K by varying $x$ in the solid solution and this although the ionic radii of $Nd^{3+}$ and $Sm^{3+}$ differ by only 0.03 Å. For example, $Sm_{0.6}Nd_{0.4}NiO_3$ (SNNO) is a semiconductor at low temperature and becomes a metal around room temperature thus offering a promising suitability for applications.

In this paper, we investigate the correlation between the electrical behavior and the structural/microstructural characteristics of SNNO films prepared by "liquid injection" Metal-Organic Chemical Vapor Deposition (MOCVD) with various thicknesses. Given the fact that SNNO, namely the $Ni^{3+}$ state, is thermodynamically unstable at the pressure and temperature deposition conditions, our films are synthesized on a single crystalline $LaAlO_3$(100) substrate. The use of this substrate with a lattice parameter close to that of the nickelate allows stabilizing the phase by epitaxial strain. In the presented study the thickness has been varied between 20 to 240nm.

We show that the temperature dependence of the electrical conductivity is strongly influenced by the film thickness: the sharpness of the semiconductor/metal transition decreases with thickness and disappears for the thickest film. Investigations by scanning electron microscopy and X-ray diffraction (teta/2teta scanning mode and reciprocal space mappings) have been performed in order to understand the structural evolution of the films with thickness. Gradual changes are observed in the structure and the microstructure of the films with increasing thickness; we show how these changes can be related to the evolution of the transport properties and the loss of the metallic behaviour for the thickest film.

# Comparison of the Properties of a New Nickel-Copper Nitride with those of Nickel or Copper Nitrides

**C. Petitjean, J.F. Pierson, D. Horwat**
LSGS, Ecole des Mines, Parc de Saurupt, CS 14234, 54042 NANCY cedex, France

Nickel and copper nitrides are thermally unstable: they decompose into metal and nitrogen after vacuum annealing. Copper nitride ($Cu_3N$) exhibits an anti-$ReO_3$ cubic structure whereas nickel nitride ($Ni_3N$) is isostructural of $Fe_3N$. Although copper nitride films have been widely studied, the literature reports little information about nickel nitride films. Recently, the effect of titanium or silver addition into $Cu_3N$ films has been reported. To the best of our knowledge, there is no information about nickel addition into copper nitride films. This presentation aims to show that for the first time nickel-copper nitride films can be synthesised. The properties of this new material are compared with those of copper or nickel nitrides.

Nitride films were deposited on glass substrates by magnetron sputtering of nickel, copper and nickel-copper (50/50 at. %) targets in various Ar-$N_2$ reactive mixtures. The film structure was studied by X-ray diffraction. The film composition was measured by secondary neutral mass spectrometry. Room temperature electrical resistivities are deduced from square resistance measurements using the four point probe method. Optical reflectance was determined by UV-visible spectrometry.

The increase of the nitrogen flow rate induces a variation of the films nitrogen concentration. In the Cu/N system, only the $Cu_3N$ phase has been evidenced by X-ray diffraction. On the other hand, $Ni_3N$ and $Ni_2N$ phases can be deposited. Ni-Cu-N films crystallise in a cubic structure with a lattice constant lower than that of stoichiometric $Cu_3N$, suggesting that copper atoms can be substituted by nickel ones. The electrical and optical properties of nickel-copper nitrides are ranging between those of nickel and copper nitrides. These results clearly show that the properties of such binary nitrides can be tuned by the addition of a second metal.

# Submicronscale Patterning of Organic Semiconductors by Self-Organization

**O. Karthaus, K. Kai**
Chitose Institute of Science and Technology, Department of Bio- and Material Photonics, Bibi 65-758, Chitose, 066-8655, Japan

Patterning of organic semiconductors is necessary to fabricate next-generation organic electronic and photonic devices. Ilya Prigogine found tht so-celled 'dissipative structures' can form in open systems that are in a non-equilibrium state. The flow of matter and energy through the system leads to spatio-temporal ordered structures. Here we present two examples of solution-based fabrication of in-plane mesoscale ordered semiconductor structures, using pentacene for organic field effect transistors and aromatic amines for organic light emitting diodes. The central step in the fabrication process is the casting by a roller apparatus. The semiconductor is dissolved in a volatile organic solvent that is placed in an air gap between the device substrate and a glass roller. The solution can evaporate along a thin stripe along the three-phase line (contact line of liquid, solid and air). This evaporation leads to dissipative structures, via fluctuations in surface tension and a 'fingering instability'. Organic compounds with a metastable amorphous state, such as aromatic amines used in OLEDs, can form submicron-size droplets (left figure) , while easily crystallizable compounds like pentacene from crystal needles (right figure).

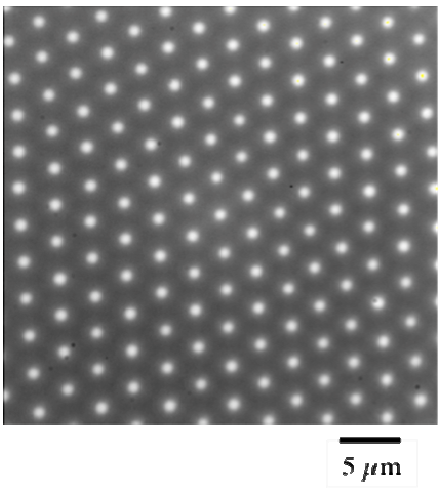


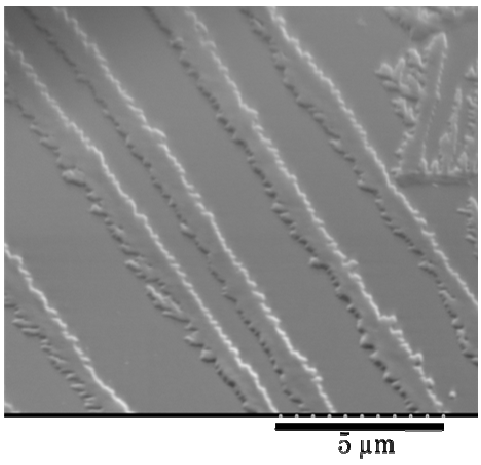

# Growth mode of organic thin films and its impact on device performance

**Y. Wakayama, R. Hayakama, T. Chikyow**
Advanced Electronic Materials Center, National Institute for Materials Science, 1-1 Namiki, Tsukuba 305-0044, Japan

We demonstrate a comprehensive study of organic thin film growth, including structural characterization and device performance. In particular, an emphasis will be placed on an impact of the film evolution on the properties of field-effect transistors (FET). For this study, we employed quaterrylene molecule, which is an aromatic hydrocarbon consisted of total eleven fused-rings. The thin films were formed on $SiO_2$/Si substrates in vacuum by an original technique, "hot-wall deposition". This technique makes it possible ultra-slow deposition, resulting in high crystallinity of the films and allowing detail discussion of growth mechanism. A series of AFM observation of the films with different thicknesses showed the films started growing with two-dimensional (2D) layered films at initial stage followed by three-dimensional (3D) islands formation. This is comparable to so-called Stranski-Krastanov growth mode, which is commonly observed in producing self-assemble quantum dots of semiconductors. For this growth mode, the stress caused by lattice mismatch between substrate and film is a trigger for 3D island growth. In fact, thorough analysis by in-plane and out-of-plane XRD measurements revealed that the 2D layers of the quaterrylene films involved compressive stress and the stress was released with increasing thickness by forming 3D islands. That is, transition from 2D to 3D morphology was driven by the lattice strain. We suppose a relatively high surface energy of the $SiO_2$ is a possible reason for the lattice strain around the interface. In contrast, a surface treatment by octadecyltrichlorosilane (OTS), which is effective to reduce surface energy, was found to suppress the transition from 2D to 3D. Correlation of the film evolution with transistor properties was investigated. Basically, the quaterrylene thin films show a p-type semiconductor, i.e., holes are majority carriers in the FET. A main finding is that the carrier mobility of the FETs was strongly related to the film evolution; the mobility increased with 2D layer thickness and saturated when the film morphology transformed to 3D. These results elucidate that only 2D layers can work as effective transistor channels. In general, it is known that an increase in grain size of the organic thin films is critical to improve the carrier mobility because grain boundaries hamper the carrier transport. Our study suggests that to increase in 2D layer thickness is another essential approach to upgrade device performance. Then, the ultra-slow deposition for improving film quality, as well as the appropriate surface treatment for reducing interface energy, is effective for this purpose.

# Deposition of allylamine plasma polymer films:Correlation between plasma diagnostic and thin film characteristics

**L. Denis [1], D. Cossement [2], T. Godfroid [2], F. Renaux [2], C. Bittencourt [1], R. Snyders [1,2] and M. Hecq [1,2]**

1. Laboratoire de Chimie Inorganique et Analytique, Université de Mons-Hainaut, Place du Parc 20, B-7000 Mons, Belgium

2. Materia Nova Research Center, Parc Initialis, Avenue N. Copernic 1, B-7000 Mons, Belgium

Plasma polymerization is a very attractive process to synthesize organic thin films referred to as "plasma polymer films" (PPF). Usually, PPF present strong adherence on numerous surfaces, good mechanical properties and high thermal resistance. Among the most promising PPF, amine-based ones have drawn a lot of attention due to their applications in the biomedical field. However, despite numerous studies, strong efforts are still needed to understand the relationship between plasma chemistry and PPF characteristics.

In this work, continuous wave (CW) and pulsed radio-frequency (RF) plasma polymerization of allylamine have been investigated. Plasma chemistry, studied by residual gas analysis mass spectrometry, reveals that the maintenance of the chemical precursor structure, necessary to synthesize PPF with high primary amine content, is a function of the equivalent power ($P_{eq}$) whatever the plasma is sustained in CW or pulsed mode. On the other hand, film chemistry, evaluated by a combination of X-ray Photoelectron Spectroscopy (XPS) measurements and chemical derivatization (by trifluoromethyl-benzaldehyde, TFBA), reveals that the primary amine content of the films (%$NH_2$) is inversely proportional to $P_{eq}$ and, if $P_{eq}$ is fixed, is independent on the method used to sustain the plasma (CW or pulsed RF).

Surprisingly, PPF synthesized at different $P_{eq}$ but having relatively close %$NH_2$, reveal strong differences in the derivatization reaction kinetics. The latter has been evaluated by following %$NH_2$ as a function of exposure time to TFBA vapor. We explain this phenomenon by considering the cross-linked structure of the PPF evaluated by Time-of-Flight Secondary Ion Mass Spectrometry (ToF-SIMS) measurements and subsequent data processing by Principal Component Analysis (PCA). The data show that the PPF cross-linking degree decreases when $P_{eq}$ decreases promoting TFBA diffusion into the film network.

Moreover, as expected, cross-linked structure and chemical composition of films synthesized at similar $P_{eq}$ are not dependent on the method used to sustain the plasma (CW or pulsed RF). This result supports the XPS-derivatization data and therefore, validates our primary amine quantification method.

# A comparative study of optical properties of nanosilver dispersed into organic and inorganic matrices

**A. Babapour [1], S.H. Li [1], B. Yang [1], W. Cao [1,2], S. Bahang [1], A.Z. Moshfegh [3]**

1. Harbin Institute of Technology, Center for condensed matter sci. & Tech, Harbin, 150080, China

2. Pennsylvania State University, Materials Research Institute, University Park, Pennsylvania, 16802, USA

3. Sharif University of Technology, Department of Physics P.O. Box 11155-9161, Tehran, Iran

Noble metal nanoparticles with their associated strong surface plasmon resonance have generated great interest in various fields such as nanoscale photonics and biological sensing. Silver nanoparticles in solution, supported onto a substrate and incorporated into organic or inorganic matrices show remarkable physical and chemical properties that are size and shape dependent. In the case of optical properties, particle size and shape determine the characteristics of their surface plasmon absorption band (SPAB), which has been observed for silver particles in solution and in solids. Other factors that also affect the SPAB of silver nanoparticles are the refractive index of the surrounding medium and adsorption phenomena at the interface. In here, we report the synthesis of silver nanoparticles into two different organic (PVP) and inorganic ($SiO_2$) matrices using sol-gel method. The optical properties of these films depend on the size and aging time. The effect of different matrices on the optical properties of silver nanoparticles was also studied. The absorption of nanosilver in PVP for the same concentration of Ag precursor is higher than that in silica. The maximum peaks occur in lower wavelengths around 418 nm while this is 440 nm in the silica matrix. By increasing the concentration of silver in both silica and PVP, the absorption maximum peaks moved to higher wavelengths (red-shifts) indicating formation of larger nanoparticles. In silica matrix, we have observed a limitation for increasing the silver concentration up to 8%, however we have synthesized nanoparticles in PVP matrix with much higher silver concentration up to 50%. The aging time for synthesis of nanosilver in silica matrix was about 6-10 hours depending on different concentration. But the aging time for PVP matrix was used about 1-2 days. The effect of aging time on the optical absorption was also studied. It was found that intensity of absorption peak was changed without any variation on their position. As the aging times increased to more than 2 days, the absorption intensity decreased. The effect of addition of $HNO_3$ (as a catalyst) on the reduction of nano silver was investigated. However, by adding $HNO_3$ to Ag-PVP sol, we did not obtain any absorption peak. After 4 days, we observed only a small change in the absorption peak measured at about 410 nm. This shows that we have silver nanoparticles after 4 days. Surface morphology of the synthesized thin films was also studied utilizing Scanning Electron Microscope and Atomic Force Microscope. We have observed well-dispersed nanoparticles on the surface and the average diameter of the particles increased by increasing the $AgNO_3$ content. For the same concentration of silver for both matrices, the particle size in the PVP is smaller. For the 1.6% Ag in $SiO_2$ films, we have found nanosilver with average diameter of about 65 nm while this is only 11 nm for the same concentration in the PVP matrix.

# Introducing a newly synthesized organic-inorganic hybrid nanocomposite to the realm of nonlinear optics

**Y. Aghili [1], M. Mohseni [1], E. Mohajerani [2], H.R. Shirvani [2], S. Moradian [1] A.R. Khosravi [1]**

1. Department of Polymer Eng., Amirkabir University of Technology, Hafez St., Tehran, Iran
2. Laser Research Institute, Shahid Beheshti University, Evin St., Tehran, Iran

The current study introduces a novel organic-inorganic hybrid nano structure synthesized via the sol-gel method with improved physical and mechanical properties. Utilizing the typical mild preparation conditions and the facile manufacture process were eventually led to the production of hybrid glasses with high optical qualities, starting from functional silica-based precursors. In addition, the studied matrix was also employed as a host network incorporated with a renowned optically nonlinear organic dye, Disperse Red 1, as the guest component. Finally, a series of photoinduced studies, focused on birefringence and dichroism measurements were carried out on the prepared dye-doped hybrid thin films. The almost high birefringence intensities and the more efficient dichroic responses along with the lower chromophore aggregations obtained for the easy-preparing sol-gel samples would obviously represent the sufficient potential for the new generation of the guest-host system, accompanied with the hybrid structures in order to be one of the reliable fields of future studies for further designing of nonlinear optical devices.

## 1. INTRODUCTION

Current trends in information technology (IT) suggest that light, rather than electricity has been labeled as one of the most important 21$^{st}$ century technology. However, the development of the photonic science largely relies on the progress achieved in fabrication of the new optical materials with better performance. In that respect, materials with a nonlinear optical (NLO) response are expected to play a major role in enabling optoelectronic and photonic technologies. On the other hand, organic-inorganic hybrid materials have increasingly become an important field of research during the recent years, due to their extraordinary properties attributed to the synergistic effects of their components. In addition, the interest of organic-inorganic hybrid materials in telecommunication devices has constantly grown, thanks to the ease with which functionalized hybrid materials can be processed into practical devices having low electric constant and high nonlinear optical coefficients [1-3].

In our previous work [4], we introduced a new hybrid organic-inorganic nano composites synthesized via the sol-gel route with lots of improved physical, mechanical and morphological properties. In the current study, we have actually applied the proven consequent matrix in the realm of nonlinear optics in order to examine its behaviors as a hybrid host component incorporated into the dye-doped guest-host NLO systems; focused on the photoinduced birefringence and dichroism analyses. The silica-based thin films were produced by sol-gel technique doped with Disperse Red 1 (DR1) molecules.

## 2. EXPERIMENTAL

The organic monomer, 2-hydroxyethylmethacrylate (HEMA) obtained from Degussa and the organic-inorganic precursor, 3- (trimethoxysilyl) propyl methacrylate (MPTMS) purchased from Wacker, were used as received. Ethanol and acetone, as the solvents, were both gained from Merck. The thermal initiator, α, α'-azoisobutyronitrile (AIBN), was supplied from Akzo-Nobel and purified by recrystalization from ethanol prior to use. Disperse Red 1 (DR1), utilized as the NLO dye, and was obtained from Sigma-Aldrich. The organic-inorganic host was prepared in two consecutive steps. The first step was included the free radical copolymerization of HEMA and MPTMS monomers and in the second step, a traditional sol-gel process was carried out which could, in turn, be divided into two stages: hydrolysis and condensation. The synthesis's route and the details of the sol-gel preparation process were completely done according to our previous work, described in [4]. It should be mentioned that the 50 mol% content of the silane monomer (i.e. PHM50) was chosen as the synthesized composition ratio in order to prepare the hybrid network participating in the current study. This was due to the highest cross-linking density and the optimum value of the other enhanced properties which the mentioned composition had formerly achieved among the other applied ratios [4].

Furthermore, Disperse Red 1, with 3 wt% concentration, was being completely dissolved in acetone by the help of a magnetic stirrer prior to impregnating into the hybrid network in order to avoid aggregation of the dye molecules. The resulting solution was then added to the polymeric prepared precursor and again stirred to obtain a homogeneous true dispersion. Consequently, a series of thin films were deposited from the final colored solution onto pre-cleaned glass-slide substrate by the help of a homemade dip-coater rig, using the withdrawal speed of 5 mm/sec (leading to the thickness of ~2μm measured with a Dektak profilometer). Actually, the obtained films were highly transparent in the visible region of the spectrum which suggests the formation of compatible uniform sol-gel network having nano particle sizes well below the visible wavelengths.

To mainly determine the influence of the samples curing process on the birefringence and dichroism measurements; the photoinduced studies were carried out, in which the prepared hybrid thin films were encountered a specific heating procedure, according to Table 1.

| Sample | Curing State |
|---|---|
| 1 | Uncured |
| 2 | Curing up to 140°C without exposing time |
| 3 | Curing @ 140°C for 45 min |
| 4 | Curing @ 140°C for 90 min |
| 5 | Curing @ 140°C for 135min |

Table 1. Curing state of the studied samples in the heating procedure.

## 3. RESULTS AND DISCUSSION

All the investigations represent that the three concerning parameters, means the saturated signal level (or the maximum probe transmission), the rise time and the fall time of both photoinduced effects (according to the definition given by the IEEE society); obviously have a flourishing trend by increasing the heating time and completing the curing procedure. These behaviors may be attributed to the greater cross-linking density of the hybrid host structure according to the more complete hydrolysis and condensation reactions of the alkoxy groups, resulting from the continual process of curing. It implies that chromophore dipoles need some kind of free space (known as the free volume or cavity) for their molecular rotation. In thermoplastic polymeric systems (without any cross-linking reaction), since the host polymer chains around the guest chromophores can be re-oriented after the dye excitation, therefore,

the mentioned rate constants depends on the number of cavities with sufficient free volumes to allow the back and forth reactions. In such organic host structures, chromophore molecule should just get over the molecules interaction energy with the cavity walls in order to change the orientation, it which accordingly results in fast orientation and re-orientation mechanisms during the Rise Time and Fall Time, respectively [5, 6]. In fact, the current thermoset nano composite structure approximately behaves as a thermoplastic polymer at its uncured state; means the state of just being deposited from a fresh synthesized solution which may only have a negligible cross-linking density. In this case, the chromophore molecules can extensively undergo thermal fluctuation in the existing free volumes. These easily thermal fluctuations cause more randomized alignments, leading to lower saturated signal intensity (or the probe transmission value) in both photoinduced birefringence and dichroism measurements. But, the obtained diagrams of the present work demonstrate that the concerning parameter increases by performing the curing procedure (see Fig. 1 and 2).

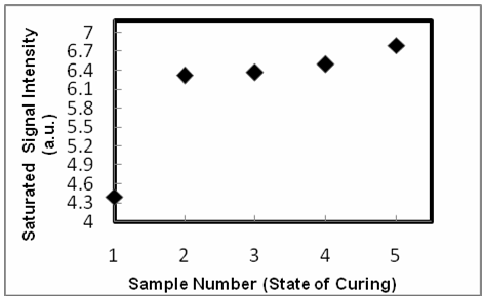


Figure 1. Variation of the saturated signal intensity as a function of the curing state, obtained in the birefringence measurements.

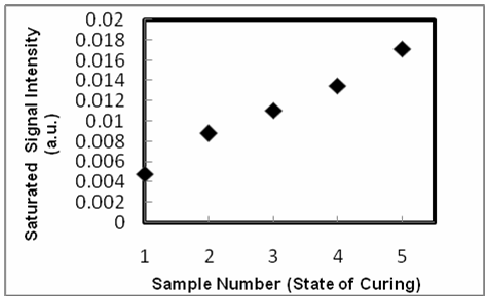


Figure 2 : Variation of the saturated signal intensity as a function of the curing state, obtained in the dichroism measurements.

This is undoubtedly attributed to the improving tendency of the cross-linking reactions between the silanol groups achieved by evaporating more side product (i.e. water or alcohol) through an endothermic process. Reaching higher cross-linking density will give rise to a drastic reduction of the size and the amounts of pores (free volumes), increasing therefore the steric hindrance for randomized molecular orientation. Consequently, the pump power will be more efficient to subdue the fluctuation motions, in order to achieve the desired alignment with higher saturated signal intensity which actually results in receiving desired variations of the refractive indices. Moreover, this increasing trend is coincided with higher photoisomerization time parameters (i.e. the R.T. and F.T.).

Fig. 3 and 4 show the changing trend of the photoinduced birefringence and dichroism, respectively. By decreasing the free volume of the polymer matrix, the thermal rotation (also known as the diffusion rotation) of both cis and trans molecules (more in the cis form) will hardly occur. Thus, the diffusion rotation procedure will happen with a slower rate, i.e. a higher Rise Time constant, compared to the uncured sample.

Qualitatively, the relaxation (i.e. the Fall Time duration) of the probe transmittance could also be analyzed by two steps: an initial fast decay related to the thermal cis-trans isomerization and a slow decay related to the angular redistribution of the oriented trans molecules [7]. It should be also mentioned that the obtained Fall Time duration always has a greater order of magnitude comparing with the relating Rise Time. This stems from the lower probability of the thermal rotation for the stable perpendicular trans molecules in order to get back to the randomized orientation.

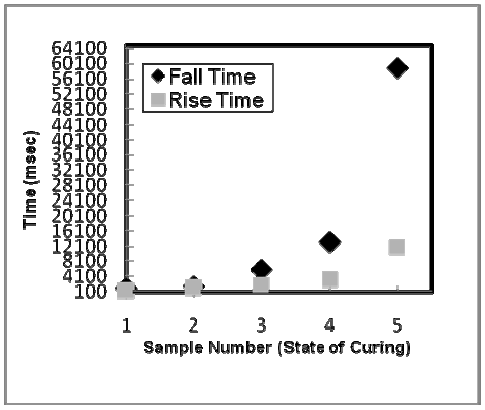


Figure 3. The changing tendency of R.T. and F.T. due to state of curing, observed for the birefringence effects.

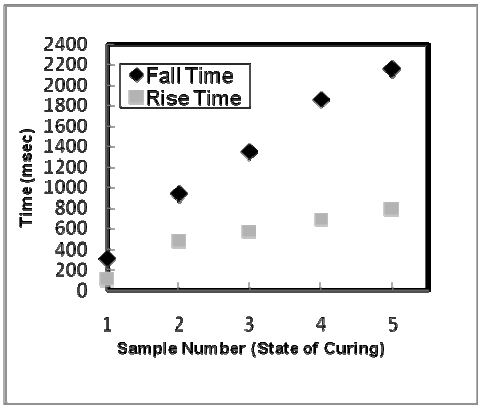


Figure 4. The changing tendency of R.T. and F.T. due to state of curing, observed for the dichroism effects.

## 4. CONCLUSION

The almost high birefringence intensity of the sol-gel films and, therefore, the higher refractive index obtained in this study is comparable to some other conventional polymeric guest-host systems. So, in the prospect of future, there would be a promise achievement for such systems in optical applications, especially the waveguides and the switchers. Moreover, the more efficient dichroic dye-doped films obtained via the easy and inexpensive sol-gel process accompanied by lower chromophore aggregation and, of course, with no covalent bonding incorporation would be also a reliable field of future study for designing the new devices and appliances. In addition, it should be also mentioned that the new generation of the guest-host (G/H) system with a hybrid organic-inorganic structures do have the enough potential to be one of the active area in the nonlinear optics, especially using the corona-poling procedure. This is due to its several modifying behaviors and advantages accompanied with the existing benefits of the conventional G/H systems; i.e. the low cost production of NLO materials, the possibility of applying a wide variety of centrosymmetric NLO chromophores along with a wide range of operating frequencies, the ease of fabrication onto a large area of any dimension and also the facile processing into thin films by spray coating, dipping or spinning. In other words, applying the sol-gel hybrid matrices in the field of G/H systems with highly stable NLO properties can hopefully overcome the drawbacks of the conventional G/H systems involved the all-organic thermoplastic polymers as the host may have a low glass transition temperature (Tg) or the dye molecules can easily diffuse to the surface of the film at elevated temperatures; e.g. during the corona-poling procedure.

## 5. References

[1] N. Prasad, J. Williams “Introduction to Nonlinear Optical effects in Molecular and Polymers” Wiley Interscince, New York 1991 (ISBN 0-471-51562-0)
[2] C. Sanchez et al., *Adv. Mater.*, 23 15 (2003)
[3] K. Yesodha et al., *Progress In polymer Science,* 29 45 (2004)
[5] M. Ganjaee et al., *J. Opt. & Adv. Mater.*, 10 575 (2008)
[6] C.R. Mendonca et al., *Optical Matt.*, 30 216 (2007)
[7] I-G. Marino et al., *J. Non-Cryst. Solids*, 354. 688 (2008)
[8] A. Vembris et al., *Thin Solid Films*, article in press (2007)

The Kurt J. Lesker Company is an international and world class manufacturer and distributor of high (HV) and ultra-high vacuum (UHV) components and thin film deposition systems, used by university, government, and industrial R&D facilities, OEMs, semiconductor processors, industrial vacuum coaters, and others thin film deposition companies. Our range of products includes:

- Flanges & Fittings
- Valves
- Electrical Feedthroughs
- Pumps
- Traps & Filters
- Fluids & Greases
- Pressure Measurement
- Sample Manipulation & Motion
- Evaporation Sources
- Deposition Materials
- Deposition Sources
- Process Instrumentation
- Vacuum Chambers and Vacuum Systems

Our in-house design, engineering and manufacturing capabilities (2800 m2 production facility in Pittsburgh, USA) allows us to supply fabricated items such as beamline components, chambers, specials, sub-assemblies, part of space simulators, complex manipulators, and complete deposition systems to customers across Europe and North America.

Olivier COSTA
Kurt J. Lesker
Manager Pays Francophones
77, cours Albert Thomas
69003 LYON
tél/fax: +33 (0)4-72-35-02-38
portable: +33 (0)6-14-19-60-83
e-mail: olivierc@leskerltd.com
www.lesker.com

# A Quantum-stabilized mirror for atoms

**D. Barredo [1], F. Calleja [1], P. Nieto [1], J.J. Hinarejos [1], G. Laurent [1], A.L. Vazquez de Parga [2], D. Farias [1], R. Miranda [2]**

1. Universidad Autónoma de Madrid, Spain
2. IMDEA Nanociencia

Helium atom scattering is a powerful, well-established technique for investigating the structural and dynamical properties of surfaces. Because of the low energies used (~100 meV), neutral He atoms probe the topmost surface layer of any material in an inert, completely nondestructive manner. This means that a Scanning Helium Atom Microscope using a focused beam of He atoms as imaging probe, would be a unique tool for reflection or transmission microscopy, with a potential lateral resolution of ~50 nanometers. It could be used to investigate insulating glass surfaces, delicate biological materials and fragile samples which are difficult to examine by other methods because of sample charging or electron excitation effects. The practical realization of such a microscope requires the development of a mirror able to focus a beam of low energy He atoms into a small spot on the sample to be examined. Holst and Allison demonstrated that electrostatic bending of a thin, H-passivated Si(111)-(1x1) crystal was able to focus a 2 mm-He beam to a spot diameter of 210 microns. A serious limitation, however, to improve the resolution was the low intensity obtained in the focused peak, which is a consequence of the poor reflectivity of such surfaces, less than 1%.

Here we show that Quantum Size Effects can be exploited to produce an ultraperfect, atomically flat film of Pb of magic thickness on a highly perfect Si(111) thin wafer. The metal film reproduces the structural perfection of the substrate, is atomically flat over micron-wide areas and stable up to 250 K. As a consequence, more than 15% of the incoming He atoms are scattered from this quantum-stabilized surface in the specular direction, which allows its use as an ultra smooth, mirror for neutral atoms, a device of interest also for atom optics in order to manipulate matter waves coherently.

# Frequency doubling between specular and diffuse x-ray intensity oscillations observed in situ during Ti and TiN heteroepitaxy

**M. Beckers [1,2], J. Grenzer [3], F. Eriksson [1], C. Baethz [3], L. Hultman [1]**

1. Linköping University, Sweden
2. Leoben University, Austria
3. Forschungszentrum Dresden-Rossendorf, Germany

The time-resolved study of x-ray intensity oscillation has emerged as a new technique to in situ monitor thin film growth. The oscillations are mostly recorded at the so called “anti- Bragg” (00½) position of the specular crystal truncation rod, and considered as roughness oscillations during nucleation and coalescence of individual monolayers. Their amplitude decay by roughening is fitted by kinematical scattering, mostly parameterized by diffusion-rate equation models for the coverage of each monolayer. In another approach, measurements are carried close to the total external reflection limit and (000). The obtained oscillations are treated as Kiessig thickness oscillations and fitted employing dynamical scattering using the Parratt formalism together with Nevot-Croce and Debye-Waller roughness models.

In the work presented here, we aimed to distinguish between roughness and thickness oscillations by simultaneous real-time measurement of specular and diffuse x-ray scattering during Ti and TiN growth for different film-substrate combinations, giving rise to different roughening behaviors. This includes heteroepitaxy with high adatom mobility onto smooth substrates (Ti onto $Al_2O_3$(0001) and TiN onto MgO(001)), heteroepitaxy with high adatom mobility onto rough substrates (Ti onto MgO(111)), heteroepitaxy with low adatom mobility onto smooth and rough substrates (TiN onto $Al_2O_3$(0001) and MgO(111)) and polycrystalline film growth (Ti and TiN onto amorphous SiO2). All depositions were carried out at 300 °C with deposition rates of 0.5 and 0.7 Å/s for Ti and TiN, respectively. The specular reflectivity was close to (00 1/4), (11 1/6) and (000 recorded at $\theta/2\theta$ = 1.75°/3.5°, 1/3) for TiN and Ti, respectively, and the diffuse scattering was measured in grazing exit configuration at $\theta$ = 1.95°, on the Ti and TiN Yoneda wing. For all film-substrate combinations, we observe the expected diametric evolution of specular and diffuse scattering signal during growth, with typical roughening factors for each combination. However, only for the case of rough substrates we observe oscillations in the diffuse scattering signal. Despite anticipation they are not out of phase to the specular signal, but exhibit a doubled oscillation period, which will be discussed during the presentation on the basis of a dynamical scattering model and correlated roughnesses..

# From Dynamic Roughening to Dynamic Smoothening: the Growth Behavior of Nanocomposite Films Controlled by Concurrent Ion Impingement

**Y.T. Pei [1], K.P. Shaha [1], C.Q. Chen [1], R. van der Hulst [1], A.A. Turkin [2], J.Th.M. De Hossson [1]**

1. Department of Applied Physics, the Netherlands Materials Innovation Institute, University of Groningen, Nijenborgh 4, 9747 AG Groningen, the Netherlands
2. National Science Center, Kharkov Institute of Physics & Technology, 1 Akademicheskaya str., UA-61108 Kharkov, Ukraine.

In film growth, the competition between interface roughening and smoothening essentially determines the nano-/microstructure and consequently the properties of a deposited film. This paper reports some striking findings on the breakdown of dynamic roughening in film growth under intensively concurrent ion impingement. With increasing the intensity of concurrent ion impingement by raising the frequency of pulsed DC sputtering, a transition from dynamic roughening to dynamic smoothening is observed in the growth behavior of TiC/a-C nanocomposite films, in correspondence with a transition of the film microstructure from strongly columnar to columnar-free. In the case of dynamic smoothening, TiC/a-C nanocomposite films exhibit a negative growth exponent and ultra-smoothness (RMS roughness ~0.2 nm at film thickness of 1.5 μm). As the first experimental proof of the impact-induced downhill flow model [1] and subplantation model [2-4], an amorphous front layer of 2 nm thickness has been observed with high resolution cross-sectional TEM to always cover the bulk nanocomposite film and thus leads to ultrasmoothness. The formation of such an amorphous front layer excludes any influence of nanocrystallites on the dynamic growth behavior of the nanocomposite films. The simulated interface evolution based on the Edwards-Wilkinson model and the Mullins model is in a good agreement with the atomic force microscopy measurements of roughness evolution.

[1] M. Moseler, P. Gumbsch, C. Casiraghi, A.C. Ferrari, J. Robertson. Science 309 1545 (2005).
[2] Y. Lifshitz, S.R. Kasi, J.W. Rabalais. Phys. Rev. Lett. 62 1290 (1989).
[3] D.R. McKenzie, D.A. Muller, B.A. Pailthorpe. Phys. Rev. Lett. 67 773 (1991).
[4] J. Robertson. Philos. Trans. R. Soc. London. A 342 277 (1992).

# Mound formation and step edge barriers in organic thin film growth

**C. Teichert [1], G. Hlawacek [1], P. Puschnig [2], C. Ambrosch-Draxl [2], P. Frank [3], A. Winkler [3]**

[1]Institute of Physics, Montanuniversität Leoben, Franz Josef Straße 18, 8700 Leoben, Austria

[2]Chair of Atomistic Modelling and Design of Materials, Montanuniversität Leoben, Franz Josef Straße 18, 8700 Leoben, Austria

[3]Institute of Solid State Physics, Graz University of Technology, Petersgasse 16, 8010 Graz, Austria

In inorganic epitaxy it is well known that kinetically hindered interlayer mass transport due the existence of an additional energy barrier at step edges - the so-called Ehrlich Schwoebel barrier (ESB) [1,2] - results in the formation of terraced mounds [3] instead of layer-by-layer growth. For the growth of rod-like para-sexiphenyl (6P) molecules on mica(001) - where usually the 6P molecules lie on the surface [4] - we found that on a pre-ion-bombarded substrate indeed such mounds composed by almost upright standing molecules do form.

Atomic force microscopy Analysis of the mound cross sections for different film thicknesses showed that the layer distribution follows almost ideally a Poisson distribution indicating an absence of mass transport between adjacent layers. The observed deep trenches separating the mounds are in agreement with the predictions of the Zeno effect [5]. From the mound separation and the size of the top terraces the Ehrlich Schwoebel barrier was estimated following a procedure developed originally for metal homoepitaxy [6]. The obtained value of 0.67 eV has been verified by a combination of first-principles density functional calculations with an empirical force field approach which yields further insight into the details of the preferential diffusion path including changes in molecular conformation during step edge crossing. A careful analysis of the AFM measurements revealed in the first few monolayers a higher tilt angle of the molecules with respect to the surface normal (up to 43°) as compared to the bulk value observed in thicker films (17°). This leads to a lower value of the ESB of only 0.26 eV for the first layer. This level dependence of the ESB could be explained by transition state theory calculations as the result of an interplay between different molecule orientation and necessary molecule bending during terrace edge crossing [7].

[1] G. Ehrlich, F. Hudda, J. Chem. Phys. **44** (1966) 1039.
[2] R. Schwoebel, E. Shipsey, J. Appl. Phys. **37** (1966) 3682.
[3] K. Meinel, M. Klaua, H. Bethge, J. Cryst. Growth **89** (1988) 447.
[4] C. Teichert, G. Hlawacek, A. Andreev, H. Sitter, P. Frank, A. Winkler, N.S. Sariciftci, Appl. hys. A 82 (2006) 665-669.Appl. Phys. A **82** (2006) 665.
[5] I. Elkinani, J. Villain, Solid State Commun. **87** (1993) 105.
[6] T. Michely and J. Krug; Islands, Mounds and Atoms (Springer, Berlin 2004).
[7] G. Hlawacek, P. Puschnig, P. Frank, A. Winkler, C. Ambrosch-Draxl, C. Teichert, Science **21** (2008) 108.
This work is supported in the framework of the Austrian Science Fund (FWF) within the National Research Network "Interface controlled and functionalized organic films" (S9707+S97014).

# Growth and characterization of Scandium Aluminium Nitride Nanowires

**T. Bohnen [1], A. E. F. de Jong [1], G. W. G. van Dreume [1]l, P. R. Hageman [1], R. Algra [3], M. A. Verheijen [3], J. H. Edgar [2], G.R. Yazdi [4], R. Yakimova [4]**

1 Applied Materials Science, Institute for Molecules and Materials, Radboud University Nijmegen, P. O. Box 9010, 6500 GL Nijmegen, the Netherlands
2 Kansas State University, Department of Chemical Engineering, Durland Hall, Manhattan, KS 66506-5102, U.S.A.
3 Philips Research Laboratories, Professor Holstlaan 4, 5656 AA Eindhoven, the Netherlands
4 Department of Physics, Chemistry and Biology, Linköping University, SE-581 83 Linköping, Sweden

The formation of ScAlN nanowires during the HVPE deposition of ScN on the silicon face of (0001) 6H-SiC was analyzed. Scanning Electron Microscopy studies revealed that the nanowires had an average length of approximately 1 μm with a diameter between 50 to 150 nm. Energy dispersive analysis of X-rays indicated that the wires contained the elements Al and Sc with a 95 : 5 Al : Sc ratio. Cathodoluminescence studies on the individual wires showed a sharp emission near 2.4 eV. Due to the low Sc content we compared the alloy to the pure AlN and found the most probable emission centers for these emissions to be the scandium atoms. Fast Fourier Transforms of the high resolution Transmission Electron Microscopy images of a wire, viewed from the side, yielded a periodicity of 4.9 Å along the length of the wire and a 2.7 Å repeating cell structure perpendicular to that, suggesting the same periodicity as wurtzite AlN. The out-of-plane orientations of the sample's surface were determined by θ-2θ X-ray diffraction using copper $K_\alpha$ radiation: only (111) and (222) peaks of the ScN and (0001) of the AlN were detected. Volatile Al (possibly AlCl) produced from a reaction between on one hand the alumina reactor tube and the scandium metal source, and on the other side hydrogen chloride, reacted with ammonia in the deposition zone to form ScAlN nanowires. A tentative model, based on catalyst-induced growth, was discussed to explain the formation of nanowires on the ScN film.

# Diverse Dopants in GaN nanowires

**B. D. Liu [1], Y.Bando [2], C. Tang [1], M. Mitome [1], D. Golberg [1,2]**

1. Nanoscale Materials Center, National Institute for Materials Science (NIMS), Namiki, 1-1, Tsukuba, Ibaraki 305-0044, Japan

2. World Premier International Center for Materials Nanoarchitectonics (MANA), National Institute for Materials Science (NIMS), Namiki 1-1, Tsukuba, Ibaraki 305-0044, Japan

In this work, various dopants including P, Mn, Si and Zn were successfully doped into GaN nanowires prepared by a simple chemical vapour deposition process.[1-3] These nanostructures were characterized and analyzed by XRD, a scanning electron microscope (SEM), a high-resolution transmission electron microscope (TEM), a field emission measurement instrument and it was found that the dopants do not only have an effect on the morphology of GaN nanowires, but also show strong influence on properties. A detailed effect of various dopants on the structure, morphology and properties of GaN nanowires will be presented later.

[1] B. D. Liu, Y. Bando, C. C. Tang, F. F. Xu, D. Golberg, J. Phys. Chem. B. 109 21521 (2005)
[2] B. D. Liu, Y. Bando, C. C. Tang, D. Golberg, K. Yamaura, E. Takayama-Muromachi, Chem. Phys. Lett. 405 127 (2005)
[3] B. D. Liu, Y. Bando, C. C. Tang, M. Mitome, D. Golberg, (unpublished)

# Three-dimensional Ge/Si quantum dot crystals with small periodicities

**G. Mussler [1], D. Grützmacher [1], C. Dais [2], H.H. Solak [2], T. Fromherz [3], J. Stangl [3]**

1. Forschungszentrum Juelich, Germany
2. Paul Scherrer Institute, Switzerland
3. Johannes Kepler University Linz, Austria

Templated self assembly of Ge quantum dots on Si substrates has been employed to fabricate 3-dimensional quantum dot crystals with high perfection and lateral periodicities ranging from 280 down to 35 nm. Extreme ultra-violet interference lithography (EUV-IL) at a wavelength of 13.2 nm was harnessed to realize prepatterned Si substrates. After exposure and resist development, shallow holes (4-10 nm in depth) were etched into the Si substrates by reactive ion etching. Subsequently, the resist was removed and the substrates were cleaned to subsequently use them for the deposition of Si and Ge by means of molecular-beam epitaxy (MBE) in order to realize the Si/Ge quantum dot structures. By choosing suitable growth conditions, perfect alignment of Ge dots in the etched grooves is found. Stacking of quantum dot layers separated by narrow Si spacer layer leads to the formation of 3-dimensional arrays of ordered Ge quantum dots, i.e. quantum dot crystals (QDC). Previously we reported on QDC having lateral and vertical periodicities of 90-100 nm and 7-10 nm, respectively. Here we reduced these dimensions substantially, achieving minimum feature sizes of 35 nm and 5 nm for lateral and vertical dimension. Even for the smallest periodicitiy close to perfect alignment of Ge dots in a 3 dimensional lattice is observed.

# Morphology of three-dimensional Ge nanoclusters growing on $SiO_x$ ($x$<2) film and efficiency of photoelectromotive force in this structure

**Yu.N. Kozyrev [1], S.V. Kondratenko [2], M.Yu. Rubezhanska [1], V.S. Lysenko [3] A.V. Sushyi [1], C. Teichert [4], C. Hofer [4]**

[1]Institute of Surface Chemistry, Generala Naumova Str. 17, UA-03164, Kiev, Ukraine

[2]National Taras Shevchenko University, Physics Department, Acad. Glushkov Ave 2, UA-03022, Kiev, Ukraine

[3]Institute of Semiconductor Physics, Prospect Nauki 45, UA-03028, Kiev, Ukraine

[4]Institute of Physics, Montanuniversitaet Leoben, Franz Josef Str. 18, A-8700 Leoben, Austria

Newly elaborated optoelectronic and nanoelectronic devices require more and more small sizes of their structural components. This explains the interest in Ge nanosize formations in $SiO_2$ matrix. Three-dimensional Ge nanoclusters about 20 nm in height and 30 nm in the basis were prepared by molecular-beam epitaxy on initially amorphous $SiO_x$ ($x$<2) film of the thickness varying from 2 to 8 nm. A possibility of epitaxial formation of such nanostructures on initially amorphous silicon oxide layer is considered. Possible formation mode of three-dimensional Ge nanoclusters on initially amorphous $SiO_x$ film is a question under discussion. Photo-emf dependences were investigated for different samples with different Ge nanocluster distribution density over the substrate surface.

Silicon oxide nanofilms on Si (111) and (100) substrates are supposed to be one of the most prospective materials in the view of their possible application in new microelectronic devices. The increasing demand for newly elaborated optoelectronic devices based on silicon is driving the silicon microelectronics world to miniaturization of their structural components, so the thickness of investigated silicon oxide layers was reduced to several nanometers [1-2]. This explains the interest in Ge nanosize formations in $SiO_2$ matrix by scientists all over the world today [3-4]. Such structures can be regarded as a type of SOI structures widely used in microelectronics.

A possibility of epitaxial formation of such nanostructures on initially amorphous silicon oxide layer is considered in this paper. To do this, information concerning growth mode, in particular, initial stages of germanium nanoisland formation during molecular-beam epitaxy is required. After the substrate was thermically cleaned heated to the temperature 750 $^oC$, Ge flux was directed to the substrate at the temperature 700-750 $^oC$. Three-dimensional Ge nanoclusters appeared to originate and form on the initially amorphous $SiO_x$ ($x$<2) film of the thickness varying from 2 to 8 nm. To investigate different stages of such nanocluster formation, the epitaxial growth process was stopped at different stages corresponding to different RHEED-images for different samples. Then these samples were extracted from the growth chamber and their surface structure was investigated using atomic-force microscopy. Ge nanoclusters were about 1-2 nm in height and 10-20 nm in the basis for the initial stage of their formation with a very low distribution density about $5 \cdot 10^8$ $cm^{-2}$ (fig.3, insert). As the epitaxial growth went on for other samples, Ge nanoclusters grew larger: about 20 nm in

height and 30 nm in the basis (fig.1,*a*). Their distribution density over the substrate surface exceeded $10^{11}$ $cm^{-2}$.

In contrast to traditional heteroepitaxial formation of Ge quantum dots on Si(100) [5] or epitaxial growth of Si nanoclusters on $SiO_x$ [6], which seem to show monocrystalline features: {113} side facets with characteristic angles of about 25° and top (100) terraces that correspond to Si(100) epitaxial formation, despite the presence of initially amorphous oxide layer (fig.1,*b*), Ge nanoclusters formed on the initially amorphous $SiO_x$ ($x$<2) were almost hemispherical in our case with the correlation between the nanocluster height and lateral size about β~5-6.

Possible formation mode of three-dimensional Ge nanoclusters on initially amorphous $SiO_x$ film is a question under discussion. We suppose that complicated physical and chemical processes occur on the surface at Ge epitaxy on $SiO_x$ so that a variband $Si_{1-x}Ge_xO_y$ structure is formed with gradually increasing Ge concentration in the growth direction. The presence of oxygen in this layer even at a low concentration may essentially enlarge the strain relaxation. In such a way the centers of Ge crystallization were formed randomly in this $Si_{1-x}Ge_xO_y$ layer.

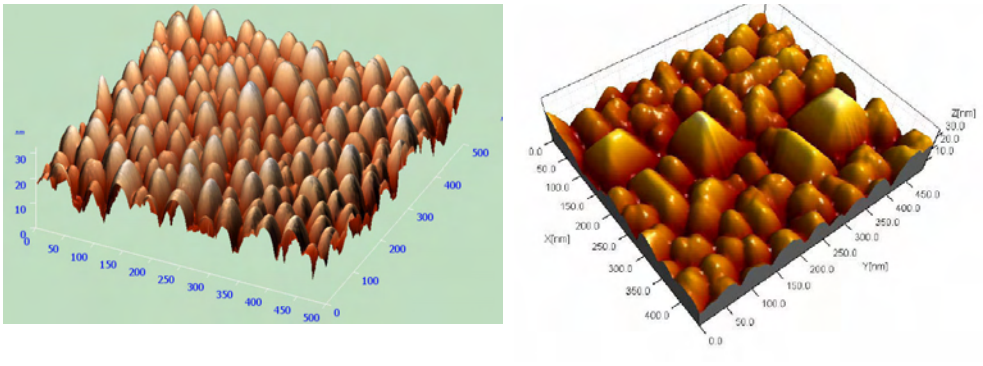


(a) (b)

Fig.1. Ge nanoclusters (*a*) and Si nanoclusters (*b*) grown on initially amorphous $SiO_x$ film.

Taking into consideration the fact that adhesion of Ge adatoms may be rather essential at high growth temperatures, the mechanism of $2D \rightarrow 3D$ transformation corresponds to the conditions of Stranski-Krastanov epitaxial growth realized in the presence of a lattice mismatch between the growing surface $Si_{1-x}Ge_xO_y$ with very low oxygen concentration and Ge. Due to their random polycrystalline nucleation the forming Ge nanoclusters take a shape of hemispheres with a low β coefficient and high distribution density over the surface.

Earlier we have investigated lateral photoconductivity from different types of Ge on Si structures, as well as photo-emf in them [5,7]. Then we studied heterostructures with Ge nanoclusters formed on initially amorphous $SiO_x$ film. It was revealed that the efficiency of photo-emf in our last samples with Ge nanoclusters on initially amorphous $SiO_x$ film appeared to be more intensive than in typical monolayer or multilayer Ge quantum dot structures on Si (fig.2). Such photo-emf dependences were investigated for different samples with different distribution density of Ge nanoclusters over the substrate surface. Photo-emf efficiency seems to depend on the nanocluster distribution density: it is smaller for the samples with smaller distribution density of Ge nanoclusters (fig.3).

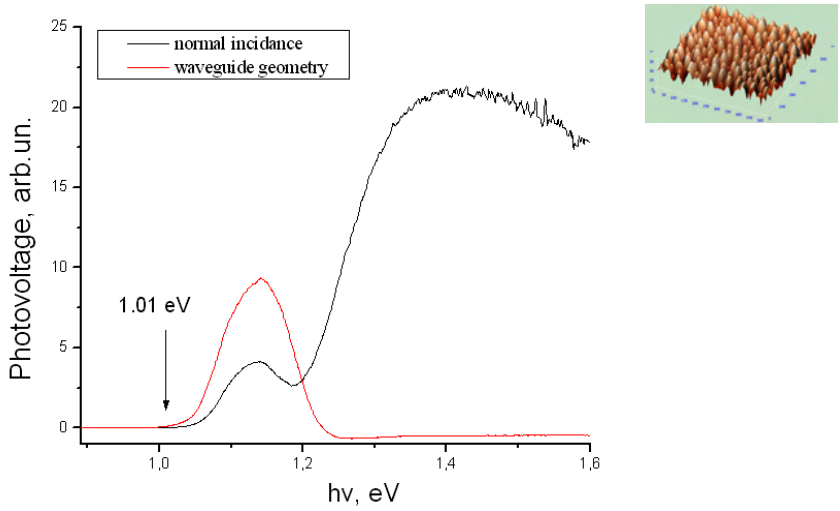


Fig.2. Photo-emf spectra of Ge nanoclusters grown on initially amorphous $SiO_x$ film at 290 K for normal incident and lateral irradiation.

Besides that, the influence of p- and n- doping of the structures Ge nanosize formations in $SiO_x$ matrix on lateral photoconductivity and photo-emf efficiency in such structures was investigated. It appeared to be that the presence of B and Sb doping almost showed no affect on morphological properties of such structures. As regards photo-emf efficiency, it was revealed that B doping (*p-i-p* heterojunction) almost did not influence on photo-emf spectra shape, while Sb doped Ge on $SiO_x$ structures (*p-i-n*$^+$ heterojunction) showed higher intensities of photo-emf efficiency spectra (fig.3).

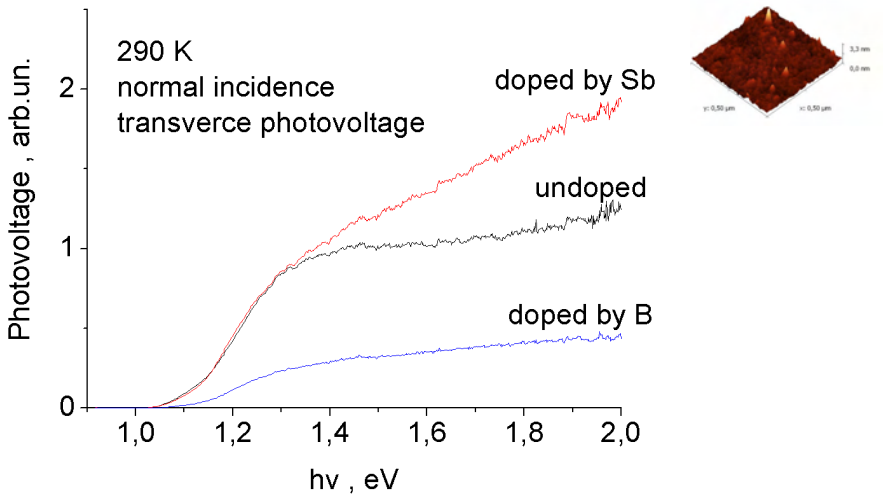


Fig.3. Photo-emf spectra of Ge nanoclusters grown on initially amorphous $SiO_x$ film doped by Sb, undoped and doped by B measured at 290 K.

A nature of these effects is a question under discussion and may be explained considering several aspects. The essential increase of the photo-emf efficiency observed in these structures, in our opinion, may be attributed to formation of a three-layer solid system containing superthin Ge layer on partially isolated $SiO_x$ layer from Si(100) substrate. The most important aspect is that many additional surface localized states for electrons and holes

are formed in the interfaces of the isolating $SiO_x$ layer. The presence of such surface localized charged states leads to formation of so called surface double space-charge layer that essentially influence interface conductivity, capacitance, electron-hole recombination in Ge/Si heterojunction. Besides that, the heterojunction capacitance is increased because of a contribution of the dielectric conductivity of $SiO_x$ barrier layer. All these aspects, may change parameters of energy-band structure and, possibly, essentially affect the efficiency of electron-hole pair recombination in Ge/Si heterojunction reducing losses and optimize processes at spatial charge separation.

This work is only the first attempt to characterize photo-emf behaviour in heterostructures with Ge nanoclusters on initially amorphous $SiO_x$ film and requires further investigation to understand a nature of these processes better. The research was implemented within the bilateral ÖAD Project UA No 2007/05 and supported by the program of fundamental research of the National Academy of Sciences of Ukraine "Nanostructured systems, nanomaterials, nanotechnologies" through the Project No 9/07 and by the Ministry of Education and Science of Ukraine through Project No M/139-07.

## References

[1] A. Athanassouli, F.Klose and S. Messoloras, Semicond. Sci. Technol. 17: 65 (2002)

[2] A. Bongiorno, A. Pasquarello, Phys.Rev. B. 70: 195312 (2004)

[3] Y. Wu, H. Xing, L. Zhang, Mat. Chem. Phys. 84: 234 (2004)

[4] J. Lee, S. Kim, B. Lee, J. Moon. Appl. Surf. Sci. 228: 271 (2004)

[5] S.V. Kondratenko, O.V. Vakulenko, A.S. Nikolenko, S.L. Golovinskiy, Yu.N. Kozyrev, M.Yu. Rubezhanska. Surf. Sci. 601: L45 (2007)

[6] Yu.N. Kozyrev, M.Yu. Rubezhanska, S.V. Kondratenko, A.V. Sushyi, C. Teichert, C. Hofer. 15th International Winterschool on New Developments in Solid State Physics, Bad Hofgastein, Austria, February 18-22, 2008.

[7] S.V. Kondratenko, O.V. Vakulenko, A.S. Nikolenko, S.L. Golovinskiy, Yu.N. Kozyrev, M.Yu. Rubezhanska. Nanotechnology 18: 185401 (2007)

# Peculiarities of sol-gel phase change as seen in effectively two-dimensional hydrophobic biopolymer aggregations

**N. Kruszewska, A. Gadomski**
Department of Modeling of Physicochemical Processes, Institute of Mathematics and Physics, University of Technology and Life Sciences, Kaliskiego 7, 85796 Bydgoszcz, Poland

HP aggregations [1] under two-dimensional confinement have been obtained by means of a Monte Carlo computer simulation [2]. The obtained aggregations involve two main tendencies prevailing systematically over our computer experiment. The first tendency reveals that the system is driven towards sol-gel phase change [3], though the gel state looks more of chemical (H-H interaction involved) nature than when obtained by changing the temperature. The second tendency, in turn, can preliminary be judged for phase separation, when the effect looks rather viscoelastic than diffusion-driven (non Lifshitz-Slyozov), where again the viscoelasticity can arise from some asymmetric distribution of H-H contacts [4]. We examine the system's behavior in a quite versatile way in a space of properly selected order vs. control parameter(s). We are able to interpret crudely some of the results by means of a two-state Kramers-type process, stated properly in such an entropic milieu. A certain rationale of the studied aggregations in terms of their creeping properties and stresses' accumulations can also be revealed, at least in some preliminary but promising way [5].

[1] R.I. Dima, D. Thirumalai, Protein Sci. 11 1036 (2002)
[2] N. Kruszewska, A. Gadomski, Act. Phys. Pol. B 38 1819 (2007)
[3] L. Arcangelis, E. Gado, A. Coniglio, Fractals 11 9 (2003)
[4] A. Gadomski, J. Łuczka, R. Rudnicki, Phys. A 325 284 (2003)
[5] I. Santamaría-Holek, J. M. Rubí, A. Gadomski, J. Phys. Chem. B 111 2293 (2007)

# Deposition of Plasma Polymerized Allylamine Films by DC magnetron sputtering

**N. Moreau [1], G. Genard [1], C. Michiels [2], B. Masereel [3], O. Feron [4], B. Gallez [5], T. Vander Borght [6], S. Lucas [1]**

1. University of Namur (FUNDP), Research center in Physics of Matter and Radiation (PMR), Rue de Bruxelles 61, 5000 Namur, Belgium
2. University of Namur (FUNDP), Unité de Recherche en Biologie Cellulaire (URBC), Rue de Bruxelles 61, 5000 Namur, Belgium
3. University of Namur (FUNDP), Department of Pharmacy, Rue de Bruxelles 61, 5000 Namur, Belgium
4. University of Louvain-La-Neuve (UCL), Unit of Pharmacology and Therapeutics (FATH), Avenue E. Mounier 53, 1200 Bruxelles, Belgium
5. University of Louvain-La-Neuve (UCL), Biomedical Magnetic Resonance Unit (CMFA), Avenue E. Mounier 74, 1200 Bruxelles, Belgium
6. University of Louvain-La-Neuve (UCL), Center for Molecular Imaging and Experimental Radiotherapy (IRME), Dr. G. Therasse 1, 5530 Yvoir, Belgium

Surface modifications induced by plasma treatments are involved in many applications. Most of them are related to biology and biochemistry. Through the presence of amine functions on their surface, Plasma Polymerized Allylamine (PPAA) films exhibit a high binding capacity with antibodies, allowing immunoassays with very high selectivity and sensitivity. PPAA is also suitable for enzyme immobilization: production of high fructose syrup from starch by immobilization of glucose isomerase can be cited as an example. Concerning the production of biohybrid organs, the PPAA serves as cell support as well as barrier protecting the tissue from environment, with oxygen and nutrients delivering. In this work, we show a simple method designed to produce PPAA films, by the use of conventional DC-magnetron sputtering set-up. The deposited layers were characterized by X-Rays Photoelectron Spectroscopy (XPS), FEG-SEM, Nuclear Reactions Analysis (NRA) and Elastic Recoil Detection (ERD). Evidences of the presence of $-NH_2$ functions were obtained by XPS. Furthermore, the functionalized polymers obtained by the described method are very stable in many organic solvents and water.

# Influence of Si on the Structure and Properties of Multifunctional Bioactive Nanostructured Films

**I.A. Bashkova [1], A.N. Sheveiko [1], N.A. Gloushankova [2], B.N. Mavrin [3], C. Rojas Ruiz [4], D.V. Shtansky [1]**

1. State Technological University "Moscow Institute of Steel and Alloys", Moscow, Russia
2. Cancer Research Center of RAMS, Moscow, Russia
3. Institute of Spectroscopy of RAS, Troitsk, Moscow region, Russia
4. Instituto de Ciencia de Materiales de Sevilla-CSIC/UNSE, Sevilla, Spain

One possible solution to the problem of producing load-bearing implants is to coat a film with multifunctional properties. In this study new ceramic Ti-Ca-Si-C-O-(N) films were evaluated as perspective biomaterials for implants. The films were deposited by magnetron sputtering in an Ar atmosphere or reactively in a gaseous mixture of argon and nitrogen ($\xi=N_2/(N_2+Ar)=0.15$ and 0.25). The films were characterized in terms of their structure, chemical composition, hardness, Young's modulus, elastic recovery, resistance to plastic deformation and long elastic strain to failure, wettability, surface topography, friction coefficient, wear- and corrosion resistance. The biocompatibility of the films was evaluated by both in vitro and in vivo experiments. In vitro study involved the investigation of adhesion, spreading and proliferation of MC3T3-E1 osteoblasts and IAR-2 epithelial cells, morphometric analysis, actin cytoskeleton and focal contacts staining of the cells cultivated on the films. Alkaline phosphatase activity and von Kossa staining of osteoblastic culture were also investigated. In vivo studies were fulfilled by subcutaneous implantation of Teflon plates coated with the tested films in mice and analysis of the population of cells on the film surface. The results obtained show that the multifunctional Ti-Ca-Si-C-O-(N) films possess a combination of chemical, mechanical, tribological, and biological properties required for orthopedic and dental implants.

# Structural and antibacterial properties of $TiO_2$-Cu thin films elaborated by DLI-MOCVD process

**Mungkalasiri J. [1,3], Bedel L.[1], Renaud F.[2], Sarantopoulos C.[3], Maury F.[3]**

[1] Laboratoires des Technologies des Surfaces (LTS), LITEN/DTNM, CEA Grenoble

[2] Nosoco.Tech®, Université Lyon 1, EA 3090, Lyon.

[3] Centre Interuniversitaire de Recherche et d'Ingénierie des Matériaux (CIRIMAT) UMR CNRS 5085

The bacteria are present in our environment, a part of them is very helpful for health but some of them are pathogenic and could be harmful and very dangerous in many fields due to their rapid proliferation such as in hospital area (nosocomial infection), food industry, cooling tower, public area and air conditioning... The principal origin of infection comes from the free bacteria which are released by the biofilms. To limit these surface contaminations, many researches deal with the curative treatment of the surfaces covered with biofilms by using chemical and/or physical cleaning methods. A great effort is developed to understand the formation of biofilms on solid surfaces and as a result there is huge interest to produce bactericidal surfaces to limit or avoid the development of bacteria and biofilm.

In this objective, this work aims to elaborate transparent nanostructured thin films which are composed of nanometric metallic particles of antibacterial element (Cu) embedded in an oxide matrix ($TiO_2$). The DLI-MOCVD process (Direct Liquid Injection-Metal Organic Chemical Vapour Deposition) was used to elaborate these thin films. The advantage of this process is its ability: to control the quantity of precursors injected into the CVD reactor and to coat porous body. Titanium dioxide was used as a matrix and its microstructure and growth mechanisms are influenced by the presence of the antibacterial molecular precursor during the deposition process. Based on SEM, SIMS, XPS, XRD, image analysis, the morphology and structural properties of these $TiO_2$-Cu thin films were analyzed and correlation between process parameters and structural properties appeared. The molar fraction of copper precursor modifies the crystallite size and the crystallographic structure of the $TiO_2$ matrix. Different sizes of copper particles are present in the film from 20 to 250 nm and an enrichment of copper closed to the surface was detected.

The antibacterial activity was tested by the standard JIS Z 2801: 2000 with many bacteria and specific tests were optimised in order to evaluate their activity closed to real condition. The structure of coatings impacts strongly the antibacterial activities from bacteriostatic effect to bactericidal effect, i.e. more efficient, by the control of the metallic content in the matrix. No diffusion of the metallic element was detected according to the ISO 20645: 2005 standard. This coating is non toxic for the environment. The efficiency to limit the development of biofilms on these surfaces was also investigated. Correlations between the microstructure and composition of the films and their antibacterial properties are discussed.

It was found that 100 nm thick coatings with a copper content of 4at% exhibit an important potential to limit significantly the surface contamination.

# ST Instruments

Enhance your Quality

## Surface Science & Nanotechnology

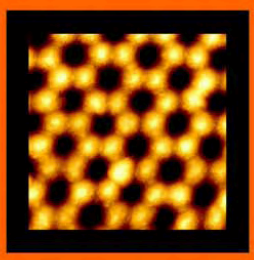

for Training or Research.

**Easyscan 2**

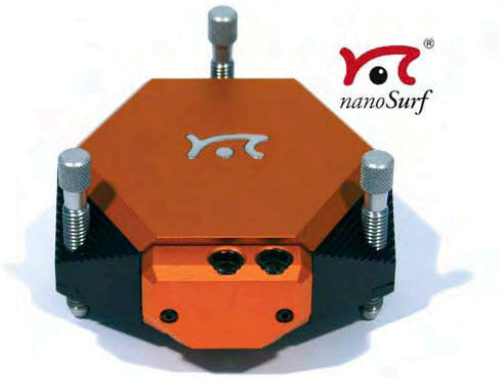


**ST Instruments provides innovated technologies for surface analysis and nanotechnology.**

**Our products are used in scientific research and high tech industries. To ensure innovative technologies ST Instruments partners with world leading manufactures focused on development.**


Broad range of research and Industrial AFM.

**XE-series**

**ST Instruments B.V.**
T: +31-(0)184-640000
F: +31-(0)184-640001
info@stinstruments.com
www.stinstruments.com

# Efficiency of high-power pulsed magnetron sputtering: experiments and modelling

**J. Vlcek, K. Burcalova**
Department of Physics, University of West Bohemia, Univerzitni 22, 306 14 Plzen, Czech Republic

High-power pulsed magnetron sputtering of copper and titanium films was systematically investigated. The depositions were performed using a strongly unbalanced magnetron system with a target of 100mm in diameter. The repetition frequency of the pulsed dc power supply (with a maximum voltage and current of 1kV and 120A, respectively) was 1kHz at a 20% duty cycle. A completely different trend in measured values of the deposition rate per average target power density obtained for these two technologically interesting materials and the same trend in their values of the ionized fraction of sputtered atoms in the flux onto the substrate (up to 56% for copper and 81% for titanium) were explained on the basis of model predictions. We present a qualitative model based on that developed recently by Christie (2005). The original model was modified and supplemented by a balance equation for secondary electrons near the sputtered target. This makes it possible to evaluate the fraction of ionized sputtered atoms directed back to the target to sustain the magnetron discharge under the experimental conditions investigated. The effects of self-sputtering of target material, losses of the target material ions during transport to the substrate and additional ionization of sputtered atoms in a plasma bulk on the deposition rate per average target power density and on the ionized fraction of sputtered atoms in the flux onto the substrate are shown.

# Structural, electronic and mechanical properties of TiTaN thin films

**G. Abadias [1], L. Koutsokeras [2], P. Patsalas [2], C. E. Lekka [2], C. Kosmidis [3], S.N. Dub [4]**

1. Université de Poitiers-CNRS, Laboratoire PHYMAT, UMR 6630, SP2MI, Téléport 2, Bd Marie et Pierre Curie, 86962 Chasseneuil-Futuroscope, FRANCE
2. University of Ioannina, Department of Materials Science and Engineering, Ioannina, 45110, GREECE
3. University of Ioannina, Department of Physics, Ioannina, 45110, GREECE
4. Institute of Superhard Materials, National Academy of Sciences, 04074 Kiev, UKRAINE

Transition metal (TM) nitride thin films find widespread applications in various fields, such as diffusion barrier or metallization layers in advanced microelectronics, hard protective coatings or decorative over-layers. If binary compounds of group IV-B and V-B crystallizing in the rock-salt structure (TiN being the prototype of these TM nitrides) have been largely studied, less has been done so far for ternary compounds combining different TM elements. In the present work, we investigate the phase stability of a new ternary system, Ti-Ta-N, by implementing PVD film growth and ab-initio calculations and show the possibility to tune the electronic and mechanical properties by appropriate choice of Ta content x.

$Ti_{1-x}Ta_xN$ thin films were deposited by Dual Ion Beam Sputtering (DIBS) and Pulsed Laser Deposition (PLD) on Si substrates. The structure and chemical composition were characterized by X-ray Diffraction (XRD) and Auger Electron Spectroscopy, respectively. It is shown that solid solutions $Ti_{1-x}Ta_xN$ films with rock-salt structure are stabilized in the whole composition range investigated ($0 \leq x \leq <1$) for both deposition conditions. Films grown by DIBS exhibited a [100] preferred orientation, while pure TiN films of the same thickness (300 nm) showed a [111] texture. For the PLD-grown films the texture is reverse; thus, pure TiN and TaN are textured along the [100] and [111] orientations, respectively, and the TiTaN are less textured.

The electronic properties of TiTaN have been studied experimentally and theoretically using spectroscopic ellipsometry and ab-initio calculations within the density functional theory scheme, respectively. We show that the TiTaN films are electrical conductors and their optical properties resemble TiN. The density of conduction electrons and the resistivity are correlated with the Ta content.

The evolution of residual stress of TiTaN films grown by DIBS was examined by XRD as a function of atomic fraction of Ta. Analysis was performed using the $\sin^2\psi$ method implemented on as-grown and annealed samples in order to induce a stress relaxation and determine the stress-free lattice parameter $a_0$. Additional experiments were performed using real time wafer curvature measurements to study the stress evolution during film growth. Nanoindentation was used to determine the hardness and elastic modulus of the films. Hardness enhancement is observed with increasing Ta content and is retained after annealing at 850°C, suggesting that these coatings are intrinsically hard. This is also suggested by our ab-initio calculations, which revealed a significant enhancement of elastic modulus with increasing Ta content.

# Investigation of the ion energies at the substrate in d.c. and pulsed d.c. magnetron sputtering

**F. Richter [1], T. Welzel [1], R. Kleinhempel [1,2], T. Dunger [1]**

1. Chemnitz University of Technology, Institute of Physics, D-09107 Chemnitz, Germany
2. present address: Southwall Europe GmbH, Southwallstraße 1, D-01900 Großröhrsdorf, Germany

An energy dispersive ion mass spectrometer has been applied to magnetron sputtering to measure the ion energy distribution functions (IEDFs) at the substrate. Mainly d.c. but also pulsed d.c. discharges were investigated with two different target materials (steel and aluminium doped zinc oxide) on the planar magnetron. IEDFs of positive ions from the target material exhibit a peak at few eV according to the plasma potential and a high energy tail due to the sputtering which is, however, much lower than the sputter energy distribution even for 0.1 Pa working pressure. The tail is strongly decreasing with pressure due to the thermalisation of the sputtered species. The IEDFs of the negative ions are dominated by a strong peak which corresponds to the target voltage and has an energy of several 100 eV. It does not change its energy with pressure but is exponentially decreasing with pressure in its intensity. Concurrently, the flux of positive ions is increasing with pressure due to growing ionisation in the bulk plasma offering the possibility to control the impact of positive and negative ions on the growing film, however, at the expense of the deposition rate.

## 1. INTRODUCTION

Magnetron sputtering is a convenient method to deposit thin films of high quality. As it offers the possibility of high rate and large area coating it has been established in several industrial branches. Although much progress has been achieved during the last years (see [1] and references therein) the physical understanding of the interplay of the processes involved is up to date still rather lacking preventing an efficient optimisation of the coating process in many cases. One such mechanism is the bombardment of the growing film with high energetic ions from the adjacent plasma which is an inherent feature of the process. This bombardment may strongly affect the film properties, especially in films for electronic usage. Positive ions can be typically used to improve the film properties by the application of a negative bias voltage onto the substrate electrode. However, for sensitive substrates where the energy must be kept low this is often complicated. When electronegative gases are used for the deposition, negative ions may bombard the growing film with high energies and cause damage. To reduce their influence, knowledge about their origin and how they can be affected is necessary. To measure the ion energy distribution functions (IEDFs) at the substrate, energy dispersive mass spectrometers can be used. The devices are capable of separating ions according to their mass and energy which is hardly possible with other methods. Moreover, such plasma monitors can directly detect negative ions. In this paper we present an investigation of the IEDFs of positive and negative ions at the substrate in a d.c. magnetron with special emphasis on their pressure dependence.

## 2. EXPERIMENTAL DETAILS

The experiments were performed in a high-vacuum chamber with a base pressure of $5 \cdot 10^{-4}$ Pa. It contained a circular planar magnetron source 100 mm in diameter which was operated in d.c. or asymmetric-bipolar pulsed d.c. mode with 100 W or 200 W and was either equipped with a steel (V2A) or an aluminium doped zinc oxide (AZO) target. The discharge was run in pure argon or oxygen at a fixed flow rate of 100 sccm. The total pressure was varied between 0.1 Pa and 3.0 Pa during the experiments by means of a throttle valve. The plasma monitor (PPM 422, Inficon) was placed at the typical substrate distance, 100 mm from the target with its entrance (100 µm diameter) facing the target to detect directed ion flux from there. The entrance was held at floating potential to disturb the discharge as less as possible. IEDFs could be measured of positive and negative ions against ground potential up to 500 eV.

## 3. RESULTS AND DISCUSSION

### *3.1 Positive Ions*

Apart from positive ions of the gas ($Ar^+$, $Ar^{2+}$), those of the target material were detected. For the steel target, the relation of the ion count rates of $Fe^+$, $Mn^+$, $Cr^+$, and $Si^+$ approximately reproduced the target composition revealing no significant differences in the ionisation behaviour. All their IEDFs in the d.c. discharge show essentially the same behaviour which is shown in Fig. 1 for $Fe^+$. The IEDFs exhibit a low energy peak at few eV which corresponds to the plasma potential ($V_P$). A more or less distinct high energy tail is observed for the ions of sputtered species. This is a remnant of the original sputter energy distribution when the atoms leave the target. It is observed most significantly at low pressure while with increasing pressure it is strongly reduced due to collisions which finally produce thermalised atoms which form the peak in the distribution. However, the sputter energy distribution should vary $\propto E \cdot U_0/(E+U_0)$, $U_0$ being the surface binding energy [2], as given by the dotted line in Fig. 1. Even for the lowest pressure of 0.1 Pa, the high energy part is much weaker than expected showing that most atoms have already lost energy by collisions. For high pressure the IEDFs look similar to that for $Ar^+$ which generally has no high energy tail because it is produced of the cold working gas. For the AZO target, positive $Al^+$, $Zn^+$, $O^+$, and $AlO^+$ ions have been observed which show essentially the same IEDFs as described for the V2A target. There, it was additionally found that the thermalisation of the sputter energy distribution is strongest for species with a mass closest to the working gas Ar [3].

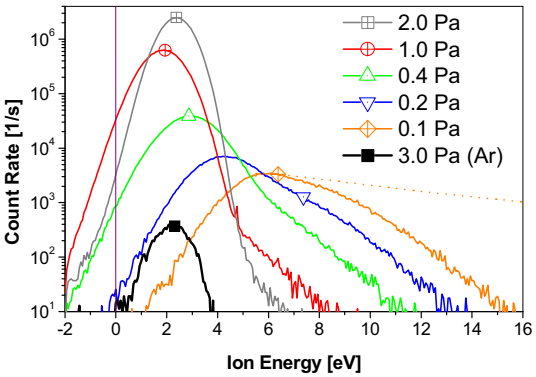


Figure 1: IEDFs of $Fe^+$ for different pressure (V2A target, 200 W, Ar, d.c.)

### 3.2 Negative Ions

Negative ions were not detected with the steel target sputtered in argon as no electronegative species were involved. With the AZO target which contains oxygen, significant count rates were observed of $O^-$ (dominating) and $O_2^-$. This was the case in both gases with $O_2$ even producing slightly less negative $O^-$ than Ar. The high energy parts of the IEDFs of $O^-$ are shown in Fig. 2 for different pressure. Scans of the complete energy range from 0 to 500 eV revealed that the peak shown is by far the dominant one. Small signals which can be attributed to $O^-$ as fragments of larger molecules were found at lower energies but they are at least 2 orders of magnitude lower. The peak has its maximum at an energy which is exactly at $eV_T$ ($V_T$ – target voltage) meaning that $O^-$ is formed directly at the target surface. The high energy tail of the peak has been shown to be much closer to the original energy distribution because colliding $O^-$ is completely removed from the shifted distribution by scattering or neutralisation [3]. Due to that the count rate is, however, drastically decreasing with increasing pressure.

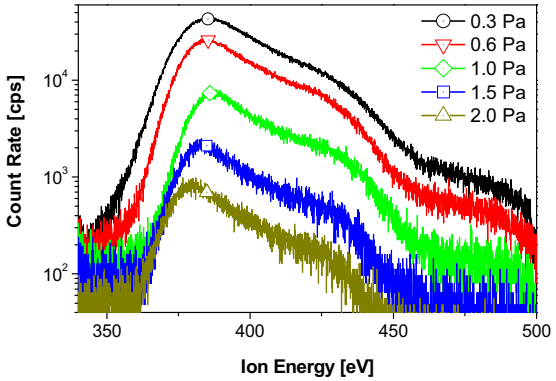


Figure 2: IEDFs of $O^-$ for different pressure (AZO target, 100 W, $O_2$, d.c.)

### 3.3 Comparison of Positive and Negative Ions

Fig. 3 shows the average ion energy and the total count rate (integrated over energy) for positive ions of sputtered material ($Fe^+$) and negative ions ($O^-$) obtained from Figs. 1 and 2, resp., as a function of the pressure. According to the thermalisation, the average ion energy is decreasing until it settles at about 2 eV, the equivalent to $V_P$. The energy of the neutral flux is thus 2 eV less than that of the ion flux. The value at 0 Pa in Fig. 3 represents the energy expected for the original sputter distribution, i.e. 17 eV average energy of the neutrals plus 2 eV from $V_P$. In contrast, the highest average energy measured for 0.1 Pa is with 6 eV much lower, showing, that the ionised neutral flux has been significantly cooled down. Parallel to the energy decrease, the flux of positive ions is strongly increasing with pressure due to increased ionization in the plasma bulk. For the negative ions, the average energy is almost unaffected by pressure as it is determined by the target voltage only which remains constant. Their flux is decreasing exponentially. Thus by increasing the pressure one can reduce high energetic negative ion impact but simultaneously increase or control the energy input by positive ions, however, at the expense of the deposition rate.

### 3.4 Pulsed Discharges

Pulsing the discharge asymmetric-bipolar leads to a variation of $V_T$ and thus $V_P$ [4]. As a consequence, the plasma potential attains positive values in the “off” phase which in most of the time range at several +10 V and for a very short time reach more than +100 V. The result for the IEDFs of the positive ions is that they still consist of the low energy peak (Fig. 1) but

contain additional structures at several 10 eV and even considerable count rates for up to 100 eV.

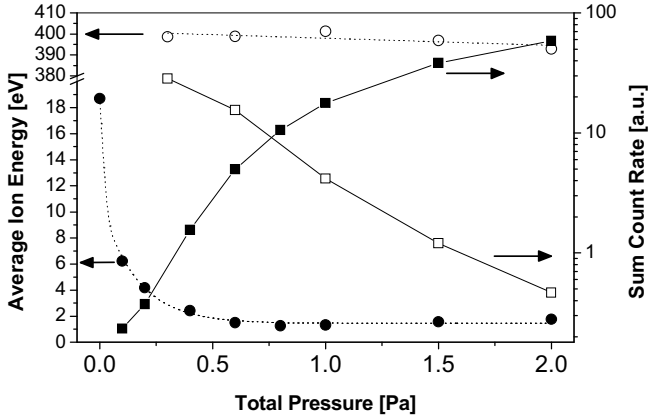


Figure 3: Dependence of the average ion energy and ion flux (sum of the count rate) on the pressure for positive ($Fe^+$, filled symbols) and negative ($O^-$, open symbols) ions. Note that the average energy of $O^-$ has been obtained from the range displayed in Fig. 2 only.

These high energy structures vary in intensity and energy with the pulse parameters while the low energy peak stays constant in energy but changes its intensity. The IEDFs of the negative ions also span a wider energy range in the pulsed case. The target voltage waveform was not rectangular but had an overshoot of up to 900 V in the "on" phase before it started to settle at about 200 V. Consequently, the peak shown in Fig. 2 appears in pulsed d.c. at about 200 eV but a broad extension is observed up to the detection limit of 500 eV which probably even extends to 900 eV considering the $V_T$ overshoot reported in Ref. 3. The IEDFs have not been investigated in dependence on pressure for the pulsed discharge but it is very likely that the trends in average energy and ion flux as described above hold also for this discharge type as the physical mechanisms are the same.

## 4. SUMMARY

IEDFs have been measured in d.c. and pulsed d.c. magnetron sputtering discharges with either a steel or AZO target. The IEDFs in pulsed d.c. are much more complex than in d.c. and generally contain ions with higher energies. For negative ions, these may range up to 900 eV in the pulsed mode. The IEDFs of both positive and negative ions strongly depend on the discharge pressure but in a different way. For the positive ions the flux of ions is increased by the pressure and the energy of the sputtered species is decreased. Generally, the energy of the positive ions including those of the working gas can be controlled by the substrate bias voltage. On the other hand, the average energy of negative ions is independent of the pressure as long as the target voltage is unchanged but their flux is decreasing with it.

## 5. REFERENCES

[1] J.W. Bradley, Th. Welzel, Process Diagnostics, in: D. Depla, S. Mahieu, Reactive Sputtering Deposition (Springer Series in Materials Science 109), Springer-Verlag, Berlin, Heidelberg, 2008, ch. 7, p. 255-300 (ISBN: 3540766626).

[2] J. A. Thornton, J. E. Green, Sputter Deposition Processes, in: R. F. Bunshah (ed.), Handbook of Deposition Technologies for Films and Applications, Noyes Publications, Park Ridge, 1994, ch. 5, p. 249.

[3] T. Welzel, R. Kleinhempel, T. Dunger, F. Richter, Ion Energy Distributions in Magnetron Sputtering of Zinc Aluminium Oxide, Plasma Processes and Polymers, submitted.

[4] Th. Welzel, Th. Dunger, B. Liebig, F. Richter, Spatial and temporal development of the plasma potential in differently configured pulsed magnetron discharges, New. J. Phys., submitted.

# The Deposition of Titania Coatings by Reactive Pulsed Sputtering: Film Structures and Process Characteristics

**PJ Kelly [1], JW Bradley [2], GT West [1], GCB Clarke [2]**

1. Surface Engineering Group, Manchester Metropolitan University, Manchester UK

2. Dept. of Electronic and Electrical Engineering, University of Liverpool, UK

Titania coatings are used as functional films in a number of commercial applications due to their high refractive index and photocatalytic properties. However, these properties are governed by the physical and crystalline structures of the films, which are in turn strongly influenced by deposition parameters, including the energy delivered during growth. In this study, titania coatings have been deposited by reactive magnetron sputtering, with the magnetrons driven in DC, pulsed DC (100-350 kHz pulse frequency), mid-frequency AC (40 kHz) and HIPIMS (50-1000 Hz) modes. Additionally, alternative magnetron designs, including full face erosion planar magnetrons and rotatable magnetrons, were used. The impact of these widely varying deposition modes on film structures, their properties and process characteristics, such as hysteresis behaviour, deposition rate and substrate heating rate, have been compared. A range of time-averaged and time-resolved plasma diagnostic tools have also been used to characterise the discharges obtained in the various modes of operation. Selected results from this extensive study will be presented.

# Investigations on High Power Impulse Magnetron Sputtering by Optical Emission Spectroscopy of NiCr in different compositions (40/60 and 80/20)

**H. Gerdes, M. Schmidt, J. Wellhausen, R. Bandorf, G. Bräuer**
Fraunhofer Institute for Surface Engineering and Thin Films IST,
Bienroder Weg 54 E, 38108 Braunschweig, Germany

In many technical applications additional information about the resulting loading or actually applied forces are gained by the use of strain gauges. Besides polymer based strain gauges which are glued to the surface improved signal quality is gained by use of directly sputtered strain gauges, avoiding creeping and swelling due to temperature and humidity. For improved properties, like thermal stability and adhesion, High Power Impulse Magnetron Sputtering (HiPIMS) is used. Due to the increased degree of ionization of the target material by HiPIMS also the resulting film properties e.g. the film structure can be modified by process parameters like voltage, current, duty cycle, or pulse packages. Actually investigations using only single pulses are reported. Besides the use of single pulses this paper also discusses the influence of pulse packages, i.e. several single pulses in short sequence followed by a long off-time. Modifications of the electrical fingerprint of the processes (current, voltage behaviour) and the plasma emission, measured by time resolved optical emission spectroscopy (OES) will be presented for two NiCr targets with different stoichiometry. It turned out that the optical intensity of the ionized material is direct proportional to the induced power.

## 1. INTRODUCTION

Strain gauges for measurement of applied forces or the loading status of workpieces are commonly used in many industrial applications. While polymer based strain gauges can lead to errors due to the influence of humidity on the polymer foils, thin film strain gauges are deposited directly on the surface of the workpiece. Therefore the influence of creeping and swelling of the glue and the polymer foil can be avoided [1]. Further improvement of the sensoric behaviour can be realized by HiPIMS [2]. HiPIMS processes are characterized by high degree of ionization of the sputtered material. Therefore an intense bombardment by target ions on the substrate surface can be realized, leading to superior properties, like high density, smooth surface, high refractive index, or high electrical conductivity [2-8]. This paper will present the characteristic current behaviour. Furthermore the correlation between the pulse current and the optical emission intensity of $Ni^0$ is discussed. As target material NiCr in two compositions (40/60, 80/20) was investigated.

## 2. EXPERIMENTAL SET-UP

The experiments were carried out in a Balzers BAS 450 sputtering plant, located in a cleanroom. For energy supply an Advanced Energies Inc. 10/10 dual pinnacle dc generator was used to charge the Melec GmbH SPIK 2000 pulsing unit. For our experiments the charging voltage was the reference parameter. The output voltage of the SPIK 2000 is limited

to 1000 V. The minimum pulse width is 5 µs at pulsing frequency up to 20 kHz. For the deposition a single magnetron was used. The base pressure was well below $1x10^{-5}$ mbar, while all the measurements were performed in an argon atmosphere at $5x10^{-3}$ mbar. For plasma spectroscopy investigations an AOS 4µchron from IFU GmbH was used. The spectral resolution ranges from 0.05nm@250nm up to 0.5nm@800nm. The optical signals were measured with 0.2 µs time resolution. The spectral information was captured from a side view of the racetrack.

## 3. EXPERIMENTAL RESULTS and DISCUSSION

### *3.1 Current characterization*

Using HiPIMS processes for film deposition not only the typical discharge voltage but also the current is increased compared to dc operation. Especially the voltage is responsible whether or not the so called self-sputtering runaway occurs [9]. In case of the runaway the target ions dominate and take over the discharge by self sputtering. For the investigations a variation of single pulses with length from 50 to 500 µs and pulse packages of 3 and 5 pulses, each of 50 µs length were chosen. In figure 1 (left) the resulting current curves of the HiPIMS pulses at constant charge voltage of 500 V are shown. In this case NiCr in the composition 40/60 was used. It is obvious that the rise of the current of each pulse is exactly the same. For long pulses, like 500 µs the current shows a maximum while the current than saturates at a lower plateau, i.e. no runaway process. For a pulse package each single pulse reached as maximum value the level of the 500 µs pulse.

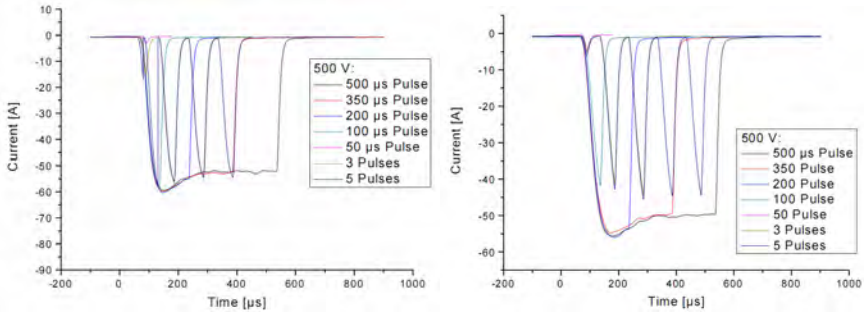


Figure 1. Current development of different pulses, $U_{Charge}$: 500 V; left: NiCr 40/60; right: NiCr 80/20.

Additionally NiCr in the stoichiometry 80/20 was chosen. On the one hand it is expected that the current characteristic will be similar to NiCr 40/60 and on the other hand this material obtains superior properties for strain gauge application. In figure 1(right) the current properties of NiCr 80/20 are shown. Again the slope of the single pulses is similar, but in difference to NiCr 40/60 the rise of the current is slower. Therefore, the pulse length of 50 µs is too short for reaching the current level of the 500 µs pulse. This may be due to the different sputter yields of Cr (1.32) and Ni (1.098) [10].

### *3.2 Optical Emission Spectroscopy (OES)*

The spectra of the optical emission were measured in the so called “Single Shot Time Spec” mode. This means that the intensity is not only measured in dependence of the wavelength but also in dependence of the time during the pulse. This gives the opportunity to determine the excitation-levels of the elements. Furthermore a threshold current for different ions can be appointed [3]. An example of a Single Shot Time Spec is shown in figure 2. For emissions of 340 to 350 nm the intensity profiles in dependence of the time during the pulse are measured.

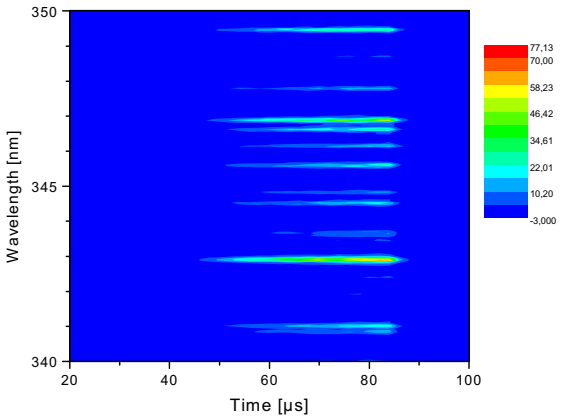


Figure 2. Time evolution of emission lines 340-350 nm during a single pulse, pulse length: 50 µs, color scheme: Intensity of emission lines.

In figure 3 the current characteristic of NiCr 80/20 at a charge voltage of 640 V and the corresponding time development of one emission line (341.5 nm, $Ni^0$) for two different pulses is shown. The pulse length was 50 µs and 500 µs. The shape of the intensity profile of the Ni neutrals is similar to the current profile since no runaway was present for this pulse setting. The intensity of the neutrals follows the current shape during the pulse. If ions would dominate the process the single and higher order ionized particles would also ionize a high fraction of neutral Ni or Cr, leading to a significant drop of neutrals with the current towards the end of the pulse. Therefore current and emission profile should differ strongly.

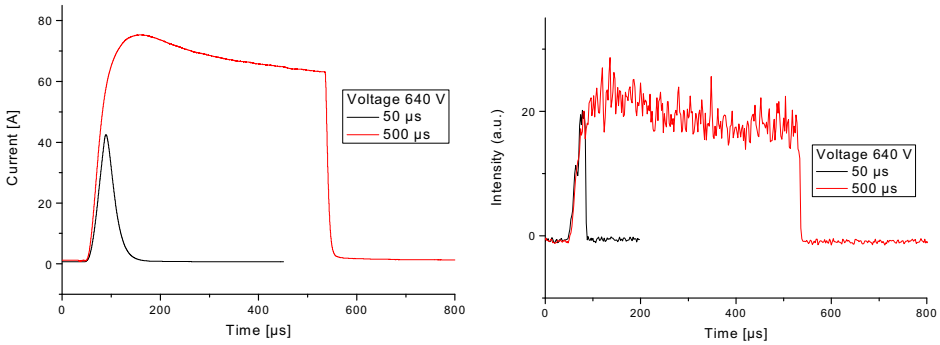


Figure 3. Variation of the pulse length at 640 V charge voltage; left: current characteristic; right: intensity of Ni-emission line (341.5 nm).

Figure 4 shows the intensity in dependence of the wavelength for the two compositions. The peaks regarding element and position were fitted and compared to a database [11]. The intensities of the emission spectra correlate to the target composition. For NiCr 80/20 a higher fraction, i.e. higher intensity of Ni emission was found in the spectrum, while the peak at 358 nm decreased. This peak can be ascribed to Cr, therefore mirroring the lower Cr content of NiCr 80/20 compared to NiCr 40/60.

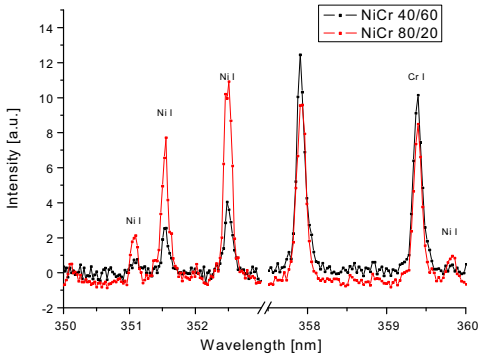


Figure 4. Comparison of the OES-spectra from NiCr 40/60 and 80/20.

## 4. SUMMARY

For NiCr alloys in different stoichiometry (40/60 and 80/20) the characteristic current curves for fixed charge voltage were measured. These curves give a fingerprint of the discharge. For the presented investigation no self-sputtering runaway occurred. In correspondence with the electrical parameters the intensity of optical emission was further shown. The OES data correlate to the resulting current during the pulse. Also the composition is mirrored by the emission lines of the sputtered elements.

## 6. Acknowledgement

This work was funded by the German Federal Ministry of Education and Research (BMBF) by the project 13N8920, supervised by the funding agency VDI Technolgiezentrum.

## 7. References

[1] K. Bethe, D. Schön: Thin-film strain gauge transducers; Philips tech. Rev. 39; 94-101 (1980).

[2] B.M. DeKoeven, P.R. Ward, R.E. Weiss, R.A. Scholl, W.D. Sproul, F. Tomasel, A. Anders, “Carbon Thin film deposition using high power pulsed magnetron sputtering”, 46th SVC TechCon 2003, 158.

[3] R. Bandorf, M. Vergöhl, P. Giesel, T. Wallendorf, G. Mark, “Investigation of HPPMS titania thin films prepared by unipolar, DC-superimposed and bipolar sputtering”, 50th SVC TechCon 2007, 160.

[4] U. Helmersson, J. Alami, P. Eklund, J.M. Andersson, M. Lattemann, E. Wallin, J. Bohlmark, P. Persson, “Phase tailoring of Ta thin films by highly ionized pulsed magnetron sputtering”, Thin Solid Films 515 (2007) 3434.

[5] K. Sarakinos, J. Alami, and M. Wuttig, “Process characteristics and film properties upon growth of TiO(sub x) films by high power pulsed magnetron sputtering”, J. Phys. D: Appl. Phys. 40 (2007) 2108.

[6] J.A. Davis, W.D Sproul, D.J. Christie, M. Geisler, “High Power Pulse Reactive Sputtering of TiO2”, 47th SVC TechCon (2004) 215.

[7] J. Alami, P. Eklund, J. Emmerlich, O. Wilhelmsson, U. Jansson, H. Högberg, L. Hultman, U. Helmersson, “High power impulse magnetron sputtering of Ti-Si-C thin films from a Ti3SiC2 compound target”, Thin Solid Films 515 (2006) 1731.

[8] D.A. Glockner, M.M. Romach, D.J. Christie, W.D. Sproul: “High Power Pulsed Reactive Sputtering of Zirconium Oxide and Tantalum Oxide”, Proc. of 47th SVC TechCon 2004, 183.

[9] A. Anders:” Self-sputtering runaway in high power impulse magnetron sputtering: The role of secondary electrons and multiply charged metal ions”, Appl. Phys. Lett. 92 (2008) 201501.

[10] http://www.iap.tuwien.ac.at/www/surface/script/sputteryield.html

[11] http://physics.nist.gov/PhysRefData/ASD/lines_form.html

# Chromium oxide and aluminum oxide coatings deposited by reactive pulsed dc magnetron sputtering

**P. Eklund [1,2], M. Sridharan [1], M. Sillassen [1], J. Bøttiger [1]**

1. iNano, Interdisciplinary Nanoscience Center (iNANO) and Department of Physics and Astronomy, University of Aarhus, DK-8000 Aarhus C, Denmark

2. Thin Film Physics Division, IFM, Linköping University, SE-58183 Linköping, Sweden

Chromium oxide and aluminum oxide thin films were deposited by reactive inductively coupled plasma magnetron sputtering at substrate temperatures from room temperature to 600 °C. X-ray diffraction and electron microscopy showed that the as-deposited chromium oxide coatings crystallized in a corundum structure, while aluminum oxide thin films deposited at low ion flux during growth were amorphous in the substrate-temperature range 200 to 600 °C. At 200 °C, with ion bombardment, 100 nm large clusters of small crystalline grains of γ-alumina with sizes of the order of 5 nm were embedded in the amorphous matrix. A higher ion flux and/or temperature resulted in predominantly crystalline γ-alumina. For chromia, the hardness was 29 GPa, while the hardness values of the as-deposited alumina films varied from 8–20 GPa, with the highest values corresponding to larger crystalline volume fractions. The thermal stability of the as-deposited alumina films was investigated by an ex-situ annealing study in ambient air. For fully amorphous films and films containing a small fraction of γ-alumina in the as-deposited state, initial γ grain growth was observed at 800 °C, followed by nucleation of transient θ-alumina phases concurrently with α at 1100°. At 1200°, only α-alumina was present. For as-deposited films containing predominantly crystalline γ-alumina, no transient alumina phases were observed. This indicates a direct γ -to-α phase transformation at about 1100°. All as-deposited films were smooth as indicated by their shiny optical appearance and evidenced by atomic force microscopy, which yielded rms roughness values of 2-3 nm. The roughness was higher for the annealed films; the films annealed at 1200° had a grey milky appearance and rms roughness values of 13-15 nm. Finally, the growth of α-alumina at 450 C could be promoted by depositing onto chromia templates. Here, the texture of the template was observed to have a strong influence on the nucleation and growth of α-alumina. Extended growth of α-alumina at a substrate temperature of 450 °C was obtained using a predominantly <104>-textured chromia template layer, while only limited α-alumina nucleation was seen on a <001>-textured chromia template.

[1] P. Eklund, et al Thin Solid Films 516 7447 (2008)
[2] P. Eklund et al Surface and Coatings Technology 203 156 (2008)
[3] M. Sridharan et al Surface and Coatings Technology 202 920 (2007)
[4] P. Eklund et al, submitted for publication

# Bimetallic nanoparticles of silver and copper in $SiO_2$ thin films: RF reactive co-sputtering synthesis and characterization

**P. Sangpour [1], A.Z. Moshfegh [1,2], O. Akhavan [1]**

1. Department of Physics. Sharif University of Technology, P.O. Box 11155-9161,Tehran, Iran.
2. Institute for Nanoscience and Nanotechnology, Sharif University of Technology, P.O. Box 14588-8969, Tehran, Iran.

Recently, much effort has been devoted to the fabrication of nanocomposite metals, including alloy, core-shell and mixed particles. Specifically, the optical properties of bimetallic nanoparticles (NPs) synthesized from free-electron like metals, such as Au, Ag and Cu has been studied intensively [1]. In this work, we report fabrication and characterization of Ag-Cu:$SiO_2$ thin film. Transparent $SiO_2$ thin films containing Ag-Cu NPs were deposited on quartz substrates by reactive magnetron co-sputtering technique. Two pieces of Ag and Cu strips (1 mm in length) were placed symmetrically on Si target. The concentration of Cu in the samples was altered by varying the length of the Cu wires (2, 3, 5 and 8 mm) with the same diameter on the surface of Si target. The as deposited films were annealed in range of 400-800°C for 1h in an Ar+H2 environment. The optical UV-visible analysis of Ag-Cu bimetallic showed that for the samples annealed at 400°C with Cu:Ag=0:1 ratio, only one sharp peak is visible at 400 nm, which is attributed to surface plasmon of silver Nps. But, for the samples with Cu:Ag ratio of 3:1 a shift of the peak towards the higher wavelength was observed, and peak was centred at 448 nm. By further increasing the fraction of copper, this plasmon peak does not shift much and another very weak peak appears at the wavelength ranging from 540 to 565 nm. For the samples exclusively copper, only one absorption peak at 565 nm was observed, which can be attributed to the surface plasmon peak for copper NPs. Since the absorption edge in pure Cu and other noble metals is mainly determined by transition from the top of the d-bands to the conduction band at Fermi level, the upper part of the Cu d-band must be little affected by alloying with Ag [2]. By increasing annealing temperature, we have a mixture of Ag-Cu in $SiO_2$ matrix. X-ray photoelectron spectroscopy results showed that the alloys have greater tendency to lose electrons as compared to their monometallic state for the ratio of Cu:Ag,3:1. Negative shift of Ag(3d) binding energy to lower values relative to monometallic state suggests formation of alloying Ag with Cu. Also, it was found that the Ag-Cu alloying makes the Cu(2p) binding energy shift to lower values. But for the ratio up to 3:1, we have not measured valuable shift. Using atomic force microscopy, we have found that some particles with a size of about 30 nm on the surface. Therefore, these surface topography observations along with our XPS and UV-visible analyses confirm that formation of Ag-Cu alloy NPs and mixture of Ag and Cu NP in low Cu:Ag ratio and reduced annealing temperature.

[1] K.H. Chung, L.Y. Hsiao, Y. Sheng Lin, J.G. Duh Acta Biomaterialia 4 717 (2008)
[2] Yu.V. Bokshits, G.P. Shevchenko,V.S. Gurin, A.N. Ponyavina, S.K. Rakhmanov Materials Science and Engineering C 27 1149 (2007)

# Observing Film Growth During Deposition With Video-Rate STM

**V. Fokkema, M. den Heijer, A. C. Geluk, G. Verdoes, M. J. Rost**
Leiden University, Kamerlingh Onnes Laboratory, P. O. Box 9504, 2300 RA Leiden, The Netherlands

We developed a scanning tunneling microscope (STM) that is capable, for the first time, of monitoring film growth during the deposition of films with significant thicknesses. To capture the dynamics involved in film growth, both high spatial and temporal resolution are required. The wish to image a growing surface during physical vapor deposition (PVD) or during ion bombardment demands an open structure of the microscope, which contradicts the desired stability for high speed imaging. Bearing this in mind, we optimized the rigidity of the scanner to not be hampered by mechanical resonances, which would render the system incontrollable. To this end we modeled the complete STM with finite elements analysis (FEA), of which the results were compared with laser vibrometer characterization on the built-up microscope, yielding new insights regarding the design rules for fast STM. Equipped with the new microscope we aim for a detailed understanding of film growth, at deposition rates relevant for industrial processes, on which we expect to present first results.

# Structure Formation in Co-deposited $Cr_{1-x}Al_xN$ Thin Films in the 0<x<1 Composition Range

**Gy. Lestyán [1], J.L. Lábár [1], L. Székely [1], O. Geszti [1], Gy. Sáfrán [1], D. Biró [2], P.B. Barna [1]**

1. Research Institute for Technical Physics and Materials Science, HAS, Konkoly Thege ut 29-33, H-1525 Budapest, Hungary

2.Sapientia University, Technical and Human Science Faculty, Road Sighisoarei 1C, OP.9, RO-540485 Targu-Mures, Romania

It has been verified that the addition of Al to CrN improves the coatings properties [1, 2]. However at higher Al concentrations the structure is changing from fcc to hcp modifying also the properties [3]. In the present experiments the micro-combinatorial method was used to investigate the formation of the structure and phases in co-sputtered polycrystalline $Cr_{1-x}Al_xN$ thin films in the $0 < x < 1$ composition range. The films were deposited by unbalanced magnetron sputtering on amorphous C layer substrates supported by Mo microgrids at $550^0$C. Two unbalanced magnetron sources were used with Cr and Al targets of 99.99 purity. The thickness of the films was in the range of 20 – 100 nm. The base pressure in the all metal UHV vacuum system evacuated by turbo molecular pump was $3.10^{-5}$ Pa. The pressure of Nitrogen was varied in the range of 0.9-$2.4.10^{-1}$ Pa, while the total pressure of Nitrogen and Argon was 2.3 – $5.10^{-1}$ Pa. The micro-combinatorial method [4] made possible to prepare and investigate the films in the $0<x<1$ range of composition in the area of a transmission electron-microscopic microgrid. The structure of the films was investigated by analytical and high resolution transmission electron microscopy and by selected area electron diffraction (SAED). SAED patterns were evaluated by the ProcessDiffraction computer program for determining the volume fraction of phases together with their orientational (texture) conditions [5]. The results supported the high mutual solubility of elements in the fcc- CrN and hcp (wurzit)-AlN phases determined by recent detailed XRD investigations, but the co-existence of the two phases could be detected in a broader composition range ($0.45 < x < 0.85$) by HR-TEM and SAED analysis. The lower edge of this range proved to depend on the Nitrogen pressure. The structure evolution is interpreted by the mutual dissolution of the AlN and CrN at lower Al and Cr concentrations respectively. In the composition range where the fcc and hcp phases co-exist we suggest the competitive nucleation and growth of phases together with the mutual segregation of excessive (not dissolved) species. A delayed nucleation of the second phase due to the accumulation of the excessive species on the growth surface is also considered in the description of the structure evolution.

The work was supported by the Hungarian National Science Foundation, OTKA No. 048699 and by the European Commission within Framework Program 6. Grant NMP3-CT-2005-515944

[1] S. Hofmann Thin Solid Films 193/194 367 (1990)
[2] H.C. Brashili, N. Salvacumar, B. Deepthi, K.S. Rajan Surf. Coat. Technol. 201 2193 (2006)
[3] S. Venkataraj, D. Severin, R. Drese, F. Koerfe, M. Wuttig Thin Solid Films 502 235 (2006)
[4] A. Kovács, P.B. Barna, J.L. Lábár Thin Solid Films 433 78 (2003)
[5] J.L. Lábár Microscopy and Microanalysis 41 155312 (2008)

# Reactive DC magnetron sputtering deposition of titanium oxide nanoparticles : influence of the process parameters on the morphology and the surface coverage

**L. Dreesen, F. Cecchet, S. Lucas**
University of Namur (FUNDP), Research center in Physics of Matter and Radiation (PMR), rue de Bruxelles 61 , 5000 Namur, Belgium

Since the discovery of its photocatalytic properties by Fujishima and Honda, titanium dioxide ($TiO_2$) is under continuous investigation. The reasons stem in the high potentialities offered by this material for the development of numerous applications that are susceptible to improve our daily life. For instance, it is involved in the development of photochromic devices, solar cells, anti-bacterial and self-cleaning coatings, etc. Numerous papers have been devoted to this material deposited as thin films but there is only a few works on its deposition as nanoparticles albeit these latter ones possess interesting advantages compared to $TiO_2$ thin films: increased active surface area, reduced electron-hole pair recombination and quantum size effects. These advantages are especially useful to improve the photocatalytic efficiency of $TiO_2$ and thus properties such as the self-cleaning or anti-bacterial ones.
$TiO_2$ nanoparticles are usually produced by methods such as laser pyrolysis, spray deposition, laser ablation, RF induction plasma or sol-gel techniques. In our laboratory, we choose another synthesis strategy based on reactive DC magnetron sputtering which is a suitable technique for potential industrial applications. In the present work, we focus on the role of process parameters such as the substrate temperature, the chamber pressure or the deposition time, that are expected to affect the morphology of the deposited nanoparticles layer and the surface coverage by the nanoparticles. This is made by using AFM microscopy which is a suitable tool to investigate surface properties at the nanometre scale.

# Preparation of Ge nanogranules embedded in Anatase-dominant $TiO_2$ thin films by RF sputtering

**S. Abe [1], M. Ohnuma [2], D. Hai Ping [2], S. Ohnuma [1]**

1. The Research Institute for Electric and Magnetic Materials, Sendai 982-0807, Japan
2. National Research Institute for Materials Science, ibaraki, 305-0047, Japan

This paper investigates preparation of Ge nanogranules embedded in $TiO_2$ matrix by rf sputtering. Small angle X-ray scattering suggested that nanogranules with mean size of 3.8nm were embedded in the matrix. X-ray diffraction result revealed that lattice constant of the matrix decreased with respect to Ge content, suggesting formation of a solid solution of $Ge_xTi_{1-x}O_2$. Thus, the added Ge partially formed the solid solution of the matrix. Direct image of the matrix with the size of ~30nm was clearly observed by high resolution electron microscopy. The solid solution exhibited the optical absorption at ultraviolet region. Consequently, such embedded Ge nanogranules reasonably exhibited the VIS-NIR absorption due to the quantum size effect.

## 1. INTRODUCTION

Quantum-dot solar cells have attracted much attention because of their potential to increase conversion efficiency [1]. Specifically, the optical-absorption edge of a semiconductor nanocrystal often shifts due to the quantum-size effect. The optical band gap can then be tuned to the effective energy region for absorbing maximum intensity of the solar radiation spectrum. $TiO_2$ sensitized by semiconductor nanocrystal is a candidate material for such use. $TiO_2$ can only absorb the ultraviolet part of the solar radiation spectrum, since its energy band gap is 3.2 eV for anatase structure and 3.0 eV for the rutile structure [2]. The semiconductor nanocrystal supports absorbing visible (VIS)-to-near-infrared (NIR) light. Up to now, various nanocrystalline materials (InP [3], CdSe [4], CdS [5], PbS [6], and Ge [7]) have been investigated as the sensitizer for $TiO_2$. Most of these composite materials were synthesized through chemical techniques, however, physical deposition, such as sputtering, is also useful. In that case, the composite material of $TiO_2$ sensitized by Ge nanocrystal ($Ge/TiO_2$) is the most compositionally simple, so that it would be relatively easy to prepare. In addition, it is believed that the anatase structure is favorable for the matrix, since carrier mobility and photoconductivity in the anatase structure exceed those in the rutile structure [2]. In our previous study, $Ge/TiO_2$ thin films were prepared by rf sputtering, and the matrix formed anatase-dominant structure at a quite restricted Ge concentration range from 6 to 9 at% [8]. In addition, an onset of optical absorption could be confirmed in the vicinity of 1.0eV in contrast to UV absorption of $TiO_2$ thin films due to its energy band gap of 3.2eV [2]. Thus, $Ge/TiO_2$ films favorably covered the energy region for high conversion efficiency [9]. Therefore, valuable characteristics of the VIS-NIR absorption and the anatase-dominant structure of TiO2 matrix were simultaneously retained in the $Ge/TiO_2$ composite thin films. However, it was not clear whether or not the VIS-NIR absorption was actually due to the presence of Ge nanogranules, since an X-ray diffraction peak of Ge was not observed in the optimized composition range. In the present study, we have investigated the presence of Ge

nanogranules embedded in the anatase-dominant structure of $TiO_2$ thin films, and clarified the reason for the VIS-NIR absorption.

## 2. EXPERIMENTAL

A composite film of Ge nanogranules embedded in $TiO_2$ ($Ge/TiO_2$) was prepared by rf sputtering with a composite target. Specifically, 5×5mm2 Ge-chips with 6N purity were set on a TiO2 4-inch-diameter target with 4N purity. This study adopted 3 Ge chips. The chamber was first evacuated to a vacuum of 1.5×10-7 Torr before introducing argon gas. The $Ge/TiO_2$ thin films were deposited on a Corning #7059 substrate grass water-cooled. The distance between the target and the substrate was kept constant at 73mm. The total gas pressure of argon and additional oxygen was fixed to 2.0×10-3 Torr. Rf power was kept constant at 200W, deposition time was kept at 90min, and no rf bias was applied to the substrate. The $Ge/TiO_2$ thin films thus deposited were successively post-annealed at 873 K for 60min in vacuum to crystallize Ge nanogranules and the $TiO_2$ matrix. The $Ge/TiO_2$ thin film was structurally characterized by small angle X-ray spectroscopy (SAXS). Direct observation of the film was performed by high resolution electron microscopy (HREM). Lattice constant of the film was estimated by X-ray diffraction (XRD). The composition of the film was analyzed by energy dispersion spectroscopy (EDS).

## 3. RESULTS AND DISCUSSIONS

As a reason for the above mentioned VIS-NIR absorption, we considered two possibilities: appearing the quantum size effect due to presence of Ge nanogranules, or forming a solid solution of $Ge_xTi_{1-x}O_2$ (GTO) as the matrix. Accordingly, the latter was first investigated. Since the films thus prepared probably forms multi phases, it is difficult to focus on a phase of the matrix. Thus, GTO solid solution was bulk synthesized as a preliminary experiment, i.e., heat-treating at 1273 K for 4 days in order to achieve thermal equilibrium state. A standard powder of GeO2 and a anatase structure of TiO2 were adopted as a starting materials, but the production of GTO solid solution resulted in rutile structure due to phase transition in the vicinity of 973 K. The lattice constant of the synthesized powders was first decreased linearly from 0.2958 to 0.2944nm at (002) reflection in proportion to Ge content, and became constant

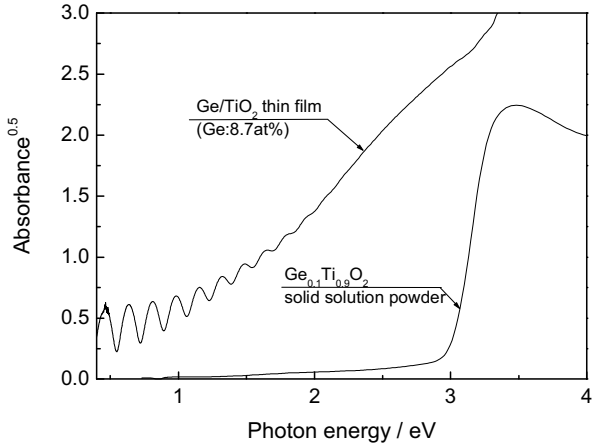


Figure 1. Absorption spectra of the Ge/TiO2 thin film and a solid solution of the GeTiO powder.

irrespective of x in the range exceeding 0.25, indicating two phases of GTO and $GeO_2$ in XRD pattern. Thus, the solubility limit of Ge at 1273 K was estimated to be ~0.22. In

contrast, the lattice constant of the Ge/$TiO_2$ thin films decreased with increasing Ge concentration, raging from 0.9495 to 0.9400 nm estimated at (004) reflection. Such decreasing tendency of the lattice constant was found to be the same as the result of GTO powder. Therefore, it was strongly suggested that the matrix of the film thus prepared reasonably formed a solid solution of GTO. However, solubility amount of Ge was actually unclear in each film, since the analyzed concentration included an unavoidable EDS signal from the other phase, such as Ge nanogranules. Figure 1 depicts the optical absorption spectra of the Ge/TiO2 thin film and a solid solution of the GTO powder. Here, Ge concentration in the film was analyzed to be 8.7 at%, and a similar concentration of x=0.1 in the powder was also presented for comparison. The absorption spectrum of the GTO powder was obtained by means of the Kubelka-Munk function [10] through a diffused reflectance spectrum. The VIS-NIR absorption was clearly observed in the Ge/TiO2 film, while an optical absorption edge of the synthesized powder was observed at ultraviolet region. It was therefore concluded that the GTO solid solution unexhibited such VIS-NIR absorption.

The possibility of forming Ge nanogranules was successively investigated. Figure 2 depicts the size distribution of nanogranules in the films. These profiles were estimated from SAXS analysis of Guinier fitting for an experimental result (the inset in Fig.2). In this case, Ge chips of 3 and the oxygen ratio of 0.3% was adopted during the deposition, and Ge concentration was analyzed to be 8.7 at%, and the film exhibited the VIS-NIR absorption (Fig.1). In the pinhole-collimated apparatus of SAXS measurement, X-ray was injected perpendicularly to the film surface, providing in-plane structural characteristic. As can be seen in the figure, the size profile distributed broadly, and mean radius of nanogranules was estimated to be 1.9 nm (3.8nm in diameter), ranging the radius from ~0.5 to 8nm. The SAXS analysis therefore strongly suggested that nano-scale material was embedded in the film, possibly attributing to Ge nanogranules or another phase of the GTO matrix. Successively, the size of GTO matrix was estimated by HREM. Figure 3 presents the HREM image of the anatase-structured matrix at an oxygen ratio of 0.3%. Lattice image of the anatase structure was clearly observed, and size of their grains was estimated to be ~30nm. The size exceeded that of the nanogranules estimated by SAXS. Furthermore, Ge nanocrystals were clearly observed at a different area with mean size of ~2nm [8]. The sizes derived from the SAXS and the HREM results were found to be close each other, and to be small sufficiently to occur the quantum size effect because of the exciton Bohr radius of 24.3nm in Ge [11]. Therefore, it was concluded that the optical absorption edge of the films could reasonably shift towards a higher energy region, and resulted in the VIS-NIR absorption due to the Ge nanogranules embedded in the GTO matrix.

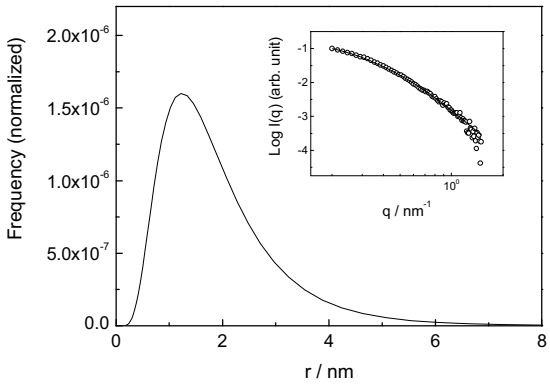


Figure 2. Size distribution of nanogranules derived from the SAXS analysis. The inset depicts SAXS spectrum.

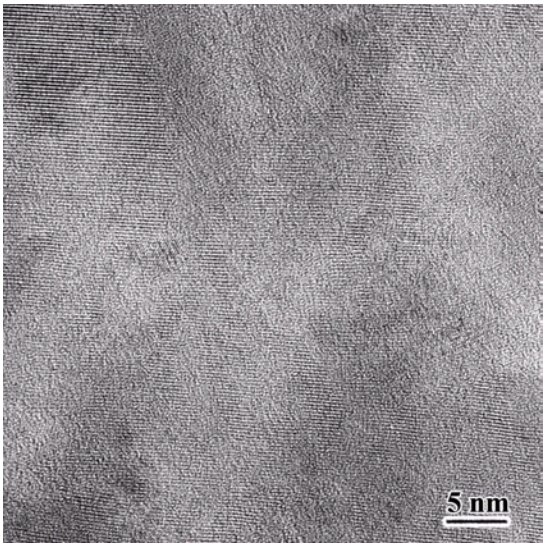


Figure 3. HREM image of anatase structure of the matrix in Ge/TiO2 thin films.

## 4. CONCUSION

This paper focused on the VIS-NIR absorption of Ge/TiO thin films deposited by rf sputtering. The matrix was found to be formed a solid solution of GTO, exhibiting optical absorption in ultraviolet region. In contrast, SAXS and HREM results clearly indicated that the Ge nanogranules were embedded in the matrix. The size was sufficiently small to appear the quantum size effect. Therefore, the VIS-NIR absorption of the $Ge/TiO_2$ thin films was concluded to be due to the presence of the Ge nanogranules embedded in the matrix.

## ACKNOWLEDGEMENT

The present work was supported by a Grant-in-Aid for Scientific Research from the Japan Society for the Promotion of Science (No.18360338). We gratefully acknowledged the valuable comments and continuous encouragement of President K. Masumoto and Director T. Masumoto [The Research Institute for Electric and Magnetic Materials (RIEMM), Sendai, Japan]. We are also grateful to Mr. Y. Sato (RIEMM) for assisting in the experiments.

## References

[1] A. J. Nozik: Physica E 14 115 (2002).
[2] H. Tang, K. Prasad, R. Sanjinès, P. E. Schmid, and F. Lévy: J. Appl. Phys. 75 2042 (1994).
[3] A. Zaban, O. I. Micic, B. A. Gregg, and A. J. Nozik: Langmuir 14 3153 (1998).
[4] D. Liu and P. V. Kamat: J. Phys. Chem. 98 3183 (1994).
[5] H. Weller: Ber. Bunsen-Ges. Phys. Chem. 95 1361 (1991).
[6] P. Hoyer and R. Könenkamp: Appl. Phys. Lett. 66 349 (1995).
[7] S. Chatterjee, A. Goyal, and I. Shah: Mater. Lett. 60 3541 (2006).
[8] S. Abe, M. Ohnuma, D. H. Ping, and S. Ohnuma: Appl. Phys. Express 1 095001 (2008).
[9] J. J. Loferski: J. Appl. Phys. 27 777 (1956).
[10] P. Kubelka and F. Munk: Z. Yech. Physik 12 (1931)593.
[11] Y. Maeda, N. Tsukamoto, Y. Yazawa, Y. Kanemitsu, and Y. Masumoto: Appl. Phys. Lett. 59 3168 (1991).

# Synthesis of Radioactive Nanoparticles by DC Magnetron Sputtering and Gas Aggregation Techniques

**S. Lucas [1], O. Feron [2], B. Gallez [3], B. Masereel [4], C. Michiels [5], T. Vander Borght [6], V. Bouchat [1]**

1. University of Namur (FUNDP), Research center in Physics of Matter and Radiation (PMR), Rue de Bruxelles 61, 5000 Namur, Belgium
2. University of Louvain-La-Neuve (UCL), Unit of Pharmacology and Therapeutics (FATH), Avenue E. Mounier 53, 1200 Bruxelles, Belgium
3. University of Louvain-La-Neuve (UCL), Biomedical Magnetic Resonance Unit (CMFA), Avenue E. Mounier 74, 1200 Bruxelles, Belgium
4. University of Namur (FUNDP), Department of Pharmacy, Rue de Bruxelles 61, 5000 Namur,Belgium
5. University of Namur (FUNDP), Unité de Recherche en Biologie Cellulaire (URBC), Rue de Bruxelles 61, 5000 Namur, Belgium
6. University of Louvain-La-Neuve (UCL), Center for Molecular Imaging and Experimental Radiotherapy (IRME), Dr. G. Therasse 1, 5530 Yvoir, Belgium

Due to their unique structural, chemical and physical properties, nanosized particles have shown promising interests in various fields such as electronics, optics and energy. More recently, nanoparticles have attracted considerable interest in medicine and biology. Quantum dots as fluorescent agents, gold nanoshells as cancer therapeutics, C60 as drug delivery system and metallofullerenes as radiotracers are some examples of possible biomedical applications of nanomaterials. When combined with radioactive atoms, these nanomaterials are very promising for cancer detection and treatment.

We propose a new method to produce isolated radioactive nanoparticles composed of radioactive material such as 99mTc mixed with carbon, inert and biocompatible element. Their sizes can vary between 10 and 20 nm and could be used to enhance diagnostic sensitivity in medical imaging of cancer. This new method is based on a physical vacuum deposition (PVD) process which combine DC magnetron sputtering and gas aggregation techniques in order to control their morphology, their size and their dispersion on any substrate. The samples are then analyzed by Transmission Electron Microscope (TEM). Firstly, tests were performed with a simple graphite cathode to find the best parameters to produce pure carbon nanoclusters. Secondly, radioactive nanoclusters were synthesised. Results will discuss the synthesis parameters and the goal of incorporation of radioactive atoms in the carbon nanoparticles.

# Development of Multilayer Optics for modern X-ray analytics

**J. Wiesmann [1], F. Hertlein [1], U. Heidorn [1], M. Störmer [2], C. Michaelsen [1]**
1. Incoatec GmbH, Max-Planck-Str. 2, 21502 Geesthacht, Germany
2. GKSS Research Centre, Max-Planck-Str. 1, 21502 Geesthacht, Germany

In this contribution, we give an overview on the state-of-the-art beam-shaping multi-layer and total reflection optics for diffractometry in the lab and for synchrotron beamlines. Nowadays a large variety of 1D and 2D optics are available with opti-mized properties for the customer's applications. We explain the manufacturing process of multilayer and total reflection optics, summarize the different type of op-tics and give some examples of typical applications which benefit from the new pos-sibilities.

The optics for lab-instrumentation consist of bent substrates with shape tolerances below 100 nm, upon which multilayers are deposited with single layer thicknesses in the nanometer range and up to several hundreds of layer pairs. Additionally these multilayers were designed with lateral thickness gradients within ± 1% deviation of the ideal shape. This means that a deposition precision in the picometer range is needed. We use magnetron sputtering methods for deposition, optical profilometry in order to characterize the shape and X-ray reflectometry to characterize the multilay-ers. The microstructure is investigated by transmission electron microscopy. The beam parameters like monochromaticity, flux, brilliance and divergence demonstrate the quality of the multilayer optics for different lab applications.

The second part will be on our special capabilities for the production of synchrotron optics for beam-shaping. For the FLASH at Hasylab we developed special carbon films used as total reflection mirrors. They are now available with lengths up to 1.5 meter. Our second synchrotron application demonstrates the possibilities for design and production of multi-stripe multilayer optics for sophisticated beamlines. One exam-ple shows a two-stripe optics for a tomography beamline. A Ru/C multilayer was choosen for energies between 10 and 22 keV and a W/Si multilayer for energies be-tween 22 and 45 keV.

# Growth and Optical properties of Amorphous Beryllium Nitride Thin Films Prepared by Radio Frequency Magnetron Sputtering

**J. M. Khoshman** [1], **M. E. Kordesch** [2]

1. Department of Physics, Al-Hussein Bin Talal University, Ma'an, Jordan
2. Department of Physics and Astronomy, Ohio University, Athens, Ohio 45701, USA

The optical properties of amorphous beryllium nitride (a-$Be_3N_2$) thin films deposited on crystalline Si (100) and quartz at temperature < 50o C using reactive radio frequency sputtering deposition were examined in the wavelength range 280 – 1600 nm. X-ray diffraction (XRD) of the films showed no structure, suggesting the $Be_3N_2$ films grown on the substrates are amorphous. The thicknesses and optical constants of the films were derived from variable-angle spectroscopic ellipsometry measurements using the Cauchy-Urbach model. Refractive indices and extinction coefficients of the films were determined to be in the range n = 1.98 – 2.28 and $\kappa = 9.3 \times 10\text{-}5$ - 0.097, respectively. Analysis of the absorption coefficient shows the optical absorption edge "optical bandgap energy" of a- $Be_3N_2$ films to be 4.12 ± 0.015 eV. These values were in excellent agreement with the photoluminescence measurements (4.18 eV). The surface morphology was characterized by atomic force microscopy (AFM). The surfaces of the films were very smooth and their average roughness were measured to be in range 0.36 – 2.4 nm. An effective medium approximation model of 50% $Be_3N_2$ and 50% voids was used in the ellipsometric fitting procedure. The effect of the surface roughness on the optical constants was examined. From the angle dependence of the polarized reflectivity we deduced a Brewster angle of about 64o. The spectral dependence of the polarized transmissivity of the films was investigated at different angles of incidence (20o – 80o). The a- $Be_3N_2$ films exhibit the least reflectance (< 3%) and highest transmittance (> 95%) over a broadband of wavelength (i.e., Visible – near infrared). Therefore, the a- $Be_3N_2$ films could be a good candidate for a broadband antireflection (BBAR) optical coating under a condition of optimized the angle of incidence with respect to normal.

# Native donor defect formation at a near-surface delta layer in epitaxial InAs thin film

**K. Kanisawa, T. Fujisawa**
NTT Basic Research Laboratories, NTT Corporation, 3-1, Morinosato Wakamiya, Atsugi, Kanagawa, 243-0198, Japan

It is well known that the epitaxial InAs surface has the native two-dimensional electron accumulation layer. Recently, we have found that the accumulated electron density at the InAs(111)A surface was dominated by the donor-type point defects; excess In atoms remained as adatoms and point defects in the near-surface region of the crystal [1]. In this paper, we characterize the depth profile and the crystallographic location of the near-surface point defects using low-temperature scanning tunneling microscope (LT-STM). After the InAs thin film was grown by molecular beam epitaxy on undoped InAs(111)A substrate, the sample was transferred to the LT-STM stage at 5 K and the clean surface was characterized in ultra-high vacuum. The near-surface defects (Ds) were always found below the In vacancy site of the (2×2) reconstruction at the density in the order of $10^{11}$ $cm^{-2}$. The depth profile was explored by imaging standing waves of local density of states (LDOS) around the defects. The observed standing waves always showed the same lateral ripple profile and wave phase at the same bias voltage V. This indicates the defect D is always formed at a certain depth in InAs with a delta-functional profile along the axis vertical to the InAs(111)A surface. To measure the depth Z of such delta layer, two spectroscopic methods were used. When we first measured the bias voltage dependence of relative LDOS standing wave intensity just above the defect D at $V > 0$, oscillatory intensity change was observed. Assuming free electronic LDOS = 0 at the defect position, each intensity minimum means $Z = (\lambda/2) \cdot n$ ($\lambda$ : electron wavelength, n = 1, 2, 3, ...). The depth Z was estimated about 1.5 nm from the surface. Since the intensity was measured with the tip few angstrom above the surface and the LDOS > 0 at the real defect site, this value might overestimate Z. We also measured the LDOS spectra of the (2×2) reconstruction just above the defect D, which was few nm far from the closest In adatom. Sharp peaks were found split into two at around 1.0 eV above the Fermi level. Such splitting was found as a result of coupling of donor bound surface states. When an In adatom was located 1.6 nm far from the surface projected location of the defect D, the measured splitting at the In adatom was 0.12 eV and smaller than expected 0.14 eV. Since the corresponding distance is 1.9 nm for the measured splitting according to the dependence on the distance between two In adatoms, the defect D was estimated about 1.0 nm below the surface. From these results, the crystallographic location of the defect D was estimated. If we adopt the accepted self-diffusion mechanism of In atom in the InAs crystal, interstitial position is found unfavorable. For the In rich condition, therefore, the most possible defect at the substitutional lattice site is the In antisite; In atom at the substitutional As site in the 3rd As layer, which is 0.79 nm below the surface.

[1] K. Kanisawa, S. Perraud, Y. Hirayama. International Conference on Nanoscience and Technology (ICN+T 2006), 171, 2006.

# Coordination and configuration analysis of local structures of B-C-N hybrid thin films

**I. Shimoyama [1], Md. N. Uddin. [2], Y. Baba [1], T. Sekiguchi [1], M. Nagano [3]**

1. Japan Atomic Energy Agency, Quantum Beam Science Directorate, Surface chemistry Research group, Tokai-mura 2-4, Ibaraki, Japan 319-1195

2. Shahjalal Univ. of Sci. and Technol., Sylhet-3114, Bangladesh

3. Saga University, Department of Chemistry and Applied Chemistry, Faculty of Science and Engineering, Honjo-machi 1, Saga-city, Saga Japan 840-8502

B-C-N hybrid thin films prepared by ion beam deposition are characterized by NEXAFS. B and N K-edge NEXAFS spectra show multiple π* components that show graphite-like polarization dependence. Different magnitude of polarization dependences are observed among the π* components. Semi-empirical molecular orbital calculation is used to clarify the configuration of local structures in the films. From the comparison of heat of formation for some B-C-N clusters, configuration difference of local structures is attributed to fullerene-like structure in which pentagons are introduced in graphite network.

## 1. INTRODUCTION

Graphite-like B-C-N hybrid materials have intermediate composition between semimetallic graphite and insulating hexagonal boron nitride (*h*-BN), and are expected to have semiconducting property. Despite much effort, there are still some obstacles for synthesis of the material. In most cases, various kinds of $B_xC_yN_z$ are formed with graphite and *h*-BN. Most products have poor crystallinity and include variety of chemical bonding states. X-ray photoelectron spectroscopy (XPS) was widely used for characterization, and multiple components were observed for B1s, N1s, and C1s peaks [1]. This implies that these components originated from combination of B-N, B-C, C-N, and C-C bonds, however, the interpretation of XPS is still ambiguous.

Local structure analysis is indispensable in this context. Near edge x-ray absorption fine structure (NEXAFS) spectroscopy is powerful tool for this purpose. One of the characteristics of NEXAFS is polarization dependence analysis. When a system has anisotropic orientation, its configuration can be clarified by polarization dependence. It is known that B-C-N material can have both planner ($sp^2$) and cubic ($sp^3$) configurations. So far, it is supposed that π* peaks observed in electron energy loss spectrum indicate planner configuration, however, the spectral shape was similar to the spectra of *h*-BN and graphite, and B-C-N compounds were not distinguished from *h*-BN and graphite due to the limit of energy resolution [2]. To our knowledge, the configuration of B-C-N materials was not closely investigated because of the difficulty to synthesize oriented B-C-N materials.

Recently, our group succeeded to synthesize two-dimensional oriented B-C-N films [3]. In this work, we investigate configuration difference between B-C-N hybrid and *h*-BN by closely analyzing these films with NEXAFS spectroscopy.

## 2. Experimental

Experimental detail is described in elsewhere [3]. B-C-N films were synthesized by ion beam deposition (IBD). Fragment ions of borazine ($B_3N_3H_6$) were implanted in highly oriented pyrolytic graphite (HOPG) with acceleration energy of 3 keV. HOPG was heated at 500 ˚C during irradiation. Samples A, B, and C were prepared with different fluences of $0.4\times10^{16}$, $2.7\times10^{16}$, and $8.3\times10^{16}$ ions/cm$^2$. The nominal composition of the samples was estimated from XPS as $B_{0.07}C_{0.88}N_{0.05}$, $B_{0.26}C_{0.55}N_{0.19}$, and $B_{0.52}C_{0.1}N_{0.38}$, respectively. NEXAFS measurements were performed at the BL-11A of the Photon Factory in the High Energy Accelerator Research Organization (KEK-PF) with linearly polarized x-ray. All the measurements were carried out *in-situ* to avoid contamination. Incidence angle of x-ray was defined as an angle between the polarization vector of x-ray and the surface normal of the HOPG. All the NEXAFS spectra of the B-C-N hybrid films were obtained by subtracting the background spectra measured before ion beam irradiation. Photon energy was calibrated by $\pi^*$ peak energies of bulk *h*-BN, which were 192.1 eV at B K-edge and 401.6eV at N K-edge.

## 3. Results and Discussion

Top and bottom in figure 1 show N and B K-edge NEXAFS spectra. Solid, broken, and dotted curves correspond to the samples A, B and C, respectively. Vertical broken lines show the π* peak positions of bulk *h*-BN. Polarization dependence is cancelled with magic angle [4]. B K-edge spectra are normalized at 250 eV, and N K-edge spectra are normalized at 450 eV. Both N and B NEXAFS spectra changed depending on the ion fluence and π* peak of *h*-BN became dominant with fluence. This result is consistent with previous interpretation that *h*-BN layer was finally formed and some B-C-N compounds were formed at the interface between HOPG and BN layer [1].

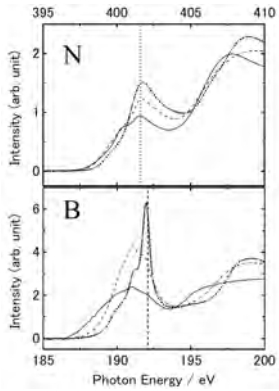


Figure 1.

Figure 2 (left) shows polarization dependence of NEXAFS for the sample A. Left and right figures correspond to B and N K-edge regions, respectively. Lateral axes are energy and incidence angle of x-ray in the upper figures. Spectra at 20º and 90º are compared in the lower figures. Peak intensities are normalized at 191 eV and 400 eV in the lower left and lower right figures, respectively. In both K-edge regions, low-energy components were enhanced at grazing incidence and high-energy components were enhanced at normal incidence. This graphite-like polarization dependence immediately suggests that the B-C-N compounds had

graphite-like orientation and the low energy components are assigned to π* peaks. Furthermore, a close analysis indicates that polarization dependence also influence relative intensities of the low-energy π* components. For the B NEXAFS spectra, solid curves (20º)

have higher relative intensity than dotted curves (90º) at the position of broken lines. This means that the π* peaks of *h*-BN have larger polarization dependence than those of B-C-N compounds.

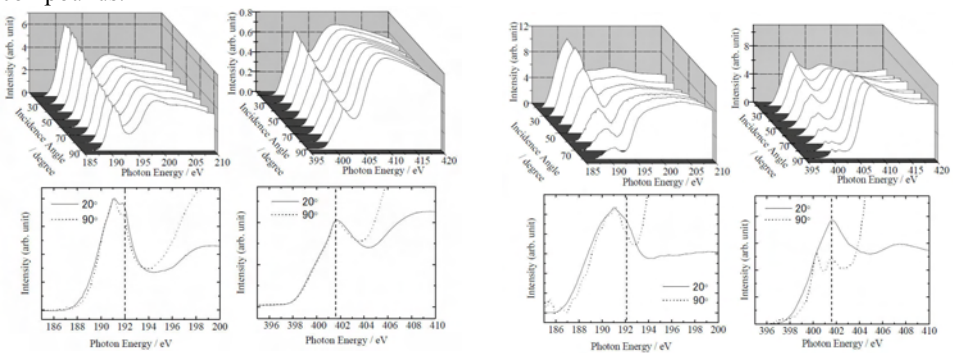


Sample A Sample B

Figure 2. Polarization dependence of NEXAFS for sample A (left) and for sample B (right)

Figure 2 (right) shows the results of the sample B. Although it was weakened, polarization dependence was still observed in the figure. π* peaks show different magnitude of polarization dependences also for the sample B. However, the difference is smaller than the case in Fig.2(left). For the sample C, the polarization dependence was almost lost.

The reason why the polarization dependence decreased with fluence is mainly due to the disorder of crystal structure which was induced by ion irradiation. Since *h*-BN has planner configuration, the π* peaks of *h*-BN disappear at normal incidence (90º) if the sample has intact flat-lying orientation. However, disorder can not explain the different polarization dependences between the π* peaks of *h*-BN and B-C-N compounds because the effect would be same for *h*-BN and B-C-N compounds which were formed with same condition. Therefore, above results suggest that the configurations of B-C-N compounds were different from that of *h*-BN when ion fluence was small.

This result reminds us of the case of carbon nitride ($CN_x$). We have measured polarization dependence of NEXAFS for $CN_x$ films which were prepared by $N_2^+$ ion implantation in HOPG at 800 ºC. Despite the π* peak in C K-edge NEXAFS showed clear polarization dependence, dominant π* peak in N K-edge NEXAFS showed no polarization dependence [5]. This result is explained by formation of "fullerene-like structure" which was proposed by Sjöstrem *et al*. [6]. According to their report, substitution of N for C induces pentagon in graphite network. Since pentagons corrugate planner structure, two-dimensional orientation is degraded at N sites. Therefore, only N sites at which pentagon was formed showed no polarization dependence.

We investigate substitution effect on configuration using two $C_{24}H_{15}$ clusters as shown in figure 4 referring the report of Sjöstrem *et al*. [6]. Cluster A consists of only hexagon and has planner configuration. Cluster B includes a pentagon and has a buckled structure. We partially substitute B and N atoms for C atoms in the clusters because different polarization dependences were observed at low fluence. Heat of formation (HOF) is calculated for the clusters using AM1 semi-empirical molecular orbital calculation with WinMOPAC package. Table 1 shows the substitution position and heat of formation for each clusters.

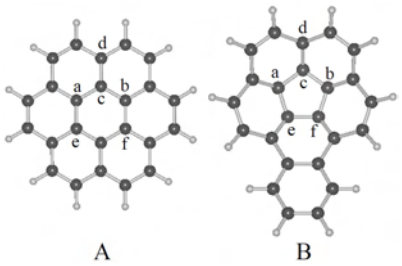


Figure 4.

| Cluster | Substitution Sites | | | | | | Heat of Formation (kcal/mol) | | |
|---|---|---|---|---|---|---|---|---|---|
| | a | b | c | d | e | f | $\Delta H_A$ | $\Delta H_B$ | $\Delta H_B$-$\Delta H_A$ |
| $C_{24}H_{15}$ | — | — | — | — | — | — | 95.95 | 169.84 | 73.9 |
| $C_{22}N_2H_{15}$ | N | N | — | — | — | — | 176.03 | 222.23 | 46.2 |
| $C_{22}B_2H_{15}$ | B | B | — | — | — | — | 191.76 | 235.01 | 43.4 |
| $BC_{20}N_3H_{15}$ | N | N | B | N | — | — | 117.26 | 132.50 | 15.2 |
| $B_3C_{20}NH_{15}$ | N | N | B | N | — | — | 68.08 | 123.26 | 55.3 |
| $BC_{22}N_2H_{15}$ | B | B | N | B | — | — | 107.65 | 173.85 | 66.2 |
| $B_2C_{20}N_2H_{15}$ | N | N | B | — | — | — | 61.28 | 128.17 | 66.9 |
| $BC_{22}NH_{15}$ | B | B | N | — | N | — | 102.52 | 175.55 | 73.0 |
| | N | B | — | — | — | — | 102.52 | 183.19 | 80.7 |
| $B_2C_{21}NH_{15}$ | — | — | — | — | B | N | 77.69 | 175.17 | 97.5 |

Table 1.

Difference of HOF ($\Delta H_B$-$\Delta H_A$) between the clusters A and B decreases when C atoms are substituted by N atoms at a and b sites in the clusters [6]. This means that pentagon is likely formed in graphite by N substitution. Alternatively, we substitute B for C in the clusters and observe that $\Delta H_B$-$\Delta H_A$ value is similar to the case of N substitution. This result indicates that B substitution also tends to form pentagon as well as N substitution. Furthermore, we attempt other B and N substitutions and find that the $\Delta H_B$-$\Delta H_A$ value is smaller than the case of $C_{24}H_{15}$ when N/B ratio is larger than unity. This result is explained as follows. Since B-N bond has isoelectronic structure to C-C bond, BN bond substitution for CC bond is stable and planner configuration of graphite is conserved. On the other hand, surplus electrons are formed by deviation from the ratio of N/B=1, and occupy $\pi^*$ anti-bonding states. Since this makes unstable the planner structure, buckled configuration is likely formed.

Local deviation from N/B=1 is prone to occur at low fluence and N/B ratio is close to unity at high fluence. This would be the reason why large difference of polarization dependence among the $\pi^*$ components was observed at low fluence. This means that fullerene-like structure is likely formed as ion fluence decreases, and graphite-like structure is preferentially formed as ion fluence increases.

Above results clarify that B-C-N compounds can have buckled configuration with fullerene-like structure when N/B ratio deviates from unity. This knowledge suggests that N/B ratio should be unity to achieve two-dimensional structure. Therefore B and N must be simultaneously supplied to synthesize highly oriented B-C-N hybrid.

## 4. References

[1] I. Shimoyama, Y. Baba, T. Sekiguchi, and K. G. Nath, J. Vac. Sic. Technol. A 21, 1843 (2003).
[2] J. Kouvetakis, T. Sasaki, C. Shen, R. Hagiwara, M. Lerner, K. M. Krishnan, and N. Bartlett, Synth. Met. **34**, 1 (1989).
[3] Md. Nizam Uddin, I, Shimoyama, Y. Baba, and T. Sekiguchi, J. Appl. Phys. 99, 084902 (2006).
[4] J. Stöhr: "NEXAFS Spectroscopy", Springer, Berlin, 1996 (ISBN-10: 3540544224).
[5] I. Shimoyama, Y. Baba, and T. Sekiguchi, Vacuum, vol. 78, 563-568 (2005).
[6] H. Sjöström, S. Stafström, M. Boman, and J. –E. Sundgren, Phys. Rev. Lett.;75:1336 (1995).

# Calculation of electron scattering of carbon atom clusters and fullerene cages – interpretation of electron diffraction of amorphous and fullerene-like carbon allotropes.

**Zs. Czigány [1], L. Hultman [2]**

1. Research Institute for Technical Physics and Materials Science of the Hungarian Academy of Sciences P.O.Box 49. H-1525 Budapest. Hungary

2. Thin Film Physics Division, Department of Physics, Chemistry and Biology (IFM), Linköping University, S-581 83 Linköping, Sweden

Amorphous carbon and carbon-based coatings show a broad variety of properties regarding mechanical hardness, elasticity as well as electronic and optical properties. The difference in properties is due to different chemical bonding and the consequent different atomic short range ordering. An interesting group of carbon-based materials are the so called fullerene-like (FL) solid phases like CNx and CPx where the solid is composed of FL fragments and/or packages. Multishell fullerene structures - so called nano-onions - were observed in CNx by high resolution transmission electron microscopy (HRTEM) [1], but CPx has amorphous appearance in HRTEM images [2]. However, the electron diffraction showed structural differences both between the CNx and CPx FL phases and compared to other amorphous carbon allotropes. Here, we report on the calculated electron scattering of graphite and diamond nanoclusters, fullerene molecules and fragments as a function of the number of atoms. Amorphous phases are interpreted as ultrafine random nanocrystalline or nanoclustered structures with characteristic cluster size of 10-30 atoms. The short range order of amorphous carbon allotropes and FL-CNx and CPx can be determined based on the relation between the calculated scattering of carbon nanoclusters and measured selected area electron diffraction (SAED) patterns.

[1] Zs. Czigány, I. Brunell, J. Neidhardt, K. Suenaga, and L. Hultman Growth of fullerene-Like Carbon Nitride Thin solid Films Consisting of Cross-Linked Nano-Onions Appl. Phys. Lett. 79 2639 (2001)

[2] A. Furlan, G.K. Gueorguiev, Zs. Czigány, H. Högberg, S. Braun, S. Stafström, L. Hultman, Synthesys of Phospho Carbide Thin Films By Magnetron Sputtering. Rapid Research Letter in Physica Status Solidi 2 190 (2008)

# Graphene on Ru(0001): Spatially resolved electronic structure by means of scanning tunneling microscopy/spectroscopy

**A.L Vazquez de Parga [1], B. Borca [2], F. Calleja [2], M.G.C. Passeggi [3], J.J. Hinarejos [2], F. Guinea [4], R. Miranda [1]**

1. IMDEA Nanociencia, Spain
2. Universidad Autonoma de Madrid, Spain
3. INTEC
4. Instituo de Ciencia de Materiales, Spain

The possibility to produce single layers of graphene has opened a fascinating new world of physical phenomena in two dimensions. While ultra-thin epitaxial films of graphite and even "monolayergraphite" have been grown on solid surfaces by Chemical Vapor Deposition for quite some time, the degree of characterization of the films was hampered by experimental limitations. Systems made up of a few graphene layers have been grown on SiC substrates. We report on a method to fabricate highly perfect, periodically rippled graphene monolayers and islands on Ru(0001) under Ultra High Vacuum conditions. The graphene layers were produced by thermal decomposition at 1000 K of ethylene molecules pre-adsorbed at 300 K on the sample surface. The epitaxial layer of graphene covers completely the surface of the single-crystal Ru substrate over distances larger than a micron and presents a triangular periodicity of 2.4 nm that is due to the coincidence lattice of graphene and Ru, i.e. the lattice of graphene has a size relation with the underlying Ru lattice that implies that 11 carbon honeycombs will adjust almost exactly with 10 Ru-Ru interatomic distances. The weakly interacting, laterally undistorted graphene structure rides on top of the lattice of the substrate, resulting in some C atoms being slightly higher than others. The periodic charge inhomogeneities in the graphene layer can be visualized directly in the real space by by means of scanning tunnelling microscopy/spectroscopy imaging the spatial distribution of dI/dV close to the Fermi energy. In our case, the inhomogeneities in the charge distribution are spatially correlated with the ripples in the graphene layer. The reason behind is the periodic modulation of the potential, due to changes in the metallic screening from the substrate. This inhomogeneity can be simulated with a tight-binding model which incorporates a periodic potential associated with the structural ripples that induces a shift of the electronic levels and a corresponding charge transfer from conduction to valence bands for some atoms and the opposite in the others. In agreement with the experiments, the calculations show that the occupied LDOS is larger on the "high" regions of the superlattice, where the potential is at a minimum, while the empty LDOS is larger at the "low" regions of the graphene layers.

# Pulsed Laser Deposition of functionally graded alumina/Ti protective coatings

**D.Tonini [1], F. Di Fonzo [1], C.S. Casari [1] A. Li Bassi [1], E. Bertarelli [2], D. Gastaldi [2], P. Vena [2], M.G. Beghi [1]**

1. NEMAS - Center for NanoEngineered MAterials and Surfaces, Dipartimento di Chimica, Materiali e Ingegneria Chimica "G. Natta", Politecnico di Milano, Piazza Leonardo da Vinci 32, 20133 Milano, Italy

2. Dip. Ing. Strutturale, Politecnico di Milano, Piazza Leonardo da Vinci 32, 20133 Milano, Italy

Pulsed Laser Deposition (PLD) offers undoubted advantages in deposition of nano-engineered coatings, namely accurate stoichiometry and thickness control and low substrate temperature, that allow deposition of multilayer films with sharp interfaces between each layer and functionally graded coatings with the desired composition profile along thickness. In this work we exploited PLD's unique features to realize three different Al2O3-based systems: homogeneous nanocrystalline aluminum oxide coatings, AlxOy/Ti multilayers and functionally graded coatings in which the composition change from pure Ti at substrate interface to pure AlxOy on the film surface. Aluminum oxide represents a suitable material to realize high quality protective coatings, due to its chemical inertness, hardness and optical transparency, nevertheless its usage is limited by the high temperatures needed to obtain coatings with the highest mechanical properties. In the PLD process the depositing species have high kinetic energy, thus it is possible to obtain smooth and dense films with the desired mechanical properties even at room temperature, extending the range of suitable substrates also to heat-sensitive materials like polymers. Multilayered coatings of alternating ceramic and metal represent a way to enhance the toughness of the coating because crack propagation is inhibited by the sharp interfaces between the two materials, whereas functionally graded materials (FGM) with Young's modulus increasing from the interface to surface avoid stress concentration at the film – substrate interface thus increasing the adhesion of the coating. Homogeneous AlxOy, multilayer and FGM coatings were deposited on Ti6Al4V and Si at room temperature in pure oxygen atmosphere (pressure in the range 0.1-0.5 Pa) using a nanosecond UV (266 nm) Nd:YAG laser. After ultrasonic cleaning in isopropanol Ti6Al4V substrates were ion beam treated with Ar+ ions at 600V accelerating voltage in order to remove contaminants and assure better adhesion of the coatings. Film's morphology was investigated using scanning electron microscopy (SEM), the elastic-plastic behavior was characterized with nano-indentation techniques, toughness was determined with high-load indentation and adhesion and failure modes were studied using nano-scratch test followed by SEM investigation of the produced track. Deposited films have high hardness (11GPa) and at the same time reduced brittleness; in fact even at high indentation load, the coatings do not develop cracks at the apexes of indentation track. Films deposited on titanium alloy are well adherent to the substrate and no catastrophic failure of the system was observed up to the maximum achievable load of the nano-scratch apparatus.

# The structure of amorphous-nano-crystalline Si thin films by Raman spectroscopy, HRTEM and GISAXS

**D. Gracin [1], K. Juraić [1], A. Gajović [1], P. Dubček [1], S. Bernstorff [2], M. Čeh [3]**

1. Ruđer Bošković Institute, 10000 Zagreb, Croatia
2. Sincrotrone Trieste, Basovizza (TS), Italy
3. Jožef Stefan Institute, Sl1000 Ljubljana, Slovenia

The amorphous - nano-crystalline silicon thin films, with various crystal to amorphous phase volume ratio were deposited by plasma enhanced chemical vapour deposition method using radio frequency discharge in silane gas diluted by hydrogen. The variation of crystal fraction and individual crystal size distribution were obtained by variation of dilution. The samples were analysed by Raman spectroscopy, high resolution transmission electron microscopy (HRTEM) and grazing incidence small angle x-ray scattering (GISAXS).

The Raman crystallinity, obtained as the ratio of areas under corresponding TO phonon peaks in Raman, was between 0 and 50%. The crystalline TO peak positions varied between 500 and 521 cm-1 which corresponds to average crystal sizes between 2 and 20 nm, considering only phonon confinement due to nano-size of crystals. However, the TO line was asymmetric and line-width was broad suggesting also the existence of smaller and larger crystals. HRTEM micrographs showed that up to highest degree of crystallinity used here, the structure corresponds to individual nano-crystals embedded in amorphous matrix. At low crystal volume contribution the peak of individual size distribution was close to 1.5 nm. For higher crystal fraction, peak shifts slightly towards 2 nm and number of lager crystals with sizes 5- 20 nm increase. The comparison of size distributions of nano-crystals estimated from HRTEM and Raman showed excellent match in average individual sizes when results of both methods were fitted as two size distributions. However, HRTEM distributions were slightly different than those obtained by Raman and suggested larger contribution of smaller crystals. Furthermore, HRTEM micrographs suggested presence of certain strain in the nano- crystals. GISAX of deposited samples indicated particles with Gyro radii between 2 and 6 nm. Larger particles were present in the samples with higher crystal fraction and larger crystals. However, the samples were porous to certain degree (as concluded from optical measurements) and direct correlation between particles and crystals were not easy to establish. GISAXS obtained under variation of incidence angle allowed estimating in depth distribution of particles. For growing conditions that favour smaller nano-crystals, the individual sizes of particles were uniform going from surface towards depth of the sample and shape was spherically symmetric. For growth that resulted in larger crystals the particles were elongated parallel to the surface and smaller in the "bulk" of the samples. The differences in results obtained by applied methods were discussed as a consequence of oversimplified models that neglects influence of strain and shape of nano-crystals (Raman) and possible in-homogeneity of samples that makes Raman and GISAXS not straight forward comparable to microscopic methods (HRTEM).

# High rate deposition of hard hydrogenated amorphous carbon for tribologic applications

**T. Zaharia [1], S.V. Singh [1], M. Creatore [1], R. Groenen [2], K. Van Hege [2], M.C.M. van de Sanden [1]**

1. Eindhoven University of Technology, Department of Applied Physics, P.O. Box 513, 5600 MB Eindhoven, The Netherlands

2. NV Bekaert SA, Dept. of Advanced Coating Technologies, Bekaertstraat 2, 8550 Zwevegem, Belgium

Hard diamond-like hydrogenated carbon deposited at high rates (>15 nm/s) utilizing the expanding thermal remote $Ar/C_2H_2$ plasma is reported. The downstream of expanding thermal plasma is characterised by a low electron temperature which leads to ion driven chemistry and negligible physical effect like ion bombardment (< 2 eV) on the substrate. Discounting any possibility of high energy ion bombardment, the material properties are studied with respect to a range of argon to acetylene gas flow ratios depicting the influence of residence time. Distinct from previous works, relatively low argon to acetylene gas flow ratio has been extensively studied. Under these conditions Infrared (IR) absorption shows reduced CH stretching strength and, in addition, it is also evident that the endgroups ($sp^2$ - $CH_2$ and $sp^3$ – $CH_3$) are absent characterising a novel material. These films posses relatively low optical band gap and hydrogen content, high refractive index and a nanohardness exceeding 16 GPa. The hydrogen content extracted from IR spectra indicates substantial decrease in bonded hydrogen concentration. From Threshold Ionization Mass Spectrometry we have clear indications that the atomic hydrogen to $C_3H_x$ radical flux is paramount in understanding the deposition process and is key in the formation of this hard carbon based material [1] under these low ratios of argon to acetylene gas flow conditions. The film properties will be interpreted in view of the specific plasma chemistry taking place in the expanding thermal plasma.

[1] J. Benedikt, D.C. Schram, and M.C.M. van de Sanden, J. Phys. Chem. A **109**, 10153-10167 (2005).

# Tribological behaviour of reactively sputtered DLC and DLC-based coatings on rubber substrates under dry and oil-lubricated conditions

**X.L. Bui, Y.T. Pei, J.Th.M. De Hosson**
Materials Innovation Institute, University of Groningen, Nijenborgh 4, 9747 AG, Groningen, The Netherlands

Hydrogenated diamond-like carbon (DLC) and metallic doped DLC coatings have been deposited on ACM (acrylate) and HNBR (hydrogenated nitrile butadiene) rubbers via unbalanced magnetron reactive sputtering. The random crack network, which facilitates the flexibility, was always observed on the coatings. The tribological behavior of uncoated and coated rubbers has been studied via ball-on-disc tribotesting against ø6 mm 100Cr6 ball counterpart under dry and boundary oil-lubricated conditions. Under dry sliding condition, uncoated rubbers exhibited very high coefficient of friction (CoF > 1) and the rubbers surface was heavily damaged with deep wear tracks and large amount of rubber adhering on the counterparts after tribotests. With 1μm Me-DLC coating, the CoF of coated rubbers was brought down to the range of < 0.22-0.25 even at high applied load of 5 N. The tribological performance was even better when a thin coating (300 nm) of pure DLC was coated on rubbers. The CoF was further lowered to less than 0.17 and the wear track on the coating and the wear scar of the counterpart were almost unobservable after tribotests. The surface graphitization, which is well-known as a main contribution to the low friction of DLC and DLC-based coatings, seems to be limited in the case of rubber substrate due to the "soft contact" characterized by a very low contact pressure between the coating and the counterpart. Under boundary oil-lubricated condition, the CoF of uncoated, Me-DLC coated and pure DLC coated rubbers were in the range of 0.25-0.30, 0.18-0.22 and 0.10-0.12, respectively. After 100000 laps, scratches on the counterpart sliding against Me-DLC coated rubber were seen but that sliding against DLC coated rubbers were very smooth.

# Synthesis and Characterization of Hard and Tough Ti-Zr-C Nanocomposite Coatings

**D. Martinez-Martinez, O. Kubova, E. Santos-Junior, M.P. Delplancke-Ogletree**
ULB, Belgium

Nanocomposite structures formed by small crystallites (generally, of a hard metal carbide or nitride) embedded in a lubricant matrix are optimal candidates for protective applications, since they present moderate-high hardness, good toughness, and also low values of friction coefficients and wear rates. These properties make them attractive for being used as the protective layer of the hip implants. However, selection of biocompatible constituting elements is also important factor for this kind of application. In principle, good choices are elements with good bulk biocompatibility properties. As a result, we have selected Ti, Zr and C as base elements for our nanocomposite coatings. The coatings are prepared by magnetron sputtering operating in dc mode. The base pressure is $2x10^{-5}$ mbar, which is increased up to $3x10^{-3}$ mbar while depositing. A metallic underlayer of cca. 200 nm is deposited to improve the adhesion. Coatings prepared by sputtering of a Ti target in a $CH_4$/Ar atmosphere were used to study the effect of the main synthesis parameters ($CH_4$ flow, bias voltage and power applied to the target) on the chemical composition and crystallinity of the coatings (measured by X-ray photoelectron spectroscopy (XPS) and X-ray diffraction (XRD), respectively). The Ti/C ratio and the TiC crystal size increased when lower $CH_4$ flow and higher power and bias voltage were used. Besides, increasing the power applied to Ti target reduces the oxygen contamination due to the higher sputtering rate. The optimal deposition conditions have been also used with TiZr and Zr targets. It has been observed that the carbon/metal ratio and oxygen contamination are dramatically reduced due to the higher sputtering rate of Zr-containing targets. Ti-C and Ti-Zr-C samples showed hardness of cca. 30 GPa and H/E* ratio (which can be used as a film toughness estimation) of cca. 0.15, while sample Zr-C showed hardness of cca. 20 GPa and H/E* ratio of cca. 0.11. This different behaviour is probably related to the different structure present in the films: both Ti-C and Ti-Zr-C samples show TiC/a-C and TiC/ZrC nanocomposite structures, while the Zr-C coating is found to be a polycrystalline ZrC. The macrostresses of the presented coatings were also measured by the curvature method.

# Effect of Metal Substitution by Magnesium in Arc-Evaporated TiN and NbN Coatings

**A. Hodroj, J.F. Pierson**
LSGS, Ecole des Mines, Parc de Saurupt, CS 14234, 54042 NANCY cedex, France

Since the 80's, titanium nitride films are widely used as protective coatings for cutting and forming tools. During the 90's, silicon and/or aluminium were added to improve the properties of TiN-based films: oxidation resistance, hardness, tribological properties… Furthermore, the effect of transition metal addition (Cr, Zr, V…) has been also studied. Recently, Fenker et al. [1] showed that magnesium addition in TiN-based films induces a change in their colour and improves the oxidation resistance in air. The present work aims to study the effect of magnesium addition into transition metal nitride coatings.

The films were deposited on stainless steel and silicon substrates by a hybrid process. Titanium and niobium were supplied by reactive cathodic arc evaporation of a metallic target while magnesium was supplied by reactive magnetron sputtering. The Mg concentration was controlled by the current applied to the target. The film structure was studied by X-ray diffraction and the film morphology was observed by scanning electron microscopy. The chemical composition was estimated from energy dispersive X-ray spectroscopy. In the 0 - 20 at. % range, the incorporation of magnesium into TiN or NbN films did not change the structure. Optical reflectance measurements in the visible range were performed to study the effect of magnesium content on the film optical properties. Oxidation resistance was evaluated after air annealing in the 400 – 800 °C range. Secondary neutral mass spectrometry was used to determine the concentration profile along the film depth and to estimate the oxide layer thickness. Finally, the hardness of 3-µm thick films was measured using the depth sensing microindentation method.

[1] M. Fenker, M. Balzer, H. Kappl, O. Banakh Surf. Coat. Technol. 200 227 (2005)

# Deposition of $SiO_xC_y$ layers on polymer films by Magnetron-PECVD

**M. Fahland, J. Fahlteich, T. Vogt, B. Meyer**
Fraunhofer Institute for Electron Beam and Plasma Technology, Department Coating of Flexible Products, Winterbergstrasse 28, 01277 Dresden, Germany

Magnetron-PECVD is a new process tool which allows the deposition of plasma polymer coatings at process pressures below 1 Pa. The striking features of this technology are the relatively easy realisation of large area deposition as well as the possibility of the combination with sputtering processes for multilayer coating designs. The deposition process is compared to other common PECVD-technologies.
The $SiO_xC_y$ coatings were deposited on PET film in a roll-to roll deposition machine. Dynamic deposition rates of more than 250 nm*m/min were achieved. The film deposition is strongly dependent on the gas composition. XPS analysis revealed that the carbon content of the films is strongly dependent on gas composition during the process.
The coatings were analysed by ERDA and by infrared absorption spectroscopy. These methods identified the existence of both chain-like und network-like Si-O bonding in the layer. The results show how the layer properties are linked to the plasma parameters of the deposition process. The properties are compared to sputtered $SiO_2$ and to HF-PECVD.
Magnetron-PECVD can be tuned by different kinds of monomer inlet. It is shown that the local plasma density plays a crucial role for film formation. Investigations with the monomer hexamethyldisiloxane (HMDSO) and with the monomer tetraethylorthosilicate (TEOS) are presented.
The coatings have a lower internal stress compared to sputtered $SiO_2$ layers. Applications examples in multilayer optical stacks and in permeation barrier stacks are given.

# Growth and properties of atmospheric pressure MOCVD titanium oxynitride

**R. Hausbrand [1], F.-D. Duminica [2]*, F. Maury [2]**

1. ArcelorMittal R&D Industry Gent – OCAS N.V., Surface Functionalisation, Pres. J.F. Kennedylaan 3, 9060 Zelzate, Belgium

2. CIRIMAT, CNRS/INPT/UPS, ENSIACET, 118 Route de Narbonne, 31077 Toulouse, France

Films in the ternary system Ti-O-N have numerous technological applications because of their chemical, optical, and mechanical properties. While titanium dioxide is most widely known for its optical and photo-catalytic properties, titanium nitride is well known for its mechanical properties. The incorporation of nitrogen into titanium oxide generates a wide range of functional materials with various properties adjusted from those of their binary parent compounds, such as materials with photo-catalytic activity in the visible light, materials with selective light absorption and very hard materials.

Atmospheric pressure metal-organic chemical vapour deposition (AP-MOCVD) is a comparatively low cost technique for the deposition of a wide range of materials on substrates such as glass, metal and silicon. It offers a good control over the growth parameters and thus over the stoichiometry and the microstructure of the films. The deposition of titanium dioxide with AP-MOCVD is well known, especially for the manufacture of self-cleaning glass.

In this paper, we report the deposition of titanium oxynitride films by AP-MOCVD using titanium tetraisopropoxide (TTIP) as base precursor and hydrazine ($N_2H_4$) as nitrogen source. The composition and the microstructure will be discussed in relation with the growth conditions. Depending on the concentrations of the precursors and the substrate temperature, dense and amorphous oxynitride films (a-$TiO_xN_y$) or crystalline films with a low nitrogen content were deposited (N-doped $TiO_2$). The films were grown on stainless steel to a thickness between a few hundred nanometers and a few micrometers. The N-doped titanium oxide films exhibited photo-catalytic activity in the visible light, while the amorphous $TiO_{1.5}N_{0.5}$ films showed good wear behaviour. The paper will focus on the properties of the amorphous oxynitride films, such as tribological behaviour, hardness and adhesion.

* now ArcelorMittal Liège, Research and Development - New Coatings Technologies, Rue Sompré 1, 4400 Flémalle, Belgium

# Conformality of thermal and plasma enhanced ALD

**D. Deduytsche, J. Dendooven, J. Musschoot, C. Detavernier**
Ghent University, Department of Solid State Sciences, Krijgslaan 281 (S1),9000 Gent, Belgium

Its ability for conformal coating of high-aspect ratio features is one of the most important advantages of atomic layer deposition (ALD). In this work, we have attempted to quantify and model the conformality of thermal and plasma enhanced ALD processes.

ALD depositions were performed in a home-built system consisting of two ALD chambers, two loadlocks and a chamber for sputter deposition. Both ALD chambers are equipped with 6 gas lines for reactants (e.g. $N_2$, $NH_3$, $H_2$, $O_2$) and 5 or 7 heated lines for precursors. The ALD chambers are pumped by turbomolecular pumps, resulting in a base pressure of $10^{-7}$ mbar. Substrates can be heated using a resistive heating plate, providing temperatures up to around 400°C. Both ALD chambers are equipped with a home-built RF plasma source. The reactant gases can flow either directly into the growth chamber (thermal ALD) or through the plasma chamber (plasma enhanced ALD).

The conformality of ALD processes is usually characterized by test depositions into high-aspect ratio trench or via structures. After deposition, a cross-section is prepared, and electron microscopy is used to verify the presence of a film on the bottom part of the structure. This method is quite time- and labour-intensive, and it is difficult to obtain a quantitative measurement of the film thickness as a function of depth into the structure.

For sufficiently low pressure ($10^{-3}$mbar), the mean free path of gas molecules is > 1cm, allowing the use of macroscopic test structures to quantify conformality. We have used a test structure consisting of two pieces of a Si wafer, which are mounted facing each other, with an adjustable gap defining the aspect ratio of the structure. This results in a hole with e.g. a depth of 5cm, a width of 0.5cm and an adjustable gap (i.e. separation between the Si wafers) of 0.9mm to 0.1mm, corresponding to an aspect ratio of 10 to 100. After deposition and disassembly of the test structure, one is left with two planar pieces of Si, and standard thickness measurement techniques such as ellipsometry can be used to determine the layer thickness as a function of depth into the hole.

The conformality of both thermal and plasma enhanced ALD was measured as a function of pulse and pump time and aspect ratio. The well-known TMA-H2O process was used for thermal ALD of $Al_2O_3$, while a combination of TMA and $O_2$ plasma was used to test the conformality of PE-ALD. A model was developed to predict the film thickness as a function of depth into the test structure. The model is based on earlier work by Gordon et al. [1], which has been extended to also take into account a variable sticking coefficient for the precursor molecules.

[1] R. G. Gordon, D. Hausmann, E. Kim and J. Shepard, Chem. Vap. Dep. 1, 73 (2003)

# Characterization of GaAs metal-oxide-semiconductor structure with $TiO_2$ as gate oxide prepared by atomic layer deposition

**MK. Lee, T.-H. Kuo**
National Sun Yat-sen University, Department of Electrical Engineering, Taiwan, R. O. C.

Atomic layer deposition (ALD) provides an excellent way to grow high-quality gate dielectrics on III-V compound semiconductors. In this study, $TiO_2$ films were grown on p-type GaAs(100) by ALD using $Ti(i\text{-}OC_3H_7)_4$ and $O_2$ as precursors in the deposition temperature range from 300 $^oC$ to 550 $^oC$. The physical, chemical and electrical characteristics of ALD-$TiO_2$ films grown on GaAs were investigated. The steady growth rate is 0.15 nm/per cycle and is almost independent of the deposition temperature. But the growth rate per cycle is larger in the first few cycles. From the X-ray diffraction (XRD) results, they indicate that the anatase phase dominates the structure in the deposition temperature range from 300 $^oC$ to 500 $^oC$. The structure is transformed to the rutile phase at the deposition temperature of 550 $^oC$. The leakage current density of Al/$TiO_2$/GaAs MOS structure is $2.7\times10^{-4}$ A/cm$^2$ at the applied electric field of -1.0 MV/cm. The high leakage current of as-deposited $TiO_2$ films is mainly from the grain boundary of polycrystalline $TiO_2$ and the $TiO_2$/GaAs interface state. In order to improve the electrical property of ALD-$TiO_2$ films, thinner $TiO_2$ films and the sulfidation passivation of GaAs were used.

From the XRD results, the structure of $TiO_2$ films thinner than 30 nm is like amorphous under the same growth conditions. The leakage current density of amorphous $TiO_2$ films can be decreased effectively to $4.38\times10^{-6}$ A/cm$^2$ at the applied electric field of -1.0 MV/cm.

Furthermore, thinner TiO2 films grown on $(NH_4)_2S_x$ passivated GaAs can decrease the leakage current density effectively. The $(NH_4)_2S_x$ treatment can assist the reconstruction of its crystalline structure of GaAs surface and improve the interface properties of $TiO_2$/GaAs. The leakage current density can be further improved to $2.05\times10^{-6}$ A/cm$^2$ under the applied electric field of -1.0 MV/cm.

[1] Y. Dong, X. Ding, and X. Y. Hou, Appl. Phys. Lett., 77 3839(2000)
[2] Jung Wook Lim, Sun Jin Yun, and Jin Ho Lee, Electrochemical and Solid-State Letters, 7 F73(2004)
[3] M.C. Marco de Lucas, F. Fabreguette, S. Collin, S. Bourgeois, International Journal of Inorganic Materials, 2 255( 2000)
[4] M. M. Frank, G. D. Wilk, D. Starodub, T. Gustafsson, E. Garfunkel,Y. J. Chabal, J. Grazul, and D. A. Muller, Appl. Phys.Lett., 86 152904(2005)
[5] Jung-Wook Lim, Hyung-Sang Park, and Sang-Won Kang, Journal of Applied Physics, 88 6327(2000)
[6] K. Vydianathan, G. Nuesca, G. Peterson, E. T. Eisenbraun, A. E.Kaloyeros, J. J. Sullivan, and B. Han, J.Mater. Res., 16 1838(2001)
[7] B. C. Kang, S. B. Lee, and J. H. Boo, Surf. Coat. Technol., 131 88(2000)

# Atomic layer deposition of TiN and Ru

**J. Musschoot [1], Q. Xie [2], D. Deduytsche [1], K. De Keyser [1], J. D'Haen [3]**
**R. L. Van Meirhaeghe [1], C. Detavernier [1]**

1. Ghent University, Department of Solid State Sciences, Krijgslaan 281 (S1), B-9000 Gent, Belgium
2. State Key Laboratory of ASIC and Systems, Department of Microelectronics, Fudan University, Shanghai 200433, China
3. Hasselt University, Institute for Materials Research – IMOMEC, Wetenschapspark 1, B-3590 Diepenbeek, Belgium

Titanium nitride (TiN) is used as a copper diffusion barrier in microelectronics. In order to electroplate copper (Cu) on the TiN, ruthenium (Ru) adhesion layers with low resistivity can be used. As the conductivity of interconnects depends on their Cu content, it is important that the diffusion barrier and adhesion layers are as thin as possible. This is why atomic layer deposition (ALD) is an interesting technology for both TiN and Ru films.

TiN and Ru were grown plasma enhanced ALD from tetrakisdimethyltitanium (TDMAT) [1] and ruthenium diethylcyclopentadienyl ($Ru(EtCp)_2$) [2], respectively. Ammonia ($NH_3$) plasma was used as reactive gas. The purity of the TiN films was greatly improved with plasma ALD over thermal ALD films, which have high oxygen and carbon contamination levels [1].

The resistivity of the Ru films was as low as 10 μOhm cm. Ru layers deposited on HF cleaned Si(100) were polycrystalline, as was determined by x-ray diffraction (XRD). However, after annealing for one minute at 600°C, the texture changed to Ru(002). The average grain diameter grew considerably (about 100 nm diameter for a height of about 10 nm), as evidenced by electron backscatter diffraction (EBSD) and transmission electron microscopy (TEM).

[1] J. Musschoot, Q. Xie, D. Deduytsche, S. Van den Berghe, R. L. Van Meirhaeghe, C. Detavernier, Microelectronic Engineering (2008), doi: 10.1016/j.mee.2008.09.036
[2] O.-K. Kwon, S.-H. Kwon, H.-S. Park, S.-W. Kang, Electrochemical and Solid State Letters 7, C46 (2004)

# Nano-smooth diamond coatings for ultralow friction with green lubricants

**T. Gries [1], C. Matta [2], M.I. De Barros Bouchet [2], B. Vacher [2], L. Vandenbulcke [1]**

1 CNRS, UPR3021 Institute of Combustion Aerothermic Reactivity and Environment, 45071 Orléans cedex 2, France, and Université d'Orléans, BP 6749, 45067 Orléans Cedex 2, France

2 Laboratory of Tribology and System Dynamics, Ecole Centrale de Lyon, 69134 Ecully, France

Titanium alloys and titanium-coated alloys are important materials for aerospace, mechanical, chemical and biomedical applications; however their applications could be extended by improving their tribological behaviour. This can be done by using diamond-based coatings which are outstanding materials for changing their surface properties. We have shown that adherent nano-smooth fine-grained diamond coatings could be deposited on titanium alloys or titanium-coated substrates at moderate temperature, equal to or lower than 600°C, from $CH_4$-$CO_2$ species. These coatings are in fact duplex coatings with an external diamond film, a titanium carbide sub-layer and a diffusion layer forming a titanium solid-solution. They exhibit isotropic biaxial residual stresses, in the 2-5 GPa range, depending on the diamond purity. These coatings exhibit particularly strong adherence with the substrates as shown by various mechanical tests and very high induced stresses without peeling off.

These nano-smooth diamond coatings are first described in terms of $sp^2$-hybridized carbon contents relatively to the $sp^3$-C ones. This important parameter which influences the structure and the intrinsic properties of the coating (surface roughness in the 15-35 nm range, micro-hardness, Young's modulus and residual stresses) is correlated to the plasma enhanced CVD process through the formation of different concentrations of the gaseous precursors in the plasma. These precursors which include both radicals and stable species are revealed by molecular beam mass spectrometry and corroborated by kinetic calculations in the C-H-O plasmas.

These coatings are studied by micro-Raman spectroscopy and their structure is revealed by transmission electron microscopy (TEM) studies. Their extreme surface structure is especially evidenced by Energy-Filtering TEM on transverse cross-sections prepared by the Focus Ion Beam technique. A $sp^2$-C enriched layer is revealed which is important for tribochemical reactions. While the friction coefficient is high under ultra high vacuum, ultralow friction is obtained in saline corrosive solution. Ultralow friction with no wear is also obtained with gas phase lubrication by glycerol under boundary lubrication regime. This gas phase lubrication allows a better identification of the friction mechanism from advanced surface characterizations. These studies allow concluding that gas phase and liquid phase lubrication of these diamond coatings can permit new or improved applications in various fields, when OH-containing green or friendly molecules are used as lubricants. Some examples of ultralow friction and low wear are provided when nano-smooth diamond coatings or alumina are sliding on nano-smooth diamond in saline solution. Nano-smooth diamond on nano-smooth diamond with glycerol lubricant as a model molecule is another example which is reported.

# Templated growth of europium-doped sulfide thin films by a solvothermal method

**P.F. Smet, D. Poelman**
LumiLab, Department of Solid State Sciences, Ghent University, Krijgslaan 281-S1, 9000 Gent (Belgium)

We recently optimized a low-temperature, solvothermal synthesis method which yields luminescent, single-crystalline (Ca,Sr)S:$Eu^{2+}$ particles. We now modified the process to allow direct growth onto templated substrates. The as-grown layers emit a bright and homogeneous photoluminescence, peaking at 615nm and 650nm for SrS:Eu and CaS:Eu respectively. x-ray diffraction measurements showed that the layers grown at a temperature of only 200°C are strongly crystalline, with almost perfect (200) out-of-plane orientation. Using silicon substrates, almost epitaxial growth could be obtained. Scanning electron microscopy was used to study the morphology of the thin films. The main advantages of this innovative approach for the production of sulfide layers are the low-temperature process and potential scalability.

## 1. INTRODUCTION

Rare earth doped sulfides are an important class of luminescent materials, with applications in thin film electroluminescence [1] and wavelength-converted white-light emitting diodes [2]. The deposition of high quality sulfide thin films is not so straightforward. Electron beam evaporation often leads to sulfur deficient thin films [3] and the reproducibility of RF sputtering sulfides is far from evident. In both cases, high deposition and/or annealing temperatures are required to obtain well-crystallized luminescent thin films and $H_2S$ is needed. Hence, research efforts towards new low cost and easily scalable deposition techniques are required. Furthermore, sulfides have a rather high refractive index (e.g. 2.1 for SrS), which leads to optical outcoupling problems in thin film applications. Consequently, the possibility of obtaining a textured thin film surface could be advantageous as well. Recently, Van Haecke et al. optimized a low temperature solvothermal synthesis method for (Ca,Sr)S:Eu particles [4,5]. Depending on the synthesis conditions, regular octahedron-shaped particles are obtained, with size ranging from a few hunderd nanometers to a few micrometers. The method uses a low temperature ($T_{max}$ = 200°C), does not involve toxic $H_2S$ and presumably is easily scalable. In this paper we describe a modification of this method for the deposition of crystalline, textured and luminescent thin films.

## 2. EXPERIMENTAL SETUP

The solvothermal synthesis process uses ethylenediamine as a solvent and a mixture of dried chlorides ($CaCl_2$, $SrCl_2$, and $EuCl_3$) and sulfur. Capping agents, such as thioglycerol, are added as well. Then the mixture is put in an autoclave and heated to a temperature in the range from 180 to 200°C. More details on this synthesis method, as used for the production of europium-doped alkaline earth sulfide particles can be found elsewhere [4,5]. Undoped

sulfide thin films with a thickness of 20 to 50nm were deposited by electron beam evaporation on silicon or vycor and used as template layers. Then, the substrates with a typical size of 1 by 4 cm² were inserted in the autoclave for a synthesis process under conditions similar to those used for particle production. The crystallinity of the as-obtained thin films was measured with θ-2θ x-ray diffraction. Pole figures were recorded with a diffractometer (Bruker D8) equipped with an Euler cradle to study the crystallographic orientation of the thin films. The morphology of the layers was studied by means of scanning electron microscopy (FEI Quanta 200F). Luminescence was studied with a fluorescence spectrometer (FS920, Edinburgh Instruments).

## 3. RESULTS AND DISCUSSION

### *3.1 Luminescence*

First of all, we discuss the results of solvothermally deposited CaS:Eu thin films on templated silicon substrates. Upon recovering the samples from the autoclave, a bright and homogeneously luminescent layer was observed under UV excitation. Fig. 1 shows the photoluminescence spectrum with a single emission peak at 650nm (FWHM = 68nm), which is identical with the emission from bulk material [6].

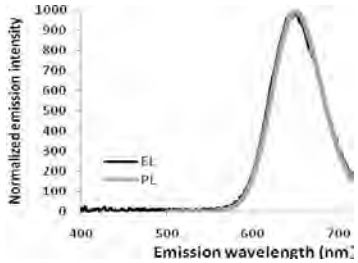


Figure 1: PL and EL emission spectrum of a CaS:Eu thin film solvothermally deposited onto a templated Si substrate.

The thin films were also electrically contacted to evaluate if the films can be used for electroluminescence applications. Fig. 1 shows the EL emission spectrum, obtained at a driving frequency of 1kHz. For SrS:Eu the emission peaks at 610nm, in line with bulk material (not shown).

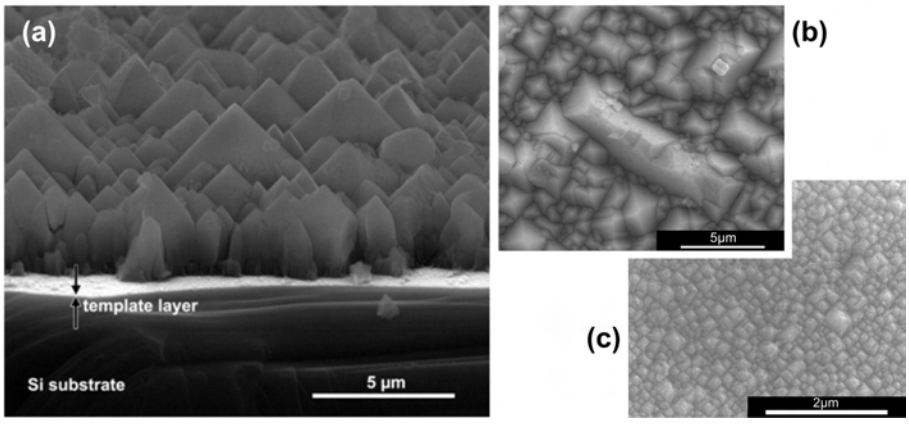


Figure 2: SEM images of solvothermally grown CaS:Eu thin films on templated Si substrates. (a) cross-section, (b) top-view and (c) top-view of a thin film with much smaller grain size.

### *3.2 Morphology*

The morphology of the layers was studied with scanning electron microscopy. From the edge-on view shown in Fig. 2, one readily observes the strongly textured surface of the solvothermally deposited thin film. The average thickness is about 2.5µm, with the surface terminated by pyramid-shaped crystallites. In Fig. 2 the template layer is barely visible, given its small thickness of about 40nm. The deposited thin film is densely packed and no voids between the crystallites are visible with SEM. Furthermore, we observed a homogeneous growth of the deposited thin film over large parts of the templated substrate.

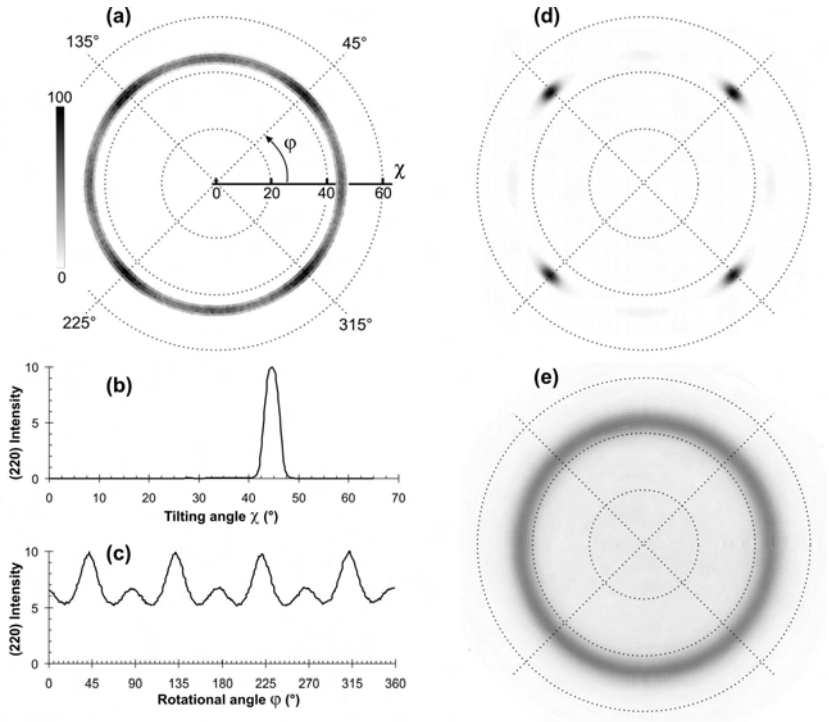


Figure 3 (a) Pole figure for the (220) diffraction of a CaS:Eu thin film deposited on template Si; (b) (220) diffraction intensity at $\varphi$ = 45° as function of the tilt angle (rocking curve); (c) (220) diffraction intensity at $\chi$ = 45° as a function of the rotation angle ($\varphi$-scan); (d) (220) pole figure for an almost epitaxially grown CaS:Eu thin film on templated Si and (e) (220) pole figure for a CaS:Eu thin film grown on a template vycor substrate.

In the x-ray diffraction pattern, recorded in a $\theta/2\theta$ configuration, only the diffraction peaks belonging to the (200) planes are visible. This points to a strong preferential orientation of the CaS crystallites. Pole figures were recorded for the (220) diffraction (Fig. 3) to further analyse the crystallographic orientation of the thin film. This confirms the preferential orientation, with all the diffraction intensity observed at a tilt angle $\chi$ of 45°. Fig. 3(c) shows the diffraction intensity at $\chi$ = 45°, depending on the in-plane rotation $\varphi$. Next to a contribution from a random orientation, 4 minor peaks (at $\varphi \sim 0$, 90, 180 and 270°) and 4 major peaks (at $\varphi \sim$ 45, 135, 225 and 315°) are observed. From SEM images of the thin film surface, this tendency for in-plane orientation was confirmed by evaluation of the orientation of the pyramid-like crystallites (Fig.2(b)). By variation of the synthesis conditions, the degree of in-plane orientation could be changed to an almost epitaxial growth (Fig. 3(d)), as the lattice constant of CaS (0.5695 nm) is only 4.8% larger than that of Si (0.5431 nm).

### *3.3 Growth mechanism*

To understand this preferential growth, the template layer was studied separately by x-ray diffraction. Due to the small thickness of the layer (tens of nm only), the x-ray diffraction intensity was very low, but a slight preferential orientation of the template layer was observed as well. CaS is known to show a preferential orientation upon deposition with electron beam evaporation. Importantly, a fully crystallized and well oriented solvothermal thin film is obtained, even if the crystallinity of the template layer is relatively poor. As the x-ray diffraction data on the template layers were not conclusive, transmission electron microscopy was performed as well to study the solvothermal growth process on the template layer. The template layer consists of small grains with a random orientation, although a bias towards (200) out-of-plane orientation is observed. By using selected area diffraction and dark field imaging, it could be proven that the pyramid-terminated grains are single-crystals, extending from the substrate to the surface of the thin film. Furthermore, the large grains originate from small seed crystals in the template layer, with the (200) out-of-plane oriented grains overgrowing grains with deviating orientation. At the interface of the large solvothermally grown particles, the secondary growth of (small) crystallites could be observed, often with a 45° orientation, in line with Fig. 3.

The influence of the substrate on the solvothermal growth was investigated by inserting templated Vycor (Corning 7913) glass substrates into the autoclave. On Vycor, the solvothermally deposited layer was again oriented with (200) parallel to the substrate surface, but no in-plane orientation was observed. Given the amorphous structure of the Vycor substrate, this could be expected. Hence we can conclude that the growth of the thin films with (200) out-of-plane orientation and (111) faceted pyramids is thermodynamically driven, as this is similar to the habitat observed for the solvothermal synthesis of single particles (i.e. octahedrons). Whether in-plane orientation is present or not, depends on the type of substrate and the microstructure of the template layer.

Finally, we patterned the template layer to allow the spatially controlled solvothermal growth of the sulfide layer. This was verified in two ways, as (1) no growth occurs on bare Si or Vycor substrates and (2) no growth occurs on e-beam deposited $Al_2O_3$ on top of the sulfide template layer. The latter effect was verified by deposition of small dots of $Al_2O_3$ through a mask. It was observed in SEM after the solvothermal deposition that the $Al_2O_3$ dots remained clear of thin film growth.

## 4. ACKNOWLEDGMENTS

PFS is a post-doctoral fellow of the Fund for Scientific Research - Flanders (FWO). This research was carried out under the Interuniversity attraction poles programme IAP/VI-17 (INANOMAT) financed by the Belgian State, Federal science policy office.

## 5. REFERENCES

[1] P. F. Smet, D. Poelman, and R. L. Van Meirhaeghe, J. of Appl. Phys. 95 (2004) 184-190
[2] P. F. Smet, K. Korthout, J. E. Van Haecke, and D. Poelman, Mat. Sci. Eng. B 146 (2008) 264-268
[3] K. Onisawa, M. Fuyama, K. Taguchi, K. Tamura, and Y. A. Ono, J. Electrochem. Soc. 135 (1988) 2631-2634
[4] J. E. Van Haecke, P. F. Smet, K. De Keyser, and D. Poelman, J. Electrochem. Soc. 154 (2007) J278-J282
[5] C. R. Wang, K. B. Tang, Q. Yang, C. H. An, B. Hai, G. Z. Shen, and Y. T. Qian, Chem. Phys. Lett. 351 (2002) 385-390
[6] P. F. Smet, J. E. Van Haecke, F. Loncke, H. Vrielinck, F. Callens, and D. Poelman, Phys. Rev. B 74 (2006).

# Hierarchical nanostructured $TiO_2$ with enhanced photocatalytic activity.

**F. Di Fonzo [1,2], V. Russo1 [2], C.S. Casari1 [2], A. Li Bassi1 [2], F. Brunella [1], C.E. Bottani [1,2]**

1. Dipartimento di Chimica, Materiali e Ingegneria Chimica 'G. Natta'
2. NEMAS - Center for NanoEngineered MAterials and Surfaces
Politecnico di Milano Piazza Leonardo da Vinci, 32 I-20133 Milano, Italy

Nanostructured titanium oxide is a relevant material for a number energy scavenging technologies: Dye Sensitized Solar Cells (DSSC), organic photovoltaics (OPV), photocatalysis for direct hydrogen production and environmental remediation [1-4]. For all these applications several requirements are of desire: very high specific surface area, well defined path for electron conduction, and optimized optical ed electronic properties. A fine control over these wide class of material characteristics is a very challenging and largely unsolved task. In this work, we report on the production, by Pulsed Laser Deposition (PLD), of a peculiar nano and mesostructured architecture resembling a "forest of trees". Noticeably, deposition is performed at room temperature in a bottom-up approach allowing the assembling of ultra-fine nanoparticles (<10 nm) in 1D "tree like" structures and these in a "forest" superstructure. In much the same way a forest has a hierarchical structure starting from the single tree with trunk, branches and leaves up to the entire tight forest assembly, this superstructure maximizes the gaseous exchange with the atmosphere maximizing specific area, while optimizing exposure to light. Ablating a titanium target by means of an excimer laser (KrF, 249 nm) in an oxygen rich atmosphere, it is possible to create different hierarchical organizations of $TiO_2$ nanoparticle by varying deposition conditions. Very high void fractions are achievable, up to 92% at 40 Pa, with a corresponding drop in density down to a tenth of the bulk value, while preserving the hierarchical order. Parallel to the change in morphology, a well-defined evolution in phase and grain size occurs. Raman spectroscopy and X-ray diffraction indicate as-deposited films being prevalently amorphous. After annealing the dominant crystalline phase is anatase with an increasing rutile content with pressure. Parallel to morphology and phase change, grain size gets smaller with increasing deposition pressure: from 20 nm to 6 nm. HRSEM observations show negligible grain growth and suggest that crystalline domains coincide with the constituents nanoparticles. Enhanced photocatalytic activity was demonstrated with respect to standard P25 powder even for as deposited samples. The "forest of trees" superstructure holds promise not only for photocatalysis, but also for advanced PV technologies (DSSC and OPV) thanks to the tunable and accessible porosity and to the interconnected 1D path for efficient charge collection [5]

[1] B. Oregan and M. Gratzel, Nature 353, (1991) 737–740
[2] G. Yu, J. Gao, J.C. Hummelen, F. Wudl, A.J. Heeger, Science, 270 (1995), 1789-1791
[3] K. Honda and A. Fujishima, Nature 238, (1972) 37−39.
[4] O. Carp, C.L. Huisman, A. Reller Progress in Solid state Chemistry 32(2004), 33-177
[5] M. Adachi, Y. Murata, J. Takao, J. Jiu, M. Sakamoto, F. Wang, J. Am. Chem. Soc. 126 (2004), 14943

# Comparison between wet deposition and plasma deposition of silane coatings on aluminum for surface passivation

**A. Batan [1, 2], F. Brusciotti [3], I. De Graeve [3], J. Vereecken [3], H. Terryn [3], M. Wenkin [4], M. Piens [4], J.J. Pireaux [2], F. Reniers [1]**

1. Université Libre de Bruxelles (ULB), Faculty of Sciences - Analytical and Interfacial Chemistry, Brussels, Belgium, abatan@ulb.ac.be, tel 0032 2 6505953 fax 0032 2 6502934.
2. University of Namur (FUNDP), Research center in Physics of Matter and Radiation (PMR), Namur, Belgium, abdelkrim.batan@fundp.ac.be.
3. Vrije Universiteit Brussel (VUB), Department of Metallurgy, Electrochemistry and Materials Science (META), Pleinlaan 2, 1050 Brussels, Belgium;
4. Coating Research Institute (CoRI), Limelette, Belgium.

The need to develop new environmentally friendly pre-treatments in the surface engineering of aluminum substrates has become more and more important. This is mainly due to the toxic and carcinogenic properties of the chromium-based surface pre-treatments frequently used in this industry. During the last decade, simple solution-dip silane-based pre-treatments have emerged as promising candidates for the replacement of the currently used pre-treatments of aluminum. Such silane systems act as a barrier for the corrosion protection. In addition to deposition from wet aqueous solutions (dip-coating, for example) more and more often plasma deposition is considered for several reasons such as health and environmental issues, flexible deposition, etc. One of the aims of this work is to determine whether plasma deposition can result in innovative properties and compete with traditional wet methods. Hybrid organic/silicon-based coatings were deposited on Al 99.99% substrates using three different techniques: wet aqueous solution deposition, atmospheric plasma and vacuum plasma deposition. The silane selected was a non-functional one, i.e. Bis-1,2-(triethoxysilyl)ethane (BTSE). The structure and composition of the deposited coatings have been investigated as a function of the deposition process parameters. Fourier-transform infrared spectroscopy, X-ray photoelectron spectroscopy and FEG-SEM were used to characterise the structure, composition and surface morphology of the silane coatings. Of special interest is to compare the different deposition technologies with each other. The FTIR evidences groups such as Si-O-Si, Si-O-C, Si-$CH_3$, and $CH_3$. The deposited layers can be considered as polymer-like coatings, comparable to the silane layers obtained by wet deposition methods.

## 1. INTRODUCTION

Silanes are mostly investigated as an alternative for the chromium-VI containing conversion treatments [1] for corrosion protection and adhesion promotion of metals. Silane coatings are environmentally sound, multi-metal [2-11] surface pre-treatments.

Silanes are hybrid molecules containing organic groups such as methoxy or ethoxy ones bound to silicon atoms. Additional functional groups, such as amines, epoxides or others, may be present to promote adhesion with covering organic coatings. Films are mostly deposited

from solutions through dipcoating or rollcoating. In these wet deposition methods, addition of water to the silane molecules is required to hydrolyse the methoxy or ethoxy groups to form functional silanol groups i.e. $X\text{-}SiOCH_2CH_3 + H_2O \rightarrow X\text{-}SiOH + CH_3CH_2OH$. Silanol groups are essential to form a covalent Si-O-metal bond at the metal/film interface [12] and for cross-linking in the bulk of the silane layer upon thermal curing. Cross-linking is due to the condensation of silanol groups i.e. $X\text{-}SiOH + HOSi\text{-}X \rightarrow X\text{-}SiOSi\text{-}X + H_2O$.
In the present work silane films will be deposited by different methods. Traditional wet deposition will be compared to plasma deposition where no solutions or solvents are required.

## 2. EXPERIMENTAL

For wet deposition (dipcoating), films were formed from 5% water-based solutions of BTSE (bis-1,2-(triethoxysilyl)ethane), provided by Chemetall GmbH. BTSE is considered as a basic silane in various commercial silane mixtures for thin-film deposition.
The atmospheric plasma apparatus consisted of a SurfX Technologies LLC, A-250D deposition system. The system was operated at 13.56 MHz (RF). The geometry is a cylindrical plasma torch, ending with a 5 $cm^2$ showerhead. The plasma was formed by feeding the process gas, argon, into the system, upstream of the electrodes at a flow rate of 30.0 L/min. The BTSE (98 wt%) precursor was kept in a temperature controlled bath at 100 °C and introduced into the plasma, downstream of the electrodes (in the post-discharge), by bubbling argon through the liquid monomer. Samples were processed at different deposition times, and at different plasma powers at a distance of 0.5 cm from the showerhead.
For vacuum plasma deposition, inductively coupled radio frequency glow discharge plasma deposition is used on BTSE vapour monomer. The plasma chamber consisted of a grounded steel chamber, with in the center a sample holder, and a 13.56 MHz plasma source (ICP-P 200, JE PlasmaConsult GmbH, Germany).
The metal under investigation is 99.99% aluminium, electropolished and alkaline pre-treated.

## 3. RESULTS AND DISCUSSION

### *3.1. Films formed by wet deposition*

In figure 1A silane films deposited by dipcoating from water-based solutions of 5 wt% BTSE is shown in cross-section using FEG-scanning electron microscopy. The morphology of the water-based dipcoating BTSE layers is depending on the solution concentration used, with a higher concentration resulting in a denser and more compact layer. The BTSE film thickness is generally between 50 nm and 1 μm, depending on the concentration used [13, 14].

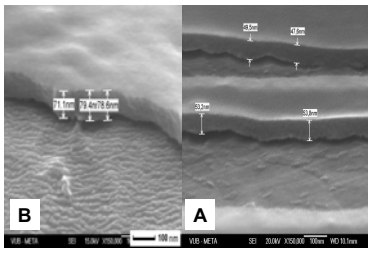


Figure 1. SEM picture of the film cross-section of a BTSE film deposited on Al by wet deposition (A), vacuum plasma (B)

In figure 2 (trace A) the IR spectra shows the typical IR absorption bands of a BTSE silane layer. Upon thermal curing of these layers the IR absorption signal of the Si-O-H bonds decreases and the one of the Si-O-Si bonds increases [15], indicating condensation reactions between silane molecules in the bulk of the layer, resulting in a cross-linked network. This network formation increases the barrier properties against hydration and corrosion of the

substrate, as was observed using electrochemical impedance spectroscopy [15] (not shown). The composition within the polymer measured by XPS (figure 3 (trace A)) corresponds to $SiO_{1.6}C$.

### *3.2. Vacuum plasma deposition*

Films were deposited at plasma powers of 200 W, 0.3 Torr, with a deposition time of 5 min. Figure 2 (trace B) presents the infrared (IR) survey spectrum of pp-BTSE film, about 70 nm thick (see Figure 1B). One can observe a significant amount of dimethylsilyl groups in the polymer which can only be formed by the cleavage of the Si-C bond. Siloxane (Si-O-Si), dimethylsilyl (Si-$(CH_3)_2$), trimethylsilyl (Si-$(CH_3)_3$) are clearly visible. Possible $CH_2$ wagging vibrations of Si–$CH_2$–Si groups at 1000–1020 $cm^{-1}$ overlap with the Si–O–Si stretching vibration at 1200–1000 $cm^{-1}$. However, by the comparison of the relative intensities between $CH_3$ ($\nu_{as}(CH_3)$ 2960 $cm^{-1}$, $\nu_s(CH_3)$ 2903 $cm^{-1}$) and $CH_2$ ($\nu_{as}(CH_2)$ 2928 $cm^{-1}$, $\nu_s(CH_2)$ 2860 $cm^{-1}$) stretching vibrations, the concentration of $CH_2$ is rather low.
The composition within the polymer measured by XPS (figure 3 (trace B)) corresponds to $SiO_{1.7}C_{0.7}$. In agreement with the IR spectra, the oxygen in the polymer is found to be mainly bound to silicon (deconvolution not shown).

### *3.3. Atmospheric plasma deposition*

Films were deposited at different plasma powers with a different deposition time. Three bands are present at: 1154, 912, 712 $cm^{-1}$ in the infrared spectra of pp-BTSE films (figure 2 (trace C)). By varying the input power (not shown), a small shift of these bands is observed. This could be a consequence of the local environment of the Si–O groups which varies with the coating nature. Indeed, Si–O bonds exist both in Si–O–Si where Si atoms are bound to H atoms or $CH_3$ groups and Si-O-C groups with the same vibrations frequency. No significant shift is observed by varying the deposition time (not shown).

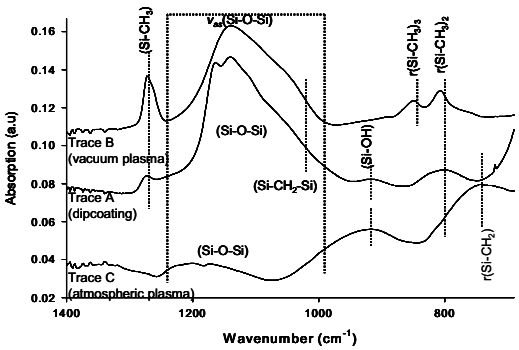


Figure 2. Infrared spectra of BTSE film deposited on Al by wet deposition (trace A), vacuum plasma (trace B), atmospheric plasma (trace C)

The composition within the polymer measured by XPS (figure 3 (trace C)) corresponds to $SiO_{1.8}C_{0.2}$. In agreement with the IR spectra, the oxygen in the polymer is found to be mainly bound to silicon (deconvolution not shown). The concentration of oxygen measured by the ex situ XPS spectrum might be slightly higher than the one extracted from the IR-spectrum, because of the XPS sensitivity to the surface and of film surface oxidation when the sample was exposed to air before it could be introduced into the ultra high vacuum chamber of the XPS. It is known from the literature that the residual free radicals within the plasma polymer react with water and oxygen from the atmosphere and thus increasing the oxygen content in the polymer network.

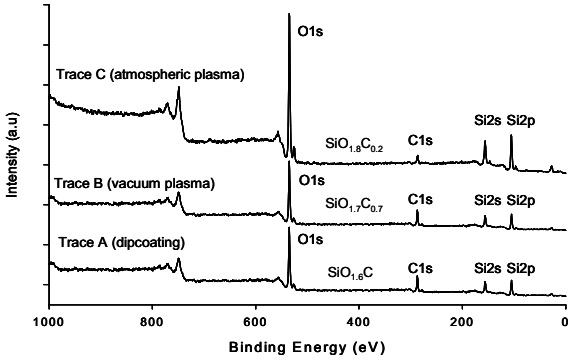


Figure 3. XPS survey spectra of BTSE film deposited by wet deposition (trace A), vacuum plasma (trace B), atmospheric plasma (trace C)

## 4. CONCLUSIONS

Using wet deposition, thin silane polymeric layers are formed with a uniform morphology depending in porosity on the solution concentration and deposition method used. The films can be cured to create barrier properties for corrosion protection.

BTSE coatings can be deposited by plasma (both atmospheric and vacuum) deposition. It should be emphasized that the literature did not report any previous deposition of PP-BTSE films by atmospheric and vacuum plasma. XPS and IR measurements attest for the presence of silicon under Si-O state in the layers deposited by the different methods. The FTIR evidences groups such as Si-O-Si, Si-O-C, Si-$CH_3$, and $CH_3$. The deposited layers can be considered as polymer-like coatings, comparable to the silane layers obtained by wet deposition methods. SEM images of coatings cross-sections show that the film deposited by wet and vacuum plasma deposition look comparable.

Additional work is currently going on to optical constant measurements of the BTSE films depending on the deposition methods by Visible Light Spectroscopic Ellipsometry (VISSE). Corrosion properties for films deposited by plasma will also be performed.

## ACKNOWLEDGEMENTS

The project partners VUB, ULB, FUNDP and CoRI gratefully acknowledge the Belgian Science Policy for funding of the FOMOS project (P2/00/04) in the “Programme to stimulate knowledge transfer in areas of strategic importance”. www.belspo.be

## REFERENCES

[1] R.W. Hinton, Metal Finishing 89 55 (1991)
[2] M.A. Petrunin, A.P. Nazarov, Y.N. Mikhailovski, J. Electrochem. Soc. 143 251 (1996)
[3] A.M. Beccaria, L. Chiarttini, Corros. Sci. 41 885 (1999)
[4] W.J. van Ooij, D. Zhu, Corrosion 57(5) 413 (2001)
[5] A. Cabral, R.G. Duarte, M.F. Montemor, M.L. Zheludkevich, M.G.S. Ferreira, Corr.Sci. 47 (3) 869 (2005) [6] A.M. Beccaria, C. Bertolotto, Electrochim. Acta 42 1361 (1997)
[7] R. Tremont, H. De Jesus-Cardona, J. Garcia-Orozco, R.J. Castro, C.R. Cabrera, J. Appl. Electrochem. 30 737 (2000)
[8] V. Subramanian, W.J. van Ooij, Corrosion 54 204 (1998)
[9] W. Trabelsi, L. Dhouibi, E. Triki, M.G.S. Ferreira, M.F. Montemor, Surface & Coatings Techn. 192, 2-3 284 (2005)
[10] W.J. van Ooij, A. Sabata, Surf. Interface Anal. 20 475 (1993)
[11] F. Zucchi, G. Trabanelli, V. Grassi, A. Frignani, Proc. Eurocorr01, Associazione Italiana di Metallurgia (2001).
[12] E.P. Plueddemann, “Silane Coupling Agents”, 2nd ed., Plenum Press., New York, (1990)
[13] A. Franquet, C. Le Pen, H. Terryn, J. Vereecken, Electrochimica Acta 48 1245-1255 (2003)
[14] A. Franquet, J. De Laet, T. Scharam, V. Subramanian, W. J. Van Ooij, J. Vereecken, Thin Solid Films 384 37-45 (2001)
[15] I. De Graeve, J. Vereecken, A. Franquet, T. Van Schaftinghen, H. Terryn, Progress in Organic Coatings 59 224 (2007)

# Study of nanoparticles formation in pulsed plasma polymerization of acetylene

**V. De Vriendt [1], F. Maseri [2], A. Nonet [1], S. Lucas [1]**

1. University of Namur (FUNDP), Research center in Physics of Matter and Radiation (PMR), Rue de Bruxelles 61, 5000 Namur, Belgium

2. ArcelorMittal Liège, Research and Development, Boulevard de Colonster 57, 4000 Liège, Belgium

The plasma polymerization is an established technique for the dry deposition of thin polymeric films. Films deposited by plasma polymerization are free of pinholes and remnants of initiator or solvents used in conventional polymerization. Moreover, it is of technological interest that, in principle, the deposition of plasma polymer coatings is possible on any material of any shape in the desired thickness. More precisely, this work concerns the pulsed plasma polymerization. In pulsed discharges the power input is delivered periodically to the plasma ($t_{ON}$), and switched off, or reduced to a certain fraction, during off time ($t_{OFF}$). Pulsed plasma deposition processes offer a rather low power input, a reduced extent of fragmentation of the monomer in the gas phase, combined with a lowered UV damage and a less energetic ion bombardment at the film surface. The aim of this work is to study at $10^{-1}$ Torr, the influence of $t_{OFF}$ parameter (and discharge power) on roughness, morphology and wettability of films deposited on silicon substrate, by pulsed magnetron discharge from a carbon target with acetylene gas precursor. By using a low power discharge (long $t_{OFF}$ and short $t_{ON}$); a roughness is induced and increases the hydrophobic properties of films. The coating is formed of nanoparticles and fractal agglomerates (called "flowers" of micrometric size). The growth mode of fractal agglomerates occurs in several steps as revealed by different scanning electron microscope (SEM) pictures. First, nanoparticles are observed on the substrate. Secondly, a filament-like structure develops from a nanoparticle interface to form later flowers-like objects. In order to understand growth mechanisms of hydrocarbon nanoparticles and fractal agglomerates, mass spectrometry analyses in acetylene plasma were achieved. These analyses highlight that hydrocarbon nanoparticles are formed in gas phase and contain several (tens of) carbon atoms.

# Electrochemical Nucleation and Growth of Copper

**A. Radisic**
IMEC vzw, Kapeldreef 75, B-3001 Leuven, Belgium

Electrodeposition is the current method used in forming copper interconnects in integrated circuits, primarily due to the ability of this technique to fill high aspect ratio features with complex geometries at high deposition rates, leading to high throughput and lower manufacturing costs. Important processing steps prior to electroplating involve the deposition of a thin diffusion barrier layer, to prevent copper diffusion into silicon, and deposition of a copper seed layer by means of physical vapor deposition (PVD). The copper seed layer provides good electrical contact and improved adhesion to the diffusion barrier layer. As the feature sizes in integrated circuits continue to decrease, industry is forced to explore the possibility of electrochemical deposition of high quality copper films without the use of a copper seed layer. It is not a priori clear that it will be possible to achieve the "superfilling" effects without the copper seed layer.

The growth of copper films on diffusion barrier materials typically occurs through Volmer-Weber (3D island) mode of growth. As a result, high island densities are essential in depositing continuous thin films. For complex structures with small length scales, such as trenches and vias in integrated circuits, a detailed understanding of nucleation and growth, and the influence of parameters such as potential and solution chemistry on the deposition mechanism is critical in designing processes for obtaining the void-free features.

The primary goal of this research project is to improve the understanding of the electrochemical nucleation and growth processes necessary for successful electrodeposition of copper onto other substrates (TiN or TaN, for example). The mechanism of nucleation and growth of copper deposited from different plating solutions is studied using electrochemical techniques such as cyclic voltammetry, chronoamperometry, and rotating disc electrode techniques. Deposited films are characterized using scanning electron microscopy (SEM), atomic force microscopy (AFM), and other appropriate surface characterization techniques. Using the results from these experiments we will optimize procedures for electrodeposition of continuous, high quality copper films on different substrates.

# Stacking fault suppression in ion assisted growth of Ir on Ir(111)

**S. Bleikamp**[1], **T. Michely**[1]
1. Physikalisches Institut, Universität zu Köln, Germany

Due to their low energy, stacking faults are among the most frequent defects in thin films. They critically influence the properties of thin films and devices and strategies for their avoidance are needed.
In homoepitaxy of Ir on Ir(111) around room temperature, stacking faults are formed in large numbers, which propagate through the growing film, causing extended defect structures. Eventually thin Ir films become heavily twinned and grow rough due to the twin associated defects.
Here we present kinetic strategies for the avoidance of stacking fault propagation and defect structure formation based on ion assistance. Ir is evaporated with ion assistance of 100eV $Ar^+$ ions at normal incidence with an ion to atom arrival ratio of R=1:2 or with ion assistance of 500eV $Ar^+$ ions incident at an angle of 85° with respect to the surface normal with R=1:10. Based on scanning tunneling microscopy investigations we find that this treatment transfers the growth mode to layer-by-layer growth and no twin crystallites are formed. The result is backed up by low energy electron diffraction measurements. Annealing shows that a significant amount of noble gas is incorporated in the films during growth. Gas incorporation could be avoided, if the necessary energy could be supplied to the Ir atoms themselves.
Analysis of the atomic processes involved indicates that the key action of the ions is to destroy the defect structures stabilizing the faults, rather than to suppress fault nucleation.

umicore
Thin Film Products

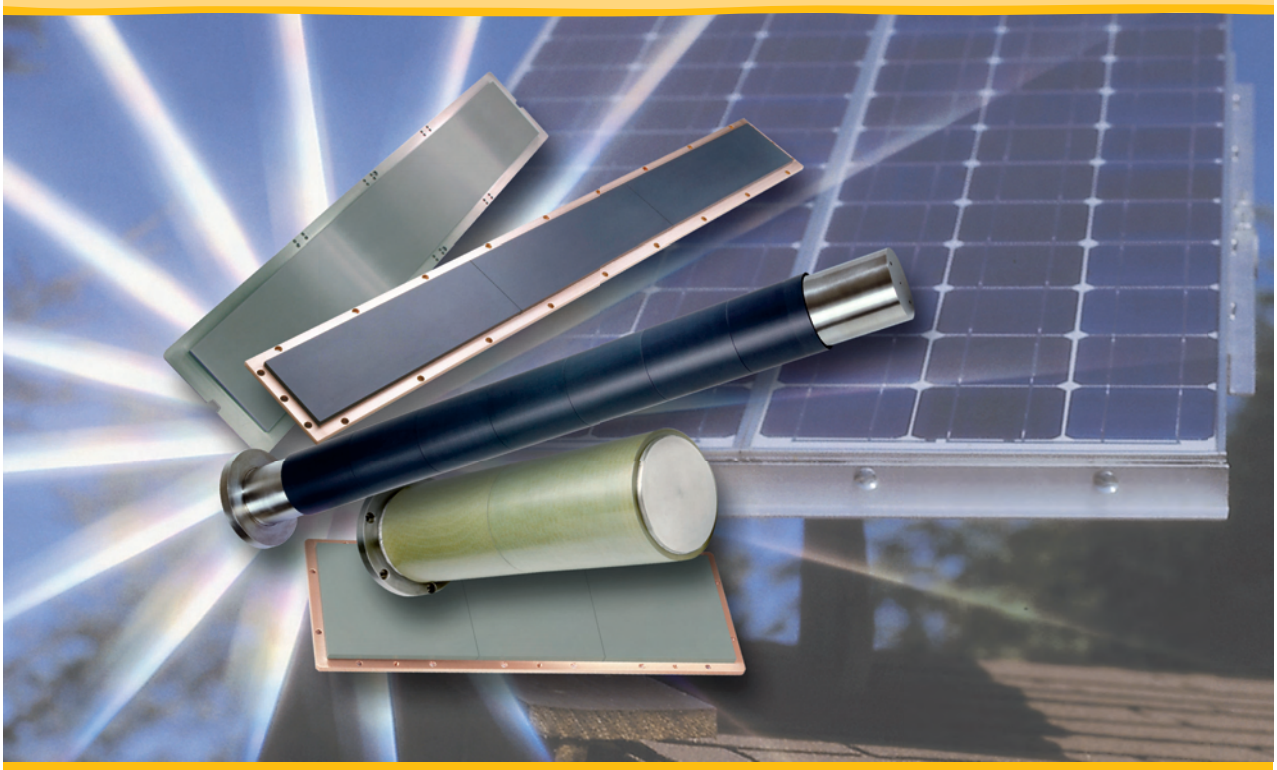

# Umicore Thin Film Products – Excellence in the field of Large Area Coating

Umicore Thin Film Products is a leading developer and manufacturer of sputtering targets and evaporation materials for all displays, photovoltaics, and glass coating applications.

The extensive product portfolio – including large rotatable target configurations – is supported by a closed recycling loop program, state-of-the-art R&D, local sales offices and customer service centers around the world.

Thanks to innovation, creativity, and a worldwide close co-operation with customers, system manufacturers, and research laboratories, Umicore Thin Film Products offers a unique expertise in the development of materials for current and future customer needs.

sales.materials@umicore.com

**www.thinfilmproducts.umicore.com**

Your Partner in Vacuum

**VACOTEC b.v.b.a**
Stationstraat 180 bus 21
3110 Rotselaar
Belgium

Tel. +32 16 622766
Fax +32 16 353539
info@vacotec.be
www.vacotec.be

VACOTEC, founded in 1993, is a customer-oriented 'Sales & Services Company' in the field of vacuum technology for the 'BENELUX Market'. VACOTEC the expert partner for installation & maintenance of vacuum equipment, including components, vacuum pressure measuring instruments, auxiliaries for production plants, consumables and spare parts.

VACOTEC's product range covers standard and customized vacuum connections and vacuum chambers with 'state-of-the-art' components for quick fastening and sealing, valves, flexible welded bellows and all materials required for high- or ultra-high vacuum.

**VACOTEC offers**
- Vacuum components, pumps and lubricants
- Custom-made bellows and vacuum chambers
- Maintenance and repair of installations and pumps
- Re-engineering of existing installations

**Partners**

**www.vacotec.be**

# Film microstructure control and characterization of plasma- deposited $SiO_2$-like films

**M.C.M. van de Sanden, N.M. Terlinden, G. Aresta, M.Creatore**
Plasma and Materials Processing group, Department of Applied Physics, Eindhoven University of Technology, Den Dolech 2, 5600 MB Eindhoven, the Netherlands

The ultimate control on film growth represents a challenge in PECVD: the film structure/ growth mode and the surface roughness evolution are affected by parameters such as the surface energy, growth and ion fluxes, and ion energy. In this contribution routes for microstructure control in PECVD $SiO_2$- like layers are described.
$SiO_2$ layers have been deposited in a remote expanding thermal plasma (ETP) setup enabling a good control of both the ion flux (by changing the deposition chemistry and the arc plasma parameters) as well as the ion energy by an additional RF substrate biasing or a so-called tailored ion biasing technique. The role of ion energy and ion-to-growth flux ratio on the film microstructure and densification at low substrate temperature (100ºC) has been investigated by means of ellipsometric porosimetry, which monitors the refractive index change due to the adsorption (and desorption) of ethanol vapors in the volume of macro-meso-micro pores in the $SiO_2$ layer. From the analysis of the adsorption isotherm and the presence of hysteresis during the desorption step as a function of the equilibrium partial pressure, the open porosity in the layer can be determined. In the absence of ion bombardment, an increase in growth flux is responsible for an increase in layer porosity and the transition from micro- (pore diameter < 2 nm) to mesopores (pore diameter > 2 nm). In the presence of ion bombardment, both biasing techniques lead to densification of the deposited layer, which experiences a transition from micro-/ mesoporosity to microporosity and eventually non-porosity. Although both biasing techniques also lead to a comparable critical ion energy value per deposited $SiO_2$ unit (≈ 100 eV), the ion-to-growth flux ratio and ion energy are not found to be interchangeable parameters. In fact, while the rf biasing technique allows the above-mentioned transition in a relatively small bias voltage range (down to –50V), the layers densified via the tailored ion biasing technique require a larger voltage range (down to –240V) to quantitatively remote microporosity from the deposited layer. This difference is attributed to the increasing ion-to-growth flux ratio accompanying they rf biasing, as a consequence of the rf plasma generation in front of the substrate.

# A Two-Step Process for the Preparation of Photoactive Tungsten Disulfide Layers: An Real-Time, *in situ* X-Ray Diffraction Study

**S. Brunken [1], R. Mientus [2], K. Ellmer [1]**

1. Helmholtz Centre for Materials and Energy, Dept. Solar Energetics, Glienicker Str. 100, 14109 Berlin, Germany

2. Opto-Transmitter-Umweltschutz-Technologie e.V., Köpenicker Str. 325b, 12555 Berlin

Tungsten disulfide ($WS_2$) is a possible absorber material for thin film solar cells, due to its suitable band gap (1.7 eV) and its high absorption coefficient (> $10^5$ $cm^{-1}$). Caused by the weak van der Waals bonding along the c-axis in $WS_2$, with strongly (001)-textured $WS_2$ films a recombination-inactive heterojunction can be built and used for thin solar cells.

Recently, we could show that by rapid crystallization of X-ray amorphous, sulfur-rich $WS_{3+x}$ films, strongly (001)-textured $WS_2$ films can be prepared [1]. The $WS_{3+x}$ films were deposited by reactive magnetron sputtering from a tungsten target in $Ar/H_2S$ mixtures. The crystallization is performed by rapid radiation heating of a double layer metal/$WS_{3+x}$ in an $H_2S$ atmosphere at temperatures around 700 °C. By a solid-liquid-solid process (SLS) $WS_2$ crystals are rapidly grown (within seconds), where liquid drops of metal sulfide eutectica strongly promote the crystallization by acting as nucleation seeds [1]. Different metals like nickel or cobalt can be used as crystallization promoters. The structural and morphological properties of the (001)- $WS_2$ films have been investigated by *in situ*, time-resolved energy-dispersive X-ray diffraction (EDXRD).

The electronic quality of the films has been analyzed by Hall and conductivity measurements and by time-resolved microwave conductivity (TRMC) analysis. The $WS_2$ films exhibit p-type conduction with hole mobilities up to about 80 $cm^2/Vs$. The TRMC signals are comparable to that of $WS_2$ single crystals, proving the photoactivity of these rapidly SLS-crystallized $WS_2$ films.

Besides on insulating oxides or nitrides, we were able to crystallize $WS_2$ films for the first time also on metallic films, i.e., on back contacts, a necessary prerequisite for the preparation of a thin film solar cell with a $WS_2$ absorber film. The crystallization process on insulators and metallic films is somewhat different, which was detected by the EDXRD analysis.

The window layer ZnO/ZnO:Al was deposited directly on the $WS_2$ film, as well as with an intermediate buffer film, like CdS or $ZnO_xS_y$ in order to check, if the van der Waals surfaces of $WS_2$ are recombination-inactive. The role of the metal sulfide ($NiS_x$, $CoS_x$) crystallites, which are interspersed within the $WS_2$ film, on the electrical characteristics of the cells is investigated. Selective etching of these $MeS_x$ crystallites has been investigated, too.

First results of thin film solar cells are presented, including I-V characteristics and spectral external quantum efficiency measurements.

[1] S. Brunken, R. Mientus, S. Seeger and K. Ellmer, J. Appl. Phys. 103 063501 (2008)

# Complex XRD studies of crystallization of amorphous and nanocrystalline magnetron-deposited $TiO_2$ films with different thickness

**R. Kužel [1], L. Nichtová [1], Z. Matěj [1], J. Šícha [2], J. Musil [2]**

1. Charles University, Faculty of Mathematics and Physics, Department of Condensed Matter Physics, Ke Karlovu 5, 121 16 Prague 2, Czech Republic

2. University of West Bohemia, Faculty of Applied Sciences, Department of Physics, Univerzitní 22, 306 14 Pilsen, Czech Republic

Titanium dioxide films have many remarkable properties, for example photocatalytic activity and hydrophilicity. However, these properties depend significantly on the crystallinity, phase composition and microstructure of the films. Many of the microstructural features can be investigated by X-ray diffraction (XRD) and X-ray reflectivity measurements. Crystallization of amorphous and nanocrystalline thin films with different thickness (50−2000 nm) deposited on silicon and glass substrates was studied on post-annealed samples as well as by in-situ XRD measurement. Phase composition and transitions, stresses, strains, crystallite size, textures and surface roughness were investigated. It was found that the crystallization depends strongly on the film thickness. Anatase crystallites larger than 100 nm grow rapidly in amorphous films at about 250 °C while in nanocrystalline films they remain small (below 10 nm) to relatively high temperatures (600 °C). Biaxial tensile residual stresses were found in crystallized amorphous films and gradient of phase composition was revealed by XRD depth profiling in nanocrystalline films.

## 1. Introduction

The applications of titanium dioxide in powder or thin film form are very broad and of high interest. The films are used as ultra thin film coatings, nanostructured membranes, in electrochemistry and electrocatalysis, in microoptics and electrooptics, medicine, cosmetics and in photocatalysis. These applications particularly depend on the layers properties (stability, transparency, photoconductivity, photoactivity, etc.) and their microstructure (surface area, pore size distribution, particle size, crystallographic structure). The films can be prepared by several techniques but the magnetron deposition is favourable from the point of view of mechanical durability required for practical applications. Depending on the deposition conditions, the films can be prepared as amorphous or nanocrystalline. Most of experiments show that crystalline or even better nanocrystalline form is required for obtaining desired properties. Therefore, the study of crystallization is of large interest.

Many of the microstructural characteristics can be investigated by X-ray diffraction (XRD) and X-ray reflectivity measurements (XRR). As it has been indicated previously, the crystallization depends significantly on the film thickness. Therefore sets of films with different thickness were prepared and studied during post-annealing and also by in-situ measurements in high-temperature chamber in X-ray diffractometer.

## 2. Experimental conditions

### *2.1 Film deposition*

$TiO_2$ films were sputtered by dual magnetron equipped with two Ti(99.5) targets of 50 mm in diameter and supplied by a dc–pulsed Advanced Energy Pinnacle Plus+ 5kW power supply unit operating in bipolar asymmetric mode at repetition frequency $f_r$ = 100kHz and duty cycle $\tau/T = 0.5$; here $\tau$ and T are the length of pulse and the period of pulses. Films were deposited on unheated silicon (100) substrates and also on microscope glass substrates (26 × 26 × 1 mm, for in-situ high-temperature XRD measurements 15 × 10 × 1 mm) at substrate to target distance $d_{s\text{-}t}$ = 100 mm, total working pressure $p_T$ = 0.5−0.9 Pa, average pulse discharge current $I_{da1,2}$ = 1.5−3 A and average pulse power density $W_{da} \approx 20-55$ Wcm$^{-2}$. Further details on dual magnetron system are given elsewhere [1].

### *2.2 XRD measurements and evaluation*

The measurements were performed mainly on Panalytical horizontal X'Pert MRD and X'Pert Pro vertical diffractometers in parallel beam setup, 2θ scans with the angles of incidence 0.5−1.5°, the Goebel mirror in the primary and parallel plate collimator in the diffracted beam, respectively. Residual stresses were measured by the $\sin^2\psi$ method for several different peaks using a point focus, polycapillary and Eulerian cradle. In-situ high-temperature measurements were performed in MRI high-temperature chamber with both direct and radiant heating.

Two methods of evaluation of XRD profiles were applied – *fitting of peak clusters* and *total pattern fitting*. In the former method the diffraction peaks were fitted with the Pearson VII or pseudo-Voigt functions. The correction for instrumental broadening was performed with the aid of a NIST $LaB_6$a standard. Due to severe peak overlap a method of total patter fitting is required. We have developed a new program, an extension of Fox program (see [2, 3]). This program includes now the effects of texture, stress, crystallite size distribution, strains in terms of both phenomenological and dislocation models, instrumental corrections, absorption.

## 3. Results

### *3.1 Crystallization and phase composition*

Diffraction patterns of the nanocrystalline films with different thickness were essentially distinct. The patterns for thin films (thickness 100 and 220 nm) showed dominating rutile phase with a small indication of anatase while in thicker films (above 500 nm) mainly anatase was observed (Fig. 1) [4, 5]. With annealing there were no significant changes neither in phase composition nor the microstructure of the films up to the temperatures of 600-700 °C. Then the transformation of anatase into rutile begins. XRD depth profiling by changing the angle of incidence in the range 0.3−0.5° confirmed that the rutile grows on the interface with the substrate while anatase is on the top. By isochronal post-anealing of amorphous films (in the air, step 50 °C, time 0.5 hr) it was found that the films crystallize into anatase at about 250 °C [4] and that for the films thinner than about 200 nm higher temperature is required for the crystallization. In thicker films (above 1000 nm) small amount of nanocrystalline rutile could be detected as well.

### *3.2 Strain and crystallite size*

In most cases, the values of mean crystallite size that is the dominating effect on XRD line profile broadening for the films investigated. For amorphous films the line profile analysis after both post- and in-situ- annealing showed the growth of relatively large crystallites (larger than 100 nm) already at the beginning of crystallization. By contrast, in as-deposited nanocrystalline films with the crystallite size of 5−10 nm the crystallites remained small to

relatively high temperatures (600 ºC). This was true for both phases – anatase and rutile. The dependence of crystallite size and microstrain of anatase on the annealing temperature is shown on Fig. 2. In two-phase films the rutile often forms smaller crystallites than anatase. The mean crystallite size in the as-deposited nanocrystalline rutile is 5−7 nm, for anatase the mean value is slightly higher (7−10 nm).

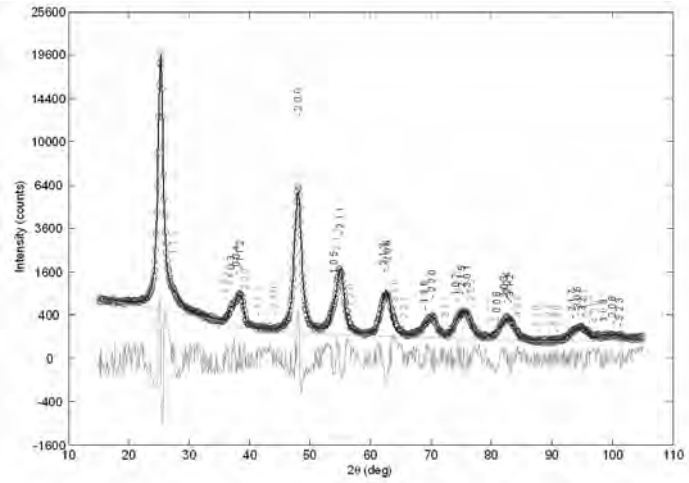


Figure 1. Example of total pattern fitting for nanocrystalline anatase (thicker indices) with small amount of rutile (thinner indices).

### *3.3 Residual stresses*

Significant shifts of diffraction peaks were observed and tensile residual stresses were confirmed by the $\sin^2\psi$ method for different diffraction peaks. They decrease with the increasing film thickness and usually are removed by annealing above 500 °C. The tensile stresses arise in particular during the crystallization of amorphous films, as it has been confirmed by high-temperature in-situ XRD measurements [6]. The stresses of the order of hundreds of MPa are of simple bi-axial type as follows from the linearity of the $\sin^2\psi$ plot of interplanar spacing $d$ but the strain show systematic anisotropy ($hkl$ dependence) [4]. For nanocrystalline films the stresses are small but complicated with strongly nonlinear $d$ vs. $\sin^2\psi$ plots. This is caused by general non-fiber texture.

### *3.4 Textures*

After crystallization of amorphous films the anatase indicated nearly random grain distribution except very thin films. However, variations of texture were observed at the beginning of crystallization when the crystallites with the (00l) orientation were developed (on Si single crystal substrates). The texture was symmetrical – fiber. Pole figure measurement for nanocrystalline films showed more complicated textured which is related to the dual magnetron geometry.

### *3.5 Reflectivity, surface roughness*

Reflectivity measurements were used for study of changes of surface roughness and for thinner films also as a check of the film thickness (from the Kiessig oscillations). As it can be expected, the surface roughness increased after crystallization of amorphous films and increased further with annealing temperature. The roughness was also increasing significantly with the film thickness.

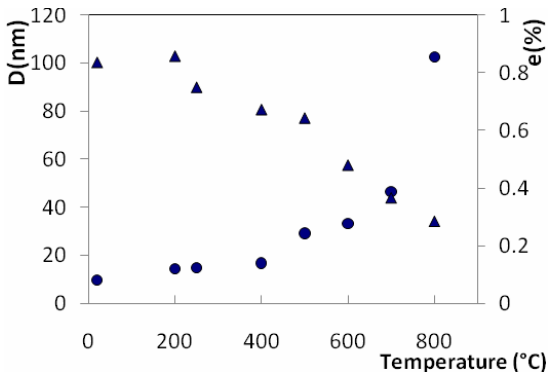


Figure 2. Dependence of the mean crystallite size (D, left axis, triangles) and microstrain (e, right axis, dots) on annealing temperature. The values were obtained by total pattern fitting.

### *3.6 In-situ high-temperature measurements*

In-situ HT XRD measurements confirmed that crystallization of amorphous $TiO_2$ films begins above 220 °C for thicker films but only above 260 °C for the films thinner than about 100 nm. Time dependences of peak intensities, widths and positions were studied in detail at somewhat lower temperatures where the crystallization is slow. XRD peak widths were quite narrow from the beginning of crystallization, peak position were changing due to the tensile stress arising and the intensities proportional to the volume fraction of crystalline anatase phase were changing in accordance with the Avrami equation. Initial time of crystallization is increasing and the speed of crystallization decreasing significantly with the decreasing of the film thickness, in particular below about 500 nm. More details are given in [6].

## 4. Summary

X-ray diffraction in different geometries and reflectivity measurements proved to be very useful methods for characterization of titanium dioxide thin films, since they can reveal many of their important microstructural features – crystallization, phase transitions, phase gradients, evolution of crystallite size, microstrain, residual stress and texture, surface roughness. Strong dependence of some of them, in particular – crystallization process, on the film thickness has been found. This was further confirmed by detailed high-temperature XRD measurement of time dependence of crystallization.

## 5. References

[1] J. Musil, D. Heřman, J. Šícha , J. Vac. Sci. Technol. A, Vol. 24, No.3 (2006).
[2] R. Kužel, L. Nichtová, Z. Matěj, J. Šícha, J. Musil, Z. Kristallogr. (2008) in press.
[3] Z. Matěj, L. Nichtová, R. Kužel, Materials Structure, Vol. 15, No. 1, (2008), open acces at http://www.xray.cz/ms.
[4] R. Kužel, L. Nichtová, Z. Matěj, D. Heřman, J. Šícha, J. Musil, Z. Kristallogr. Suppl. 26 247-252 (2007).
[5] R. Kužel, L. Nichtová, Z. Matěj, D. Heřman, J. Šícha, J. Musil, Z. Kristallogr. Suppl. 26 241-246 (2007).
[6] L. Nichtová, R. Kužel, Z. Matěj, J. Šícha, J. Musil, in this issue.

### Acknowledgements

The work is supported by the Grant Agency of the Czech Republic under number 106/06/0327, Grant Agency of Academy of Sciences (KAN400720701) and also as a part of the research plans MSM 0021620834 and MSM 4977751302 financed by the Ministry of Education of the Czech Republic.

# Analysis of soft X-ray multilayer interfaces by grazing incidence small angle X-ray scattering

**E. Majkova [1], P. Siffalovic [1], M. Jergel [1], L. Chitu [1,] S. Luby [1], T. Harada [2], T. Hatano [2], M. Yamamoto [2], G. A. Maier [3], J. Keckes [4]**

1. Institute of Physics SAS, 845 11 Bratislava, Slovakia
2. IMRAM, Tohoku University, 2-1-1 Katahira, Aobaku, Sendai 980-8577, Japan
3. Materials Center Leoben Forschung GmbH, Roseggerstraße 12, A-8700 Leoben, Austria
4. Erich Schmid Institute for Materials Science AAS and Department of Materials Physics University of Leoben, Jahnstrasse 12 A-8700 Leoben, Austria

Reliable quantitative analysis of multilayer interfaces is important for soft X-ray multilayer mirror applications. A well established approach relies on specular X-ray reflectivity (XRR) and X-ray interface diffuse scattering (XRIDS) measurements in coplanar geometry. The present work demonstrates that new information on interface morphology can be obtained by non-coplanar grazing incidence small-angle X-ray scattering (GISAXS) technique. Using GISAXS, a considerably larger volume of the reciprocal space is mapped which gives access to structural features on a scale of several nm. The potential of GISAXS is demonstrated on short-period Co/C and Cr/C multilayers with the nominal multilayer period of 2.3 nm.

Periodic multilayers with nominal metallic sublayer thickness of 0.7 or 1.15 nm and number of periods 200 (Co/C) or 300 (Cr/C) were prepared by ion beam sputtering. At 276 eV (soft X-ray range), the samples showed reflectance up to 18%. For interface analyses, the XRR, XRIDS (measured on BRUKER D8 Discover SSS with Cu rotating anode) and GISAXS (measured on Bruker Nanostar equipped with X-ray microsource IμS and VANTEC-2000 detector) were applied. The measurements confirmed regular layering and low interface roughness of all samples. The differences in terms of the lateral correlation length, Hurst parameter, rms roughness and vertical correlation length of interfaces determined from the simulation of experimental data are discussed.

The GISAXS experiments on the Co/C multilayer with Co layers 0.7 nm thick revealed the presence of nanoclusters. Considering the published data on Co film growth, one can assume that at 0.7 nm layer thickness, the coalescence of islands is not finished yet and free (pinhole-like) space is filled by carbon when the next carbon layer is deposited. Under stable deposition conditions, the size of islands forming Co layers will be accessible from GISAXS. This effect is much less visible for Cr/C multilayer though both Co/C and Cr/C multilayers with thinner metallic sublayers exhibit soft X-ray reflectivities not far below the theoretical limit. GISAXS technique thus proves to be a very efficient tool for tailoring subtle structural details in high-quality soft X-ray multilayers.

# Characterization of solid-state reactions and crystallization in thin films using in-situ X-ray diffraction.

**W. Knaepen [1], D. Deduytsche [1], J. Demeulemeester [2], D. Smeets [2], J. Jordan Sweet [3], A. Vantomme [2], R.L. Van Meirhaeghe [1], C. Detavernier [1], C. Lavoie [3]**

1. Ghent University, Department of Solid State Sciences, Krijgslaan 281 (S1),9000 Gent, Belgium
2. Kat. Univ. Leuven, Inst. Kern & Stralingsfys, Celestijnenlaan 200D, B-3001 Heverlee, Belgium
3. IBM Thomas J. Watson Research Center, Yorktown Heights, New York 10598, USA

X-ray diffraction (XRD) is a well-known characterization technique for studying the phase composition and texture of thin films. The technique is often used to study solid-state reactions in thin films, as it allows for a relatively straightforward identification of the reaction products. Most frequently, an 'ex-situ' approach is applied, whereby several identical small specimens are submitted to different heat treatments. After cooling down to room temperature, the individual samples are then characterized one-by-one. This ex-situ approach is quite time consuming and only provides data for discrete points during the reaction.

A more efficient approach consists of collecting XRD spectra during the heat treatment, i.e. 'in-situ'. In this work, we report on a set-up for in-situ XRD on thin films, consisting of a Bruker D8 diffractometer, a linear Vantec detector and a home-built annealing chamber. X-rays are generated by a standard Cu tube (CuKα $\lambda = 0.1540$ nm). In the annealing chamber, powders or thin films can be heated in a He-, Ar- or $N_2$-atmosphere from 20 to 1100°C. The linear Vantec detector allows for the acquisition of an XRD spectrum over a 2θ range of up to 20°. The system provides a sufficiently large signal to noise ratio to collect a single scan every 2s for films with a minimal thickness of about 20 nm. At an annealing rate of 0.5°C/s, this corresponds to one XRD spectrum per degree Celsius. In addition, a 4-point probe can be installed on the system which allows the simultaneous measurement of sheet resistance and XRD data.

Examples will be shown for Pt/Ge, Pd/Ge, Ni-Yb/Si thin film reactions, where the lab-based in-situ XRD data are compared to in-situ data obtained at a synchrotron. We will present a detailed analysis of the reaction kinetics of Pd thin films with Ge that can be performed through measurements at different ramp rates or during isothermal anneals at various temperatures. Apart from thin film reactions, we will discuss other applications, such as. crystallization [1], melting and thermal expansion studies.

[1] W. Knaepen, C. Detavernier, R. Van Meirhaeghe, J. Sweet, and C. Lavoie, Thin Solid Films 516, 4946 (2008)

# Real-time RBS to study thin film growth kinetics: the use of artificial neural networks for instantaneous data analysis

**J. Demeulemeester [1], D. Smeets [1], N. P. Barradas [2], A. Vieira [3], C. M. Comrie [4], K. Temst [1], A. Vantomme [1]**

1. Instituut voor Kern-en Stralingsfysica, Department of Physics and Astronomy and INPAC, KU Leuven, Belgium

2. Instituto Tecnológico e Nuclear, Estrada Nacional 10, Apartado 21, 2686-953, Sacavém, Portugal and Centro de Física Nuclear da Universidade de Lisboa, Av. Prof. Gama Pinto 2, 1699, Lisboa Codex, Portugal

3. Instituto Superior de Engenharia do Porto, R. António Bernardino de Almeida 431, 4200 Porto, Portugal

4. Department of Physics, University of Cape Town, Rondebosch 7700, South Africa

Rutherford backscattering spectrometry (RBS), a quantitative technique to probe the thin film compositional profile with depth sensitivity, has proven most useful in thin film research. RBS has been applied in numerous subfields of thin film growth; most notably in studies of the solid phase reaction between a thin film and its substrate. Conventionally, specimens are exposed to different treatments (being thermal, chemical, physical or implantation) and subsequently analyzed ex situ to examine the induced change in the compositional depth profile. The advantages of characterization in real time, i.e. performing the analysis during thin film growth or modification, are well-known and apply for real-time RBS as well as for any other real-time technique. As such real-time in situ RBS has been applied to sputter processes, implantation studies, diffusion experiments and solid phase reactions. In the case of a solid phase reaction it has been demonstrated that kinetic parameters such as the apparent activation energy for growth and the diffusion coefficient can be obtained from a single real-time RBS measurement. However, the large number of RBS spectra obtained during a typical real-time RBS experiment and the time consuming analysis associated with that, has so far obstructed the breakthrough of this technique for real-time analysis. Artificial Neural Networks (ANNs) may solve this issue.

We will demonstrate that the use of ANNs for the analysis of real-time RBS data drastically decreases the analysis time, without losing accuracy. Neural networks are based on neuron-like program blocks, which learn to link input (e.g. RBS spectra) to a desired output (e.g. thickness and compositions of layers within a thin film). For the analysis of real-time data these networks are trained to analyse RBS spectra by a set of theoretically simulated RBS spectra (training set) covering a range of experimental conditions and thin film compositions. The training of an artificial neural network is dedicated to a specific system, but covers all experiments performed on that system. Once the training is completed, the network allows instantaneous analysis of all experimental data. In this contribution we will present the progress in real-time RBS credited to the routine use of ANNs. We will demonstrate specific real-time RBS studies analyzed by ANNs, i.e. studies of silicide growth kinetics, marker experiments and elemental redistributions during thin film reactions, and discuss the construction, training, and quantitative analysis capabilities of those specific neural networks.

# In-situ and real-time investigations of ultrathin oxide-film growths

**L.P.H. Jeurgens, E.J. Mittemeijer**
Max Planck Institute for Metals Research, Heisenbergstraße 3, D-70569, Stuttgart, Germany

The electronic and chemical properties of ultrathin (< 2 nm) oxide films, utilized in many microelectronic and catalytic technologies, are determined by their microstructure (i.e. thickness, composition, morphology, crystallographic and defect structure), which in turn depends on the growth conditions, such as temperature, time, partial oxygen pressure and on the composition and crystallographic structure of the parent substrate. In this study, a state-of-the-art combinatorial approach of in-situ surface-sensitive analytical techniques under UHV conditions is presented to establish and tailor the relationships between the developing microstructure and the growth conditions of ultrathin oxide films grown on parent metal substrates by thermal oxidation. To this end, the oxide-film growth kinetics is monitored in real-time by in-situ spectroscopic ellipsometry. In-situ angle-resolved X-ray Photoelectron Spectroscopy is applied to deduce the local chemical state of the ions in the grown oxide films. Structural analysis by in-situ Low Energy Electron Diffraction provides details on oxygen-induced surface reconstructions, crystallographic structures of epitaxially grown oxide films, as well as on amorphous-to-crystalline transitions of initially amorphous oxide films. After in-situ capping of the grown oxide films, ex-situ characterization of the grown oxide film and its interface with the parent substrate is performed on an atomic-scale by cross-sectional High Resolution Transmission Electron Microscopic analysis. Detailed results on the microstructural evolution as a function of the growth conditions will be presented for thermally grown oxide films on bare Al, Zr and MgAl substrates.

# The role of mass transport rates in establishing layer-by-layer growth in homoepitaxial systems

**D. Adamovic [1], E. P. Münger [1], V. Chirita [1], L. Hultman [1], J.E. Greene [2]**

1. Linköping University, IFM, Thin Film Physics, Linköping 581 83, Sweden
2. University of Illinois, Materials Science Department, Champaign-Urbana, USA

We employ multi-billion time step embedded-atom method molecular dynamics simulations to study homoepitaxial growth of Pt(111) using low-energy (0.2 - 50 eV) hyperthermal Pt fluxes. We deposit 5 monolayers at 1000K and with deposition rates approaching experimental conditions. The results reveal a transition from a three-dimensional (3D) multilayer growth mode to layer-by-layer growth at ~ 20 eV which is maintained for energies of up to 50 eV [1]. In order to determine the mechanisms responsible for the observed change in the growth mode, we resolve, with picosecond resolution, both irradiation-induced and thermally activated processes. This allows us to determine, with unprecedented accuracy, the energy dependence of the net intra- and interlayer migration rates during the deposition process. Results show, that for all energies, irradiation events are completed within 10 ps following energetic impacts and that these processes dictate the growth mode. As expected, thermal migration is not affected by the deposition energy. For Pt deposition energies above 20 eV, the net interlayer migration induced by irradiation is towards the surface. This type of mass transport occurs via exchange mechanisms between surface and sub-surface atoms. On the growing layers, we observe primarily the descent of adatoms at step-edges and the recombination of adatoms with surface vacancies, i.e. mainly thermally activated processes. However, thermally activated net downward migration is an order of magnitude less than irradiation-induced upward migration. Intralayer migration is shown to depend strongly on adatom surface coverage. Results show that adatoms are the primary source of in-layer mass transport, which is observed to peak at a coverage of ~ 0.05 ML. Sputtering is observed to occur for energies higher than 25 eV. However, the yield is too small, less than 1% at 50 eV, to have a significant effect on island nucleation and coalescence kinetics.

[1] D. Adamovic, V. Chirita, E. P. Münger, L. Hultman, J.E. Greene Phys. Rev. B 76 115418 (2007)

# Optical emission spectrometry and characterization of pulsed-DC reactively sputtered TiC/a-C:H nanocomposite films

**K.P. Shaha, Y.T. Pei, C.Q. Chen, J.Th.M. De Hosson**
University of Groningen, Department of Applied Physics and Netherlands Materials Innovation Institute, Nijenborgh 4, 9747 AG Groningen, The Netherlands.

Diamond-like carbon (DLC) based nanocomposite films have attracted wide interests in fundamental research and industrial applications during the last decade [1]. Surface and bulk properties of these films prepared by different deposition techniques have been of great concern. Pulsed-DC (p-DC) unbalanced magnetron sputtering is proved to be a prominent technique. Pulsing magnetrons in the mid frequency regime (100-350 kHz) leads to much extended energy distribution and high ion flux density of impinging ions on the growing films. Such an impingement with high flux of Ar+ ions during deposition is crucial in the control and optimization of the microstructure and properties of various films [2]. In order to study the effect of pulse frequencies on the plasma properties and thus the composition, structure and properties of TiC/a-C:H nanocomposite films, reactive pulsed-DC magnetron sputtering of Ti targets in Ar/acetylene plasma has been used to deposit the films, together with in-situ plasma characterization by optical emission spectrometry. The pulse frequencies used ranges from 0 Hz (DC) to 350 kHz p-DC. ERD, SEM, HRTEM and nanoindentation were used to characterize the films. A summary of the deposition rate, composition including hydrogen content, microstructural evolution, mechanical and tribological properties as a function of the pulsed-DC frequency and the plasma property will be presented. The nanocomposite coatings exhibit superb toughness, wear resistance and ultralow friction.

[1] J. Robertson, Mater. Sci. Eng. R37 129 (2002).
[2] Y.T. Pei, C.Q. Chen, K.P. Shaha, J.Th.M. De Hosson, J.W. Bradley, S.A. Voronin, M. Cada, Acta Mater. 56 696 (2008)

# Sputter Process in-situ Monitoring by optical Reflectance Measurement

**E. Steimetz [1], S. Uredat [1], T. Trepk [1], H. Bartzsch [2], J. Weber [2], B. Ocker [3], K.-H. Schuller [3], J.-T. Zettler [1]**

1. LayTec GmbH, Helmholtzstr. 13-14, D-10587 Berlin, Germany

2. Fraunhofer-Institut für Elektronenstrahl- und Plasmatechnik (FEP), Winterbergstr. 28, D-01277 Dresden, Germany

3. Singulus Nano Deposition Technologies (NDT) GmbH, Hanauer Landstr. 103, D-63796 Kahl am Main, Germany

In this paper we present new results regarding the application of in-situ reflectance for process development in two different sputter applications: a single wafer sputter tool for advanced optical filters and coatings and a large multi-wafer production tools for giant magnetoresistive (GMR) heads for hard disk drive applications.

For the optical filter application we have monitored the spectral reflectance of silicon oxide / silicon nitride multilayer stacks on glass during a reactive Pulse Magnetron Sputtering (PMS) process. Data analysis was performed using the measured reflectances at four probe light wavelengths simultaneously. The data could only be interpreted by assuming non constant layer densities and sputtering rates for all layers, revealing time delays and occurrence of mixed interface layers upon material change. This report represents an excellent example of how unexpected phenomena influencing the layer quality can be monitored and localized in-situ within the process development.

For reflectance monitoring at the multi-wafer production-tool, for deposition of very thick $Al_2O_3$ films we have chosen the two optimum wavelengths of 633 and 950 nm for double-wavelength reflectance monitoring, The $Al_2O_3$ thickness was permanently determined in real-time for each individual wafer. By the data presented in this paper we show how the growth of even very thick aluminum oxide layers (0.5 to 30 µm) on silicon can be monitored. Growth-rate feed-back to the sputter system compensates slightly drifting deposition rates and enables the deposition of accurate thicknesses in an industrial process, where very high deposition rates and high material quality are the preferential aims.

[1] U. Schulz, U. Schallenberg, N. Kaiser: Reflection-reducing coating, Patent WO 02 043 74, 2002

# Hard X-ray Photoelectron Spectroscopy up to 15 keV: A novel tool for non-destructive characterization of bulk and buried interfaces

**J. Rubio-Zuazo [1,2], G.R. Castro [1,2]**

1. SpLine Spanish CRG BM25 beamline at the ESRF, ESRF B.P. 220, F-38043 Grenoble, France
2. Instituto de Ciencia de Materiales de Madrid, ICMM, CSIC, Cantoblanco E-28049 Madrid, Spain

Hard X-ray photoelectron spectroscopy (HAXPES) is a powerful novel emerging technique for bulk compositional, chemical and electronic properties determination in a non-destructive way. It benefits from the exceptionally large escape depth of high kinetic energy photoelectrons enabling the study of bulk and buried interfaces up to several tens of nanometres depth. Its advantage over conventional XPS is based on the long mean free path of high kinetic energetic photoelectrons. Using the advantage of tuneable X-ray radiation provide by the synchrotron the photoelectron kinetic energy, i.e. the information depth can be changed and consequently electronic and compositional depth profiles can be obtained. At SpLine, the Spanish CRG beamline at the European Synchrotron Radiation Facility (ESRF) we have developed a novel and exceptional set-up that combine surface X ray diffraction (SXD) and HAXPES. Both techniques can be operated simultaneously on the same sample and using the same excitation source. The set-up includes a heavy 2S+3D diffractometer and UHV chamber and electrostatic analyzer. The UHV chamber has also MBE evaporation sources, an ion gun, a LEED optic, a sample heating and cooling device, an electron gun, a UV discharge lamp, leak valves and a load-look port. The photon energy ranges between 7 and 45 keV. The HAXPES analyzer is an electrostatic cylinder-sector (FOCUS HV CSA), with a compact geometry and high transmission due to second order focusing. The analyzer is capable to handle kinetic energies both up to 15 keV and down to a few eV with the same analyzer setup and power supply.

## 1. INTRODUCTION

The photoemission and the Auger electron spectroscopies play a preponderant role in the study of the electronic properties of solids [1]. These techniques have been extensively used in the last 40 years and have reached a high degree of sophistication [1]. Overall, their application has been limited to the investigation of surface phenomena by using energies between 40 and 2000 eV for both the excitation sources and detected electrons. The low electron inelastic-mean-free-path (IMFP) and/or the effective attenuation length (EAL) [2] in the solid materials, at the energies used is responsible for their surface sensitivity. Particularly, buried interfaces are not accessible for the great majority of the techniques of surface physics. However, using hard X-rays as excitation source which has a macroscopic penetration depth in the materials, high kinetic energy photoelectrons can be produced [3]. Consequently, HAXPES benefits from the exceptionally large escape depth of high kinetic energy photoelectrons enabling the study of bulk and buried interfaces up to several tens of

nanometres depth [4]. Its advantage over conventional XPS is based on the long mean free path of high kinetic energetic photoelectrons. The information depth can reach several tens of nanometres for 15keV electron kinetic energy. Using the advantage of tuneable X-ray radiation provided by the synchrotron the photoelectron kinetic energy, i.e. the information depth can be changed and consequently electronic and compositional depth profiles can be obtained. HAXPES is a powerful emerging technique for bulk compositional, chemical and electronic properties determination. HAXPES is a novel method for non destructive and bulk sensitive electronic and chemical characterization of solids. At SpLine, the Spanish CRG beamline at the European Synchrotron Radiation Facility (ESRF) we have developed a novel and exceptional set-up that combine HAXPES and X-ray diffraction XRD (surface and bulk X-ray diffraction and X-ray reflectivity). Both techniques can be operated simultaneously on the same sample using the same excitation source.

## 2. Experimental

### *2.1 HAXPES-XRD set-up*

The experimental set-up is placed on branch B of the Spanish CRG BM25 beamline SpLine [5] at the European Synchrotron Radiation Facility (ESRF), Grenoble, France. The Branch B is located on the hard edge of the bending magnet D25 device with a critical energy of 20.6 keV and a horizontal angular divergence of 2 mrad. Two Si (111) crystals placed at ~30 meters from the source serve as a double-crystal monochromator, which gives an energy resolution of $\Delta E/E=1.5x10^{-4}$. The horizontal focusing is achieved by the second monochromator crystal through a sagittal cylindrical bending. A cylindrical bent mirror placed after the monochromator is used to focus in the meridional plane. In all the energy range the beam spot size is around 300x100 $\mu m^2$ in the horizontal and vertical direction, respectively. A first mirror, Rh coated, is located before the monochromator that cuts-off the higher-order-harmonics reducing the heat load on the monochromator. The beamline X-ray energy ranges between 5 keV and 45 keV with a X-ray flux of $10^{13}$ photons/s flux, that is well adapted for the HAXPES and XRD requirements.

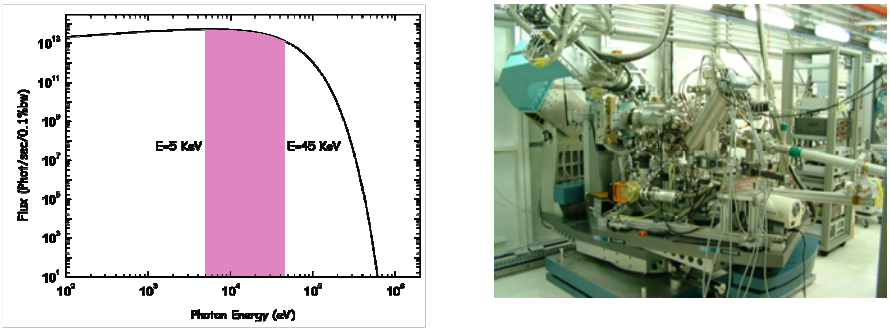


(a) (b)

Figure 1. (a) SpLine branch B photon flux in photons/sec/0.1% bandwidth in dark the achievable energy range (5-45 keV). (b). a picture of the whole experimental HAXPES and XRD setup.

Figure 1(a) shows the beamline photon flux at 01% bandwidth obtained at the branch B with a storage ring current of 200 mA. The bending magnet D25 of the ESRF generates the X-rays provided by the SpLine beamline. A high-resolution channel-cut (Si(311), Si(333), and Si(400)) post-monochromator is located close to the vacuum chamber for cases where a better excitation source resolution in the HAXPES measurements is required. The experimental set-up includes a heavy 2S+3D diffractometer, a UHV chamber and an electrostatic analyzer [6, 7]. The UHV chamber has also MBE evaporation sources, an ion gun, an electron gun, a UV

discharge lamp, a LEED optic, a sample heating and cooling device, leak valves and a load-look port. In figure 1(b) a picture of the UHV experimental set-up is displayed. In our set-up design we have chosen an analyzer with the wider angular acceptance, keeping in mind that a great effort has to be done in optimizing the transmission and the energy resolution. The analyzer is an electrostatic cylinder-sector (FOCUS HV CSA), with a compact geometry and high transmission due to second order focusing. The analyser is based on a cylinder sector with 90° deflection and 300mm slit-to-slit distance and an entrance lens with 50mm sample distance [7, 8]. This gives a very compact design of the analyser that is easily integrated into a multipurpose experiment with different techniques. The analyzer is capable to handle kinetic energies both up to 15 keV and down to a few eV with the same analyzer setup and power supply.

## 3. EXPERIMENTALS RESULTS

Representative HAXPES 3s, 3p and 3d Au core level spectra (see Fig. 2a) and Cu and Au valence band (see Fig. 2b) obtained at the SpLine HAXPES-SXD set-up measured on a 21 nm thick Au film growth on a Cu polycrystalline sample. The spectra displayed on fig. 2 are representative photoemission data and were obtained with a photon energy of hν = 9 keV ($E_{kin}$ = 5.40 - 6.90 keV), hν = 17 keV ($E_{kin}$ = 13.40 - 14.90 keV), hν = 7.5 keV ($E_{kin}$ = 7.36 - 7.50 keV) and hν = 15 keV ($E_{kin}$ = 14.86 - 15.00 keV), respectively. The bottom (Fig. 2a) and the upper spectrum (Fig. 2b) are multiplied by a factor 3 and 14.26, correspondingly. Note the absolute and relative cross section differences in the spectra.

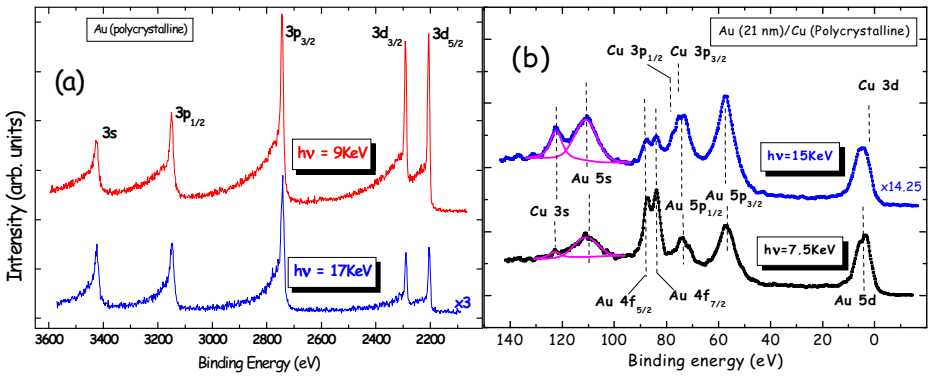


Figure 2. (a) HAXPES Au 3s, $3p_{1/2}$, $3p_{3/2}$, $3d_{3/2}$ and $3d_{5/2}$ spectra recorded at 9 and 17 keV photon energy. (b) Cu and Au valence band spectra taken at 7.5 and 15 keV photon energy.

Using the advantage of tuneable X-ray radiation the photoelectron kinetic energy, i.e. the information depth can be changed. Figure 3 shows the experimentally obtained photoemission peak intensities as a function of their kinetic energy for the Au overlayer and the buried Cu substrate. The signal is normalized with the corresponding bulk photoemissions peak (scatter symbols). The displayed data was obtained by measuring the 1s, 2s, 2p, 3s, 3p and 3d subshells from Cu and 2s, 2p, 3s, 3p, 3d, 4s, 4p, 4d, 4f, 5s, 5p and 5d subshells for Au for a photon energy range between 7.5 and 17 keV. The normalized signal is only a function of the EAL and of the atomic density N(z) functions of the corresponding measured element, i.e. Cu and Au [8, 9]. The compositional depth profile analysis has been obtained by fitting the measured data with general polynomial depth dependence. The fit results are shown in Figure 3 as continuous line that match with a uniform Au over layer of 21 nm and an inter layer diffusion region of 2.4 nm. The obtained composition depth profile is in very well agreement with equivalent results obtained from X-ray reflectivity measurements performed in the same system and set-up.

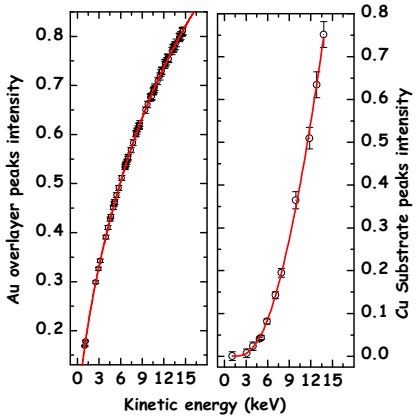


Figure 3. Photoemission peak intensity dependence with kinetic energy. Scatter symbols experimental data. Continues line fit results.

## 4. Conclusions and outlook

We have developed a novel outstanding tool for non-destructive characterization of bulk and buried interfaces that combine XRD and HAXPES. The implementation of HAXPES open a direct way to correlate surface and bulk properties and in combination with XRD is opens a new research field.

The developed set-up offers a unique opportunity to obtain, on a same sample and under identical experimental conditions, simultaneous information about the electronic properties, geometric structure and chemical composition of bulk, buried interfaces and surfaces. The exceptionally large escape depth of high kinetic energy photoelectrons increases the sampling depth up to several tens of nanometres. Even more, using the advantage of tuneable X-ray radiation provided by the synchrotron the photoelectron kinetic energy, and hence the information depth can be changed and consequently electronic and compositional depth profiles can be obtained in a non-destructive way. HAXPES is a powerful emerging technique for bulk compositional, chemical and electronic properties determination.

## Acknowledgements

We thank the SpLine and Focus GmbH staff for their precious help in the development of the electron analyzer. Financial support was provided through Spanish ministry of Education and Science (MEC) Grants nos. FAP-2001-2166 and MAT1999-0241-C01.

## 5. References

[1] S. Hüfner, "Photoelectron Spectroscopy", Springer Verlag (1994), ISBN number 3-540-41802-4

[2] S. Tanuma, C. J. Powell, D. R. Penn, Surf. Interf. Anal. 25 25 (1997)

[3] J. Rubio-Zuazo and G.R. Castro, Journal of Physics: Conferences Series, 100 012042 (2008)

[4] J. Rubio-Zuazo, E. Martinez, P. Batude, L. Clavelier, F. Soria, A. Chabli and G.R. Castro."Hard X-ray photoemission experiments on novel Ge-based metal gate / high-k stacks", AIP Conference Proceedings-2007: International Conference on Frontiers of Characterization and Metrology for Nanoelectronics. pp. 329-333

[5] G.R. Castro, J.Synchrotron Rad 5, 657 (1998)

[6] J. Rubio-Zuazo and G.R. Castro, Nuclear Instruments and Methods in Physics research, Section A, 547 64 (2005)

[7] M .Escher, M. Merkel, J. Rubio-Zuazo and G.R. Castro, "An energy analyser for Hard X-ray Photoelectron Spectroscopy", Proceedings of Recent Trends in Charged Particle Optics and Surface Physics Instrumentation, Brno 2006, Czech Republic

[8] J. Rubio-Zuazo and G.R. Castro "Hard X-Ray Photoelectron Spectroscopy and X-Ray Surface Diffraction station". Pico, Vol 10. No2 (2006)

[9] J. Rubio-Zuazo and G.R. Castro, Reviews on Advanced Materials Science, 15 79 (2007)

# Development and study of growth mechanism of anatase crystallized titanium dioxide thin films prepared on steel substrates by reactive DC magnetron sputtering process

**D. Wicky [1], M.-H. Berger [2], C. Archambeau [3], R. Cloots [1], B. Vertruyen [1]**

1. Laboratory of Structural Inorganic Chemistry, University of Liège, Chemistry Department B6a, Sart-Tilman, B4000 Liège, Belgium

2. Centre des Matériaux Pierre-Marie Fourt, Ecoles des Mines de Paris, RN 446 SNECMA, B.P. 87, 91003 Evry, France

3. ArcelorMittal Liège Research, Sart-Tilman B57, B4000 Liège, Belgium

It is well-known that $TiO_2$ photocatalyser absorbs UV-light so that electron-hole pairs are generated. These pairs contribute to redox- reactions and decompose organic compounds that are adsorbed on the $TiO_2$ surface. The functionalization of steel substrate surfaces by titanium dioxide photocatalytic coatings allows the development of new steel products with high added value and new properties such as air or water purification, deodorizing, bactericidal effect and self cleaning.

Titanium dioxide films have been deposited on steel substrates by a d.c. reactive magnetron sputtering process which is a dry and environmental friendly coating technology. In addition, this vacuum process is industrialized by ArcelorMittal Group in order to make steel products with new properties in a large scale.

$TiO_2$ deposits have been prepared on stainless steel substrates in a laboratory batch reactor. We have studied the influence of different process parameters like work pressure, substrate temperature and oxygen quantity on structural characteristics of film.

Titanium dioxide coatings have been characterized by :

- X-ray diffraction at grazing incidence and micro-Raman spectroscopy to evaluate crystallinity
- X-ray fluorescence and step measurement to determine thickness
- Scanning Electron Microscopy and Atomic Force Microscopy to study the morphology.

Moreover, in order to understand the growth of the $TiO_2$ film, we have studied the morphology and crystalline structure evolution of coating as a function of the film thickness by Transmission Electron Microscopy.

First, we have made transverse section of coated steel samples. By this way, the columnar structure of the coating can be revealed.

Secondly, we have prepared PVD $TiO_2$ coating on carbon membranes fixed on stainless steel substrate. This technique provides a top view of the $TiO_2$ film. Membranes with increasing $TiO_2$ thicknesses have been observed. The growing mechanism of a $TiO_2$ film prepared by reactive PVD has been followed step by step :

-First, the deposition on the substrate of amorphous clusters of 5 to 15 nm in width ;

-Then the crystallization of anatase isolated clusters on the substrate followed by the crystallization of the adjacent clusters, keeping the same crystal orientation ;

-After that, the deposition of amorphous clusters on crystalline ones, their crystallization being leaded by the orientation of the cluster beneath, inducing the growth of columns ;

-Finally the development of a continuum of anatase crystallized grains.

# Deposition and Diffusion Processes and Barriers on Rutile $TiO_2$ (110)

**L. Vernon, E. Sanville, S. Kenny, R. Smith**
Department of Mathematical Sciences, Loughborough University

With an aim to model surface growth over long time scales, the deposition and diffusion of titanium oxide clusters on the $TiO_2$ rutile (110) surface have been modelled. The growth of $TiO_2$ is of particular interest to the optical coatings industry where the photocatalytic and hydrophilic properties along with the absorption spectra offer many commercial uses.

Diffusion events were found using the Dimer method along with the climbing nudged elastic band (CNEB) and the associated prefactors were calculated using the Vineyard equation. In order to combine the millisecond frequency of deposition events and the duration of the intermediate diffusion transitions a combination of on-the-fly kinetic Monte Carlo method and molecular dynamics was employed.

The variable charge SMB-Q potential of Halil et al. and the Matsui-Akaogi fixed charge potentials were employed. In order to assess the accuracy of the empirical potentials intuitive transition barriers were found using the CNEB method were compared to density functional theory (DFT) results where applicable.

The fixed charge model can only be employed to study TiO2 ad-clusters; due to the requirement of charge neutrality. For this case the DFT, variable charge and fixed charge models are in good agreement. The SMB-Q model allows for more realistic modelling with most DFT binding sites having empirical equivalents with two exceptions. There is no angular component in the Ti-O empirical potential, this leads to the O adatom sitting directly above the 5-fold co-ordinated Ti surface atom. Whilst in the DFT simulations 2 equivalent sites are found, with the O adatom above the 5-fold co-ordinated Ti atom in 2 symmetrically displaced configurations. Additionally in DFT an O adatom is found to bind to one of the O atoms in the O ad-row, while this configuration is not stable in the variable charge model due to the purely repulsive O-O Buckingham potential.

With a single ad-cluster most surface diffusion barriers are large in magnitude, greater than 2eV. Thus implying that diffusion of these ad-species would not take place. The exception being the barrier for O adatom diffusion on the surface with a DFT barrier of 0.3eV and a SMB-Q barrier of 0.78eV where the discrepancy between results can be explained due to the 2 stage process evident in the DFT calculation.

Whilst the SMB-Q potential could be applied unchanged, for most transition calculations the lack of a Ti-Ti potential resulted in un-physical behaviour during deposition and some Ti and TiO diffusion processes. Initially the Ti-Ti Morse potential parameterised by Thomas was applied, however the steep potential wall led to problems with the dynamics and as such the ZBL potential was introduced enabling calculation of Ti transitions barriers along with sensible deposition simulations.

# Reactive sputter deposition of TiN layers, simulated with a Particle-in-cell/Monte Carlo Collisions model.

**E. Bultinck [1], S. Mahieu [2], D. Depla [2], A. Bogaerts [1]**

[1] Research Group PLASMANT, Department of Chemistry, University of Antwerp, Universiteitsplein 1, 2610 Antwerp, Belgium

[2] Department of Solid State Sciences, Ghent University, Krijgslaan 281 (S1), 9000 Ghent, Belgium

Magnetron plasma sources are intensively applied since the 1970s for the sputter deposition of thin metal or compound films [1], and play nowadays a very important role in industry. Most of the deposited thin films are metal nitride or metal oxide layers, because of their interesting mechanical [2-5] and electrical properties [2, 6]. By adding nitrogen or oxygen to the argon sputter gas, a metal nitride or oxide layer can be formed by reaction between the reactive plasma species and the sputtered metal particles. Aside to experimental investigations, numerical simulations are often applied in order to understand and improve the applications of (reactive) magnetron sputtering. In the case of the low-pressure magnetron discharges, the so-called particle-in-cell/Monte Carlo Collisions (PIC/MCC) model is most accurate. A 2d3v PIC/MCC model was constructed for an $Ar/N_2$ reactive gas mixture in a balanced planar magnetron. A titanium target is sputtered and a TiN thin film is deposited. The model includes the following species: electrons, $Ar^+$, metastable Ar atoms, fast Ar atoms, $Ti^+$, Ti, $N^+$, $N_2^+$ and N. The $Ar/N_2$ ratio was varied from pure argon (60 sccm) to a 60/10 sccm $Ar/N_2$ gas mixture. The model has an external electrical circuit, consisting of an external voltage source and resistor. This current limiting device occurs to be inevitable in a PIC/MCC code for an accurate and correct description of magnetron discharges [7]. When nitrogen gas is added to the argon sputter gas, a thin nitride layer can also be formed on the cathode surface [8]. Due to this surface modification, which is called poisoning, the secondary electron emission coefficient (SEEC), given as the number of secondary electrons produced by an ion striking the cathode surface, will change. This results in a change of the cathode potential, and consequently, all other plasma characteristics will be influenced [8, 9]. Therefore, target poisoning is taken into account in the model by varying the value of the SEEC. Typical results include for example the plasma potential distribution and particle densities. To investigate the sputter deposition, the particle fluxes to the cathode (sputtering) and the anode (deposition) are calculated. The influence of the gas mixture ratio on the sputter deposition process is investigated.

[1] R. K. Waits, J. Vac. Sci. Technol. 15 179 (1978)
[2] H. Bartzsch et al., Surf. Coat. Technol. 174 774 (2003)
[3] P. J. Kelly et al., Surf. Coat. Technol. 174-175 795 (2003)
[4] P. S. Henderson et al., Surf. Coat. Technol. 174 779 (2003)
[5] J. O'Brien et al., Surf. Coat. Technol. 142 621 (2001)
[6] A. Mahmood et al., Diam. Relat. Mater. 12 1315 (2003)
[7] E. Bultinck et al., J. Appl. Phys. 103 013309 (2008)
[8] D. Depla et al., Plasma Sources Sci. Technol. 10 547 (2001)
[9] D. Depla et al., Surf. Coat. Technol. 201 848 (2006)

# Spatially resolved thickness determination of metal and oxide coatings using optical consumer electronic components

**M. Horkel [1], H. Mahr [1], J. Hell [1], C. Eisenmenger-Sittner [1], E. Neubauer [2]**

1. Vienna University of Technology, Institute of Solid State Physics Wiedner Hauptstrasse 8-10, A-1040 Vienna, Austria

2. ARC Seibersdorf Research GmbH, Department of Materials and Production Engineering, A-2444Seibersdorf, Austria

Film thickness determination by optical methods is an established and well known field. A huge variety of high precision optical instruments, ranging from spectro-photometers via confocal microscopes to spectroscopic ellipsometers are commercially available.On the other hand, in recent years also the sector of consumer electronics begins to offer high precision optical instruments such as digital cameras and high resolution scanners at very low costs. This paper describes the use of consumer electronic components to determine the thickness of metallic and dielectric coatings in the nm range by using easily available consumer electronic components. Two examples are presented:

(i) Thickness determination of Mo coatings on Diamond granulates: Industrial diamonds with grain sizes of 50 - 200 µm were uniformly coated with molybdenum by DC magnetron sputtering in a specially designed mixing device. The Mo thickness was determined by the measurement of optical density using a Reflecta CrystalScan 7200 optical scanner working in transmission mode with Silverfast AFL-SE software. A correlation between the deposition time and the measured coating thickness was achieved.

(ii) Transparent coatings of Al-oxide with variable thickness were deposited on natively oxidized Si wafers. The thickness variation leads to the formation of interference patterns with a lateral extension of some centimetres. The interference patterns were imaged by a digital camera and quantitatively evaluated at three different wavelengths using RGB-splitting. The film thicknesses obtained from the interferometric measurements were compared to profilometric measurements and found to be in good agreement

These two examples show that quite demanding tasks related to film thickness determination may be executed with high accuracy by present day consumer electronic devices.

The financial support of the Austrian "Fonds zur Förderung der Wissenschaftlichen Forschung" (FWF), Grant No. P-19379-N16 and the IWT Flanders, Grant No. SBO-060030 is gratefully acknowledged.

# A MC-simulation of the metal flux from a rotating cylindrical magnetron

**K. Van Aeken [1], S. Mahieu [1], M. Horkel [2], D. Depla [1]**
**C. Eisenmenger-Sittner [2]**
1. Ghent University, Department of Solid State Sciences, Krijgslaan 281 (S1),9000 Gent, Belgium
2. Vienna University of Technology, Institute of Solid State Physics, Wiedner Hauptstrasse 8-10, 1040 Wien, Austria

Knowledge and optimisation of the metal flux towards the substrate during magnetron sputtering is a requisite for the controlled deposition of complex layers with desired stoichiometry and microstructure. To this end the authors developed a test particle MC-code, SIMTRA[1], to describe the transport of neutral particles through the gas phase.
The code was applied to the study of a small scale rotating cylindrical magnetron. First the metal flux was experimentally characterized for Cu, Al and Ti sputtered at different pressures by measuring deposition rates with a quartz crystal microbalance mounted on a rotatable and translatable feedthrough. These experiments were compared to simulations taking into account the full 3D geometry of the set-up. The sputtered particles starting positions were obtained by simulating the ion current density on the target using a MC test-electron code. The magnetic field, an important input, was calculated either using 3D finite elements or analytical formulas for an optimised equivalent set of cubical magnets, and a comparison was made. As verification, erosion profiles on stationary sputtered targets were also measured. It was found that the nascent angular distribution must significantly deviate from cosine in order to reproduce the measurement. This distribution was not considered given (by sputter simulation or analytical formula) but instead reconstructed from low pressure experimental deposition profiles. A comparison with results from literature and sputter simulations was made. The spatial, pressure and material dependence of the metal flux was also studied.
As an additional verification to the code, simulated arriving angular distributions for sputtering from a planar 2" magnetron were compared to experimental ones measured with a flux monitor, being a small differentially pumped pinhole camera.

[1] K. Van Aeken, S. Mahieu, D. Depla J. Phys. D: Appl. Phys. 41 205307 (2008).

# Angular Resolved Determination of the Particle Flux Towards a Substrate for Magnetron Sputtering

**C. Eisenmenger-Sittner[1], M. Horkel [1], K. Van Aeken [2], S. Mahieu [2], D. Depla [2]**

1. Vienna University of Technology, Institute of Solid State Physics, Vienna, Austria
2. Ghent University, Department of Solid State Sciences, Krijgslaan 281 (S1),9000 Gent, Belgium

Magnetron sputtering offers a wide range of deposition parameters because of the free choice of target parameters and due to the possibility to tune the angular and energy distribution of the ejected particles by variation of the working gas pressure. In addition reactive working gases may be chosen to allow the formation of compound materials. This paper focuses on the experimental determination of the angular distribution of metallic sputtered particles upon impingement on a substrate and on the comparison of these experiments with Monte Carlo simulations of the gas phase transport. For the experiments a special Metal Flux Monitor (MFM) based upon the principle of a differentially pumped pinhole camera was designed. The particles are collected either on transparent or highly reflecting plane substrates and the film thickness is determined spatially resolved by optical methods. The metals chosen were Cu and W as examples for non reactive materials with different masses and Al as a metal highly inclined to oxide formation. The distance target to pinhole was kept constant at approx. 95 mm and Ar with pressures in the range from 0.3 – 3 Pa was chosen as working gas. Cu and W formed thin metallic coatings, while in the case of Al the oxygen background pressure was sufficient of lead to the formation of transparent Aluminium Oxide. The experimentally determined film thicknesses and Monte Carlo Simulations showed very good agreement in both cases, metallic and oxidic coatings. Therefore both, the experimental and the simulation technique can be extended to the more complex case of the deposition from different sputter sources and also to the intentional introduction of reactive gases, thus allowing for the formation of compound materials using different reactive gases.

The financial support of the IWT Flanders, Grant No. SBO 060030 is gratefully acknowledged.

# Ordered growth of Si nanostructures by glancing angle deposition

**C. Patzig [1], J. Zajadacz [1], R. Fechner [1], B. Rauschenbach [1], B. Fuhrmann [2]**
1. Leibniz-Institut für Oberflächenmodifizierung Leipzig, Germany
2. Martin-Luther-Universität Halle, Germany

In most physical vapour deposition processes, the vapour flux that contributes to the deposition of the thin film reaches the substrate parallel to the substrate normal, resulting in the growth of a dense, compact layer. If, however, the substrate is tilted with respect to the vapour source, the particle flux will reach the substrate under a highly oblique angle to the substrate normal. Under those glancing angle deposition conditions, self-shadowing of the particles on the substrate surface leads to the growth of highly underdense films that consist of needle-like structures which are slanted into the direction of the incoming vapour flux. A suitable substrate rotation during deposition enables the forming of those needles into nearly arbitrary shapes such as zigzags, vertical posts, spirals or screws. If the deposition is performed on patterned substrates, the template can be used as an array of artificial seeds that capture the incoming vapour flux and shadow the region in between, thus giving the possibility to grow periodically arranged nanostructures. Here, the growth of Si nanostructures by ion beam sputter glancing angle deposition on bare substrates as well as on patterned substrates with different template geometries (square lattice, hexagonally close packed, honeycomb-like) will be shown, and the influence of the periodicity and form of the used pattern on the growth of the structures will be discussed. Additionally, the experimental results will be compared with Monte Carlo simulations of glancing angle deposited thin films on patterned substrates.

# Optical anisotropy induced by oblique incidence ion bombardment of Ag(001)

**F. Everts, H. Wormeester, B. Poelsema**
University of Twente, Solid State Physics, MESA+ Institute for Nanotechnology, Veldmaat 10
7522 NM Enschede, The Netherlands

Oblique incidence ion sputtering has become a widely used method for the creation of highly regular patterns of lines and dots [1-2]. This technique has great potential, since it enables a fast and easy way to create large homogeneous areas with highly ordered features. Most common is the formation of a pattern with a height modulation in one direction, a nanoripple pattern [3]. On a Ag(001) surface oblique incidence sputtering creates a ripple pattern that exhibits plasmonic features. The photon energy of this plasmonic feature depends on the ripple periodicity. The development of these anisotropic features is measured in-situ with the optical technique Reflection Anisotropy Spectroscopy (RAS) [4].

The ion induced nanopatterns are prepared using 2 keV Ar ions with a flux of a few $\mu A/cm^2$ in a temperature range of 300 - 420K. With RAS, a periodicity of ripples above 200 nm is measured by a shift in photon energy of the plasmon resonance. Features with a smaller periodicity show a plasmon resonance around 3.65 eV. For very grazing incidence sputtering, 80° polar angle of incidence, only a resonance feature around 3.65 eV is observed. High resolution LEED measurements after sputtering confirm the formation of 1D nanoripples.

For a polar angle of incidence of the ion beam of 70° a shift in the maximum of the plasmon resonance feature is observed. These spectra can be well described within the Rayleigh-Rice description for scattering from a slightly rough surface [5]. The formation of nanoripples, i.e. a 1D roughening of the surface perpendicular to the direction of the ion beam, suffices to describe the measured optical data. The evolution of the rms, wavelength and wavelength distribution of the ion bombardment induced nanoripples is obtained from in-situ measurements. For a polar angle of the ion beam of 61.5° we find that also the roughening in the direction along the nanorippels has to be taken into account to describe the optical spectra.

[1] S. van Dijken, D. de Bruin, B. Poelsema, Phys. Rev. Lett. 86, 4608 (2001)
[2] U. Valbusa, C. Boragno, F. Buatier de Mongeot, J.Phys. Cond. Matt. 14 8153 (2002)
[3] R. M. Bradley, J. M. E. Harper, J. Vac. Sci. Technol. A 6, 2390 (1988)
[4] F. Everts, H. Wormeester, B. Poelsema, Phys. Rev. B. 78, 155419 (2008)
[5] D. Franta, I. Ohlídal, Opt. Commun. 248, 459 (2005)

# The effects of residual strain on the structure of ultra-thin ZnO films on Ag(111) surfaces: a first principles study

**C. L. Phillips, P. D. Bristowe**
University of Cambridge, Department of Materials and Metallurgy, Pembroke Street, Cambridge CB2 3QZ, United Kingdom

In the manufacture of solar-control windows, optical multilayers containing thin films of oxides and metals are deposited on glass using magnetron sputtering. Typically, these optical coatings contain Ag layers buffered by layers of ZnO. Due to the sputtering process and the effects of lattice and thermal mismatch between the various layers and the glass, a residual compressive stress of 1-3GPa, sufficient to cause de-lamination at the metal/oxide interfaces, develops. The weakness of these interfaces motivates an examination of the effect of strain on the structure and bonding of ultra-thin films of oxides on transition metals. This paper presents first principles calculations of the structures of ultra-thin films of ZnO on Ag(111) over the typical range of strain occurring in ZnO/Ag/ZnO stacks in optical multilayers.

When ZnO is deposited on Ag (111) in an oxygen-rich magnetron sputtering chamber, we expect the first ZnO layer to be oxygen with the subsequent layers of zinc and oxygen creating a ZnO structure. Experimental evidence suggests that the first few ZnO layers have a graphitic structure rather than the expected wurtzite [1] when deposited on unstrained Ag(111). In the present computational study various amounts of in-plane compressive stress are applied to ZnO/Ag interfaces and the structures allowed to relax using a plane-wave, pseudopotential, density-functional approach. The chosen periodicity in the Ag (111) plane is such that the ZnO film forms a 30° rotated epitaxial relationship with it as observed in electron diffraction studies of Ag/ZnO systems.

Results show that in the absence of in-plane compression the ZnO film forms a graphitic structure on the Ag surface similar to that seen experimentally [1]. The application of a small compressive stress produces rippled graphitic sheets of ZnO. These results are compared with calculations on freestanding ultra-thin ZnO slabs [2] where similar results are observed.

[1] C. Tusche, Phys. Rev. Lett. 99 026102 (2007)
[2] F. Claeyssens, J. Mater. Chem., 15 139-148 (2005)

# Kinetic Monte Carlo simulation of homoepitaxial growth of magnesium oxide thin films by molecular deposition

**E. Antoshchenkova [1], M. Hayoun [1], F. Finocchi [2], G. Geneste [3]**

1. Ecole Polytechnique, Laboratoire des Solides Irradiés, 91128 Palaiseau, France
2. Universités Paris 6 – Paris 7, Institut des Nanosciences de Paris, Campus de Boucicaut,140 rue de Lournel, 75015 Paris, France
3. Ecole Centrale Paris, Laboratoire Structures, Propriétés et Modelisation des Solides, Grande Voie de Vignes, 92295 Châtenay-Malabry, France

The aim of our study is to build up a realistic model of the growth of metallic oxides layers. We present the first stage the work*:* the simulation at the atomic scale of MgO homoepitaxial growth. Magnesium oxide is a model material that is often used as epitaxially grown thin films on various substrates, as substrate, or both of them. The resulting film properties are very sensitive to the structure and morphology of the surface and interfaces. The understanding of growth mechanisms is also required to determine and control the growth conditions.

For this first stage, we have developed a Kinetic Monte Carlo (KMC) code adapted to the homoepitaxial growth of MgO. The KMC approach is an efficient tool for modeling a complex sequence of simple events. The events, which form the growth of the oxide, are the followings: deposition, various diffusion mechanisms, evaporation and chemical reactions. These events and their probabilities obtained from their frequencies are the input data of the KMC simulations. We have used *ab initio* calculations (Density Fonctional Theory) at T=0 K [1] and Molecular Dynamics (MD) computations based upon phenomenological potentials at T=1000 K [2] to guess and discover the possible events occurring and their corresponding frequencies.

KMC allows us to bridge the time scale gap between diffusion events (nanoseconds) and deposition events (seconds). Our KMC code simulate the homoepitaxial growth by Molecular Beam Epitaxy. The simulations where carried out on a MgO(001) monocrystalline substrate using a cell with periodic boundary conditions. The dimensions of the system can reach a few hundred thousand of molecules.

We simulated the MgO homoepitaxial growth at different temperatures and pressures of the molecular beam and at a chosen roughness of the MgO substrate. We investigated and compared the effects of each event in order to estimate the role of diffusion in crystal growth and the contribution of every diffusion mechanism. To obtain a realistic model, we varied the event probabilities as a function of the neighboring of the migrating molecule: near defects (steps, vacancies) and centers of nucleation (clusters). We have also used MD as a tool to check the validity of some hypothesis made within KMC.

[1] G. Geneste, J. Morillo, F. Finocchi, Appl. Surf. Sci. 188 122 (2002)
[2] G. Geneste, J. Morillo, F. Finocchi, M. Hayoun, Surface Science 601 5616 (2007)

# Transition Pathways Of Small Titanium Oxide Clusters On The Rutile (110) Surface: *Ab Initio* And Qeq Calculations Using The Nudged Elastic Band Method

**E. Sanville, L. Vernon, R. Smith, S. Kenny**
Loughborough University, Department of Mathematical Sciences, Loughborough, UK LE11 3TU

We present calculated surface and interstitial transition barriers for Ti, O, $O_2$, TiO, and $TiO_2$ atoms and clusters at the rutile (110) surface. Defect structures involving these small clusters, including adcluster and interstitial binding sites, were calculated by energy minimization using density functional theory. Transition energies between these defect sites were calculated using the nudged elastic band (NEB) method. Additionally, a modified SMB-Q charge equilibration empirical potential, and a fixed-charge empirical potential, were used for a comparison of the transition energy barriers. Barriers of 1.2 to 3.5 eV were found for all studied small cluster transitions upon the surface, except for transitions involving $O_2$. By contrast, the $O_2$ diffusion barriers along the [001] direction upon the surface are only 0.16 eV. The QEq charge equilibration model gave mixed agreement with the DFT calculations, with the barriers ranging between 0.8 and 5.8 eV.

# Description of the cross magnetron effect as a local variation of the process operation point

**H. Kupfer [1], R. Kleinhempel [2], F. Richter [1]**

1. University of Technology Chemnitz, Institute of Physics, D-09107 Chemnitz, Germany
2. Southwall Europe GmbH, D-09100 Grossröhrsdorf, Germany

For economic reasons and to get optimized functional parameters of indium tin oxide (ITO) films a strong homogenous lateral distribution of the process parameters in magnetron sputter technologies is an indispensable precondition. We have investigated the influence of the cross magnetron effect (CME) on the homogeneity of the process parameters in comparison to the film properties using pulsed reactive magnetron discharges. Especially we have measured the lateral plasma parameters at the substrate position. A distinct effect of the CME on the charge carrier density $n_i$ is indicated. As a result, the lateral distribution of the functional film properties reflects the effect of the CME too. We discuss the film property distribution in terms of the flux $j_{O^*}$ of the reactive atomic oxygen particles to the substrate surface, which depends strongly on the charge carrier density and the electron temperature. Additionally, the deposition rate R has to be taken into account. We found that an increasing ratio $j_{O^*}/R$ causes a increasing specific electrical resistance and a reduced optical absorption. It could be demonstrated that the lateral variation of the electrical, optical and structural film properties qualitatively equals to the change of the film properties achieved by the variation of the operation point of the sputter process at different oxygen flow rates $F_{O2}$. Therefore we describe the locally changed film properties in terms of a local shift of an ideal homogeneous process operation point.

## 1. Introduction

Transparent conductive oxide (TCO) films are a key component in many opto-electronic devices like touch panels, photovoltaic cells or display elements. For many purposes indium tin oxide (ITO) films are used. In case of industrial applications they are mainly deposited by reactive sputtering technologies.

Different technical applications require varied sheet resistances of the ITO films. For instance the usage as an electrode for touch panels needs 400 ... 600 $\Omega_{sq}$ [1]. In contrast, as an electrode for OLED elements a sheet resistance of only 20 $\Omega_{sq}$ is required. For economically reasons the desired sheet resistance has to be obtained at a film thickness as low as possible to reduce the deposition time. At first, this implies the requirement for optimized film resistivity values. They can be obtained only at a well defined operation point of the deposition process, where a minimal electrical resistance and an acceptable optical transparency are obtained at the same time. At a given discharge power the operation point depends of the reactive gas flow rate ($F_{O2}$). Secondly, for dynamic deposition processes with moving substrates the requirement of a strong homogeneity of the lateral distribution of the process parameters can be concluded.

Our investigations were focused on the influence of the cross magnetron effect (CME) on the process parameter distribution, the film growth and the resulting functional film properties using a dual magnetron assembly. We have measured the lateral distribution of the plasma

parameters using Langmuir double probes and the deposition rate distribution. The electrical and optical properties as well as the structur of the ITO films will be discussed in relation to the process parameters. Local deviations of the electrical and optical film properties will be compared with those caused by a certain lateral variation of operation point of the process.

## 2. Experimental

The ITO films were deposited by reactive pulsed magnetron sputtering in a vertical inline sputtering system (type DMS 400, FHR Anlagenbau, Germany). The sputtering system was equipped with a dual magnetron, consisting of two spatially separated single magnetron sources at a distance of 210 mm. Two In:Sn alloy targets (400 x 130 $mm^2$) containing 10 wt.-% of tin were mounted on the dual magnetron source which was powered in the bipolar mode by a mid frequency (70 kHz) sine-wave generator. All experiments were performed at a constant power of 2 kW per target with the target operating in the transition mode. The magnetron sources were optimized regarding the target erosion, i.e. they did not show the anomalous target erosion usually connected to the CME.
The argon flow rate was fixed at 40 sccm and the oxygen flow rate was adjusted between 35 and 70 sccm depending on the desired operation point. The total pressure was kept constant at 0.4 Pa using a shutter.
Investigation of the plasma properties has been done by using a self-developed Langmuir double probe system [2]. The electrical resistivity of the ITO films was measured using a four-point probe, while the films thickness was taken from profilometer results. Optical properties of the films have been determined by transparency and reflectivity measurements. Experiments and modelling were done in the spectral range of 400 nm up to 830 nm. The refractive index n and the extinction coefficient k were determined on the basis of a Drude–Lorentzian double oscillator model using the software VWASE.

## 3. Results

### *3.1 Film properties*

We have deposited ITO films on glass and silicon substrates applying a static deposition process. In such experiments the lateral distribution of the films properties reflects the process parameter distribution like a finger print. It allows the correlation of the electrical, optical and structural properties to the measured plasma parameters, the thermal load on the substrates due to the particle bombardment of the growing film and the plasma radiation, and the deposition rate R.
Figure 1 exhibits the distribution of the specific electrical resistivity and - for a better overview - qualitatively the optical absorption. The extinction coefficient of these samples varied between $10^{-2}$ and $6 \cdot 10^{-1}$ (see also figure 3). The electrical resistivity and the optical absorption of the ITO films show a diagonal asymmetry, whereby a high transparency, for instance at the position P7 at source 2, is connected with a high electrical resistivity value. On the other hand, beyond a minimum at the center position P5 the electrical resitivity seems to increase again, connected with the increasing optical absorption of the films (see position P3). The assymmetry correlates with the appearance of the CME.
The lateral diagonal asymmetry of the film properties is confirmed by the structure analysis of the ITO samples. The REM pictures of the cross section and partially of the film surface of the ITO samples on position P7 (a) and P3 (b) of source 2 (figure 2) prove a different crystalline structure on these positions, mainly a different grain size. A small grain size is obtained at position P7, where transparent, but low conductive ITO films were deposited. More detailed results of XRD investigations are published in [3].

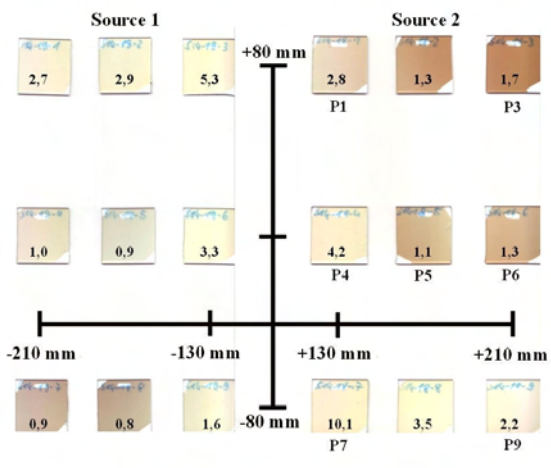


Figure 1. Electrical resistivity (in $10^{-3}$ Ωcm) and a qualitative display of the optical absorption of reactive sputtered ITO films. Source 1 and source 2 designate the components of the dual magnetron. P1 to P9 are position numbers.

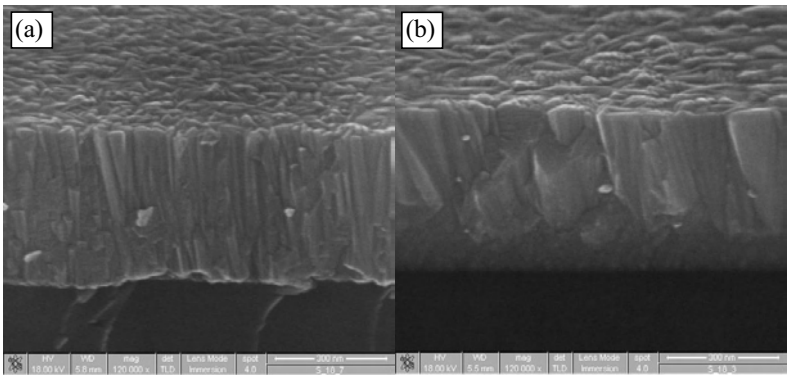


Figure 2. REM pictures of ITO samples on different positions. (a) is sample on P7, (b) is on position P3

### *3.1 Process properties*

Careful measurements of the film thickness along horizontal lines (e.g. from sample 1 to sample 3 etc.) have always shown thickness profiles which were symmetric with respect to the longitudinal axis of symmetry. This confirms that the magnetron sources of the dual magnetron were optimized in respect to the target erosion, which is not influenced by the CME.

In contrast, Langmuir probe measurements of the charge carrier density $n_i$ and the electron temperature $T_e$ clearly have revealed a CME influence on the plasma properties. At positions showing transparent ITO films we have measured $n_i$ up to $6 \cdot 10^{10}$ $cm^{-3}$, on the other hand a high optical absorption correlates to $n_i$-values of about $2 \cdot 10^{10}$ $cm^{-3}$ [3]. The behavior of the plasma parameter measurements corresponds to the thermal load of the samples during the film growth, which grows monotonously with the measured charge carrier density [3]. The thermal load at low $n_i$ values was 0.21 $J \cdot s^{-1} \cdot cm^{-2}$ and at high $n_i$ values about 0.17 $J \cdot s^{-1} \cdot cm^{-2}$.

## 4. Discussion

We discuss the strongly different film properties at equal deposition rates in terms of a different concentration of dissociated oxygen O* at the substrate position. We consider any atomic oxygen species, i.e. ions or atoms in the ground as well as in an excited state as components of O*. The flux $j_{O*}$ of dissociated oxygen towards the substrate depends on the charge carrier density, the oxygen partial pressure ($p_{O2}$) and a value $k(T_e)$ depending strongly on the electron temperature $T_e$. Therefore we get

$$j_{O*} \propto n_e \cdot p_{O2} \cdot k(T_e) \qquad (1)$$

Furthermore, the total particle flux to the substrate surface $j_{tot}$ is proportional to the growth rate R. Following this, any deviation of the ratio $j_{O*}/R$ from that value which results in optimized functional film properties indicates a certain surplus or a lack of reactive oxygen particles. At a given R the ratio $j_{O*}/R$ can be changed by the variation of the $p_{O2}$, correlating to the variation of the operation point of the integral process. On the other hand, the $j_{O*}/R$ can be also varied due to the locally different plasma properties, which result in a varied $j_{O*}$ corresponding to Eq. (1), or due to a locally different flux of target particles to the substrate.
This equivalence of both possibilities could be demonstrated by comparing the dependence of the optical absorption and the electrical resistivity in dependence on the reactive gas flow $F_{O2}$ [3] or, on the other hand, on the locally different $j_{O*}/R$ (figure 3). Both parameters result in qualitatively equal curves. Therefore we interpret the locally changed film properties in terms of a local shift of the process operation point. An detailed analysis of the variation of the local film properties leads to an shift, which corresponds to a deviation of $F_{O2}$ by ±1.8 sccm.

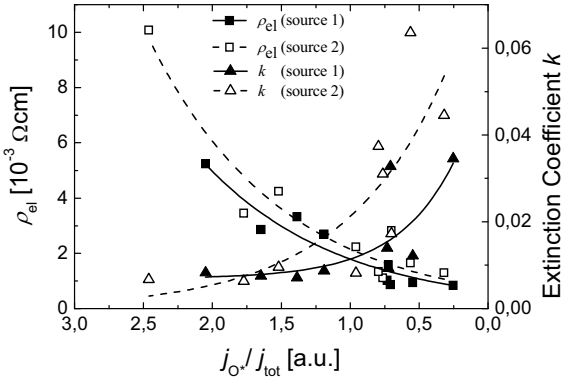


Figure 3. Dependence of the electrical resitivity and the optical absorption on the ratio jO*/jtot for both components of the dual magnetron.

## 5. References

[1] M. Fahlandt, T. Vogt, W. Schoenberger, Thin Sol. Films 516 5777 (2008)
[2] R. Pintaske, Th. Welzel, N. Kahl, M. Schaller, J. Hahn and F. Richter, Surf. Coat. Technol. 90 275 (1997)
[3] H. Kupfer, F. Richter, Reactive Magnetron Sputtering of Indium Tin Oxide Thin Films, in: D. Depla, S. Mahieu, „Reactive Sputter Deposition“ (Springer Series in Materials Science 109), Springer-Verlag, Berlin, Heidelberg, 2008, ch. 10, p. 337-366 (ISBN-10: 3540766626)

## 6. Acknowledgements

The authors appreciate financial support of the State Ministry of Economic Affairs and Labour of Saxony as well of the European Union and the Federal Ministry of Education and Research of Germany.

# Improvement of the structural quality of reactively sputtered ZnO:Al thin films by means of advanced seed layers.

**D. Koehl, M. Wuttig**
RWTH Aachen University, I. Institute of Physics (IA), Sommerfeldstr. 14, 52074 Aachen, Germany

Reactively sputtered ZnO:Al thin films exhibit structural deficiencies when deposited at unheated substrates. This is mainly due to the energetic impact of the highly energetic oxygen ions bombarding the growing film, a subject of research for the last few decades. To promote structural self-healing during growth, films are usually deposited onto heated substrates at temperatures of about 200-300°C to yield high quality ZnO:Al films. However, this technique suffers from drawbacks such as increased process costs and limitations in the choice of substrates with sufficient temperature stability. Therefore it would be very desirable to have techniques that enable room temperature deposition of ZnO:Al films with exceptionally high structural qualities.
We will show that the growth of ZnO:Al thin films can be well separated into a nucleation stage and a post-nucleation growth stage. It is the structure of the nucleation stage which governs the quality of the final film. We will furthermore show a special technique to tailor the structural properties during the nucleation stage by employing an advanced seed layer for the growth of high quality ZnO:Al films on cold substrates.

# The Stoney Equation for Silicon (001) and (111) wafers

**G.C.A.M. Janssen**
TU Delft, Materials Science and Engineering, Mekelweg 2, 2628CD Delft, Netherlands

Stress in a thin film on a flexible substrate induces a curvature of the substrate. Usually the substrate is orders of magnitude thicker than the film, leading to small and purely elastic deformation of the substrate. In this case, the Stoney equation yields the stress in the film from the measured curvature of the substrate. The Stoney equation contains thickness of film and substrate and the elastic properties of the substrate. Typically the elastic properties of the substrate are specified by E (Young's modulus), and $\nu$ (Poisson's ratio). E and $\nu$ provide a valid description for elastically isotropic substrates, e.g. polycrystalline steel strips, as used by Stoney in 1909.
Today the Stoney equation is still used for relating substrate curvature to film stress. However, in the majority of thin film stress measurements by means of substrate curvature, Si wafers are used as the substrate. Silicon wafers are cut from single crystals and are thereby elastically anisotropic. In the present paper, a modified form of the Stoney equation, well known for elastic isotropic substrates, is derived for Si(001) and Si(111) wafers, using the elastic stiffness constants of silicon, $c_{ij}$, instead of the orientation averaged values E and $\nu$, which do not have a meaning for elastically anisotropic single crystal materials.
Curvature measurements of thin films on Si(001) and Si(111) wafers are presented. The difference in film-stress-induced curvature of Si(001) and Si(111) wafers is discussed.

# In situ evolution of the growth stress during the early stage of sputter deposition of Mo/Si thin films

**A. Fillon [1], G. Abadias [1], A. Michel [1], C. Jaouen [1]**
1. Laboratoire PHYMAT, Université de Poitiers-CNRS, SP2MI, Téléport 2, Bd Marie et Pierre Curie, 86962 Chasseneuil-Futuroscope, FRANCE

Stress evolution during magnetron sputtering deposition of Mo thin films onto Si was monitored with in situ real-time curvature measurements. The data show the presence of a large tensile stress in the early stage of the growth for deposition onto a crystalline Si substrate prepared by ion etching, while a more complex evolution is observed when the metallic film is grown on an amorphous Si layer. In the latter case, the features of the evolution are ascribed to the amorphous to crystalline phase transformation taking place at a critical thickness and to a related negative volume change. Finally, for higher thickness, a steady-state stress regime is attained which, depending on the deposition conditions, is either compressive or tensile.

## 1. INTRODUCTION

The origin of stress in polycrystalline thin films has gained a renewed interest with the potentiality offered by real-time techniques to measure stress evolution during growth [1,2]. Such in situ measurements not only yield the magnitude of the growth stress, but also provide insights into the growth mechanism itself. Stress models have been proposed to explain the complex behavior of high-mobility materials (like Ag, Al) grown by evaporation. A typical three-stages stress evolution reported by many groups [2-6], is related to microstructural evolution during Volmer-Weber (3D) growth: in the pre-coalescence stage, a small compressive stress is found, at coalescence the stress turns tensile, and finally reaches a constant value. This post-coalescence steady-state stress depends on growth flux and adatom mobility. For high mobility metals and low growth flux, the stress is compressive and a reversible tensile change is observed during growth interruption [2-6]. Many models have been proposed to account for these evolutions but their physical origins are still under debate.
Stress evolution during sputtering has been less investigated [7-9], although stress producing or relaxation mechanisms like intermixing, phase stabilization and defect formation may be favored due to the higher energetics of sputtering deposition compared to thermal evaporation. For low-mobility metals like molybdenum (Mo), the atomic peening mechanism [10,11] may contribute significantly to the stress build-up, making the overall stress compressive due to incorporation of defects [12]. However, the stress evolution in the early stage of metal sputtering remains largely unexplored, in particular the interplay between stress and reactivity with the substrate. We show that in situ stress measurements during growth of Mo on silicon (Si) or on Si oxide layers allows to address this issue, which is also of technological relevance for fabrication of devices for microelectronics or optoelectronics.

## 2. EXPERIMENTAL DETAILS

Mo thin films are deposited at room temperature by dc magnetron sputtering on Si (001) wafer covered with native oxide (oxidized Si) using Ar as the working gas in a deposition chamber equipped with three independent planar magnetron sources. Layer thicknesses are controlled by magnetron power and deposition time. Samples are deposited at Ar working pressure varying from 0.1 Pa to 0.6 Pa and deposition rates are between 0.56 Å/s and 1.3 Å/s. Additionally, films are grown on amorphous Si buffer layers ( $a-\mathrm{Si}$ ) deposited in situ and on Si wafers (etched Si) that are treated in situ for 90 s at ~ -70 V to remove the native oxide.
Stress evolution during growth is monitored using a multibeam set-up [13]. The sample is mounted, facing downward, onto substrate holders which allow unconstrained bending of the substrate. The force per unit width, $F/w$, given by the product between the average stress <σ> and film thickness $h$ according to the well-known Stoney's equation [14] is calculated from the change between adjacent laser spots. By convention, positive σ refers to a tensile stress state. The standard deviation in the spacing measurement is determined to be $\sigma_D = 2.10^{-4}$, giving a typical sensitivity of ~ 8 MPa for a 10 nm film on a 0.1 mm-thick Si substrate.

## 3. RESULTS AND DISCUSSION

### *3.1 Stress evolution in pure Mo films: Influence of deposition conditions*

Figure 1 displays the evolution of the intrinsic force per unit width versus thickness for Mo thin films grown onto oxidized Si (001) substrates, for working pressures in the range 0.1 Pa to 0.6 Pa. The influence of a negative bias voltage (-60 V) on the substrate is also shown. The incremental stress at a given thickness is deduced from the local slope of these curves.

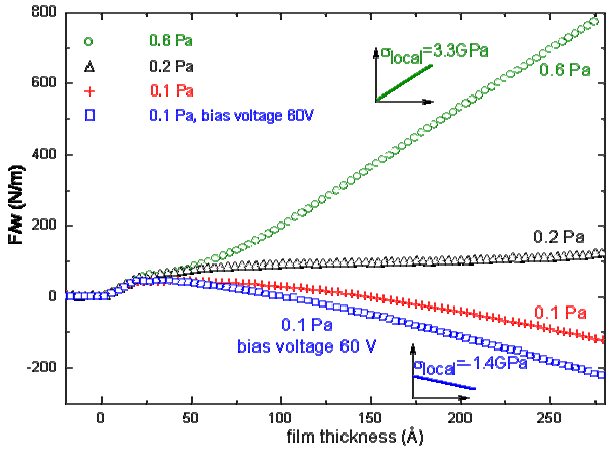


Figure 1. Force per unit width versus thickness during growth of a Mo thin film on (001) Si wafer at different Ar working pressures and substrate bias voltage (deposition rate: 0.56 Å/s).

Three main stages can be distinguished: in the initial stage (h < 2 nm), the force change can be attributed to either surface stress change or possible interfacial effects; second, an intermediate stage with constant force (that will be discussed in the next section) is observed. In the third stage, the steady-state stress can be compressive or tensile depending on Ar working pressure. When the growth flux is interrupted, no relaxation is detected, neither in the compressive nor in the tensile regime, independent of the deposition conditions (see for example Fig. 2b)). Such behavior is consistent with the low mobility character of refractory metals like Mo. The drastic change in the stress magnitude, from 3.3 GPa to –1.4 GPa could result from the competition between two stress generation mechanisms. In the low pressure

regime, contribution of atom insertion prevails: this mechanism is related to the high energy of incoming particles (sputtered atoms, backscattered Ar neutrals) and induces compressive stress[10, 11]. At higher pressure, grain boundary formation in polycrystalline thin films generates tensile stress[15-16].
Nevertheless, a detailed structure investigation would be required in order to correlate this transition from compressive to tensile stress with the corresponding evolution to a less dense microstructure.

### *3.2 Stress evolution in pure Mo films: effect of substrate reactivity*

The tensile force plateau visible in the second stage (film thickness of 2.0 – 3.0 nm) in Fig. 1 recalls the behavior associated with the nucleation, growth and coalescence of islands in the Volmer-Weber growth mode. However, AFM observations of the initial growth stages indicate no island growth. To get a better insight on these first stages, stress evolutions are compared for Mo growth on different substrates. Figure 2.a) reports the stress evolutions observed for oxidized Si, etched Si and $a-\mathrm{Si}$ substrates. During the preliminary $a-\mathrm{Si}$ sputtering deposition, a constant compressive stress (-1.6 GPa) is observed, a well known effect in amorphous high mobility films, which is attributed to a cumulative action of surface stress [17].

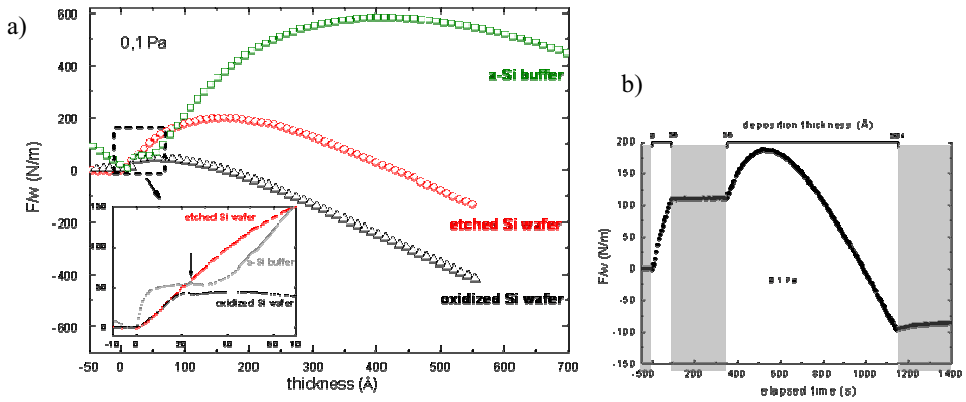


Figure 2. a) Force per unit width versus thickness for Mo thin films grown on differently prepared substrates (deposition rate 0.56 Å/s). b) Force per unit width versus elapsed time for a Mo thin film (deposition rate 0.56 Å/s) deposited on a (001) etched Si wafer. The grey rectangles indicate growth interruptions.

While all curves tend towards a similar compressive steady-state regime, the early growth stages present dissimilar stress developments (see inset of Fig. 2.a)). For etched-Si and oxidized-Si substrates, the curves start with an identical tensile stress, pointing to a similar interfacial reaction with the substrate. The Mo film reaches its steady-state compressive stress at a smaller thickness for oxidized-Si than for etched-Si. Indeed, the presence of oxygen seems to counterbalance the tensile stress generation, acting as a relaxation mechanism. In contrast, deposition onto $a-\mathrm{Si}$ presents a steep force variation clearly related to the surface stress change, followed by a constant-force plateau where a transient effect occurs (see arrow in the inset). This phenomenon is attributed to the prompt transformation from an amorphous into a crystalline phase at a critical thickness of $\sim 2$ nm. Both XRD and TEM observations performed on Mo/a-Si multilayers allow to confirm this amorphous to crystalline transition. This phase transformation should involve a negative volume change, which in turn might induce the development of a tensile stress during subsequent coherent growth.
It is worth to emphasize that in all cases, despite the large stress variations observed, the same steady-state stress is attained.

All the previously described experiments contribute to bring into light the essential factors involved in the development of stress during growth, such as interfacial reactions and deposition conditions. Moreover, this study allows to discuss the connections between growth, microstructure and stress evolution. The next step of the work is to explain the stress evolutions during the deposition of Mo/a-Si multilayers.
Figure 3 presents the stress evolution of a Mo/a-Si multilayer deposited by magnetron sputtering, and shows the multiplicity of phenomena taking place during the growth. The general evolution is quite consistent with the data obtained previously by Freitag and Clemens [7]. For each sublayer, the abrupt variation of stress in the initial deposition stage is attributed to surface stress change. The different stages during the Mo layer deposition can be explained according to the previous analyses; however, here, the limited Mo thickness does not permit the evolution to a steady state.

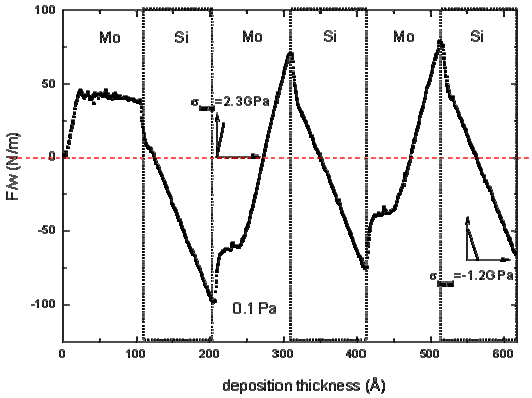


Figure 3. Force per unit width versus thickness measured during the growth of a Mo 10 nm/a-Si 10 nm multilayer on an oxidized Si substrate (deposition rate 0.56 Å/s for both Mo and Si layers).

Nevertheless, the mechanisms taking place at the interfaces still need to be clarified, as the interfacial effects are of prime importance for the phase transformation and the microstructure of the multilayers. Understanding the stress in Mo/a-Si multilayers can elucidate the details of the growth process and the consequences on the structural and physical properties.

## 4. References

[1] R. Abermann, R. Kramer, and J. Mäser, Thin Solid Films 52 215 (1978)
[2] J. A. Floro, E. Chason, R. C. Cammarata, and D. J. Srolovitz, MRS Bull. 27 19 (2002)
[3] E. Chason, B. W. Sheldon, L. B. Freund, J. A. Floro, and S. J. Hearne, Phys. Rev. Lett. 88 156103 (2002)
[4] C. Friesen, S. C. Seel, and C. V. Thompson, J. Appl. Phys. 95 1011 (2004)
[5] A. L. Del Vecchio and F. Spaepen, J. Appl. Phys. 101 063518 (2007)
[6] R. Koch, D. Hu, and A. K. Das, Phys. Rev. Lett. 94 146101 (2005)
[7] J. M. Freitag and B. M. Clemens, Appl. Phys. Lett. 73 43 (1998)
[8] M. Pletea, W. Brückner, H. Wendrock, R. Kaltofen, J. Appl. Phys. 97 054908 (2005)
[9] I. Fernandez-Martinez, J.L. Costa-Krämer, F. Briones, J. Appl. Phys. 103 113902 (2008)
[10] F. M. d'Heurle, Metall. Trans. 1 725 (1970)
[11] H. Windischmann, Crit. Rev. Solid State Mat. Sci. 17 547 (1992)
[12] A. Debelle, G. Abadias, A. Michel, C. Jaouen, Appl. Phys. Lett. 84 5034 (2004)
[13] J.A. Floro, E. Chason, L.B. Freund, R.D. Twesten, R.Q. Hwang, Phys. Rev. B 59, 1990 (1999)
[14] G.G. Stoney, Proc. R. Soc. London, Ser. A 82, 172 (1909)
[15] R.W. Hoffmann, Phys. Thin Films 3, 211 (1966)
[16] W.D. Nix and B.M. Clemens, J. Mat. Res. 14, 3467 (1997)
[17] J.A. Floro, P.G. Kotula, S.C. Seel and D.J. Srolovitz, Phys. Rev. Lett. 91, 0961101 (2003)

# Direct determination of surface stress during Bi-mediated Ge growth on Si

**H. Asaoka [1], T. Yamazaki [1,2], S.N. Filimonov [3], S. Shamoto [1]**

1. Quantum Beam Science Directorate, Japan Atomic Energy Agency (JAEA), Tokai, Ibaraki 319-1195, Japan

2. Eiko Engineering Co., Ltd., Hitachinaka, Ibaraki 312-0024, Japan.

3. Tomsk State Univ., Lenin Prospekt, Tomsk 634050, Russia

We report stress evolutions during Bi adsorption on Si(111) 7x7 and initial stages of Bi-mediated Ge growth on Si(111). Surface stress is determined by using a real-time measurement of the substrate curvature. We find a difference in the surface stress between clean Si(111) 7x7 surface and Si(111) √3x√3 surface covered with one monolayer of Bi, and an increase in the surface stress accompanied by RHEED intensity oscillation of the specular beam during ideal pseudomorphic Ge layer growth with Bi. For Ge coverage of up to 2 bilayers, the stress evolution shows a clear stress relaxation due to formation of trenches on the Ge surface and injection of misfit dislocations into the Ge/Si interface.

## 1. INTRODUCTION

Interplay of surface stress and surface free energy determines the growth mode of heteroepitaxial layers. Therefore, surface morphology is sensitive to the presence of a third species on the surface, so-called surfactant. For instance, it is well known that the Stranski-Krastanow (SK) growth mode of Ge on Si [1-3] can be suppressed with the surfactant [4-6]. In such a surfactant-mediated epitaxy (SME), a flat Ge layer grows on Si while the surfactant floats up to the growth front and always covers the Ge surface. The stress in the Ge layer is relaxed by injection of dislocations into the Ge/Si interface [7,8].

Recently, Bi has attracted a lot of attention as a surfactant in Ge/Si(111) heteroepitaxy due to its ability to suppress Ge-Si intermixing [9] and provide a chemical contrast between Ge and Si in a Scanning Tunneling Microscope (STM), allowing fabrication of self-organized Ge/Si nanostructures on the Si(111) surface [10]. In addition, low incorporation of Bi in the Ge layer [11] allows to remove it from the surface after Bi-mediated growth [12].

In this work, we have focused on the stress evolution during the initial stages of Bi adsorption on Si(111) 7x7 and Bi-mediated growth of Ge on Si(111). The stress behavior and surface morphology were observed simultaneously by using real-time measurements of the substrate curvature and Reflection High Energy Electron Diffraction (RHEED). We find a difference in the surface stress between the clean Si(111) 7x7 surface and the Si(111) √3x√3 surface covered with one monolayer of Bi (1 ML = $7.8 \times 10^{14}$ atoms/cm$^2$), and an increase of the compressive surface stress accompanied by RHEED intensity oscillation of the specular beam during Bi-mediated Ge growth. For Ge coverage of up to 2 bilayers (1 BL = 2 ML), the stress evolution shows a clear stress relaxation due to formation of trenches on the Ge surface and injection of misfit dislocations into the Ge/Si interface.

## 2. Experimental procedures

Real-time stress and RHEED measurements were performed in an ultrahigh vacuum (UHV) system with a base pressure of $1x10^{-8}$ Pa. Substrates were both side mirror polished Si(111) wafers with a diameter of 25 mm and a thickness of 0.1 mm. They were chemically treated before introduction into the UHV system in the following way: the substrates were boiled in a solution of $H_2SO_4$:$H_2O_2$ = 3:1 for 10 min to grow a clean oxide layer on the surfaces. Then the oxide layer was removed by etching the samples by 1% HF solution for 5 min. After this process, they were dipped in a 40% $NH_4F$ aqueous solution for 30 s to terminate the surfaces. The temperature in the final process was maintained at 80 ˚C. They were checked with Auger Electron Spectroscopy (AES) to see that no contamination remains on the surfaces. The deposition amount and the rate were monitored by a quartz crystal oscillator located close to the substrate position. The values from the quartz crystal oscillator were corrected by using X-ray reflectivity profile of Bi surfactant-mediated Ge layer on Si. Bi (99.99%) and Ge (99.999%) atoms were deposited on Si(111) surfaces at 500 ˚C. Stress behavior during growth was observed by means of a substrate curvature measurement using a multiple parallel laser beam technique [13,14]. This system consists of a diode laser, beam-splitters, and a position detector as shown in Figure 1. The incident beam on the beam-splitters forms an array of parallel beams which are simultaneously reflected off the surface and onto the position detector. If a thin film under stress leads to bending of a substrate, the parallel beams of light that strike it at different positions will be reflected at different angles. The relationship between the stress in film, $\sigma_f$ and the radius of curvature, $R$ is given by the following equation developed originally by Stoney [15]:

$$\sigma_f h_f=(M_s h_s^2)/(6R) \qquad (1)$$

where $M_s$ and $h_s$ are the substrate's biaxial modulus and the thickness, respectively, and $h_f$ is film's thickness. The product of the film stress and the film thickness is inversely proportional to the radius of curvature, which can be measured by the deflection of parallel light beams:

$$1/R=(\delta d/d_0)(\cos\alpha)/2L \quad (2)$$

where $\delta d$ is the measured change in beam spacing, $d_0$ is the initial spacing, $L$ is the distance from the sample to the detector and $\alpha$ is the angle between the incident beams and the surface.

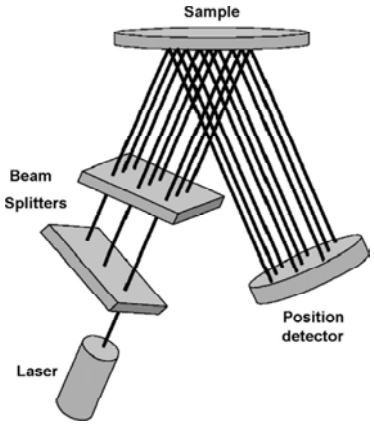


Figure 1. Schematic setup of a substrate curvature measurement technique.

## 3. Results and discussion

The H-terminated Si(111) surface prepared by the chemical treatment shows a 1x1 streaky RHEED pattern. After heating this surface up to 600 ˚C, the pattern changes to a 7x7 reconstructed surface. The initial substrate shows zero curvature because both sides of the substrate have the same surface structure and surface stress. At the beginning of Bi adsorption on Si(111) 7x7, the substrate starts to bend (Figure 2) due to the surface stress difference between the front and rear sides. Simultaneously, a √3x√3 structure appears in the RHEED pattern indicating formation of a Bi-terminated surface. The Bi-terminated Si(111) surface transforms from the √3x√3-α reconstructed surface at 1/3 ML to the √3x√3-β reconstructed surface at saturated Bi coverage of 1 ML [16,17] at 500˚C (Figure 3a and b). The surface stress ($\sigma_f h_f$ in equation (1)) also saturates at the completed 1 ML Bi coverage on Si(111) after 200 s in Figure 2. The measured surface stress difference between the clean Si(111) 7x7 surface and the Si(111) √3x√3-β surface covered with 1 ML Bi is -1.8 N/m (-1.4 eV/(1x1 unit cell)).

At the beginning of the Ge deposition, the substrate continues to bend. As can be seen from Figure 2, the surface stress increases almost linearly with the Ge coverage which indicates formation of a compressively strained two-dimensional Ge layer on Si(111) covered with Bi. The observed stress gradient matches with the calculated stress value of 2.30 (N/m)/BL estimated for an ideal pseudomorphic strained Ge layer structure on Si(111). Simultaneous RHEED measurement shows clear intensity oscillations of the specular beam during growth of the pseudomorphic strained layer indicating the layer-by-layer growth mode of the Ge layers (Figure 4). The period of oscillation corresponds to the deposition of a single Ge BL. When the coverage approaches the critical value around 2 BL, the stress evolution shows a clear stress relaxation. This is consistent with STM reports on the onset of the trench formation with an increase in surface roughness, and with the interfacial misfit dislocation injection in the Ge/Si(111) leading to the stress relaxation at the coverage of 2 BL [18,19].

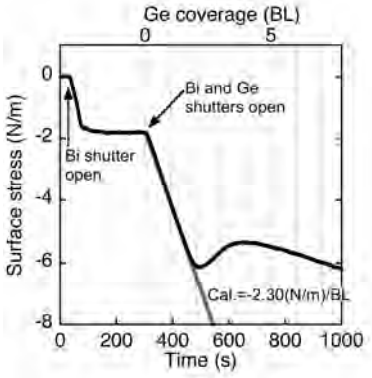


Figure 2. Real-time surface stress measurement during Bi adsorption on Si(111) 7x7 and initial stages of Bi-mediated Ge growth on Si(111) at 500 ˚C.

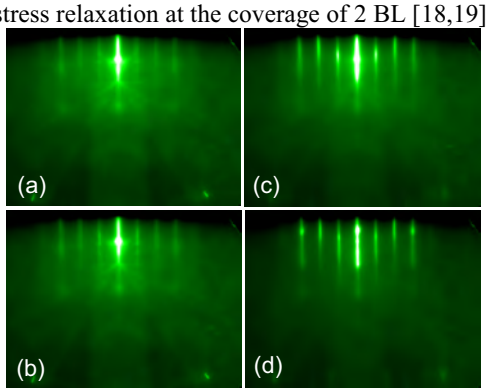


Figure 3. Evolution of the RHEED patterns during (a,b) Bi adsorption on Si(111) 7x7 and (c,d) initial stages of Bi-mediated Ge growth on Si(111) at 500 ˚C. The orientation of incident electron beam is parallel to the [] azimuth of Si(111) substrates. The coverage is (a) 1/3 ML of Bi, (b) 1 ML of Bi, (c) 1 BL of Ge with Bi, and (d) 5 BL of Ge with Bi.

The relaxed Ge layer with dislocations can grow on Si in the layer growth mode. During the Ge growth, the surface structure doesn't show the characteristic 5x5 RHEED pattern, but the √3x√3 pattern is preserved (Figure 3c and d) indicating 1 ML Bi termination of the Ge surface is also preserved. The observed stress evolution reveals the surfactant-mediated growth with a

variety of stress relief processes, which can drive changes in the growth mode during the Ge heteroepitaxial growth with Bi.

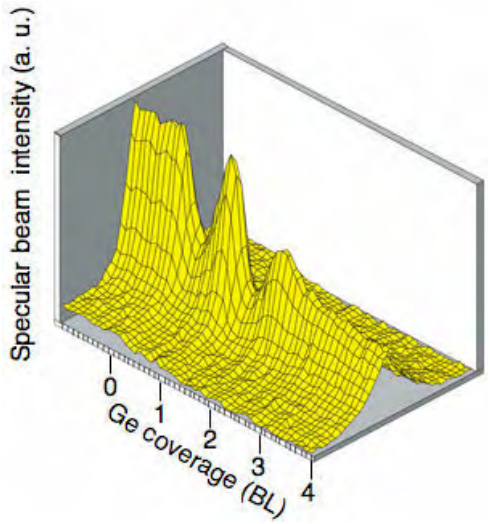


Figure 4. RHEED intensity oscillation of the specular beam during Bi surfactant-mediated Ge growth at 500 ˚C. The orientation of incident electron beam is parallel to the [] azimuth of Si(111) substrates.

## 4. Conclusion

Stress evolutions during initial stages of Bi adsorption on Si(111) 7x7 and Bi-mediated growth of Ge on Si(111) are studied by using real-time measurements of substrate curvature and RHEED. It shows the surface stress difference is -1.8N/m (=-1.4eV/(1x1 call)) between a Si(111) 7x7 and a Si(111) $\sqrt{3}$x$\sqrt{3}$-β with 1 ML Bi adsorption. When Ge is deposited with Bi, an increase in compress surface stress accompanied by RHEED intensity oscillation of the specular beam is followed by clear stress relaxation at the coverage of 2 BL due to trench formation on the Ge surface and injected misfit dislocation into the Ge/Si interface.

## References

[1] D. J. Eaglesham, M. Cerullo, Phys. Rev. Lett. **64**, 1943 (1990).
[2] Y.-W. Mo, D.E. Savage, B.S. Swartzentruber, M.G. Lagally, Phys. Rev. Lett. **65**, 1020 (1990).
[3] U. Köhler, O. Jusko, G. Pietsch, B. Müller1, M. Henzler, Surf. Sci. **248**, 321 (1991).
[4] M. Copel, M.C. Reuter, E. Kaxiras, R.M. Tromp, Phys. Rev. Lett. **63**, 632(1989).
[5] M. Copel, M.C. Reuter, M. Horn-von Hoegen, R.M. Tromp, Phys. Rev. B **42**, 11682(1990).
[6] M. Horn-von Hoegen, M. Copel, J.C. Tsang, M.C. Reuter, R.M. Tromp, Phys. Rev. Lett. **67**, 1130(1991).
[7] F.K. LeGoues, M. Horn-von Hoegen, M. Copel, R.M. Tromp, Phys. Rev. B **44**, 12894(1991).
[8] G. Meyer, B. Voigtländer, N.M. Amer, Surf. Sci. Lett. **274**, L541(1992).
[9] N. Paul, S.N.Filimonov, V. Cherepanov, M. Çakmak, B. Voigtländer, Phys. Rev. Lett. **98**, 166104(2007).
[10] M. Kawamura, N. Paul, V. Cherepanov, B. Voigtländer, Phys. Rev. Lett. **91**, 096102(2003).
[11] M. Horn-von Hoegen, F.J. Meyer zu Heringdorf, M. Kammler, C. Schaeffer, D. Reinking, K.R. Hofmann, Thin Solid Films, **343-344**, 579 (1999).
[12] N. Paul, B. Voigtländer, Surf. Sci. **551**, 80 (2004).
[13] R.E. Martinez, W.M. Augustyniak, J.A. Golovchenko, Phys. Rev. Lett. **64**, 1035 (1990).
[14] J. A. Floro, E. Chason, S.R. Lee, R. D. Twesten, R. Q. Hwang, L. B. Freund, J. Electeon. Mater. **26**, 983(1997).
[15] G.G. Stoney, Proc. Roy. Soc. **A82**, 172(1909).
[16] K.J. Wan, T. Guo, W.K. Ford, J.C. Hermanson, Phys. Rev. B **44**, 3471(1991).
[17] S. Nakatani, T. Takahashi, Y. Kuwahara, M. Aono, Phys.Rev. B **52**, R8711(1995).
[18] N. Paul, H. Asaoka, J. Mysliveček, B. Voigtländer, Phys. Rev. B **69**, 193402 (2004).
[19] N. Paul, H. Asaoka, B. Voigtländer, Surf. Sci. **564**, 187 (2004).

# Influence of plasma parameters and structural properties on the stress behaviour in thin AlN films deposited by Magnetron Sputtering

**B. Abdallah [1, 2], M-A. Djouadi [1], P-Y. Jouan [1], C. Ewels [1], A. Soltani [3], J-C. Gerbedoen [3], S. Rahmane [4]**

1. Institut des Matériaux Jean Rouxel, IMN-LPCM, UMR CNRS 6502, 2 rue de la Houssinière BP 32229, 44322 Nantes, France.

2. Atomic Energy Commission Syria (AECS), P.O.Box 6091, Damascus, Syrian Arab Republic.

3. Institut d'Electronique, de Microélectronique et de Nanotechnologie (IEMN/DHS) CNRS Cite Scientifique Avenue Poincaré BP69 59652 Villeneuve d'Ascq Cedex, France.

4. Département de Physique, Université de Biskra, BP 145 RP, 07000 Biskra, Algérie.

The thermal, acoustic, dielectric and piezoelectric properties of aluminium nitride make it a good candidate for many applications in electronics and telecommunications devices [1]. AlN is a wide band gap material ($E_g$=6.2 eV) with high electrical resistance, high breakdown voltage and low dielectric loss [2].

The stress of AlN films is very important in device manufacturing, especially for SAW and FBAR devices. We have therefore chosen to consider more carefully the evolution of the residual stress in AlN films depending on the thickness for experimental conditions.

A fine structural study was conducted by high-resolution electronic microscopy (HRTEM) to identify the orientation of crystal AlN films and their texture, and we conducted a mathematical calculation to estimate surface [3] and strain energy [4] for several crystallographic orientations. We have developed a model capable of explaining the reduction of the residual stress with thickness, taking into account the surface energy and the grain size.

Finally we link the stress behaviour to plasma parameters. Starting with Windischmann and Davis models, we propose a model to express the stress including the plasma parameters (ion flux, bombardment energy), the mechanical and structural properties and grain size of the film.

[1] Saravanan, S.; Berenschot, E.; Krijnen, G.; Elwenspoek, M., The 13th International Conference on Vol 2, Issue , 5-9 June 1362 (2005)

[2] S. Strite and H. Morkoc, J. Vac. Sci. Technol. B 10 1237 (1992)

[3] J.P. Zhao et al, J. Phys. D: Appl. Phys. 30 5 (1997)

[4] G. F. Cardinale et al, J. Vac. Sci. Technol. A 15(1) 196 (1997)

# Formation of patterned GaInAs/GaAs hetero-structures using amorphous arsenic mask in molecular beam epitaxy

**Y. Suzuki [1], K. Motoki [1], M. Tabuchi [2], Y.Takeda [2]**

1. Graduate School of Engineering, Nagoya University, Nagoya, 464-8603, Japan

2. Venture Business Laboratory, Nagoya University

In order to form patterned GaInAs hetero-structures on GaAs, we proposed a new fabrication process using amorphous As (a-As) layer as a mask for electron beam (EB) lithography. An amorphous As layer is easily deposited in a normal molecular beam epitaxy chamber and is removed by only heating it at about 350ºC. In this work, we attempted to find a condition to remove In on the a-As layer selectively. It was demonstrated that selective removing of In on a patterned a-As layer was achived by annealing at 450ºC in a UHV environment. AES analysis of the sample after annealing showed that In remained in the 170×140μm² area, where the a-As layer was removed by an electron beam, while In on the a-As masked region was removed selectively.

## 1.Introduction

An amorphous As (a-As) layer can be utilized for protection of III-V compound semiconductor surface, which was first reported by Kowalszyk, et al. [1]. It enables us to transfer samples of III-V compound semiconductors from an molecular beam epitaxy (MBE) growth chamber to the other chamber through the air without surface oxidation and contamination. The amorphous As (a-As) layer can be removed easily by annealing it at about 350ºC in UHV environment[2]. Many investigations have been conducted on the properties of the amorphous As layer for the use of passivation layer[3-7]. Further, using the amorphous As layer as a mask, Husby, et al. achieved photolithographic patterning[8].

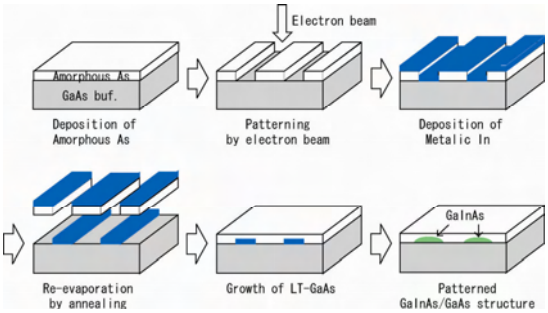


Fig. 1 New fabrication process of patterned GaInAs/GaAs hetero-structures using a-As layer as a mask. (1) an a-As layer is deposited on a GaAs substrate, (2) desigend patternes are drawn on the a-As layer by electron beam, (3) metalic In is deposited on the patterned a-As layer, (4) the substrate is annealed to remove the a-As layer together with the metalic In on top while In on bare GaAs surface remains, (5) a GaAs cap layer is grown, and (6) In diffused into the GaAs layer forms patterned GaInAs.

A technique to fabricate nano-patterned hetero-structures of GaAs-base III-V compound semiconductors, such as GaInAs nano-disks and nano-lines on GaAs substrate is important,

since the technique can be utilized to fabricate integrated quantum devices and circuits. In order to form the patterned GaInAs hetero-structures on GaAs, we proposed a new fabrication process using the a-As layer as a mask for the electron beam (EB) lithography. As shown in Fig.1, the process consists of six stages all in one chamber: (1) an a-As layer is deposited on a GaAs substrate, (2) designed patterns are drawn on the a-As layer by electron the EB, (3) metallic In is deposited on the patterned a-As layer, (4) the substrate is annealed to remove the a-As layer together with the metallic In on top while In on the bare GaAs surface remains, (5) a GaAs cap layer is grown, and (6) In diffused into the GaAs forms patterned GaInAs. We had already studied on the stages (1), (2), and (3) and found the best conditions to form a-As layer, to draw patterns on the a-As by the EB, and to deposit In. In this work, we attempted to find a condition to remove In on the a-As layer selectively at the stage (4).

## 2. Investigation of annealing condition to remove In on a-As mask selectively.

Samples were prepared using solid-source MBE system on GaAs(001) substrates. Before the depostion of a-As, 0.5μm of GaAs buffer layer was grown at 580ºC under As flux of $2\times10^{-x}$ Torr with the growth rate of 0.25nm/s. Two groups of samples, groups-A and B, were fabricated to find a condition to selectivly remove In on the a-As layer while In on the bare GaAs remains. For the samples of group-A, In was deposited on GaAs masked by a-As layer that was formed by exposing the GaAs surface to As molecular beam of 3×10□□Torr for 180 seconds at room temperature. For the samples of group-B, In was deposited directly on the GaAs buffer layer without the a-As layer. 10 monolayer of metallic In was deposited on both of the samples.

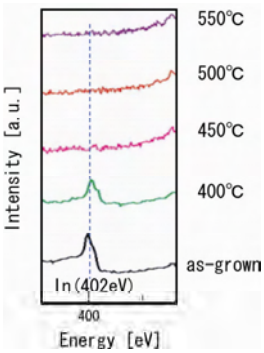


Fig. 2 AES spectra obtained from the surface of the samples of group-A.

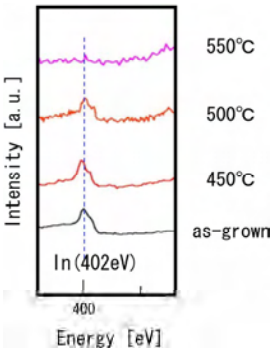


Fig. 3 AES spectra obtained from the surface of the samples of group-B.

The samples were annealed to find a proper annealing temperature at which In deposited on the a-As layer is removed and while In deposited on the bare GaAs surface remains. The samples of group-A were annealed at 400, 450, 500, and 550ºC. The samples of group-B were annealed at 450, 500, and 550ºC. The surfaces of the samples were analyzed by AES and SEM after the annealing.

Figures 2 and 3 shows the results of the AES analysis for the samples of groups-A and B, respectively. The signal from In appears at 402eV in these spectra. As shown in Fig. 2, In on the a-As layer was removed when the annealing temperature was 450ºC and above. Fig. 3 shows that In on the bare GaAs substrate still remained when the annealing temperature was 500ºC and below. The results indicated that it should be possible to remove In selectively between 450ºC and 500ºC.

## 3. Selective removing of In on the a-As layer

As the appropriate annealing condition was found in section 2, an experiment of selective removing of In on patterned a-As layer was performed.
In this experiment, In was deposited on a patterned a-As layer formed on a GaAs substrate with the same process described in section 2. After the formation of the a-As layer, the sample was taken out from the MBE chamber, and introduced into an Auger electron spectroscopy (AES) system. The AES system was utilized to draw patterns on the a-As layer by EB and to analyze the surface. The EB-gun of the AES was operated at 25kV and 10μA to draw patterns of 170×140μm² on the a-As layer. It was confirmed by the AES and an SEM that the a-As was perfectly removed in the EB irradiated area as shown in Fig. 4. After the EB drawing, the sample was re-introduced into the MBE chamber. 10 monolayer of In was deposited in the MBE chamber on the patterned a-As layer. Then, the sample was annealed at 450ºC in order to remove In selectively.
Fig. 5 shows the surface of the sample after the annealing. The AES analysis showed that In remained in the 170×140μm² area where the a-As layer was removed while In on the a-As masked region was removed selectively.

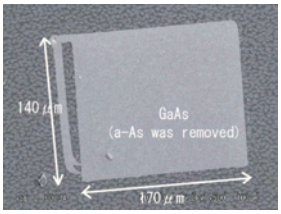


Fig. 4 SEM observed surface of patterned a-As layer.

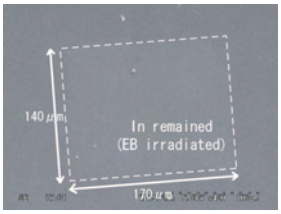


Fig. 5 SEM observed surface of sample after the selective removing of In on patterned a-As layer.

## 4. Conclusions

In order to form patterned GaInAs/GaAs hetero-structures, we proposed a new fabrication process using amorphous As layer as a mask. We have discussed on the condition to remove In on the patterned a-As layer selectively. The analysis showed that In on the a-As layer was removed when the annealing temperature was 450ºC and over, and In on the bare GaAs surface remained when the annealing temperature was 500ºC and under. The results indicated that it should be possible to remove In selectively between 450ºC and 500ºC.
We performed selective removing of In on a patterned a-As layer by annealing at 450ºC in the UHV environment. The AES analysis of the sample after annealing showed that In remained in the 170×140μm² area, where the a-As layer was removed by the EB, while In on the a-As masked region was removed selectively.

## References

[1] S.P. Kowalczyk, D.L. Miller, J.R. Waldrop, P.G. Newman, R.W. Grant, J. Vac. Sci. Technol. 19 (1981) 255.
[2] R.W. Bernstein, A. Borg, H. Husby, B.-O. Fimland, J.K. Grepsted, Appl. Surf. Sci. 56-58 (1992) 74.
[3] H. Wilheim, W. Richter, U. Rossow, D. Zahn, D.A. Woolf, D.I. Westwood, R.H. Williams, Surf. Sci. 556-560 (1991) 251
[4] I. Karpov, N. Venkateswaran, G. Bratina, W. Gladfelter, A.Franciosi, L. Sorba, J. Vac. Sci. Technol. B. 2041-2048 (1995) 13
[5] K. Knorr, M. Pristovsek, U. Resch-Esser, N. Esser, M. Zohn, W. Richter, J. Crystal Growth 230-236 (1997) 170
[6] A. Balzarotti, E. Placidi, F. Arciprete, M. Franfoni, F. Patella, Phys. Rev. B. 115332 (2002) 67
[7] C. Riedesel, C. Meier, P. Schafmeister, D. Reuter, A.D. Wieck, Physica E 503-504 (2003) 17
[8] H. Husby, J.K. Grepstad, R.W. Bernstein, Appl. Phys. Lett. 64 (1994) 2124.

# Formation of epitaxial nanocomposite in Cu-Ag eutectic thin films

**F. Misják, P. B. Barna, G. Radnóczi**
Research Institute for Technical Physics and Materials Science (MFA) of the Hungarian Academy of Sciences, H-1525 Budapest, P. O. Box 49, Hungary

Eutectic composition Cu-Ag alloy thin films were prepared by co-deposition at room temperature onto oxidised Si substrates by thermal evaporation. Morphological development, structure and phase state of the films was investigated by transmission electron microscopy, high resolution microscopy and electron diffraction. The few hundred nm thick films possess fibre morphology corresponding to zone I in the structure zone diagrams. The fibre diameter is 10-30 nm and strong <111> texture is simultaneously present. The fibres are nanocrystalline composed of nm size domains of Cu and Ag reach solid solution phases. The concentration of the dissolved component is about 10 at% in both phases. The size of the domains is 5-6 nm in the growth direction and 2-3 nm perpendicular to it. High resolution images show, that the domains are epitaxial to each other and the domain (phase) boundaries are semicoherent. Lattice planes are curved suggesting high non-uniform lattice strain in the films. As a result, each fibre can be considered as a three dimensional epitaxial nanocomposite built from few nm sized epitaxially grown domains of Cu and Ag reach solid solution phases. A model for morphological development and phase separation in eutectic Cu-Ag films based on the structural information will also be described.

# Laser-nanopatterning of thin films for templated nanostructure growth of ZnO and GaN

**M. Maeder [1], T. Hoeche [1], J.W. Gerlach [1], L. Neumann [1], C. Czekalla [2], M. Lorenz [2], M. Grundmann [2], B. Rauschenbach [1]**

1. Leibniz Institute of Surface Modification, Germany
2. Leipzig University, Germany

The growth of well ordered nanostructures, as for example nanowires requires pre-patterned substrates for most of the different techniques. Common methods to create such pre-patterns are for example electron beam lithography (EBL), nanosphere lithography (NSL) or other lithographic techniques. Most of those methods are very time-consuming, complex and last but not least costly. Diffraction mask projection laser ablation (DiMPLA), however, is a versatile, fast, and relatively easy technique to create patterned templates for nanostructure growth. For this method, a 5-15 nm thick metal film (for e.g. Au or Ti) is illuminated by a laterally varying intensity pattern of an excimer laser (248 nm wavelength, 25 ns pulse duration). The film is structured by choosing the intensity appropriately, resulting in one- (dots) or two-dimensional (gratings) metal structures on the substrate. The highly regular intensity pattern is achieved by sending the laser beam through a phase mask which imprints the corresponding pattern onto the intensity distribution. By demagnifying the lateral pattern, using a reflective objective, structures, that are small enough to act as catalysts for nanostructure growth, can be created. In this paper the DiMPLA technique is introduced as well as typical results are shown. Experiments were done using DiMPLA-patterned substrates for the catalytic nanostructure growth of ZnO using pulsed-laser deposition (PLD) and GaN using ion-beam assisted molecular-beam epitaxy (IBA-MBE). Results for the two materials and further analysis of the structures are presented.

# Multiferroic nature of the BLZT-CFO composite thin films

**C. Ostos [1], M.L. Martínez-Sarrión [1], L. Mestres [1], E. Delgado [2], D. Lederman [2], P. Prieto [3], G. Abril [1], J.M. Hernandez [1], J. Tejada [1]**

1. University of Barcelona, Spain
2. University of West Virginia, USA
3. Excellence Centre for Novel Materials, Colombia

Ferroelectric materials are attractive candidates for the next generation of non-volatile memories (FRAM) [1]. Lead-free ferroelectric materials have emerged to form part of the same family, such as barium lanthanide zirconate titanate (BLnZT; Ln = La, Nd) compounds, which have very high dielectric constants and good ferroelectric response [2-3]. The potential impact on society of recent advances in magnetic materials is also extensive. Some examples, such as dramatic increases in data storage density, are already evident [4] and are already commercially available. In this work we explore an astonishing class of materials known as magnetoelectric multiferroics, where the ability to couple to either electric or magnetic polarization allows an additional degree of freedom in device design, and therefore, a whole range of new applications can be envisaged [5]. New BLZT –CFO composite thin film were prepared by RF-magnetron sputtering from a 0.68 $Ba_{0.90}La_{0.067}Ti_{0.91}Zr_{0.09}O_3$ – 0.32 $CoFe_2O_4$ mixed target at 1033 K. The system was deposited on $Pt/TiO_2/SiO_2/Si$ substrate under high oxygen-pressure atmosphere. The composite was successfully deposited according to XRD and AFM results. The separated CFO phase mixed into BLZT matrix was shown by SEM and TEM micrographs. The thin films showed epitaxial growth and are composed of randomly dispersed CFO nanopillars in the BLZT matrix. XPS analysis in depth profile mode confirmed the presence of all constituent elements through the film and the favourable octahedral $TiO_6$ distortion in the structure showing the difference from $BaTiO_3$ in chemical titanium environment. The magnetization curves were measured between 2 K and 300 K at a constant magnetic field of 10 mT applied normal to the film plane (out-of-plane). The Zero Field Cooled (ZFC) and Field Cooled (FC) magnetization curves converge around 300 K showing that magnetic irreversibility should disappear around this temperature. The CFO thin film magnetic transition (ferrimagnetic to paramagnetic) occurs at higher temperatures and was not observed. At lower temperatures (T<15 K) the magnetization behaviour could be due to two separate surface phenomena resulting from the nanostructure of the multiferroic film. The multiferroic nature of the composite thin film was demonstrated through the variation of measured ferroelectric polarization with the application of external field and vice versa.

[1] J. F. Scott, C. A. Paz de Araujo, Science 246 (1989) 1400.
[2] C. Ostos, M. L. Martínez-Sarrión, L. Mestres, A. Cortes, E. Delgado, P. Prieto, Braz. J. Phys. 36 (2006) 1062.
[3] E. Delgado, C. Ostos, M. L. Martínez-Sarrión, L. Mestres, P. Prieto, Phys. Status Solidi C 4(11) (2007) 4099.
[4] H. Coufal, L. Dhar and C. D. Mee, MRS Bull 31(5) (2006) 374.
[5] W. Eerenstein, N. D

# Amorphous Silicon Carbo-Nitrides created by ion sputtering

**V. Vishnyakov [1], A. Ehiasarian [2], V.V. Vishnyakov [1], R. Valizadeh [1], P. Hovsepian [2], J. Colligon [1]**

1. Dalton Research Institute, Manchester Metropolitan University, Manchester, M1 5GD, UK
2. Nanotechnology Centre for PVD Research, Sheffield Hallam University, Sheffield, S1 1WB, UK

Silicon carbo-nitrides with boron were deposited using the ion beam assisted deposition (IBAD) method. Sputtering was from a combined elemental Si, B and C target and was performed in a Nitrogen/Argon atmosphere. The film composition was adjusted by changing the relative area of materials in the sputtering beam. The $N_2$/Ar ratio and degree of ion assistance was varied. Deposition was carried out onto unheated and heated to 720K silicon, glass and Stainless Steel substrates. The layers were examined by means of X-Ray Diffraction, Scanning Electron microscopy, Energy Dispersive X-Ray analysis, Atomic Force Microscopy and Nano-indentation. The films show composition and chemical bonding variation dependant on deposition conditions. All coatings were amorphous, fully dense and showed high hardness up to 32GPa. A low friction coefficient of about 0.3 was measured using the pin-on-disk method and the films on Stainless Steel Substrates were able to withstand oxidation in air up to 1420K.

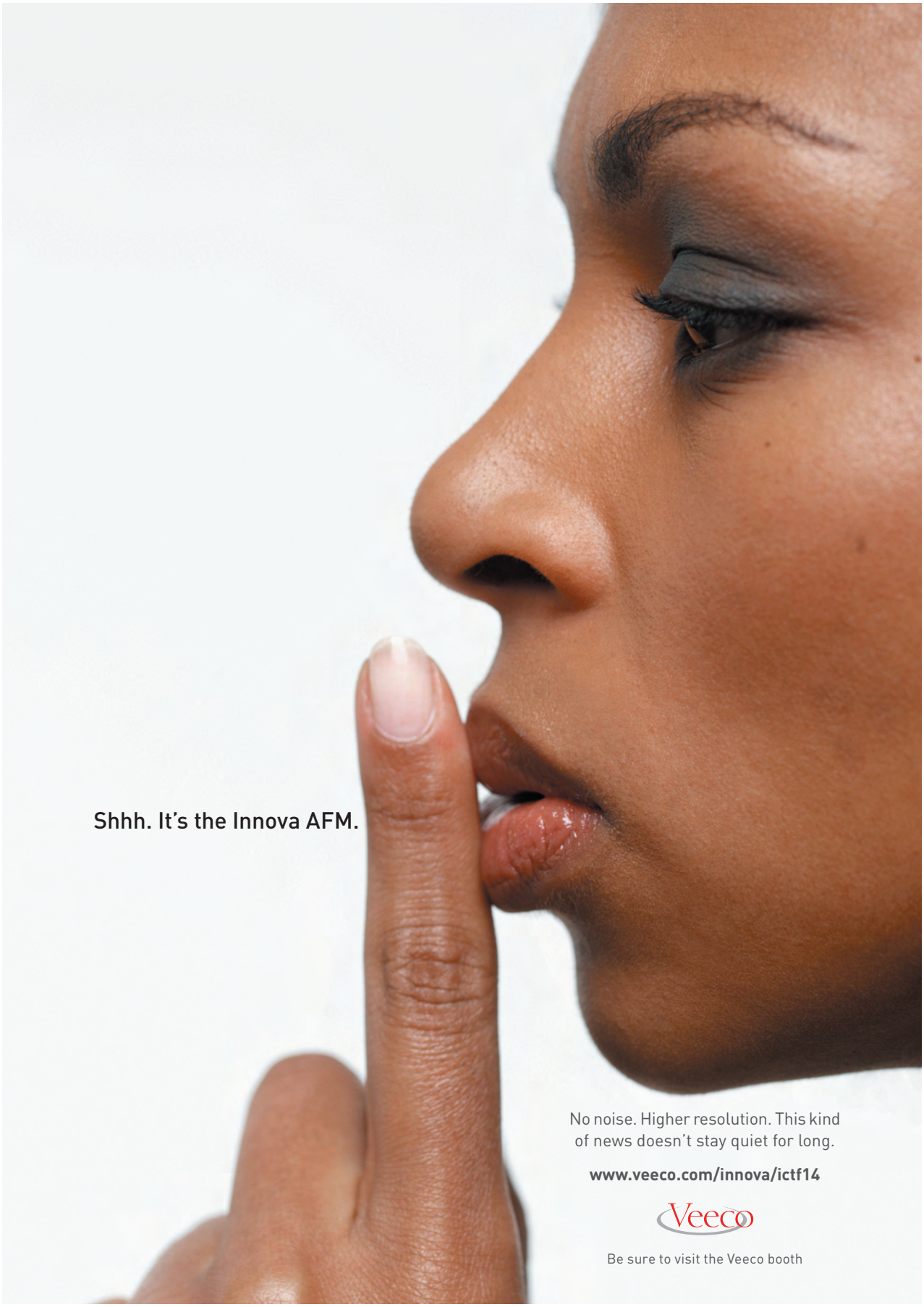
Shhh. It's the Innova AFM.
No noise. Higher resolution. This kind of news doesn't stay quiet for long.
www.veeco.com/innova/ictf14
Veeco
Be sure to visit the Veeco booth

BEKAERT

better together

# better together

Bekaert believes that *better together* is the key to success.

Bekaert is active worldwide in selected applications of its two core competences: advanced metal transformation and advanced materials and coatings. The combination of these competences makes Bekaert unique.

The power of combination is also reflected in the way Bekaert works.

Over 22 000 employees around the world work together as one company, serving customers in over 120 countries.

Their combined efforts enable the company to offer a wide array of high-tech products, systems and services, designed to give customers an edge in their markets. Together they create added value. They build win-win relationships, based on equal partnerships, in an atmosphere of mutual trust and respect.

In pursuit of its goal of sustainable profitable growth, Bekaert aims for market leadership and technological leadership and strives to be world number one or two.

**www.bekaert.com**

# Preferred orientation and film structure of Ti-Zr-N hard coatings grown by reactive magnetron co-sputtering

**G. Abadias [1], Ph. Guerin [1], P. Villechaise [2]**

1. Université de Poitiers -CNRS, Laboratoire PHYMAT (UMR 6630), SP2MI, Téléport 2, Bd Marie et Pierre Curie, BP 30179, 86962 Chasseneuil-Futuroscope, France

2. ENSMA, Laboratoire de Mécanique et de Physique des Matériaux (UMR 6617), 1 av. Clément Ader, Téléport 2, BP 40109, 86962 Chasseneuil-Futuroscope, France

$Ti_{1-x}Zr_xN$ films with $0 \leq x \leq 1$ were grown at 0.18 Pa and 300°C by reactive dc unbalanced magnetron co-sputtering in $Ar/N_2$ atmosphere onto oxidized Si substrate. The deposition conditions were optimized according to the $N_2$ partial pressure vs. $N_2$ flow rate hysteresis curves, as determined using a mass spectrometer. X-ray Diffraction (XRD) was used to identify film structure and preferred orientation as a function of Zr content and film thickness, while *in situ* wafer curvature technique was implemented during deposition to determine the stress state. It is shown that solid solution thin films with Na-Cl structure are stabilized in the whole composition range investigated. The stress is found to be compressive and increases with Zr content. No interdependence between stress and preferred orientation is observed, the (111) texture being predominantly enhanced with film thickness and Zr content for $x<0.5$.

## 1. INTRODUCTION

Transition metal (TM) nitride thin films, the most representative being TiN, find widespread applications due to their unique physical, electronic and mechanical properties. They can be used as hard and wear-resistant protective coatings, decorative coatings or diffusion barriers in ULSI circuits. To achieve the desired properties, it is crucial to understand and control film formation, and in particular the texture development during growth [1] since film properties are very often anisotropy-dependent. A possible route to design thin films with more functional properties consists in growing ternary or multinary nitride-based films, which exhibit superior mechanical or chemical properties compared to their binary counterparts. Depending on the chemical properties of the elements, these systems may form a nanocomposite material or a solid solution. For example, solid solution could be stabilized in the whole composition range for Ti-Ta-N [2] and Ti-Zr-N [3] systems, although these systems exhibit a miscibility gap in the bulk state. If texture formation has been largely investigated in binary TM nitride films like TiN, very limited data exist for ternary ones. In the present work, we study the phase stability, texture development and stress state in Ti-Zr-N thin films deposited by magnetron sputtering (MS).

## 2. EXPERIMENTS

$Ti_{1-x}Zr_xN$ thin films with $0 \leq x \leq 1$ were deposited on Si substrates covered with native oxide (~2 nm) at 300°C using reactive d.c. unbalanced magnetron co-sputtering. The UHV chamber (base pressure of $\sim 2 \times 10^{-6}$ Pa) was equipped with one Ti (99.995% purity) and one Zr (99.2%

purity) target with a diameter of 7.5 cm and placed at a distance of 18 cm from the substrate. The magnetrons were operated in constant power mode, the power of the respective targets being adjusted to obtain the required composition (see Table 1). Substrates with a bias of –58 V were kept at temperature of 300°C in an $Ar/N_2$ atmosphere. The working pressure was fixed at 0.18 Pa and the $N_2$-flow was adjusted so as to sputter the targets in metallic mode [4], resulting in relatively high deposition rates (see Table 1). The $N_2$ partial pressure was measured using a mass spectrometer and the growth rate deduced from the measurement of the film thickness by X-ray Reflectivity.

| | Ti target | | Zr target | | P $N_2$ (Pa) | Growth rate (Å/s) |
|---|---|---|---|---|---|---|
| Sample | power (W) | disch volt. (V) | power (W) | disch volt. (V) | | |
| TiN | 300 | 458 | / | / | $4.5\times10^{-3}$ | 1.40 |
| $Ti_{0.75}Zr_{0.25}N$ | 300 | 501 | 54 | 382 | $3.0\times10^{-3}$ | 1.86 |
| $Ti_{0.5}Zr_{0.5}N$ | 300 | 450 | 154 | 436 | $2.0\times10^{-3}$ | 3.06 |
| $Ti_{0275}Zr_{0.75}N$ | 195 | 430 | 301 | 480 | $1.2\times10^{-3}$ | 3.80 |
| ZrN | / | / | 300 | 525 | $4.0\times10^{-3}$ | 2.50 |

Table 1. Deposition parameters for the growth of Ti-Zr-N films by reactive unbalanced MS at a working pressure of 0.18 Pa, substrate bias of -58V and substrate temperature of 300°C.

X-ray Diffraction (XRD) technique was used in various configurations to characterize film's crystallographic structure and preferred orientation, grain size and residual stress [1]. Finally, a multi-beam optical setup [5] was used during deposition in order to determine the stress of the growing film from the measurement of the wafer curvature, according to the well known Stoney's equation.

## 3. RESULTS

### *3.1 Film growth*

Figure 1 shows the typical morphology of films obtained at 0.18 Pa. A characteristic columnar microstructure is observed, evolving from 'V-shaped' columns to a more dense and homogeneous microstructure with increasing Zr content. The microstructure of pure ZrN film resembles more a globular profile corresponding to zone III of structure zone models [6], which could be related to its lower melting temperature.

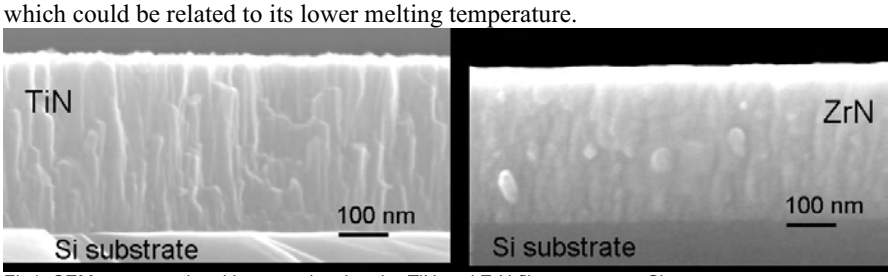


Fig1. SEM cross-sectional images showing the TiN and ZrN films grown on Si

The evolution of the $N_2$ partial pressure exhibits a characteristic hysteresis effect with the $N_2$ flow rate (see fig.2a), typical of reactive sputtering [4]. A hysteresis is also observed for the variation of the discharge voltages of Ti and Zr targets with supply of reactive gas (zone 1 and 2 in fig.2b). Interestingly, a shift towards larger values in the upper limit of the $N_2$ flow rate for sputtering in metallic mode is noticed during co-sputtering compared to sputtering of a single target, suggesting changes in plasma properties during co-sputtering. In particular a coupling of hysteresis effect from Zr target is visible on the Ti target (see shaded area of fig.2b). All the films investigated in this study were sputtered in metallic target mode, as

checked from the measurement of the $N_2$ partial pressure from mass spectrometer. For $Ti_{0.5}Zr_{0.5}N$ film, this corresponds to a $N_2$ flow rate of 0.9 sccm (point A of fig.2a) and $N_2$ partial pressure of ~$2\times10^{-3}$ Pa (see Table 1), which is typically one order of magnitude lower than in poisoned target mode (see fig.2a).

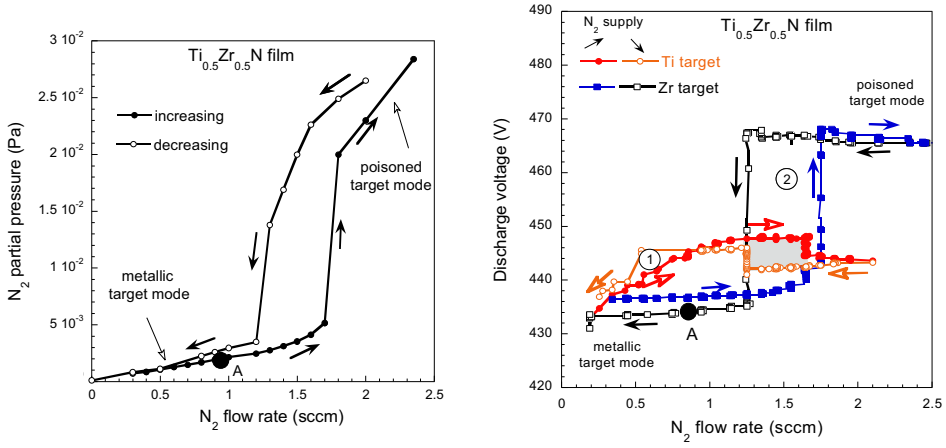


Fig.2: a) Typical experimental variation of the partial pressure of the reactive gas vs. reactive gas flow during co-sputtering of $Ti_{0.5}Zr_{0.5}N$ film, b) Corresponding evolution of the discharge voltages of Ti and Zr targets. The $N_2$ gas supply is expressed in standard cubic centimeters per minute (sccm), the Ar gas flow being fixed at 9 sccm.

### *3.2 Structure stability and preferred orientation*

All the $Ti_{1-x}Zr_xN$ films ($0<x<1$) exhibited the characteristic XRD lines of a single-phase solid solution with cubic rock-salt structure. Both (111) and (002) textures were found, the (111) texture becoming predominant with increasing film thickness (see fig.3).

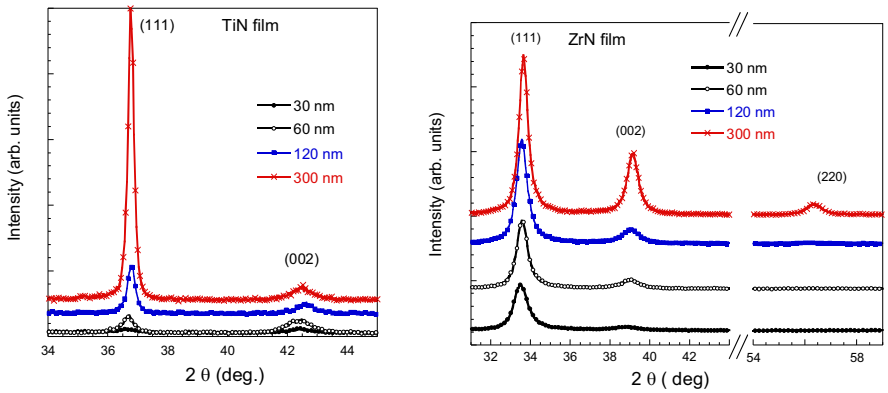


Figure 3: Evolution of XRD patterns as a function of film thickness for a) TiN film and b) ZrN film.

For pure TiN film, a transition from (002) to (111) preferred orientation occurred at a thickness of ~ 60 nm, while for pure ZrN film, the (111) texture develops since the early growth stages (below 30 nm). However, other orientations, like (220), develop with further deposition (at ~300 nm), which is consistent with the globular microstructure of fig.1: the crystal growth is repeatedly blocked, making the nucleation of grains with more random orientations possible. For ternary nitrides, the (111) texture is also observed since the early stages and is enhanced with increasing Zr content up to x~0.5 (see fig. 4a).

### *3.3 Stress state*

Stress data obtained for three TM nitride films grown at low pressure (0.18 Pa) are presented in Fig.4b. A monotonous compressive stress is observed for ZrN (with a steady-state value of 4.2 GPa), while for TiN and TiZrN films grown under the same deposition conditions a stress evolution is noticed: the compressive stress decreases with further film growth. This effect was related to the presence of stress gradients due to two competing stress producing mechanisms, namely growth-induced point defects (compressive stress) as a consequence of atomic peening, and void formation (tensile stress) as a consequence of surface roughness and shadowing effects [5]. For ZrN, no stress gradients are observed at low pressure (0.18 Pa), in agreement with dense globular microstructure of fig.1. Increasing the working pressure to 0.31 Pa leads to a ZrN stress*thickness curve very similar to that of TiN or TiZrN obtained at 0.18 Pa, i.e. with the evidence of stress gradients.

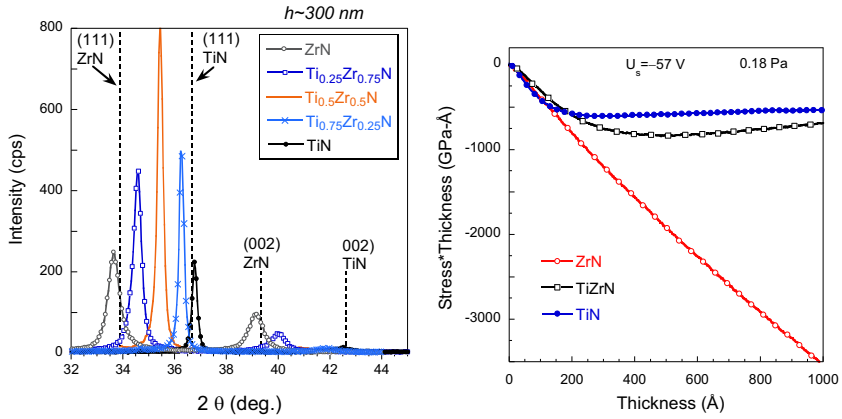


Fig.4. a) Evolution of XRD patterns in $Ti_{1-x}Zr_xN$ films as a function of Zr content (film thickness is ~300 nm) b) In situ stress evolution during growth of $Ti_{1-x}Zr_xN$ films.

## 4. DISCUSSION AND CONCLUSIONS

In a previous study [7], we have shown that TiN films grown by dual ion beam sputtering (DIBS) exhibited a mixed (002)+(111) texture, the (111) texture becoming predominant at large film thickness (>200 nm). It was shown that the texture change was not driven by a strain energy minimization. In the present work, similar observations are found for magnetron sputtered TiN. The real time stress data of fig.4b show that the stress change observed at ~20 nm is not correlated with a change in preferred orientation (fig. 3a). We ascribed this stress evolution to change in film morphology (inter-column void formation). Additional experiments are required to investigate the kinetics effects (temperature, growth rate) which are expected to be dominant in these nitride-based systems [8].

## 5. References

[1] G. Abadias, Surf. Coat. Technol. 202 2223 (2008)
[2] L. E. Koutsokeras, G. Abadias, Ch. E. Lekka, G. M. Matenoglou, D. F. Anagnostopoulos, G. A. Evangelakis and P. Patsalas, Appl. Phys. Lett. 93 011904 (2008)
[3] A. Hoerling, J. Sjölen, H. Willmann, T. Larsson, M. Oden, L. Hultman, Thin Solid Films 516 5421 (2008)
[4] S. Berg, T. Nyberg, Thin Solid Films 476 215 (2005)
[5] G. Abadias and Ph. Guerin, Appl. Phys. Lett. 93 111908 (2008)
[6] P. B. Barna, M. Adamik, Thin Solid Films 317 27 (1998)
[7] G. Abadias, Y.Y. Tse, Ph. Guerin, V. Pelosin, J. Appl. Phys. 99 113519 (2006)
[8] M. Beckers, N. Schell, R.M.S Martins, A. Mücklich, W. Möller, J. Appl. Phys. 98 044901 (2005)

# Study of the nature of states and optoelectronic properties in random dimer $In_xGa_{1-x}As/InAs$ superlattices

**S. Bentata** [1], **S. Terkhi** [2], **Z. Aziz** [1]
Mostaganem University, Mascara University

We study the optoelectronic and transport properties of one-dimensional disordered structures. We examine analytically and numerically the effects of short-range correlated disorder in Random Dimer Barrier Superlattices (RDBSL). Various physical quantities such the conductance, the localization length, the resistance and its probability distribution are statistically computed within an average procedure by means a transfer matrix formalism to discriminate the nature of the electronic states and the miniband structure. We consider InxGa1-xAs layers having identical thickness where the (In) composition x takes at random two different values with the constraint that one of them appears only in pairs, thus forming a RDBSL. We demonstrate that the superlattice supports two types of extended states, one of them comes from resonance effects at dimer barriers, as it was reported for dimer well superlattices, while the other type is due to the commuting nature of the transfer matrices describing the system at certain energies. The states close to the resonance can be viewed as consisting of extended states. In the band tails, i.e. for vanishing conductance, the states are strongly localized. The nature of the transition between theses two regimes is quantitatively investigated through relevant physical quantities.

# Structural and electrical properties of bismuth films deposited by pulsed D.C. magnetron sputtering

**M. D. Cropper, S. Stanley**
Loughborough University, Department of Physics, Loughborough, LE11 3TU, UK

Thin films of bismuth attract attention due to the interesting electronic properties of this semi-metal and due to several possible modern applications. There have been a few studies of the deposition of such films by evaporation radio frequency sputtering and pulsed laser deposition. In the work reported here, thin films of bismuth have been deposited onto glass substrates by pulsed D.C. sputtering. They were deposited from a three-inch target at a substrate distance of 23 cm, using base pressures below 5×10-7 mbar. The deposition utilised a variety of target conditions and substrate temperatures. We present the results of measurements of carrier mobility, magnetoresistance, carrier concentration, resistivity and physical structure.
Initial investigations of the influence of sputtering power and gas pressure, revealed that mobility is highest when relatively low sputtering powers of 50 W and relatively high argon gas pressure of 10 mTorr are used. Under these conditions a systematic investigation of the variation of properties with deposition temperature and thickness has been carried out. With regard to structure, films of the order of 500 nm thickness show a preferred orientation to the (003) plane for deposition at, and close to room temperature. However, for deposition temperatures above 120ºC a change in orientation to the (012) plane is observed. At this deposition temperature there is a step-wise change in the measured carrier mobility.
In general, increasing the deposition temperature gives an increase in mobility up to 490 cm2V-1s-1 at 180°C with a decrease in carrier concentration to 2.7×10-19 m-3. Magnetoresistance follows mobility up to 2.5% at 0.55 T in the films deposited at 180°C when measured at room temperature. Increasing thickness gives an increase in resistivity and decrease in carrier concentration.

# Muscle cell growth on allylamine plasma polymer films

**L. Denis [1], C. Vanderplanck [2], C. Bittencourt [1], R. Snyders [1], A. Belayew [2], M. Hecq [1]**

1. Laboratoire de Chimie Inorganique et Analytique, Université de Mons-Hainaut, Place du Parc 20, B-7000 Mons, Belgium.
2. Laboratoire de Biologie Moléculaire, Université de Mons-Hainaut, Avenue du Champ de Mars 6, B-7000 Mons, Belgium.

Interactions between artificial materials and biological environments are strongly related to the physico-chemical properties of the material surface. Consequently, for several applications, the possibility to tailor surface properties allows engineering of highly optimized systems. Among the various thin film synthesis techniques, plasma polymerization has already shown its great potential to engineer high quality films with tailored surface. Plasma polymer films (PPF) show good adherence to different surfaces, good mechanical properties and high thermal resistance. Among the most promising PPF, primary amine-based films have shown their high potential for applications in the biomedical field. For instance, DNA single strands have been successfully immobilized on allylamine PPF while cell adhesion and growth were also promoted.

In this work, allylamine PPF were deposited on standard glass slides using pulsed radio-frequency plasma aiming to study their potential for human cell immobilization and growth. Film-substrate adherence properties and resistance to sterilization procedures as well as cell adhesion, proliferation and differentiation were studied. The composition of the films, and the primary amine content, was inferred by combining X-ray photoelectron spectroscopy with chemical derivatization. The primary amine content was 20%, i.e., one nitrogenous chemical group out of five is a primary amine. Seeding, adhesion, proliferation and differentiation of muscle cancer cells on PPF-coated slides were studied and compared to results obtained on standard uncoated glass slides.

PPF-coated slides were found to be sterilizable in isopropanol (20 min) as well as by autoclave (120°C, 20min). By optical microscopy, it was observed that cell morphology and growth are similar on both allylamine PPF-coated slides and standard glass slides. In a further experiment, the cells were transfected with the pCIneo-EGFP vector that express a green fluorescent protein and with the pCIneo-DUX4c for which the protein was detected by immunofluorescence. Fluorescence microscopy analysis revealed that higher amounts of cells were immobilized on PPF-coated slides suggesting a better cell adherence than on the standard glass slides. Furthermore, cell differentiation, induced by changing the culture medium, was found to occur faster for cells growing on allylamine PPF-coated slides.

Differentiation experiments were also performed on immortalized primary myoblasts. Similar rates of desmin expression and myoblasts fusion were observed on allylamine PPF- and collagen-coated dishes. Cell cytoskeleton structure was also observed by immunofluorescence with actin antibody.

In conclusion, the results suggest that allylamine PPF-coated substrates are suitable for the culture of supported human cells.

# The features of protective coating in low pressure power discharge lamps.

**L. A. Drozdov**
LIT Technology, Moscow, Russia.

At the present time a mercury or amalgam low pressure gas discharge lamps are widely used in different areas of human's activity. Some areas of such light sources application require the high UV intensity irradiation of lamp. It achieves by means of lamp electric power increasing. Several types of low pressure discharge lamps are able to operate with specific power up to 5 W/cm. Serious disadvantage of power amalgam lamp is UV intensity drop during the operating time. For example, the lamp with specific UVC power 0.65W/cm loses 50% of the UV intensity after 4000 hr of operating. The coating from $Al_2O_3$ on inner surface of the lamp bulb can decrease the velocity of the UV intensity dropping. But this effect is extremely depending on coating quality. It is very difficult to investigate this dependence because of relatively big operating time of amalgam lamps – al least 3000-5000 hr, up to 15000 hr. For save investigation time we have implemented the coating test on quartz lamps without mercury with the inert gases pressure much lower than in typical amalgam lamps. This kind of lamp is spontaneously becoming dim during the operation. And the lifetime of such lamps is extremely depending on coating quality. For example, when we didn't use coating on these lamps, the operating time is about 2 hr, but with coating it can increase up to 1000 hr. In our opinion the main reason of the lamp senescence is the plasma and lamp bulb inner wall interactions. In case of pure quartz inner wall, plasma particles can easily destroy quartz and some oxygen came into discharge. When the quartz wall coated by relatively thin (about 100 nm) layer of $Al_2O_3$ the plasma should destroy it and only after that quartz would able to interact with plasma particles. Of course plasma can destroy $Al_2O_3$ molecular and take oxygen from it, but $Al_2O_3$ is more stable formation than quartz. We made the experiments with surface tests on dektak 6M profilometer. We have got surface profile on the pure quartz, on coated by $Al_2O_3$ quartz, on quartz after 2 hr plasma treatment and on coated by $Al_2O_3$ quartz after 100 hr plasma treatment. We obtain the roughness of the quartz surface always increasing after plasma treatment. And the treatment time defines the roughness level – the more time the more roughness level. The main conclusion is to provide greater lifetime of this lamp we should use enough thickness of the film and use chemical components with big decomposition energy. This approach can be used on amalgam lamps – the coating that provided big (long) lifetime of the mercury free lamp can show low UV intensity drop when it used on amalgam lamps.

## INTRODUCTION

The application of germicidal low pressure amalgam lamps is very multifarious. This type of lamps is replacing the mercury lamps with increasing frequency. The main advantage of amalgam lamps is much greater power per unit of lamp length without any lose of efficiency. In many cases we can use one amalgam lamp instead of five or six mercury lamps [1]. From the other side ecological aspect – these lamps don't contain the free mercury only solid

amalgam. The pressure of harmful mercury vapours over the free metallic mercury at room temperature by to orders grater than this value over the amalgam in the same conditions. But it is not enough to provide safety level of mercury pressure. It is very important, that solid amalgam easily can be collect in case of the bulb damage unlike the metallic mercury. And after all the quantity of the mercury in one amalgam lamp can be much lower than in mercury lamp.

The great electrical power of amalgam lamps is provided by means of using electronic ballasts and amalgam. These ballasts can supply the discharge tube with high frequency current that is impossible with the simple electromagnetic ballast because of fixed line voltage and frequency. The amalgam provides the optimal level of mercury vapours in the discharge in conditions of relatively big current of the lamp. The wall of the powerful lamp has a big temperature about 100°C and more. In this case the usage of free mercury is impossible because the mercury vapours pressure will be out of optimal values [2].

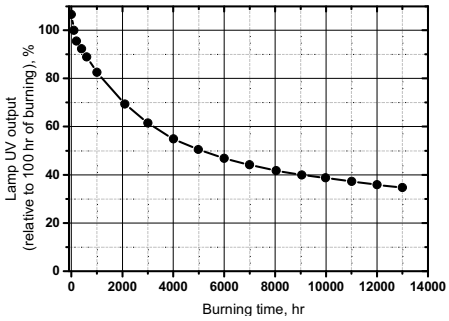


Figure 1. The dependency of UV power from time of burning for quartz amalgam lamp [3].

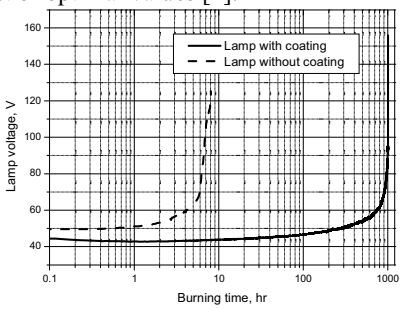


Figure 2. The typical curves of voltage evolution on mercury free experimental lamps from pure quartz and coated quartz.

In amalgam lamps the load on the bulb wall is extremely bigger than in traditional mercury lamps. That's why during the quartz amalgam lamps burning we observe a speedy bulb modification: the wall loses the clarity and getting to be fragile. In the figure 1 we can see the dependency of UV power on the time of burning for quartz amalgam lamp [3]. Although the quartz glass is one of the strongest materials from all glasses but the load on the wall is so great that this material can't make enough resistance. It is necessary to use additional protective coating on the inner surface of the lamp bulb to increase the quartz wall resistance to the influence of the discharge plasma. This coating is very effective but the final result is depending of coating quality. It is very difficult to investigate this dependence because of the experiments time until we can make some conclusions is relatively big – from 3000 hr to 15000 hr.

We implement the coating test on quartz lamps without mercury with the noble gases pressure much lower than in typical amalgam lamps to save the research time. In this case we are obtaining the plasma with greater particles energy than in the standard lamps. This kind of lamp is spontaneously becoming dim during the operation. And the lifetime of such lamps is extremely depending on coating quality. For example, when we didn't use coating on these lamps, the operating time is about 2 hr, but with coating it can increase up to 1000 hr. In this work we are investigating the inner surface of the quartz bulb changes during the experimental lamps without mercury operating.

## EXPERIMENTS

For investigations we take the lamps made of the quartz tube with inner diameter 25 mm. On the ends of this tube we have pinched oxide electrodes. The discharge distance between them is 50 cm. These lamps was pumped and filled by neon argon mixture in proportional 3:2, with

pressure 0.3 torr. All samples are made by the same technology. One group of the experimental lamps was made with protective layer from $Al_2O_3$ with thickness about 100 nm, and another group was made from pure quartz
After making, the lamp samples were connected to the electronic ballast and power analyser YOKOGAWA PZ4000. This ballast provides the stabilized 3.0 A lamp current with frequency 45 kHz. During the lamp burning the voltage between electrodes and discharge current was fixed every five minutes.
We have made some numbers of measurements of the surface profile by means of stylus profiler Veeco Dektak 6M to find out the result of discharge plasma treatment on lamp bulb inner surface. Step by step we obtained the profiles of quartz with and without coating before plasma influence and after it. Due to special features of quartz tube production technology we could measure a profile along the tube generatrix to find small roughness. In case of pure quartz the time of plasma treatment is about 2 hr, it is enough to make non able to burn lamp. In case of coated by $Al_2O_3$ quartz the time of treatment is much greater - about 900-1000 hr. This time is necessary to experimental lamp with quartz protective coating to become dim.

## RESULTS

The typical curves of lamp voltage evolution on experimental lamps from pure quartz and coated quartz are represented in the figure 2. They have two parts: at first the relatively slow linear rise of the voltage and then the quick non-linear voltage rise and lamp extinction. The presence of protective coating seriously influences on the first part of the voltage curve and makes the tilt angle much smaller.
On the figure 3 we can see the results of profiles measurements. There are four groups of samples: pure quartz, quartz with $Al_2O_3$ layer, quartz from experimental lamp which became dim after about 2 hr of burning, quartz with $Al_2O_3$ layer from experimental lamp which became dim after 900-1000 hr of burning. We can observe that the surface roughness in case of coated is grater than in case of not coated quartz. After the plasma treatment the surface roughness increasing and we can suppose roughness level is depending on treatment time.

## DISCUSSION

The fact of spontaneous experimental lamps extinction after raising a lamp voltage we can explain in terms of limited ballast power. When the lamp current is stabilized and the properties of discharge plasma are changing during the lamp burning, the lamp voltage is increasing. In some moment lamp power increases over the ballast limit and it automatically turn off. But the main question is the reasons of plasma changing during the lamp burning and why the relatively thin layer of $Al_2O_3$ makes the velocity of this evaluation much lower. It is significant that in presence of small quantity of mercury in discharge makes the lamp life time increase to thousands of hours and burning time is not extremely depend on coating layer it define the velocity of bulb darkening.
When arc discharge is glow the positive ions are falling on the inner bulb surface due to ambipolar diffusion. They are recombined on the wall and lose the energy which is equal to ionization potential. In case of lamp filled by neon and argon it is 21.5 and 15.8 eV (in accordance). We suppose that this energy is sufficient to destroy the quartz structure and make oxygen atoms out of it. So the lamp filling is changing and lamp voltage is increased, by the way oxygen can connect with the free Barium on the oxide electrodes this fact also can cause the rise of the lamp voltage. The greater voltage we have between electrodes, the more atoms of neon ionized in plasma. So, the processes of inner wall destroy are intensifying. When we have the $Al_2O_3$ layer on inner surface the plasma firstly should destroy it. This substance is stronger than $SiO_2$, and it decomposes only by neon atoms as we think and

velocity of inner wall destroy fall down. The inner bulb wall after plasma treatment has a bigger roughness level than in new bulb (fig. 3).

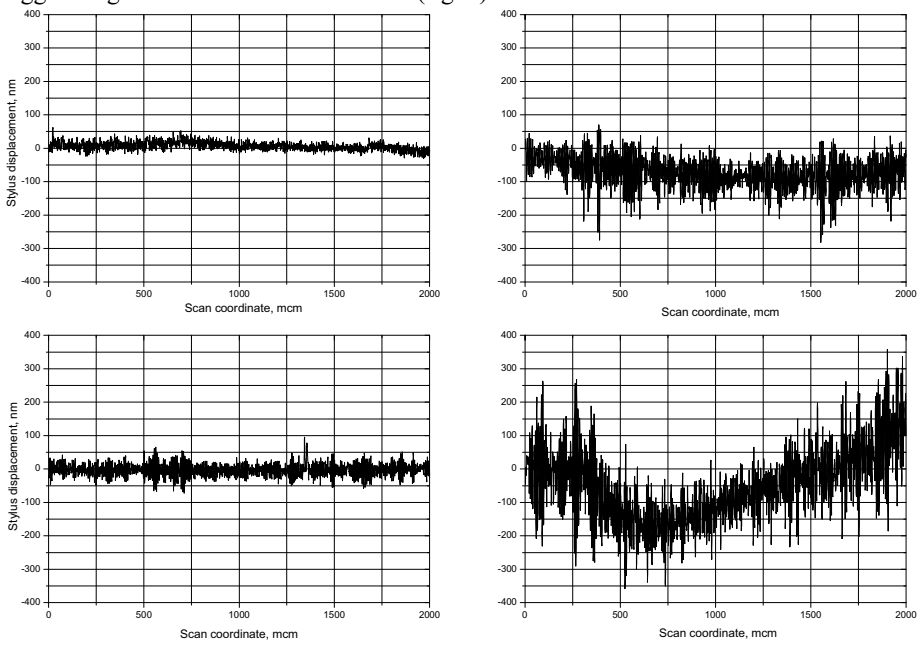


Figure 3. Results of profile measurements for pure (left side) and coated with $Al_2O_3$ (right side) quartz before (up side) and after (down side) plasma treatment.

It is possible to say the main part of the plasma positive ions is $Hg^+$ if there is small mercury amount in discharge. So the inner wall interacts with mercury ions as Hg ionization potential is only 10.4 eV (besides most part of mercury ions arises by multi-step ionisation acts). It is small value in comparison with neon and argon and this energy is not enough to make oxygen out of quartz structure. But mercury have an ability to connect on inner wall with quartz structure and makes it non transparent for UV irradiation. The coating from $Al_2O_3$ is making smaller the velocity of this quartz modification.

## CONCLUSSIONS

The thin (about 100 nm) layer of $Al_2O_3$ on inner surface of the quartz bulb of low pressure lamp with neon and argon is seriously increasing the resistance of wall from arc discharge plasma influence.

During the lamp burning the roughness level of inner surface became bigger and depends on burning time.

To provide greater life times of these lamps it necessary to increase the protective layer thickness.

We can suppose that protective coating made for these lamps can work in amalgam low pressure lamps and provide low level of UV intensity drop.

## REFERENCE

[1] Light Technical reference book under Julian B. Aizenberg redaction, Znack publishing house, Moscow, 2006 (on Russian).

[2] Waymouth J F Electric "Discharge Lamps", The MIT Press, Cambridge, Massachusetts and London, 1971.

[3] Kostiouchenko S and Giller H 3-nd Int. Congress of Ultraviolet Technologies (Whistler, British Columbia), C1-7, 2005.

# Optical detection of organic vapours on thin films of polymethylmetacrylate

**V. Myslik [1], P. Fitl [1,2], M. Vrnata [2], F. Vyslouzil [2], D. Kopecky [2], O. Ekrt [2]**

1. Institute of Chemical Technology in Prague, Department of Solid State Engineering, Technicka 5 , 166 28 Prague, Czech Republic

2. Institute of Chemical Technology in Prague, Department of Physics and Measurements, Technicka 5 , 166 28 Prague, Czech Republic

The detection principle is based on interference effects observed on a thin layer at different wavelengths of radiation. The change of reflectance of thin polymethylmethacrylate (PMMA) film for wavelengths from $\lambda$ = 400 to 580 nm (Range 1) and $\lambda$ = 520 – 620 nm (Range 2) was evaluated during changing atmosphere from pure air to a given concentration of toluene in the air. These two ranges were selected for given layer thickness on the basis of a wide-spectral reflectance measurement to ensure increasing reflectance at Range 1 and simultaneously decreasing in Range 2. Sensor response for the given range was evaluated as an integrated absolute value of reflectance change after alternating of atmosphere. Resulting sensitivity was calculated as a sum of the partial responses.

Thin films of PMMA were deposited onto polished silicon wafers. The source PMMA was diluted in 1,2-dichlorethane (7 wt.%) and subsequently deposited by spin-coating technique. The as-deposited layers were dried at 25°C for 48 hours. The thickness of resulting layers was 750 nm. The measurement was carried out in a shielded Teflon chamber. The source of radiation was pink LED with two emission maxima at 460 and 625 nm. Reflected radiation was detected by fiber-optic spectrometer ($\lambda$ = 350 – 1000 nm). The radiation is leaded by optical fiber and passes through the collimation lens. The same lens serves as a reflected radiation collector.

In the presented contribution there are three main mechanisms of polymeric thin layer reflectance changes utilized for optical detection: a) change of refraction index resulting from penetration of toluene vapors into PMMA volume; b) increase of layer thickness as a result of volume dilatation; c) changes of the surface light dispersion and absorbance in volume of the layer.

The sensor response to toluene vapors in Range 1 is negative and in Range 2 is positive. It is apparent that desorption process has longer time constant than sorption one. Experimental setup depicts the dependence of both sensitivity and response as a function of toluene vapors concentration. Sensitivity values ranges from 0.24% to 2.0% for concentration of toluene from 2.5 to 40‰. The estimated detection limit is in the order of hundreds ppm. There are still two possibilities of detection improvement: increasing integration time and number of averaged samples or enhancement of selectivity due to suppression of common-mode signals

# Rectifying Characteristics and Transport Behavior of $La_{0.9}Hf_{0.1}MnO_3$/Nb-doped $SrTiO_3$ Heteroepitaxial Junctions

**L. Wang, J. Gao**
The University of Hong Kong

La0.9Hf0.1MnO3 (LHMO) films were grown on (001) $SrTiO_3$ (STO) and (001) 0.7% Nd-doped $SrTiO_3$ (STON) substrates, respectively, at the same conditions by using pulsed laser deposition technique. The x-ray diffraction and rocking curve measurement demonstrate highly epitaxy and crystallinity obtained in our films. The resistance vs temperature curves indicate that the as grown LHMO film remains a semiconductor behavior from room temperature to 20 K due to oxygen deficiency. The LHMO/STON junction exhibits an asymmetric current-voltage relationship similar to a diode and a typical temperature-dependent rectifying property in a wide temperature range from 20 to 300 K. The diffusion voltage (Vd) of the junction decreases with decreasing temperature for the temperature dependence of splitting eg gap. The most remarkable discovery is that, at negative bias voltage, as the voltage is decreased from -2 V to -7 V, temperature dependence of the junction resistance (dV/dI) show an insulator-metal transition below 200 K. This behavior is quite different from the previous reports on heterojunctions composed of manganites and Nb-doped $SrTiO_3$ [1-2] in which no insulator-metal transition occurs at negative bias voltage. The results were discussed by considering the depletion layers in both LHMO and STON, and the tunneling current through the junction.

[1] Z.H. Wang, G.L. Yu, Y. Nie, Z.F. Wu, L. Qiu, Z. Luo, J. Gao, Journal of Applied Physics, Vol. 103, pp. 07A913: 1-3, 2008.
[2] J.R, Sun, B.G. Shen, H.F. Tian, J.Q. Li, Y.X. Weng, Applied Physics Letters, Vol. 87, Issue: 20 Article Number: 202502, 2005.

# Study of the interaction between the surface of polymeric substrates and chromium thin coatings grown by RF and DC sputtering

**R. Gazia [1], P. Rivolo [1], P. Mandracci [1]**

1. Politecnico di Torino - Physics Department - Materials and Microsystems Lab - Corso Duca degli Abruzzi, 24 - 10129 - Torino (Italy)

The deposition of chromium thin films on polymeric substrates is a subject of great interest for several industrial applications, especially for the substitution of galvanic deposition processes, which are presently used in some industrial fields, such as the automotive industry, for the fabrication of chromium plated components.

While the growth processes that can be used for the deposition of chromium on polymeric substrates are well known and have been reported to a great extent in the scientific and patent literature, fewer information can be found concerning the effects of the morphological and chemical properties of the surfaces of polymeric substrates on the growth of chromium films.

The present work deals with an experimental study of the interaction between the surface of different polymeric substrates, such as ABS and ABS/PC, and chromium coatings. Several chromium thin films, of thickness varying from 5 nm to more than 1000 nm, were deposited by means of DC and RF sputtering techniques at room temperature. Different types of surface modification, such as plasma-assisted surface activation and deposition of polymeric interlayers, were also applied to the polymeric substrates before the chromium films deposition in order to investigate their effect on the chromium layers growth mechanism.

Several characterization techniques were used in order to analyze the physical and chemical properties of the materials involved in the study. High resolution mechanical profilometry and field emission scanning electron microscopy (FESEM) were used to analyze the surface morphology of the polymer surfaces, before and after the surface modifications, and to investigate the effect of different surface properties of the substrates on the morphology of chromium films. Attenuated total reflection Fourier transform infrared spectroscopy (ATR-FTIR) and contact angle measurements were used to analyze the chemical characteristics of the polymer surface and to investigate the effects of the surface modification processes. Energy dispersive X-ray spectroscopy (EDX) was also used to analyze the composition of polymer surface and chromium films.

# Characterization of RF magnetron sputtered $Ge_2Sb_2Te_5$ thin films towards PC-RAM application

**J. Gutwirth [1], T. Wágner [1], P. Bezdička [2], J. Přikryl [1], Mil. Vlček [3], M. Frumar [1]**

1. University of Pardubice, Faculty of Chemical Technology, Department of General and Inorganic Chemistry & Research Centre LC 532, nám. Čs. legií 565, 53210 Pardubice, Czech Republic, e-mail: Jan.Gutwirth@upce.cz

2. Institute of Inorganic Chemistry, Academy of Sciences of the Czech Republic v.v.i., 25068 Husinec-Rez, Czech Republic

3. Joint Laboratory of Solid State Chemistry of the Institute of Macromolecular Chemistry, Academy of Sciences of the Czech Republic v.v.i. and University of Pardubice, Studentská 84, 53210 Pardubice, Czech Republic

Thin amorphous Ge-Sb-Te films were deposited by RF (f = 13.56 MHz) magnetron sputtering in argon plasma. Feasibility of prepared thin GST films for Phase-Change Random Access Memory (PC-RAM) application was tested via four-point probe measurement of temperature dependence of sheet resistance known as Van der Pauw technique. As-deposited and thermally treated thin films were characterized by the same way. Composition, chemical homogeneity and surface morphology were studied by Energy Dispersive X-Ray analysis coupled with Scanning Electron Microscopy (SEM-EDX). Crystallinity was determined by X-Ray diffraction (XRD). Optical properties and deposition rate were evaluated on basis of spectroscopic ellipsometry measurements.

Influence of deposition conditions (RF power, Ar pressure, deposition geometry) to composition, crystallinity and surface morphology was established. Profile of temperature dependence of sheet resistance and obtained characteristic temperatures (e.g. crystallization temperature and/or phase transformation temperature) were discussed.

## 1. INTRODUCTION

Non volatile rewritable data storage is one of the recent applications of chalcogenide thin films [1 - 4]. Especially phase-change based data storage technology is commercially succesfull. This technology consists in reversible phase change between amorphous and crystalline state and vice versa. These phase changes could be induced optically (commercially widespread rewritable optical discs as CD-RW, DVD±RW, DVD-RAM, HD DVD-RAM and BD-RE discs) [5, 6] or electrically (denoted as Ovonic Unified Memory (OUM) or Phase Change Random Access Memory/Chalcogenide Random Access Memory (PC-RAM, P-RAM, C-RAM)) [2, 7, 8].

Principally, phase changes are caused by laser or electrical pulses with different power and duration. Detection consists in reflectivity difference (optical memories) or electrical resistance difference (PC-RAM) between amorphous and crystalline phase.

Active materials in phase change based memories are currently chacogenide materials [9]. The benefit of these materials consists in possibility of easily feasible reversible phase

change. In addition, the rates of phase changes are high and stability of both phases in ambient conditions is relatively good. Widely used active recording films are based on doped Sb-Te alloys [2, 6, 9, 10]. Mostly used materials are from Ge-Sb-Te (GST) [11, 12] and Ag-In-Sb-Te (AIST) [13, 14] system, respectively.

## 2. EXPERIMENTAL

Vacuum deposition system UP 858 (Tesla, Czech Rep.) equipped with 1 inch magnetron Torus 1 (Kurt J. Lesker, USA) was used for thin film deposition. The system is pumped down by rotary and diffusion pump, Ar pressure was monitored by Pirani gauge VPR 1 (Lavat, Czech Rep.) The system is designed for three off-axis substrate holders (angle divergences from normal direction: position A - $\alpha_{DEP} = 2.4°$, position B - $\beta_{DEP} = 18.0°$, position C - $\gamma_{DEP} = 24.0°$ ); target – substrate holders configuration is plane-parallel in normal distance $l = 12$ cm. Substrate holders rotate at a speed of 20 rpm. Microscope slides, silica glasses and silicon wafers $1.5 \times 1.0$ cm were used as substrates. The system is equipped with RF power source RFX 600 (Advanced Energy, USA) operate at frequency 13.56 MHz coupled with matchbox ATX 600 (Advanced energy, USA). 1 inch target of $Ge_2Sb_2Te_5$ composition fixed to copper backplate supplied by Umicore (Liechtenstein) was used.

Depositions were done under Ar pressure of 1 - 4 Pa and RF power 10 - 40 W. Typical thicknesses of deposited thin films were 50-500 nm.

Composition and chemical homogeneity of target and prepared thin films were studied by SEM-EDX using JSM-5500 LV apparatus (Jeol, Japan) equipped with analyzer IXRF Systems (USA) and detector Sirius 10 (Gresham, Japan). The same apparatus was used for observation of surface morphology of prepared thin films. Accelerating voltage U = 20 kV, SE signal, high vacuum mode (target) or low vacuum mode (thin films) were applied.

The character (crystalline/amorphous) of target and prepared thin films was studied by XRD. Measurement was realized via diffractometer X'PertPRO (PANalytical, The Netherlands) with Co Kα X-ray tube (U = 40 kV, I = 30 mA) and Fe β filter. Primary as same as secondary optics was Soller slits (0.04 rad). Multichannel semiconductor detector PANalytical X'celerator with anti-scatter shield was used for detection. Qualitative analysis was performed with HighScore software package (PANalytical, The Netherlands, version 1.0d), Diffrac-Plus software package (Bruker AXS, Germany, version 8.0) and JCPDS PDF-2 database [15].

Optical properties (refraction index n, optical band gap energy $E_g^{opt}$) and some particular properties (film thickness, deposition rate) were evaluated on basis of spectroscopic ellipsometry measurements, which were carried out on V-VASE apparatus (J. A. Woolam, USA) equipped with NIR extender and focusing windows. Measurement range was 300 – 2300 nm with measuring angles $\alpha = 60°$, 65° and 70° . Software W-VASE (v. 3.445) and Tauc-Lorentz dispersion formula [16, 17] were used for data evaluation.

Temperature dependence of sheet resistance was measured by four point probe technique via source/digital meter 2602 (Keithley, USA) in furnace S 02 (Vezas, Czech Rep.) equipped with digital thermometer GMH 3230 (Greisinger Electronic, Germany). Temperature gradient was 2 $°C \times min^{-1}$.

## 3. RESULTS AND DISCUSSION

Sputtering target is chemically homogeneous with stoichiometry close to $Ge_2Sb_2Te_5$ in terms of SEM-EDX technique accuracy. Nevertheless, XRD study leads to detection of several crystalline phases (i.e. hexagonal $Ge_2Sb_2Te_5$ , rhombohedral $Ge_{0.95}Sb_{2.01}Te_{4.00}$ and rhombohedral $Ge_1Sb_2Te_4$). Thus, the target microstructure is more complicated than usually expected without any influence of overall stoichiometry.

Deposited thin films are chemically homogeneous (SEM-EDX), nevertheless composition vary from nominal stoichiometry of target with deposition conditions. Generally, tendencies

to Ge enrichment and Te depletion of thin films could be observed. Composition differences between samples prepared under the identical conditions on to silicon or silica glass substrates were observed. Trends to composition interval reduction with deposition rate increasing could be seen. Thus, sputtering equilibrium with highly angle resolved sputtering yields for particular elements could be expected when the deposition rate is sufficiently slow. This resolution disappears where deposition rate as well as particles flux in plasma increases.
Amorphous character of deposited thin films was proved by XRD measurements. The position of broad peak of amorphous phase is in good correspondence with positions of the most intensive peaks of crystalline phases mentioned above.
Refractive indices of deposited thin films increase with increasing of deposition rate, i.e. among others refractive index increase with decrease of angle divergence to normal deposition direction. This fact is probably caused by higher energies as well as higher number of deposited particles in normal direction which results in higher compactness of thin films. Reached values of refractive indices are lower in comparison to other studies deals with optical properties of $Ge_2Sb_2Te_5$ materials [12]. This is probably partially caused by low deposition rate in comparison with other studies [12]. Also, our latest results of Elastic Recoil Detection Analysis (ERDA) implies relatively high content of hydrogen.
Measurement of sheet resistance temperature dependence not resulted in huge change of crystallization temperature region as well as curve shape with deposition conditions. More significantly changes namely in $T_c$ region is observed between samples deposited under same conditions and different deposition angle as depicted in fig. 1.

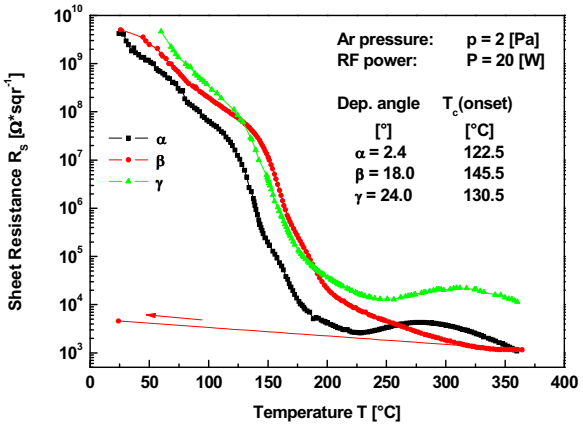


Figure 1. Temperature dependence of sheet resistance.

Structure of thermally treated thin films determined by XRD is crystalline. Nevertheless, crystalline phases are identified as rhombohedral $Sb_2Te_3$ and hexagonal Te in contrary to other works (e.g. [12]). This fact could be caused by presence of hydrogen and low compactness of deposited thin film which resulted in different pressure impingement during phase transformation [18].

## 4. CONCLUSIONS

Target of nominal composition $Ge_2Sb_2Te_5$ was found to be chemically homogeneous in both macroscopic and microscopic scale, however contrary to expectation three crystalline phases were detected by XRD.
Thin films prepared under different conditions are chemically homogeneous with smooth surface. Generally, tendencies to Ge enrichment and Te depletion of thin films were seen.

There were found differences in stoichiometry of thin films deposited onto silicon or silica glass substrates under the identical conditions. It was found that the composition differences between thin films deposited on different substrates (Si or $SiO_2$) as well as composition differences between particular deposition positions (A, B and C) decrease with increase of deposition rate.
Deposition yield is angle dependent, the maximum deposition rate occurs in normal direction to target as expected. Ratio of deposition rates in particular deposition angles is constant over all deposition conditions.
Generally, refractive index of deposited thin films is lower in comparison to other studies. Decrease of refractive index with decrease of deposition rate and namely increase of angle divergence to normal direction is observed.
The structure of all deposited thin films is amorphous. Thermal treatment leads to crystallization, crystalline phases were identified as rhombohedral $Sb_2Te_3$ and hexagonal Te. No significant change of crystallization temperature with Ar pressure or RF power was observed in contrary to influence of deposition angle.

## 5. ACKNOWLEDGEMENT

The authors thanks to the Ministry of Education, Youth and Sports of the Czech Republic (research centre LC 523 project, project MSM 0021627501), to Czech Science Foundation (project GA 203/06/1368) and to European Commission (FP 6 project IST 2004 017406) for financial support.

## 6. REFERENCES

[1] T. D. Milster in: Th. G. Brown, K. Creath, H. Kogelnik, M. A. Kriss, J. Schmit, M. J. Weber (eds.), The Optics Encyclopedia – Basic Fundations and Practical Applications Volume 1, Wiley-VCH, Weinheim, Germany 2004 p. 227 – 274 (ISBN-978-3-527-40320-2)
[2] M. Wuttig in: R. Waser (ed.), Nanoelectronics and Information Technology, Advanced Electronic Materials and Novel Devices, Wiley VCH, Weinheim, Germany 2003 p. 645 – 658 (ISBN-3-527-40363-9)
[3] M. Wuttig, Nat. Mater. 4 265 (2005)
[4] C. Steimer, W. Welnic, J. Kalb, M. Wuttig, J. Optoelectron. Adv. Mater. 8 2044 (2006)
[5] H. J. Borg, R. van Woudenberg, J. Magn. Magn. Mater. 193 519 (1999)
[6] G. F. Zhou, Mater. Sci. Eng. A – Struct. Mater. Prop. Microstruct. Process. 304 73 (2001)
[7] G. Purvis, III-Vs Review 19 39 (2006)
[8] A. L. Lacaita, Solid-State Electron. 50 24 (2006)
[9] T. Ohta, J. Optoelectron. Adv. Mater. 3 609 (2001)
[10] T. Ohta, K. Nishiuchi, K. Narumi, Y. Kitaoka, H. Ishibashi, N. Yamada, T. Kozaki, Jpn. J. Appl. Phys. 39 770 (2000)
[11] B. Hyot, L. Poupinet, V. Gehanno, P. J. Desre, J. Magn. Magn. Mater. 249 504 (2002)
[12] H. Dieker, M. Wuttig, Thin Solid Films 478 248 (2005)
[13] J. Li, L.Hou, H. Ruan, Q. Xie, F. Gan, Proc. SPIE 4085 125 (2001)
[14] J. Li, F. Gan, Thin Solid Films 402 232 (2002)
[15] JCPDS PDF-2 database, International Centre for Diffraction Data, Newtown Square, PA, U.S.A., release 54, (2004)
[16] G. E. Jellison, Jr., F. A. Modine, Appl. Phys. Lett. 69 371 (1996)
[17] G. E. Jellison, Jr., F. A. Modine, Appl. Phys. Lett. 69 2137 (1996)
[18] P. Fons, A. V. Kolobov, J. Tominaga, Y. Katayama, Nucl. Instrum. Methods Phys. Res. Sect. B-Beam Interact. Mater. Atoms 238 160 (2005)

# Study of thin hard coating of tantalum carbides on steel substrates

**R. Halimi, Y. Hadjar**
Université Mentouri Constantine

Hard tantalum carbide coatings were elaborated by depositing a tantalum layer (4 µm thickness), on carbon steel substrates and, subsequently, annealing the system in vacuum at temperatures from 600 to 1100°C. Structural characterization was assessed using X-ray diffraction, scanning electron microscopy and Auger electron spectroscopy. Mechanical characterization was performed by measuring microhardness and adhesion. It is found that at annealing up to 800°C two carbides ($Ta_2C$ and TaC) are formed. Moreover, the microhardness and adhesion of the films increase significantly with increasing annealing temperature. At a given temperature, the microhardness increases, with the rise of the annealing time, to reach a maximum and then decreases. This behavior is discussed.

# Structural properties of evaporated thin Cu-In bilayers on silicon and glass substrates

**A. Bouchetiba [1], A. Bouabellou [2], R. Halimi [2], M. Boudissa [3], C.Benazzouz [4]**

[1] Département de Physique, Université de Jijel, Jijel 18000, Algérie

[2] Laboratoire Couches Minces et Interfaces, Université Mentouri Constantine, Route Ain El Bey, Constantine 25000, Algérie

[3] Département de Physique, Université de Sétif, Sétif 19000, Algérie

[4] CRNA Alger, 2 Bd F. Fanon, Alger 16000, Algérie

Thin copper-indium (Cu-In) bilayers were deposited by thermally vacuum co-evaporation method on monocrystalline silicon, polycrystalline silicon and glass substrates at room temperature. The solid state reaction at the Cu-In interface was studied by using X-ray diffraction (XRD), scanning electron microscopy (SEM) and Rutherford backscattering spectrometry (RBS) techniques. It was shown that, independently of the substrate nature, the reaction between as-deposited Cu and In films occurs during the evaporation and leads to the formation and growth of CuIn and $CuIn_2$ phases. The substrate was found to influence the microstructure and surface morphology of the samples. The results of the investigation obtained on Cu/In bilayers prepared with various atomic compositions were consistent with the phase diagrams.

## 1. INTRODUCTION

The Cu-In compounds in thin films have attracted much interest these last years because of their very promising applications [1,2]. They are largely used as precursors in the manufacturing of solar cells in which thin Cu(In-Ga)(Se,S) layers are significant materials in the photovoltaic field [3,4].

This work reports structural properties of evaporated thin Cu-In bilayers on silicon and glass substrates.

## 2. EXPERIMENTAL DETAILS

Polycrystalline copper and indium thin films were sequentially thermal evaporated under vacuum on unheated glass, poly-and monocrystalline silicon Si(111) substrates. The Cu films thickness is fixed equal to 1000 Å. Whereas, the values of In films thicknesses are equal to 2600 Å (S1) and 1500 Å (S2), corresponding to 67 at.% and 50 at.% In respectively. The crystalline structure of the films was investigated by X-ray diffraction (XRD) using $CuK\alpha$ ($\lambda$=1.5405 Å) radiation. The formed intermetallic Cu-In phases were identified by using JCPDS data files. The morphology of the samples surface was investigated by scanning electron microscopy (SEM). The chemical composition of the samples and the in-depth distribution of the species were investigated by the Rutherford Backscattering Spectrometry (RBS).

## 3. RESULTS AND DISCUSSION

Figure 1 shows the XRD patterns for the S1 samples. The registered peaks are therefore characteristic of the polycrystalline CuIn, $CuIn_2$, Cu, In and CuO phases independently on the

nature of the substrate. The peaks assigned to In and CuO have relatively weak intensities. It is interesting to underline here that the JCPDS data files relative to the two phases CuIn and $CuIn_2$ give very similar lines of diffraction. Consequently, it is difficult to distinguish between these two compounds. This result shows that the thin Cu and In films interact during their deposition. This interaction leads to the formation and growth of the intermetallic $CuIn_2$ and CuIn.

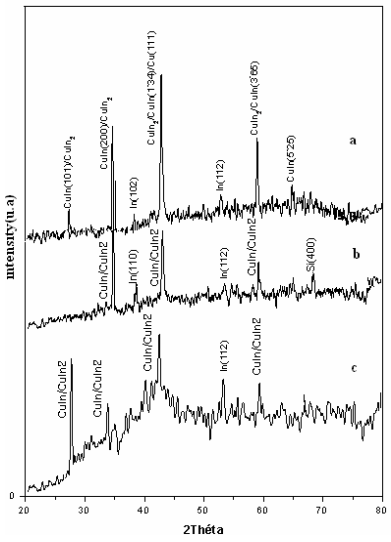


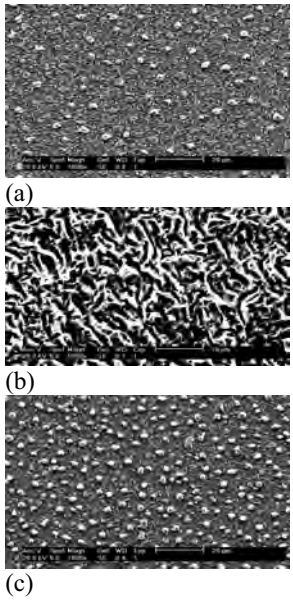


Figure 1. XRD spectra of as deposited Cu-In bilayers on glass (a), poly-silicon (b) and mono-silicon (c) .Figure 2. SEM micrographs of as deposited Cu-In bilayers on glass (a), poly-silicon (b) and mono-silicon (c).

However, the solid state reaction between Cu and In is not total since the elementary starting Cu and In compounds still remain. Figure 2 consists of the surface SEM micrographs of the S1 samples surface. It is easy to see that the observed microstructures are characteristic of a polycrystalline structure. The grains, more or less spherical form, are fine, perfectly connected and uniformly distributed on surface. The average size of the grains is considered equal to approximately 1 and 2 μm on glass and Si(111) substrates respectively. Also, one notices the formation of small islands in a uniform way on all the surface of the analyzed samples. On the other hand, the morphology of the Cu-In sample on polycrystalline silicon (Figure 2 b) is completely different. It is homogeneous, rough, and the grains form parallel connected columns. The energetic RBS spectra obtained for the S1 samples are given in figure 3. The main characteristic of these RBS spectra is the absence of the two distinct signals corresponding to two separate Cu and In films. The energy position of signal RBS of copper is clearly shifted towards the energy position of the copper signal on the surface. This fact proves that the films Cu and In are not distinct. Also, the report of the heights of the signals RBS relative to indium and copper is not consistent with the signals associated with indium and copper pure. Moreover, RBS analysis shows that copper is present at the surface of the samples. The no symmetrical shape of the two copper and indium signals is obvious. It reveals thus that a significant interfacial mixing has taken place, which testifies to a very strong atomic interdiffusion between the thin Cu and In layers of copper and indium during the co-evaporation process. RBS results are compatible with those obtained by XRD and SEM techniques. Previous studies, carried out on both sputtered and thermally evaporated Cu-

In bilayers onto glass substrate with In content varying in the range 50 – 75 at.%, have reported the formation of $CuIn_2$ and $Cu_{11}In_9$ phases [5,6].

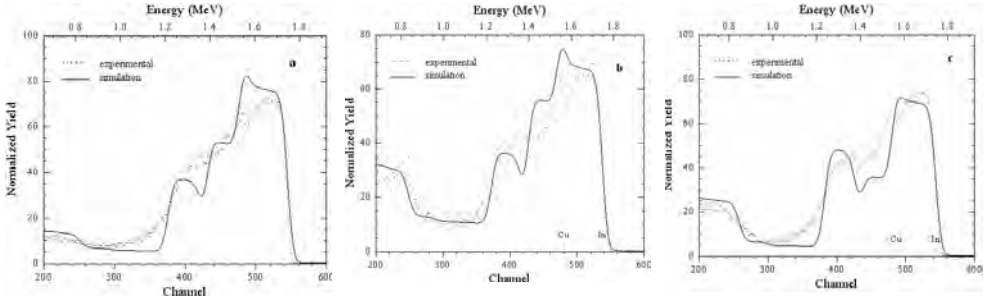


Figure 3. RBS spectra of as deposited Cu-In bilayers on glass (a), poly-silicon (b) and mono-silicon (c).

The increase in the atomic indium content leads to the formation of the same CuIn and $CuIn_2$ phases, but modifies the morphological properties of the Cu-In system. Indeed, the results of XRD nalysis of the S2 samples (no shown) are fully similar to those of the S1 samples. In RBS spectra of the S2 samples (no shown), on only notices that the recorded tails on the side of low energy of RBS copper signal are reduced. This result supports the SEM observations (Figure 4) which show a reduction of the films roughness.

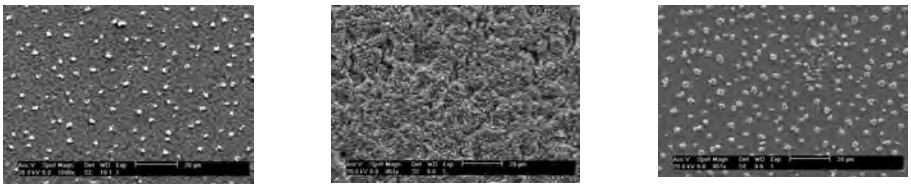

Figure4. SEM micrographs of as deposited Cu-In bilayers (S2 samples) on glass (a), poly-silicon (b) and mono-silicon (c).

It has been reported that the metastable CuIn phase is formed as deposition Cu-In bilayers regardless of the employed process deposition, and annealing induces the formation of copper-rich $Cu_9In_4$ and $Cu_7In_4$ compounds [7]. However, the co-existence of CuIn and $CuIn_2$ at room temperature, not reported previously, is confirmed here. This results is consistent with the phase diagrams corresponding to the considered 67 - 50 at. indium contents.

## 4. SUMMARY AND CONCLUSION

Thermally evaporated Cu-In bilayers on glass and silicon substrates are strongly mixed at room temperature. The Cu and In atomic interdiffusion leads to the formation and growth of CuIn and $CuIn_2$ phases for 67 – 50 at.% In independently on the used glass and silicon substrates. This is well consistent with the Cu-In phase diagrams. The nature of the substrate has a notable influence on the morphology of the samples surface. The density and the grains size are strongly influenced by the atomic In content.

## 5. References

[1] P. .Parrelta, M..L. Addonizio, S. Loreti, L. Quercia. M..K. Jayaraj, Crystal Growth 183 196 (1998)
[2] C.H. Chung, S.D. Kim, H.J. Kim, F.O. Adurodija, K.H. Yoon,J. Song, Sol. Stat. Com. 126 185 (2003)
[3] A. Ihlal , K. Bouabid , D. Soubane , M. Nya , O. Ait-Taleb-Ali , Y. Amira ,A. Outzourhit , G. Nouet .Thin Solid Films 515 5852 (2007)
[4] S. Jost, F. Hergert, R. Hock, J. Schulze, A. Kirbs, T. Vox, M. Purwins, Solar Energy Mater. Solar Cells 91 1669 (2007)
[5] F.O. Adurodija, J. Song, I.O Asia,K.H. Yoon, Solar Energy Mater. Solar Cells 58 287 (2007)
[6] T. Nakana, T. Suzuki, N. Ohnuki, S. baba, Thin Solid Films 334 192 (1998).
[7] J.S. Chen, E. Kolaw, M._A. Nicolet, Solar Cells, 30 451 (1991).

# Influence of UV exposure on cytotoxicity of luminescent nanocrystalline silicon particles

**M. Hiruoka [1], K. Fujioka [2], K. Yamamoto [2], K. Sato [3], K. Hirakuri [1]**

1. Tokyo Denki University, Graduate school of Science and engineering, Saitama, Japan

2. International Clinical Research Center Research Institute,

International Medical Center of Japan, Tokyo, Japan

3. International Center for Materials Nanoarchitectonics,

National Institute for Materials Science, Ibaraki 305, Japan

Luminescent semiconductor nanoparticles consisting of group IV have been expected for various biomedical applications. We have been currently preparing luminescent nanocrystalline silicon (nc-Si) particles dispersed in pure water in order to apply the nanoparticles to various kinds of biomedical application fields. However, it should clarify the safety of ingestion by living organisms to utilize the nc-Si particles in the biomedical fields. In this paper, the cytotoxicity tests of nc-Si particles using mitochondrial activity (MTT) assays and lactate dehydrogenate (LDH) release assays is discussed.

The nc-Si particles having a diameter of 2.2 nm were formed in $SiO_2$ thin films by radio frequency sputtering method and subsequent thermal annealing. The sample was treated with hydrofluoric acid solution to extract the particles from the $SiO_2$ thin films. After HF treatment, the nc-Si particles were uniformly dispersed in the pure water using supersonic vibration technique. The nc-Si particles in the pure water then added in HeLa cells which were sensitive to toxicity test, and were co-cultured for 48 hours. The concentration of nc-Si particles varied from 1.12 to 112 μg/mL. The cytotoxicity tests was examined from the viability and cellular membrane damages of HeLa cells with the nc-Si particles as a function of the particle concentration using the MTT and LDH release assays, respectively. Moreover, it was also performed the cytotoxicity tests of nc-Si particles after ultraviolet (UV) light irradiation for 2 hours in order to investigate the toxicological effect of UV exposure.

The viability and cellular membrane damages of cells did not quite depend on the particle concentration. These tendencies were almost same as those of cells without nc-Si particles. Furthermore, when the nc-Si particles after UV exposure added in cells, the cellular membrane damages were less in addition to the stable viability compared with the cells having the particles before UV exposure. These results imply that the cytotoxicity can improve by the use of nanoparticles based on the silicon materials for application in various environments, because of the good biocompatibility between the harmless crystalline silicon and cellular tissue. Moreover, the cells with nc-Si particles exhibited green luminescence by irradiating UV light.

# The interface behavior of $Bi_2Te_3$ thermoelectric cooler under load and heat condition

**J. Y. Huang, H. L. Hsieh**
China Steel Corporation, 81233, Kaohsiung, Taiwan

The connection integrity of thermoelectric module (TEM) under load and heat condition was investigated. In this study, 10 V was applied on TEM and the temperature of hot side TEM was maintained at 110℃. The integrity of TEM was regularly checked by measuring the resistance of TEM at room temperature. For a long period of time (166 hours), the resistance decreased slowly, from 2.14 to 1.71 Ω. However, the resistance increased to 17.99 Ω just before the failure of TEM. The SEM and EDX results suggested that two mechanisms causing the degradation of the connection of TEM. One is the diffusion of Cu and Sn at interface causing small change in TEM resistance. The path way of Cu diffusion is through Sn rich area in Bi-Sn solder. The other is the diffusion of Sn through micro-cracks causing a total failure of TEM.

## 1. INTRODUCTION

Thermoelectric module (TEM) is a solid-state energy converter or heat pump. It can be used for cooling, heating, temperature control, and electric generation. A large amount of researches focus on developing more advance materials and model for optimizing thermoelectric modules[1,2,3]. Less effort probes into the reliability issue of TEM. It has been reported that commercially available TME are very reliable as cooler operated around room temperature[4]. However, it is less reliable when operated at higher temperature. Ni layer is normally deposited between thermoelectric and electrode to block the interdiffusion of one or more thermoelectric element and a soldering material into each other which would degrade the thermoelectric characteristics over a long time usage.
The objective of this paper is to understand the interface behavior and failure mechanism of $Bi_2Te_3$ TEM under load and heat condition.

## 2. EXPERIMENT

The TEM tested in this study is a commercial thermoelectric cooling module. It composed of 127 pairs of bismuth telluride thermocouple that are connected electrically in series and thermally in parallel between two $Al_2O_3$ substrates. The overall resistance of this TEM is 2.14Ω. The connection structure between thermoelectric element and conductor strip is $Bi_2Te_3$(doped)/Ni/Bi-Sn(solder)/Ni/Cu. Ni is used for better weldability and as diffusion barrier. The hot side of TEM is attached to a heat sink to remove heat that draws from cold side. A fan with adjustable speed is attached to the heat sink in order to maintain the hot side temperature at a desired temperature. 10 V was applied on TEM and the temperature of hot side TEM was kept at 110℃ to expedite failure mechanism while preventing solder melting. The integrity of TEM was regularly checked by measuring the resistance of TEM at room temperature.

## 3. RESULTS AND DISCUSSION

Under the load and heat condition, the resistance of TEM slowly decreased from 2.14 to 1.71Ω for a long period of time (166 hours). However, the resistance radically increased to 17.99 Ω just before failure. To further analyze the cause of failure, cross-section sample was prepared and the connection of TEM was analyzed by SEM and EDX. SEM revealed that some thermoelectric elements of TEM showed severe splitting at center (Fig. 1). At hot side of TEM, Sn diffused into the TE element through micro-cracks causing an expansion perpendicular to heat flux, as shown at lower part of Fig. 1. These micro-cracks were created by the weak Van der Waals forces perpendicular to the c-axis of $Bi_2Te_3$. As more Sn diffused into TE element, the strain increased further, causing some large splits at center and the detachment of TE element at cold side of TEM. Consequently, it is the cause of the radical increase of TEM resistance.

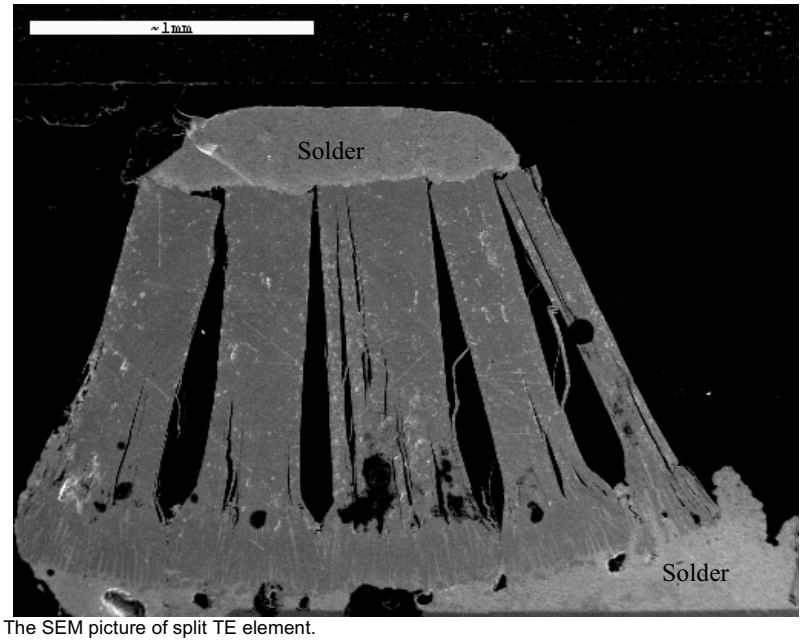


Figure 1. The SEM picture of split TE element.

Fig. 2 shows SEM picture, element distribution, and a brow out picture at connection interface of TE element which is still intact. Table 1 lists the Cu, Ni, Sn, and Bi ratio at A, B, C, D spots in Figure 2. A 7μm of reaction layer was formed due to inter-diffusion of Cu and Sn at solder/Cu interface. The ratio of Cu to Sn at spot A is around 1.18 suggeting a $Cu_6Sn_5$ formation. At solder region, it is clear that there are two types of structure: darker and lighter areas. The darker area is a Sn-rich area and lighter area is a Bi-rich area. Cu contain is much larger at Sn-rich area (darker area) than Bi-rich area (lighter area). It suggested that not only Ni at Cu/solder interface was unable to block Cu diffusing into solder, Cu diffused farther into the $Bi_2Te_3$/Ni/Bi-Sn interface through those Sn-rich area in solder. Furthermore, a Cu-rich layer was accumulated at Ni/solder interface. These interface diffusions and solder migration into microcracks were the leading cause of slow resistance decrease of TEM.

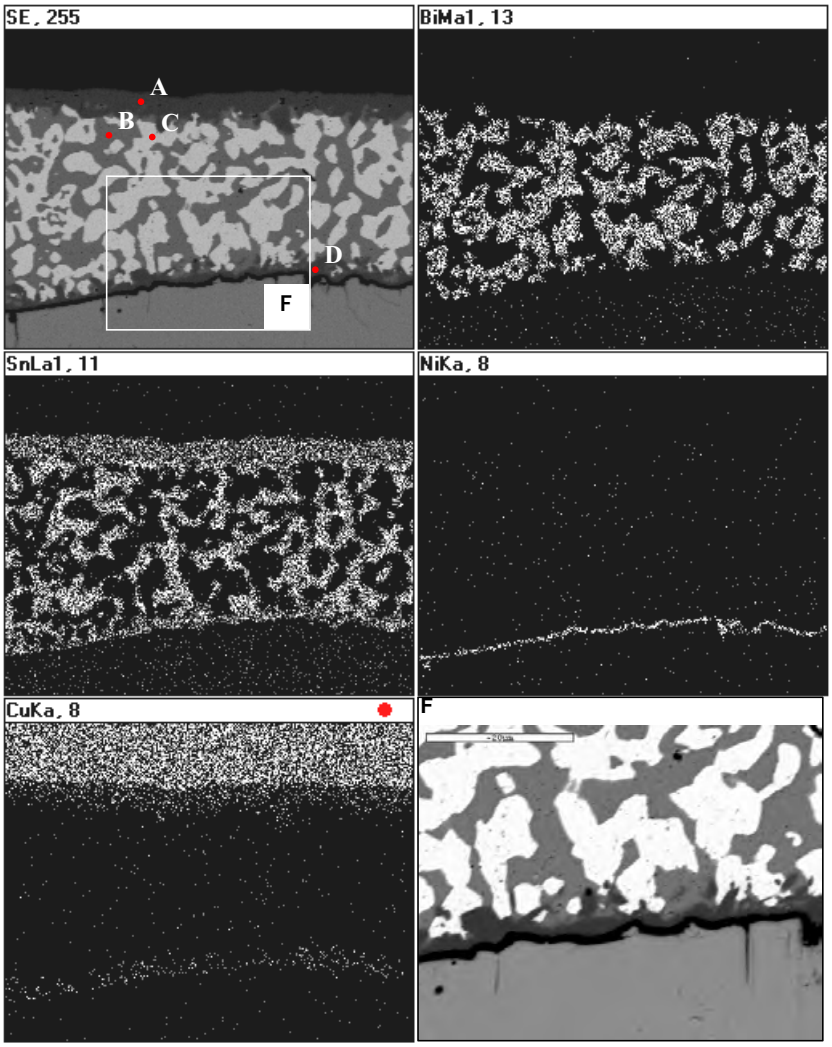


Figure 2. The SEM and element distribution pictures at the connection area of TEM and blow out picture white square area.

| Element | A (at.%) | B (at.%) | C (at.%) | D(at.%) |
|---|---|---|---|---|
| Cu | 53.9 | 5.2 | 2.5 | 34.7 |
| Ni | 0 | 0 | 0 | 18.3 |
| Sn | 45.6 | 82.6 | 0 | 46.3 |
| Bi | 0.5 | 12.2 | 97.2 | 0.7 |

Table 1. The Cu, Ni, Sn, and Bi, ratio at A, B, C, D spots in Figure 2.

## 4. CONCLUSION

In conclusion, there are two mechanisms causing the degradation of the connection of TEM. One is the diffusion of Cu and Sn at interface causing small change in TEM resistance. The path way of Cu diffusion is through Sn rich area in Bi-Sn solder. The other is the diffusion of Sn at micro-cracks leading to the split of TE element and detachment from solder resulting in a total failure of TEM.

## 5. References

[1]T.M. Tritt and M.A. Subramanian, MRS Bulletin 31 188(2006)
[2]Q.J. Zhang, X.F. Tang, P.C. Zhai, M. Niino, and C.Endo, Mat. Sci. Forum 492-493 135(2005)
[3]Gao Min and D.M. Rowe, J. Power Sources 38 253 (1992)
[4]D.M. Rowe and Gao Min, J. Power Sources 73 193 (1998)

# Influence of the dopant activation on the electrical properties of reactively sputtered Al:ZnO film

**M. Jullien [1], J.F. Pierson [1], B. Lenoir [2], J.Ph. Bauer [1], D. Horwat [1]**

[1] Laboratoire de Science et Génie des Surfaces (UMR CNRS 7570), Ecole des Mines, Parc de Saurupt CS 14234 F-54042 Nancy Cedex France

[2] Laboratoire de Physique des Matériaux (LPM) (UMR-CNRS 7556), Ecole des Mines Parc de Saurupt CS 14234 F-54042 Nancy Cedex France

AZO (ZnO:Al) semi-conductor thin films exhibit a high transmittance in the visible region and a good electric conductivity making it a really good candidate for transparent electrodes in electro-optics based devices.

AZO films were deposited on glass slides and silicon substrates by pulsed DC reactive sputtering using a Zn/Al (96/4 at.%) composite target. An oxygen/argon flow rates ratio of 4/20 and a total pressure of 6 Pa allowed the synthesis of highly transparent films. The film structure was characterized by X-ray diffraction. Room temperature electrical conductivity of films deposited on glass substrates was measured using the four point probe method. Finally, the film optical transmittance was studied by UV-visible spectrometry.

Both optical transmittance and electrical conductivity are strongly dependent on the position of the samples in the deposition chamber. Moreover, it is not simply ruled by the grain size [1]. ZnO:Al is a n-type semi-conductor and its electrical conductivity is very sensitive to a slight shift of the oxygen concentration. The variation of the Al dopant activation can also explain this conduction heterogeneity. Additionally, the fact that the optical band gap energy is very slightly affected by the samples positions suggests an evolution of the density and mobility of charges carriers. To solve the origin of the heterogeneity, the values of the charge carrier densities and mobilities obtained from Hall measurements are discussed in relation to the elaboration parameters and plasma reactivity.

[1] D. Horwat, A. Billard, Thin Solid Films. 515 (2007) 5444-5448.

# Optical and electrical characteristics of boron-doped nanocrystalline silicon particles

**K. Niino [1], K. Sato [2], K. Hirakuri [1]**

1. Tokyo Denki University, Graduate of science and engineering, Saitama, Japan
2. International Center for Materials Nanoarchitectonics,National Institute for Materials Science, Ibaraki, Japan

Nanocrystalline-Silicon (nc-Si) particles have been expected for application in industrial and medical fields because they have many excellent features for multicolor luminescent phenomenon, production cost and environmental influence. In order to apply the nc-Si particles to an EL (Electro Luminescence) device, it is necessary to improve carrier injection efficiency to the nc-Si particles. We have been previously confirmed the improvement of the electrical characteristics of the EL device by reducing the defects and etching the insulating layer ($SiO_2$ layer) on the surface of nc-Si particles. In this study, the effect of boron doping on the optical and electrical characteristics of the boron-doped nc-Si particles will be discussed.

The boron-doped nc-Si particles were prepared on the p-type Si (100) substrate by co-sputtering of boron chips/silicon chips/silica mixture targets and post-annealing at the temperature of 1100 °C. The boron concentration was controlled from 0.4 to 2.3 atm.% by changing the number of boron chips from 2 to 9 chips in the composite targets. The composite targets were sputtered in an argon (Ar) gas atmosphere at a gas pressure of 5 Pa and a RF power of 100 W for 120 min. The annealed samples were then treated in hydrofluoric (HF) acid steam to remove the defects and the $SiO_2$ layer on the surface of nc-Si particles. After HF treatment, ITO (Indium tin oxide) and aluminum electrodes were deposited on the top of nc-Si layer and back of Si substrate, respectively, using radio frequency sputtering method.

The series resistance of boron-doped nc-Si particles was lower about 50 % than that of the non-doped one. The lowering of the series resistance may be due to effective boron doping. The series resistance was decreased from 96.2 to 50.0 Ω with increasing the boron concentration from 0.4 to 2.3 atm.%. The lower series resistance brought about the increase of the carrier injection efficiency to the nc-Si particles. The carrier injection of the sample with boron concentration of 2.27 atm.% was improved about 2 times higher than sample without boron doping.

# High photocatalytic activity of tungsten oxide nanowalls synthesized by combined Sol-gel/ thermal method

**P. Khosravi [1], R. Azimirad [1], O. Akhavan [1], A. Z. Moshfegh [1, 2]**

1. Sharif University of Technology, Department of Physics, P.O.Box 11155-9161, Tehran, Iran
2. Sharif University of Technology, Institute for Nanoscience and Nanotechnology, P.O.Box 14588-8969, Tehran, Iran

Recently, Quasi-one-dimensional (Q1D) structures with high surface-to-volume ratio and small grain size have been attracted extensive studies due to their unique properties and various applications in nanoscale device fabrication. As an important wide band gap semiconductor, the tungsten oxides $WO_x$ (x=1-3) have been applied to photocatalysis, photochromic and electrochromic devices, as well as humidity, temperature and gas sensors for many years. In this research, initially tungsten oxide thin films were prepared on cleaned soda lime glass substrate using sol-gel dip-coating method. All the films were dried in air at 100$^o$C for 1h. Some of the deposited films heat treated in a controlled conditions (temperature 700$^o$C for 60 min under $N_2$ environment with a constant flow rate of 100 sccm) producing $WO_3$ nanowalls. The grown samples containing the tungsten oxide nanostructures were characterized and analyzed by scanning electron microscopy (SEM), X-ray diffractometry (XRD), X-ray photoelectron spectroscopy (XPS) and Ultra Violet UV-Visible spectrophotometry. In addition, the photocatalytic activity of the samples was evaluated through the degradation reaction of Methylene Blue (MB) under UV irradiation. According to SEM observations, length and width of synthesized nanowalls were measured between 10-30 μm and 100-300 nm, respectively. Based on XRD analysis, the crystallization phase of nanowalls was identified as non-stoichiometric monoclinic $W_{17}O_{47}$ with strong (500) diffraction peak. XPS analysis also determined that the W (4f) core level peak shifted from $W^{+6}$ chemical state to a lower binding energy ($W^{+5}$) indicating reduction of oxygen on the surface of the sample after the annealing process. Optical transmission and reflection of the annealed samples were measured around 10% and <1%, respectively. Moreover, absorption edge was also determined at 310 nm for the samples. Photocatalytic experiments indicate that the synthesized nanowall samples show much higher photoactivity than $WO_3$ thin film dried at 100$^o$C during photodegradation reaction of MB. It was found that 96% of MB was degraded after 200 min UV-irradiation on the heat treated films containing nanowalls, while only 55% of MB was degraded on $WO_3$ thin films dried at 100$^o$C.

[1]S. J. Yoo, Y. H. Jung, J. Y. Lim, H. G. Choi, D. K. Kim, Y. E. Sung, Sol. Energy Mat. Sol. Cells 92 (2008) 179
[2] S. Berger, H. Tsuchiya, A. Ghicov, P. Schmuki, Appl. Phys. Lett. 88 (2006) 203119
[3] Y. Guo, X. Quan, N. Lu, H. Zhao, S. Chen, Environ. Sci. Technol. 41 (2007) 4422

# Structural and Discharging Properties of MgO Thin Films Prepared by Pulsed Laser Deposition

**M. Kodu [1], J. Raud [1], M. Aints [1], T. Avarmaa [1], V. Denks [1], J-S. Choi [2], E. Feldbach [1], R. Jaaniso [1], M. Kirm [1], M-S. Lee [2], A. Maaroos [1], Y. T. Matulevich [2], H. Mändar [1], V. Sammelselg [1]**

1. Institute of Physics, University of Tartu, Riia 142, 51 014 Tartu, Estonia
2. Electronic Materials Development Team, Corporate R&D Centre, Samsung SDI, 428-5, Gongse-dong, Giheung-gu, Yongin-si, Gyeonggi-do 446-577, Korea

Polycrystalline MgO layer with typical thickness of 500 nm have two major functions in plasma display panels (PDPs). Firstly, this film protects the dielectric layer deposited onto the electrodes from plasma erosion due to gas discharge. Secondly, it ensures the favourite energetic conditions for discharge. Some of the actual problems that concern PDPs presently are relatively short lifetime and high electric power consumption. The key elements to overcome these disadvantages are the increase of the sputtering resistance against ion bombardment and the reduction of the discharge voltage. Previously MgO layers were made mainly by electron beam deposition (EBD) method and also by various sputtering techniques. For studying possible replacement materials for currently used MgO, it is useful to apply a suitable deposition method for materials engineering and research. PLD is a method that not only produces high quality films but is very versatile at the same time – combinatorial deposition, ability to transfer complex stoichiometry from target to film, easy to deposit layered structures with the use of multiple targets.

In this work, 200-250 nm thick MgO films were deposited by pulsed laser deposition (PLD) method on fused silica substrates and on special electrode substrates for firing voltage (FV) measurements. High quality MgO single crystals grown by the arc-fusion method were used as targets. PLD deposition parameters of the films were as follows: excimer laser wavelength 248 nm, laser pulse energy density on the target ~7 J/cm$^2$, substrate temperature (T) 260 – 600 $^o$C, and oxygen pressure (p) in the chamber $2*10^{-4}$ - $5*10^{-2}$ mbar. Structural and morphological characterisation of the films was performed by XRD, XRR, and AFM. The results were compared to the data of FV measurements.

Discharge and structural properties of the samples were strongly dependent on PLD growth parameters. At a fixed temperature, the crystallinity and density of the films were higher when oxygen pressure was lower. At a fixed oxygen pressure, the crystallinity and density of the films increased with increasing substrate temperature. Surface roughness of the films increased with increasing oxygen pressure and substrate temperature. Practically all crystalline samples obtained were highly (200) oriented and showed only one reflection at $2\Theta = 43$ deg. It has been reported that EBD grown (200) oriented MgO films are more resistant to ion sputtering as compared to (111) oriented films. FV values were correlated with structure properties and surface morphology of the samples. At a given substrate temperature, lower FV values were obtained for the films grown at lower oxygen pressures. At a fixed oxygen pressure, the FVs of the samples decreased when substrate temperature increased. Samples with the lowest FV values had high crystallinity and density close to theoretical value of bulk MgO (3.58 g/cm$^3$), but moderate surface roughness.

# Pd-doped $TiO_2$ Thin Films as Gas Sensors

**D. Mardare [1], F. Iacomi [1], N. Iftimie [1], M. Crisan [2]**
Al.I.Cuza University
Institute of Physical Chemistry

Titanium dioxide ($TiO_2$) films can detect a large category of harmful gases that affect our environment and, as a consequence, the quality of life, being used in gas sensor applications. A semiconducting gas sensor change its electrical conductivity when exposed to different gas atmosphere. The mechanism usually depends on the operating temperature, which is optimal depending on the sensor material properties and on the selected gas atmosphere. Nanosized grains of the sensing materials are preferred, because they increase the specific surface exposed to gas. In this paper we refer to the influence of substrate nature and doping (0.5% Pd) on the phase composition and morphology of titanium oxide films and, as a consequence, on their gas sensing properties. The sensitivity of these films and the optimum operating temperature were investigated for some reducing gases (formaldehyde, methane, acetone, ethanol and liquefied petroleum gas). The structure of the films and the microstructure were investigated by X-ray diffraction (XRD) and Atomic Force Microscopy (AFM) respectively. The results presented in this paper clearly show a high selectivity of all the films to formaldehyde, with a special remark for the titanium oxide films deposited onto Si[100]p substrates.

# Enhancement of the photovoltaic performance of dye-sensitized solar cells by application of a visible light-responsive $TiO_2$ thin film electrode prepared by RF magnetron sputtering deposition method

**M. Minakata [1], H.C Chen [2], W.T Lin [2], M. Takeuchi [1], M. Matsuoka [1], M. Anpo [1]**

1. Graduate School of Engineering Osaka Prefecture University, Department of Applied Chemistry, 1-1 Gakuen-cho, Naka-ku, Sakai, Osaka 599-8531, Japan

2. Taiwan Textile Research Institute (TTRI), No. 6, Chen-Tian, Rd., Tu-Chen City, Taipei County, 236 Taiwan

Vis-$TiO_2$ and UV-type $TiO_2$ (UV- $TiO_2$) thin films were prepared by a RF-MS method on conducting ITO-glass substrates at a substrate temperature of 873 K and 473 K, respectively. $TiO_2$ was used as the source material and Ar as the sputtering gas. Hereafter, these electrodes will be denoted as Vis- $TiO_2$ and UV- $TiO_2$. Characterization of these $TiO_2$ electrodes were performed by XRD, UV-Vis, BET and SEM measurements. The DSCs were fabricated using these $TiO_2$ electrodes sensitized by a N719 dye and Pt counter electrode deposited on the conducting ITO-glass substrate. Acetonitrile solution including 0.5M LiI, 0.05M I2 and 0.5M TBP (4-tert butylpyridine) was used for the DSC electrolyte. IPCE and photocurrent-voltage measurements of the DSCs were performed in air at room temperature under illumination with an AM 1.5 simulated lamp (100mW cm-2). UV-Vis investigations showed that the absorption band edge of Vis- $TiO_2$ electrode shifted significantly to the visible light region at around 600 nm as compared to the UV-$TiO_2$ electrode. Furthermore, flat band potential measurements revealed that the conduction band edge (ECB) of the Vis- $TiO_2$ electrode (-1.02V) shifted positively as compared to that of UV-TiO2 (-1.11V). Photovoltaic performance measurements were performed on two types of DSCs using the Vis- $TiO_2$ (DSCVis) and UV- $TiO_2$ electrodes (DSCUV). DSCVis exhibited remarkably higher IPCE and photoconversion efficiency than DSCUV, showing that the ECB of the $TiO_2$ electrode affects the photovoltaic performances of the DSC, i.e., the lower the position of ECB, the more efficient the electron transfer is from the photo-excited N719 dye to the conduction band of the $TiO_2$ electrode. Furthermore, it was found that the photovoltaic performance of DSCVis greatly depend on the deposition time of Vis- $TiO_2$. The highest IPCE and photoconversion efficiency was obtained for Vis- $TiO_2$ deposited for 700 min. The details of this research will be reported.

[1] M. Kitano, M. Takeuchi, M. Matsuoka, J.M. Thomas, M. Anpo, Catal. Today, 120, 133 (2007).
[2] H. Kikuchi, M. Kitano, M. Takeuchi, M. Matsuoka, M. Anpo, P. V. Kamat, J. Phys. Chem. B, 110, 5537 (2006).

# Ion irradiation stability of Ta/Ti nanostructured multilayers

**V. Milinović [1], D. Peruško [1], S. Petrović [1], M. Milosavljević [1], A. Zalar [2], J. Kovač [2], C. Jeynes [3]**

1. VINČA Institute of Nuclear Sciences, POBox 522, Belgrade 11001, Serbia
2. Jožef Stefan Institute, Jamova 39, Ljubljana 1000, Slovenia
3. Surrey Ion Beam Centre, ATI, University of Surrey, Guildford, Surrey GU2 7XH, UK

Ion beam processing is a very powerful and widely applied technique for preparation and modification of thin film materials. It can enhance the adhesion of hard coating materials to the substrate, and in general improve their tribological properties. On the other hand, multilayered structures provide numerous advantages over single component coatings, such as much higher hardness and strength due to a large number of interfaces, possibilities to form super lattices, graded composition, more dense and less porous structures. Multilayers are also interesting as radiation protective materials and for gas storage, such as hydrogen, in which case mutually immiscible materials are of primary interest. In this paper we have studied ion irradiation stability of Ta/Ti multilayered structures, deposited on Si substrates by ion sputtering in a single vacuum run. The starting structures consisted of 10 alternate Ta and Ti layers, with individual layer thickness of ~20 nm. Hence, the total thickness of the multilayered structures was ~200 nm. After deposition the structures were irradiated with $Ar^+$ ions, at 200 keV, to the fluences from $5x10^{15}$ to $2x10^{16}$ ions/cm$^2$. The projected ion range was around mid-depth of the multilayered structures. An area of 2.5x2.5 cm$^2$ was irradiated, with a beam current of ~1 μA/cm$^2$. Structural analyses of the samples were performed by transmission electron microscopy (TEM), Rutherford backscattering spectrometry (RBS), Auger electron spectroscopy (AES) and X-ray diffraction (XRD). It was found that in the as-deposited structures the interfaces between individual layers are very sharp, and the surface is flat and uniform. Individual layers have a very fine polycrystalline structure, with a grain size of up to a few tens of nm. After ion irradiation we observe practically no change in the depth profiles of the components. TEM analysis showed only a slight increase of the mean grain size in individual layers, while the interfaces remained sharp as in the case of as-deposited layers. Hence, there was no observable interface mixing, as typical for the applied fluences on systems which can form solid solutions, or can interact chemically. Such behavior of Ta/Ti multilayers is assigned to their mutual immiscibility.

# Photocatalytic and hydrophilic properties of sol-gel nanocomposite $TiO_2$-$SiO_2$ thin films

**S. Ganjoo[1], R. Azimirad [1], O. Akhavan [1], A. Z. Moshfegh [2]**

1. Sharif University of Technology, Department of Physics, Tehran, Iran.
2. Sharif University of Technology, Institute for Nanoscience and Nanotechnology, Tehran, Iran.

Titania has excellent photocatalytic and hydrophilic properties under UV-irradiation [1]. One way to enhance these properties is to decrease the recombination rate of the electron-hole pair by increasing the band-gap energy. This can be accomplished by adding $SiO_2$ to $TiO_2$ base matrix[2]. In this work, both photocatalytic and hydrophilic properties of nanocomposite $(TiO_2)0.80$-$(SiO_2)0.20$ thin films have been studied as compared to pure $TiO_2$ prepared films. The thin films, at first, were dried at 100°C and then annealed in a range of 200-500°C in air for 1 h. Some of the samples were also dried at room temperature for comparision . In order to determine properties of the synthesized thin films, various characterization techniques were used. Based on AFM analysis, averagesurface roughness of the $TiO_2$ and $TiO_2$-$SiO_2$ thin films increased from 0.4 to 4.3 nm and 0.6 to 2.4 nm by increasing the annealing temprature from room temprature to 500°C, respectively. XRD analysis revealed that the titania thin film annealed at 500°C has mainly anatase structural phase with (101) crystallographic orientation and average crystalline size of 31 nm, while the $TiO_2$-$SiO_2$ composite thin film showed no crystalline peak. In fact, $SiO_2$ can form a Si–O bond in the $TiO_2$-$SiO_2$ thin film preventing formation of the anatase phase [3]. XPS analysis showed that concentration of silica relative to titania at the surface was much higher than the ratio of initial prepared sol. At 500 °C, using XPS the Ti/Si ratio was estimated about 2 which means diffusion of the Si atoms into the surface [3]. Optical properties of the thin films showed that, by adding $SiO_2$ to $TiO_2$, the transmission increased and reflection decreased [4]. To examine photocatalytic and hydrophilicity activities of the films photodegradation reaction of Methylene blue (MB) was considerably increased and contact angle (CA) of water droplets decreased for the both types of the films by increasing annealing temperatures. It was found that 77% of MB was degraded after 200 min UV-irradiation on the $TiO_2$-$SiO_2$ surface annealed at 500°C, while only 30% of MB was degraded on the pure $TiO_2$ thin film dried at room temperature. The CA of the compound thin film annealed at 500°C after 1 h UV-irradiation was about 4°, while it was measured 8° for the dried titania thin films under the same conditions. After keeping the samples for 1 h in a dark, CA of the dried titania films increased to 58° while it remained as small as 6° for the nanocomposite $TiO_2$-$SiO_2$ films.

[1] A. Murakami,T. Yamaguchi, S. Hirano, K. Kikuta Thin Solid Films 516 3888 (2007)
[2] C. Shifu, C. Gengyu, Surface & Coating Technology, 200 3637(2006)
[3] K. J. Saini, S. D. Sharma, Chanderkant, M. Kar, D. Singh, C. P. Sharma J. Non-Crystalline Solids 353 2469 (2007).
[4] M. Ohring "Materials Science of Thin Films" Academic Press, New York (2002)

# Stability enhancement of hydrophilic RF co-sputtered $Ti_xSi_{1-x}O_2$ thin films in dark

**A. Z.Moshfegh [1,2], M. Mirshekari soleimani [1], R. Azimirad [1] O. Akhavan [1]**

[1] Department of Physics, Sharif University of Technology, P.O. Box 11155-9161, Tehran, Iran.

[2] Institute for Nanoscience and Nanotechnology, Sharif University of Technology, PO Box 14588-89694, Tehran, Iran

It is established that the contact angle of water for pure $TiO_2$ becomes almost zero during UV irradiation. It was found that by adding $SiO_2$ to $TiO_2$, the initial contact angle of water is reduced and become more hydrophilic in dark as compared to pure $TiO_2$. In this regard, many researches were reported sol-gel derived Titania–Silica thin films [1,2]. But in this paper, for the first time, we investigate the effect of Si concentration on photo-induced hydrophilicity of $Ti_xSi_{1-x}O_2$ thin film system (x = 1, 0.8, 0.6, 0.3 and 0) were formed in Argon (60%) and Oxygen (40%) by reactive RF co-sputtering technique without any annealing process. The degree of hydrophilicity of the prepared samples is assessed by measuring $H_2O$ contact angle with the surface. These measurements were performed before, during and after UV irradiation. It was found that the films with $Ti_{0.6}Si_{0.4}O_2$ composition possess the best hydrophilic properties among all the grown samples. The initial contact angle of water on the surface of this type of sample has the lowest value (~20˚) and it becomes about 3˚ after 1 hour UV irradiation and their angle slightly increased to (~7˚) after they remained about 50 hour in dark. The optical properties of the samples were investigated by measuring the transmittance and reflectance by a UV-Visible spectrophotometer. It was found that transmittance and reflectance of the $Ti_xSi_{1-x}O_2$ compound films decreased and increased with increasing Ti content (x) in the films, respectively. Moreover, Based on our optical data analysis, the average thickness of the samples were determined about 140 nm and their band gap energy for the pure $TiO_2$ films (3.2eV) and the $Ti_{0.8}Si_{0.2}O_2$ (3.7eV) obtained. The surface ratio, average roughness and grain size of the deposited thin films were also studied by atomic force microscopy (AFM). It was found that the roughness of compound samples varied between 1.5-2 nm and in the pure $SiO_2$ and $TiO_2$ thin films, roughness is 3.5 and 7 nm, respectively. According to XRD data analysis for the pure $TiO_2$ films, the polycrystalline anatase phase was formed with an average grain size of about 15 nm without any annealing process. Moreover, amorphous phase was also formed for the $Ti_xSi_{1-x}O_2$ compound system due to presence of Si in the films. To determine the surface stoichiometry, chemical state and the concentration of Ti in the compound $Ti_xSi_{1-x}O_2$ thin film system we have applied XPS surface analysis technique. O(1s), Ti(2p) and Si(2p) core level binding energies were measured with reference to C(1s) peak. In addition to $SiO_2$ and $TiO_2$ oxide formation, we have also revealed the presence of mixed oxide (Ti-O-Si) at the surface of compound films [3] which is effective for enhancing hydrophilicity of the $Ti_xSi_{1-x}O_2$ compound films [1].

[1] K. Guan, B. Lu, Y.Yin, Surf. Coat. Tech 173. 219 (2003)

[2] M. Maeda, S. Yamasaki, Thin Solid Films 483. 102 (2005)

[3] R. P. Netterfield, P. J. Martin, C. G. Pacey, W. G. Sainty, J.Appl. Phys 66, Issue 4. 1805 (1989)

# $In(OH)_xS_y/Pb(OH)_xS_y$/PEDOT:PSS Solar Cell

**J.M. Mwabori, B.O. Aduda, R.J. Musembi**
University of Nairobi

A new highly structured $In(OH)_xS_y/Pb(OH)_xS_y$/PEDOT:PSS solar cell has been developed based on the novel eta concept, and characterized by X-ray photoelectron and Auger electron spectroscopies, photovoltaic response and quantum efficiency spectroscopy. In this system, $In(OH)_xS_y$,/$Pb(OH)_xS_y$ and PEDOT: PSS serve as electron conductor, light photon absorber material and hole conductor respectively. The electron conductor and absorber layer were prepared by chemical bath deposition, while the hole conductor was prepared by spin coating technique. The band gap of as prepared $In(OH)_xS_y$ has been found to vary with PH of the solution, also the band gap of $Pb(OH)_xS_y$ can be engineered to make it suitable as absorber material for solar cell application. At present, a solar cell device has been realized with efficiency up to over 1%, Jsc =8 mA/cm2 and Voc=3.0 V

# The Electrochromic Performance of Sol-gel Deposited $WO_3$-$SiO_2$ Compound Thin Films

**N. Naseri [1], R. Azimirad [1], O. Akhavan [1], A. Z. Moshfegh [1,2]**

1. Department of Physics, Sharif University of Technology, P.O. Box 11155-9161, Tehran, Iran
2. Institute for Nanoscience and Nanotechnology, Sharif University of Technology, P.O. Box 14588-89694, Tehran, Iran

In this investigation, the physical and electrochromic properties of $WO_3$-$SiO_2$ compound thin films with various $SiO_2$ contents including 0, 25, 50 and 70 mol% has been studied. Optical properties of the samples were investigated by the UV-visible spectrophotometry in a range of 300-1100 nm. It was found that the transmittance and the band gap energy of the compound films increased with increasing the $SiO_2$ concentrations. X-ray photoelectron spectroscopy (XPS) was used to study surface chemical composition of the samples. Based on the XPS analysis, the formation of stoichiometric $SiO_2$ and $WO_3$ in the compound films was verified. The electrochromic properties of the $WO_3$-$SiO_2$ compound films were investigated on the ITO/glass substrates using a 1 M $LiClO_4$ in propylene carbonate (PC) as the electrolyte and pure graphite as the counter electrode in a two electrode system. By measuring the coloration transmittance of the compound films as a function of time at different coloring voltages, it was found that the samples with 25 and 50 mol% of $SiO_2$ show the shortest bleaching and coloration time, respectively.

## 1. INTRODUCTION

Research in the field of electrochromic transition metal oxide films has gained a lot of attention in the past several decades. Electrochromism phenomenon in transition metals can be explained as making changes in optical properties of materials by applying an electric field. [1]. Among the transition metal oxides that exhibit electrochromic properties, $WO_3$ has been investigated most extensively [1-4]. This was due integrally to its fast response times, coloration efficiencies, long life times and etc. These properties tendered $WO_3$ desirable for use in information displays [5], anti glare rear view mirrors of automobiles [6,7] and the so-called “smart windows” [8]. However, there are many efforts to improve its coloration performance for practical applications. An important factor for electrochromic films which are used as a smart window is their transmittance in the bleached state should be high enough. For this purpose, addition of materials with high transmission to the electrochromic layer can be useful. Silicon oxide has attracted much attention due to its unique properties such as high transmission, porosity, and unreactivity [9] but there is not any report about the effcet of $SiO_2$ addition on the electrochromic performance of the $WO_3$ thin films. In this paper, we have presented optical properties and surface chemical state of $SiO_2$ doped $WO_3$ thin films synthesized by easy and low cost sol-gel method. In addition, electrochromic behavior of $WO_3$-$SiO_2$ thin films under various applied voltages has been also studied.

## 2. EXPERIMENTAL DETAILS

Sol-gel dip-coated $WO_3$-$SiO_2$ compound thin films were grown using the procedure mentioned in our recently published paper [10]. The molar concentration of $SiO_2$ in the

compound was varied by values of 0, 25, 50 and 70% and the deposition process was performed by dipping microscope slide glass and indium tin oxide (ITO) coated glass substrates in the solution for 60 s and pulling them out with a rate of 1 mm/s. All films, at first, were dried at 100 °C and then annealed at 200 °C in air for 1 h. By using the optical method, thicknesses of the dried films was measured about 200nm.
A UV-visible spectrophotometer (Jascow-V530) was used to investigate the optical properties of the films in the wavelength range of 300-1100 nm. X-ray photoelectron spectroscopy (XPS) was employed to characterize the surface chemical composition of the films. All binding energy values were calibrated by fixing the C(1s) core level to the 285.0 eV.
The electrochromic properties of the $WO_3$-$SiO_2$ thin films were investigated on ITO/glass substrates. The $WO_3$-$SiO_2$ films, as working electrodes, were electrochemically cycled in a 1 M $LiClO_4$ in propylene carbonate (PC) electrolyte in a glass test vessel, using pure graphite as the counter electrode. Experimental details of the electrochromic test have been reported recently in our recent work [11]. The coloration transmittance of the $WO_3$-$SiO_2$ thin films was studied in two states. In the first state, it was measured as a function of time at a fixed wavelength of 500 nm (in which eye has a high sensitivity) at different coloring voltages, and then negative voltages applied for bleaching the films. Furthermore, during the electrochromic process, the magnitude of the current between the two electrodes was recorded. In the second state, the transmittance was measured by the spectrophotometer in a range of 300-1100 nm wavelength for the films colored after a constant time (500 s) at the different coloring voltages.

## 3. RESULTS AND DISCUSSIONS

### *3.1 Optical Measurments*

The optical transmission and reflection spectra of the $WO_3$-$SiO_2$ films were measured in a range of 300-1100 nm wavelength ( Fig. 1). The transmittance of the pure $WO_3$ thin film reached to 70% in the visible region of the spectrum. The transmission spectra show that the transmittance of the compound films increased with increasing the $SiO_2$ concentration and it became ~ 90% in the visible range for the compound film containing 70% $SiO_2$. This increase was occurred because silicon oxide has a lower extinction coefficient than tungsten oxide.

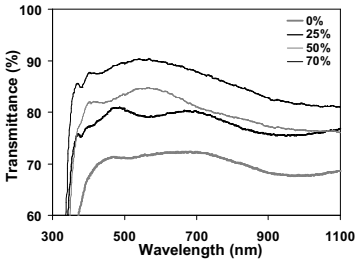


Figure 1. Transmittance spectra of $WO_3$-$SiO_2$ compound thin films containing different concentration of $SiO_2$.

### *3.2 XPS analysis*

To determine the surface stoichiometry and chemical state of the samples, $WO_3$–$SiO_2$ thin films were studied by XPS analysis. Figure 2a shows the deconvoluted XPS spectrum of the W(4f) core level peak for the sample containing 50 mol % of $SiO_2$. It consists of the W($4f_{7/2}$) peak at 35.6 eV and the W($4f_{5/2}$) peak at 37.7 eV with a full-width at half-maximum (FWHM) of 1.84 ± 0.04 eV for both of the peaks. The area ratio of these two peaks was fixed at 0.75 which is consistent with the spin-orbit splitting theory of 4f levels. Moreover, the two-peak structure was shifted by ~ 5 eV toward a higher binding energy relative to $W^0$ metallic state. It

is thus clear that the main peak in our XPS spectrum represent the $W^{6+}$ state on the surface [12,13]. To determine the chemical state of the silica in this film, the Si(2p) peak was also studied in more details, as illustrated in Fig. 2b. The Si(2p) peak was deconvoluted into two peaks ($2p_{3/2}$-$2p_{1/2}$) with fixed separation energy of 0.6 eV and area ratio of 2 calculated from the theory of splitting of 2p levels. It has been reported previously that the Si($2p_{3/2}$) core level binding energy of elemental Si is at 99.8 eV and the binding energy of SiO, $SiO_2$ and $SiO_2 + nH_2O$ films are 102.3, 102.7 and 103.2 eV, respectively [14]. The binding energy of the Si($2p_{3/2}$) peak in Fig. 2b was determined at 103.0 eV with FWHM of 2.09 ± 0.04 eV which is in agreement with stoichiometric formation of $SiO_2$ in the film. It should be noted for the other samples, data analyses for the W(4f) and Si(2p) peaks in the XPS spectra were coincidence with these results.

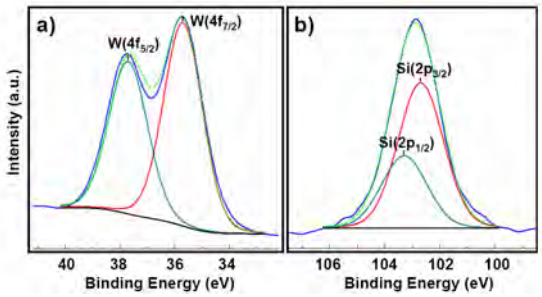


Figure 2. Deconvoluted XPS spectra of a) W($4f_{7/2,5/2}$) and b) Si($2p_{3/2,1/2}$) photoelectron lines of the $WO_3$-$SiO_2$ films with 50 mol % $WO_3$ concentration.

### *3.4 Electrochromic measurements*

The coloration–bleaching kinetics and the optical modulation of the samples were followed by putting the graphite and $WO_3$-$SiO_2$ electrodes in the prepared electrolyte, and then applying different coloring voltages to them. Figure 3 illustrates the changes in optical transmission as a function of time for the pure $WO_3$ film and the compound sample whith 25% $SiO_2$ at a constant wavelength (500 nm) in various applied coloring voltages. By applying the coloring voltage to the electrode at t = 10 s, the transmittance of the films continuously decreased and they were colored. For all the samples, the considered coloring voltages were disconnected at t = 500 s, and then, the polarity of the applied voltages was inverted 10 s later. By changing the polarity, the transmittance of the films was increased and they were bleached. All the samples were almost colorless before cathodic polarization, whereas they turned colored after the polarization. When a negative bias was applied, some $W^{V}$ ions were produced, due to the electron transfer from the electrode to $W^{VI}$ ions, and cations were inserted into the films simultaneously so as to maintain electroneutrality. Tungsten bronze ($Li_xW^{VI}_{1-x}W_x{}^{V}O_3$) was thus produced and a blue color appeared due to the optical intervalence charge transfer between tungsten atoms having different valance [15]. The equal transmittance of the films before coloration and after bleaching showed that the electrochromic reaction of the samples for that coloring voltage was reversible. It is clear from figure 3 that by increasing the coloring voltage up to its optimum value, the transmittance of the colored film decreased and the rate of the coloration increased. But after dispensing a higher voltage, the transmittance of the bleached film did not represent the reversible process. This is because of an effect called “site saturation” in which reversibility of optical effects at large Li+ intercalations in $Li_xWO_3$ is not valid [15]. The optimum value of coloring voltage for the films containing 0 and 25 mol% of $SiO_2$ was determined 2.5 V while it was measured to be 3 V for the samples containing 50 and 70 mol% $SiO_2$. A determinant factor in fabrication of electrochromic films is their response time. It is so critical to decrease the time interval needed for coloration and bleaching process, in practical

applications. The coloration time can be defined as the requisite time for reduction of the transmittance of the layer from 10% to 90% of the final reduction [16]. The coloration time of the samples was determined 215, 278, 224 and 316 for the films containing 0, 25, 50 and 70 mol% $SiO_2$, respectively. It can be found that the film with 50 mol% $SiO_2$ has the shortest response time between the compound samples which is near to one for the pure $WO_3$ thin film, while the transmittance of that is 15% more than the transmittance of the pure film in the visible range.

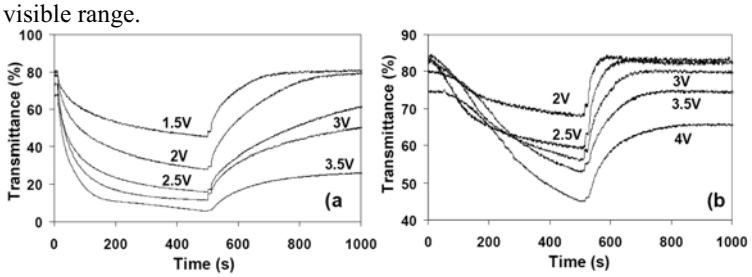


Figure 3. The transmittance variation of the films containing a)0 and b)50% $SiO_2$ at different voltages.

## 4. CONCLUSIONS

In summery, $WO_3$-$SiO_2$ compound thin films contaning different concentration of $SiO_2$ were synthesized. The optical analysis showed that they have high transmittance in the visible range. According to the electrochromic measurments, the films contsining 50% $SiO_2$ have the shortest coloration time between the compound films whith a transmittance more than pure $WO_3$ pure thin film.

## 5. References

[1] C.G. Granquvist "Handbook of Inorganic Electrochromic Materials" Elsevier, Amsterdam, 1995()
[2] N.S. Giakwad, G. Waldner, A. Bluger, A. Belaidi, S.M. Chaqour, M. Neumann-Spallart, J. Electrochem. Soc. 152 G411 (2005).
[3] M. Deepa, M. Kar, S.A. Agnihotry, Thin Solid Films 468 32 (2004).
[4] M. Hepel, H. Redmond, I. Dela, Electrochim. Acta 52 3541 (2007).
[5] W. Lu, A.G. Fadeev, B. Qi, B.R. Mattes, J. Electrochrem. Soc. 151 H33 (2004).
[6] H.N. Cui, M.F. Costa, V. Teixeira, I. Porqueras, E. Bertran, Surf. Sci. 532 1127 (2003).
[7] G. Liu, T.J. Richardson, Sol. Energy Mater. Sol. Cells 86 113 (2005).
[8] C.M. Lampert, Mater. Today 7 28 (2004).
[9] L. Ovari, F. Solimosi J. Mol. Catal. 207 35 (2004).
[10] N. Naseri, Re. Azimirad, O. Akhavan, A.Z. Moshfegh, J. Phys. D 40 2089 (2007).
[11] R. Azimirad, O. Akhavan, A.Z Moshfegh, J. Electrochem. Soc. 153 E11 (2006).
[12] R. Azimirad, O. Akhavan, A. Z. Moshfegh J. Electrochem. Soc. 153 E11(2006).
[13] . Taghavinia, T. Yao Physica E 21 96 (2004).
[14] A. Babapour, O. Akhavan, R. Azimirad, A. Z. Moshfegh Nanotechnology 17 1 (2006).
[15] P.R. Somani, S. Radhakrishnan, Mater. Chem. Phys 77 117 (2002).
[16] S. Heusing, D.L. Sun, J. Otero-Anaya, M.A. Aegerter, Thin Solid Films 502 240 (2006).

# Effects of thermal annealing on structural and electrical properties of sputtered WTi thin films

**S. Petrovic [1], D. Perusko [1], B. Gakovic [1], M. Mitric [1], J. Kovac [2], A. Zalar [2], V. Milinovic [1], I. Bogdanovic-Radovic [3], M. Milosavljevic [1]**

1. Instute of Nuclear Science - Vinca, P.O.Box 522, 11001 Belgrade, Serbia

2. Jožef Stefan" Institute, Jamova 39, 1000 Ljubljana, Slovenia

3. Department for experimental physics, Ruđer Bošković Institute, P.O. Box 180, 10002 Zagreb, Croatia)

Thermal and chemical stability of WTi thin films are needed for their efficient use as diffusion barriers in contact structures in microelectronic devices. In this work we have studied the influence of thermal annealing on the properties of tungsten – titanium thin films, deposited on n-type (100) silicon wafers. The films were deposited at 130 $^{o}$C by d.c. sputtering from a 90:10 wt% W–Ti target, using Ar ions. Post-deposition thermal annealing of the samples was performed at various temperatures, ranging from 400 to 700 $^{o}$C for 60 min, in a nitrogen ambient. Structural characterization of the samples was performed by X-ray diffraction (XRD), X-ray photoelectron spectroscopy (XPS), cross–sectional and plane view transmission electron microscopy (TEM) and by Rutherford backscattering spectrometry (RBS). For point probe was used for electrical characterization. It was found that annealing at temperatures up to 600 $^{o}$C leads to an increase of the mean grain size in the films and a decrease of sheet resistance. For these annealing temperatures we did not register any interaction between the WTi films and the Si substrate. Depth profiles of the components remained practically the same as in the as-deposited films. However, after annealing at 700 $^{o}$C, an interaction between the film and the substrate was detected. Structural analyses suggested the formation of both W and Ti silicides. Also, the sheet resistance of the films increased rapidly after annealing at 700 $^{o}$C due to fact that the $WSi_2$ phase is a semiconductor. Similar contribution to sheet resistance can be attributed to the presence of Ti-silicides, though the concentration of Ti in the as-deposited films in much lower then the concentration of W. The estimated thickness of the formed metal-silicide layer is approximately 80 nm. The results to be presented in this paper can be interesting for application of WTi thin films in contact metallization schemes in Si electronic devices. Combined results obtained by the different analytical techniques will be compared and discussed.

# High performance $Si_xGe_{1-x}$ thin film electrodes for lithium ion micro-batteries

**V.P. Phan [1], B. Pecquenard [2], F. Le Cras [3], P. Bouillon [1], C. Delmas [2]**

1. ST Microelectronics SAS
2. CNRS, Université de Bordeaux 1, ICMCB
3. CEA Grenoble – LITEN

All-solid-state lithium microbatteries are on the way to replace regular lithium cells in numerous applications and/or to become a necessary component to power new microdevices including RTC controllers, RFID tags, stand-alone MEMS, medical implants. In some cases, constraints from the manufacturing process (solder reflow) or from the application (cell storage at 0 V) disqualify metallic lithium as active material for the negative electrode. Elements forming alloys with Li and having melting temperatures above 300°C constitute substitutes to lithium in these systems. Among them, silicon which is extensively studied as negative electrode material for Li-ion conventional cells, is an interesting candidate due to its high volumetric specific capacity (880 $\mu Ah.cm^{-2}.\mu m^{-1}$ for $Li_{15}Si_4$). Nevertheless, it presents a high volumetric expansion during Li insertion (> 280 % in the bulk form). Germanium which also forms a series of defined compounds with lithium (up to the Li-richest composition $Li_{22}Ge_5$) has received little attention due to its cost. Even if Ge films have a theoretical volumetric capacity (864 $\mu Ah.cm_{-2}.\mu m_{-1}$) and a mean charge voltage close to silicon ones, this material offer potential additional operating advantages: i) Li diffusivity at room temperature calculated to be 400 times higher allowing higher current rates, ii) a thinner native oxide layer on its surface leading to lower irreversible capacity during the first cycle, iii) a lower volume expansion during Li insertion. This work reports on the electrochemical behavior of amorphous $Si_xGe_{1-x}$ thin films (100-400 nm thick) obtained by physical vapor deposition (DC magnetron sputtering) on copper foils or on tungsten-coated silicon wafers (400 nm films corresponding to actual capacities around 150-200 $\mu Ah.cm_{-2}$ targeted for the applications). Different film morphologies were obtained depending on the sputtering parameters. It was found that Ge films exhibit a more stable capacity during cycling in liquid electrolyte than Si ones. A film having a more dense morphology was also found to be beneficial to the cycle life. The capacity stability of negative electrode materials involving large volume expansion during lithium insertion is known to be mainly governed by the electrode/electrolyte interface properties. Thus, in addition to experiments in a conventional liquid electrolyte, a comparative evaluation of the electrochemical behavior of electrodes in different environments was carried out: in liquid electrolyte containing VC additive, covered by a lithium phosporus oxynitride (LiPON) protective layer, and in all-solid-state half-cells ($W/Si_xGe_{1-x}$ /LiPON/Li). The first results in all-solid-state cells demonstrate that high cycle life, low initial irreversible loss, and high coulombic efficiency can be achieved with $Si_xGe_{1-x}$ films. Rate capability measurements of these electrodes in half cells will be also reported.

# Co-sputtering Process: a Method to Tune the Ni/P Ratio in Nickel Phosphide Coatings

**J.F. Pierson [1], C. Petitjean [1], F. Robert [2], L. Monconduit [2], M.C. Marco de Lucas [3], D. Horwat [1]**

1. LSGS, Ecole des Mines, Parc de Saurupt, CS 14234, 54042 NANCY cedex, France
2. ICG-AIME, Université de Montpellier II, Place E. Bataillon, 34095 Montpellier cedex, France
3. ICB, Université de Bourgogne, 9 Av. A. Savary, BP 47870, 21078 Dijon Cedex, France

The Ni-P phase diagram contains several defined compounds: $Ni_3P$, $Ni_5P_2$, $Ni_{12}P_5$, $Ni_2P$, $Ni_5P_4$, NiP, $NiP_2$ and $NiP_3$. Although the sputtering processes are well-known for their ability to synthesise films with various compositions, the literature reports few articles on the synthesis of nickel phosphide films.

Ni-P films were deposited on glass and steel substrates by co-sputtering of nickel and nickel phosphide targets. The nickel concentration in the deposited films was adjusted by the variation of the current applied to the nickel target. The film chemical composition was estimated from energy dispersive X-ray spectroscopy and the structure was studied by X-ray diffraction. Micro-Raman spectrometry was used to confirm the film structure. Optical and electrical properties were studied using UV-visible spectroscopy and the four point probe method, respectively. Finally, the electrochemical performance of nickel phosphide films was evaluated vs lithium in a classical swagelock cell.

Within the deposition conditions tested in this study, the Ni/P atomic ratio is ranging between 0.1 and 3. Except for Ni/P = 2, the deposited films are X-ray amorphous. Furthermore, only $Ni_2P$ films exhibit a Raman spectra with well defined peaks. Depending on the chemical composition, the film electrical resistivity at room temperature is ranging between 100 and 1000 μΩ cm. Then, nickel phosphide films are highly reflective in the visible range.

The preliminary electrochemical measurements show promising results as negative electrode for Li-ion battery. The $Ni_2P$ film/Li battery can retain a 0.2 mAh $cm^{-2}$ capacity during 50 cycles, while the $Ni_2P$-powder (prepared by ceramical route) did not show any electrochemical reactivity versus Li.

# Structure and molecular orientation of polytetra-fluoroethylene coatings, formed from active gas phase

**A.A. Rogachev [1], M.A. Yarmolenko [1], A.V. Rogachev [2], I.I. Prosycevas [3]**

1. Belarusian State University of Transport
2. Francisk Scorina Gomel State University
3. Kaunas University of Technology

Thin polymer coatings of polytetrafluoroethylene (PTFE) obtained by vacuum methods have an outstanding combination of chemical and physical properties, excellent electrical properties low dielectric constant and dielectric loss tangent, high insulation and a breakdown voltage. The structure formations of PTFE coating nucleation and growth from the active gas phase, formed by electron beam dispersion of initial polymer in vacuum were examined. The morphology and molecular structure of the deposited fluoropolymer films were analyzed by atomic force microscopy (AFM), scanning electron microscopy (SEM) and polarized attenuated total reflection Fourier transform infrared spectroscopy (ATR-FTIR). Àn additional mathematical analysis of the cluster formation images was carried out. Using dichroic ratio the thin PTFE films were found to have polymer chains highly oriented with molecular axes aligned to be parallel to substrate surface. The order parameter (in case unaxially orientation) nonmonotonic depended from thickness of formed layers. The maximal orientation, maximal angle between the helix axis and surface normal occur in the thin interface layer disposed at a distance from frontier substrate-coating. This structural feature has been analyzed from the standpoint of the polymerization-diffusion growth mechanism.

# Infrared spectroscopic ellipsometry for characterization of functionalized thin films

**D.M. Rosu, G. Sun , N. Esser, K. Hinrichs**
ISAS – Institute for Analytical Sciences, Department Berlin, Albert-Einstein-Str. 9, 12489 Berlin, Germany

Infrared Spectroscopic Ellipsometry (IR-SE) was used for identification of adsorption of ultrathin biomolecular films on functionalized surfaces as well as for investigation of molecular orientation and lateral homogeneity in different organic-GaAs hybrid diodes. The FT-IR synchrotron ellipsometer at the IRIS beamline at BESSY II [1], for the mid infrared range, enables investigation of samples with monolayer sensitivity and a lateral resolution below 1 $mm^2$. Being equipped with a mapping table, the set-up allows the investigation of heterogeneous organic thin films. Results from mapping ellipsometry of biosensors [4] and self assembled monolayers, with thicknesses between 2 nm and 100 nm, will be presented in this work. Evaluation of measured spectra with optical models gives informations about thickness, homogeneity and orientation of the molecules on the substrates.

[1] M. Gensch, N. Esser, E. H. Korte, U. Schade, K. Hinrichs, Infrared Physics and Technology 49 (1-2) 39-44 (2006)

# Relationship between Nano-structure and Dielectric Properties of CSD-derived $BaTiO_3$ Thin films

**N. Sakamoto [1], K. Uchida [1], N. Wakiya [1], T. Suzuki [2], H. Suzuki [3]**

1. Department of Materials Science, Shizuoka University, 3-5-1 Johoku, Naka-ku, Hamamatsu 432-8561, JAPAN

2. Taiyo Yuden Co.,Ltd., 6-16-20, Ueno, Taito-ku, Tokyo 110-0005, JAPAN

3. Graduate School of Science and Technology, Shizuoka University, 3-5-1 Johoku, Naka-ku, Hamamatsu 432-8561, JAPAN

$BaTiO_3$ films oriented to [100] direction are expected of high-k dielectric thin films. In the present study, we fabricated $BaTiO_3$ (BT) dielectric thin films using $LaNiO_3$ (LNO) seed layer on $Pt/SiO_2/Si$ substrate via Chemical Solution Deposition (CSD) method. Both of the BT film and the LNO seed layer were fabricated from alchoxide precursor solutions. The precursor solutions of them were spin coated, dried at 150 °C, and pre-annealed at 400 °C, followed by Rapid Thermal Annealing at 700 °C. The film with thickness of ca. 180nm showed smooth surface with the RMS ca. 2.6nm observed by AFM. The BT film fabricated on the LNO seed layer showed [100] orientation normal to the substrate plane, whereas the film without seed was polycrystalline BT film. Permittivity of the film fabricated on the LNO seed layer was ca. 550 pF/m whereas the film without seed layer was ca. 300 pF/m measured at 10kHz. XRD pole figure showed both of the BT film and the LNO seed layer had no particular orientation parallel to the plane. Relationship between nano-structure and dielectric properties regarding crystal orientation for the BT film fabricated on the LNO seed layer was studied by SEM, HRTEM and STEM-EELS. Although the morphology of the LNO seed layer was porous, the BT film on the seed layer was dense and well crystallized without voids by HRTEM and SEM observation. Each BT grain was ca. 80 nm in size and some of them were columnar structure. HRTEM image and Selected Area Electron Diffraction (SAED) pattern of the BT grains implied no particular relation among the neighboring BT grains, which might indicate the BT grain growth were strongly affected by the LNO seed layer rather than neighboring BT grains. Electron Energy Loss Spectrum (EELS) of the TEM image indicated Ba rich particle penetrating into the LNO seed layer, which might decrease the Ba/Ti ratio of the BT film and decrease the permittivity of the film. Ba rich precursor solution may increase the Ba/Ti ratio therefore be expected to increase dielectric properties.

# Study of preferential sputtering and segregation on the surface composition of icosahedral Al-Pd-Mn quasicrystals

**F. Samavat**
Bu-Ali Sina University

Using 2keV noble gas ions (He and Ne), it was found that the Al/Pd concentration ratio at the surface, as determined by low energy ion scattering (LEIS), of a nominally Al69.9Pd20.5Mn9.6 quasicrystal, decreases smoothly to a steady state under bombardment as a result of preferential sputtering. The steady state under sputtering was attained quicker for Ne+ than for He+. Sputtering of an annealed surface results in a significant amount of Mn on the surface. The surface enriched in Mn was annealed and it was found that at temperatures above 575K the surface Mn had diffused away. Variations of the Mn/Pd and Al/Pd ratios have been measured by LEIS as a function of temperature in the range 295-975K for a clean annealed surface and also clean surface sputtered to equilibrium. The results show that Al/Pd ratio does not significantly change from 295K to 575K for both He and Ne ion beams. Then, they increase with sample temperature until around 875K. At temperatures in excess of 875K, the Al/Pd ratio is approximately constant or it decreases slightly.

# Hydrogenography: identifying the thermodynamic properties of metal hydrides.

**H. Schreuders [1], R. Gremaud [2], B.Dam [1], C.P. Broedersz [1], M. González-Silveira [1], M. Slaman [1], R. Griessen [1]**

1. VU University Amsterdam, Department of Physics and Astronomy, De Boelelaan 1081, 1081 HV, Amsterdam, The Netherlands.
2. EMPA, Dept. of Mobility Environment & Energy, Ueberlandstrasse 129, 8600, Dubendorf, Switzerland.

For a sustainable society, the development of a reliable and safe energy carrier is essential. The use of hydrogen as such a carrier has many advantages. However, hydrogen storage at sufficiently high density and specific energy is still a problem. While metal hydride storage is ideally suited for mobile applications, the use of PEM fuel cells impose specific conditions on the desorption pressure and temperature. Thus, the search for new lightweight metal-hydride storage materials is essentially that for a needle in a haystack. Experimentally, the determination of the plateau pressures of many different bulk samples is a very time consuming procedure. This explains the renewed interest in high-throughput experimental methods.

We demonstrate that the change in optical properties on hydrogenation make metal hydrides perfectly suited for a thin film combinatorial search for new hydrogen storage materials [1]. Sputtering of several materials from different angles on a wafer will result in a wafer with gradient(s) in the composition. By changing the sputter angles and sputter rates we change the steepness and position of the gradients and this allows us to investigate a particular part of the phase diagram. After deposition, the glass wafer is being characterized in a special furnace set-up. The transmission of thousands of compositions is monitored with a CCD camera while we change hydrogen pressure and temperature in the furnace. In this way the plateau pressure for loading and unloading at different temperatures are determined, as well as the enthalpy of formation for all the compositions. Here we will present the deposition and measuring method and show how Ti dopants affect the thermodynamics of $Mg_2Ni$-hydrides [2]. Thus we demonstrate the power of this technique to identify the interesting regions in the phase diagram.

[1] Gremaud, R., Ch.P. Broedersz, D.M. Borsa, A. Borgschulte, P. Mauron, H. Schreuders, J.H. Rector, B. Dam and R. Griessen , Adv. Mat. 19 2813 (2007)
[2] Broedersz, C.P., R. Gremaud, B. Dam, R. Griessen, O.M. Lovvik, Phys. Rev. B77 024204 (2008)

# Single-molecular layer surface modification on top of vapor phase deposited silica clad metallic surfaces using silazane treatments

**S. Siau, O. Van den Berg**
OCAS

Due to environmental concerns, there is a requirement for passivation layers on steel and metallically clad steel surfaces that does not contain any potential harmful elements. A coating of vapor phase deposited Si-oxide has been developed with the goal of fulfilling this objective. This Si-oxide passivating coating may also be used as a platform for surface modifications on top of this coating, so that the modified Si-oxide exhibits specific tailored surface properties like improved wettability, improved oil or water repellency, improved corrosion resistance, anchoring improvement for paints, etc... A well known and much employed scheme for modifying the surface of silica's is to employ silane and siloxane compounds. These can bring various types of surface properties, but in general yield coatings that have multiple molecule-thickness aspects. An alternative surface modification scheme has been developed using silazane compounds that yield surface modifications that exhibit single molecular layer properties on the surface and still can bring the effects of the silane and siloxane compounds. The combination of the silica coating and the surface modification on top of this Si-oxide layer with the silazane compounds enables to tailor the passivation layer to a specific customer requirement based on a similar platform. The surface treatment with the silazane compounds can also be tailored to improve the corrosion properties of the passivating Si-oxide film. The silazane surface modified Si-oxide films were characterized by corrosion tests and analyzed by means of angle-dependent XPS and contact angle measurements. The XPS measurements confirmed that the modification with the silazane compounds of the Si-oxide passivation layer exhibit near single-molecular-layer-type properties.

# Structural changes induced in a molecular layer by resonant photoexcitation of nanocomponents differing in structures

**E.N. Kaliteevskaya, V.P. Krutyakova, T.K. Razumova, A.A. Starovoytov**
St. Petersburg State University of Information Technologies, Mechanics and Optics,
Kronverkskii av. 49, St. Petersburg, 197101 Russia

The study is concerned with the mechanisms of the changes in the conformational composition and spatial reorientation of nanocomponents of an organic layer under the action of laser radiation. The model of the change in the layer structure owing to resonant photoexcitation was developed. Two monomeric stereoisomers and two aggregated forms were found simultaneously in layers of symmetric polymethines on glass. Each layer component can have two spatial orientations differing in the tilt angles of their optical transitions. The photoexcitation causes irreversible transformation of the orientation type of the layer and the mutual transformation of layer nanocomponents. This leads to the change in relative and absolute concentrations of components. As a result, the optical density, absorption spectrum, and absorption dichroism of the layer change. Objects of study were layers of dicarbocyanines bearing different heterocyclic end groups. Irreversible spatial reorientation of components of various structures was excited by a nanosecond laser radiation at various wavelengths. The results obtained were compared with the available experimental data on the heating-induced layer reconstruction. The regularities of the processes of irreversible change in the structure of molecular layers were determined depending on exciting radiation (wavelength, energy, and kinetic parameters). The results of the study can be used for the development of new methods for long-term recording of information on organic molecular layers and for selection of most promising media.

## 1. INTRODUCTION

Molecular layers compising nanocomponents are used in designing solar cells, diodes, dichroic color light filters for liquid crystals devices and in field transistors for optoelectronics [1]. Also, they are applied for recording of data by photo- [2] or thermally-induced destruction [3] of layer components. The photostimulated processes in organic molecular layers (change in spatial orientation of molecular components with respect to the surface and change of component composition of the layer) show that it is, in principle, possible to write and read out the information by the optical methods without layer destruction [4]. In this work, the processes of the photostimulated rearrangement of molecular layers are studied by the example of polymethine dyes (PDs) on glassy substrates [5].

## 2. SAMPLES AND METHODS

Objects of study were layers of symmetric dicarbocyanine compounds with heterocyclic end groups of varied structure and electron-donating ability Φo (Fig. 1a). Layers were spin coated onto rotating glass substrates from a PD solution in ethyl alcohol. The spatial orientation of a dipole moment transition of molecular components was evaluated by the polarized absorption

spectra. The surface concentration of molecules in all components (Nsm) was determined from the PD concentration in ethanol solution, which was obtained by washing off layer. Photostimulated rearrangement of the layer structure was done with a radiation of single pulse lasers (pulse length ~ 20 ns, surface energy density falling onto the sample Es ≤ 100 mJ).

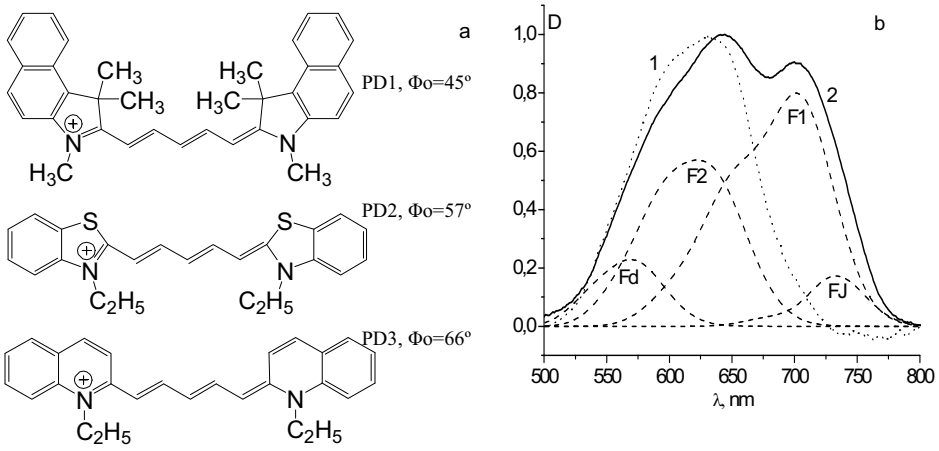


Figure 1. a) Structure of PDs studied; b) Normalized absorption spectra and spectra of molecular components of PD1 layers. Maximum optical absorption density Dmax: 0.00357 (1), 0.04071 (2).

## 3. RESULTS OF A STUDY

The comparison of the absorption spectra for layers of varied thickness showed that their component composition depends on Nsm and Φo. The spectra of thick PD1 layers (Fig. 1b) contain bands associated with two monomeric stereoforms (F1 and cis-isomer F2), a band associated with a dimer (Fd), and a band associated with a J aggregate (FJ).

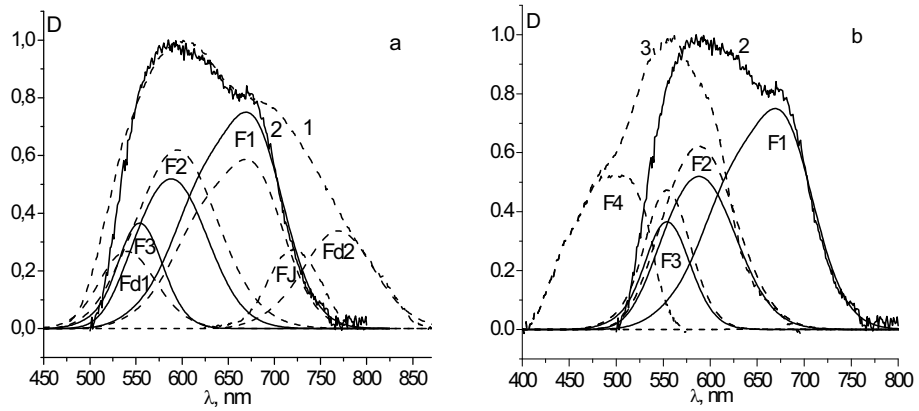


Figure 2. Normalized absorption spectra and spectra of molecular components of PD2 layers. Maximum optical absorption density Dmax: 0.0405 (1), 0.0052 (2), and 0.0027 (3).

In thin layers, only monomers are present. As Nsm decreases, the relative concentration of F1 decreases too, whereas the concentration of F2 grows. In PD1 submonolayers (Nsm < $3x10^{13}$ mol/(cm·cm)), only F2 form exists. The total regularities of the effect exerted by surface concentration on the layer component composition are the same for PD2 and PD3. The absorption spectra of PD2 layers are demonstrated in Fig. 2. Thick layers contain F1 and

F2 forms and Fd and FJ associates. Increasing Φo of the end groups leads to the appearance of another long-wave band (Fd2) that is, on all probability, associated with the second band of the dimer. As Nsm decreases, the F1 concentration decreases, the F2 concentration increases, and two (first, F3 and then, F4) short-wave bands appear. When a thick PD1 layer is irradiated by single pulses at λexc = 694 nm, which preferentially excite F1 form, then for the layer components the angles (θi) between the absorption transition dipole moment and the normal to the substrate surface change. At Es ≥ 10 mJ/(cm·cm) θ1, θ2, and θJ grow, whereas θd decreases. The dependences of θi on the total excitation energy density (ΣE) are saturating curves (Fig. 3a). The limiting angles θisat in the saturation region and ΣEsat, corresponding to the saturation, depend on Es and on the ratio of the absorption density D694 to the initial Nsm value, which determines extent to which layer temperature increases upon absorption of radiation energy (Fig. 3b). At Es ≤ 8 mJ/(cm·cm) the relative changes of the orientation angles are considerably lower for F2 and Fd than for F1 and FJ.

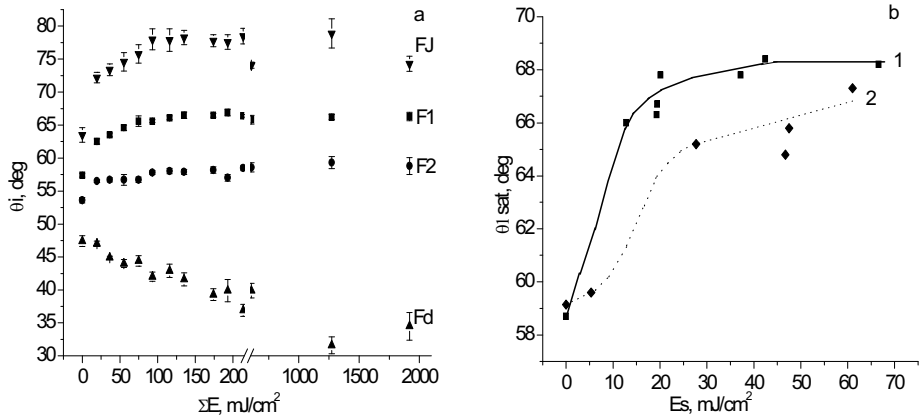


Figure 3. a) Change in orientation angle of the components of PD1 layer excited by a single-pulse radiation λexc = 694 nm, Es=19 mJ/(cm·cm); b) Limiting orientation angle (θ1sat) of F1 for PD1 layer vs. Es. (D694/Nsm)·E17 = 5.45±0.5 cm·cm/molecules (1) and 3.91±0.6 cm·cm/molecules (2).

On passing to pulsed radiation at λexc =730 nm that excites FJ in the Stokes absorption region and F1 in the anti-Stokes region the rearrangement character changes slightly. Only quantitative ratios between Es and θisat vary. At (D694/Nsm)·E17 = 4.3 cm·cm/molecules no changes in the θ2 and θd angles were observed at Es < 30 mJ/(cm·cm). At Es = 100 mJ/(cm·cm) all angles changed, whereas the θ1sat value (65.5º) was markedly lesser than limiting θ1sat values at λexc =694 nm. Resonance excitation of the PD1 layer components leads to the drop of F2 and Fd concentrations with respect to their initial values and results in the growth of the F1 and FJ concentrations (Fig. 4a). At low Es values the Ni/Nsm = f(ΣE) dependences are saturating curves. At large Es values the relative concentration of the excited components first, increases and then, decreases with increasing ΣE. Evidently, the regularities observed are due to the destruction of excited components. Upon irradiation of a PD3 layer the optical density in the F1 and FJ absorption bands increases and the density in the F2, Fd1, and Fd2 bands decreases (Fig. 4b). This confirms a conclusion that Fd2 band is due to dimers.

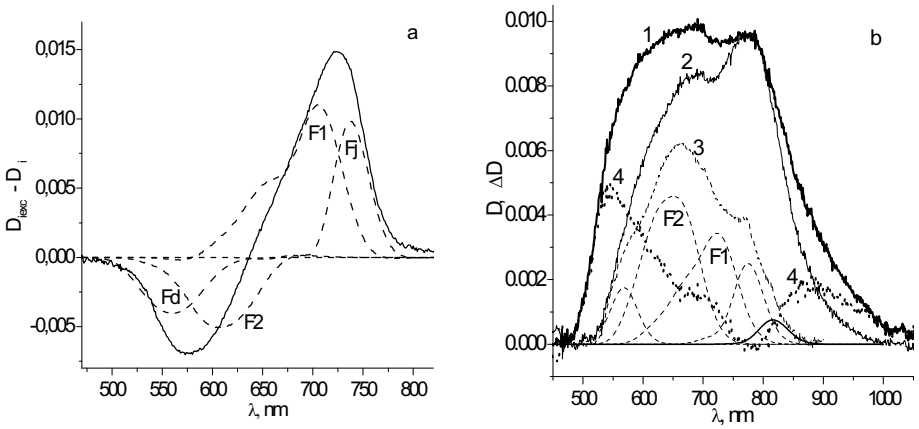


Figure 4. a) Difference between absorption spectra of a PD1 layer and spectra of molecular components before and after excitation single pulse radiation, λexc = 694 nm, Es = 19 mJ/(cm·cm); b) Absorption spectra of PD3 layers before (1,3) and after (2) irradiation. 4 – difference between 1 и 2. Layers were deposited from a solution with Kmax (1/cm): 583 (1,2) and 449 (3).

## 4. DISCUSSION OF RESULTS AND CONCLUSION

1. The observed dependences of component composition on the layer thickness are associated with the asymmetry of interaction of the molecular components with the substrate, which results in the asymmetry of intramolecular distribution of electron density. The asymmetry degree grows with increasing Φo and with decreasing layer thickness. From the comparison with asymmetric PDs solutions [6] we may conclude that F2, F3, and probably F4 forms are monomolecular cis-stereoisomers, whose equilibrium concentrations grow as the electron asymmetry of a PD molecule in a layer increases.

2. Spatial reorientation of the molecular forms (Fd and F2), that are beyond excitation wavelength, an increase in probability of these forms' rearrangement with increasing Es, and increase of the D694/Nsm ratio, warrant a conclusion that heating is responsible for the change in the orientation angles of these forms.

3. The fact that the probability of rearrangement of the layer components in the case, when all-trans isomer F1 is excited in preference, is larger than in the case, when F1 and J aggregate are excited simultaneously, shows that the initial steps of the rearrangement are related to the processes of stereoisomerization in the F1 excited state. The probability of the above processes increases with heating.

## 5. References

[1] J.D. Wright "Molecular Crystals" Cambridge University Press, Cambridge 1995 (ISBN-10 0521477301)

[2] Yang Wang, Donghong Gu, Fuxi Gan, Proc. SPIE, 5060 15 (2003)

[3] V.G. Kravets, K.L. Vinnichenko, O.V. Prygun Semicond. Phys., Quant. Electron.s & Optoelectron. 3 520 (2000)

[4] E.N. Kaliteevskaya, V.P. Krutyakova, T.K. Razumova, A.A. Starovoytov, Proc. SPIE, 6728 (2007)

[5] A.A. Ishchenko "Structure and Spectral-Luminescence Properties of Polymethine Dyes" Naukova Dumka Kiev 1994

[6] T.K. Razumova, A.N. Tarnovskii, Opt. Spektrosk. 73 1113 (1992)

# Influence of spatial sputtering distribution on TCO thin film properties

**V. Tvarozek [1], S. Flickyngerova [1], I. Novotny [1], A. Rehakova [1], P. Sutta [2], M. Netrvalova [2], P. Gaspierik [1]**

1. Slovak University of Technology, Ilkovicova 3, 812 19 Bratislava, Slovak Republic
2. New Technology Center, West Bohemian University, Univerzitni 8, 306 14 Plzen, Czech Republic

ZnO thin films codoped by Al and Sc prepared by RF/DC magnetron sputtering were depended on the deposition conditions [1]. One of the problems, which have not been resolved completely, is associated with obtaining the low resistivity: what parameters are dominantly influencing on it and how to improve the homogeneity of spatial distribution of resistivity in the real sputtering system. It was also studied an effect of substrate position and content of oxygen on the properties of AZO films prepared by reactive co-sputtering from Zn and Al targets [2]. To accelerate our investigation of suitable thin film properties of ZnO:Al and ZnO:Sc, we used the RF diode sputtering where the bombardment of a growing film during deposition with energetic particles of various types (negative ions, reflected atoms, secondary electrons) has to be taken into consideration. We have applied the model and simulations of spatial distribution of sputtered particles in our diode system (so-called deposition profile) to get continual changes of thin film thicknesses in one deposition run. Corning glas substrates were placed on different positions under the target, in diameter of 6“ (ZnO+2 wt. % $Al_2O_3$) or 4“ (ZnO+2 wt. % $Sc_2O_3$). Changes of thin film thicknesses were less then 15% in the central substrate holder region of diameter value $\leq$ 1/3 of target diameter. In distances equal target radius, the thin film thickness decreased down to 40% of the maximal value. Properties of sputtered thin films were significantly influenced by the local placement of substrates on the substrate holder. All films were polycrystalline with a strong texture in the [001] direction perpendicular to the substrate, but sputtering in outer substrate holder region caused changes of thin film lattice parameters and stresses. Their resistivities have also varied in the range of $10^{-3}$-$10^{-13}$ Ωcm. Results led to conclusion that the carrier transport (in the range of concentrations $\leq$ $10^{20}cm^{-3}$) is particularly determined by crystal imperfections such as interstitials, point defects and dislocations. Spatial distributions of both fluxes, sputtered particles and energetic species (Ar ions neutralized at the target and reflected from it, negative oxygen ions coming from sputtered targets and secondary electrons) and their mutual ratios were responsible for both opposite effects on TCO thin film properties: an improvement of composition (e.g. breaking-up oxide compounds of Al, Sc dopands and to replace Zn by them in the lattice) or the degradation of structure (e.g. to cause extended defects in the film crystalline structure (intersticials, lattice expansion, grain boundaries).

[1] Jing-Chie Lin, Kun-Cheng Peng, Hsueh-Lung Liao, Sheng-Long Lee, Thin Solid Films 516 5349 (2007)
[2] T. Minami, T. Yamamoto, T. Miyata, Thin Solid Films 366 63 (2000)

# Impedance Characteristic of Thin Polypyrrole Layers for Sensor Application

**F. Vysloužil [1], D. Kopecký [1], M. Vrňata [1], V. Myslík [2], P. Fitl [1], O. Ekrt [1], J. Hofmann [1]**

1. Institute of Chemical Technology in Prague, Department of Physics and Measurement, Technická 5,166 28 Praha, Czech Republic

2. Institute of Chemical Technology in Prague, Department of Solid State Engineering, Technická 5,166 28 Praha, Czech Republic

An impedance measurement was used in the range of 10 Hz to 100 MHz to describe AC electrical and sensing properties of thin (~hundreds of nm) polypyrrole (PPY) layers. Sensitive layers were prepared by the advanced laser deposition method - Matrix Assisted Pulsed Laser Evaporation (MAPLE). The layers were deposited onto an alumina substrate with Pt electrodes. These sensors were studied by impedance measurement under testing atmospheres (dry synthetic air, water vapor in synthetic air, hydrogen in synthetic air) containing different concentrations of detected gases. An interesting electrical behavior was found in Nyquist diagrams of sensors for low frequency of AC signal. Further, some long term drift of AC electrical parameters was found. Phase sensitivity was evaluated for all PPY layers. The ATR-FTIR spectra of prepared layers were also studied and interpreted. The results of both impedance and spectral measurement were given into the consequence with deposition conditions.

## 1. INTRODUCTION

Polypyrrole is useful substance for chemical gas sensors construction. The doped polypyrrole (PPY) exhibits electrical properties similar to inorganic semiconductors. Furthermore this polymer has good affinity to various gases and vapours.

Ionic conductivity of doped PPY increases with its humidity (in connection with humidity of surrounding atmosphere) [1,2], similar behaviour was observed for other conductive polymers such as polyaniline [3,4]. Increasing content of water leads to higher electrical conductivity due to enhanced mobility of the dopant counter-anions. In moist PPY the mechanism of conductivity can be dominating, especially in the case of inorganic dopants. Surprisingly, water molecules, even at trace concentrations, reduce the conjugation effect in double bonds of polymer backbone (due to hydroxylation and formation of hydrogen bonds) and simultaneously they reduce the polarons mobility [5].

This paper is focused to testing of gas sensors with PPY active layers. AC electrical field was used. This work presents some consequences among a long term drift of Nyquist diagrams, ionic conductivity, phase-angle sensitivity and relative humidity or temperature.

## 2. Text

### *2.1 Experimental*

The sensitive layers were deposited by MAPLE technology from PPY/$H_2O$ or PPY/DMSO (dimethylsulfoxide) targets by laser beam with different energy density and number of pulses. The substrates for the layers were made from alumina plates equipped with intedigital Pt electrodes on the one side and with the Pt heating meander on the other side (Fig. 1). The measurement of the impedance was carried out by impedance analyzer HP4191A and verified by HP4194A. A phase shift θ between voltage applied to the layer and corresponding current through the layer is a basis for the definition of phase sensitivity. The phase sensitivities Spa were evaluated from phase shift of signal in synthetic air θair and phase shift of signal in different atmospheres θgas:

$$S_{pa} = \left|\theta_{air} - \theta_{gas}\right| \quad (1)$$

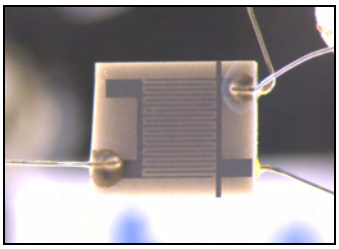

Figure 1. The polypyrrole sensor.

### *2.2 Results*

The main results of this work are in measurement of Nyquist diagrams (Fig.2) and interpretation of the phase sensitivities of sensitive layers.

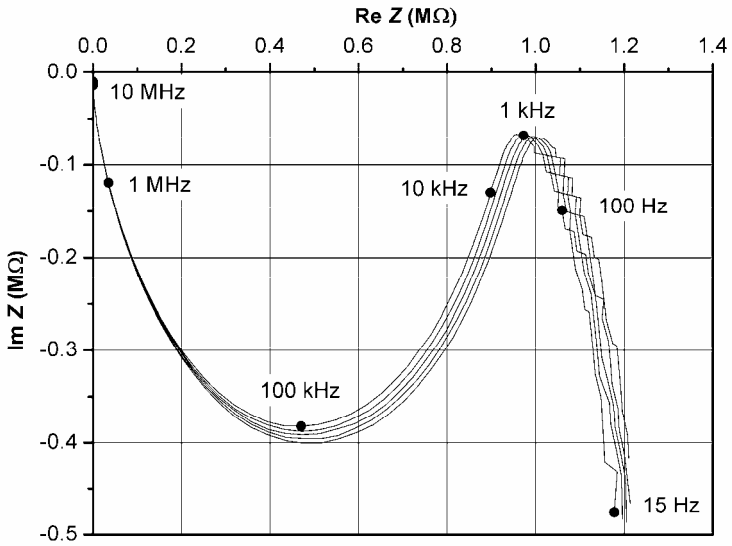


Figure 2. Nyquist diagram of PPY-based sensor in synthetic air containing 90% r.h. at isothermal conditions (t = 22°C) - measured repeatedly during 5 min.

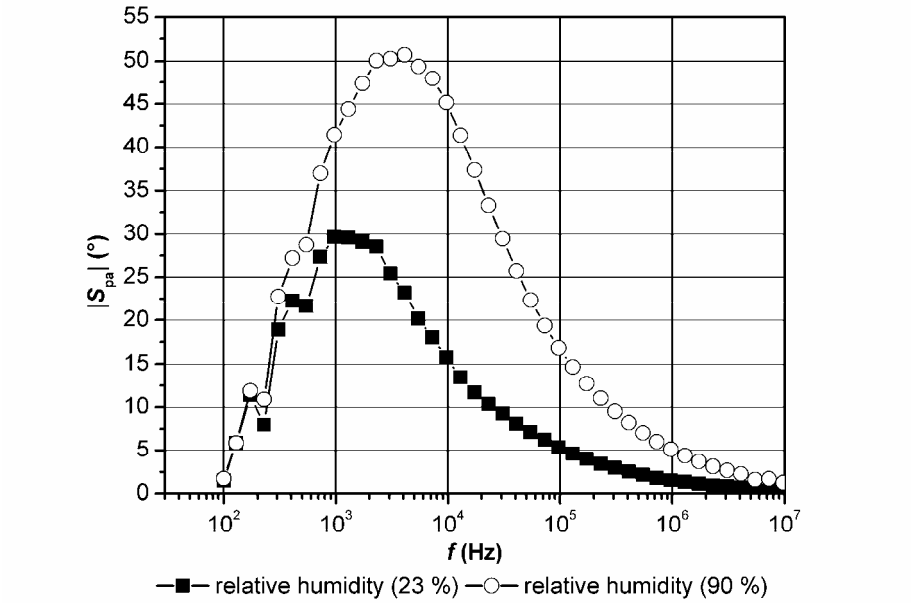


Figure 3. Phase-angle sensitivity of PPY sensor synthetic air containing 23% r. h. and synthetic air containing 90% r. h. at isothermal conditions (t = 21°C). Reference gas - dry synthetic air.

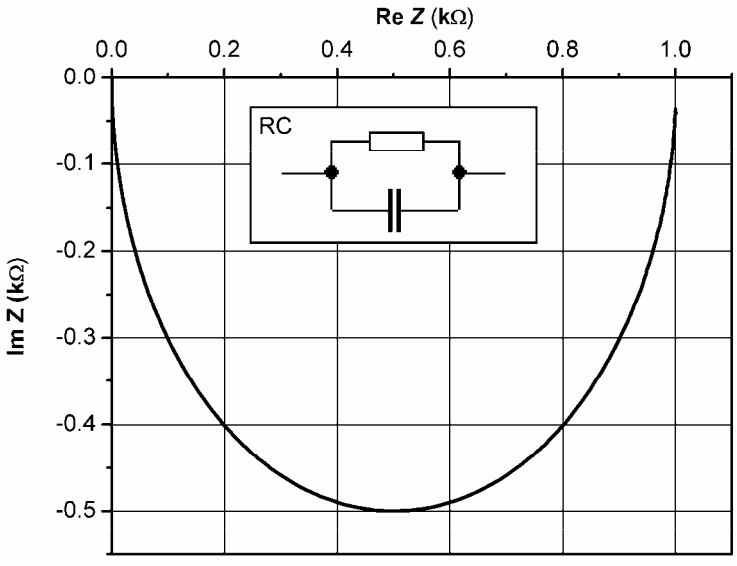


Figure 4. Typical Nyquist diagram and equivalent circuit of Resistor-Capacitor.

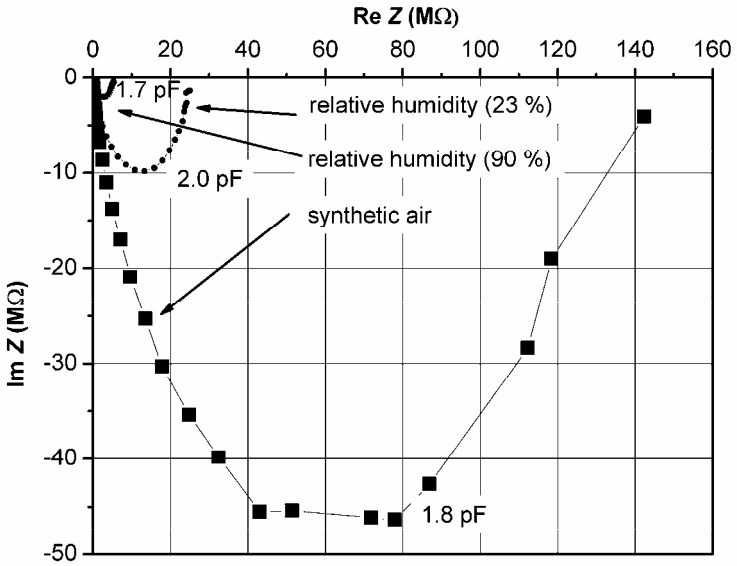


Figure 5. Nyquist diagram and equivalent circuit parameters of PPY-based sensor at isothermal conditions (t = 22°C) in different atmospheres.

An example of phase sensitivity (Fig. 3) shows that it depends on the frequency of testing signal. The frequency corresponding to maximum of phase shift, is for the PPY layer by two orders of magnitude lower than that for inorganic materials (SnO2). This is the noticeable property of polymeric material. Further, the equivalent circuit of the layers was found. It is represented by the parallel RC term (Fig. 4). The drift of parameters is caused only by drifting the resistivity R but not the capacity C (Fig. 5). This is probably caused by the long term persisting of water molecules in the layer. Water molecules increase the mobility of doping anions and by this way they increase the conductivity of the PPY sensors. By evaporation of the water molecules in dry air the resistivity slowly increases.

## 3. References

[1] J. H. Cho, J. B. Yu, J. S. Kim, S. O. Sohn, D. D. Lee, J. S. Huh, Sens. Actuators, B, Vol. 108 389 (2005)
[2] R. P. Tandon, M. R. Tripathy, A. K. Arora, S. Hotchandani, Sens. Actuators, B, Vol. 114 768 (2006)
[3] S. T. McGovern, G. M. Spinks, G. G. Wallace, Sens. Actuators, B, Vol. 107 657 (2005)
[4] N. Parvatikar, S. Jain, S. Khasim, M. Revansiddappa, S. V. Bhoraskar, M. V. N. A. Prasad, Sens. Actuators, B, Vol. 114 599 (2006)
[5] H. S. Nalwa "Handbook of Organic Conductive Molecules and Polymers: Vol. 3 Conductive Polymers: Spectroscopy and Physical Properties", John Wiley & Sons, Inc. New York (ISBN-10 0471968137)

## 4. Acknowledgements

This work was supported by the Ministry of Education of the Czech Republic - projects MSM 604 613 7302 and MSM 604 613 7306.

# Determination of the electron inelastic mean free path for poly[methyl(phenyl)silylene] films

**J. Zemek [1], J. Houdlova [1], P. Jiricek [1], A. Jablonski [2]**

[1] Institute of Physics Academy of Sciences of the Czech Republic, Cukrovarnicka 10, 162 53 Prague 6, Czech Republic

[2] Institute of Physical Chemistry, Polish Academy of Sciences, ul. Kasprzaka 44/52, 01-224 Warszawa, Poland

Thin films of aryl-methyl-substituted polysilane chain, poly[methyl(phenyl)silylene], (PMPSi), were prepared by casting from benzene solution under He protecting atmosphere in a small preparation chamber attached to a photoelectron spectrometer and were characterized by X-ray and UV-induced photoelectron spectroscopy. The inelastic mean free path of electrons, the basic parameter for the quantitative analysis using electron spectroscopy [1], has been determined from the measurements and calculations of the elastic electron backscattering probability. Monte Carlo calculations utilize the theoretical model of the electron transport, accounting for the multiple elastic scattering events in the analyzed films. In the present work, calculations were performed using the software packet EPESWIN [2]. The inelastic mean free path values have been determined in the energy range 200 – 1600 eV and compared to the predictive TPP-2M formula [3] and to the quantitative structure-property relationship [4].

[1] C.J. Powell, A. Jablonski, J. Phys. Chem. Ref. Data 28 19 (1999)
[2] A. Jablonski, Surf. Interface Anal. 37 1035 (2005)
[3] S. Tanuma, C.J. Powell, D.R. Penn, Surf. Interface Anal. 21 165 (1994)
[4] P.J. Cumpson, Surf. Interface Anal. 31 23 (2001)

# Effect of interfacial roughness configuration on exchange bias in NiO-based spin valves

**A.M. Zhang [1], H.L. Cai [2], X.S. Wu [2], L. Wang [3], J. Gao [3]**

1. Hohai University
2. Nanjing University
3. The University of Hong Kong

Exchange-bias (EB) effect between ferromagnetic (FM) and antiferromagnetic (AFM) thin films has attracted increasing attention for its important role in pinning the FM layer in giant magnetoresistance heads or spin valves. The properties at the interface of FM/AFM play a key role in affecting the EB effect. In order to systematically study the interface dependence of the EB effect, in the present paper, two batches of NiO-Co-Cu based spin valves with different deposition conditions were fabricated. The nominal structure for the two batches is the same. Each batch of samples includes a TSV, with a NiO layer at the top of the Co/Cu/Co, and a BSV, with a NiO layer at the bottom of Co /Cu/Co. For batch 1 (SV1), the base pressure was $1.95\times10^{-5}$ Pa and the sputtering Ar pressure remained 0.1Pa during the sample growing. The deposition rate for NiO was 0.034nm/s. For batch 2 (SV2), the base pressure was $3\times10^{-5}$ Pa, the sputtering Ar pressure raised to be 0.3Pa, and the deposition rate for NiO was 0.020nm/s. Phases and textures for each film were identified by X-ray diffraction (XRD). The thickness, surface & interface microstructures were characterized by the grazing incident X-ray reflectivity (XRR) and transverse X-ray scattering measurement (TXS). For TSV2, the Co, Cu and NiO sub-layers are all in the texture of (111), but for others, there are no textures observed. EB effect is only observed in batch 2. We believe that textured structure is not a prerequisite factor for EB effect in NiO/Co/Cu/Co spin valves. For all samples, the averaged roughness of NiO/Co interface are almost the same (0.3nm for BSV, 1.2nm for TSV), which indicates that there is no obvious relationship between the EB effect and interface average roughness. However, TXS fitting clearly showed that the correlation length of the interface roughness for SV2 is about 100nm, which is much larger than that for SV1. The dimension of the roughness for SV2 is also a little different from that for SV1 (about 10nm). We, therefore, conclude that the correlation length and dimension of the interface roughness may be the key factors of affecting the EB effect in NiO based Co/Cu/Co spin valves.

VG SCIENTA
a gammadata company

## About VG Scienta

**VG Scienta** is the merger of the former Vacuum Generators and Gammadata Scienta businesses. By combining the expertise and knowledge from both companies **VG Scienta** is uniquely suited to meet the current and future needs of our customers.

Both are world renowned and respected companies in their own right; our combination means we are one of the world's premier suppliers of quality products to meet the demanding standards of the scientific market.

### *Surface Physics*

The inquisitive and methodical approach to problem so lving and solution creation that permeates the whole of the natural sciences also permeates operations within the **VG Scienta** Group. In many respects, **VG Scienta** represents a link between the academic community and a wide range of businesses, governmental authorities and other research and development facilities across the globe.

### *Ultra High Vacuum*

Established in 1964, **VG Scienta**'s vacuum component business (formerly Vacuum Generators) built a name for itself based on high quality and technical innovation in UHV applications. **VG Scienta** continues to pioneer and innovate to go beyond the high standards demanded by the vacuum market. This has led to opportunities in semiconductor, surface science and synchrotron applications, maintaining the company's position at the forefront of ultra high vacuum (UHV) technology.

### *Quality*

Our customers, their needs and expectations, are the starting point for all we do. Our task is to create satisfied customers by delivering products and services within the areas of surface physics, atomic physics and UHV technology that will exceed our customers' expectations.

# Correlation between plasma parameters and coating structure in reactive HIPIMS discharge

**Y. Aranda Gonzalvo [1], A.P. Ehiasarian [2], A. Vetushka [2]**

1. Plasma & Surface Division, Hiden Analytical Ltd., 420 Europa Boulevard, Warrington, WA5 7UN, UK

2. Nanotechnology Center for PVD Research, Materials and Engineering Institute, Sheffield Hallam University, Howard Street, Sheffield, S1 1WB, UK

HIPIMS (HIPIMS (High Impulse Power Magnetron Sputtering) discharge is a new PVD technique for the deposition of high-quality thin films. In this method, a high power density is applied at the cathode yielding a higher degree of plasma ionization than in conventional magnetron sputtering.

In this study, the operation of HIPIMS in an Ar and N2 atmosphere with a Ti target was investigated. Plasma was operated at a pressure of 0.24 Pa and an Ar:$N_2$ partial pressure ratio of 10:1 was used to operate at the metallic to poisoned transition point. The peak current was varied from 5 to 30 A with a pulse duration of 200 μs. The frequency was adjusted between 200 and 1000 Hz to maintain a constant average power of 0.4 kW. Time-resolved measurements of the plasma parameters near to the substrate were carried out using energy resolved mass-spectrometry and Langmuir probe (LP) at a distance of 170 and 100 mm from the target respectively. The influence of the gas-metal ratio, plasma composition and plasma density on film structure was investigated.

Mass spectrometry measurements showed that the reactive HIPIMS discharge produced a deposition flux with a significantly increased content of ionised film-forming species, such as Ti+, $Ti_2^+$ and $N^+$. Increasing the discharge current from 10 to 30 A resulted in an enhanced activation of the atomic ion $N^+$. $Ti^+$ ions with energies up to 50 eV were detected during the pulse with reducing energy in the pulse-off times. Results from LP showed that the plasma density generated during the pulse was in the range of $3x10^{16}$ $m^{-3}$.

TiN films deposited by HIPIMS were analysed by X-ray diffraction, atomic force microscopy and electron microscopy. The films were highly textured with a strong [220] orientation. The roughness reduced from 10 to 5 nm and grain size reduced from 30 to 20 nm as function of discharge current. The effects of the significant activation of the deposition flux observed in the HIPIMS discharge on the film structure are discussed.

# Influence of Mechanical Properties on the Cracking and Failure Behaviour of $TiN/Si_3N_4$, TiN, TiFeN and TiFeN/Mo Films on Si

**B.D. Beake [1], J. Freneat [1], A. Harris [1], V.M. Vishnyakov [2], R. Valizadeh [2], J.S. Colligon [2]**

1) Micro Materials Ltd., Willow House, Yale Business Village,
Ellice Way, Wrexham LL13 7YL, UK

2) Dalton Research Institute, School of Biology, Chemistry and Health Science, Manchester Metropolitan University, Manchester M1 5GD, UK

$TiN/Si_3N_4$, TiN, TiFeN and TiFeN/Mo films were produced on silicon substrates using a dual ion beam system. Their mechanical properties have been determined by nanoindentation and tribological behaviour assessed by nano-scratch testing. Harder nitrides exhibited higher ratios of hardness to modulus, H/E and resistance to plastic deformation, $H^3/E^2$. Whilst ion assist during deposition was beneficial for producing harder $TiN/Si_3N_4$ films this was not the case for TiFeN films. We have shown previously that the H/E ratio can be a critical index controlling deformation and film failure in nano-scratch tests.

Although coatings and thin films are often designed with H/E as high as possible, we found that nanocomposite thin films of Ti-Si-N with very high H/E ratios failed dramatically at low critical load. Similar behaviour has now been observed for TiN, TiFeN and TiFeN/Mo films. The frictional force was strongly correlated to the failure location. Failures behind the moving indenter barely registered in the friction signal whilst failures in front were associated with the onset of oscillations.

We have introduced a new parameter for assessing film durability and toughness. The new parameter, coating/substrate toughness parameter (CSTP), is the ratio $(Lc_2\text{-}Lc_1/Lc_1)$ where $Lc_1$ and $Lc_2$ are the critical loads associated with cracking and delamination. It is shown that use of the new parameter may enable comparison of data on films of different thickness and when using probes of differing radius.

# Electrical behaviours and structural properties of GLAD chromium thin films sputter deposited

**A. Besnard [1], N. Martin [1], B. Gallas [2], A. Vignal [3], A. Billard [4]**

1. Institut FEMTO-ST, 26 Chemin de l'épitaphe, 25030 Besançon, France
2. Institut des NanoSciences de Paris, 140 rue de Lourmel, 75015 Paris, France
3. Institut Carnot de Bourgogne, BP 47870, 21078 Dijon, France
4. LERMPS, Université Technologique de Belfort-Monbéliard, 90010 Belfort, France

This study reports on obliquely sputtered chromium thin films 1 µm thick deposited by GLancing Angle Deposition [1]. The angle of incidence of sputtered atoms varied from $\alpha = 0$ to 85° with respect to the substrate normal. An inclined columnar film microstructure was produced with column angles $\beta$ showing significant deviations from the empirical tangent rules [2] or taking into account conventional geometrical models [3], especially for incident angles $\alpha$ higher than 40°. Such discrepancies were correlated with the mean free path of sputtered atoms and assuming the process parameters. The influence of the deposition at oblique incidence on the surface morphology and microstructure was also investigated by atomic force microscopy and by scanning electron microscopy. A structural anisotropy is developed on oriented columns due to self-shadowing in the growing film. Similarly roughness and shape analyses on the cross section or surface topography support some anisotropic behaviours found in films at deposition angles close to 50°. The evolution of the crystallographic structure was examined by X-ray diffraction versus the angle $\alpha$. A strong preferential orientation along the (110) direction was observed for any incident angle of the sputtered atoms. Measurements of the dc electrical conductivity as a function of temperature and for various incidence angles $\alpha$ were performed. The monotonous decrease of conductivity from $\sigma_{300K} = 1.10\times10^{6}$ to $3.50\times10^{5}$ S.m$^{-1}$ as $\alpha$ increases from 0 to 85°, was connected to a porous structure favoured at high incidence angle.

## 1. INTRODUCTION

Functional thin films are gaining scientific interest since the last tens years and the development of new methods of synthesis became a technological requirement. In the well-known race for multifunctional materials, an enhancement of the material behaviours due to the modification of its surfaces or thanks to the synthesis of coatings appears as an attractive way. Among the panel of deposition methods, a very innovative approach has recently been proposed by Robbie and Brett [1] for films prepared by vacuum processes, namely, the GLancing Angle Deposition technique (GLAD).

In this article, we investigate electrical and structural properties of chromium thin films with close correlations with their architecture. The films are obtained by GLAD sputtering and the deposition conditions are set in order to produce a columnar structure [4]. A systematic change of the incidence angle $\alpha$ of sputtered atoms is carried out. The resulting angle of columns $\beta$ is measured and exhibits some discrepancies with empirical rules previously developed for evaporated films, especially for high incidence angles. Similarly, electrical

behaviours of such oriented chromium films are strongly influenced by the architecture. Transport properties are discussed taking into account some significant changes of morphology, surface topography and porous structure with the incidence of the sputtered atoms.

## 2. EXPERIMENTAL

Chromium thin films were deposited at room temperature by magnetron sputtering. The chromium target (purity 99.95%) was dc powered with a constant current J = 66 A.m$^{-2}$. The substrates, glass and silicon (100), were grounded and distanced from the target by 8 cm. Incidence flux angle α and column angle β were measured from the substrate normal. The substrate holder allowed the incidence flux angle to vary from 0 to 85°, and the column angles were obtained from cross section observations of the films by scanning electron microscopy (SEM). The thickness was determined by profilometry. The surface topography was viewed by atomic force microscopy (AFM) in non contact mode and SEM. Crystallographic structure was examined by X-ray diffraction (XRD) in θ/2θ configuration using Co Kα radiation. Measurements of the dc electrical conductivity versus temperature of the films deposited on glass and for various incident angles α were performed in the Van der Pauw geometry.

## 3. RESULTS AND DISCUSSIONS

### *3.1 Architecture*

The evolution of the column angle versus incidence angle deviates from classical models (Fig. 1) [2-3]. The tangent rules (dash) is an empirical model, and gives correct values for α lower than 40-50°. The Tait's model (dot) is based on geometrical consideration from growth simulation in ballistic mode. In our work, because of the weak mean free path (1.25 cm), obtained with work pressure and argon atoms diameter [5], compared to the substrate-target distance (8 cm), the trajectory of all sputtered atoms can not be considered as linear. A major part of the flux keeps the incidence angle required, and the rest comes from other directions. The SEM observations show a more defined and distinct columnar microstructure (individual columns separate by voids and less in contact) with the increase of incidence angle. This is in agreement with the prediction of porosity based on the tangent rules [6].

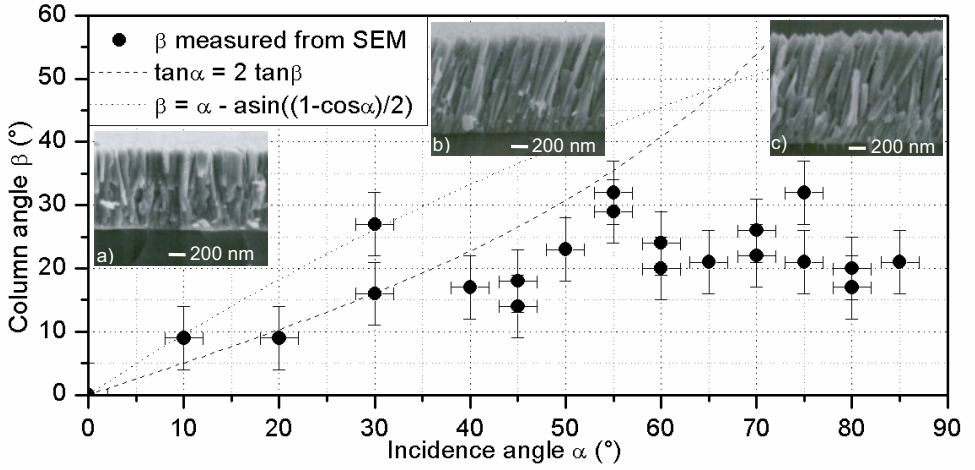


Figure 1. Column angle β versus incidence angle α: a) 0°; b) 50°; c) 85°.

### *3.2 Surface topography and structure*

Surface analyses by AFM (Fig. 2a) and SEM (Fig. 2b) show similar surface morphologies, i.e. structures at two different scales. The smallest one corresponds to the top of the columns, with an average size around 100 nm. The second one consists of elongated blocks of ten columns perpendicular to the direction of the atoms flux. Such elongated forms, produced for high incident angles, are in agreement with experimental and theoretical results published by Tait *et al.* [3]. The authors showed that oriented columnar coatings exhibit an elliptical section as the column angle increases. A structural anisotropic growth is developed parallel to the substrate surface due to the shadowing effect, which is predominant following the direction of the deposited atoms. The growth of islands connected to each others progresses perpendicular to the atoms flux. Similarly, the surface roughness, determined from AFM measurements, takes value from $R_q$ = 11 nm at α = 0° to 20 nm at 85° [7]. This roughening effect has already been reported by others [8, 9] and corresponds to a more porous structure versus incidence angle.

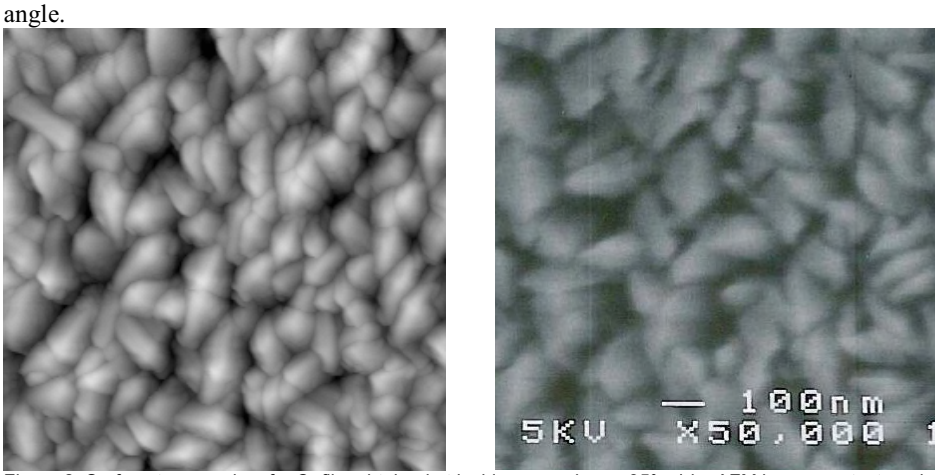


Figure 2. Surface topography of a Cr film obtained at incidence angle α = 85°: a) by AFM in non contact mode; b) by SEM.

The crystallographic structure was examined for several angles of incident flux from α = 0 to 85°. For any angle a strong preferential orientation along the (110) direction was observed. Crystallite size was determined with the Scherrer's method. It takes value around 35-40 nm, with a weak tendency to increase with incidence angle α (Table 1).

| Incidence angle α (± 2°) | 0 | 20 | 40 | 50 | 60 | 85 |
|---|---|---|---|---|---|---|
| Crystallite size (± 5 nm) | 35 | 31 | 34 | 32 | 39 | 44 |

Table 1. Crystallite size versus incidence angle α.

### *3.3 Electrical behaviours*

For all chromium films, the dc electrical resistivity shows a linear evolution versus temperature with a positive slope, which is characteristic of a metallic-like behaviour (Fig. 3a). It is also worth of noting the difference of resistivity measured for various incidence angles. Thus, the reduced conductivity $\sigma/\sigma_0$ determined at 300 K, with $\sigma_0$ at $7.74\times10^6$ $S.m^{-1}$ (bulk conductivity of chromium at 300 K) decreases significantly from 0.14 to 0.04 with the incidence angle. This result is closely linked to the porosity of the films. For bulk metallic compounds, resistivity is related to temperature with TCR (temperature coefficient of resistivity) according to (1):

$$TCR = \frac{1}{\rho}\frac{\partial \rho}{\partial T} \quad (1)$$

For thin films, crystallite size and barriers potential at the grain boundaries mainly influence the TCR value [10], because of the electron scattering. TCR tends to be improved from $0.5\times10^{-3}$ $K^{-1}$ to $0.9\times10^{-3}$ $K^{-1}$ as α changes from 0 to 85°. In our case, the most important factor is not the crystallite size (nearly constant as shown in table 1) or the number of interfaces due to grain boundaries, but the height of the barriers potential at the grain boundaries, which are enhanced due to a favoured porosity as the incidence angle increases.

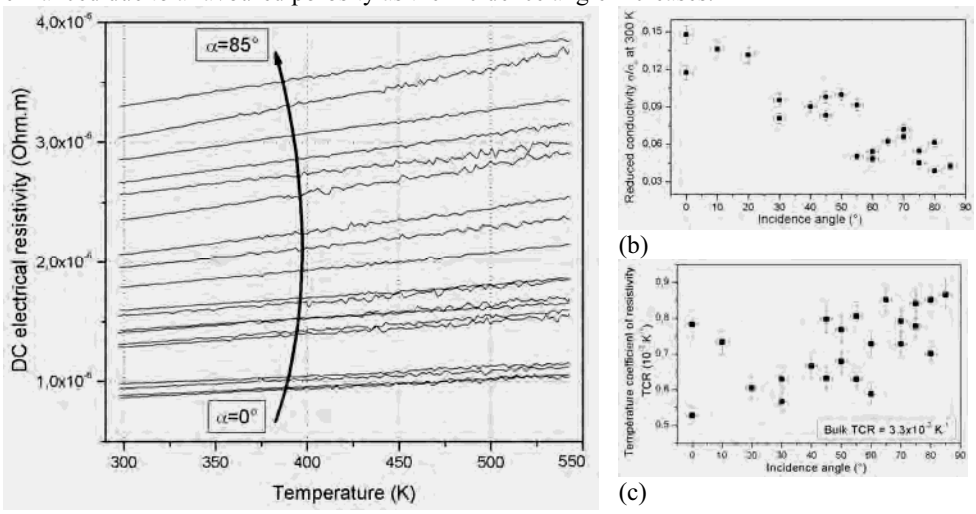


Figure 3. a) Electrical resistivity versus temperature for different incidence angles; b) Reduced conductivity at 300 K and; c) Temperature coefficient of resistivity at 300 K (TCR) versus incidence angle.

## 4. Conclusion

Chromium thin films, deposited by GLAD sputtering exhibit an oriented columnar microstructure. Column angle changes from β = 0 to 25° in spite of an incidence angle variation of the sputtered atoms from α = 0 to 85°. Scattering in the vapour flux (low mean free path) restricts the achievable column angles. The electrical resistivity is enhanced for high incidence angles of the atoms. This effect is mainly attributed to the height of the barriers potential at the grain boundaries. Such barriers potential are promoted with a porous structure.

## 5. References

[1] K. Robbie, M.J. Brett J. Vac. Sci. Technol. A13 1460 (1995).
[2] J. M. Nieuwenhuizen, H. B. Haanstra Philips Tech. Rev. 27 87 (1966).
[3] R.N. Tait, T. Smy, M.J. Brett Thin Solid Films 226 196 (1993).
[4] J. A. Thornton J. Vac. Sci. Technol. 11 666 (1974).
[5] J. E. Mahan "Physical vapor deposition of thin films", Wiley-Interscience New York 2000 (ISBN 0-471-33001-9)
[6] L. Dong, R. W. Smith, D. J. Srolovitz J. Appl. Phys. 80 5682 (1996).
[7] M. Mansour, A. Keita, B. Gallas, J. Rivory, A. Besnard, N. Martin e-J. Surf. Sci. Nanotechnol. to be published (2009).
[8] J. Lintymer, N. Martin, J. Gavoille, J. Takadoum Surf. Coat. Technol. 174-175 316 (2003).
[9] H. Lui, G. Cheng, Y. Zhao, R. Zheng, C. Liang, F. Zhao, T. Zhang Surf. Coat. Technol. 201 938 (2006).
[10] A. F. Mayadas, M. Shatzkes Phys. Rev. B 1 1382 (1970).

# Thin Films of Al-Nb Intermetallic Compounds

**T. Car [1], N. Radic [1], J. Ivkov [2], A. Tonejc [3]**

1. Rudjer Boskovic Institute, Division of Materials Science, Bijenicka cesta 54, 10 000 Zagreb, Croatia,

2. Institute for Physics, Bijenicka cesta 46, 10000 Zagreb, Croatia

3. Faculty of Science, Department of Physics, Bijenicka cesta 32, 10 000 Zagreb, Croatia

Thin films of $Al_xNb_{1-x}$ ($95 \geq x \geq 20$), have been prepared by magnetron codeposition in the CMS-18 sputtering system at room temperature. The structure of the as-deposited films was examined by the XRD and the AlNb films were amorphous in the range of composition from 30% to 85% aluminum content. $Al_{95}Nb_5$, $Al_{90}Nb_{10}$ and $Al_{20}Nb_{80}$ films were nanocrystalline. For the purpose of examination of thermal stability the samples were deposited onto glass and alumina ceramics. Thermal stability and phase transformation of the Al-Nb amorphous and nanocrystalline films under isochronal conditions were examined by continuous in situ electrical resistance measurements in vacuum. Estimated values of $\rho$ and $\alpha$ are in accordance with the Mooij correlation, and reflect typical properties of the amorphous alloys containing early transition metals. As determined by the XRD method, the first dominant component after phase transformation is the $AlNb_3$ intermetallic compound for Nb-rich alloys and the $Al_3Nb$ intermetallic compound for Al-rich alloys. The rate of extraction of intermetallic phase is dependent on composition. Amorphous Al-Nb films with composition closer to stoichiometric ratio of intermetallic compounds exhibit lower crystallization temperatures.

# The Effects of RF power on the physical properties of AZO thin film deposited on glass Substrates by RF sputtering

**H. Monoochehr [1], N. Fatemeh Dehghan [1], K. Mohammad Reza [2], S. Ebrahim Asl [1], M. Shamsoddin [1]**

Thin Film Laboratory, ECE Department, University of Tehran, Tehran, Iran.
Atomic Energy Organization of Iran , Exploration Division X-Ray Lab

Aluminum zinc oxide (AZO) has attracted much attention recently for use in transparent oxide films compared with the ITO film. AZO films were deposited by an RF sputtering system using a AZO (99.99% purity) target with a diameter and a thickness of 76 and 3 mm, respectively. The sputtering was carried out in an Ar (99.99% purity) gas atmosphere by supplying 100-300 W RF power at a frequency of 13.56 MHz. The flow rate of the Ar gas was set to 20 sccm. The distance between target and substrate was about 80 mm. The chamber was down to $8.10^{-6}$ Torr using a turbo-molecular pump before introducing the Ar sputtering gas into the chamber. The AZO film was grown at room temperature at a pressure of $5.0.10^{-2}$ Torr. The physical structure of the films (crystalline structure or microstructure) were analyzed by XRD using CuKa1 radiation (k = 0.154056 nm) in θ-2θ scan mode and by SEM. The films exhibited a high degree of preferred orientation which depends on the various RF power. The θ-2θ scan data of AZO films exhibit a strong 2θ peaks at 34.53˚, corresponding to the (002) peaks of AZO. C-Axis (002) diffraction peaks were distinguishably observed in the grown AZO films; we surmise that the c-axis oriented AZO film is obtained. It is noteworthy that the intensity of AZO (002) diffraction peak increases with increasing the RF power. We surmise that at higher RF power and at low substrate temperature, enhanced high energetic ion bombardment leads to improve, resulting. The electrical resistance was measured by a four-point probe method. The experimental results show that sheet resistance of as- grown films deposited with the RF power of 200 to 250 W can be decreased to 2.5 Ω/(Square) with post deposition annealing at 500 ºC for 1h in vacuum pressure of 105 torr. Optical transmittance measurements were carried out using a UV–VIS–NIR spectrophotometer. All these films demonstrate good optical transmittance (over 80%) in the visible and near infrared spectrum. It is observed from the spectrum that the transmittance of the film reaches its maximum when RF power is at 250 indicating that it is the optimal RF power to prepare the transparent AZO films.

# Real-time RBS to study thin film growth kinetics: the use of artificial neural networks for instantaneous data analysis

**J. Demeulemeester [1], D. Smeets, [1], N.P. Barradas [2], A. Vieira [3], C.M. Comrie[4], K. Temst [1], A. Vantomme [1]**

1. Instituut voor Kern-en Stralingsfysica, Department of Physics and Astronomy and INPAC, KU Leuven, Belgium

2. Instituto Tecnológico e Nuclear, Estrada Nacional 10, Apartado 21, 2686-953, Sacavém, Portugal and Centro de Física Nuclear da Universidade de Lisboa, Av. Prof. Gama Pinto 2, 1699, Lisboa Codex, Portugal

3. Instituto Superior de Engenharia do Porto, R. António Bernardino de Almeida 431, 4200 Porto, Portugal

4. Department of Physics, University of Cape Town, Rondebosch 7700, South Africa

Rutherford backscattering spectrometry (RBS), a quantitative technique to probe the thin film compositional profile with depth sensitivity, has proven most useful in thin film research. RBS has been applied in numerous subfields of thin film growth; most notably in studies of the solid phase reaction between a thin film and its substrate. Conventionally, specimens are exposed to different treatments (being thermal, chemical, physical or implantation) and subsequently analyzed ex situ to examine the induced change in the compositional depth profile. The advantages of characterization in real time, i.e. performing the analysis during thin film growth or modification, are well-known and apply for real-time RBS as well as for any other real-time technique. As such real-time in situ RBS has been applied to sputter processes, implantation studies, diffusion experiments and solid phase reactions. In the case of a solid phase reaction it has been demonstrated that kinetic parameters such as the apparent activation energy for growth and the diffusion coefficient can be obtained from a single real-time RBS measurement. However, the large number of RBS spectra obtained during a typical real-time RBS experiment and the time consuming analysis associated with that, has so far obstructed the breakthrough of this technique for real-time analysis. Artificial Neural Networks (ANNs) may solve this issue. We will demonstrate that the use of ANNs for the analysis of real-time RBS data drastically decreases the analysis time, without loosing accuracy. Neural networks are based on neuron-like program blocks, which learn to link input (e.g. RBS spectra) to a desired output (e.g. thickness and compositions of layers within a thin film). For the analysis of real-time data these networks are trained to analyse RBS spectra by a set of theoretically simulated RBS spectra (training set) covering a range of experimental conditions and thin film compositions. The training of an artificial neural network is dedicated to a specific system, but covers all experiments performed on that system. Once the training is completed, the network allows instantaneous analysis of all experimental data. In this contribution we will present the progress in real-time RBS credited to the routine use of ANNs. We will demonstrate specific real-time RBS studies analyzed by ANNs, i.e. studies of silicide growth kinetics, marker experiments and elemental redistributions during thin film reactions, and discuss the construction, training, and quantitative analysis capabilities of those specific neural networks.

# Growth of Ge nanostructures with different methods

**P. Dubcek [1], B. Pivac [1], I. Capan [1], N. Radic [1], H. Zorc [1], S. Bernstorff [1]**
R. Boskovic Institue
Sincrotrone Trieste

The growth and the self-organization of Ge nanostructures on Si substrate have been extensively studied in the last few years because of their technological potential in the field of Si-based quantum optical devices. In particular, the self-organization of nanostructures with quantum dot properties could be used for the new light emitting diodes and for solar cells. From the fundamental point of view, growth of Ge islands on Si has been studied very extensively as a result of a modified Stranski-Krastanov growth process. Samples were prepared with two different techniques, namely, high-vacuum evaporation of a thin Ge layer on Si(100) or silica substrate held at different temperatures and subsequently annealed and magnetron sputter deposition of thin Ge layer on Si(100) substrate held at C.°C up to 700 °different temperatures from 400. We present a study of Ge islands formation morphology on different substrates using atomic force microscopy (AFM), grazing-incidence small-angle X-ray scattering (GISAXS) and photoluminescence. From the GISAXS pattern it is possible to determine the size, the shape, the inter-island distance and the size distribution of islands and compare the results with AFM analysis. The analysis of the experimental 2D GISAXS pattern for both growth techniques has shown that nano-sized Ge islands were formed but with different average inter-island distance. With increase of the temperature islands evolved into dome clusters.

# Development of the oxide films prepared by reactive sputtering

**E. G-Berasategui, R. Bayon, B. Fernandez-Diaz, U. Ruiz de Gopegui, J. Goikoetxea, C. Zubizarreta, I. Ciarsolo, J. Barriga**
Tekniker Research Centre Eibar, 20600 Guipuzcoa, Spain

Due to their high application as antireflective coatings, TiO2 and Al2O3 films have been investigated in this paper. Different growth conditions of titanium and aluminium oxide coatings synthesized by reactive unbalanced magnetron sputtering have been analysed and the influence of these conditions on the mechanical and optical properties of the coatings has also been studied. With this purpose, different power and voltage, which influence the pressure and deposition rate, have been chosen for the deposition process on unheated substrates. Knowing this correlation is of key importance for the preparation of theses two films with the best properties (optical and mechanical) for solar systems application.
It has been observed that the selected parameters do not affect in the same way neither the deposition rate nor the optical properties for both the coatings investigated.

## 1. INTRODUCTION

Nowadays solar systems are being subject of great quantity of studies which try to improve their efficiency (both solar cells and thermal collectors). Decreasing the reflection of visible light while transmitting the rest of the sunlight spectrum to minimize energy loss is a way of improving this efficiency. A compromise between the visible reflectance and the solar transmission has to be found. But in order to warranty the performance of the coating in use, besides the optical properties the mechanical ones and durability are also key factors of these coatings.
$TiO_2$ films and $Al_2O_3$ films have a wide optical band gap that results in an excellent optical transmittance in the visible and near infrared regions [1], making them ideal candidates for antireflective coatings [3]. Their insulating and mechanical properties are also key factors for improving wear resistance and durability of the antireflective coatings [3,4]. Moreover, $TiO_2$ films have applications in dye sensitized photovoltaic cells [5], as well as biomaterials [6]. These are the reasons why $TiO_2$ films and $Al_2O_3$ films have been chosen for this study among all the oxide films (high index and low index).
In the present work, $Al_2O_3$ and $TiO_2$ coatings have been deposited by DC reactive magnetron sputtering under different growing conditions which entail different locations in the hysteresis curve for the poisoning of the targets for two different power levels.

## 2. EXPERIMENTAL PROCEDURE

The industrial equipment MIDAS 450 developed by Tekniker was used to deposit the $Al_2O_3$ and $TiO_2$ PVD coatings by pulsed reactive sputtering method. The power of the magnetrons varies between 1 and 4 kW. Titanium grade II target and aluminium (purity 99.99%) and Ar (flow rate, 30-60 sccm) and $O_2$ (flow rate, 8-110 sccm) gas mixture were used during process. A constant argon flow rate was maintained and the $O_2$ flow rate was feedback controlled so as

to keep the voltage of the sputtering discharge constant at a prefixed value. The base pressure in the chamber was 5x10-5 mbar. 2.9 W/cm$^2$ and 4.4 W/cm$^2$ (corresponding to 2000 and 3000 W) were used as power levels to investigate the mechanism of $Al_2O_3$ and $TiO_2$ thin film growth.
The target voltage was set to 50%, 75% of the turn down set point and fully poisoned condition, at different pressures for the different power levels so that corresponds respectively to 572, 441 and 330 V for the titanium target at both power levels , and to 520, 375 and 220 V for the aluminium target at both power levels. Table 1 collects the deposition conditions.

| | N1 $TiO_2$ | N2 $TiO_2$ | N3 $TiO_2$ | N4 $TiO_2$ | N5 $TiO_2$ | N6$TiO_2$ |
|---|---|---|---|---|---|---|
| Sputtering Pressure (*10 $^{-3}$ mbar) | 6.5 | 2.55 | 2.4 | 7.5 | 3.2 | 2.9 |
| Sputtering Power W/cm$^2$ | 2.9 | 2.9 | 2.9 | 4.4 | 4.4 | 4.4 |
| Cathode potential (V) | 330 | 451 | 572 | 330 | 451 | 572 |
| Deposition rate (nm/m) | 0.49 | 0.58 | 0.72 | 0.76 | 0.85 | 1.47 |

| | N7 $Al_2O_3$ | N8 $Al_2O_3$ | N9 $Al_2O_3$ | N10$Al_2O_3$ |
|---|---|---|---|---|
| Sputtering Pressure (*10 $^{-3}$ mbar) | 4.8 | 3.2 | 4.8 | 3.8 |
| Sputtering Power W/cm$^2$ | 2.9 | 2.9 | 4.4 | 4.4 |
| Cathode potential (V) | 220 | 375 | 220 | 375 |
| Deposition rate (nm/m) | 0.8 | 6.65 | 1.16 | 14.5 |

Table 1. Deposition conditions for TiO2 films (above) and Al2O3 films (below).

A Jasco V-570 NIR spectrophotometer equipped with a 60mm diameter integrating sphere was used to measure the transmittance and diffuse reflectance. From these experimental data, and with the help of the Thin Film software package FilmWizard Professional, the refractive index and the optical thickness of the films has been characterized. Wear resistance measurements were carried out with the ***CSM Nanotribometer, using*** a ball on disc oscillating configuration. A 2mm diameter $Si_3N_4$ ball was used as counterbody. The tests were run for 300 cycles reaching a maximal sliding speed of 5mm/s with a fixed stroke of 700µm. During the test the normal load was maintained at 25mN. In order to have statistical information about the results each test was done by duplicate. The evolution of the friction coefficient through time was recorded and after the test, the wear scars were analyzed my means of confocal microscopy (PLµ from Sensofar).

## 3. RESULTS AND DISSCUSION

All the samples described in table 1 were first characterised by means of the refractive index and optical thickness. Table 2 collects the values for the optical thickness and refractive index for all the samples analysed. The alumina coatings deposited at the highest voltage, which corresponds to the middle of the hysteresis curve, have not been tested because in these cases they were not fully transparent, as was the aim of this study. In view of the very high growing speed of the film, some improvements in the gas delivery method should be made to assure the complete oxidation of all the evaporated aluminium.

| | N1 $TiO_2$ | N2 $TiO_2$ | N3 $TiO_2$ | N4 $TiO_2$ | N5 $TiO_2$ | N6$TiO_2$ |
|---|---|---|---|---|---|---|
| Refractive index (550nm) | 2.25 | 2.46 | 2.44 | 2.39 | 2.40 | 2.47 |
| Optical thickness (nm) | 157 | 143 | 148 | 123 | 110 | 139 |

| | N7 $Al_2O_3$ | N8 $Al_2O_3$ | N9 $Al_2O_3$ | N10$Al_2O_3$ |
|---|---|---|---|---|
| Refractive index (550nm) | 1.59 | 1.58 | 1.61 | 1.67 |
| Optical thickness (nm) | 168 | 133 | 153 | 158 |

Table 2. Values of the optical thickness and refractive index fotTiO2 films (above) and Al2O3 films (below)

The refractive index of $TiO_2$ films varies from 2.25 to 2.47 at 550nm. Most of the films have refractive index values about 2.40. The only exception corresponds to sample N1, with the lowest value, 2.25, obtained using lowest voltage and power. Anyway, all these values are consistent with literature and are close to the maximum values report to date for amorphous layers [7]. X-ray Diffraction has been performed to check the amorphous structure. The significantly increase in refractive index has been attributed to films densification [8,9].
Growth conditions have less influence in the refractive index of $Al_2O_3$ than in $TiO_2$ films. For $Al_2O_3$ films only a 5% of variation has been observed between sample N7 (n= 1.59) and sample N10 (n=1.67). But in all the cases the indexes are consistent with literature values and have a high index for $Al_2O_3$ amorphous films.
Results in table 1 show that the voltage of the cathode has a very big influence on the growth rate of the alumina films. Despite 375 Volts is only 25% higher than the voltage corresponding to the fully poisoned mode, the growth rate is multiplied by a factor about ten in respect of the fully poisoned state. But this faster growth, far from having any deleterious effect on the quality of the film, for those films grown at 4.4 $W/cm^2$, improves the optical properties (higher refractive index).This effect of increasing growth speed when changing the conditions from a fully poisoned state to a point in the middle of the hysteresis curve is less pronounced for the $TiO_2$ films. The films grown at high deposition rate, 1.47nm/m, also show the higher refractive index (2.47). Even if the deposition rates of these films are those reported in the literature for oxide mode of Ti films, it is believed that changing the experimental set up of our machine, higher deposition rate could be achieved with the same quality films.
Ball on disc bidirectional tests were used to study the wear resistance of the samples. Figure 1 shows the evolution of the friction coefficient for the $Al_2O_3$ films (N7-N10).

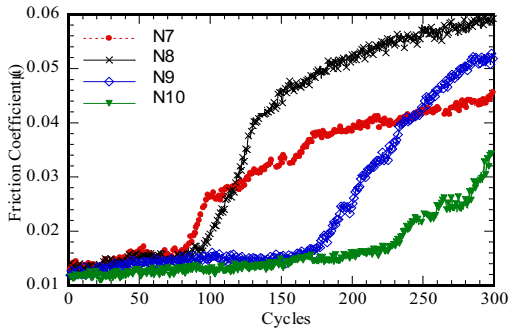


Fig 1. Evolution of the friction coefficient as a function of the cycles for the different Al2O3 samples

A general behaviour is observed for all the $Al_2O_3$ samples. The initial friction coefficient (around 0.012) increases gradually after a certain number of cycles. This increase is directly related to the fail of the coating thus, to its lifetime. The lower the cathode potential the shorter the lifetime (compare N7 with N8 and N9 with N10) and the higher the sputtering power the longer the lifetime (compare N7 and N8 with N9 and N10).
During the first cycles of the tests the samples are scratched by the counterball. This abrasive wear provokes the formation of wear debris which affected the tribological behaviour of the system causing an increase of the friction coefficient as described above.
$TiO_2$ showed a different qualitative tribological performance compared with $Al_2O_3$ films, as it can be seen in figure 2. In most of the samples, the friction coefficient increases from the very beginning of the test. There is only sample, N1, grown at 2.9 w/cm and 330V, where the friction coefficient is low and stable during the whole test. This result indicates that this sample has better wear resistance than the rest of $TiO_2$ samples.

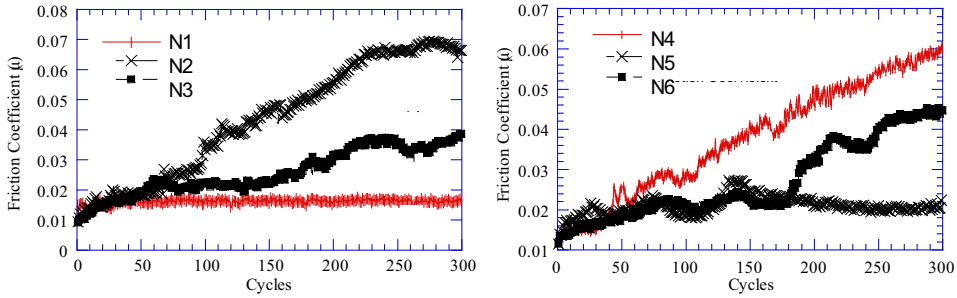


Fig 2. Evolution of the friction coefficient as a function of the cycles for TiO2 samples grown at 2.9 W/cm2 (left) and at 4.4 W/cm2 (right)

## 4. CONCLUSIONS

The influence of the growth conditions, cathode potential and sputtering power on the optical properties (refractive index) and mechanical properties (wear resistance) of Titanium oxide and Aluminium oxide films deposited by dc reactive pulsed magnetron sputtering has been investigated.

It has been observed that both voltage and power have a big influence on the deposition rate for the $Al_2O_3$ films. However, the refractive index is less affected.

Considering $TiO_2$ films, the studied parameters have less influence on the deposition rate. While the refractive index shows bigger changes.

As far as wear resistance is concerned, $Al_2O_3$ coatings have shown the degradation of the films when increasing the number of cycles. The lower the cathode potential, the shorter the lifetime and the higher the sputtering power, the longer the lifetime.

No clear relation between the evolution of the friction coefficient and the wear of the films has been found for the $TiO_2$ films.

## 5. REFERENCES

[1] L-j. Meng, V. Teixeira, H. N. Cui, F. Plcido, Z. Xu, M. P. Dos Santos Applied Surface Science 252 7970 (2006).
[2] G. San Vicente, A. Morales, M.T. Gutierrez Thin Solid films 403/404 335 (2002).
[3] M.T. Li, H. Tan, L. Chen, J. Wang S.Y. cchou J.Vac. Sci. Technol. B 21 2 660 (2003)
[4] J. Wang, Y-H Yu, s. C. lee, Y-W Chung Surf. Coat. Technol, 146-147 189 (2001)
[5] B. S. Richards Prog. Phtovoltaics 12 4 253 (2004)
[6]Y. X. leng, P. yang, j. Y. Chen, L. X. Xu, A. S. Zhao, H. Sun Key Eng. Mater 288-289 311 (2005)
[7] M Zhang, G. Lin, C. Dong, L. Wen, Surf. Coat. Technol. 201 7252 (2007)
[8] S. Konstantinidis, J. P. Dauchot, M. Hecq Thin Solid Films 551 1182 (2006)
[9] J. A Davis, W.D. Sproul, D. J. Christie, M. Geisler 47th Annual Tech. Conference Proceedings, SVC, Albuquerque 215 (2004)

# Anisotropic stresses in diamond coatings on titanium alloys by polarized micro-Raman spectroscopy

**T. Gries [1], L. Vandenbulcke [1], P. Simon [2], D. Bormann [2], A. Canizares [2]**
1 CNRS, UPR3021 ICARE, 45071 Orléans cedex 2, France,
2 CNRS, UPR3079 CEMHTI, 45071 Orléans Cedex2, France, and Université d'Orléans, BP 6749, 45067 Orléans Cedex 2, France

Adherent nano-smooth fine-grained diamond coatings can be deposited on titanium alloys or titanium-coated substrates at moderate temperature equal to or lower than 600°C. These coatings exhibit isotropic biaxial residual stresses, in the 2-5 GPa range, which are principally from thermal origin and depend on the diamond purity of the coating. In service conditions, the modification of such stresses greatly influence the lifetime of parts. These stresses can be studied by Raman spectroscopy; however a complete simulation of the generated anisotropic stresses is first necessary.

Such advanced study of the anisotropic stresses is reported here after a tensile test which has induced permanent deformation of a polycrystalline diamond-coated titanium alloy specimen. The influence of the in-plane orientation of each grain relatively to the stress directions is shown experimentally by polarized micro-Raman spectroscopy and deduced theoretically. Considering the dynamical equations under small strains, the solutions of the secular equation permits the determination of the triply degenerate phonon frequency of strained polycrystalline diamond which splits into three singlets for each crystallite. The calculation is carried out here for six textures and for all in-plane orientations normal to these textures. For an isotropic polycrystalline diamond film, this Raman spectroscopy of strained cubic polycrystals approximates the complete solution for all crystallite orientations relatively to the anisotropic biaxial stresses. It allows calculating theoretical Raman spectra which fairly well compare to the experimental ones. The determination of the anisotropic stresses is then obtained with a better accuracy than with the previous average procedures used for isotropic cubic polycrystalline materials.

Adherent diamond coatings with anisotropic stresses as high as 1 GPa in the tensile direction and -18 GPa in the perpendicular to tensile direction have been evidenced. This result is explained by a sufficient plastic deformation of the titanium substrate at the end of the test which has finally induced a residual moderate tensile stress and a high compressive component in the transversal direction. Besides, this is an evidence of the very strong adherence of the diamond film on the metallic substrate. This residual stress level occurs in diamond because it depends both on the thermal expansion mismatch between diamond and titanium and on the plastic deformation induced by the tensile test, the final forces at play being dominated by the substrate as the film thickness is much smaller than the substrate thickness.

This approach could be applied to strained/stressed Raman-active materials with in-situ or ex-situ Raman spectroscopy techniques including Raman imaging. In-situ polarized micro-Raman spectroscopy during the tensile test should permit to deduce very accurate information about the interfacial properties of the coatings.

# New microfocus source for X-ray diffractometry of thin films and nano-sized materials

**U. Heidorn, J. Wiesmann, C. Michaelsen**
Incoatec GmbH, Max-Planck-Str. 2, 21502 Geesthacht, Germany

The increasing importance of X-ray diffractometry with 2-dimensional detectors for materials research has lead to a rising demand for highly intense X-ray sources enabling the analysis of very small and weakly scattering samples in the home-lab within a reasonable time frame. Therefore, various microfocusing sealed tube X-ray sources with focal spot sizes below 100µm are now available.
We present the new low-maintenance high-brilliance Incoatec Microfocus Source IµS. The source incorporates an optimized combination of an extremely bright and very durable stationary air-cooled 30 W microfocus source and the newest type of 2-dimensional beam shaping multilayer optics, the so called Quazar optics.
Measurements of thin films and nano-sized materials demonstrate the possibilities of new microfocus solutions for X-ray diffractometry. The comparison of IµS with typical sealed tube fine focus systems shows data of outstanding quality in diffractometry applications using a 2-dimensional detector. A huge improvement in intensity and resolution by factors of about 15 was observed. Especially for the measurements of powders in transmission geometry the IµS delivers very promising results. A focusing on the detector enables better crystallite statistics and better resolution. For some applications there are even intensity gain factors in the range of 100 achievable. For small angle scattering a factor of 5 in comparison to a typical sealed tube instrument was observed when using an IµS with optics for a parallel beam.

# Comparison of silicon nitride thin films deposited by plasma magnetron in an $Ar/N_2/H_2$ and an $Ar/NH_3$ gas mixture

**F. Henry, A. Batan, F. Reniers**
Université Libre de Bruxelles, Bd Triomphe, B-1050 Brussels, Belgium

Silicon nitride films are useful for functional device applications due to their attractive mechanical properties and chemical inertness. Silicon nitride thin films can be deposited by different techniques such as CVD and PVD techniques. Among these, the reactive magnetron sputtering technique has many advantages: low temperature deposition, large choice of the composition of the deposited films, environment friendly. In this present study, silicon nitride thin films were deposited by DC magnetron sputtering from a silicon target in an $Ar/NH_3$ and an $Ar/N_2/H_2$ gas mixture. The composition, the purity and the structure of the films has been investigated as a function of the plasma parameters. X-ray photoelectron spectroscopy (XPS) and XPS-depth profiling was used to investigate the composition and the purity. Infrared reflection-adsorption spectroscopy (IRRAS) was used to study the nature of the chemical bonds of the deposited films. The plasma gas phase was characterized by optical emission spectroscopy (OES). A comparison between the $Ar/NH_3$ and the $Ar/N_2/H_2$ plasma was performed. The nature of the species and their intensities were followed as a function of the deposition parameters. The XPS results show that the N/Si ratio of the films could be tuned between 0.49 and 1.21 for $Ar/NH_3$ gas mixture and 0.56 and 1.33 for $Ar/N_2/H_2$ gas mixture, this ratio depends on the deposition conditions. The presence of the transverse optical (TO) and longitudinal optical (LO) phonons in IRRAS attest for the presence of Si-N bonds for both gas mixtures ($Ar/NH_3$, $Ar/N_2/H_2$). The OES highlights the presence of Ar+*, Ar*, Si*, N2*, H*, N2+*, NH*, N*, SiN* and SiH* excited species. The evolution of the lines of these species with the deposition parameters, normalized by the Ar* line, give us qualitative information about the plasma composition. The same species are detected in the $Ar/NH_3$ and in the $Ar/N_2/H_2$ plasma but the intensity of these lines vary greatly between the two kind of plasma. The most significant differences are the intensity of these species : N2*, N2+*, NH*, H*. The N2* and N2+* lines and the NH* and H* lines are more intensive in the $Ar/N_2/H_2$ plasma and in the $Ar/NH_3$ plasma respectively.

# Effects of Sc-Additive on Properties and Structure of ZnO:Al Transparent Conductive Thin Films

**Fu-Yung Hsu, Hung-Li Yeh**
Dept. of Materials Engineering, Mingchi University of Technology, Taipei 24301, Taiwan, ROC

Aluminum-doped zinc oxide (AZO) transparent conductive thin-films with or without scandium additive were deposited on STN-glass substrates by an asymmetric bipolar pulsed DC reactive magnetron sputtering system. Three different alloys, Zn-1.6wt.%Al, Zn-2.0wt.%Al and Zn-1.6wt.%Al-0.4wt.%Sc, were used as the sputtering targets. The sputtering power was fixed at 100 W and the substrate temperature at 200°C. The oxygen flux ratio ($O_2/(O_2+Ar)$) of the sputtering gas was regulated from 5% to 20%. Effects of the Sc-additive and the oxygen flux ratio were fully discussed. The lowest resistivity of $6.03\times10^{-4}$ Ω-cm was obtained from the film deposited with Zn-1.6wt.%Al-0.4wt.%Sc target at the oxygen flux ratio of 10%. The transparency in the infrared region is affected significantly by the oxygen flux ratio, but not by the Sc-additive. Energy band gaps decreased obviously with the increase of the oxygen flux ratio, but had little relationship with the addition of Sc.

# Investigation of the Influence of Energy Deposition on the Microstructure of Reactively Deposited Aluminum Nitride Film

**F. J. Jimenez, S. D. Ekpe, S. K. Dew**
Department of Electrical and Computer Engineering, University of Alberta, Edmonton Alberta, Canada, T7G 2V4

Aluminum nitride (AlN) is a material with many applications (optical, optoelectronic, electronic, structural, etc) due to its many attractive properties, such as low electrical conductivity and low dielectric constant, high thermal conductivity, high acoustic wave conductivity, etc. Process conditions, which determine the energy deposition, greatly influence the microstructure of the growing film. In this work, AlN was reactively deposited in a DC magnetron sputtering system at different proportions of nitrogen in the process gas mixture. The microstructure and composition of the films were analyzed using X-ray diffraction data, energy dispersive spectroscopy and scanning electron microscopy. Energy deposition was measured using a MEMS sensor. The energy deposition was then determined in terms of the energy per deposited atom, and related to the structural formation of the film. For the process condition under studies, this energy per atom was in the range of 38 – 159 eV/atom. Results show that increase in the energy per deposited atom results in a more dense fibrous structure. For the near stoichiometric AlN, (002) seems to be the preferred orientation, however increase in energy per atom tends to promote (101) and (100) growths.

# Ballistic electron emission microscopy of Co and NiFe multilayers and clusters buried in Cu

**A. Kaidatzis, S. Rohart, A, Thiaville, J. Miltat**
Laboratoire de Physique des Solides, UMR 8502, Université Paris-Sud et CNRS, Bât. 510 - 91405 Orsay cedex

The demonstration of hot electron devices like the spin transistor [1], made necessary the further study of hot electron transport in such hybrid metal/semiconductor structures. Ballistic electron emission microscopy (BEEM) [2] is a three terminal extension of Scanning Tunnelling Microscopy (STM) on metal/semiconductor structures. Hot electrons injected from the STM tip, after crossing the thin metal layer, are energy filtered at the metal/semiconductor interface to be collected from the semiconductor terminal. The collector (BEEM) signal depends on the metal layer thickness with a typical hot electron attenuation length λ. Here we report on a BEEM study of Co and $Ni_{80}Fe_{20}$ multilayers and isolated clusters buried in Cu.

The samples were thermally evaporated in a UHV chamber on hydrogenated Si(111) substrates. After the deposition of a Au layer in order to form a smooth metal/semiconductor growth template, two kinds of structures were fabricated. The first are Co or NiFe single layers or Co/Cu/NiFe spin-valves buried in Cu. The second are self assembled Co or NiFe clusters buried in Cu, grown by nominally depositing a fraction of an atomic layer. All the experiments were performed at room temperature using a UHV STM.

Due to the spin dependence of λ in magnetic materials, the BEEM signal on the spin-valve samples depends as well on the relative magnetization orientation of the two magnetic layers. Parallel orientation yields high signal, while anti-parallel orientation yields low signal. The spin dependent λ in Co and NiFe was determined by BEEM measurements. In the energy range 1-2 eV above the Fermi level, the hot electron attenuation length is 3.2 (0.9) nm for Co and 4.9 (1.3) nm for NiFe, for the majority (minority) electrons.

The existence of the Co and NiFe buried clusters is revealed by BEEM imaging, because of the lower hot electron transmission that they exhibit. The cluster widths are 10 to 20 nm. The ability of determining where such a buried structure exists, allows us to perform BEEM spectroscopy on single clusters. Extremely intense hot electron attenuation occurs in these buried structures, considering the attenuation lengths measured before in Co and NiFe. The origin of this effect is still under investigation.

[1] R. Jansen, J. Phys. D: Appl. Phys. 36 R289 (2003)
[2] M. Prietsch, Phys. Rep. 253 163 (1995)

# Size control and multicolored luminescence of diamond-like carbon coated nanocrystalline silicon particles

**K. Sato [1], M. Hiruoka [2], K. Hirakuri [2]**
1. National Institute for Materials Science
2. Tokyo Denki University

Multicolored luminescence from the nanocrystalline-silicon (nc-Si) particles can easily obtain by changing the size owing to the quantum size effects. However, the intensity of the multicolored luminescence is rapidly degraded by aging after a short period of exposure in a highly oxidizing environment. The degradation of luminescence intensity is caused by the presence of an unstable chemical element as hydrogen atoms, which was adsorbed on the surfaces of nc-Si particles. Therefore, it should passivate the surfaces of nc-Si particles with a stable chemical element in order to improve the stability of luminescence intensity with a highly oxidizing environment. Diamond-like carbon (DLC) coating on the surfaces of nc-Si particles is an effective technique for preventing the degradation of luminescence intensity, because of the formation of silicon-carbon bonds with high chemical resistant. In this study, the size control and multicolored luminescence of DLC coated nc-Si particles will be discussed. The DLC coated nc-Si particles were fabricated on the Si substrate by co-sputtering of graphite chips/Si chips/silica composite targets and subsequent annealing at 1100 °C and hydrofluoric (HF) acid steam treatment. The formation quantity of the DLC layer was controlled by changing the number of graphite chips in the composite target. The size and luminescence property of the DLC coated sample were estimated using X-ray diffraction and photoluminescence (PL) measurements, respectively. The size of nc-Si particles with DLC layer was reduced from 3.2 to 1.8 nm with increasing the number of graphite chips from 4 to 18 pieces. This was due to the decrease of Si concentration in the as-sputtered sample with the increase of the number of graphite chips, because the nc-Si particles form by the coagulation of excess Si atoms by annealing. The reduction of size resulted in the continuous blue-shift of luminescence color from red light to blue light. The intensity of each luminescence color from the sample with DLC layer was stable for the exposure in a highly oxidizing environment. This was attributed to the suppression of the reformation of dangling bonds on the surface of nc-Si particles by DLC coating. These results indicated that the DLC coated nc-Si particles can be realized stable multicolored luminescence.

# Al-$W_x$ coatings as an alternative for corrosion protection of Al-alloys

**D. Kek Merl, I Milošev, P. Panjan, E. Blaževič**
Jožef Stefan Institute, Thin Films and Surfaces Department, Jamova 39, SI-1000 Ljubljana, Slovenia

PVD hard coatings (metals, alloys, nitrides and oxides, carbides) are prepared by vacuum deposition techniques and they are, in many cases, promising alternatives to galvanic protective coating, that they are coming under increasing pressure due to environmental and worker safety issues.
They show a good mechanical, optical and wear properties to compare hard chrome plating. However, corrosion properties of the thin PVD-coatings do not always match all the requirements due to growth-related defects, e.g. pores and pinhols. It is known, that properties of coatings are many-sided related to their microstructure. Therefore, the microstructural characterisation of coatings is extremely important. Many highly effective techniques are available to examine the surface of coatings (SEM, AFM and XPS). The state-of-the-art techniques to investigate internal microstructure, sub-surface and the deformation mechanism in coating is focus ion beam work station (FIB).
In this work coatings of Al-$W_x$ on aluminium substrates were prepared by physical vapour deposition. The corrosion testing of coatings, using electrochemical methods (potentiodinamic data and with electrochemical impedance spectroscopy), were performed in chloride medium. Surface and sub-surface characterization were perforemed before and after corrosion testing by SEM and FIB. Properties such as hardness, roughness were determined for each coating. The results are discussed and compared to the surface defects density.

# Boron-doped hydrogenated amorphous silicon (a-Si:H(B)) thin films properties studied with infrared, optical absorption and electrical measurements

**N. Khelifati [1], A. Rahal [1], R. Cherfi [1],A. Keffous [2] , M. Kechouane [1]**
1. University of Sciences and Technology Houari Boumedienne
2 Research Center (UDTS)

The effects of the boron incorporation on the physico-chemical, optical and electric properties of hydrogenated amorphous silicon (a-Si:H) films are presented. Boron-doped hydrogenated amorphous silicon (a-Si:H(B)) thin films were deposited on two kinds of substrates : corning glass and crystalline silicon by DC magnetron sputtering of a silicon target under hydrogen and argon plasma. Boron was incorporated into the host material by a co-sputtering technique. Deposited films (~0.4 μm thick) were characterized by Secondary Ion Mass Spectrometry (SIMS), infrared, optical absorption and electrical conductivity measurements. SIMS measurements clearly showed evidence for boron incorporation with a concentration varied between 1.3 $10^{17}$ $cm^{-3}$ and 1.6 $10^{22}$ $cm^{-3}$. The boron incorporation induced an increase in the refractive index and a decrease in the optical gap. This incorporation is followed by a decrease of the hydrogen film content. Infrared absorption measurements were made by Perkin Elmer spectrometer. These measurements showed that the increase of the boron concentration induced an decrease of the Si-H stretching band at 2000 $cm^{-1}$ and the Si-H wagging band at 640 $cm^{-1}$ followed by an increase of the infrared absorption between 700 $cm^{-1}$ and 900 $cm^{-1}$ attributed to Si-B and/or B-B stretching vibrations. A significant shift of 2000 $cm^{-1}$ band towards the lower wave number was also observed. Consequently, this evolution of different bands leads us to conclude that hydrogen lies preferentially to silicon rather than boron, and that the boron incorporation increases the structural disorder. These explanations were confirmed by the contracting of the optical gap ($E_g$) and the reduction in the Tauc's factor ($B_0$), determined from optical measurements. The electrical conductivity measurements, under darkness ($\sigma_d$) and under illumination ($\sigma_{ph}$), according to the temperature allowed following the evolution of the activation energy (Ea) as well as the light sensitivity of the films. An increase of $\sigma_d$ and a decrease of $E_a$ were observed. This result can be related to the shift of the Fermi level towards the valence band due to boron doping. The effect of annealing temperature on electrical conductivity was also studied. It shows that boron atoms passivated by hydrogen can be activated for the annealing temperature range between 200°C and 350°C through bridging Si-H---B bonds dissociation.

# Enhancement-mode Si MOSFET with MOCVD-$TiO_2$ as gate oxide improved by oxygen annealing and fluorine passivation

**M.-K. Lee, C.-F. Yen, C.-H. Fan**
National Sun Yat-sen University, Department of Electrical Engineering, Taiwan, R. O. C.

As the dimension is continuously scaled down in integrated circuit (IC) fabrication, the leakage current of silicon oxide ($SiO_2$) via direct tunneling becomes excessive in metal-oxide-semiconductor (MOS) devices and the device reliability is an issue. The replacement of $SiO_2$ with higher dielectric constant (high-k) materials can have an increased physical thickness and significantly reduce the direct tunneling leakage current to improve the reliability. Among binary high-k materials, titanium dioxide ($TiO_2$) is a potential candidate (bulk ε is 180 along the c axis and 90 along the a axis in the rutile phase) and has good thermal stability. Usually, the leakage current of polycrystalline $TiO_2$ is high mainly from the grain boundaries. The oxygen ($O_2$) annealing can decrease oxygen vacancies and passivate the grain boundaries. Fluorine ions ($F^-$) form fluorinated LPD-$SiO_2$ films can be used to passivate the grain boundaries of polycrystalline $TiO_2$ film and the interface of MOCVD-$TiO_2$/Si. Furthermore, the nitrogen ($N_2$) annealing can be used to strengthen Ti-F, Ti-O-F in MOCVD-$TiO_2$ films. For the MOS structure of fluorinated $O_2$-annealed MOCVD-$TiO_2$ on Si with $N_2$ annealing at 300°C, the dielectric constant is 61 and the leakage currents are 7.2 x $10^{-9}$ and 9.7 x $10^{-7}$ A/cm$^2$ at ± 5 MV/cm. The interface state density is 7.2 x $10^{10}$ cm$^{-2}$eV$^{-1}$ at the mid-gap. The fabricated e-mode Si NMOSFET has high $g_m$, high $\mu_{FE}$ and good $I_D$-$V_D$ characteristics. The maximum $g_m$ is 1.54 x $10^{-4}$ (A/V) at $V_G$ = 1.11 V and $V_D$ = 0.1 V. The maximum derived electron $\mu_{FE}$ at $V_{DS}$ = 0.1 V is 192 cm$^2$/V·s. The subthreshold swing (S) is 153 mV/decade. It shows high potential to use fluorinated $O_2$-annealed MOCVD-$TiO_2$ as gate oxide for MOS IC fabrication in the future.

[1] Q. X. Jia, L. H. Chang, and W. A. Anderson, Thin Solid Films., 259 264(1995)
[2] Y. H. Lee, K. K. Chan, and M. J. Brady, J. Vac. Sci. & Technol., 13 596(1995)
[3] K. Vydianathan, G. Nuesca, G. Peterson, E. T. Eisenbraun, A. E. Kaloyeros, J. J. Sullivan, and B. Han, J. Mater. Res., 16 1838(2001)
[4] C. W. Wang, S. F. Chen and G.T. Chen, J. Appl. Phys., 91 9198(2002)
[5] S. A. Campbell, D. C. Gilmer, X. C. Wang, M. T. Hsieh, H. S. Kim, W. L. Gladfelter, and J. H. Yan, IEEE Trans. Electron Devices, 44 104(1997)
[6] D. M. Shang and W. Y. Ching, Phys. Rev. B, 51 13023(1995)
[7] S. R. Kasi, M. Liehr, and S. Cohen, Appl. Phys. Lett., 58 25(1991)

# HarmoniX microscopy: A new scanning probe technique for high resolution, quantitative mapping of material properties like adhesion and elastic modulus.

**P. Markus**
Veeco Instruments BV, Verlengde Poolseweg 34-46, 4818 CL, Breda, The Netherlands

Scanning Probe Microscopy (SPM) is a common used technique to observe different kind of surfaces. The high resolution, non-destructive imaging capabilities of Tapping Mode Scanning Probe Microscopy have made it the first choice for the study of soft materials at the nanoscale since its introduction in 1993. The addition of phase imaging has made tapping mode even more popular by enabling the mapping of non-topographic properties of the sample. This often allows discrimination between different components in composite systems and sometimes allows qualitative comparisons between mechanical properties of components. For more quantitative measurements of local mechanical properties, SPM users have commonly turned to contact mode force distance curves. While this has the benefit of simpler interpretation, and the ability to decouple the effects of different mechanical properties such as elasticity and adhesion, it has much lower speed and resolution and can damage soft samples.
HarmoniX microscopy is a brand new mode of SPM that provides independent, nanoscale mapping of material properties such as elasticity, adhesion, and dissipation. By analyzing the full spectrum of motion of special probes designed for high bandwidth measurement of force on the tip, HarmoniX produces force-distance curves that represent the variation in tip-sample force that occurs when the tip goes through a period of tapping oscillation. These curves are then analyzed to obtain the material properties of the sample. HarmoniX microscopy is hundreds of times faster than other quantitative material mapping techniques such as force volume, but retains the high resolution, non-destructive qualities of TappingMode Imaging.

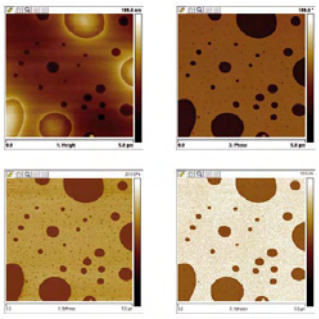

# Ga:La:S amorphous thin films prepared by pulsed laser deposition

**P. Němec [1], M. Pavlišta [2], V. Nazabal [3], A. Moreac [4], M. Frumar [1], M. Vlček [5]**

1. University of Pardubice, Department of General and Inorganic Chemistry & Research Center, nám. Čs. Legií 565, 53210 Pardubice, Czech Republic

2. University of Pardubice, Department of Physics, Studentská 84, 53210 Pardubice, Czech Republic

3. University of Rennes 1, Sciences Chimiques de Rennes (SCR), UMR-CNRS 6226, Equipe Verres et Céramiques, 35042 Rennes, France

4. University of Rennes 1, GMCM, UMR 6626, 35042 Rennes, France

5. Joint Laboratory of Solid State Chemistry of the University of Pardubice and the Institute of Macromolecular Chemistry of Acad. Sci. of the Czech Republic, Studentská 84, 53210 Pardubice, Czech Republic

Amorphous thin films based on chalcogenides play an important role in optics, electronics, and optoelectronics. For applications, a perspective suitable technology for the thin film growth has to be developed. Pulsed laser deposition (PLD) is a promising thin films preparation technique which can be widely used to fabricate thin films with required and/or interesting properties and/or composition.

Thin amorphous gallium-lanthanum-sulphide films were prepared by pulsed laser deposition method. The prepared layers were characterized in terms of the structure (using Raman scattering spectroscopy), chemical composition (by energy-dispersive X-ray analysis), and optical properties. The photosensitivity of amorphous chalcogenides was studied.

## 1. INTRODUCTION

Amorphous chalcogenides, typically formed by chalcogens (S, Se or Te) in combination with suitable elements – As, Ge, Ga, Sb, etc. –, are important class of inorganic materials due to their interesting properties applicable in different fields of optics and optoelectronics [1].

From a variety of amorphous chalcogenides' compositions, gallium-lanthanum-sulphide (GLS) family is of large interest because of its wide transmission window (0.5-10 μm), low-phonon energy, good rare-earth solubility, large non-linearity, high values of glass transition temperature, photoinduced phenomena and non-toxicity [2-3].

Typically, for the thin films preparation, different deposition techniques are useful; vacuum thermal evaporation, sputtering, chemical vapour deposition, spin coating and pulsed laser deposition (PLD) are of importance for amorphous chalcogenides. PLD seems to be favourable according to its simplicity, easy control of the process, often stoichiometric transfer of target material to the films and possibility to fabricate films of unusual compositions [1].

In previous work [4-6], PLD with 248 nm KrF line was used for the fabrication of GLS thin films and optical properties of prepared layers were mainly investigated. This work is focused

on the PLD using 532 nm line and more complex characterization of the GLS films in terms of their structure employing Raman scattering spectroscopy.

## 2. EXPERIMENTAL

Amorphous thin films were prepared by PLD using targets of GLS glass with nominal composition of $(Ga_2S_3)_{65}(La_2S_3)_{32}(La_2O_3)_3$ supplied by ChG Southampton Ltd.
Few ns laser pulses at 532 nm with energy of 85 mJ (on target) were used for PLD of GLS targets. The laser beam was incident on the target under an angle of about 45°. The energy fluence on the target was constant (~3-4 $J.cm^{-2}$). Amorphous thin films were deposited in a vacuum chamber (background pressure ~4-5.2x$10^{-4}$ Pa). The substrates used for PLD (chemically cleaned microscope glass slides, Si wafers) were positioned parallel to the target surface at a distance of 5 cm. The number of laser pulses used for the preparation of the films was 18000-54000. Both target and substrates were rotated in order to avoid deep damage of the target and to improve the thickness homogeneity of the films, respectively.
The surface of the GLS films and their chemical composition were studied using scanning electron microscopy (SEM) with energy-dispersive X-ray analyzer (EDS). Raman scattering spectra were measured by double-monochromator Raman spectrophotometer HR800 (Horiba Jobin-Yvon) with He-Ne laser (633.8 nm) as excitation source. Refractive indices and the thicknesses of the films were evaluated using variable angle spectroscopic ellipsometry (VASE, J.A. Woollam Co., Inc.) in spectral range 500-2300 nm measuring at 65, 70, and 75° angles of incidence.

## 3. RESULTS AND DISCUSSION

Thin films obtained by PLD were amorphous and homogeneous according to optical and electron microscopy. The thickness of the films varied from ~420 to ~1670 nm depending on the number of laser pulses and PLD geometry. By SEM, we observed some droplets (with diameter of 0.01-2 μm) on the surface of the layers. The chemical composition of the films is little bit shifted from the composition of the targets as results from EDS analysis. We found ~3-4 at.% of Ga excess, ~1 at.% of La excess, and ~4-5 at.% of S deficit. Mentioned sulphur deficit is probably connected with the volatility of the element.
The Raman scattering spectra of bulk GLS glass and corresponding thin film are given in Fig. 1. In the Raman spectrum of bulk GLS glass, the main feature is broad band between ~260 and 450 $cm^{-1}$ with maximum near 330 $cm^{-1}$, which is practically without structure. There are also three nearly featureless bands of lower intensity between 90 and 250 $cm^{-1}$ at 95, 135, and 210 $cm^{-1}$ in Raman spectra of GLS glass. Raman spectra of PLD GLS thin films reveal four bands with maxima near 95, 135, 220, and 360 $cm^{-1}$ being similar in positions but differing in amplitudes in comparison with bulk glass. In accordance with previously published reports [7-9] we tentatively assign the Raman band at 330 (360) $cm^{-1}$ to $F_2$ $\nu_d$ $GaS_4$ tetrahedra vibrations overlapping with $F_2$ $\nu$ $LaS_8$ vibrations. Raman band at 210-220 $cm^{-1}$ can be attributed to $A_1$ $\nu_s$ $GaS_4$ tetrahedra vibrations overlapped with $A_1$ or E, eventually $F_2$ $\nu$ $LaS_8$ vibrations. Further, weaker bands at 135 and 95 $cm^{-1}$ we connect with $F_1(F_2)$ $\delta$ $GaS_4$ and $A_1$/E T' $LaS_8$ vibrations, respectively.
The results of VASE data analysis show an increase of thickness and refractive index values when moving ~18 mm outwards from the plasma plume centre at fixed target-to-substrate distance of 5 cm; ~30% decrease in thickness and ~4% decrease in refractive index, respectively, were found. The values of refractive index obtained at mentioned distance from plasma plume centre are quite comparable with values for bulk GLS glass (2.45 at 633 nm).
The VASE study of sensitivity of GLS thin films under irradiation/annealing shows following: i) irreversible photoinduced decrease of refractive indices of ~1% (when exposed by 473 nm cw laser with 220 $mW.cm^{-2}$ for 3 hrs) or ~2% (due to the exposure by one pulse

from 248 nm pulsed laser with 30 ns pulse and energy density of 0.038 J.cm$^{-2}$), ii) annealing-induced decrease of refractive index of ~2% (at 400 °C, 2 hrs, nitrogen atmosphere). Observed changes in refractive indices should be accompanied by changes in the structure and optical band gap values, which will be the focus of future investigations.

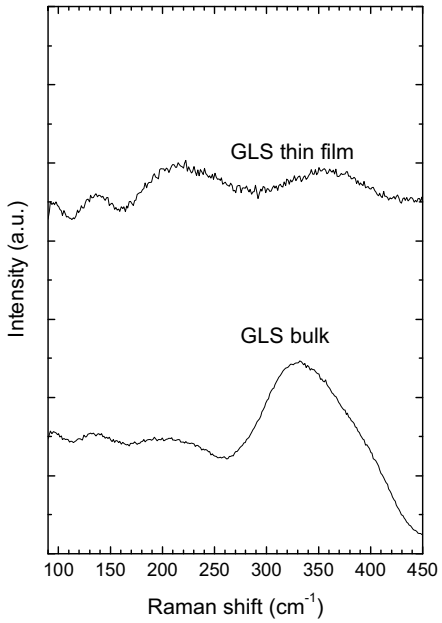


Figure 1. Raman scattering spectra of GLS bulk glass and thin PLD film.

## 4. CONCLUSIONS

Pulsed laser deposition technique was employed for the fabrication of gallium-lanthanum-sulphide thin films. The prepared layers show understoichiometric content of sulphur (~4-5 at.%), the content of gallium and lanthanum is overstoichiometric (~3-4 at.% and ~1 at.%, respectively). The structure of the films is formed by $GaS_4$ tetrahedra and $LaS_8$ structural units following preliminary analysis of Raman scattering data. Negative irreversible photorefraction phenomena (~1-2 %) was observed under cw or pulsed laser irradiation.

## 5. ACKNOWLEDGEMENT

This work was supported by the Ministry of Education, Youth and Sports of the Czech Republic (projects MSM 0021627501, LC523 and MEB020829 respectively) and by Czech Science Foundation (project No. 104/08/0229).

## 6. REFERENCES

[1] M. Frumar, B. Frumarová, P. Němec, T. Wágner, J. Jedelský, M. Hrdlička, J. Non-Cryst. Solids 352 544 (2006)
[2] A.K. Mairaj, A. Fu, H.N. Rutt, D.W. Hewak, Electron. Lett. 37 1160 (2001)
[3] J.A. Frantz, L.B. Shaw, J.S. Sanghera, I.D. Aggarwal, Opt. Express 14 1797 (2006)
[4] R. Asal, H.N. Rutt, Opt. Mater. 8 259 (1997)
[5] K.E.Youden, T. Grevatt, R.W. Eason, H.N. Rutt, R.S. Deol, G. Wylangowski, Appl. Phys. Lett. 63 1601 (1993)
[6] D.S. Gill, R.W. Eason, C. Zaldo, H.N. Rutt, N.A. Vainos, J. Non-Cryst. Solids 191 321 (1995)
[7] G. Lucazeau, S. Barnier, A.M. Loireau-Lozac'h, Spectrochim. Acta, 34A 21 (1978)
[8] G. Lucazeau, J. Leroy, Spectrochim. Acta, 34A 29 (1978)
[9] S. Barnier, G. Lucazeau, J. Chim. Phys. 73 580 (1976)

# Electrical properties of nanocomposites

**S. Novak [1], R. Hrach [1, 2], M. Svec [1]**

1. J. E. Purkinje University, Faculty of Science, Department of Physics, Ceske mladeze 8, 400 96 Usti nad Labem, Czech Republic

2. Charles University, Faculty of Mathematics and Physics, Department of Surface and Plasma Science, V Holesovickach 2, 180 00 Prague 8, Czech Republic

Nanocomposite structures are studied by the help of an analytical software tool with a view to find correlations between morphological and electrical properties. Model structures of nanocomposites are introduced, their structures are analysed by the Voronoi tessellation and the transport properties were obtained by the Monte Carlo simulation of electron tunnelling through the structures. Connections between morphology and electrical properties are discussed in the end.

## 1. INTRODUCTION

In our contribution we deal with a study of nanocomposites. Introducing nanoparticles into a material called matrix creates these materials with very enhanced mechanical, electrical, optical, and thermal properties. These properties strongly depend on methods used for manufacturing nanocomposites (e.g. thermal evaporation, ion-beam sputter deposition, laser deposition and above all by plasma deposition techniques) [1].

One of the main parameters that influence the electrical properties of these structures is metal volume fraction of the system [2]. At low values of the parameter the structures are formed by mostly isolated particles spread in the matrix. The electrical conductivity of these materials is very low. The conductivity rises up with the metal volume fraction increase. There is a critical value of the metal volume fraction called percolation threshold. Structures with the metal volume fraction below the percolation threshold comprise the tunnelling mechanism of charge transport contrary to structures close or over the percolation threshold where the ohmic type of conductivity prevails.

The next interesting parameter of such structures is a degree of objects arrangement and its incidence to electrical properties of nanocomposites. We accentuate this standpoint in this paper.

We study the morphology and electrical properties of nanocomposite structures by the help of a self-made analytical software tool. We describe the models of nanocomposite structures, then the morphological analysis of the obtained structures, transport of electric charge through them and finally we conclude with a search of correlations between the morphology and electric properties of nanocomposites.

## 2. MODELS AND METHODS

The whole computer experiment consists of three main parts: (i) generation of nanocomposite structures, (ii) study of their morphology, and (iii) simulation of charge transport through these structures.

### *2.1 Models of nanocomposite structures*

We prepared two models of nanocomposite structures, the hard sphere model and the growth model [3]. Both of them are based on the Monte Carlo method – random generation of objects to the working area obeying conditions and parameters of the models.

The main parameter of the hard sphere model is so called diffusion zone $D$ – the minimal distance between edges of two particles. Alongside it, we use a relative parameter

$$D_{\mathrm{rel}} = D / D_{\max}, \qquad (1)$$

where $D_{\max}$ is the maximal possible $D$ for a given structure. This parameter varies between values 0 and 1, whereas structures with $D_{\mathrm{rel}} = 0$ are random and structures with $D_{\mathrm{rel}} = 1$ are maximally arranged.

The growth model stems from the hard sphere model. It uses also the parameter $D_{\mathrm{rel}}$ and in addition it has next two parameters: deposition rate and the width of the growing region of the film. This model is faster that the hard sphere model and provides structure with large scale of arrangement (Fig. 1). The nanocomposite structures were simulated by spherical objects of constant radius spaced out in a three-dimensional (3D) working area. Dimensions of the area were set from 1000×1000×100 to 1000×1000×500 pixels with c. 10% margins. The usual number of objects to be generated was between $1\times10^3$ and $1\times10^4$ in order to guarantee the reasonable precision of our results.

In spite of that our task is to study and analyse 3D nanocomposite structures, these structures are not so sufficient for both the algorithms development and the visualization of results. Two-dimensional (2D) analogies were prepared because of that (see Fig. 1). The parameters of 2D structures were set to 1000×1000 pixels with margins; objects were circular with constant radii. The usual number of objects was around $1\times10^3$. Simulations were performed for both types of models, 3D and 2D, but the results are presented in following figures for 2D analogies only.

### *2.2 Morphology of nanocomposite structures*

There are several methods for study of the morphology of such structures [4]. We focused on the correlation between the degree of arrangement of objects in the structure and the electrical properties. The degree of arrangement was determined by the parameter $D_{\mathrm{rel}}$ and the morphological method used was the Voronoi tessellation [5, 6] (Fig. 2). This method divides the studied area into cells and they are analysed consequently.

### *2.3 Model of charge transport*

The Monte Carlo technique was used for the simulation of current passing through the nanocomposite structure. The complete transport algorithm consists of emission of electrons from negatively biased electrode, tunnel transport of electrons between individual objects causing their charging and finally the collecting of electrons by positively biased electrode. In every time step the given number of electrons originating from negative electrode was divided into various conduction paths according to corresponding tunnel probabilities and actual potential of objects. The simulation was very time consuming, as the simulation had a form of iterative process.

## 3. RESULTS

We present model nanocomposite structures, their morphological and electrical properties as results of our computer simulation. All the figures show results obtained for the growth model. Results for the hard sphere model are very similar.

### *3.1 Nanocomposite structures*

Fig. 1 shows the examples of 2D analogies of nanocomposite structures obtained by the growth model. One can compare the arrangement of objects in the structures depending on the parameter $D_{rel}$. The degree of arrangement of the structure grows from left to right.

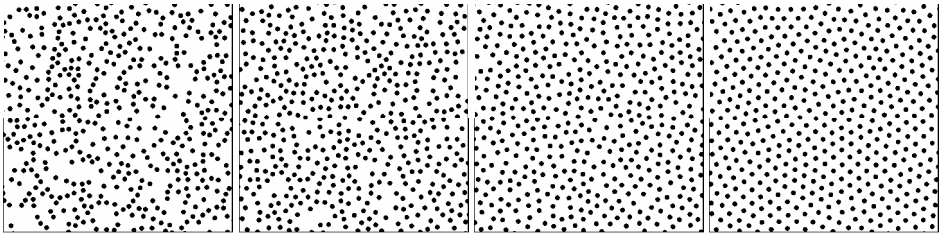

Figure 1. Examples of structures generated by the growth model. $D_{rel}$ = 0.25, 0.5, 0.75, 1.0 (from left to right).

### *3.2 Morphological properties*

Fig. 2 shows the morphological analysis of 2D analogies of nanocomposite structures by the help of Voronoi tessellation method. We analysed all areas of Voronoi cells and the frequency diagrams of them are also depicted.

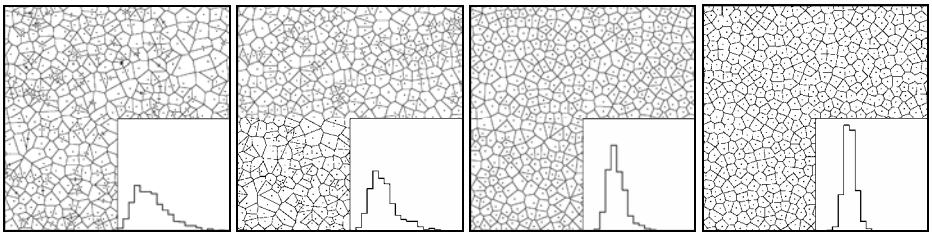

Figure 2. Morphological analysis of the structures – the Voronoi tessellation. Right bottom corners show the frequency diagrams of Voronoi cells areas. $D_{rel}$ = 0.25, 0.5, 0.75, 1.0 (from left to right).

### *3.3 Electrical properties*

Results of the simulation are shown in Fig. 3. There are 'fuzzy' clusters formed by electric current in structures with different degree of arrangement. Contrary to clusters from the common percolation theory [7], these clusters need different analysis. One of the possible ways is to determine the distribution of values of electric currents flowing between objects in the structures with various degrees of arrangement by the help of distribution functions (3D graph in Fig. 4). 2D graph in Fig. 4 shows the total amount of electric current flowing through the structure in a steady state for each degree of arrangement.

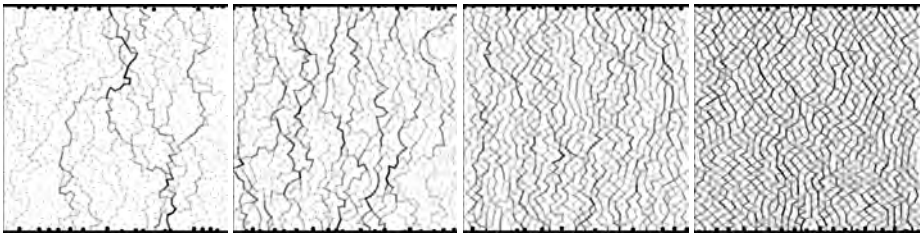

Figure 3. Infinite 'fuzzy' clusters representing currents flowing between electrodes. The positions of metal particles are depicted by the dots. The values of the electric current are proportional to the shade of lines. $D_{rel}$ = 0.25, 0.5, 0.75 and 1.0 (from left to right).

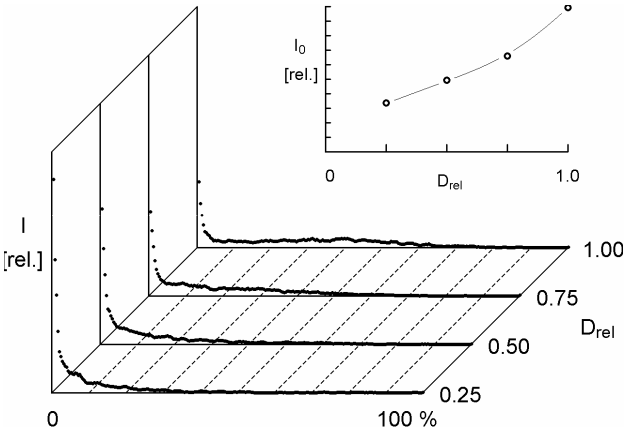


Figure 4. The distribution of values of electric currents flowing between objects in simulated nanocomposite structures (in arbitrary units) for various degrees of object arrangement characterized by relative diffusion zones $D_{rel}$ (3D graphs) and the relation between the object arrangement and the relative value of total electric current in the structure.

## 4. DISCUSSION

Fig. 1 shows the increasing arrangement of the structure when $D_{rel}$ grows from 0 to 1. This conclusion confirms the morphological analysis – the distribution of the areas of the Voronoi cells gets narrow with increasing of $D_{rel}$ (see Fig. 2), so the dispersion of distances between each object and it's nearest neighbour decreases and the structures become more arranged.
The evolution of fuzzy clusters shows Fig. 3. One can see that the current paths become shorter and more compact with increasing $D_{rel}$. The structure and size of the fuzzy clusters is different from clusters defined in common theory of percolation. Extended analysis of them has to be done. Fig. 4 shows one possible way how to obtain some information contained in these structures. The distribution functions in 3D graph show how the spectrum of the particle-particle current is determined by the arrangement of particles. The individual values of particle-particle currents are more uniformly distributed for structures with higher degree of arrangement. The upper-right corner graph depicts the integral information on how the total current increases with increasing parameter $D_{rel}$. The structures with uniform distribution of particles embody higher electric conductivity than structures with random distribution.
The computer simulation undertaken by the help of the analytical software tool unfolded some information that could be hardly obtained in the other way because the processes take place inside the nanocomposite materials.

**Acknowledgements.** The work is part of research plan MSM0021620834 financed by the Ministry of Education of Czech Republic. The authors acknowledge the support of the Czech Academy of Science, project KAN101120701 and project 1ET400720409.

## 5. References

[1] H. Biederman, L. Martinu "Plasma Deposition, Treatment and Etching of Polymers", Academic Press New York 1990
[2] P. Sheng Phil Mag B 65 357 (1992)
[3] R. Hrach, S. Novak, M. Svec Thin Solid Films 459 174 (2004)
[4] J. Serra "Image Analysis and Mathematical Morphology", Academic Press London 1982
[5] G. J. Voronoi Reine Angew Math 134 198 (1908)
[6] G. J. Voronoi Reine Angew Math 136 67 (1909)
[7] D. Stauffer, A. Aharony "Introduction to Percolation Theory", Taylor and Francics London 2003

# Elaboration of $SmNiO_3$ and $NdNiO_3$ thin films prepared by DC magnetron sputtering followed by ex-situ air annealing

**F. Capon, D. Horwat, J.F. Pierson**
Nancy University

Due to its metal–insulator transition and thermochromic properties, the rare earth nickelate perovskite $RENiO_3$ has received a great deal of attention for the last years. Such unusual electronic and optical features are all the more interesting since the metal–insulator transition temperature (MIT) can be tuned by changing the RE cation: $LaNiO_3$ is metallic while $PrNiO_3$, $NdNiO_3$, $SmNiO_3$ and $EuNiO_3$ undergo an MI transition at 130, 200, 400 and 460 K respectively. Using the sputtering method, the synthesis conditions are not as extreme as for the bulk but remains drastic. Laffez et al showed that to produce a perovskite phase $NdNiO_3$, the annealing treatment has to be performed at 800◦C during 2 days under a high oxygen pressure of 190 bars. In this work $RENiO_3$ (RE = Nd and Sm) thin films are deposited by DC sputtering and subsequent annealed in air at 800 K. The experimental device is equipped with two magnetron system associated with a rotating substrate holder to ensure the production of films with uniform thickness. The constitutive elements of the perovskite are deposited at room temperature from two metallic targets RE and Ni onto {100} undoped Si single-crystal substrate. The RE and Ni contents were controlled by the current applied to the targets. X-ray diffraction was performed before and after annealing. As-deposited films are X-ray amorphous. The chemical stoichiometry of the deposited material was checked by energy dispersive X-ray analysis. The DC electrical resistance was measured with the four-probe method scanning temperature from 20 to 420 K using Quantum Design equipment. As Catalan et al. propose, we fitted the resistivity behavior using a dual mechanism in which activated behaviour and variable range hopping are the only terms $1/R=C \exp(-D/T)+A \exp(-B/T^{1/4})$.

# Metal Decoration of Carbon Nanotubes

**A. Felten, [1] I. Suarez-Martinez, [2] J. Ghijsen, [1] W. Drube, [3] X. Ke, [4] G. Van Tendeloo, [4] C. Bittencourt, [5] M. Hecq, [5] C.P. Ewels, [2] J.-J. Pireaux [1]**

1) University of Namur, Laboratoire LISE, 61 rue de Bruxelles, Namur 5000, Belgium
2) IMN, CNRS UMR6502, 2 Rue de la Houssiniere, BP 32229, 44322 Nantes, France
3) HASYLAB, Notkestrasse 85, Hamburg D-22603, Germany
4) University of Antwerp (EMAT), Universiteitsplein 1, Antwerp 2610, Belgium
5) LCIA, Universite de Mons, Parc Initialis, Av. Nicolas Copernic 1, Mons 7000, Belgium

Composites materials based on metal decorated carbon nanotubes have gain increased interest since recent years. They are expected to play significant roles in field of nanoelectronics, bio or gas sensing, catalysis…

In this work we investigate the chemical interaction between different metals namely Au, Pd, Pt, Ni and Ti thermally evaporated onto pristine and oxygen plasma functionalized CNTs. Transmission Electron Microscopy (TEM) was used for monitoring the nucleation and evolution of the metal coating of the CNTs, while chemical interaction was monitored by X-ray photoemission using synchrotron radiation.

Metal covering pristine nanotube surface varies from continuous layer (Ti) to aggregated clusters (Ni), and to isolated clusters (Au, Pd, Pt). A qualitative trend for metal to carbon nanotube interaction binding energy is deduced from the TEM pictures: Ti > Ni > Pt > Pd > Au. Oxygen plasma treatment was found to improve the cluster dispersion and to reduce their size distribution by grafting oxygen groups on the CNT surface, which act as nucleation sites for the metal clusters. Evolution of the valence band and core levels as a function of metal amount evaporated onto the sample was then studied using photoemission spectroscopy, showing strong bonding for Ni and Ti and poor interaction in the case of Pt, Pd and Au.

The experimental results are correlated with Density Functional Theory calculations of the interaction of metal atoms with bare and oxygenated structural defects on the graphitic surface. The energetic study for the different metals is in good agreement with the experimental results showing the trend of metal to carbon binding energy with the pristine surface as Ti >> Pd > Au. In addition, we also show a dramatic increase in binding energy of the metal atom with oxygenated vacancies and divacancies with respect to the perfect graphitic surface. We discuss charge transfer in these different systems and compare this with the experimental PES results. These results give insight to the improvement of nanoparticle dispersion found for the oxygen plasma treated tubes.

This work is financially supported by Nano2Hybrids (EC-STREP-033311), the PAI 6/08, by DESY and the European Commission under contract RII3-CT 2004-506008 (IASFS).

# Sputter-Deposition Of Metal/Oxide And Oxide/Oxide Nanocomposite Thin Films From An Oxide Target

**L. Presmanes , A. Barnabe , C. Bonningue , I. Pasquet and Ph. Tailhades**
Université de Toulouse, CIRIMAT, UPS/INPT/CNRS, Bat. 2R1, 118 route de Narbonne, 31062 Toulouse cedex 9 France.

Among all the processes for producing films, the sputtering process is one of the most popular. This method allows film preparation at moderate temperatures, making it possible to deposit on various substrates with high homogeneity and good uniformity. As a consequence, the sputtering technique is widely used in research laboratories as well as in industrial production units. Sputtering deposition of iron oxide thin films leads to a combination of attractive physical properties which can be adjusted by the parameters of preparation.
The majority of authors active in the field of oxide thin films, reports the elaboration of oxide thin films by reactive magnetron sputtering from a metallic target using an $Ar–O_2$ gas mixture. The proportion of oxygen present in the plasma then determines the stoichiometry of the oxide. Another method to obtain oxide thin films is by radio frequency (RF) sputtering of an oxide target. During sputtering, the layer growing on the substrate is subjected to continuous bombardment by energetic species emitted from the target or retro-diffused. In the case of oxide deposition, oxygen atoms can even be ejected from the film when the bombardment becomes stronger. The amount of reduced phase can then be adjusted by the modification the sputtering conditions. The additional bias polarization of the substrate is another way to increase the bombardment on the growing layer. These extreme conditions of preparation lead to interesting reducing preparation conditions from which metal/oxide or oxide/oxide nanocomposites can result [1,2]. The preparation of nanocomposite thin films can lead to devices with attractive optical, magnetic, and semiconducting properties. These original compounds are generally obtained at very low partial oxygen pressure, and high temperature (>1000°C) in the classical ceramic route.
We report here the preparation and the characterization of different nanocomposites that were easily obtained, at low temperature, by rf-sputtering of ceramic targets under various reducing conditions. Scanning electron Microscopy and atomic force microscopy were used to observe these nanostructured layers. Grazing angle X-ray diffraction, electrical properties and magnetic measurements are also reported versus deposition parameters and annealing temperature.

[1] E. Mugnier, I. Pasquet, A. Barnabe, L. Presmanes, C. Bonningue, P. Tailhades, Thin Solid Films 493 49 (2005).
[2] B. Mauvernay, L. Presmanes, C. Bonningue, Ph. Tailhades, J. Magn. & Magn. Mater. 320 58 (2008).

# XRD assesment of Zn doped Si wafer surface

**V. Privezentsev**
Institute of Physics & Technology, Russian Academy of Sciences, Nakhimovskiy prosp., 34;
Moscow 117218 , Russia;

The investigation of physical properties of zinc doped silicon was made recently [1, 2]. Lately the properties of Zn doped n-Si by the electron beam induced current (EBIC) method in a scan electron microscope (SEM-EBIC) have been observed the microdefects [3]. These microdefects located in different depth and characterized by the raised recombination speed of nonequilibrium charge carriers. The revealed microdefects were connected with zinc precipitates and/or dislocations.
In present communication for analysis of such material surface the X-ray diffractometry method with employment of Cu$K_{\alpha 1}$-radiation and Bragg scheme assisted in a triple-crystal combination mode was used. As an additional technique has been used the SEM. The test Si<Zn> samples had the size 5,0*5,0*0,8mm$^3$ and plane orientation (111). The test samples surface has been subjected to finishing chemical-dynamic polishing.
At θ-scanning mode the triple-crystal difractometry (TCD) curves of scattering intensity $I(\Delta\theta)$ near a reciprocal lattice point for sample error angle α=±80 and α=±120arc sec from exact Bragg angle were obtained. There are three peaks at this curve: Bragg main peak (MP) at θ=2α, analyzer pseudo-peak (PP) at θ=α and diffusion peak (DP). The form, angular position and intensity of DP are defined by type and quantity of defects. The asymmetry of the MP intensity at positive and negative analyzer turn angles $\Delta\theta$ testifies about deformation of a crystal lattice. The deformation average value of the crystal lattice interplane distance was received from angular dependence of resulted intensity $P(\alpha)=\alpha^2 \cdot I_{MP}$. It was made $\Delta d/d \approx 1 \cdot 10^{-4}$ concerning parameter of an initial matrix $d_0$ and can be caused by vacancy character of microdefects near surface.
The MP width $\Delta\theta_{MP}$ on TCD curves increases with increase in a sample error angle α. This line spreading of MP at TCD curve presence of micro-roughness at the sample surface. They can be characterized by an angle $\Delta\psi$ between reflecting planes and the surface local The pattern of the Si<Zn> sample surface was obtained in a secondary electron mode in SEM, and the tilt was 70$^o$. From this it is well visible the surface relief characteristic, in particular, and deepenings and hollows on the the sample surfaces. They validated conclusions of X-rays diffractometry about presence of roughness at wafer surface.

## 1. Introduction

The investigation of physical properties of zinc doped silicon was made recently [1, 2], because of researching of properties of the silicon doping with deep impurity of transitive metals became again actual [3]. Later the properties of Zn doped n-Si by the electron beam induced current method in a scanning electron microscope (SEM-EBIC) have been observed the microdefects [4]. These microdefects located in different depth and characterized by the raised recombination speed of nonequilibrium charge carriers. The revealed rood-like microdefects were presumably connected with zinc precipitates and/or dislocations.

In present communication for analysis of such material surface the X-ray diffractometry method with employment of Cu$K_{\alpha 1}$-radiation and Bragg scheme assisted in a triple-crystal diffractometry (TCD) combination of crystals arrangement [5] was used. As an additional technique have been used the scanning electron microscope (SEM) and atomic force microscope (AFM).

## 2. Samples.

It was investigated the silicon, preliminary alloyed with shallow donor impurity – phosphorus with concentration $N_P=1{,}5\times10^{14}$см$^{-3}$ and compensated by deep acceptor impurity - zink. Concentration of Zn in Si was made $N_{Zn}=1\times10^{14}$см$^{-3}$. It is necessary to notice, that concentration of the mane charge carriers (electrons) was $n=5\times10^{11}$см$^{-3}$, that more, than on two orders is less, than concentration of the entered impurity (phosphorus and/or zinc). It testifies to presence of significant amount electrically inactive atoms of Zn in Si lattice. The test n-Si<Zn> samples had the sizes 5,0×5,0×0,8mm$^3$ and big plane orientation (111).

For elimination of crystal structure imperfections in near-surface region the n-Si<Zn> samples has been subjected to finishing chemical-dynamic etching. For test samples disordered orientation of investigated surface (111) rather crystallographic planes did not exceed 1ang.degr. The high-perfect Si sample with orientation (111) of big plane and sizes 20×20×1mm$^3$ was made by riveing from standard Si(111) wafer after chemical-dynamic polishing and has been investigated parallelly as a model pattern.

## 3. Experimental technique

The analysis of structural scattering in near-surface region of samples has been lead on the basis of data intensity Bragg scattering $I(\Delta\theta_{sam}, (\Delta\theta_{an})$, where $\Delta\theta_{an}$ and $\Delta\theta_{sam}$ are an angles of a crystal-analyzer and a sample deviation from exact adjustment position. It have been used the techniques TCD and were used dispersion-free (n, -n, +n) combination in triplet-crystal in the automated diffractometer, operated by the PC [4]. In the capacity of a radiation source with wave length of λ=1,54Å and power 1,2kW was used the X-rays tube with a rotating copper anode (Rigaku RU-200) with the visible focus size 0.05×10mm$^2$. This tube working served at voltage 40kV and current 25mA.

Primary bundle of $CuK_{\alpha 1}$-radiations with small angular divergence 3,5ang.sec have been generated as a result of symmetric reflection from Si (111) monochromator. As the analyzer same monocrystal Si with reflection from a plane (111) served. The sample was established in reflecting position at factor of asymmetry Bragg reflections from the sample $\beta=1$. Here $\beta = \sin(\theta_{Br} + \psi)/\sin(\theta_{Br} - \psi)$, and $\psi$ is an angle between reflecting planes and a crystal surface, and $|\psi| <\theta_{Br}=$, where Bragg angle for Si<111> is $\theta_{Br}$=14,2arc.sec. At symmetric diffraction the value $\psi=0$. Coherent Bragg scattering intensity of the main peak (MP) on TCD curves $I(\Delta\theta_{sam}, (\Delta\theta_{an})$ was registered in a mode $\Delta\theta_{sam}/2\Delta\theta_{an}$ and at the fixed angle $\Delta\theta_{an,\ sam}$ depending on angular position of crystal-analyzer $\Delta\theta_{an}$ in relation to a bundle falling on it. Measurements were made at exact adjustment of all three crystals in reflecting position. Such installation geometry leads to only insignificant RDC line broadening (in our case dispersion was D=2,5ang.sec) and does not deform at all the form and width Bragg components on TCD curves.

## 4. Experimental results and their discussion.

Primarily the electron diffraction investigation of test samples have been carried out. On Fig.1 the electron reflected diffraction pattern from the sample n-Si<Zn> (at accelerating voltage=75 кeV) is presented. The analysis of this pattern from fast electrons has shown, that for series of reflexes along a normal to the sample surface shadow the interplane distances

have been certain. They allow to determine orientation of the substrate big side along a plane (111). Presence on electron reflected diffraction pattern the Kikuchi-lines (light and dark strips) is an attribute of perfection of a test n-Si<Zn>(111) sample crystal.
For detailed elaboration of layers structure of investigated samples Zn> (111) then the map of distribution of intensity diffraction scattering near to a reciprocal lattice point 1 1 1 in a TCD mode has been obtained (Fig.2). Reception of 2D distribution of intensity $I(q_x, q_z)$ was spent by record of a series of TCD curves measured in an of corners of turn angles interval of the sample and analyzer $\Delta\theta_{sam}$, $\Delta\theta_{an}$=±500arcsec in the scheme of ω-scanning (the sample rotation at the analyzer fixed position, that corresponds to sections $q_z$=const). On Fig.2 experimental contours of equal intensity are presented in a scattering plane near the reciprocal lattice point 111. Display of dynamic effects in the form of non-uniform intensity distribution in narrow areas along a line $q_x$=0 (the Bragg main peak (MP)) is clearly visible. It is a Bragg scattering, which located along a normal to a crystal surface. The small deviation from a vertical is caused by some mismatch of the investigated surface from a crystal plane (111). Dynamic strips in narrow areas near to a line $q_z$=-ctg $\theta_{Br}$ (pseudo-peak of a crystal-analyzer (PP)) are well visible also. They arise because of use of a crystal-analyzer with unitary reflection. Let's note, that intensive dispersion along a line $q_z$=ctg $\theta_{Br}$ is not observed. It occurs because at the given crystal installation is used monochromator with quadruple reflection. An equal intensity contours in the form of the concentric closed deformed curves around ofreciprocal lattice point indicate the diffusion scattering from large-scale microdefects. Correct definition of these defects type demands the account of diffusion scattering contours distortion because of dynamic effects. This challenge is solved by approximate trimmings of the Bragg MP, PP and smoothings of heterogeneity on initial experimental curves [5].

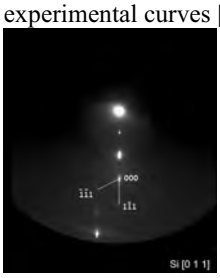

Figure 1

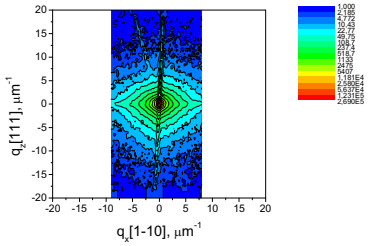

Figure 2

In TCD scheme the coherent and diffusion components of scattering from a crystal have various angular distribution: the reflection area of a coherent component is equal to several ang.sec, while the diffusion component is distributed isotropically. Therefore these scattering components are divided by the third crystal-analyzer at scanning of radiation reflected from the sample. Usually at such diffractometer geometry TCD curve consists of three maxima, which refer to as the Bragg MP, crystal-analyzer PP and diffusion peak DP. MP and PP are connected with a coherent component of scattering and in Bragg geometry located accordingly at angles $\Delta\theta=2\alpha$ and $\Delta\theta=\alpha$. Value of scattering DP depends on crystal lattice defects density, and its angular position - from defects type. Due to the high angular resolution the TCD method allows to divide contributions in full scattering from the various its component, simultaneously registered on curves DRC. These components have visualized on TCD curves (sections of a reciprocal lattice) differently. For a quantitative estimation of morphology and structure of a sample near-surface region it is necessary to consider some reasons of occurrence diffusion scattering. Among them it is possible to name the following: 1) small angle scattering, which connected with certain order of an arrangement micro-heterogeneity along a sample surface; 2) crystalline particles (clusters) gives the contribution to scattering. They incoherent connected with a sample matrix and it is necessary to consider

their sizes, forms and distribution; 3) the deformation in elastic strain local areas around crystalline particles (clusters).

Measurement of scattering intensity $I(\Delta\theta)$ near to a reciprocal lattice point at $\theta$-scanning mode is convenient for comparison of the contribution various a component of full scattering. For the proof of existence of large-scale defects TCD curves have been measured in Si<Zn>(111) samples for corners of a mismatch of the sample from exact Bragg angle α=±80 and α=±120ang.sec (on Fig.3,a and b). As mentioned above on

each of cross-sections curves the three maxima are observed. On Fig.3 it is well visible that expressed enough asymmetry of intensity MP at positive and negative analyzer turn angles $\Delta\theta_{an}$. So, MP value at analyzer turn angle $\Delta\theta_{an}$=+160 ang.sec in 2 times exceeds similar MP value at an analyzer turn angle $\Delta\theta_{an}$=-160ang.sec (at displacement angle |α|=80ang.sec) and in 1,5 times exceeds MP value at an analyzer turn angle $\Delta\theta_{an}$=+240ang.sec. in comparison with an analyzer turn angle $\Delta\theta_{an}$=-240ang.sec (at displacement angle |α|=120ang.sec). The results presented on Fig.3, confirm it and prove, that near-face the of Si <Zn> (111) sample has the reduced lattice parameter in relation to the value of other Si matrix that testifies to presence of lattice deformation in near-surface sample region. The average deformation value was obtained from angular dependence of function of normalized intensity $P(\alpha)=\alpha^2 \cdot I_{MP}(\alpha)$ [6], makes, as already has noted been above, $\Delta d/d_0 \approx 1 \cdot 10^{-4}$.

Besides this, on curves TCD (Fig.3) are observed significant on intensity diffusion peaks (DP), which practically do not differ on value both for positive, and for negative sample displacement angles. However intensity of these peaks at displacement angles |α|=80ang.sec. almost in 3 times exceeds their intensity at displacement angles |α|=120ang.sec. Intensity and FWHM of DP testifies to formation of the big number of microdefects inside of a crystal lattice. The concrete kind of these defects can be received from the analysis of a map of distribution diffusion scattering near to reciprocal lattice point. Such measurements demand big experimental time. Otherwise the effective size of these microdefects in kinematic approach can be estimated as [6] $d_{eff} \approx \lambda/(2\Delta\theta_{DP}) \approx 2{,}8\mu m$, where $\Delta\theta_{DP}$=57ang.sec is a DP linewidth on Fig.3. The MP width $\Delta\theta_{MP}$ on TCD curves increases with increase in a sample error angle α. This line spreading of MP at TCD curve presence of micro-roughness at the sample surface. They can be characterized by an angle $\Delta\psi$ between reflecting planes and the surface local relief, which caused by these roughness. Namely, [6] $\Delta\psi=0.5(\Delta\theta_{MP}|\alpha|tg\theta_{Br}=0{,}5(20*80*tg14{,}2^o=(7\pm1)$arc min. It is necessary to note also, that DP is observed at analyzer angles of the $\Delta\theta_{an}$=(7-10)ang.sec. We shall notice, that at scattering on chaotically distributed clusters of spherical defects the DP is located near to an angle [6] $\Delta\theta=2\alpha sin2\theta_{Br}=2 \cdot 80$ang.sec$\cdot 0{,}244^2=9{,}5$ang.sec. It corresponds to our experimental results. Therefore in our case it is impossible to exclude such character of microdefects. Functions of resulted intensity $P(\alpha)=\alpha^2 I_{MP}(\alpha) \approx 1$ testifies, that appreciable values of DP peaks on TCD curves (Fig.3) are caused by defects in the sample volume, instead of in a near-surface layer. Radiation penetration depth makes $L_{pen}=(\sin\theta_{Br})/\gamma=17{,}0\mu m$, where $\gamma=143 cm^{-1}$ is a of photo-electric absorption factor in Si at wave length λ=1,54Å [6]. Also it is necessary to note, that DP intensity, measured for various crystal-sample angles α, sharply falls down both at positive, and at negative angle values α.

The analysis of these TCD curves on Fig.3 allows to draw a following conclusion: the crystal lattice of investigated n-Si<Zn>(111) samples is not perfect and observable defects have the micron sizes. It is a conclusion proves to be true observable shift of DP maxima from zero position $\Delta\theta_{DP}$=0 to value $\Delta\theta_{DP}=2|\alpha|sin2\theta_{Br}$. The last value is characteristic for microdefects with spherical symmetric long-active field of atomic displacement concerning to defect nuclear.

On Fig.4 is presented the Si <Zn>sample image in SEM, tilt is 70°. This photo was obtained in a secondary electron mode in SEM, and the tilt was 70°. On Fig.4 it is well visible a surface

relief, in particular, and deepenings and hollows on the of the sample surfaces. They validated conclusions of X-rays diffractometry about presence of roughness at wafer surface.
On Fig.5 are presented the AFM image investigated sample [7]. From it follows, that the sample is heterogeneous enough, that confirms presence in it a sufficient quantity of a crystal lattice imperfections.

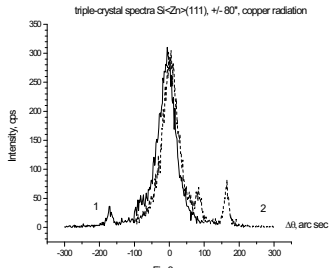


Figure 3

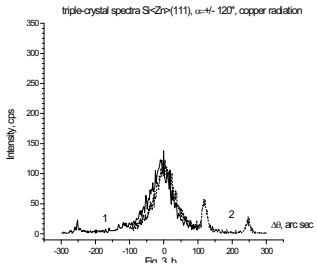


Figure 4

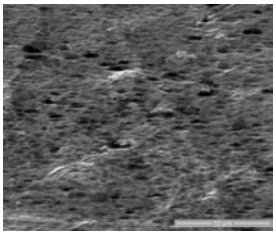

Figure 4

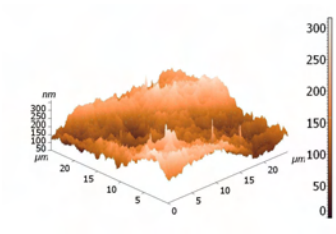

Figure 5

## 5. Conclusions.

X-ray diffractometry researchs of samples Si<Zn>(111) have result, that :

1) The interplane distance in a near-surface layer of Si crystal lattice is reduced by value of $\Delta d/d_0 \approx 1 \cdot 10^{-4}$ concerning parameter of other matrix $d_0$.
2) The samples surface are characterizied by presence of micro-roughness.
3) Crystal lattice Si<Zn> contains a plenty of microdefects: large-scale defects with micron sizes (dislocation and/or zinc precipitates) and small-scale clusters with spherical symmetric long-active field of atomic displacement with respect to defect nucleus.

## Acknowledgments.

I thank A.Lomov , K.Scherbachev and P.Ares for the help at carrying out of investigation and useful discussions.

## References:

[1] H. Schroth, K. Laßmann, S. Voß and H. Bracht. *Phys. Rev.Lett.*, **85** 417 (2000).
[2] S.N. Dobryakov, B.V. Kornilov and V.V. Privezentsev. *Russ. Microelectron.,* **36** 203 (2007).
[3] A.M. Stoneham, A.J. Fisher and P.T. Greenland. *J. Phys.: Condens. Matter.* **15** L447 (2003).
[3] E.B. Yakimov, V.V. Privezentsev. *J.Mater.Sci.: Mater.Electron.*, 2008, in press (DOI: 10.1007/s10854-008-9730-1). [4] A.A. Lomov, V.A. Bushuev, V.A. Karavanskii and S. Bayliss. C*ryst. Rep*., **48** 326 (2003).
[5] A.Shalimov, K.D.Shcherbachev, J.Bac-Misiuk and A.Misiuk. phys.stat.sol.(a) **204** 2638 (2007).
[6] D.K. Bowen and B.K. Tanner. High Resolution X-Ray Diffractometry and Topography. London, Taylor & Francis, (2001).
[7] I. Horcas, R. Fernandez, J.M. Gomez-Rodriguez, J. Colchero, J. Gomes-Herrero and A.M. Baro. *Rev. Sci. Inst.,* **78** 013705 (2007)

# Microwave plasma induced reactions of thin nickel films

**M. Quaas [1], V. Stranak [2], R. Hippler [2], H. Wulff [1]**

1. University of Greifswald, Institute of Biochemistry, Felix-Hausdorff-Str. 4, D-17489 Greifswald, Germany

2. University of Greifswald, Institute of Physics, Felix-Hausdorff-Str. 6, 17489 Greifswald, Germany

Nickel films were treated in a microwave plasma (SLAN, 2.45 GHz). In the experiments gas composition and negative substrate voltage bias were varied. Argon was used as buffer gas. Oxygen or hydrogen was chosen as reactive gases to study plasma induced oxidation and reduction reactions. The samples were investigated by means of grazing incidence x-ray diffractometry to determine the phase composition. Film thickness, density and roughness were determined by x-ray reflectometry.

Discharge was investigated by Langmuir probe measurements with the aim to estimate electron density and electron temperature. The combination of plasma and film diagnostics allows the analysis of the occurring plasma-chemical processes.

A reversible oxidation and reduction of the Ni films can be observed by changing the reactive gas from oxygen to hydrogen. Oxygen plasma treatment results in the formation of NiO layers on the metallic Ni. The effect of hydrogen plasma depends on the applied negative substrate voltage bias. Without an external voltage the reduction stops at the level of metallic Ni, whereas negative substrate voltages lead to the formation of $Ni_2H$ or NiH, respectively.

## 1. INTRODUCTION

So far there are only few experimental data showing the effect of low energy plasmas onto solid walls. Structural investigations of surface layers after plasma exposition convincingly describe surface layers with different physical and structural properties [1-4].

Caused by active species within the plasma, different reaction paths are conceivable and thus chemical reactions can be observed at comparable low substrate temperatures. To understand plasma-induced reactions, investigations of energy and particle influx onto the substrate have to be combined with analysis of structural properties of the plasma-treated surface.

The present study focuses on the microwave enhanced oxidation and reduction of thin polycrystalline Ni films. Layer characterization was done by grazing incidence x-ray diffractometry (GIXD) and x-ray reflectometry (XR). Basic plasma parameters were determined by Langmuir probe measurements. Hence, information of both, layer properties and plasma characteristics are obtained and enable a detailed description of plasma induced chemical processes in thin Ni layers.

## 2. EXPERIMENTAL

Thin pure Ni coatings (about 20 nm thickness) deposited on Si substrates with 800 nm $SiO_2$ and 1 nm Cr buffer layers were treated by a 2.45 GHz microwave plasma source (SLAN) [5]. Absorbed plasma power was kept constant at 700 W. The experiments were carried out at pressure 50 Pa without external substrate heating. Substrate bias voltage was varied from 0 up to -100 V. Reduction and oxidation cycles were performed using gas mixtures of 10 sccm Ar + 10 sccm $H_2$ or 10 sccm Ar + 10 sccm $O_2$, respectively. After every 30 minutes the samples were taken out of the plasma chamber and characterized by GIXD and XR. For GIXD and XR measurements a Siemens D 5000 θ-2θ diffractometer (Cu-$K_\alpha$ radiation) equipped with a dedicated reflectometry sample stage was used. For GIXD a special parallel beam attachment with Soller collimator and secondary monochromator was applied.

GIXD measurements (asymmetric Bragg case, incidence angle ω = 0.5°) were analyzed regarding position, profile and intensities of observed Bragg reflections. A pseudo-Voigt fit was applied to the measured profile and the domain sizes were. A detailed description of the method is given in [6]. Diffrac$^{plus}$ Leptos 3.03 program package by Bruker AXS was used to determine thickness, density and roughness of the samples from the XR measurements.

With a reference sample thermal annealing experiments were performed at 600°C for 2 h. Thus conceivable thermal induced processes could be monitored.

Langmuir probe (250 µm Cr/Ni wire with active length 3.5 mm) was used for in-situ diagnostics of basic plasma parameters. The probe was situated near by the substrate in non-perturbed plasma volume. Plasma potential $V_p$, electron temperature $T_e$ and electron density $n_e$ were determined by standard methods from measured data: plasma potential was estimated from the zero–cross section of the second derivative, mean electron energy was calculated from the integral of the second derivative of the probe characteristic and electron density was estimated from $I^2_e$ vs. V plot in the electron acceleration regime [7]. No noise-reduce techniques were applied.

## 3. RESULTS AND DISCUSSION

### *3.1 Plasma characterization*

Basic plasma parameters were calculated from Langmuir probe measurements.

Electron temperature and density reach larger values for argon/oxygen compared to argon/hydrogen discharge.

Electron density slightly decreases with increasing negative bias voltage at the substrate (Fig.1), but electron temperature slightly increases (Fig.2). Plasma potential was found to be about 12 V.

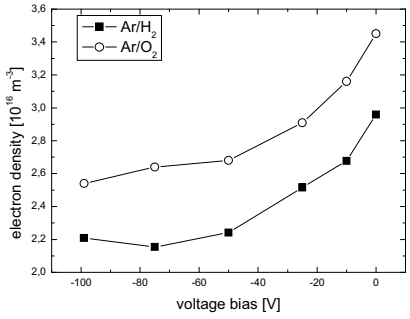


Fig. 1 Electron density depending on bias voltage

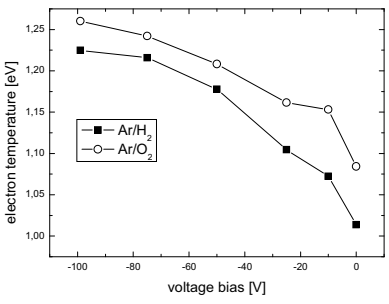


Fig. 2 Electron temperature depending on bias voltage

### *3.2 Layer characterization*

No thermal induced chemical reactions of the Ni samples occur, as could been shown by annealing experiments up to 600°C using a reference sample.

As-deposited films consist of polycrystalline Nickel with mean domain sizes of about 7 nm. However, plasma treatment of the films rapidly results in increasing domain sizes (18 nm) and a mass loss of about 25% for metallic Ni. This result can be explained by sputtering of small Ni particles.

Due to reactive species in the plasma volume like $O^*$, $O^+$, $O_2^+$ or $O^-$ an oxidation of metallic Ni is caused (Fig. 3). This reaction occurs independently of substrate bias. X-ray diffraction measurements show decreasing Ni intensity and increasing NiO reflections. The oxidation stops at a mass ratio of 40% NiO (calculated from integrated intensities). The domain sizes of the formed oxide are found to be 6 nm, i.e. distinctly smaller than size of metallic Ni. Domain sizes of Ni stay more or less constant. AFM measurements show a cauliflower-like structure of the films with small oxide crystallites surrounding the metallic grains (see reference [8]).

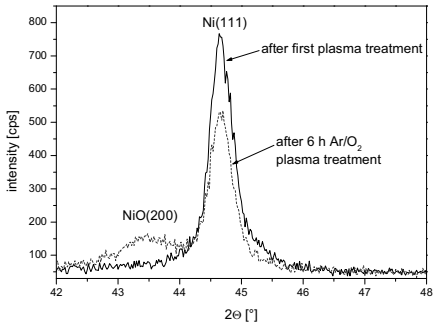


Fig. 3 Formation of NiO caused by Ar/O2 plasma treatment observed by x-ray diffraction measurements

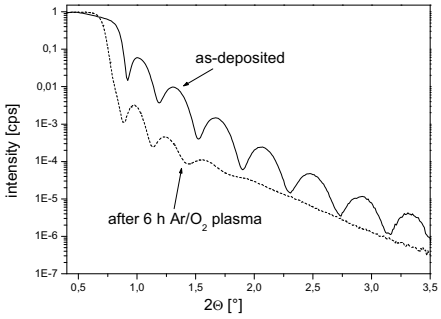


Fig. 4 Reflectometry measurement of untreated film and after 6 h Ar/O2 plasma treatment

Figure 4 compares XR measurements of the untreated (solid line) and 6 h oxygen plasma treated (dotted line) films. For the as deposited film an interference pattern, which is typical for a homogeneous layer is observed. The slow decay of the oscillations pronounced for the as deposited film indicates a small film/air roughness. After oxygen plasma treatment, the frequency of the oscillations increases, indicating a thicker film. Film thickness increases from 20 to 26 nm. Increased thickness through oxidation is expected because of the larger molar volume of NiO compared to Ni. Also, the interference pattern is damped, indicating increased film/air roughness. Furthermore, the critical angle is shifted to much lower values, which is caused by a decreased film density (8.9 g $cm^{-3}$ to 6.2 g $cm^{-3}$. The theoretical densities of NiO and Ni are 6.8 g $cm^{-3}$ and 8.9 g $cm^{-3}$, respectively. That means, the oxidized film includes a certain amount of voids, as it can be concluded from the AFM measurements [8].

The effect of hydrogen plasma treatment strongly depends on applied substrate voltage bias. Without external bias voltage no chemical reactions were observed. Obviously the energy of the impinging activated species is not sufficient enough to induce a chemical reaction. Nickel hydride formation generally requires extreme pressure conditions [9, 10].

However, applying -50 V bias voltage in our experiments induces the formation of $Ni_2H$ in a first step. Subsequently NiH is formed, probably by decomposition of $Ni_2H$ (Fig. 5).

$$2Ni + 1/2H_2 \longrightarrow Ni_2H \text{ and } Ni_2H \longrightarrow Ni + NiH$$

Increasing negative substrate bias voltage to -75 V also results in the formation of NiH besides $Ni_2H$, but NiH is formed much faster.

A possible explanation could be direct formation of NiH from metallic nickel as a second reaction path: $2Ni + H_2 \longrightarrow 2NiH$

Because of the superposition of Ni(111) and $Ni_2H$(101) reflections the reaction mechanisms can not be easily distinguished. However, kinetic investigations analogous to the isoconversional analysis suggest the occurrence of competitive reactions (not shown here, will be published in near future).

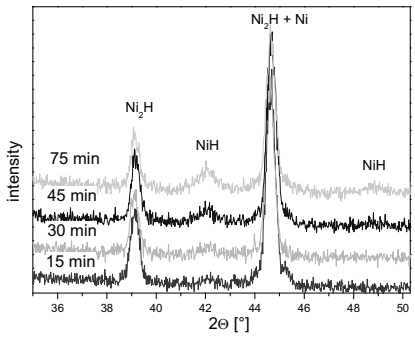


Fig. 5 Diffractometry measurements of $Ar/H_2$ plasma treated sample, substrate bias voltage -50 V

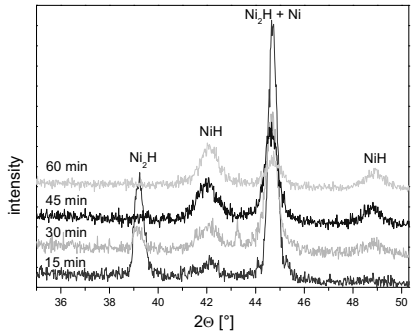


Fig. 6 Diffractometry measurements of $Ar/H_2$ plasma treated sample, substrate bias voltage -75 V

## 4. CONCLUSION

We have shown the effect of low energy plasma on solid Ni-surface layers. Nickel oxide as well as nickel hydride formation can be induced by reactive plasma species. Determination of plasma parameters gives first ideas to understand the processes. Hydride formation occurs faster at -75 V substrate bias, i.e. at smaller electron density but larger electron temperature. Obviously, not the number but first the energy of the plasma species seems to determine the reaction. Nevertheless, especially the plasma induced nickel hydride formation entails further investigations regarding its dependence on substrate voltage.

Electron densities as well as electron temperatures show a similar dependence on bias voltage for oxygen and hydrogen as reactive gases, but only in case of nickel hydride formation the plasma induced reactions change with applied bias. Hence, further investigations have to be done regarding energy and particle influx caused by ions and neutrals.

## 5. ACKNOWLEDGEMENTS

The work was supported by Deutsche Forschungsgemeinschaft (DFG) through SFB TR 24 “Fundamentals of Complex Plasmas”. We gratefully acknowledge the help of Dr. K. Ellmer, Helmholtz Centre Berlin, for preparation of the Ni samples.

## 6. REFERENCES

[1] W. Jacob Thin Solid Films 324 1 (1998)

[2] A. Quade, H. Steffen, R. Hippler, H. Wulff Anal. Bioanal. Chem. 374 720 (2002)

[3] A. N. Itakura, M. Shimoda, M. Kitajma Appl. Surf. Science 216 41 (2003)

[4] J. C. Jiang, K. Lian, E. L. Meletis Thin Solid Films 411 203 (2002)

[5] F. Werner, D. Kozec, J. Engemann Plasma Sources Sci. Technol. 3 473 (1998)

[6] H. Wulff, H. Steffen “Characterization of thin films” in R. Hippler, S. Pfau, M. Schmidt, K.H. Schoenbach (eds.) “Low temperature Plasma Physics” Vol. 2, Wiley VCH, Berlin 2008 (ISBN-978-3-527-40673-9)

[7] S. Pfau, M. Tichy “Langmuir probe diagnostics” in R. Hippler et al. (eds.) “Low temperature plasma physics”, Vol. 2, Wiley VCH, Berlin 2008 (ISBN-978-3-527-40673-9)

[8] M. Quaas, H. Wulff, O. Ivanova, C.A. Helm Surf. Interface Anal. 40 552 (2008)

[9] V.E. Antonov J. Alloys Comp. 330-332 110 (2002)

[10] B. Baranowski, S.M. Filipek J. Alloys Comp. 404-406 2 (2005)

# Surface Layer Morphology of Tungsten-Carbon Thin Films

**N. Radić [1], P. Dubček [1], M. Jerčinović [1], M. Ristić [1], S. Musić [1], A. Tonejc [2], S. Bernstorff [3]**

1. Rudjer Boskovic Institute, Bijenicka 54, HR-10000 Zagreb, Croatia
2. Faculty of Sciences, Department of Physics, Bijenicka 34, HR-10000 Zagreb, Croatia
3. Sincrotrone Trieste, I-34012 Basovizza (TS), Italy

Transition metals carbides, and tungsten carbides in particular, exhibit many properties of interest to technology - high metling point, extreme hardness, low friction coefficient, chemical inertness, oxidation resistance, and good electric conductivity. The surface conditions of these materials are critical for some applications, and preparation processes are optimized to meet such requirements. Surface layer of W-C thin films prepared by reactive magnetron sputtering (argon + benzene) on monosilicon substrates has been examined by GISAXS, AFM and SEM methods. Preparation conditions have been varied in a wide range of deposition parameter values: benzene partial pressure in the 1-10% range, substrate temperature in steps RT, 200°C, and 400°C, and beside deposition onto substrates at floating potential a substrate bias of -70 V has been applied . It was found that WC1-x is a dominant carbide in all prepared films, with (111) preferential orientation in films deposited at room temperature. The surplus/unreacted carbon forms a fine dispersion of graphitic nanoparticles imbedded in the intergranular space. The W-C grainsize is determined at about 3 nm by the GISAXS method, with a very smooth surface - roughness about 0,5 nm - and a very short height-height correlation length at the surface. The AFM examination show roughness depending upon the preparation conditions - from about 0.5 nm on films prepared at low benzene partial pressure increasing towards a few nanometers when high benzene partial pressure was used. A corresponding average lateral grainsize has been estimated at 10-20 nm, revealing a scale-like morphology of the film surface. The SEM results corroborate the surface morphology, but reveal the subsurface film structure: at the top of the film there is a 10-20 nm thick layer which clearly differs from the main body of the film beneath. The "bulk" of the W-C films (about 200 nm thick) consist of columns 50-100 nm in diameter, atop of which there is a continuous segregated fine-structured layer. The observed structural discontinuity in the prepared W-C films inevitably influence their mechanical properties.

# Mass and Energy Spectrometry of Magnetron Plasmas.

**J A Rees [1], T.Whitmore [1], J J Moore [2], J Lin [2], C Muratore [3]**
(1)Hiden Analytical, Warrington U.K.
(2) C.S.M., Colorado, USA
(3)Wright Patterson AFB, Ohio, USA.

The nature and quality of surface coatings deposited from magnetron plasmas are controlled by the mixture of particles arriving at the substrate and by their energies. Direct determination of the particle species and energy distributions as a function of the operating conditions is possible using combined mass/energy spectrometers such as the Hiden EQP and PSM instruments [1 to 4]. The measurements can be used in conjunction with analysis of the surfaces produced to optimise the deposition (or etching) process. To illustrate the range of measurements which can be made, data obtained in a number of magnetron systems are discussed. The simplest measurements allow the identification of the ions (both positive and negative) arriving at the substrate as a function of the plasma conditions, as, for example, in the deposition of hard coatings of titanium nitride and other materials and in the etching of molybdenum in a sulphur hexafluoride plasma. Of considerable assistance in understanding the quality of the films deposited in a magnetron system are measurements of the energies with which the ions arrive at the growing film. This is particularly the case for systems in which the magnetron plasma is either augmented by, for example, the output from an inductively-coupled plasma source, or in which the magnetrons are pulsed. Examples of such data for the growth of optical titanium oxide films, low friction films of molybdenum disulphide, and hard chromium-aluminium nitride surfaces are discussed and compared with selected data for the characterisation of the various surfaces. In the case of pulsed magnetron systems, the strong influence of particular features of the pulsing waveforms is clearly seen and is of considerable importance.

[1] J.A. Rees, Le Vide (Plasma, Surface, Adhesion), p441, 1999.
[2] I.T. Martin, J Zhou, and E R Fisher, J Appl Phys 100, 13301,2006.
[3] C Muratore, J J Moore and JA Rees, Surface and Coatings Tech 163/164, 12, 2003.
[4] J Lin, B Mishra, J J Moore, W D Sproul and J A Rees, Surface and Coatings Tech 201,6960,2007

# A new method for simultaneous determination of the refractive index and thickness of transparent films

**B. Šantić**
R. Bošković Institute, Bijenička 54, HR-10002 Zagreb, Croatia

A novel method is introduced for the simultaneous measurement of the refractive index and the thickness of a transparent film. As the main advantage, the refractive index is evaluated with no prior information about the material, the thickness and the substrate material. The method is based on the shift of the optical interference pattern caused by the swivel of the sample. Besides, an improved expression for the order of extreme is derived. The lowest thicknesses of the film that can be measured is in the ~40-60 nm range, while the upper limit of the thickness is determined by the resolution of the spectrometer. As a further benefit, the boundary surfaces can be slightly rough provided that the roughness does not bleach out the Fabry-Perot interference. The method is illustrated by several model examples. In the two experimental examples, the refractive indices and the thicknesses are measured for a GaN thin film and a cling-film. Although illustrated by the measurements in the 300-1100nm range, the method is by no means restricted to the visible range.

# Investigations on the interfacial strength of chromium adhesion layers in DLC coating systems

**J. Schaufler[1], K. Durst [1], R. Mertens [2], M. Göken [1]**

1. Department of Materials Science and Engineering, University Erlangen-Nürnberg, Germany
2. Oerlikon Balzers AG, Liechtenstein

DLC coatings play an important role in many high load applications. Their unique properties such as hardness, low friction coefficient and chemical inertness make them suitable for such applications. During service, the interfacial strength between the coating and the substrate is of a great importance. A chromium - chromiumcarbid adhesion layer is frequently used to enhance the adhesion between the coating and the steel substrate. Chromium ensures an adequate bonding strength between the coating and the substrate. However, the structure and quality of these adhesion layers mainly depend on the conditions and parameters of the deposition process. In this work a detailed structural characterisation of various adhesion layers with different interfacial strength, ranging from poor to very good has been conducted. The layers have been deposited in a combined physical vapor deposition – plasma enhanced chemical vapor deposition process. As usual, the interfacial strength is determined by a Rockwell-C indentation test. Using focused ion beam and transmission electron microscopy the failure mechanism of the delaminated interface regions are examined.

# Diagnostics of an argon/oxygen magnetron plasma and comparison with Monte Carlo simulation

**M. Gaillard [1], L. Schwaederlé [1], S. Mahieu [2], W. Leroy [2], D. Depla [2], A. Bogaerts [1]**

1. University of Antwerp, Belgium
2. Ghent University, Belgium

A sputter deposition process is a rather complex mechanism, specially in a reactive gas mixture. To understand it properly, it is necessary to separate the different part involved, i.e., the sputtering, the plasma chemistry, the growth of deposited layers... Our work is related to the plasma itself: what kind of chemistry, which influence of the experimental conditions and which relationship does exist between the flux/energy/angular distribution of heavy particles and the homogeneity/charateristics of the growing film. For this study, we have analysed the plasma with two powerful diagnostic tools, a Langmuir probe and a mass spectrometer. The experimental conditions are chosen as the conditions for real deposition. The results of these experiments will be compared with numerical simulation results. For this purpose, we are developing a 3D simulation code whose aim is to give as output the chemistry and flux/energy/angular distribution of heavy particles. The first part of this code is based on the Monte Carlo technique to follow the emitted secondary electrons in front of the cathode and throughout the plasma. The chemistry of the plasma is obtained through the simulation of the collisions encountered by the electrons until they are lost on the walls. The magnetic field has been simulated in 3D and compared with the real one (experimentally measured). The simulations are performed for a reactive environment of argon and oxygen. The main assumption up to now is a fixed electric field throughout the whole simulation, obtained from a particle-in-cell code, developed earlier in the group [1]. This simulation allows to obtain the electron velocity distribution function and the ionization and excitation rates. These results are compared with those obtained by the PIC-MC code mentioned above. The geometry under investigation is a unique magnetron cylindrical planar source, although the goal of the project is to implement soon a flexible geometry allowing complex deposition with two magnetron sources working together. Within this project, the balance equations for every plasma species and another Monte Carlo module for the heavy particles will also be developed in order to obtain the energy and angular distribution functions for heavy particles and their fluxes towards the substrate.

[1] I. Kolev, A. Bogaerts, R. Gijbels, Influence of the electron recapture by the target on the discharge characteristics in dc planar magnetrons, Physical Review E 72, (2005) 05642

# The effect of ITO film thickness on the microstructure evolution and crystallization kinetics during annealing

**N. Shevchenko, A. Rogozin, M. Vinnichenko, A. Kolitsch, W. Moeller**
Research Center Dresden-Rossendorf, Institute of Ion Beam Physics and Materials Research

Amorphous indium tin oxide (ITO) films have been grown by reactive pulsed medium-frequency dual magnetron sputtering on Si substrates covered with $SiO_2$. The real-time evolution of the ITO film structure during annealing has been investigated by synchrotron X-ray diffraction at ROssendorf Beam Line (ROBL) located at the European Synchrotron Radiation Facility in Grenoble, France. The annealing experiments have been carried out in a UHV annealing chamber equipped with a beryllium dome at a constant temperature of 310 °C. The XRD experiment has been performed in Bragg–Brentano geometry over a range of scattering angles of 27° to 37°. The incident X-ray beam has been monochromatized to 8.048 keV ($\lambda$=0.154 nm). An in situ four-point probe technique has been used to characterize the film resistivity. The microstructure of the annealed films has been examined by transmission electron microscopy (TEM). This work is focused on the effect of ITO film thickness on the crystallization kinetics during annealing. Three series of samples with thicknesses of ~50, 170 – 180, and 310-320 nm have been investigated. The evolution of the (222) and (400) peaks of the $In_2O_3$ phase has been monitored. The time dependence of the integral intensity of these peaks exhibits an s-like shape, which is typical of a crystallization process. The XRD data have been analyzed in the frame of the Kolmogorov – Johnson – Mehl – Avrami (KJMA) model. The activation energy and the kinetic parameters of the crystallization process have been determined. The value of the KJMA exponent of about 2 obtained for all ITO films points toward two-dimensional grain growth in the site saturated mode. However, detailed TEM studies of partly crystallized ITO samples display two-dimensional grain growth only during the crystallization of the 50 nm ITO films. In contrast, the thicker films show two stages of crystallization. During the first stage, the single grains grow from the film surface to the interface, after which lateral growth of the grain has been observed to occur. The KJMA model is unable to predict the difference in the crystallization kinetics for films of different thicknesses. The specific film anisotropy and the limited thickness are discussed as the main reasons for the change in the crystallization kinetics. The film resistivity decrease correlating with the film crystallization depends non-linearly on the degree of crystallization.

# Investigation of Ta-Ti-silicide films prepared by magnetron cosputtering and radio-frequency heating

**S. Rosenberg, M. Sinder, J. Pelleg**
Materials Engineering Department, Ben Gurion University of the Negev

The formation of disilicides of titanium and tantalum on silicon substrate is of interest because of their low resistivity which is an important quality in microelectronics. Previous studies have reported the formation of titanium and tantalum disilicides without any phase separation. On the other hand, no ternary compound formation was reported. Characterizing the nature of such film is important for determining whether a truly ternary phase (Ti, Ta)$Si_2$ is formed or just solution of Ti or $TiSi_2$ (up to 50%) in the $TaSi_2$ phase occurs. Co-deposited Ta and Ti on Si (111) and Si (100) substrates were fabricated using high vacuum sputtering equipment. Post deposited samples have undergone XRD, sheet resistance, AES characterization, optical microscope (OM) and SEM techniques. Thin conducting films were heat treated by induction heating which is a rapid thermal process (RTP). Basically the process consists of placing a film on a silicon substrate and applying a radio-frequency magnetic field perpendicular to the film surface [1]. The above mentioned analysis was also applied to the samples following RTP. In samples which were heated up to the melting point of silicon parallel strips were observed by OM. The causes of the strip formation are discussed.

[1] M. Sinder, J. Pelleg, V. Sokolovsky, V. Meerovich, RF heating of the conductor film on silicon substrate for thin film formation, Materials Science and Engineering A 302, pp. 31–36 (2001)

# Periodically arranged tin and tin oxide nanoparticles

**Z. Stryhal [1], M. Stofik [2], J. Maly [2], J. Pavlik [1]**
1. J. E. Purkinje University, Department of Physics, Ceske mladeze8, 40096 Usti nad Labem, Czech Republic
2. J. E. Purkinje University, Department of Biology, Ceske mladeze8, 40096 Usti nad Labem, Czech Republic

We report fabrication of highly organized nanostructured tin and tin oxide layers on silicon, silica and glass substrates by combination of nanospheric lithography and PVD tin deposition. Template mask was prepared by self-assembling of carboxylated polystyrene (PS) nanoparticles (NPs) of variable diameters by dip-coating method. The process of mask assembling was optimized and highly reproducible deposition of organized mono and bilayer of PS nanoparticles was achieved in several tens square millimeters. Vacuum evaporation of tin and subsequent mask displacement resulted in highly organized, trigonally or hexagonally arranged arrays of tin NPs. Diameter, shape and interparticle distance varied depending on type of mask used. Almost spherical NPs were prepared by treatment of nanostructured surfaces in RF argon plasma. Tin oxide nanostructured layers were subsequently obtained by plasma oxidation in $Ar/O_2$ mixture. Both types of nanoarrays were characterized for their topographic (AFM) and chemical (XPS) properties. Presented nanostructures can be utilized for development of sensitive sensors as well as model system for research in gas sensing, catalysis and biosensing principles

## 1. INTRODUCTION

Tin oxides are used for decades in wide range of applications, mostly in transparent conductive layers, gas sensors and catalysts. Although this material is frequently utilized, mechanism of its functionality is not well understood in many cases, so there is still place for research which can improve qualities and performance in many applications.
Sensing performance can be significantly improved when the sensor consist of periodic arrays of active structures and empty regions. There are several important requirements for manufacturing of nanostructured surfaces for gas sensors or biosensors. Generally, submicron resolution, high-throughput and low cost fabrication method is necessary for analytical devices production. Nanotopographic pattern should usually occur over a large surface area (even several sq. centimeters) and it should be well reproducible and without any defects.
Low cost nanopatterning technique called nano-sphere lithography (NSL) shows many applications in various fields where large numbers of periodical nanosized features are required. NSL method employs self-assembling processes of nanometer scale spherical particles over large area on planar substrate and several different steps of plasma etching and deposition processes, for the creation of polymeric or metallic nanostructures. Main advantage of the method is ability to independently control the size, shape and coverage of particles over large areas ($cm^2$), low cost and simplicity of preparation.

## 2. EXPERIMENTAL

### *2.1 Materials*

Microscope glass slides, silica glass slides and boron doped silicon (100) wafers were used as substrates for PVD deposition. Carboxylated polystyrene spherical microparticles with diameter 40, 200, 600 and 1000 nm (Duke Scientific) were used for mask deposition. Argon (99.9999 %), oxygen (99.995 %) and nitrogen (99.995 %) compressed gases (Linde) were used for cleaning and plasma treatment. Solutions were prepared in ultrapure water with conductivity below 1 $\mu S.cm^{-2}$ (Goro Pharmapur system). All used chemicals were of analytical grade.

### *2.2 Polystyrene microparticles deposition*

Substrates were cut to 15×15 mm pieces and cleaned in acetone and deionized water in ultrasonic bath and dried under stream of pure nitrogen.
Template mask was prepared by self-assembling of polystyrene particles on planar substrates. Dip coating method was performed with self-made apparatus which allows to withdraw the sample from microparticle solution (volume 1.5 ml) at speed 1.25–12.5 $mm.min^{-1}$. Substrate was fixed in sample holder and immersed completely into microparticle solution and elevated by defined velocity. After completing the lift, we kept the sample for 1 hour under ambient laboratory conditions to let the remaining water evaporate.

### *2.3 Mask removal*

The mask was removed by ultrasonic bath in water (10 seconds) or in $CHCl_3$ (1 hour). Procedure was repeated 3 times in fresh liquid. We also tried dry mask removal by utilization of RF excited plasma (10 W) in argon (100 Pa) and it was found effective. Ultrasonic bath in water was mostly used for the mask removal.

### *2.4 Tin deposition*

Tin nanostructures were obtained by vacuum thermal evaporation of metallic tin over microparticle mask. Two-chamber vacuum system designed for evaporation (chamber 1) and plasma oxidation (chamber 2). The system's ultimate pressure is $10^{-7}$ Pa. Tin was evaporated from molybdenum boat heated directly by AC current (~ 100 A). The sample was fixed 15 cm above evaporation boat. Deposition rate was kept at ~ 5nm/min, controlled by crystal thickness monitor. Pressure during deposition was maintained at $10^{-2}$ Pa by turbo pump.

### *2.5 Tin oxidation*

The tin oxides were obtained by plasma oxidation of metallic tin in RF discharge (13.56 MHz, 35 W, quartz tube ø 25 mm) in $Ar/O_2$ (4:6) mixture at pressure 100 Pa (maintained by gas flow meters and rotary pump).

### *2.6 AFM measurements*

AFM characterizations were performed using atomic force microscope Integra Probe Nanolaboratory (NT-MDT). All measurements were performed in semi-contact mode in air. HA_NC ETALON silicon cantilevers with resonant frequency 280 kHz, tip radius <10 nm and force constant 11.5 N/m provided by NT-MDT were used.

### *2.7 XPS measurements*

Tin and tin oxide nanostructures were analyzed for their chemical composition by custom made X-ray photoelectron spectroscope (X-ray source: Specs XR 50, input power 200 W, Al/Mg anode, no monochromator; Electron energy analyzer: Specs PHOIBOS, hemispherical, single channeltron; System's ultimate pressure: < $10^{-8}$ Pa).

## 3. RESULTS AND DISCUSSION

### *3.1 Mask preparation*

Experiments with drop coating method for polystyrene particles deposition were not successful. We were not able to obtain mono or double layer of particles of desired quality at any conditions (concentration, solvent, amount of solution, evaporation speed).

Unlike drop coating, dip coating method was found to be usable. It is easy to get relatively large area (> 20 $mm^2$) consisting of well ordered particles. Thickness of the layer may be tuned through sample elevation speed. Monolayer of ø 200 nm polystyrene spheres may be deposited at speed 2.5 mm/min, while double layer at speed 1.8 mm/min. Comparable results may be obtained with slightly higher speeds (+10 %) for spheres with diameter of 600 nm. Solution of 40 and 1000 nm particles were not found usable due to high dispersion of particle size.

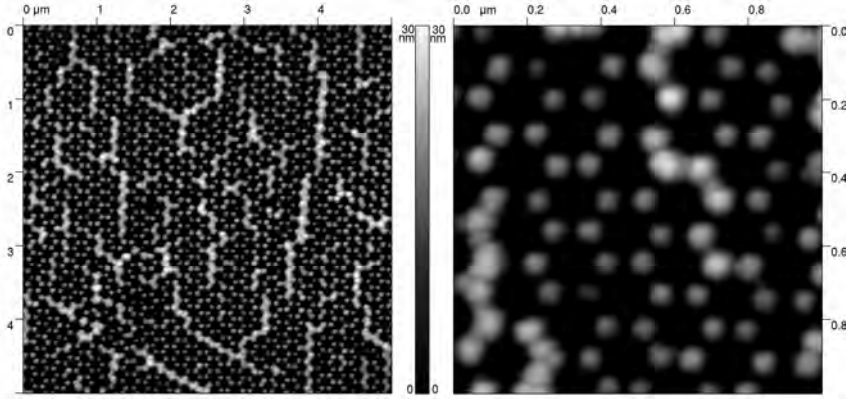


Figure 1. Tin nanoparticles prepared by evaporation over monolayer mask made of 200 nm spheres. AFM images, 5×5 µm left, 1×1 µm right.

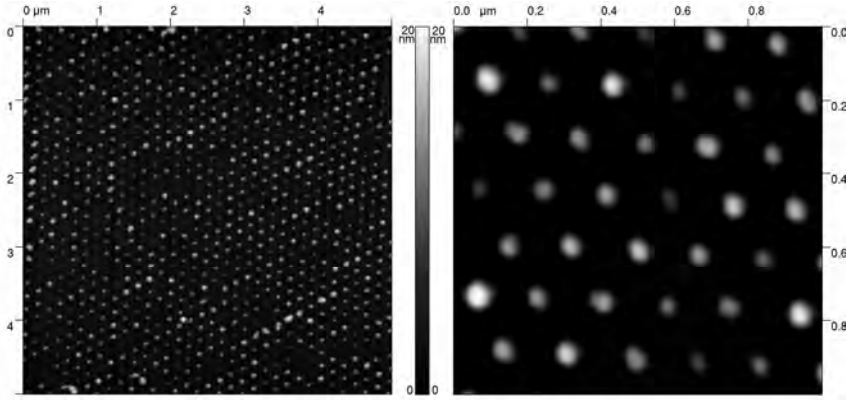


Figure 2. Tin nanoparticles prepared by evaporation over double layer mask made of 200 nm spheres. AFM images, 5×5 µm left, 1×1 µm right.

### *3.2 Tin and Tin oxide nanoparticles*

Tin layers of different thicknesses were evaporated to substrates covered by mono or double layer of polystyrene spheres (ø 200 nm spheres: 10 nm, 15 nm, 20 nm, 25 nm; ø 600 nm spheres: 25 nm, 30 nm, 40 nm). Two well defined types of periodical arrangements were observed after mask removal, hexagonal alignment for mono layer mask (Fig. 1) and trigonal alignment for double layer mask (Fig. 2).

Tin particles are round shaped in all cases when 200 nm mask is used. In case of 600 nm mask, only double layer mask usage results in round shaped tin particles. We found, tin clusters may be transformed to round shaped (Fig. 3) by combination of heat (250˚C) and argon plasma treatment (RF, 50 W, 30 Pa). Transformation does not occur just by heating above tin melting point, because surface oxide layer prevents the tin sub particles putting together.

Plasma oxidation of tin highly ordered particles was found functional. We also found that tin particles of height < 10 nm are almost fully oxidized if exposed for few hours to atmosphere (Fig. 4).

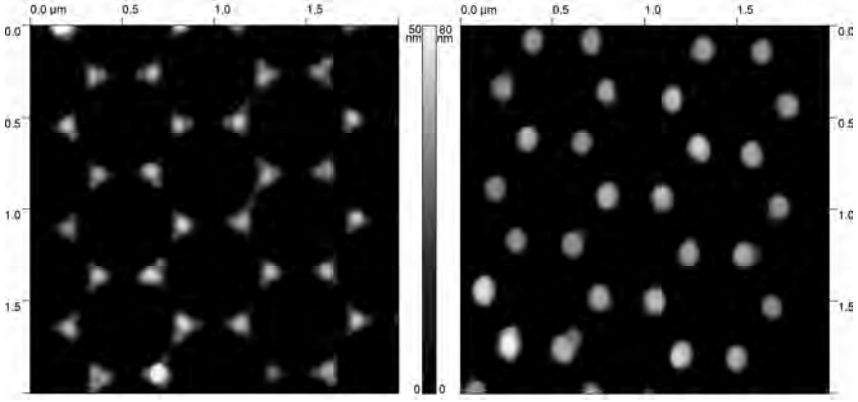


Figure 3. Tin nanoparticles prepared by evaporation over double layer mask made of 600 nm spheres, as prepared on the left, transformed to rounded shape on the right. AFM images 2×2 µm.

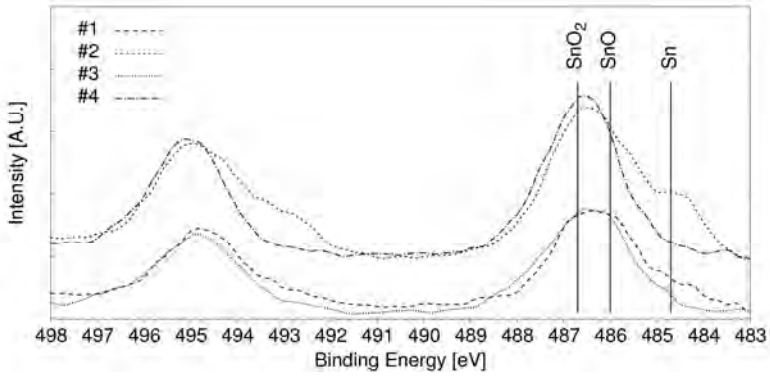


Figure 4. XPS spectrum of Sn 3d electrons. #1 particle height 8 nm, as prepared; #2 particle height 24 nm, as prepared; #3 particle height 8 nm, after plasma oxidation; #4 particle height 24 nm, after plasma oxidation.

## 4. ACKNOWLEDGMENT

This work was supported by The Ministry of Education of Czech Republic (Project LC 06041) and by AS CR (Projects KAN 400720701and KAN 200520702)

# Optical Switching Property of All-Solid-State Switchable Mirror with Proton Conductive Tantalum Oxide Thin Film Deposited by Reactive DC Magnetron Sputtering

**K. Tajima, Y. Yamada, S. Bao, M. Okada, K. Yoshimura**
National Institute of Advanced Industrial Science and Technology (AIST), Nagoya, Japan

Switchable mirrors are expected to apply for new energy-saving window. They can change their optical property from reflective to transparent states reversibly due to dehydrogenation and hydrogenation of functional thin films [1, 2]. Their states change control the inflow of heat from solar radiation into the room effectively. Recently, we develop and research two-type switchable mirrors. One is a gasochromic-type which switches its state by using dilute hydrogen gas [3, 4]. The other is an electrohromic-type which switches its state by electrically [5]. Especially, the electrochromic-type switchable mirror is composed of all-solid material in the view point of easy handling. The device has a multi-layer of Mg-Ni/Pd/Al/$Ta_2O_5$/$WO_3$/ITO on transparent substrate such as glass and polymer sheet [6, 7]. Each material of Mg-Ni, Pd, Al, $Ta_2O_5$, $WO_3$ and ITO acts as optical switching, proton injector, buffer, solid electrolyte, ion storage, transparent conductive layers, respectively. All film was fabricated by using dc magnetron sputtering at room temperature. When a voltage was supplied to the device, the protons in the ion storage layer moved to the optical switching layer, and the layer was hydrogenated to be hydrides, resulting in transparent state. Therefore, it changed its transmittance from reflective of 0.1% to transparent states of 48% within 10 s due to the hydrogenation of the film. It also had a durability of over 4000 cycles of switching. Its optical switching property was significantly affected by the electrochemical property of proton conductive $Ta_2O_5$ thin film [8]. In practical use of the device, the electrochemical property of $Ta_2O_5$ thin film is one of the most important properties for switching speed and stability. Though we researched its property suitable for the device, the evaluation was insufficient. In this research, we fabricated $Ta_2O_5$ thin film by using reactive dc magnetron sputtering, and investigated an effect of its property on the optical switching property of the device in detail.

[1] J. N. Huiberts, R. Griessen, J. H. Rector, R. J. Wijngaargen, J. P. Dekker, D. G. de Groot, N. J. Koeman Nature 380 231 (1996)
[2] T. J. Richardson, J. L. Slack, R. D. Armitage, R. Kostecki, B. Farangis, M. D. Rubin Appl. Phys. Lett. 78 3047 (2001)
[3] K. Yoshimura, Y. Yamada, M. Okada, Appl. Phys. Lett. 81 4709 (2002)
[4] S. Bao, Y. Yamada, K. Tajima, M. Okada, K. Yoshimura Jpn. J. Appl. Phys. 45 L588 (2006)
[5] Y. Yamada, K. Tajima, S. Bao, M. Okada, K. Yoshimura Jpn. J. Appl. Phys. 46 5168 (2007)
[6] K. Tajima, Y. Yamada, S. Bao, M. Okada, K. Yoshimura Appl. Phys. Lett. 91 051908 (2007)
[7] K. Tajima, Y. Yamada, S. Bao, M. Okada, K. Yoshimura Appl. Phys. Lett. 92 041912 (2008)
[8] K. Tajima, Y. Yamada, K. Yoshimura J. Electrochem. Soc. 154 J267 (2007)

# Thin hematite films: structural, microstructural and Mössbauer characterization

**C. Van Cromphaut [1], E. De Grave [1], L. Presmanes [2], A. Barnabe [2], P. Tailhades [2], V.G. de Resende [1], R.E.Vandenberge [1]**

1 Ghent University

2 CIRIMAT UMR CNRS 5085

Hematite ($\alpha$-$Fe_2O_3$) has been studied extensively in numerous papers. Special attention has been given to the Morin transition, i.e., the transition from a weakly ferromagnetic (WF) to an antiferromagnetic (AF) state in which the spins turn from the (111) basal plane to the [111] direction on lowering the temperature. The transition is influenced by particles size, pressure, and substitution by foreign elements such as Al, Mn, Ti, etc. In order to study the transition, thin films have been prepared with different thickness. Thin films can have large intrinsic and thermal stress and their properties often differ from the bulk analog. Therefore, it is believed that also the behavior of the Morin transition will be different in thin films, especially when the thickness becomes very small. For this study, $\alpha$-$Fe_2O_3$ films with different thickness (20 – 500 nm) have been RF-sputtered on quartz glass substrates from a hematite target. The sputtering was carried out in a pure argon gas flow. After the deposition stage, the samples were annealed at a temperature of 650 °C in order to recover the stoichiometry of hematite. Mössbauer spectroscopy is an excellent tool for studying hematite because both the AF and WF phase can be readily distinguished. The surface variant ILEEMS (Integral low-energy electron Mössbauer spectroscopy) is sensitive to the surface and is used to study the behavior of the Morin transition in the films. It is found that the temperature, at which the Morin transition occurs (~260 K for bulk hematite), is lowered when the film becomes thinner. For the very thin films (20 nm) the transition is even absent down to 160 K. The distribution of the hyperfine field of the WF state of the thin films has two distinct maxima, suggesting that two phases are present in the film. These two contributions can be caused by differences in defect structure, surface roughness, particle size…

# Adhesion of very thin silica passivation coatings on cold rolled steel

**T. Van der Donck [1], M. Muchlado [1], R. Hausbrand [2], J.P. Celis [1]**

1. Katholieke Universiteit Leuven, Department MTM, Kasteelpark Arenberg 44, 3001 Leuven , Belgium

2. ArcelorMittal R&D Industry Gent – OCAS N.V., John Kennedylaan 3, 9060 Zelzate, Belgium

An important trend in actual surface engineering is to achieve unique combinations of surface-related properties on common base materials. Our research aims to investigate the use of sub-micrometer thick SiOx layers for the corrosion protection of steel sheets. Dense films with good barrier properties can be deposited with vapour phase processes. In the case of steel sheets, good adhesion of passivation coatings is mandatory, because during processing the steel sheet is often subjected to mechanical stresses and even plastic deformation.

In this presentation, the focus is on the characterization of the mechanical properties and adhesion of sub-micrometer silica layers (thickness between 20 nm and 100 nm) to the steel substrate. This demanded the elaboration of a suitable scratch testing methodology, requiring mN and sub-mN normal forces. Next to SEM analysis of the scratch track, the occurring tangential forces provide additional information on the adhesion of these film/substrate systems in contact with a Berkovich indenter. The results are compared to results obtained with industrial deformation testing. First evaluation of the corrosion barrier performance of such thin films is presented based on electrochemical transient measurements.

# Structural Hierarchy in Nanotubular Oxide Films

**N.M. Yakovleva [1], A.N. Yakovlev [2], E.A. Chupakhina [1], A.N. Kokatev [1]**
1. KSPU
2. Petrozavodsk University

Anodic oxidation is a commonly used method for surface treatment especially in forming self-organized porous alumina structures. Similar to anodic alumina self-ordered titania nanotubes can be fabricated by anodization. Nanotubular anodic titania is a very promising material for applications in many scientific and technological areas. However in contrast to the anodic porous alumina detailed film growth mechanism to get such oxide semiconductor as titania by anodization has not been well understood.
In the present work we studied growing behavior of amorphous nanotubular anodic oxide films on titanium in various electrolytes with focusing on their structural analysis on two scales, atomic (mutual atom arrangement), and mesoscopic (mutual pore arrangement).
Titania nanotubes (TNT) were obtained via constant voltage anodization in fluoride containing electrolytes such as $H_2SO_4/NH_4F$ aqueous solutions and water-free electrolytes on the base of ethylene glycol and glycerol added $NH_4F$. TNT was characterized by means of x-ray diffraction (XRD), transmission electron microscopy (TEM) and atomic force microscopy (AFM) as well as Fourier transform infrared spectroscopy (FTIR). The short-range order parameters of atomic structure were calculated by pair-function method from XRD data. To obtain the qualitative data concerning the size, form and mutual arrangement of the pores (mesoscopic order parameters) observed on the oxide surfaces the computer procession of TEM- and AFM-images was developed. Finally on the base of two-levels structural analysis the views on the peculiarities of forming mechanism of self-ordered titania connected with competition of oxide growth and dissolution under assistance of the electric field were developed.

# Optical properties of switchable mirrors based on magnesium alloys measured in situ by spectroscopic ellipsometry

**Y. Yamada, K. Tajima, S. Bao, M. Okada, K. Yoshimura**
National Institute of Advanced Industrial Science and Technology (AIST), Anagahora 2266-98, Shimoshidami, Moriyama-ku, Nagoya 463-8560, Japan

Metal-hydride switchable mirrors change their optical properties reversibly between transparent and reflective states as a result of hydrogenation and dehydrogenation of the films. A promising application for these coating is in smart windows, which can save energy for air-conditioning. To estimate energy-saving effect as utilizing switchable mirrors to buildings precisely, it is necessary to evaluate the optical indices of component materials of a switchable mirror in the transparent and reflective states. In this study, we have measured the optical indices of Mg alloys and their hydride *in situ*, which are main components of switchable mirrors, using spectroscopic ellipsometry. Switchable mirrors are prepared using dc-magnetron sputtering on quartz substrates using dc-magnetron sputtering in a pure Ar atmosphere without substrate heating. Ellipsometric $\Psi$ and $\Delta$ spectra were acquired with flowing 4% $H_2$ in Ar or dry-air in the range from 0.7 to 3.3 eV using light with three different angles of incidence: 50°, 60° and 70°, to the films using a J.A. Woollam M2000 ellipsometer. Although the optical indices n and $\kappa$ of a Mg-Ni alloy increase with decreasing photon energy, those of their hydride decrease with photon energy and the k-value decreases drastically with hydrogenation. On the day we will also report the Ni concentration dependence on optical properties.

# High-speed STM for real-time observations during electrochemical deposition

**Y. Yanson, M. J. Rost**
Leiden University, Kamerlingh Onnes Laboratory, P.O. Box 9504, 2300RA Leiden, The Netherlands

Besides vacuum deposition, electrochemical deposition is an important thin film growth technique, especially if referring to its vast use in industry. Information on the surface properties (like roughness, structure, or chemical composition) of the electrochemically deposited films can be obtained by various ex-situ and in-situ techniques. However, these techniques are usually averaging over a large surface area and are clearly lacking crucial information on the atomic scale. Unrevealing the fundamentals of electrochemical deposition requires a high-speed acquisition technique that delivers spatial resolution on the atomic scale, thereby enabling the direct observations of dynamic processes that take place during the deposition process. We present our ideas on a new, high-speed electrochemical scanning tunnelling microscope (EC-STM) that allows conducting in-situ, real-time, atomic-scale observations during the plating process. Next to a high-speed electronics that allows high data acquisition rates and fast feedback, the most important part of such an instrument is its mechanical design. We applied finite element analysis (FEA) calculations to optimize the microscope as well as a special electrochemical flow cell in terms of internal resonance frequencies. Finally we discuss remaining problems that have to be solved in order to design the ultimate, high-end EC-STM.

***The organizing committee wish***

***to thank also following sponsors:***



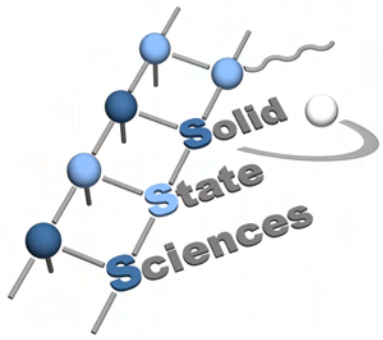



***and the research communities***

***“Surface Modification of Materials”***

***“Structural and chemical characterisation of materials on the micro and nano scale”***

# Effects on deposition rate when varying the magnetic field strength in magnetron sputtering

**M. Aiempanakit, D. Lundin, P. Larsson, D. Jädernäs, U. Helmersson**
Plasma & Coatings Physics Division, IFM-Materials Physics, Linköping University, SE-581 83 Linköping, Sweden

The effects on the deposition rate of Ti thin films, when varying the magnetic field strength, have been investigated by direct current magnetron sputtering (dcMS) as well as by high power impulse magnetron sputtering (HiPIMS). It was found that the magnetic confinement is a key parameter for controlling the deposition rate, and particularly so in the HiPIMS case. The experimental findings verify that the magnetic configuration can easily be optimized to achieve an increase in deposition rate of at least 50 % for both dcMS and HiPIMS. Moreover, it was found that the deposition rate fraction, $R_{side}$ / $R_{front}$, *i.e.* the rate at the side of the cathode (perpendicular to the target surface) divided by the rate in front of the target (parallel to the target surface), increases in HiPIMS when increasing the magnetic field strength, but not so for dcMS. This is in line with previous reports on a recently discovered anomalous transport in HiPIMS [1], which is further developed here. The results lead to the conclusion that the deposition rate in HiPIMS can be tailored by a suitable magnetic field configuration.

[1] D. Lundin, P. Larsson, E. Wallin, M. Lattemann, N. Brenning, U.Helmersson, Plasma Sources Sci. Technol. 17, 035021 (2008)

# Effect of Xe-ion irradiation on structural and magnetic properties of Co/Si bilayers

**N. Bibić [1], K. Zhang [2], N. Milinović [1], K.P. Lieb [2]**
1. VINČA Institute of Nuclear Sciences, 11001 Belgrade, Serbia
2. Physikalisches Institut, Georg-August-Universität Göttingen

Ion-irradiation of ferromagnetic thin films induces pronounced changes of their microstructure and micromagnetism, due to the high local energy deposition, which produces radiation defects and spikes. We report here on the results of a study in which Co/Si bilayers were irradiated with 200-keV Xe-ions. The 30 or 55 nm Co layers of 99.99% purity were deposited by electron-beam evaporation on crystalline Si(100) wafers or Si substrate having a thin evaporated a-Si interlayer. After deposition all irradiations were performed at room temperature to fluences of up to $1.5x10^{16}/cm^2$. The structural changes and phase formation induced by irradiation were analyzed by Rutherford backscattering spectroscopy (RBS) and X-ray diffraction analyses (XRD). The in-plane magneto-optical Kerr effect was used to investigate the changes in the magnetic properties (MOKE). The magnetic properties were correlated with the ion-induced structural changes in the Xe ion-irradiated Co/Si bilayers.

# Influence of the Magnetic Field Configuration on the Reactive Sputter Deposition of TiN

**F. Boydens, S. Mahieu, D. Depla**
Ghent University, Department of Solid State Sciences, Krijgslaan 281 (S1), 9000 Gent, Belgium

Various titanium nitride films were deposited on stainless steel samples by DC reactive sputter deposition using an unbalanced circular magnetron. The degree of unbalancing could be varied by adjusting the magnet configuration in order to investigate the influence on the film microstructure. The degree of unbalancing was characterised by the ratio of the magnetic fluxes above the inner and outer magnet, which were calculated using the FEMM software package. For each magnet configuration several depositions were carried out at different nitrogen flows. The crystallographic out-of-plane orientation of the samples was determined by X-ray diffraction. We observed the much reported transition from a [111] to a [200] out-of-plane orientation with increasing nitrogen flow as well as a shift in the critical flow due to the varying degree of unbalancing. This could be explained by measuring the ion-to-atom ratios towards the substrate. We noticed that both the magnet configuration and the nitrogen flow have a strong influence on the ion-to-atom ratio.

# Preparation of copper telluride layers by an electrochemical approach

**F. Caballero-Briones [1,2,3,a] A. Palacios-Padrós [1,2], J.L. Peña [4], F. Sanz [1,2,3]**

[1] Universitat de Barcelona, Department of Physical Chemistry, Martí i Franquès 1, 08028 Barcelona, Spain

[2] CIBER-BBN, María de Luna 11, 50018 Zaragoza, Spain

[3] Institute for Bioengineering of Catalonia (IBEC), Edifici Hèlix, Baldiri i Reixac 15-21, 08028 Barcelona, Spain

[4] CINVESTAV-IPN Unidad Mérida, Department of Applied Physics, Km 6 Car. Antigua a Progreso, 97310 Mérida, México

[a] On leave from CICATA-IPN Unidad Altamira, Km 14,5 Carr Tampico-Puerto Industrial, 89600 Altamira, Tamps, México

Cu(I) chalcogenides (Cux-X, X=O, S, Se and Te) are promising candidates to cheaper and less toxic devices that could be useful alternatives to Cd chalcogenides. $Cu_2O$ include applications such as nanocrystalline $Cu_2O$-based solar-cells, transparent conductive oxides and resistive random access memories between other. $Cu_2Se$ has also applications on energy generation.

$Cu_2Te$ is a p-type semiconductor with a band gap of 1.1 eV, suitable for solar energy applications, microwave shielding coatings and photodetectors. Particularly, $Cu_{1.4}Te$ has been proposed as a key phase that promotes the efficiency of the CdTe/CdS solar cells as back contact. The preparation of $Cu_xTe$ has been reported by modified-chemical bath deposition (MCBD), by electrodeposition (ED), and by direct reaction of Cu evaporated on the top of Te-enriched CdTe.

Preparing $Cu_xTe$ films by Cu anodization would lead to interesting advantages such as an efficient natural electronic back contact and the development of a controlled fiel-induced doping. In previous works we have prepared submicron thick, polycrystalline, p-type $Cu_2O$ films with good photoconductive properties using an electrochemical routine based on Cu anodization in alkaline media and found that the growth of a thick layer proceeds mainly by solid state reation.

In this work we prepared polycrystalline $Cu_xTe$ layers onto Cu substrates by a combined electrochemical routine that leads to $Cu_xTe$ formation in a solid state reaction. Aqueous Te (IV) was used as Te precursor and polycrystalline Cu disks as substrates. The obtained layers were characterised by X-ray diffraction and the results show the presence of single phase, crystalline $Cu_{2-x}Te$ in the weissite form when a single reduction sweep was performed. Using a combination of slow reduction and anodization, evidence of multiple phases such as $Cu_{1.75}Te$, $Cu_{2.72}Te$ and $Cu_7Te_5$ was observed, confirming the feasibility of our approach to grow $Cu_xTe$ films with a doping gradient. The morphology and optical characterization of the layers will be also presented.

# CFD simulations for a low-pressure hot wall CVD-reactor

**K. De Bruyn, P. Cosemans**
1. SIRRIS, Wetenschapspark 3, 3590 Diepenbeek, Belgium

In casting, extruding, forming and other industrial operations that use dies or moulds, thin ceramic coatings deposited by Physical Vapour Deposition (PVD) or Chemical Vapour Deposition (CVD) are often used to protect the mould surface from corrosive, abrasive or adhesive wear. In general CVD is more suitable to deposit uniform and dense coatings on complex geometries because the process operates at higher pressures than the PVD process.
However, even with CVD, obtaining a uniform coating thickness on complex geometries is not straightforward. To avoid several trial-and-error coating runs to optimize the deposition parameters, Computational Fluid Dynamics (CFD)-software can be used to simulate the CVD process. Numerical calculations have been carried out to simulate the deposition process of tungsten metal coatings in an industrial low-pressure hot wall CVD reactor with diameter 550 mm and height 700 mm.
Depositing a uniform CVD coating requires well defined deposition parameters (such as temperature, pressure, gas flow) at the surfaces to be coated. To make sure that the optimal temperature prior to the actual deposition process is reached the temperature distribution within the reactor as a function of time was simulated and compared with experimental data.
Furthermore, assuming a constant temperature, the coating thickness of the W coating as a function of time was simulated and again compared with experimental data.
Finally, the gas flows within the reactor were simulated to verify that all gasses reached all functional surfaces.

# Deposition of Metallic Nanoparticles on Carbon Nanotubes using Atmospheric Plasma

**F. Demoisson [1], A. Felten [2], A. Mansour [3], H.-N. Migeon [3], J.J. Pireaux [2], F. Reniers [1]**

1. Université Libre de Bruxelles, Faculté des Sciences, Service de Chimie Analytique et Chimie des Interfaces (CHANI), CP 255, Boulevard du Triomphe 2, B-1050 Bruxelles, Belgique
2. Facultés Universitaires Notre-Dame de la Paix, Laboratoire Interdisciplinaire de Spectroscopies Electroniques (LISE), 61 Rue de Bruxelles, B-5000 Namur, Belgique
3. Centre de Recherche Public – Gabriel Lippmann, Département Science et Analyse (SAM), 41 rue du Brill, L - 4422 Belvaux, Luxembourg

The interest of metallic nanoparticles in the nanocatalysis and nanosensors fields is growing. Carbon nanotubes decorated with metallic nanoclusters could present interesting properties in catalysis or/and in devices based on catalytic reaction such as chemical gas sensor. Indeed, carbon nanotubes have already been highlighted as promising gas sensing candidates due to their unique properties such as one dimensional electronic structure and high surface to volume ratio. In the "Nano2Hybrids" European research project (www.nano2hybrids.net), carbon nanotubes decorated with metallic cluster nanostructures are proposed as prototype systems for molecular recognition at the nanoscale. Although the sensor response from a number of pristine and functionalized single wall carbon nanotubes (SWNT) gas sensors have already been demonstrated, little attention has been paid to metal decorated nanotubes. It is generally accepted that the carbon surface must be activated, either by the creation of surface defects and/or by the adsorption of reactive species, such as oxygen containing groups. Most of the time, activation is carried out using wet chemistry techniques, such as hot nitric acid solutions. Some studies present activation and deposition experiments using vacuum techniques with ion guns, low pressure plasma, and/or thermal evaporators. The originality of this work is to operate with an atmospheric plasma torch running in the RF mode (13.56 MHz) using argon like plasma gas and metallic colloids solutions. The challenge of the proposed plasma treatment is to deposit gold, platinum, rhodium and nickel nanoparticles with an average diameter between 10 and 4 nm on multiwall carbon nanotubes (MWCNTs) at atmospheric pressure but also to realise in one treatment the surface cleaning, the surface activation of the substrate before the metal deposition. HOPG substrate has been used as a model surface that present the same chemical properties as MWCNTs. The surface composition of the resulting nanomaterials was analysed using XPS (X-ray Photoelectron Spectroscopy). Narrow region electron spectra were used to extract the chemical state information from the C 1s, O 1s and metal levels peaks. This result evidences a good agreement between experiment from Field Emission Scanning Electron Microscope (FE-SEM) images and theory. The dispersion and shape of metallic clusters on MWCNTs were observed by (High Resolution) Transmission Electron Microscopy. Some ToF-SIMS experiments have been attempted on HOPG decorated with gold clusters in order to elucidate the chemical binding between metal and carbon support.

# Adatom Surface Processes During Diamond Thin Film Growth: a combined Molecular Dynamics-Monte Carlo study

**M. Eckert, E. Neyts, A. Bogaerts**
Plasma, Laser Ablation and Surface Modelling ANTwerp (PLASMANT), University of Antwerp, Department of Chemistry, Universiteitsplein 1, 2610 Antwerp, Belgium

To obtain more insight into the different stages of (ultra)nanocrystalline diamond ((U)NCD) thin film growth, combined molecular dynamics-Monte Carlo simulations are carried out. In this study, we investigate the surface relaxation behavior of species that may contribute to the growth of (U)NCD films deposited by microwave plasmas.

The growth of thin films comprises numerous physical processes, which occur on different time scales. Surface diffusion might be an important process during (U)NCD growth, e.g. causing (re)nucleation.

Since molecular dynamics (MD) simulations enable us to study the time evolution of a system on the femtosecond to nanosecond time scale, they are not capable for describing surface diffusion, i.e. processes on a microsecond time scale, within a reasonable calculation time. Therefore, we combined our MD code with a Monte Carlo (MC) method. In this methodology, the atoms are followed probabilistically [1].

In the past, molecular dynamics (MD) simulations showed that for (U)NCD growth, C, $CH_3$, $C_2H_2$, $C_3$, $C_3H_2$ and $C_4H_2$ are the most important species of the $C_xH_y$ (x=0-4) series [2].

To study the surface relaxation behavior of those $C_xH_y$ species at diamond surfaces, we implemented an algorithm that is based on the Metropolis Monte Carlo (MMC) algorithm [3]. In MMC simulations, the system evolves from state to state. In every MMC cycle, new and randomly chosen positions are assigned to the atoms. The transition probability into the new configuration is determined by the Boltzmann distribution function, and thus by the energy difference between the old and the new configuration: $P_{old \rightarrow new} = \exp(-\Delta E/kT)$. A random number determines whether the new configuration is accepted or rejected. To overcome the difficulties of the original MMC algorithm, the simulation is limited to adatoms and their neighbors.

Preliminary results of the MMC simulations show that for the diamond (100) and (111) surfaces, carbon adatoms insert into carbon-carbon bonds at the surface, disturbing the reconstruction geometry, pursuing the diamond crystal.

[1] D. Frenkel and B. Smit, "Understanding Molecular Simulations: from Algorithms to Applications", Academic Press, San Diego 2002
[2] M. Eckert, E. Neyts, A. Bogaerts, Chem. Vap. Deposition, accepted for publication
[3] N. Metropolis, A. W. Rosenbluth, M. N. Rosenbluth, A. H. Teller and E. Teller, J. Chem. Phys. 21 1087 (1953)

# Molecular dynamics study of complex oxide thin film growth

**V. Georgieva, A. Bogaerts**
Department of Chemistry, Research group PLASMANT , University of Antwerp
Universiteitsplein 1, 2610 Antwerp, Belgium

Molecular dynamics (MD) is a technique for computing the equilibrium and transport properties of a classical many-body system. Giving an initial set of positions and velocities of a system of N atoms, Newton's equations of motion are solved for this system [1].
In the present work the growth of (Mg-Al-O) thin films formed by a magnetron sputter-deposition process is investigated by MD simulations. The MD package DL_POLY, developed in Daresbury Laboratory, U.K. [2] is used to simulate the deposition of atoms. A driving program is written which automates the deposition and relaxation. The potential describing the interaction is a classical pairwise ionic potential, i.e. the sum of a long range Coulombic interaction and a short range repulsion and van der Waals attraction [3]
The deposition is simulated at constant NVE (i.e., constant number of particles, volume, and total energy) conditions for 2ps. After that a relaxation at constant NVT (i.e., constant number of particles, volume, and temperature) conditions for another 2ps is executed before the next deposition takes place. The time step is in the order of femtoseconds in order to resolve the atomic vibrations. Hence, even with the fastest processors and parallel executing, the simulated time with MD is limited to nanoseconds or less. Therefore, the simulated deposition rates are several orders of magnitude higher than the experimental deposition rates. Thermally activated processes with rates as low as one per millisecond are excluded in the MD simulations. Therefore, other methods should be employed in order to extend the simulation time-scale and, in this way, phenomena such as terrace diffusion and interlayer transport to be considered. Recently, several accelerated dynamics methods were proposed [4]. Among them the temperature accelerated dynamics (TAD) [4] is the most studied and developed method and has been already applied to oxides [5].
Preliminary results show that the structure of the deposited film depends on the Mg content. It changes from crystal to amorphous with decreasing of Mg content in the film. Comparison of the deposited film simulated by a regular MD method and by the MD method coupled with the TAD method is carried out.

[1] D. Frenkel and B. Smith "Understanding Molecular Simulation" Academic Press, 2002 (ISBN-13 978-0-12-267351-1).
[2] C. R. A. Catlow, C.M. Freeman and R.L. Royle, Physica 131B 1 (1985).
[3] www.ccp5.ac.uk/DL_POLY/
[4 ]A. Voter, F. Montalenti, and T. Germann, Annu. Rev. Mater. Res. 32 321 (2002).
[5] D. Bacorisen et. al, Nucl. Instr. and Meth. in Phys. Res. B 250 36 (2006).

# Room temperature epitaxy of thin TiN films using hyperthermal titanium ions

**J.W. Gerlach, A. Wolfsteller, T. Höche, B. Rauschenbach**
Leibniz-Institute of Surface Modification (IOM), Permoserstrasse 15, D-04318 Leipzig, Germany

Conventional ion beam assisted deposition (IBAD) of binary nitrides, e.g. TiN, is usually done by evaporation of the metal component and simultaneous nitrogen ion irradiation of the growing film. In the literature, a lot of consequences of this ion irradiation during film growth are reported like densification, enlargement of the crystallite size, change of the preferred orientation, biaxial texturing of the films, and others. Contrary, in the present contribution the growth of thin TiN films by deposition of titanium ions, possessing hyperthermal energies of several ten eV, in a nitrogen ambient is investigated. These hyperthermal titanium ions were produced by a pulsed dc vacuum arc metal plasma source. The TiN films were deposited at substrate temperatures in the range from 700 °C down to room temperature on $Al_2O_3$(0001) and MgO(100) substrates. The surface structure of the films was monitored in situ by reflection high energy electron diffraction (RHEED). The crystallographic structure and texture was investigated by x-ray diffraction (XRD). High resolution transmission electron microscopy (TEM) was used to examine the morphology and defect structure of the films. The results show that all the deposited TiN films are epitaxial, even at room temperature, indicating the beneficial effect of the hyperthermal energy of the particles involved in the deposition process. The influence of the hyperthermal titanium ion irradiation, especially of the parameter kinetic energy, on the crystalline quality of the films is discussed.

# Recent developments in arc handling and pulsed-dc power in sputtering applications

**R.S. Hall, D. Carter**
Advanced Energy Industries

Magnetron sputtering is widely used to deposit thin films on products serving a broad range of applications and industries. Thin films are produced to exacting standards and so the processes producing them must be tightly regulated. The power systems driving these processes are some of the most critical elements for achieving necessary control. Essential in today's sputtering power supplies is the ability to deliver precise power along with the means to quickly respond to arcs that can be extremely disruptive to the control and quality of the deposition. Macro-particles are one of the most damaging byproducts of magnetron arcs. Macro-particles embedded in thin films can be damaging to both appearance and performance because they are often many times larger than films are thick. The size of these defects depends in part on the energy the power supply delivers to an arc, therefore it is important for the power supply to respond fast in order to minimize the size and also the quantity of the particles produced. Arc response duration is also an important factor in arc management. To be effective, response duration should be long enough to quench arcs but short enough to minimize process disruption. Reactive sputtering of dielectric films can be particularly problematic. Insulating films produced during reactive sputtering are highly prone to charge buildup and eventual breakdown leading to severe arcing. Further, operation in the transition region makes reactive processes highly sensitive to the arc shut-off time. In this poster we illustrate the factors that influence the formation of arcs in magnetron sputtering, the influence they can have on a process and the methods used in modern power systems to minimize their impact. Effective arc management for both DC sputtering for metals and Pulsed-dc sputtering for reactive dielectric compounds will be covered.

# Study of Initial Growth Stages of Metal Films by the Techniques of Computational Physics

**R. Hrach, J. Simek, V. Hrachova**
Charles University, Faculty of Mathematics and Physics, Department of Surface and Plasma Science, V Holesovickach 2, 180 00 Prague 8, Czech Republic

The nucleation and initial stages of three-dimensional thin-film growth were studied by a computer experiment. This experiment consisted of two parts - the preparation of simulated thin-film structures and the computational analysis of their images. The simulated structures were generated by several models with various levels of complexity ranging from simple hard-disk and soft-disk models till more realistic model combining the molecular dynamics and Monte Carlo approaches. The analysis of obtained structures was based on both standard and advanced algorithms of image processing - algorithms based on the theory of mathematical morphology, algorithms based on integral transforms as well as algorithms using the neural networks. The results obtained by the image processing of simulated structures by all these techniques were compared and the best algorithms were suggested for the image analysis of experimentally prepared thin films structures.

## 1. INTRODUCTION

In thin film physics as well as in some other fields of science and technique as in astronomy or metallurgy, the systems consisting of large number of individual objects are often studied. One of important sources of information about internal processes in these structures are their images from various types of devices specific for given branch of science - transmission electron microscopes as well as other types of microscopes as STM, AFM, ... in thin film physics or solid state physics, etc. During image analysis of such micrographs several levels of information can be derived: characterisation of whole images, size distribution of individual objects and their distribution on the substrate. Here especially the spatial distribution of objects in the studied structures can bring valuable information. However, there exist two tasks which must be solved, when processing the experimentally derived images. It is necessary

- to find or create convenient methods for the quantitative characterisation of given type of systems, and
- to properly interpret the obtained morphological characteristics in order to be able to derive hidden information about internal processes in studied systems.

For several decades the most popular technique represent algorithms based on the theory of mathematical morphology - see e.g. [1]-[5]. However, these methods have a limitation as they produce as a result of image analysis rather complicated curves, which depend besides the important parameters of studied samples also on non-physical image parameters, so the interpretation of derived characteristics is sometimes difficult. Therefore there exist attempts either to improve the informative value of these algorithms or to prepare new algorithms based on different mathematical or computational principles.

In our contribution we describe a simple computer experiment for the analysis of both well-known and modern morphological algorithms for the image analysis in thin-film physics. This computer experiment consists of several stages:

i. preparation of model structures with given properties
ii. image analysis of simulated structures by various morphological algorithms based on different principles
iii. critical evaluation of obtained results on the basis of known information about model structures.

## 2. GENERATION OF MODEL STRUCTURES

### *2.1 Hard-disk model*

Individual objects are generated randomly, but their spatial distribution is influenced by model parameter called the diffusion zone D representing the minimum distance between objects. According to values of diffusion zone the generated structures range from fully random (for D = 0) till maximally "statistically" arranged (for D = $D_{max}$) - Fig. 1.

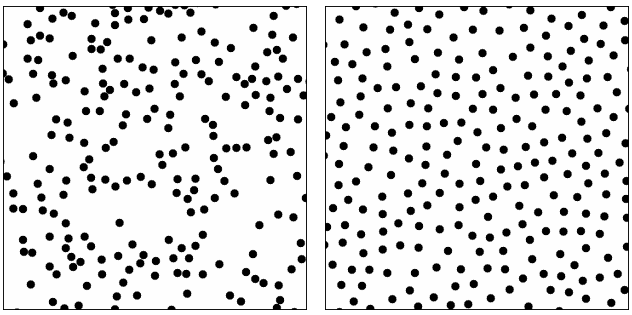

Figure 1: Structures generated by hard-disk model with parameters: D = 0 (left) and D = $D_{max}$ (right).

### *2.2 Soft-disk model*

In this model the final positions of objects in generated structures are obtained with the help of the technique of simulated annealing - the both attractive and repulsive forces originating from the Lennard-Jones potential describing the interactions between individual objects are compared with the chaotic disturbing forces characterised by the effective temperature $T_{eff}$. This parameter again influences the degree of arrangement of the structure - see Fig. 2.

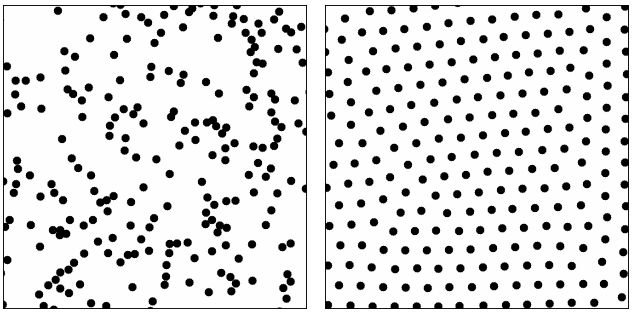

Figure 2: Structures generated by soft-disk model with parameters: $T_{eff.} = 1\times10^{8}$ (left) and $T_{eff.} = 1\times10^{-2}$ (right).

### *2.3 MD/MC model*

Contrary to previous simple models the more advanced technique for the preparation of model structures is based on the combination of molecular dynamics (MD) and Monte Carlo (MC) methods acting on atomic scale. This model starts with the deterministic simulation of

initial stages of thin film growth and continues with the MC simulation of the growth and coalescence of larger objects, when the stochastic description can be applied (Fig. 3). The link between both parts is provided by the information about the forms of nuclei and small islands and about the speed of their coalescence given by the MD part of model which is transformed into corresponding probabilities in the MC part of model. This model, contrary to simple hard-disk and soft-disk models, uses parameters with the physical meaning - substrate temperature, deposition rate, activation energies for surface diffusion and desorption, etc. [6].

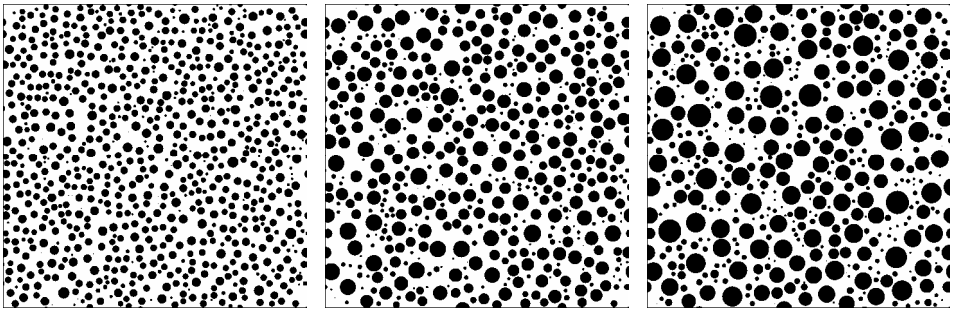

Figure 3: Structures generated by the MD/MC model. Three growth stages derived by the stochastic simulation.

## 3. MORPHOLOGICAL ANALYSIS OF MODEL STRUCTURES

For the image analysis of prepared model structures three types of algorithms were used:

i. standard algorithms based on the theory of mathematical morphology - radial distribution function, distribution of nearest neighbours, chord-length distribution, covariance function, Quadrat Counts method and Voronoi tessellation [7];
ii. algorithms based on non-localised integral transforms - Fast Fourier transform and Hartley transform [8];
iii. algorithms based on neural networks technique [9].

## 4. RESULTS

During the analysis of the results obtained by all above-mentioned methods it was found that the sensitivity of individual methods to the object arrangement in generated thin-film systems differs profoundly. Therefore,

- for the characterisation of small deviations from the completely arranged systems, the radial distribution function, the distribution of nearest neighbours and the covariance function are the best suited;
- for the analysis of small deviations from the random state, the Voronoi tessellation and the q
- Quadrat Counts methods can be used - either directly (Voronoi tessellation) or its sensitivity can be tuned by the internal parameter of the method (Quadrat Counts);
- the integral transform methods are more sensitive to the angular anisotropy of studied systems than to the spatial arrangement of their objects;
- the neural networks cannot be applied directly to the image analysis of thin-film systems, as they require enormous computer time and memory. However, when some of the standard morphological algorithms is used as a pre-processing tool, the neural networks are very suitable technique for the image analysis in thin-film physics.

The sensitivity of morphological methods to the objects arrangement in thin-film system is not the only criterion which must be taken into account. Other criteria are the sensitivity of individual methods to the variation of morphological information in samples with limited numbers of objects and the sensitivity of methods to non-physical parameters of analysed

images. For the study of these questions it is better to use the one-number features describing the most important properties of given characteristics. Typically, for single morphological method several features with different properties can be suggested.
The final part of our contribution is devoted to the critical discussion of numerical features of the most of suggested morphological algorithms. When the sensitivities of individual features to the both useful information and statistical noise are taken into account, the Voronoi tessellation method is probably the most applicable to the analysis of images in thin-film physics. The reason is, first, that it is possible to invent more than ten numerical features based either on areas or forms of individual cells and, second, that the derived results are not very influenced by the fluctuations - see Fig. 4. The second useful morphological technique is the Quadrat Counts method, as only this method is in the same time its numerical feature and this method can be tuned by the proper choice of test squares. These two methods were therefore used for the image analysis of experimental data.

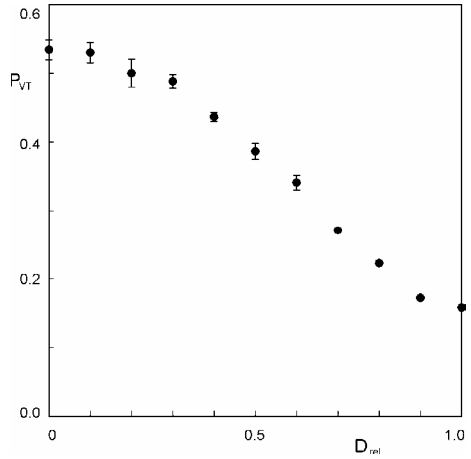


Figure 4: Voronoi tessellation of hard-disk generated model structures. $P_{VT}$ is the feature derived from areas of Voronoi cells, fluctuations correspond to 5×11 analysed structures.

## Acknowledgements

The work is a part of the research plan MSM0021620834 financed by the Ministry of Education of Czech Republic.

## 5. References

[1] J. Serra “Image Analysis and Mathematical Morphology” Academic Press London 1982
[2] B.D. Rippley “Spatial Statistics” Willey New York 2001
[3] H. Schmeisser Thin Solid Films 22 83 (1974)
[4] R. Hrach Vacuum 43 705 (1992)
[5] E. Dobierzewska-Mozrzymas, P. Bieganski, G. Szymczak Vacuum 63 59 (2001)
[6] R. Hrach, J. Simek, M. Kostern Vacuum 67 229 (2002)
[7] J. Simek, R. Hrach Thin Solid Films 466 16 (2004)
[8] D. Novotny, R. Hrach, M. Kostern Vacuum 82 282 (2008)
[9] M. Maly, R. Hrach, D. Novotny Vacuum 61 223 (2001)

# Interaction of Magnetrons in a Codeposition Mode

**M. Jerčinović [1], Z. Siketić [1], R. Grötzschel [2], N. Radić [1]**
1. Rudjer Boskovic Institute, Bijenicka 54, HR-10000 Zagreb, Croatia
2. Forschungzentrum Rossendorf, Bautzner Landstrasse 128, D-01328 Dresden, BR Deutschland

In a co-deposition mode of thin film preparation, two or more magnetrons are simultaneously operated in a deposition chamber. Cross-contamination shields are used to minimize mutual deposition of respective target materials onto each other. However, the magnetron plasmas are in contact above the shield, and the operating conditions of each magnetron are somewhat perturbed due to their interaction. A main consequence of these perturbations is the change of deposition rates of co-deposited materials, which leads to the departure of the true composition of prepared material from the prescribed composition of the film. Film composition being one of key parameters which determine material properties, its reproducibility is essential for correct interpretation of measured properties and applications. Two magnetron characteristics dominantly influence a composition of the materials prepared by a codeposition: a) magnetron discharge IU characteristics, and b) deposition rate as a function of discharge power. Difference between the IU characteristics of singularly operated magnetrons, and those of magnetrons operated simulatenously during codeposition, reveals the perturbation introduced by magnetron plasmas interaction. This interaction mostly affects the respective discharges operating voltage, and thus the average energy of sputtering (argon) ions, which allows to estimate the change of respective deposition rates of codepositing magnetrons. Here, a nominal (prescribed) and measured (RBS method) chemical composition of two series of binary alloys (Al-Mo, Ag-W) are compared, and the observed differences are correlated with the change of operating conditions of two magnetrons due to their respective plasmas interaction.

# Hydrogenated amorphous carbon (a-C:H) film coating on an inner-wall of a Artificial heart blood pump by special 3-dimensional electrode with r. f. plasma CVD technique

**K. Kanasugi, Y. Ohgoe, K. K. Hirakuri, Y. Fukui**
Tokyo Denki University, Graduate school of Science and engineering, Saitama, Japan

Hydrogenated amorphous carbon (a-C:H) films including diamond-like carbon (DLC) are considerably interesting in a variety of applications, due to their attractive properties. Especially, radio frequency (r.f.) plasma chemical vapor deposition (CVD) technique is very useful for a-C:H film deposition on most substrates that are conductor and/or insulator at room temperatures. Therefore a-C:H film coatings with r.f. plasma CVD method are possible to be applied to polymeric materials as biomedical applications. However, it is difficult to deposit to any complicated subjects with 3-dimensional structure such as artificial organs using common capacitive coupled r.f. plasma CVD system. In this study, to deposit a-C:H film uniformly on an inner-wall of polyurethane artificial heart blood pump, we have developed a special 3-dimensinal-type electrode for a complicated subject. In estimating the uniformity of the a-C:H film, the film thickness was measured using scanning electron microscopy (SEM). The surface morphology of the a-C:H film was evaluated with atomic force microscopy (AFM) and contact angle measurement. The structures of the film were evaluated with Raman spectroscopy (Raman), and X-ray photoelectron spectrometer (XPS). The uniform a-C:H film was deposited on the inner-wall with a thickness of 300 nm. Additionally, it was observed that the deposited a-C:H film had good stability adhesion on the blood pump inner-wall. In investigating the availability of the special 3-dimensinal-type electrode method, under helium (He) gas, the plasma states were measured using Langmuir double probe analysis. The He plasma was generated using the special electrode; r.f. discharge plasma surrounded an inner-wall of artificial heart blood pump. As a result, lateral profiles of the electron temperature were higher in the edges and decreased towards the center of the electrode. On the other hand, the plasma density profiles were kept uniformly on the blood pump inner-wall. Based on these results, the new technique with the special 3-dimensional-type electrode technique is expected for medical appliance including an artificial heart blood pump. Furthermore, this processing could be widely applied to film deposition industries.

# Structure of magnetron co-sputtered Fe:$SnO_2$ coatings in off-axes configuration

**M. Kormunda [1], J. Pavlik [1], P. Hedbavny [2]**

1. J.E. Purkinje University, Department of Physics, Ceske mladeze 8, 400 96 Ustí nad Labem, Czech Republic

2. VAKUUM PRAHA s.r.o., V Holesovickach 2,. 180 00 Praha 8, Czech Republic

The $SnO_2$ material combines electrical conductivity with optical transparency; it is a heterogeneous oxidation catalyst and a solid-state gas sensor. The doped $SnO_2$ gas sensors are produce by many different techniques with wide range of dopands to improve their selectivity and sensitivity. It was demonstrated that a small amount of transition metals (less than 1 at.%) significantly modifies the properties of tin oxide thin films used for the gas sensors. The magnetron deposition is known to introduce energy particles to the growing films especially in on-axes configuration and therefore the wide range control of coating's structure is possible. But the surface damages are also introduced to the film. The influence of higher energy particles reduction on film properties was investigated by the deposition in off-axes configuration. The deposition system allowed deposition temperatures control by water cooled substrate holder and afterward in-situ annealing up to 600$^{o}$C under vacuum conditions. The thin films of $SnO_2$ were deposited by RF magnetron co-sputtering of $SnO_2$ and Fe dopand using a single sputter target with variable $SnO_2$/Fe ratio in oxygen-argon gas mixture at wide range of deposition temperatures. Especially the influence of low deposition temperature on the coatings structure was investigated. The control of doped film's structure was enhanced by the epitaxy grow onto previously deposited $SnO_2$ film. The properties of those Fe:$SnO_2$ multi-layer coatings were compared to properties of $SnO_2$ coatings doped only by Fe top layer deposition; when different amount of doping metal (up to 10 at.%) was sputtered on the top of $SnO_2$ film and annealed. The surface topology was measured by AFM; chemical bonds in the coatings were characterized by FTIR and the surface chemical structure was investigated by XPS method; a crystal structure of the films was investigated by XRD technique. The depth profiles of the basic composition were taken by SIMS.

# Sputtering Ice Films at the Bombardment by $Ar^+$ Ions

**U.O.Kutliev**
Urgench State University, Department of Physics. 740000,Urgench, Uzbekistan.

Secondary ion mass spectrometry (SIMS) is a wonderful technique for providing mass spectrometric information of molecules on surfaces[1]. Theoretical studies of the keV bombardment of organic films on metallic surfaces have contributed to our understanding of the mechanisms governing these processes. Many experiments of keV bombardment, however, are performed thin films[2,3].

Below we give our choices for the interaction potentials for the $H_2O$-$H_2O$, Au-Au, and Au-$H_2O$ components of the system. At the end of this section, the details of the MD simulations are described. $H_2O$-$H_2O$ interaction potential employed to describe the $H_2O$-$H_2O$ interaction is the simple-point-charge (SPC) water potential developed by Berendsen et al.[4] This potential has been used extensively to study the properties of $H_2O$ as a solid[5,6]. It has been shown that the SPC potential is able to reproduce many of the properties of bulk $H_2O$ [7]. The Au-Au interactions are represented by the MD/Monte Carlo corrected effective medium (MD/MC-CEM) potential function for fcc metals [8]. For metal- water systems has been developed a potential by Spohr[9].

The computational results shown, that in the mass spectra a few intensive peaks are observed. In case $E_0$=0,3 keV at the mass spectra observed very intensive peak corresponding to molecule $H_2O$. After this peak are observed peaks corresponding to the water clusters. This clusters consists 2 and 3 water molecules. And this clusters no dissociated during this time. But they will have difference coordinates.

The almost same picture will present the simulation by initial energy 0,7 keV. But in this case the mass spectra observed some another peaks which performed by 5 molecules of water. Also shown that the intensity Au peak higher than the case 0.3keV.

The simulation clearly shows that the mass spectrum contains peaks of the water molecules, water clusters and Au atoms. These results are of interest for mass spectrometry of molecules, study of surfaces.

[1] B.J.Garrison, A.D.Delcorte, K.D.Krantzman.Acc.Chem.Res.33(2000) 69.
[2] S.J.Stuart, A.B.Tutein, J.A.Harrison. J.Chem.Phys.112(2000) 6472.
[3] E.S. Parilis, L.M. Kishinevsky, N.Yu. Turaev, B.E. Baklitzky, F.F. Umarov, V.Kh.Verleger, S.L.Nizhnaya and I.S. Bitensky, Atomic Collisions on Solid Surfaces. North-Holl. Publ., Amsterdam, 1993. 664 p.
[4] . J. C.Berendsen, J. P. M., Postma, W. F.van Gunsteren, J.Hermans. in Intermolecular Forces; Pullman, B., Ed.; Reidel: Dordrecht, The Netherlands, 1981.
[5] R. W.Impey, M.L.Klein, T.S. Tse. J. Chem. Phys. 1984, 81,8406.
[6] M.Lombardero,C. Martin, S.Jorge, F.Lado, E.Lomba. J. Chem.Phys. 1999, 110, 1148.
[7] A.Wallqvist, O. Teleman. Mol. Phys. 1991, 74, 515.
[8] M.S.Stave, D.S.Sanders, T.J.Raeker,A.E. DePristo. J. Chem.
[9] E.Spohr. J. Mol. Liq. 1995, 64, 91.

# PVD deposition of thermochromic vanadium dioxide thin films on metallic substrates

**A. Lafort [1], J. Colaux [2], S. Lucas [2], F. Maseri [3], R. Cloots [1]**

1. University of Liège (ULg), Laboratoire de Chimie Inorganique et Structurale (LCIS), allée de la Chimie, 3, bat B6a, 4000 Sart-Tilman, Liège, Belgium.

2. Centre de Recherche en physique de la matière, Laboratoire d'Analyses par Réactions Nucléaires (LARN), rue de Bruxelles, 61, 5000 Namur, Belgium

3. ArcelorMittal Liege Research, Boulevard de Colonster B57, 4000 Liège, Belgium

Vanadium dioxide is a thermochromic material that exhibits a reversible monoclinic to tetragonal phase transition at the critical temperature (TC) of 68°C. Below this temperature, $VO_2$ is IR transparent and semiconducting. Above, it is IR reflecting and metallic. Due to its low TC, this oxide is a promising material for smart coating in the automatic solar heat control.

While many efforts have been developed in the past to manufacture thermochromic $VO_2$ coated glasses, deposition of vanadium dioxide on metallic substrates received less interest although some interesting and concrete applications, based on reflective properties, are possible.

The stoechiometry and crystallinity are two necessary conditions to produce thermochromic $VO_2$. Due to the complex V-O system, the synthesis of a single phase of vanadium dioxide requires an accurate control of critical parameters such as the temperature of substrate and the oxygen partial pressure.

In this work, we report the successful growth of thermochromic $VO_2$ on a metallic substrate by DC magnetron sputtering. We have investigated the influence of thickness and the biasing substrate on the optical properties. Structural and compositional analyses were performed by grazing incidence X-ray diffraction and Rutherford backscattering spectrometry. The morphology of the films was study by SEM and the optical properties are measured by UV-VIS-NIR spectrometry.

This preliminary study will soon be extended to a complete parametric study of deposition conditions aiming to achieve the best quality coating with maximum optical contrast between both phases.

# Annealing effect on physical and mechanical properties of TiN films deposited by high power pulsed magnetron sputtering

**L. Mohammedi [1], R. Gheriani [1], R. Halimi [2], A. Billard [3]**

1. Laboratoire de développement des énergies nouvelles et renouvelables dans les zones arides et sahariennes, Université de Ouargla

2. Laboratoire Couches Minces et Interfaces, Campus Chaâb Erassas, Université Mentouri de Constantine

3. laboratoire d'Etudes et de recherches sur les Matériaux, les Procédés et les Surfaces, Université de Technologie de Belfort-Montbéliard

High power impulse magnetron sputtering (HIPIMS) is a technique that lately has drawn attention from both industry and academia. In the present work TiN films on high carbon substrates (Z200C12) are prepared by high power pulsed magnetron sputtering. The so prepared samples are submitted to various thermal anneals in vacuum between 300°C and 1000°C, and then characterized structurally and mechanically by X-ray diffraction (XRD), scanning electron microscopy (SEM) and Mercedes test. The analysis showed clearly the effect annealing treatment on the properties of titanium nitride coatings. The optimized conditions of TiN films synthesis were deduced. The film morphology was dense and flat, and coating layers, obtained by HIPIMS, were adherent.

# Glycine adsorption on a-C:H and Silicon doped a-C:H studied by Raman and FTIR

**A. Mukhtar, J. A. Byrne, J. A.D. McLaughlin**
Nanotechnology and Integrated Bio-Engineering Centre, University of Ulster, Newtownabbey, BT37 0QB, UK

Protein adsorption onto surfaces is of major significance in many areas of biomedical sciences. Hydrogenated amorphous-carbon thin films (a-C:H) and silicon doped a-C:H thin films (Si-DLC) were prepared by plasma-enhanced chemical vapour deposition (PECVD). Glycine ($H_2N$-$CH_2$-COOH) adsorption onto the surface of the films was investigated in order to elucidate the mechanisms involved in protein adhesion. The physicochemical nature of the surfaces, before and after adsorption of glycine, was analysed. Raman and Fourier transform infrared (FTIR) spectra were recorded at room temperature. The Raman spectra highlighted a significant decrease of ID/IG ratio with increasing Si doping ratio in film. Following exposure to solutions containing (0.01M) glycine, the vibrational assignments of the observed wave numbers have been made for the functional groups, e.g. COOR, $COO^-$, $-NH_3^+$, $NH_2$, C-H and C-C-N. The results from both FTIR and Raman spectroscopy confirm that glycine was bound to the surface of the DLC and Si-DLC films via interaction of ionized carboxyl groups and the amino group did not play a significant role in the adsorption of glycine. Extensive intermolecular hydrogen bonding has been identified by the shifting of bands due to the stretching and bending modes of the various functional groups. The carboxylate, ionized carboxylic ($COO^-$) and protonated amine ($NH_3^+$) groups have been identified on the surface suggesting multilayer glycine on the surface.

[1] Zhang, H. Du, S.E. Ong, K.N. Aung, .C. Too, X. Miao. *Thin Solid Films* **515** (2006) 66 –72
[2] S.E. Ong, S. Zhang , H. Du, D. Sun. *Diamond & Related Materials* **16** (2007) 1628-1635
[3] S. Pandiarajan, M. Umadevi, R.K. Rajaram, V. Ramakrishnan. *Spectrochimica Acta Part A* **62** (2005) 630–636
[4] T. V. Kumar, I. H. Joe, C.P. R. Nair, V.S. Jayakumar. *Journal of Molecular Structure* **877** (2008) 20–35
[5] S. Ramaswamy, R. K. Rajaram and V. Ramakrishnan. *J. Raman Spectrosc.* **34** (2003) 50–56

# XRD in-situ study of crystallization of magnetron-deposited $TiO_2$ thin films

**L. Nichtová [1], R. Kužel [1], J. Šícha [2], J. Musil [2]**

1. Charles University, Faculty of Mathematics and Physics, Department of Condensed Matter Physics, Ke Karlovu 5, 121 16 Prague 2, Czech Republic

2. University of West Bohemia, Faculty of Applied Sciences, Department of Physics, Univerzitní, Pilsen, Czech Republic

Crystallization of amorphous titanium dioxide films with different thickness (50−1000 nm) deposited on silicon substrates was investigated by in-situ isochronal and isothermal annealing in high-temperature chamber in the X-ray diffractometer. It was found that the crystallization depends strongly on the film thickness, especially below about 500 nm and it is slow for very thin films. The process can be well described by the Avrami equation modified by the initial time of crystallization. All the parameters of the equation vary with film thickness.

## 1. Introduction

In order to obtain titanium dioxide having many of its well-known remarkable properties (hydrophilicity, photocatalytic activity), the crystalline or nanocrystalline form seems to be necessary. This can be achieved either by annealing of amorphous films or by appropriate selection of deposition parameters. There are several known crystalline phases of titanium dioxide – mainly anatase, rutile and brookite. Nanocrystalline anatase is supposed to have higher photocatalytic activity than other titania phases [1].

Microstructure and crystallization of amorphous and nanocrystalline magnetron deposited films were studied for example recently for example in [2]. It was found that the amorphous $TiO_2$ films can be crystallized at approximately 250 °C and their crystallite size was then immediately above 100 nm. The films with the thickness below 200 nm crystallized at higher temperatures (350 °C) and their diffraction patterns did not change significantly after annealing up to 600 °C. Tensile residual stresses have been found in crystallized films and relaxed after annealing at 500 °C.

In this work, results of in-situ measurements of a set of titanium dioxide thin films with different thickness are presented. Both isochronal and isothermal annealing were performed in the high-temperature chamber in the X-ray diffractometer.

## 2. Experimental conditions

### *2.1 Film deposition*

$TiO_2$ films were sputtered by dual magnetron equipped with two Ti(99.5) targets of 50 mm in diameter and supplied by a dc–pulsed Advanced Energy Pinnacle Plus+ 5kW power supply unit operating in bipolar asymmetric mode at repetition frequency $f_r$ = 100kHz and duty cycle $\tau/T = 0.5$; here $\tau$ and T are the length of pulse and the period of pulses. Films were deposited on unheated silicon (100) substrates (15 × 10 × 1 mm) at substrate to target distance $d_{s\text{-}t}$ = 100

mm, total working pressure $p_T$ = 0.5 Pa, average pulse discharge current $I_{da1,2}$ = 1.5 A and average pulse power density $W_{da} \approx 20$ Wcm$^{-2}$. Further details on dual magnetron system are given elsewhere [3].

### *2.2 XRD measurements*

Two identical sets of samples with different following thickness were measured: 48 nm, 100 nm, 130 nm, 180 nm, 300 nm, 440 nm, 630 nm and 800 nm. In-situ high-temperature measurements were performed in MRI high-temperature chamber with both direct and radiant heating. The chamber was placed in Panalytical X'Pert Pro vertical diffractometer in parallel beam setup. 2θ scans with the angles of incidence 1° were carried out with parallel plate collimator placed in the diffracted beam and the Goebel mirror inserted in the primary beam. The films on Si substrate were fixed on the top of PtRh strip heater with a silver paste. Each time after the setting the temperature, alignment of the specimen was checked by measurement of primary beam and specimen position was corrected if it was necessary. For in-situ measurements only selected diffraction peaks were measured. They were fitted with the Pearson VII function and peak positions, integrated intensities and integral breadths were determined. Total pattern fitting was used for the evaluation of the whole diffraction patterns taken at room temperature. More details about the method can be found in [4, 5].

## 3. Results

### *3.1 Isochronal annealing*

Isochronal annealing experiments started always at 180 °C and were performed with a step of 20 °C. 101 peak of anatase was scanned at each temperature. These in-situ experiments confirmed previously found results on the post-annealed samples, i.e. higher temperature of crystallization for very thin films. The crystallization temperatures found in this experiment could be called “temperatures of fast crystallization” when, of course, the definition of “fast” is somewhat arbitrary. This fast crystallization of the order of minutes appeared at 220 ºC for thicker films (300 nm and more) and were higher for the thinner films with the thickness below 100 nm (290 ºC for 42 nm thick film).

### *3.2 Isothermal annealing*

For measurement of time dependences of crystallization slightly lower temperatures (180 ºC, 215 ºC) were selected than the crystallization temperatures found in isochronal annealing experiments. Then, the crystallization occured as well but it was very slow which enabled detailed measurement of time dependences. Mainly two anatase peaks − 101 and 004 were watched. Normalized intensities of 101 peak for different film thickness are shown on Fig 1. The normalization was performed with respect to the maximum value reached for each sample after full crystallization.

The evolution of the integrated intensities $I_{101}$ can be well fitted by the modified Avrami equation [6] as follows, $I = 1\text{-}\exp[-b(t-t_0)^n)]$, where $t_0$, the initial time of crystallization is related to the first appearance of any diffracted intensity above the background level at the peak position. However, the parameter values were obtained by the least-squares fits of the equation to the full intensity vs. time curve. Fits are shown in Fig. 1 by solid lines. Very good agreement could be observed for thicker films while for the thinnest one the intensity at early stage of crystallization is a little higher than expected according to the Avrami equation. The parameters of the Avrami equation fitted show clear dependence on film thickness. On Fig. 2, these dependences for $t_0$ and exponent $n$ are shown. The exponent was in the range 2−2.5 and slightly increased with the film thickness. These low values indicate two dimensional character of the crystallite growth [6]. The initial time $t_0$ of crystallization (non-zero intensity)

increases nearly exponentially with the decreasing thickness while the slope *b* increased significantly for thicker films.

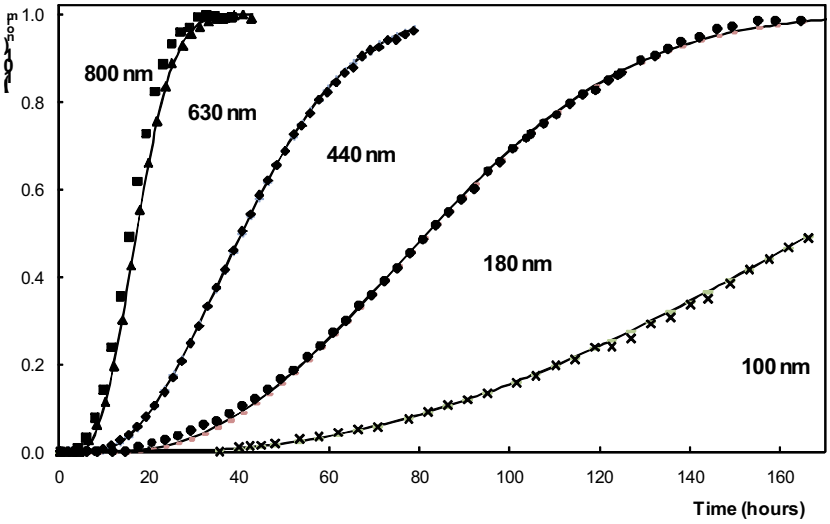


Figure 1. Evolution of normalized integrated intensity of 101 peak of anatase with time at 180 °C for different film thickness as indicated in the graph. Solid lines correspond to the fits by the Avrami equation.

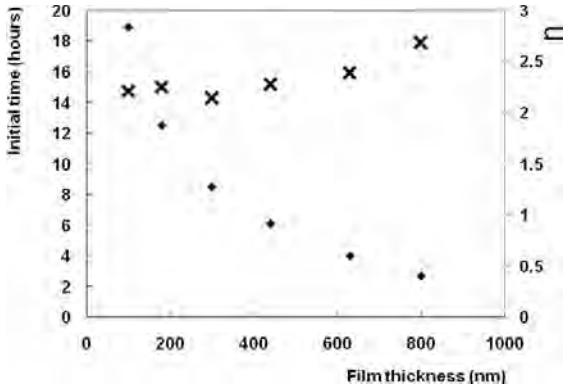


Figure 2. Dependence of parameters of the modified Avrami equation on the film thickness (initial time of crystallization − left axis, dots; exponent *n* − right axis, crosses) for annealing at 180 °C. The parameters were calculated for the integrated intensities of 101 diffraction peak of anatase.

Weak texture was changing during the crystallization. At the beginning, the crystallites with the (00l) orientation were developed but after complete crystallization, the texture was weak except the very thin films (below 100 nm). The change is visible on the evolution of ratio of integrated intensities 101/004 (Fig. 3a). Significant shifts of diffraction peaks with the temperature were observed (Fig. 3b) and tensile residual stresses were confirmed by the $\sin^2\psi$ method for different diffraction peaks. They decrease with the increasing film thickness. Line broadening was not changing significantly during crystallization. This indicates relatively fast growth of a few crystallites at the beginning of crystallization. Their possible further growth with annealing time cannot be watched by XRD since the sensitivity of the method to crystallite size is up to a few hundreds of nanometers and less.

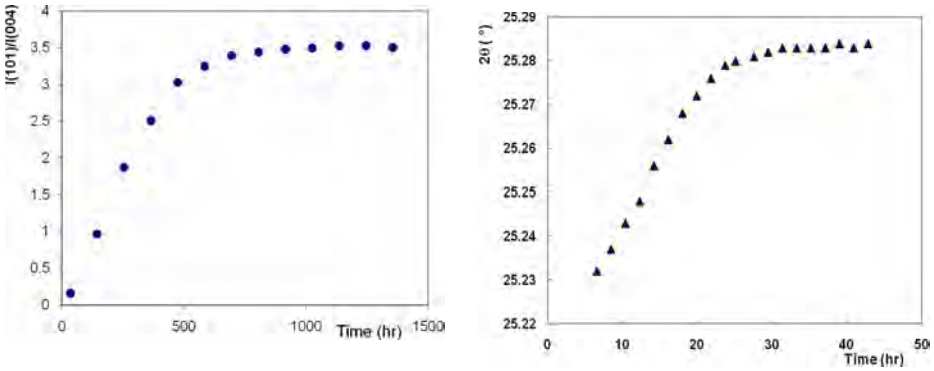


Figure 3. Dependence of ratio of integrated intensities of anatase peaks 101 and 004 on annealing time (a, film 130 nm thick, annealing temperature 220 °C) and dependence of 101 peak position on annealing time (b, film 630 nm thick, annealing temperature 180 °C).

## 4. Summary

In-situ high temperature XRD measurements of amorphous $TiO_2$ thin films confirmed strong dependence of crystallization process on the film thickness. With the thickness decreasing below about 500 nm the crystallization starts to be slow and its speed dramatically decreases with decreasing thickness. The evolution of the integrated intensities of anatase diffraction peaks with annealing time follows the Avrami equation modified by the introduction of initial time of crystallization corresponding to the appearance of an indication of the diffracted intensity above the background level. This time also increases rapidly for very thin films. Behaviour of XRD line broadening, intensities and small exponent of Avrami equation indicate continuous nucleation with 2D growth, i.e. gradual increase of number of fast growing grains. With proceeding crystallization tensile residual stress appears. This stress is higher for the thinnest films.

## 5. References

[1] L. Gaho, Q. Zhang, Scripta Materialia, 44 1195 (2001).
[2] R. Kužel, L. Nichtová, Z. Matěj, D. Heřman, J. Šícha, J. Musil, Z. Kristallogr. Suppl. 26 247-252 (2007).
[3] J. Musil, D. Heřman, J. Šícha , J. Vac. Sci. Technol. A, Vol. 24, No.3 (2006).
[4] R. Kužel, L. Nichtová, Z. Matěj, J. Šícha, J. Musil, Z. Kristallogr. (2008) in press.
[5] Z. Matěj, L. Nichtová, R. Kužel, Materials Structure, Vol. 15, No. 1, (2008), open acces at http://www.xray.cz/ms.
[6] M. J. Avrami, J. Chem. Phys. 7 1103 (1939).

### Acknowledgements

The work is supported by the Grant Agency of the Czech Republic under number 106/06/0327, Grant Agency of Charles University (258200) and also as a part of the research plans MSM 0021620834 and MSM 4977751302 financed by the Ministry of Education of the Czech Republic.

# Microstructural changes of CrN thin films induced by argon irradiation and annealing temperature

**M. Novaković [1], M. Popović [1], D. Peruško [1], V. Milinović [1], M. Milosavljević [1], M. Mitrić [1], N. Bibić [1]**

1. VINČA Institute of Nuclear Sciences

We have studied the effects of argon ion irradiation and annealing temperature on the structural and electrical changes in CrN/Si bilayers. CrN films were deposited by reactive ion sputtering on (100) Si wafers, to a thickness of ~ 280 nm. The base pressure in the chamber was in the low $10^{-6}$ mbar region, and partial pressure of nitrogen was $5x10^{-4}$ mbar. After deposition the samples were thermally treated in nitrogen atmosphere at 600°C, for 1 hour. Both as deposited and annealed samples were irradiated with 200 keV argon ions to the fluences from $5x10^{15}$-$2x10^{16}$ ions/cm$^2$. Structural characterization of the samples was performed by cross-sectional transmission electron microscopy, x-ray diffraction and Rutherford backscattering spectroscopy. The sheet resistivity of the samples was measured by a four point probe. It was found that after annealing a thin film of $Cr_2O_3$ was formed on the surface. Besides, closer analysis of the annealed and irradiated samples indicates the structural changes and intermixing of the components at the CrN/Si interface.

# Structural and electrical changes induced by ion irradiation and annealing temperature in TiN thin films

**M. Popović, M. Novaković, V. Milinović, D. Peruško, M. Mitrić, M. Milosavljević, N. Bibić**
VINČA Institute of Nuclear Sciences

This article reports investigations of the structural and electrical changes induced by ion irradiation and annealing temperature in TiN thin films. The 240 nm TiN thin films have been deposited on (100) Si substrates by reactive ion sputtering. After deposition the samples were annealed at 600°C for 1h under nitrogen atmosphere. All the samples were irradiated with $Ar^+$ ions to the fluences from $5x10^{15}$ - $2x10^{16}$ ions/cm$^2$ at room temperature. The structural changes induced by irradiation and annealing temperature were analysed by cross-sectional transmission electron microscopy (TEM), x-ray diffraction (XRD), and Rutherford backscattering spectrometry (RBS). Electrical characterization included sheet resistivity measurements with a four point probe. The results clearly show that the as deposited layers grow in a columnar structure which are partly disconnected after ion implantation. The irradiation does not induce any redistribution of the components and there is no significant intermixing at the TiN/Si interface. The structural changes are in a good agreement with electrical resistivity measurements.

# Surface Characterization of $SiO_2$ Layers Deposited using Atmospheric Pressure Plasma Enhanced Chemical Vapour Deposition (AP PECVD)

**P. A. Premkumar [1,2], S. Starostin [1,2], H. de Vries [3], R. Paffen [3], M.C.M. van de Sanden [2], M. Creatore [2]**

1. Materials Innovation Institute (M2i), P.O. Box 2008, 2600 GA Delft, The Netherlands.
2. Eindhoven University of Technology, Plasma and Materials Processing Group, Department of Applied Physics, P.O. Box 513, 5600 MB Eindhoven, The Netherlands.
3. FUJIFILM Manufacturing Europe B.V, P.O. Box 90156, Tilburg, The Netherlands.

Transparent barrier layers, such as $SiO_2$, deposited on polymers are receiving much attention in packaging industries as well as in the field of encapsulation of organic-based display applications. These layers deposited in atmospheric pressure PECVD [1,2], considered as a newly emerging technology which does not only offer advantage in cost reduction due to the lack of bulky vacuum equipment, but also it is compatible with roll-to-roll manufacturing. The control on the layer properties requires a deep understanding of the plasma physics and film deposition mechanism. In this investigation, $SiO_2$ films are deposited on a polymeric substrate in a roll- to- roll AP-PECVD set up fed with Ar-N2-$O_2$-hexamethyldisiloxane (HMDSO) mixtures. The deposited films undergo a detailed surface analysis with respect to thickness, composition, morphology, texture, surface roughness, film homogeneity and defect presence (~ 25-75 nm in height and 400-750 nm in width) by means of spectroscopy ellipsometry, x-ray photoelectron spectroscopy and large area atomic force microscopy, respectively. In order to understand the dynamics of the $SiO_2$ layer growth, films grown under static (polymer substrate held fixed and not moved) and web roll (substrate transported at a desired speed) conditions were characterized. These investigations unravelled the different stages of growth involved in the deposition of smooth and uniform layers, as being controlled by the diffusive flux of HMDSO radicals generated in the plasma as well as by the surface modification of the polymer substrate by non-depositing reactive species (such as O, OH).

[1] S. Starostine, E. Aldea, H. de Vries, M. Creatore, M.C.M. van de Sanden, Plasma Proc. Polymers 4 S440 (2007).
[2] S. Martin, F. Massines, N. Gherardi, C. Jimenez, Surf. Coat. Technol. 177-178 693 (2004).

# Study of annealing effect of $Tb^{3+}$ photoluminescence in $TiO_2$ thin films prepared by magnetron sputtering

**D. Kaczmarek, J. Domaradzki, E. L. Prociow, K. Sieradzka**
Faculty of Microsystem Electronics and Photonics, Wroclaw University of Technology,
Janiszewskiego 11/17, 50-372 Wroclaw, Poland

Thin films of $TiO_2$ doped with terbium were deposited on $SiO_2$ substrates by High Energy Reactive Magnetron Sputtering using metallic Ti-Tb mosaic target. After deposition, thin films were additionally annealed in an air ambient at the temperature of: 470 K, 670 K, 870 K and 1070 K. X-ray diffraction (XRD) results show that the obtained thin films revealed the evolution of crystal structure upon additional post-annealing and existence of nanocrystalline $TiO_2$ in the form of the rutile. Additional post-annealing of $TiO_2$:Tb thin films results in further crystallinity enhance of the thin films manifested by an increase in the intensity of observed XRD peaks. From optical transmission measurements it was found that transparency of Tb-doped $TiO_2$ thin films decreased as compare to reference $TiO_2$ and was in a range of about 80 %. Photoluminescence (PL) spectra measured at room temperature, demonstrated a broad unresolved peak with dominating green emission corresponding to 5D4-7F5 transition, centered at 545 nm. Recorded luminescence decreased with the increase of the temperature of additional post-annealing.

## 1. INTRODUCTION

Luminescence from RE ions in dielectric matrix, especially from $Eu^{3+}$ (red), $Tb^{3+}$ (green/blue), $Er^{3+}$ (NIR) is useful in phosphors and light emitting devices [1]. As the host material, for rare earth elements, $TiO_2$ is often used because of its good mechanical, optical and thermal properties [2, 3]. Improving of efficiency of advanced photonic materials fabricated from nanocrystalline materials have attracted much attention for the last few years. Successful attempts of RE doped nanocrystalline materials have been presented in the literature but only few reports are on efficient green emission from $TiO_2$:$Tb^{3+}$ thin films, so far [4, 5]. To our knowledge there were no reports, so far on fabrication of $TiO_2$:Tb thin films using magnetron sputtering from metallic Ti-Tb mosaic target and on efficient emission from $Tb^{3+}$ ions embedded in $TiO_2$-rutile host. In our recent work [6] we have shown efective PL emission from $Eu^{3+}$ embedded in nanocrystalline $TiO_2$ host and its evolution upon additional post annealing has been discussed.
In this work, $Tb^{3+}$ doped $TiO_2$ thin films were synthesized by sputtering of metallic Ti-Tb target in reactive oxygen atmosphere using energy-enhanced magnetron sputtering process [7].

## 2. EXPERIMENTAL PROCEDURE

The thin films of $TiO_2$:Tb were deposited on $SiO_2$ substrates in oxygen atmosphere from metallic Ti-Tb mosaic target by high energy reactive magnetron sputtering (HE RMS) method. The total amount of Tb in the prepared thin films, evaluated with energy dispersive

spectrometer was 2.6 at. %. The samples were additionally annealed after deposition at 470 K, 670 K, 870 K and 1070 K for 2 hours in an air ambient. The structural examinations of prepared thin films was verified by means of X-ray powder diffraction (XRD), performed with the help of DRON-2 powder diffractometer. Optical parameters, such as fundamental absorption edge and optical band gap of the thin films were determined from optical transmission characteristics. The samples were illuminated with coupled deuterium-halogen lamp at normal incidence. During optical transmission and photoluminescence experiments the measurement signal was collected in a spectral range form 250 nm to 1100 nm by a single grating CCD spectrometer.

## 3. RESULTS AND DISCUSSION

### *3.1 Structural characterization*

XRD patterns of $TiO_2$:$Tb^{3+}$ thin films deposited on $SiO_2$ for as-deposited and additionally annealed thin films have been presented in Fig. 1. Based on the XRD data, it could be noticed that investigated samples exhibit presence of nanocrystalline $TiO_2$ in the temperature stable rutile form with its preferred (1 1 0) plane orientation (Fig. 1a). Usually the rutile form is rather rarely observed in as deposited thin films. It results from relatively high energy required for transformation from amorphous or metastable the $TiO_2$–anatase and/or brookite to the rutile and additional post-annealing in the temperature of at least 900 K is required in order to get phase transformation. In our process, the nanocrystalline structure and the rutile form of the $TiO_2$ thin films directly after deposition could be achieved thanks to modification of selected parameters of the deposition process, namely HE RMS. The hot target, low pressure (below 0.1 Pa) of the oxygen as working and reactive gas and specially designed pulse power supplier were applied [7]. Additional post-annealing of $TiO_2$:Tb (2.6 at. %) thin films results in crystallinity enhance of the thin films manifested by an increase in the intensity of observed XRD peaks (Fig. 1b). The fundamental structural parameters determined from XRD measurements have been collected in Table 1. The average grain size (D) of the $TiO_2$:Tb thin films directly after deposition was 6.6 nm. Moreover, the influence of additional heat treatment on average grain size which changed from 6.6 nm to 10.2 nm is clearly seen.

### *3.2 Optical measurements*

From optical transmission measurements (Fig. 2) it could be seen that doping of $TiO_2$ with Tb results in a slight red shift of the fundamental absorption edge as compared to undoped $TiO_2$ , prepared also using HE RMS. Additional annealing of doped samples did not make any essential changes of its position (Fig. 2). Band gap energies determined for particular samples were found to be about 3.53 eV for $TiO_2$ and around 3 eV for doped-$TiO_2$. Optical results have been collected in Table 1 together with structural properties (section 3.1). Transparency of Tb-doped $TiO_2$ thin films decreased as compare to reference $TiO_2$ and was in a range of about 80 %.

Photoluminescence of prepared $TiO_2$:$Tb^{3+}$ thin films have been presented in Fig. 3 and 4. PL spectrum recorded for $TiO_2$:$Tb^{3+}$ thin films when as-deposited, exhibits a broad unresolved spectra with dominating green luminescence at 545 nm. That corresponds to the intra-4f 5D4-7F5 transition of $Tb^{3+}$. Other visible emission lines of $Tb^{3+}$ in the spectra are positioned at 431 nm (5D3-7F4), 491 nm (5D4-7F6) and 619 nm (5D4-7F3) and fulfil the radiative recombination of carriers which transits from different energy level [4, 5].

According to the literature [8], $Tb^{3+}$ ions embedded in $TiO_2$ need an excitation energy higher than that of $TiO_2$ defect states and thus sensitized luminescence for terbium in $TiO_2$ was rarely observed.

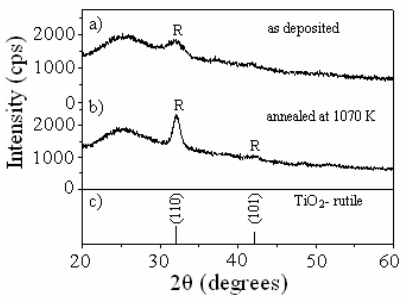


Fig. 1. XRD patterns for $TiO_2$ doped with Tb (2,6 at. %) thin films on $SiO_2$: a) as deposited and b) additionally annealed at 1070 K. At the bottom (c), standard pattern for the rutile

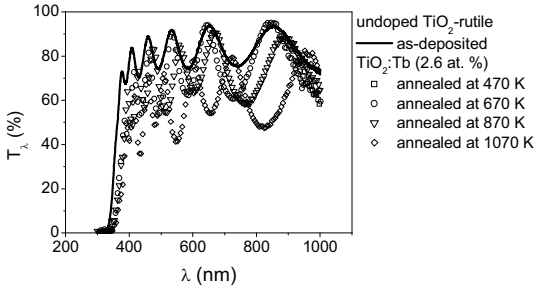


Fig. 2. Transmission characteristics of undoped-$TiO_2$ when as-deposited and $TiO_2$:Tb (2.6 at. %) thin films on $SiO_2$ when: as-deposited and additionally annealed at 470 K, 670 K, 870 K and 1070 K for 2 hours in air ambient

| Sample | D (nm) | d (nm) | $E_g$opt (eV) |
|---|---|---|---|
| $TiO_2$:Tb (2.6 at. % ) as deposited | 6,6 | 0.3247 | 2.98 |
| $TiO_2$:Tb (2.6 at. % ) annealed at 1070 K | 10,2 | 0.3236 | 2.99 |

Table 1. Structural and optical properties of the TiO2:Tb (2.6 at. %) thin films on SiO2 substrates evaluated for the (110) rutile diffraction peak. D and d stands for grain size and interplanar distance, respectively Egopt stands for width of the optical band gap determined from optical transmission characteristics

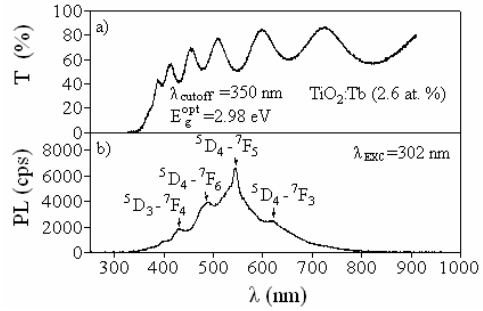


Fig. 3. Transmission (a) and photoluminescence spectra (b) of as deposited $TiO_2$:Tb (2.6 at. %) thin films on $SiO_2$

The reason of effective green photoluminescence in our samples may be that the $Tb^{3+}$ emission centers are mainly excited through the photon absorption of $TiO_2$ host and the energy transfer process directly from conduction band of the $TiO_2$ nanocrystallites to $Tb^{3+}$ ions without relaxation to defect states of titania [4]. After additional annealing the PL intensity of $TiO_2$:$Tb^{3+}$ thin films (Fig. 4) dramatically decreased. In the PL spectra, main contribution plays broad emission bands from self trapped excitons of the $TiO_2$ host (around 435 nm, 492 nm) and oxygen vacancy levels (around 535 nm and 650 nm) [9]. The peak with the center around 365 nm could be attributed to the intrinsic emission of the $TiO_2$ itself.

## 4. CONCLUSIONS

RE-doped nanostuctured titania prepared by co-sputtering of metallic RE-Ti mosaic target, has been found as an efficient host for $Tb^{3+}$ rare earth ions, when prepared thin films are as-deposited. Effective PL emission from Tb in rutile matrix, is the novelty, because up to now such effect was recorded for the $TiO_2$:Tb thin films with the anatase or amorphous matrix [6, 10]. The green (545 nm) emission was mainly excited thanks to that $Tb^{3+}$ ions were

incorporated in nanocrystalline lattice of $TiO_2$. After additional heat treatment, the average particle size of $TiO_2$-rutile increased from 6.6 nm to 10.2 nm with increasing annealing temperature and simultaneously broadening of PL response was observed.

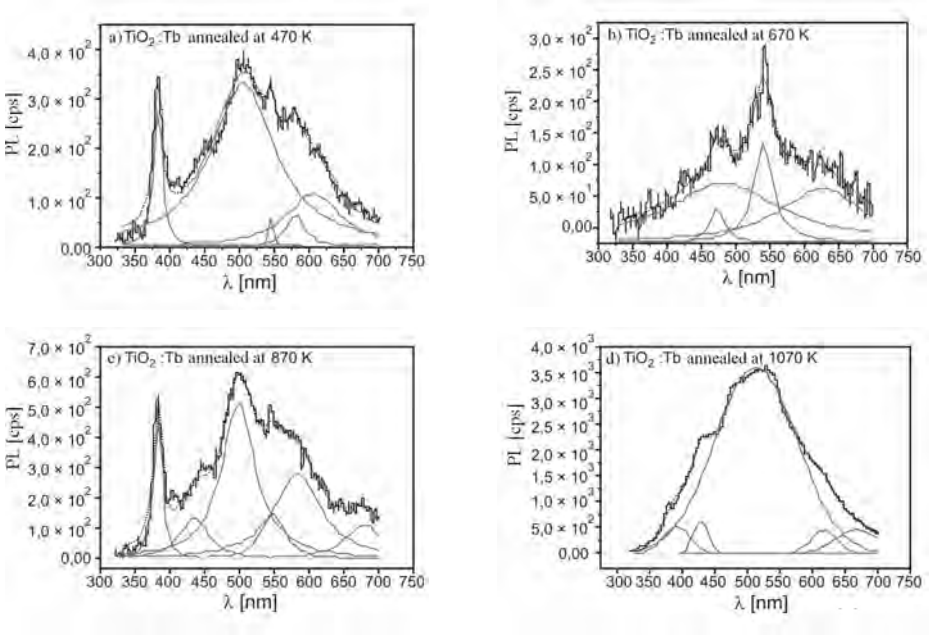


Fig. 4. Photoluminescence spectra of $TiO_2$:Tb (2.6 at. %) thin films annealed at: a) 470 K, b) 670 K, c) 870 K, d) 1070 K for 2 hours in air ambient. PL was performed upon UV (302 nm) excitation from argon laser

## Acknowledgments

This work was financed from the sources granted by the NBCiR in the years 2008-2010 as a development research project number N R02 00 1904. Authors would like to thank W. Mielcarek from Electrotechnical Institute, Wroclaw, Poland for providing experimental data from XRD and A. Podhorodecki from Institute of Physics, Wroclaw University of Technology, Poland for his help during PL experiment

## 5. References

[1] Q.G. Zeng, Z.J. Ding, Z.M. Zhang Journal of Luminescence 118 301 (2006)
[2] Z. Zhao, Q.G. Zeng, Z.M. Zhang, Z.J. Ding Journal of Luminescence 122–123 862 (2007)
[3] M.A. Omari, R.S. Sorbello, C.R. Aita J. Vac. Sci. Technol. A 23 1568 (2005)
[4] Ch. Jia, E. Xie, A. Peng, R. Jiang, F. Ye, H. Lin, T. Xu Thin Solid Films 496 555 (2006)
[5] B.K. Moon, J.H. Jeong, S. Yi, S.C. Kim, H. Choi, J.H. Kim Optical Materials 28 676 (2006)
[6] E.L. Prociow, J. Domaradzki, A. Podhorodecki, A. Borkowska, D. Kaczmarek, J. Misiewicz Thin Solid Films 515 6344 (2007)
[7] Polish Patent No P 379 365 (2006)
[8] K.L. Frindell, M.H. Bartl, M.R. Robinson, G.C. Bazan, A. Popitsch, G.D. Stucky, J. Solid State Chem. 172 81 (2003)
[9] V. Melnyk, V. Shymanovska, G. Puchkovska, T. Bezrodna, G. Klishevich, J. Mol. Struct. 744-747 573 (2005)

# Stabilization of $TiO_2$-anatase in wide temperature range by europium doping

**E.L. Prociow [1], J. Domaradzki [1], D. Kaczmarek [1], D. Wojcieszak [1], A.W. Morawski [2], M. Janus [2]**

1. Faculty of Microsystem Electronics and Photonics, Wroclaw University of Technology, Janiszewskiego 11/17, 50-372 Wroclaw, Poland

2. Institute of Chemical and Environment Engineering, Szczecin University of Technology, Piastów 42, 71-065 Szczecin, Poland

In this work influence of Eu doping on structural properties of $TiO_2$ thin films has been outlined. Thin films were prepared using high energy magnetron sputtering from Ti-Eu mosaic targets with different amount of Eu. The results from SIMS, XRD, AFM and photocatalytic activity measurements have shown that Eu at the amount of 0.1 at. % stabilize the nanocrystalline $TiO_2$-anatase structure upon annealing up to 1070 K temperature.

## 1. INTRODUCTION

Thin films based on oxides have a wide range of different applications. Especially thin films based on titanium dioxide ($TiO_2$) are often applied in gas sensors [1], gate oxides [2], photoelectrocatalysis [3] or advanced phosphors and photonic materials [4]. The range of applications is conditioned by structural properties, which depends on crystal phase of $TiO_2$, i.e. the anatase or the rutile. Anatase is thermodynamically non-stable form, which after annealing beyond 1070 K transforms in to the stable rutile. Selection of the appropriate deposition parameters, the type and the amount of dopants in the film and the temperature of post-process annealing makes possible to form the thin films with desired structural behaviors. Nowadays, the scientific investigations are conducting to receive the high-temperature stabile anatase structure. Such $TiO_2$-anatase thin films can find application, for example, as self-cleaning [5], superhydrophilic [6], bactericidal [7], antistatic films [8] or coatings for the solar cells [9]. Recently, stabilization of the anatase by doping with fluoride ion has been reported by E. P. Lokshin and T. A. Sedneva [10]. An effect of increased temperature required for the anatase-to-rutile phase transformation in sol-gel prepared $TiO_2$:Eu thin films has also been reported by Zhao et al. [11]. For the present study thin films of $TiO_2$ and $TiO_2$ doped with different amount of Eu have been prepared using modified high energy magnetron sputtering [12]. The applied process allows us to prepare the rutile $TiO_2$ directly during deposition. It was shown that using Eu, as a dopant at a specified amount, it was possible to receive the temperature stable anatase or the rutile. Additionally performed investigations of phenol degradation under UV illumination proved usefulness of prepared thin films for photocatalytic applications.

## 2. EXPERIMENTAL DETAILS

The $TiO_2$ and $TiO_2$:Eu thin films were deposited on silicon and $SiO_2$ substrates by modified High Energy (HE) magnetron sputtering method [12]. Sputtering process was carried out in low pressure (< 0.1 Pa) of oxygen as working and reactive gas using additionally heated Ti or Ti-Eu mosaic target. After deposition selected samples were also additionally annealed at 470 K, 1070 K and 1270 K for 2 hours in an ambient air. The results from Energy Disperse Spectroscopy (EDS) method reveal the total amount of Eu concentration in two selected sets of the doped thin films as: 0.1 at. % and 0.5 at. %. The thickness of examined thin films was 415 nm, 300 nm and 600 nm for undoped $TiO_2$, $TiO_2$:(0.1 at. %)Eu and $TiO_2$:(0.5 at. %)Eu, respectively. Structural investigations of manufactured thin films were carried out by X-Ray Diffraction, using DRON-2 powder diffractometer. The diversification of the surface topography was determined by Veeco atomic force microscope, working in a contact mode in an ambient air. The images of the surface were performed by using WSxM ver. 4.0 software [13]. The Secondary Ion Mass Spectroscopy (SIMS) experiments were performed using SAJW-05 instrument with the Balzers QMA-410 quadrupole-based mass spectrometer and Physical Electronics ion gun with Ar+ primary beam of about 100 μm in diameter. Photocatalytic activity of thin films was examined on the basis of the phenol decomposition by UV radiation (6 x 20 W lamps, Phillips) with intensity: VIS 167 $W/m^2$, UV 183 $W/m^2$. The volume solution was 100 ml and the process was conducting by 5 hours. The phenol concentration was 10 mg/l and it was determined by UV-VIS spectrometer using standard curve for phenol $\lambda_{max}$ = 270 nm.

## 3. RESULTS AND DISCUSSION

In table 1 structural parameters of $TiO_2$ and $TiO_2$:Eu (0.1 and 0.5 at. %) thin films, deposited on $SiO_2$ substrates have been collected. Our previous work [14] has shown that HE process allows us to obtain nanocrystalline $TiO_2$-rutile directly during deposition. However, depending on Eu-dopant concentration in the thin film, the structure can be changed into the anatase (0.1 at. %) or still keep the rutile (0.1 at. %) structure. Moreover, europium at the amount of 0.1 at. % allows the stabilization of the anatase structure, upon additional annealing up to 1070 K. Besides, XRD results (tab. 1) have shown that additional annealing caused 2-times increase of the crystallite sizes and increase of the tension stress in the film as compared to standard values [15]. The maximum tension stress in the film was obtained in case of thin film annealed at 870 K. Annealing at 1270 K caused recrystalization into the rutile and increase in the crystallite sizes up to 46 nm.

Eu at the amount of 0.5 at. % in the thin film caused that after deposition the rutile was present (tab.1). The crystallite sizes were 3-times smaller as compared to $TiO_2$:(0,1 % at.)Eu – anatase, what testifies about densification of the structure with increase of the dopant amount in the film. Additional annealing at 1070 K of $TiO_2$:(0,5 % at.)Eu caused 60 % increase of the crystallite sizes and the change of the type of stress from compression to tension.

Our previous investigations [8] of $TiO_2$:Eu (0.1 at. %) thin films performed by X-Ray Photoelectron Spectroscopy have shown that europium atoms can form Eu-O-Ti bonds at the surface of $TiO_2$ nanocrystallities. As it was reported by Zeng [16], europium remains on the surface of the $TiO_2$ grains and Eu is not incorporated inside. Stabilization of the anatase phase up to 1070 K is probably connected, with expelling $Eu^{3+}$ by $Ti^{4+}$ ions into the interstitials which block the nucleation of the rutile and inhibit the anatase-to-rutile phase transformation during annealing. In connection with that, the temperature of phase transformation considerably increase as compared to data from the literature for $TiO_2$.

In figure 1 the AFM images of $TiO_2$ thin films doped with Eu at the amount 0.1 at. % (after deposition and after additional annealing at 1070 K and 1270 K) and 0.5 at. % (after deposition) on $SiO_2$ substrates have been presented. The results have shown that examined

thin films were homogenous and nanocrystalline. In case of thin film doped with 0.1 at. % Eu annealing at 1270 K caused considerably increase of grain sizes as compared to the rest of examined films (fig. 1d). In fig. 1d very big and oblong grains are visible. As it was suggested by Pamu [17], they might be clusters formed from smaller grains upon heat treatment.

| Thin films | | Structural parameters | | | |
|---|---|---|---|---|---|
| | | Phase | D (nm) | d (nm) | Δd (%) |
| $TiO_2$ | as-deposited | rutile | 8.7 | 0.3250 | +0,09 |
| $TiO_2$:Eu 0.1 at. % | as-deposited | anatase | 18.2 | 0.3520 | 0 |
| | annealed at 470 K | | 18.7 | 0.3507 | -0.37 |
| | annealed at 870 K | | 23.9 | 0.3494 | -0.74 |
| | annealed at 1070 K | | 35.2 | 0.3502 | -0.51 |
| | annealed at 1270 K | rutile | 46.0 | 0.3237 | -0.31 |
| $TiO_2$:Eu 0.5 at. % | as-deposited | rutile | 6.1 | 0.3254 | +0.22 |
| | annealed at 1070 K | | 10.3 | 0.3242 | -0.15 |

Table 1. Structural parameters of $TiO_2$:Eu (0.1 and 0.5 % at.) thin films on $SiO_2$ substrates determined on the basis of the XRD patterns. D – average crystallite size, d – interplanar distance, $\Delta d = ((d-d_{PDF})/d_{PDF})\cdot 100$ %, $d_{PDF}$ – standard interplanar distance, $d_{PDF\ anatase} = 0.3520$ nm, $d_{PDF\ rutile} = 0.3247$ nm

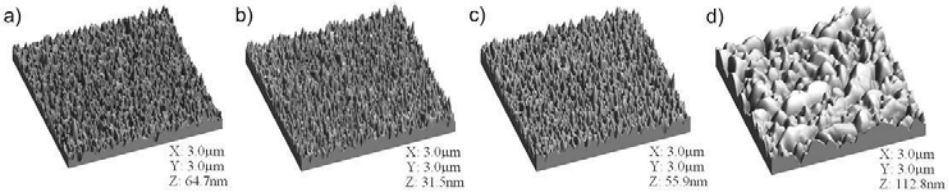


Figure 1. AFM images of $TiO_2$:Eu thin films as-deposited: a) 0.1 at. % Eu, b) 0.5 at. % Eu, and annealed (0.1 at. % Eu) at: c) 1070 K, d) 1270 K, on $SiO_2$ substrates

In figure 2 photocatalytic activity of $TiO_2$ and $TiO_2$:Eu (0.1 and 0.5 at. %) thin films, determined by the percent decrement of the phenol in time have been presented. The results have shown that after 2 hours the percent amount of decremented phenol for the thin film doped with 0.1 at. % Eu–anatase was about 7-times higher, as compared to undoped $TiO_2$ matrix. Increase of the Eu amount up to 0.5 at. % caused 4-times higher decrement of phenol as compared to undoped $TiO_2$. However this is considerably poorer result than for thin film with smaller amount of Eu. After 5 hours intensity of the reaction become saturated in case of thin films with rutile structure (undoped $TiO_2$ and $TiO_2$:0.5 at. % Eu) and the phenol decrement was about 2 %. While in case of $TiO_2$:0.1 at. % Eu – anatase, after the same period, the intensity of the reaction had still increasing tendency and the amount of phenol decrement was about 5 %. Thus, the thin film with the anatase structure exhibits the highest photocatalytic activity from the all examined films. That could be explained by the presence of potential barriers on the grain-boundary of the anatase structure which caused that the recombination time of charge carriers is loner and therefore the photocatalytic activity is better [7]. High difference of activity between $TiO_2$ doped with 0.1 and 0.5 at. % Eu is a result of specific properties of anatase and differences in surface diversification, what was observed in the AFM images (fig. 1).

In figure 3 the SIMS spectra of $TiO_2$ thin films doped with 0.1 and 0.5 at. % of Eu, as-deposited on Si substrates have been presented. SIMS results have shown that Eu-dopant in examined thin films was uniformly distributed with similar concentration in all volume. The different etching times of examined thin films are connected with different thickness of the films. The residual elements in the films, i.e. Ti and O were also distributed homogenously with constant concentration in the films.

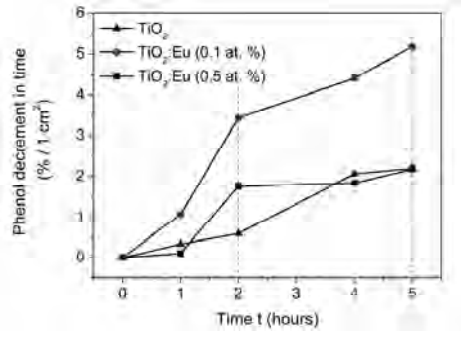


Figure 2. The photocatalytic activity of $TiO_2$ and $TiO_2$:Eu (0.1 and 0.5 at. %) thin films determined by percent decrement of phenol in time during UV radiation exposure

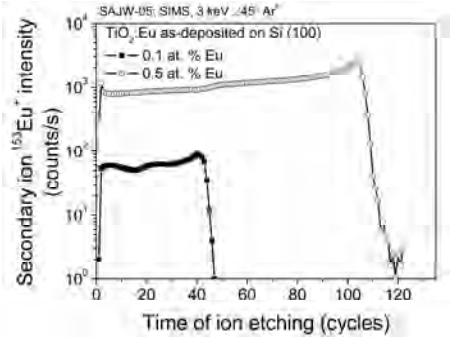


Figure 3. The SIMS spectra of $TiO_2$ thin films doped with 0.1 and 0.5 at. % of Eu, as-deposited on Si (100) substrates

## 4. CONCLUSIONS

In this work influence of Eu-doping on structural properties of $TiO_2$ thin films has been presented. Eu at the amount of 0.1 at. % stabilize the anatase structure and block rutile phase forming up to 1070 K. Also it was observed that $TiO_2$:0.1 at. % Eu – anatase has very good photocatalytic properties, considerably better than pure $TiO_2$ and $TiO_2$:0.5 at. % Eu – rutile. Possibility to obtain nanocrystalline and thermal stable up to 1070 K anatase, additionally characterized by very good photocatalytic properties, allows to application manufactured thin film as a high temperature self-cleaning coatings or sensor films.

## 5. ACKNOWLEDGEMENT

This work was financed from the sources granted by the NBCiR in the years 2008-2010 as a development research project number N R02 0019 04.

## 6. References

[1] A. Cornet, K. Shimanoe, J. R. Morante, N. Yamazoe, A.M. Ruiz Sensors and Actuators B 108 34-40 (2005)
[2] G. Lucovsky, J.G. Hong, C.C. Fulton, Y. Zou, R.J. Nemanich, H. Ade Journal of Vacuum Science & Technology B 22 (4) (2004)
[3]C. He, X.Z. Li, N. Graham, Y. Wang Applied Catalysis A: General 305 54–63 (2006)
[4] B.K. Moon, J.H. Jeong, S.-s. Yi, S.C. Kim, H. Choi, J.H. Kim Optical Materials 28 676–680 (2006)
[5] N.P. Mellott, C. Durucan, C.G. Pantano, M. Guglielmi Thin Solid Films 502 112-120 (2006)
[6] K.-R. Wu, J.-J. Wang, W.-C. Liu, Z.-S. Chen, J.-K. Wu Applied Surface Science 252 5829-5838 (2006)
[7] R.J. Tayade, P.K. Suroliaa, R.G. Kulkarnib, R.V. Jasra Science and Technology of Advanced Materials 8 455-462 (2007)
[8] G.K.L. Goh, C.P.K. Liew, J. Kim, T.J. White Journal of Crystal Growth 291 94-99 (2006)
[9] B. Park Issues in Environmental Science and Technology 24 The Royal Society of Chemistry 1-18 (2007)
[10] E.P. Lokshin, T.A. Sedneva Russian Journal of Applied Chemistry 79 1220-1224 (2006)
[11] Z. Zhao, Q.G. Zeng, Z.M. Zhang, Z.J. Ding Journal of Luminescence 122-123 862-865 (2007)
[12] E. L. Prociow, J. Domaradzki, D. Kaczmarek, T. Berlicki Polish patent No. PL 382163
[13] I. Horcas, R. Fernandez, J.M. Gomez-Rodriguez, J. Colchero, J. Gomez-Herrero, A.M. Baro Rev. Sci. Instrum. 78 013705 (2007)
[14] J. Domaradzki, D. Kaczmarek, A. Borkowska, D. Schmeisser, S. Mueller, R. Wasielewski, A. Ciszewski, D. Wojcieszak Vacuum 82 1007-1012 (2008)
[15] Powder Diffraction File Joint Committee on Powder Diffraction Standards ASTM, Philadelphia PA Card 211272 (1967)
[16] Q.G. Zeng, Z.J. Ding, Z.M. Zhang Journal of Luminescence 118 301-307 (2006)
[17] D. Pamu, M.G. Krishna, K.C.J. Raju, A.K. Bhatnagar Solid State Communications 135 7-10 (2005)

# Study of n-Type Doping GaSb Using DMTe by Metalorganic Chemical Vapour Deposition

**A.H. Ramelan [1], P. Arifin [2]**

(1) Jurusan Fisika (Physics Department), Faculty of Mathematics and Natural Sciences (FMIPA) Universitas Sebelas Maret (UNS), Jl. Ir. Sutami No. 36A, Surakarta 57126, Indonesia
Tel/Fax : +62 (271) 663375 ; Email : aramelan_uns@yahoo.com
(2) Physics Department, Faculty of Mathematics and Natural Sciences; Email: pepen@fi.itb.ac.id
Institut Teknologi Bandung (ITB), Jl. Ganesha 10, Bandung 40132, Indonesia.

Dimethyltelluride has been used as a dopant source for GaSb epilayers grown by atmospheric pressure metalorganic chemical vapour deposition (MOCVD). It has been observed that the electron concentration (n) is proportional to the Te partial pressure in the vapour phase, until n saturates at high Te partial pressure. Electron concentrations as high as $1.4x10^{18}$ $cm^{-3}$ have been measured with imperfect morphology, and as high as $1.2x10^{18}$ $cm^{-3}$ with excellent, mirror like, morphology. These appear to be the highest electron concentrations reported to date for any MOCVD-growth epitaxial n-type GaSb doped with DMTe and grown at 540°C with a V/III ratio of 1.4.

## 1. INTRODUCTION

Antimony-based III-V semiconductors grown either lattice matched or slightly strained on GaSb substrates have received much attention both due to their potential applications as optical devices in the wavelength of 1-4 μm, and for their potential use in tunnelling structures, exploiting the heterojunction offset. Although investigations in laser diodes have been carried out by many groups [1-4] problems still remain with the growth of device-quality GaSb layers [5], most significantly with doping.

Undoped GaSb usually exhibits p-type conductivity, owing to native lattice defect including Sb vacancies, antisite defects i.e., Ga atoms on Sb site, $V_{Ga}Ga_{Sb}$ [6]. The group-VI elements such as S, Se, and Te are commonly used as n-type dopants in GaSb because the group-VI elements such as Si and Sn are amphoteric and lead to heavily compensated p-type layers [7]. Researchers have investigated the n-type doping of GaSb by all major techniques [8-12]. In the course of this work, it was identified that group-VI elements have high vapour pressure and segregation coefficient, making it difficult to control the electron concentration. Therefore, the growth of GaSb doped with Te is still a challenging and worth in-depth exploration.

In this work, dimethyltelluride (DMTe) has been used as a dopant for the MOCVD growth of GaSb. The physical properties of MOCVD grown Te-doped GaSb on SI-GaAs substrates are reported. The effects of dopant flow rate on growth rate, surface morphology, and electrical properties have been determined.

## 2. EXPERIMENTAL PROCEDURE

### *2.1. Growth Condition*

Growth was carried out in the horizontal quartz atmospheric pressure MOCVD reactor. Six IR lamps were used to heat the graphite susceptor. TMGa (trimethylgallium) and TMSb (trimethylantimony) were used as metalorganic sources and kept at a constant bath temperature of -9 and 0°C, respectively which correspond to a molar flow of 2.53 and 1.82 μ mol/min respectively, for 1 sccm hydrogen flows through the metalorganics. DMTe (dimethyltellurium) was used as dopant precursor and kept at a constant temperature of 27°C. High purity $H_2$ was passed through a proprietary metal hydride filter made by Ultra Pure Systems. In this work, we have used a group V mole fraction, $X_{TMSb} = 10.1x10^{-5}$, an input V/III = 1.4, a DMTe mole fraction, $X_{DMTe} = 0.7x10^{-7}$-$7.1x10^{-6}$, a growth temperature of 540°C and the total flow rate was 8 l/min. Values of DMTe flow with corresponding mole fractions of DMTe in the input gas stream for various samples are given in table 1. Substrates used were semi insulating (SI) GaAs(100) from Freiberger (Germany). Prior to the growth, substrates were immersed for 5 min in each of trichloroethylene at a temperature of 100°C, acetone and methanol and then etched in $H_2SO_4 : H_2O_2 : H_2O = 1:1:8$ solution for 30 seconds followed by a DI water rinse. The substrate were then blown dry by $N_2$, before being loaded into the reactor.

| Sample no. | DMTe flow (sccm) | DMTe mole fraction |
|---|---|---|
| #1 | 10 | $7.08x10^{-6}$ |
| #2 | 5 | $3.54x10^{-6}$ |
| #3 | 3 | $2.12x10^{-6}$ |
| #4 | 2 | $1.42x10^{-6}$ |
| #5 | 1 | $7.10x10^{-7}$ |

Table 1. Values of DMTe flows with corresponding mole fractions of DMTe for n-type GaSb growth.

### *2.2. Characterisation*

Van der Pauw Hall measurements were performed in the temperature range of 300 - 20 K on the 3 μm thick epilayers grown on the SI-GaAs substrates. Photographs of sample morphology were taken using a Nomarski phase contrast microscope.

## 3. RESULTS AND DISCUSSION

### *3.1. Surface Morphology*

The morphology obtained from samples grown using $X_{DMTe}= 3.5x10^{-7}$ and $X_{TMSb} = 1.29x10^{-3}$ is illustrated in figure 1. The epilayers shown in figures 1a, 1b, 1c, 1d and 1e were grown with the DMTe flow rate in the range of 1 - 10 sccm for a growth temperature of 540°C. Some degradation of morphology can be seen for the samples grown with a 5 and 10 sccm DMTe flow, where hillocks and ripples are typically observed. The sample grown with 10 sccm DMTe shows pyramid-like hillocks about 10 μm across. Similar results reported for Te-doped GaAs using diethyltelluride (DETe) in low pressure organometalic vapour phase epitaxy (LPOMVPE) [13,14] show that the degradation of morphology occurs at the highest electron concentrations. Figure 1b shows the surface morphology for the GaSb sample doped with 2 sccm DMTe. The surface is mirror like and less hillocks occur. The sample shown in figure 1c was grown at 3 sccm and the surface morphology is mirror-like. For samples grown at 1 sccm, as displayed in figure 1a, small ripples and several droplets appear on the surface.

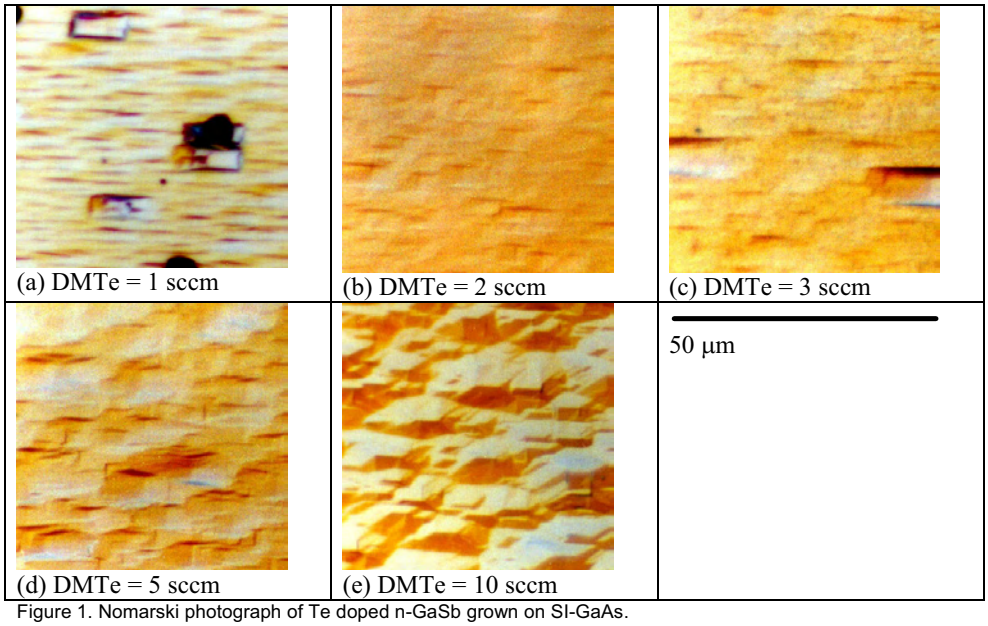


Figure 1. Nomarski photograph of Te doped n-GaSb grown on SI-GaAs.

### *3.2. Electrical Properties*

Table 2 shows the electrical properties obtained from Hall measurements of 3 μm-thick GaSb layers doped with Te. Hall concentrations from $3.5x10^{17}$ $cm^{-3}$ to $1.4x10^{18}$ $cm^{-3}$were obtained by varying the DMTe source vapour pressure. It should be noted here that the measured Hall concentration, particularly at room-temperature, is not considered to be the total free-carrier concentration. It was observed that electron concentration n is proportional to Te partial pressure in the vapour phase until it saturates at high Te partial pressure. Measured electron concentrations were as high as $1.4x10^{18}$ $cm^3$ with imperfect morphology and as high as $1.2x10^{18}$ $cm^3$ with excellent, mirror like, morphology. These appear to be the highest electron concentrations reported to date for any epitaxial n-type GaSb. The electron concentration shows a linear dependence on $X_{DMTe}$ and saturates near n = $1.4x10^{18}$ $cm^3$ when $X_{DMTe}>3.5x10^{-6}$ as shown by the circles in figure 2. A possible explanation for this behaviour is that Te incorporation results from a competition between Sb and Te atoms for Sb free-site occupation.

| DMTe flow rate (sccm) | $n_H$ (300K) ($cm^{-3}$) | $\mu_H$ (300K) ($cm^2$ /V.s) | $n_H$ (77K) ($cm^{-3}$) | $\mu_H$ (77K) ($cm^2$ /V.s) |
|---|---|---|---|---|
| 1 sccm | $5.2x10^{16}$ | 3268 | $7.6x10^{16}$ | 5437 |
| 2 sccm | $3.5x10^{17}$ | 2543 | $5.4x10^{17}$ | 4478 |
| 3 sccm | $1.2x10^{18}$ | 877 | $1.4x10^{18}$ | 1891 |
| 5 sccm | $1.4x10^{18}$ | 956 | $1.5x10^{18}$ | 1730 |
| 10 sccm | $1.0x10^{18}$ | 997 | $1.3x10^{18}$ | 1755 |

Table 2. Hall measurements on Te-doped GaSb layers as function of DMTe vapour pressure.

The squares in figure 2 show the results obtained by Wang et al. [15] using a DETe dopant MOCVD growth at a growth temperature of 550°C, and with V/III = 1.8. The higher mole fraction of DMTe in the saturation region is presumably caused by the higher vapour pressure of DMTe compared with DETe. Similar results were reported by Ehsani et al. [16] for the growth of InGaSb with DETe doping, the electron concentration was found to increase

linearly as the DETe increased, reaching a saturated concentration of $1.5x10^{18}$ $cm^{-3}$. When the DETe mole fraction was increased further, the electron concentration decreased.

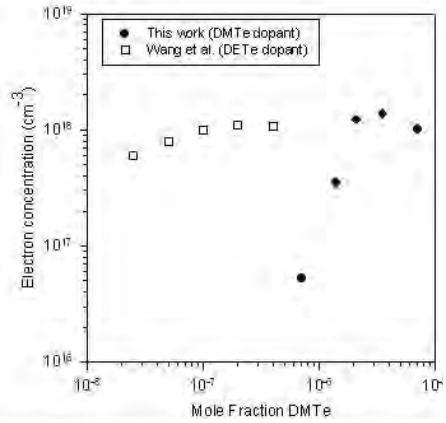


Figure 2. Electron concentration dependence on Te mole fraction.

## 4. CONCLUSION

n-type GaSb has been grown by MOCVD with DMTe as a dopant in the range of 1 and 10 sccm. It has been observed that the electron concentration (n) is proportional to the Te partial pressure in the vapour phase, until n saturates at high Te partial pressure. Electron concentrations as high as $1.4x10^{18}$ $cm^{-3}$ have been measured with imperfect morphology, and as high as $1.2x10^{18}$ $cm^{-3}$ with excellent, mirror like, morphology. These appear to be the highest electron concentrations reported to date for any MOCVD-growth epitaxial n-type GaSb doped with DMTe and grown at 540°C with a V/III ratio of 1.4.

## 5. References

[1] R.J. Menna, D.R. Capewell, R.U. Matinelli, P.K. York, and R.E. Enstron, Appl. Phys. Lett. 59, 2127 (1991).
[2] H.K. Choi and S.J. Egflas, IEEE J. Quantum Electron. QE-27, 1555 (1991).
[3] R.U. Martinelli and T.J. Zamerowski, Appl. Phys. Lett. 56, 125 (1990).
[4] A.K. Srivastava, J.C. DeWinter, C. Caneau, M.A. Pollack, and J.L. Zyskind, Appl. Phys. Lett. 48, 903 (1986).
[5] A. Sasaki, A. Ohishi, E. Sogawa, Y. Takeda, and S. Fujita, in Gallium Arsenide and Related Compounds, 1982 Institut Physics Conference, pp83-88.
[6] C. Anayama, T. Tanahashi, H. Kuwatsuka, S. Nishiyama, S. Isozumi, and K. Nakajima, Appl. Phys. Lett. 56, 239 (1990).
[7] K.F. Longenbach, S. Xin, and W.I. Wang, J. Appl. Phys. 69, 3393 (1991).
[8] I. Poole, M.E. Lee, K.E. Singer, J.E.F. Frost, T.M. Kerr, C.E.C Wood, D.A. Andrew, W.J.M. Rothwell, G.J. Davies, J. App. Phys. 63, 395 (1988).
[9] F. Pascal, F. Delannoy, J. Bougnot, L. Gouskov, G. Bougnout, P. Grosse, J. Kaoukab, J. Electron. Mater. 19, 1987 (1990).
[10] T.H. Chiu, J.A. Ditzenberger, H.S. Luftman, W.T. Tsang, and N.T. Ga, Appl. Phys. Lett. 56, 1688 (1990).
[11] J.F. Chen and A.Y. Chao, J. Appl. Phys. 70, 277 (1991).
[12] F. Nakamura, K. Tiara, K. Funato, and H. Kawai, J. Crsytal Growth 115, 474 (1991).
[13] Y.H. Houng and T.S. Low, J. Crystal Growth 77, 278 (1986).
[14] S.Z Sun, E.A. Armour, K. Zheng, and C.F. Schaus, J. Crystral Growth 113, 103 (1991).
[15] C.A. Wang, K.F. Jensen, A.C. Jones, and H.K. Choi, Appl. Phys. Lett. 68, 400 (1996).
[16] H. Ehsani, I. Bhat, C. Hitchcock, R.J. Gutmann, G. Charache, and M. Freeman, J. Crystal Growth 195, 385 (1998).

# DC and DC pulsed magnetron sputtering of dielectric materials

**G. Strauss [1], S. Schlichtherle [1], M. Stolze [2]**
1. PhysTech Coating Technology GmbH
2. Umicore Materials AG

There is an increasing interest in the last years in using oxide target materials in dc and dc-pulsed magnetron sputtering processes for the production of thin films in the application field of optical coatings, coatings for photovoltaic modules, architectural coatings, TFT displays, optical data storage and precision optics. In this work, the behavior of dielectric materials like $Nb_2O_5$ and $Ta_2O_5$ in dc continuous and dc pulsed sputter modus are discussed, the influence of some process parameters like target power, frequency, duty cycle (on and off time durations) on the deposition process and the resulting film properties will be shown. A plasma characterization of the sputter processes was done by means of a plasma monitoring system (PPM421 from Inficon), which consists of a quadrupol mass spectrometer with an additional energy analyser. The influence of the pulse frequency and the duty cycle on the plasma and deposition parameters were investigated. The correlation between the process parameters, the plasma properties (e.g. ion energy distribution) and the film properties (refractive index, stress) will be presented.

# Modeling of Phase Separation in Au-Ni Surface Alloy

**G. Zvejnieks [1], E. E. Tornau [2]**

1. Institute of Solid State Physics, University of Latvia, Kengaraga 8, LV-1063, Riga, Latvia
2. Semiconductor Physics Institute, Gostauto 11, LT-01108,Vilnius, Lithuania

We propose the kinetic Monte Carlo simulation of Au-Ni separation in Au/Ni(111) surface alloy by taking into account CO adsorption and nickel carbonyl formation reaction. We estimate Au-Au, Ni-Ni and Au-Ni pair interaction constants (v(Au-Au)=-0.08 eV, v(Ni-Ni)=-0.39 and v(Au-Ni)=-0.25) using *ab initio* calculations and find that they satisfy the inequality $|v(Au-Au)|+|v(Ni-Ni)|<2|v(Au-Ni)|$. This condition ensures an increased Au concentration on step edge after relaxation. We study the step flow rate dependence on Au-CO interaction which is one of the main factors (along with CO pressure and reaction rate) governing the process of nickel carbonyl formation. We also study the step flow rate dependence on step edge Au concentration.

## 1. INTRODUCTION

Electronic, magnetic and catalytic properties of bimetallic systems on metal surfaces attract nowadays a considerable attention. Advances in surface growth technologies allows to produce surface alloys, which are formed by two thermodynamically bulk-immicible metals only in the surface layer. Surface alloying by adatoms exchange with surface atoms in the surface layer occurs at low (submonolayer) coverages of adatom component. Au-Ni alloy on Ni(110) and Ni(111) ($c_{Au}$=0.3-0.35) [1,2], Ag-Cu on Cu(110) ($c_{Ag}$=0.2) [3] and Pb-Cu on Cu(111) ($c_{Pb}$<0.4) [4] are the examples of such bimetalic surface alloys.

In pursuit of a novel catalyst with improved properties in activity and selectivity working at industrial conditions, the Au-Ni surface alloy on Ni(111) was recently studied at high CO pressures, and phase separation was observed and recorded as STM movie [1]. Phase separation was caused by gold-catalyzed reaction producing nickel carbonyl gas and nucleation of remaining Au into islands on the reaction front.

The problem of phase separation in Au-Ni surface alloy at high CO pressure is very attractive for kinetic Monte Carlo simulations. In a first simulation reproducing experiment [1] Au-islands formation and the reaction front propogation was followed in time [5]. However, the role of CO was neglected assuming that at high pressures all Au and Ni atoms are covered by CO molecules. Neglect of CO makes it impossible to simulate the experimentally observed step flow rate dependence on CO pressure. It also contradicts the X-ray diffraction study [6] indicating the existence of strong CO-CO repulsion in CO/Ni(111) even at high CO pressures.

The effect of both CO concentration and Ni+CO reaction on step flow rate in Au-Ni surface alloy was numerically studied in our work [7]. We have noticed that step flow rate increases with CO coverage up to some critical value of CO coverage.

Here we propose kinetic Monte Carlo simulation of phase separation in Au-Ni surface alloy introducing several new aspects. First, we use “realistic” biatomic interaction parameters in our simulation. Using *ab initio* methods we calculated pair interactions of Au-Au, Ni-Ni and Au-Ni atoms. Second, we study the step flow rate dependence on Au-CO interaction which is

an important parameter governing the process of nickel carbonyl formation. And finally, we study step flow rate dependence on step edge Au concentration.

## 2. SIMULATION PARAMETERS

We perform our simulations at room temperature on a hexagonal lattice of size 100*a* (width) x 200*a*(length) with periodic boundary conditions (*a* is lattice constant). The initial lattice as in experiment [1] is randomly covered by Au (30%) and Ni (70%) concentrations. We set Au concentration on the step edge (a single border line) in a range from 30% to 95%, in order to study its effect on the step flow rate. In our model we allow Au and Ni atom jumps to the unoccupied nearest neighbor (NN) sites, as well as adsorption and desorption of CO molecules. The CO molecule is assumed to react with the neighboring Ni atom provided Ni has at least one Au atom as its NN. It should be noted that nickel carbonyl ($Ni(CO)_4$) production reaction is much more complicated [8]. In our model we consider just a single layer of atoms, i.e both jump and adsorption to an occupied site is forbiden.

The jump rate of both Au and Ni atoms, $k_{Au}$ and $k_{Ni}$, are assumed to be equal to $10^5$ $s^{-1}$. This rate can be obtained, e.g, by the activation energy around 0.4eV at pre-exponential factor $10^{12}s^{-1}$. Since the real value of the activation energy is still under debate, our value is a compromise between typical value for metals on metal (111) surfaces (0.1-0.3eV) [9] and the value 0.53eV obtained by Termenzides et al [10] for Au on Ni(111) (making adatom diffusion very slow or requiring very small pre-exponential factor). Our preliminary *ab initio* estimation indicates that activation energy of Au on Ni(111) might even be lower than 0.1eV.

In our model the diffusion of CO is neglected assuming that appropriate balance between CO adsorption and desorption effectively substitutes the CO diffusion. In the pair algorithm [11] used here atom diffusion rate is strongly affected by atom interactions. Therefore using *ab initio* VIENNA simulation package (VASP) and technique described, e.g., in Ref. [12] we calculated interactions between Au-Au, Ni-Ni and Au-Ni atoms and obtained the following attractive pair interaction constants: v(Au-Au)= -0.08, v(Ni-Ni)= -0.39 and v(Au-Ni)= -0.25 eV. It can be verified that theese constants satisfy the inequality $|v(Au\text{-}Au)|+|v(Ni\text{-}Ni)|<2|v(Au\text{-}Ni)|$. This condition ensures an increased Au concentration on step edge when one allows AuNi surface layer to relax at increased temperature values. Moreover they are very close to the phase transition estimate $|v(Au\text{-}Au)|+|v(Ni\text{-}Ni)|=2|v(Au\text{-}Ni)|$, which divides separated and mixed phases.

For our calculations we use CO pressure $p$=0.5 Torr which corresponds to CO adsorption rate $k_a=10^5$ $s^{-1}$. Desorption rate is activated and equal to $k_d=k_{d0}\exp(-E_d/k_BT)=10^{-7}s^{-1}$, where pre-exponential factor $k_{d0}=10^{13}$ $s^{-1}$ and activation energy $E_d$=1.2eV are taken from [13]. Similarly to the jump rates of Au and Ni atoms, both adsorption and desorption rates are modified [11] by CO interactions with other CO molecules and Au atoms in NN positions.

Step flow rate might be strongly affected by the interactions of CO molecules with other atoms, especially by Au-CO repulsion which can notably modify nickel carbonyl production reaction. Since at the moment these interactions are unknown, in our model we assume repulsive v(CO-CO)=0.3eV, v(Ni-CO)=0 interactions and use v(Au-CO) as a variational parameter (in limits 0.1-0.2 eV).

Finally, very important parameter of our model is the reaction rate of Ni(CO) formation, $k_r$. Here we choose $k_r$ =1 $s^{-1}$. Thus the rates chosen in our model correspond to the inequalities $k_{Au} = k_{Ni} = k_a >> k_r >> k_d$ which we consider quite appropriate: they approximately correspond to existing data on activation energies and allow to perform the calculations in a realistic time scale.

## 3. STEP FLOW RATE

Step flow rate was calculated as a derivative of parameter Δc in front propagation direction on a propagation time, where $\Delta c=h[c_{Ni}(0)-c_{Ni}(t)]/c_{Ni}(0)$ characterizes the decrease of relative Ni concentration, $c_{Ni}(t)$, with time, $c_{Ni}(0)=0.7$ and h is initial alloy length (to make the rate value independent on lattice size). Step flow rate time dependence is obtained as an average of 70-100 independent runs.

The step flow rate time dependence on Au-CO interaction constant, v(Au-CO), is presented in Fig. 1a. Interaction v(Au-CO) was chosen as a variational parameter since the CO repulsion strength by Au atom onto the neighboring Ni atom demonstrates the role of Au in effectiveness of Ni+CO reaction. It is seen that with increase of v(Au-CO) repulsion step flow rate decreases. For all curves the rate is the fastest at initial times (until Ni concentration is high), while later reaching the steady step flow rate. Note, that at reaction rate $k_r=1\ s^{-1}$, CO-CO repulsion 0.3 eV and CO pressure p=0.5 Torr we achieve the step flow rate as small as 0.005 nm/s for v(Au-CO)=0.2 eV. This value agrees well with 0.001 nm/s estimate for p=0.5 Torr [1] obtained from experimentally derived step flow rate pressure dependence.

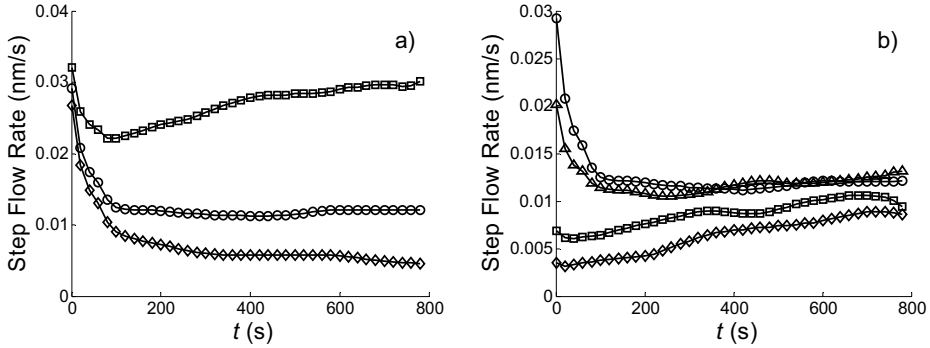


Figure 1. Step flow rate time dependences for different values of parameter v(Au-CO) (a) and concentration of Au atoms at the step edge, $c_{Au}$(edge) (b). Curves from top to bottom: (a) v(Au-CO)=0.1, 0.15 and 0.2eV at $c_{Au}$(edge)=0.3; (b) $c_{Au}$(edge)=0.3, 0.6. 0.9 and 0.95 at v(Au-CO)=0.15eV.

The time dependence of step flow rate for different concentrations of Au atoms on the step edge is shown in Fig. 1b. As might be expected, the main effect is found at initial time limit when the excess of Au atoms at the edge slows down the step flow rate. After relaxation time step flow rate becomes independ on initial Au concentration on the step edge and within the errors of calculations tends to a single value. The pronounced hindering of reaction at initial times is observed when there are more than 85-90% of Au atoms at the edge: two upper curves with 30 and 60% of Au at the edge demonstrate rather similar result. It should be noted that relaxation of Au (30%) and Ni (70%) surface with interaction constants obtained from *ab initio* estimates gives Au concentration on a step edge around 95-98%.

The snapshots of phase separation and islands formation at different v(Au-CO) values at $t$=800s are presented in Fig. 2. It is seen that considerable part of Ni atoms is still accumulated in the islands. A certain part of Ni atoms in islands outreact in later stages of reaction, but due to Au poisoning at islands edges a part of Ni will remain in islands in contradiction to experiment [1]. We obtained [7] Au islands with very small amount of screened Ni atoms, when Ni atoms were immobile with simulation parameters v(Ni-Ni)=v(Au-Ni)=0, v(Au-CO)=0.08 and v(Au-Au)=-0.05 eV. In this paper we mostly studied step flow rate dependence on both Au step concentration and v(Au-CO) interaction. The study of Ni screening problem by Au atoms is under consideration using more elaborate model.

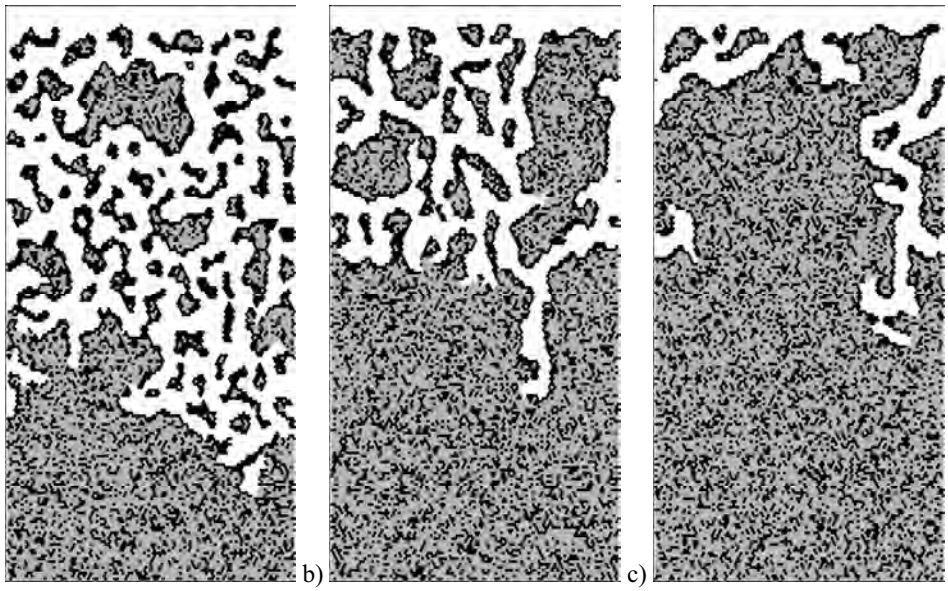


Figure 2. Snapshots at the largest step propagated distance at v(Au-CO)=0.1 (a), 0.15 (b) and 0.2 (c) at $t$=800s and $c_{Au}$(edge)=0.3. Au and Ni atoms are showed in black and grey color, respectively.

In summary, we performed kinetic Monte Carlo simulation of phase separation and Au islands growth in Au-Ni surface alloy with realistic constants of interaction between Au-Au, Ni-Ni and Au-Ni atoms and obtained step flow rate time dependences varying two important parameters hindering the reaction front propagation process: Au-CO repulsion and initial Au concentration on a step edge.

## Acknowledgement

This work was partly supported by both Latvian National Research Programme in Material Sciences and C-18 project of Lithuanian State Science and Studies Foundation.

## References

[1] E.K. Vestergaard, R.T. Vang, J. Knudsen, T.M. Pedersen, T. An, E.Laegsgaard, I. Stensgaard, B. Hammer, F. Besenbacher, Phys. Rev. Lett. 95, 126101 (2005).

[2] L. Pleth Nielsen, F. Besenbacher, I. Stensgaard, E.Laegsgaard,, C. Engdahl, P. Stolze, K. W. Jacobsen, J. K. Norskov, Phys. Rev. Lett. 71, 754 (1993).

[3] O. Kizilkaya, D.A. Hite, W. Zhao, P.T. Sprunger, E. Laegsgaard, F. Besenbacher, Surf. Sci. 596, 242 (2005).

[4] C. Nagl, O. Haller, E. Platzgummer, M. Schmid and P. Varga, Surf. Sci. 321 (1994) 237.

[5] V.P. Zhdanov, R.T. Vang, J. Knudsen, E.K. Vestergaard, F. Besenbacher, Surf. Sci. Lett. 600, L260 (2006).

[6] C. Quiros, O. Robach, H. Isern, P. Ordejon, S. Ferrer, Surf.Sci. 522, 161 (2003)..

[7] G. Zvejnieks, E. E. Tornau, Acta Physica Pol. 113, 1099 (2008).

[8] V.K. Medvedev, R. Boerner, N. Kruse, Surf. Sci. 401, L371 (1998).

[9]P.M. Agrawal, B.M. Rice, D.L. Thompson, Surf. Sci. 515, 21 (2002).

[10] K. Termentzidis, J. Hafner, F. Mittendorfer, J. Phys.: Condens. Matter 18, 10825 (2006).

[11] G. Zvejnieks, V. N. Kuzovkov, Phys. Rev. E 63, 051104 (2001).

[12] K. A. Fitchthorn, M. Scheffler, Phys. Rev. Lett. 84, 5371 (2000).

[13] P.M. Holmblad, J.H. Larsen, I. Chorkendorff, J. Chem. Phys. 104, 7289 (1996)

# Condensation of thin films HgCdTe by pulsed laser deposition

**I.S. Virt [1], T.P. Shkumbatiuk [1], I.O. Rudyi [2], I.V. Kurilo [2]**
1. Pedagogical University, 24 Ivan Franko Str., 82100, Drogobych, Ukraine
2. Lviv Polytechnic National University, 12 Bandera Str., 79013, Lviv, Ukraine

Pulsed laser deposition (PLD) has been used successfully to grow many different materials. This work reports results of experimental and theoretical investigation of $Hg_{1-x}Cd_xTe$ x~0.20 thin films structure and photoelectrical phenomena. Thin films were prepared by the PLD technique (Nd:YAG laser: $\lambda\approx$ 1064 nm; $\Delta\tau \approx$ 10 ns; f ≈ 0.5 Hz) on the Al2O3 substrates at different temperatures. The structural properties and surface morphology of films were studied by reflection high-energy electron diffraction (RHEED) method also studied by means of X-ray diffraction (XRD) technique and the lattice parameter of the transitional films was determined. The mechanical properties were investigated with microhardness method. Investigated a kinetics of growth of recordings during an (PLD). Measured the change of resistively resistance of grow thin layer $Hg_{1-x}Cd_xTe$ with the preliminary inserted Ag-contacts by the ohmmeter METEX with an output on personal computer. After the quantity of impulses of laser resistively resistance of film is translated in permittivity and its sentinel dependence is set at the Tsub = 30 °C and Tsub = 200 °C. Observed rather high specific conductivity of recordings of small thicknesses (less than 10 nm), significant diminution (~ 100 times) with a minimum value of thicknesses about 100 nm slow growth at the large thicknesses. It indicates components (increase to the coefficient of adhesion) on the prevailing process of condensation of atoms of metallic, more credible all of atoms Cd, on the initial stages of growth of films. The overlapping of a bundle of the laser during growth has enabled to place real temperature of growth of a film in a model of a nondegenerate semiconductor in the field of own conductivity. This temperature is appraised on 260 °C higher than temperature of substrates and conditioned by the local warming-up of material of films by laser plasma. Have an influence on conductivity of the as growth film also and radiation defects are generated by laser plasma. The process of annealing of such radiation defects passes at a room temperature during a few hours.

# Low Temperature Thin Films by Atomic Layer Deposition

**M. Zucca [1], I. Alessandri [1], E. Bontempi [1], L.E. Depero [1]**

1. INSTM and Chemistry for Tecnologies Laboratory, University of Brescia, via Branze 38, 25123 Brescia, Italy

Thin films can be synthesized through various chemical and physical methods; among these Atomic Layer Deposition (ALD) allows to obtain single atomic layers with excellent uniformity and conformality. An important advantage of the ALD technique is the possibility to grow oxide layers at temperatures that are significantly lower than in the chemical vapour deposition (CVD). This feature makes possible to deposit on various surfaces other than silica as some plastics or some organic substrates for interesting and innovative applications. In our research we grow layers of various oxides at very low temperatures, less than 100°C, especially titanium dioxide (TiO2), zinc oxide (ZnO) and aluminium oxide ($Al_2O_3$). These thin films have recently found several applications in optics, biomaterials and photocatalysis because of their appealing physical and chemical properties. Furthermore outstanding applications can concern the multilayer of these oxides, that can be synthesized at the same temperature. The structure and the microstructure of the oxides were analyzed through different characterization techniques such as Secondary Ions Mass Spectrometry (MiniSIMS), X-Ray Reflectivity (XRR), X-Ray Diffraction (XRD and XRD2), Scanning Electron Microscopy (SEM) and Atomic Force Microscopy (AFM). The photocatalytic activity of the multilayer films has been also investigated, evaluating the influence of the thickness of the different materials on the final properties.

Authors Index



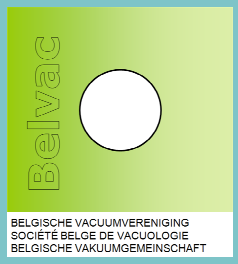












www.draft.ugent.be